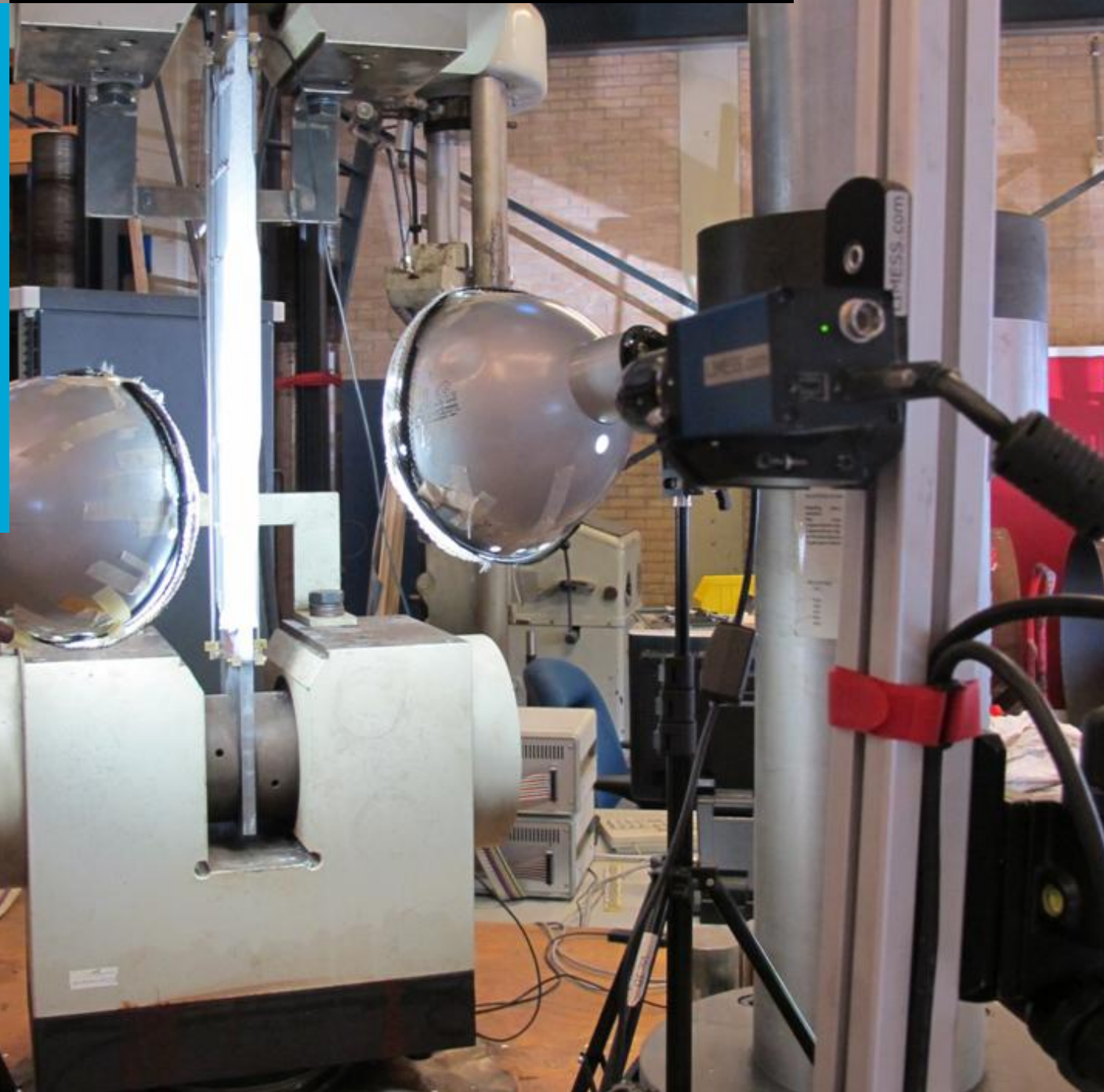


Structural Adhesive Bonded Steel-to-Steel Connections

An Introduction for Structural Engineering

Master Thesis by J.H.J. Floor

Faculty of Civil Engineering and Geosciences



Cover

This picture was taken during the tensile test of one of the five tested stepped double strap connections at the Stevin II laboratory. During this test, besides two LVDT's (linear variable differential transformer) also DIC (digital image correlation) is used for measurements. One of the two DIC camera's, mounted on a Boikon profile, can be seen in the right front. In between the lamps connection 4, mounted in the tensile test machine, is visible.

Master Thesis

Structural Adhesive Bonded Steel-to-Steel Connections

An Introduction for Structural Engineering

in partial fulfilment to the requirements for the degree of

Master of Science

in

Civil Engineering

at the Delft University of Technology,
to be defended publicly on Friday June 13, 2014 at 16h00

by

ing. Jurriaan Hildebrand Jacobus Floor

born in Maarssen, the Netherlands



Date	May, 2014		
University	Delft University of Technology Faculty of Civil Engineering and Geosciences Department of Structural Engineering Section of Structural and Building Engineering		
Author	J.H.J. Floor 4050614 (student number) jurriaanfloor@gmail.com		
Master program	Civil Engineering Structural Engineering Steel and Timber Construction		
Graduation committee	prof. ir. R. Nijse	(Chairman)	Delft University of Technology
	prof. ir. F.S.K. Bijlaard		Delft University of Technology
	ir. J. Sinke		Delft University of Technology
	dr. M.H. Kolstein		Delft University of Technology
	ir. L.J.M. Houben	(Graduation coordinator)	Delft University of Technology

I Summary

Today, there are only a few types of structural engineering applications where structural adhesives play a role, in contrast to other engineering sectors. The possibilities and difficulties of structural adhesive bonding in structural engineering, especially for steel-to-steel connections, are investigated.

Practically all structural adhesives are polymers. The cohesive properties mainly depend on their polymer structure and eventual additives. Specific adhesion covers all adhesion types through intermolecular forces (chemical, adsorptive, diffusive and electrostatic). For specific adhesion, good wetting is important. Mechanical adhesion is characterised by interlocking.

The mechanical behaviour of most structural adhesives is best described by the Drucker Prager (or related) model. Therefore the tension strength is limited, hence connections should be designed for shear and compression. Lap connections are prone to shear lag which causes a low effectiveness of long laps. Shear lag is mainly influenced by the axial stiffness of the adherents, and shear stiffness and thickness of the adhesive. Lap connections are also prone to peel, due to eccentricity of the lines of action (externally and/or internally). Peel is mainly influenced by adhesive and adherent thicknesses, bending stiffness of the adherents and axial stiffness of the adhesive.

The material properties of adhesive are strongly influenced by time-and-environmental effects, especially temperature, moisture and creep are important.

The mechanical properties of adhesive bonds provide potential for lengthening of steel beams, structures with thin elements, small tolerances or HSS, and fatigue sensitive, composite, hybrid and laminated structures. Due to the relative low weight, adhesive bonds have potential for light weight structures. Due to the appearance, aesthetics may allow the choice for adhesive bonding.

For structural engineering there are four specific points of attention. Firstly, the strength of adhesive bonds depend on the adhesive thickness. An optimal thickness exists which is relatively small. The tolerances used in structural engineering make the application of a thin bondline difficult.

Secondly, the service life of structural engineering applications is usually 50 years. At such time spans the time-and-environmental effect may lower the design strength drastically.

Thirdly, for adhesive bonding a clean working environment is needed, which is difficult to achieve on a construction site.

Finally, there is a lack in knowledge, products and code/directives for structural engineering.

For adhesive bonded beam-to-column connections a continuous beam instead of a continuous column is beneficial with respect to tension. Nevertheless, tension is hard to avoid in T- or X-shaped beam-to-column connections. An L-shaped roof connection is the most suitable beam-to-column connection for adhesive bonding. The connection can be achieved by two adhesive bonded L-shape plates to the flanges of the beam and column at the inner and outer corner. Linear elastic FEM calculations with linear elements show that, due to shear lag, the effective length of these plates is limited. Due to the large differences of axial stiffness over the width of an H-shaped profile, load transfer mainly takes place near the web. Calculations with higher order element or non-linear material behaviour are not possible with commercial computers.

To increase the efficiency of load transfer at the middle of a lap, stepped adherents can be used. The change of axial stiffness at the steps causes an uplift of the shear stress distribution. FEM and practice tests are executed for an adhesive bonded stepped double strap connection. The connection exists of two 15mm thick steel plates (S235) which are bonded (Sikadur®-30) by two bonded (Sikadur®-30) steel stepped straps. The straps exist of three 3mm thick, steel plates (S235) of 200mm, 400mm and 600mm length. FEM calculations predict a nearly linear load-displacement curve and a failure load of at least 400kN. The load-displacement curves of the practice tests are similar to the FEM curves up to $\pm 300\text{kN}$, afterwards the curve slowly flattens.

A mean failure load of 561kN, a sample standard deviation of 12.85kN and a 5th percentile failure load of 549kN have been achieved. Failure was imposed by adhesion failure; all connections show delamination near nearly all lap ends.

II Samenvatting

Vandaag de dag zijn er slechts enkele constructieve bouwtechnische toepassingen waar constructieve lijmen gebruikt worden, in tegenstelling tot in andere technische sectoren. De mogelijk- en moeilijkheden voor constructieve lijmverbindingen in de bouw, in het bijzonder staal-op-staalverbindingen, zijn onderzocht.

Praktisch alle constructieve lijmen zijn polymeren. De cohesieve eigenschappen hangen met name af van de polymeerstructuur en eventueel additieven. Specifieke adhesie omvat alle adhesie typen door inter-moleculaire krachten (chemische, adsorptie, diffusie en elektrostatische), hiervoor is goede bevochtiging van belang. Mechanische adhesie wordt gekenmerkt door interlocking.

Het mechanische gedrag van de meeste constructieve lijmen wordt het best beschreven door het Drucker Prager (of gerelateerd) model. Derhalve is de treksterkte beperkt, dus kunnen verbindingen het best op schuif en druk worden ontworpen. Lapverbindingen zijn vatbaar voor shear lag, met een lage efficiëntie van lange lappen als gevolg. Shear lag wordt hoofdzakelijk beïnvloed door de axiale stijfheid van de adherent, en afschuifstijfheid en dikte van de lijm. Lapverbindingen zijn ook vatbaar voor afpellen, door excentriciteit van de werklijnen (uit- en/of inwendig). Afpellen wordt met name beïnvloed door lijm en adherent dikte, buigstijfheid van de adherenten en axiale stijfheid van de lijm. De materiaaleigenschappen van lijm worden sterk beïnvloed door tijds-en-omgevingseffecten, met name temperatuur, vocht en kruip zijn van belang.

De mechanische eigenschappen van lijmen hebben potentie voor verlengen van stalen liggers, constructies met dunne elementen, kleine toleranties en HSS, en vermoeiingsgevoelige, composiet, hybride en gelamineerde constructies. Door het relatief lage gewicht hebben lijmen potentie voor lichtgewicht constructies. Door het uiterlijk, kan esthetica de keuze voor lijmverbindingen steunen.

Voor de constructietechniek zijn er vijf aandachtspunten. Allereerst, de sterkte van de lijmverbinding is afhankelijk van de dikte. Er bestaat een optimale dikte die relatief klein is. De toleranties die in de constructietechniek worden gebruikt maken het toepassen van een dunne lijmlaag moeilijk.

Ten tweede, de levensduur van constructies is doorgaans 50 jaar. Op deze tijdschalen kunnen de tijds-en-omgevingseffecten de ontwerpsterkte drastisch verlagen.

Ten derde, voor lijmverbindingen is een schone werkomgeving vereist, wat moeilijk te realiseren is op een bouwplaats.

Tot slot, er is een gebrek aan kennis, producten en codes/richtlijnen voor de constructie techniek.

Voor gelijkde ligger-kolomverbindingen is een doorgaande ligger in plaats van een doorgaande kolom voordelig met het oog op trek. Toch is trek moeilijk te verkomen in T- of X-vormige ligger-kolomverbindingen. Een L-vormige dakverbinding is de meest geschikte ligger-kolomverbinding voor lijm. De verbinding kan tot stand worden gebracht door twee L-vormige platen aan de flensen van de ligger en kolom in de binnen- en buitenhoek te lijmen. Lineair elastische FEM berekeningen met kwadratische elementen laten zien dat, door shear lag, de effectieve lengte van deze platen beperkt is. Door het grote verschil in axiale stijfheid over de breedte van een H-vormig profiel, vindt de belastingafdracht hoofdzakelijk plaats ter plaatse van het lijf. Berekeningen met hogere orde elementen of niet-lineair materiaal gedrag zijn niet mogelijk met commerciële computers.

Voor het verhogen van de belastingafdrachtefficiëntie in het midden van de lap, kunnen getrapte adherenten ingezet worden. Het verschil in axiale stijfheid bij de trap veroorzaakt een verheffing van de afschuifspanningsdistributie. Van een getrapte dubbele strapverbinding zijn FEM en praktijktesten uitgevoerd. De verbinding bestaat uit twee 15mm dikke staal platen (S235) welke verbonden (Sikadur®-30) zijn door twee gelijkde (Sikadur®-30) stalen getrapte straps. De straps bestaan uit drie 3mm dikke staal platen (S235) van 200, 400 and 600mm lengte. FEM voorspelt een bijna lineaire last-verplaatsingscurve en bezwijkbelasting van ten minste 400kN. De last-verplaatsingscurve van de praktijktest is gelijk aan de FEM curve tot $\pm 300\text{kN}$, hierna vlakkt deze af.

Een gemiddelde bezwijkbelasting van 561kN, een steekproefstandaarddeviatie van 12.85kN en een 5 percentiel bezwijkbelasting van 549kN zijn behaald. Bezwijken is veroorzaakt door adhesie falen; alle verbindingen vertoonden delaminatie bij bijna alle lap einden.

III Preface

This master thesis is the result of research carried out at the Structural and Building Engineering section of the Faculty of Civil Engineering and Geosciences at the Delft University of Technology. The research is an exploratory study on the applicability of structural adhesive bonding in the structural engineering.

In search for a suitable thesis topic, I encountered a flyer about 'Glued connections in steel trusses'. None of the courses which I followed throughout my student career treated adhesive bonding. I could only enumerate two applications of structural adhesive bonding in structural engineering on the spot; laminated timber and adhesive bonded carbon fibre strips for reinforcement. I wondered a few things. Why aren't there more well-known applications of structural adhesive bonding in structural engineering? What are the mechanics behind adhesive bonding? How strong are adhesive bonds? Is a full strength structural steel-to-steel connection with adhesive bonds possible? What are the possibilities of adhesive bonds? Enough questions for a graduate research and that is why I started this research.

Firstly, I would like to thank my graduation committee for giving me guidance, support and the opportunity to do this research.

Also I would like to thank Bart Wiegant, Johan Boender and Fred Bosch of the Delft Aerospace Structures and Materials Laboratory. Without their help and advice during the fabrication of the double strap connections I certainly would not have been able to fabricate the connections with the achieved quality and strength.

I am grateful to Berthil Grashof of the Delft Aerospace Structures and Materials Laboratory. Without his help and explanation with the DIC equipment, measuring with DIC was not possible.

I am grateful to Fred Schilperoort and John Hermesen of the Construction Laboratory of the Macromechanic (Stevin II) laboratory at the Faculty of Civil Engineering and Geosciences. Their help and advice during the tensile tests of the adhesive bonded double lap connections was essential for reliable test data.

I am thankful to Gérard Hagmolen of ten Have and Mark Nieuwpoort of Sika for sponsoring my research with two sets of 6kg of Sikadur®-30 and for the additional information about some of the adhesives of Sika.

Last but not least, I would like to thank my girlfriend, Judith, for her moral support and for checking all the grammar and spelling.

I hope that this thesis can take away some of the scepticism about structural adhesive bonded connections among structural engineers, architects and contractors. Hopefully this will result in an increase of adhesive bonded applications in the structural engineering.

Jurriaan Floor

Delft, May 2014

IV Contents

I	Summary	3
II	Samenvatting	5
III	Preface	7
IV	Contents	9
1	List of symbols and abbreviations	15
1.1	Greek	15
1.2	Latin	15
1.3	Subscript	17
1.4	Abbreviations	18
2	Introduction	21
2.1	Inducement	21
2.2	Objective	21
2.3	Outline	22
	Part A: Theoretical backgrounds	23
3	Advantages and disadvantages	25
3.1	Advantages	25
3.2	Disadvantages	29
4	Adhesive technology	33
4.1	Cohesion	33
4.2	Adhesion	35
5	Mechanical behaviour	39
5.1	Mechanical properties	39
5.2	Calculation methods	42
5.3	Theories	43
6	Time-and-environmental-dependent effects	53
6.1	Temperature	53
6.2	Moisture uptake	53
6.3	Creep and relaxation	54
6.4	Crazing	56
6.5	Oxidation	56
6.6	Chemicals	56
6.7	UV radiation	57
6.8	High-energy radiation	57
6.9	Biological degradation	57
6.10	Calculation method	57
7	Applications and developments	59
7.1	Composite, hybrid and laminated structures	59
7.2	Lengthening of steel beams	62

7.3	Fatigue sensitive steel structures	63
7.4	Aesthetics	63
7.5	Thin elements	63
7.6	Small tolerances	63
7.7	Light weight structures	63
7.8	High strength steel (HSS)	64
7.9	Journals	64
8	Key points of theoretical backgrounds	65
Part B: Testing of a connection		69
9	Design study of L-connection	71
9.1	Starting point	71
9.2	Types of forces on the connection	74
9.3	Analysis of a bolted T-connection	75
9.4	Analysis of a bolted L-connection	80
9.5	Analysis of adhesive bonded X- and multiple-span-T-connections	83
9.6	Choice of connection	84
9.7	Measurements and loads	84
9.8	Tolerances	88
9.9	Fabrication	94
9.10	Requirements for the adhesive and application	96
9.11	Selection of the adhesive type	97
9.12	Final design of the connection	100
10	FEM test of L-connection	103
10.1	What is FEM?	103
10.2	Cantilever length	103
10.3	Non linear calculation of the entire model	105
10.4	Redesign of the FEM model	106
10.5	Analysis of the results	108
11	Design study of double strap connection	119
11.1	Materials	119
11.2	Dimensioning	120
12	FEM test of double strap connection	123
12.1	Modelling	123
12.2	Calculation	123
12.3	Conclusion	128
13	Practice test of double strap connection	129
13.1	Design of test connection	129
13.2	Materials	131
13.3	Equipment	131
13.4	Fabrication	132

13.5	Practice test	138
13.6	Test results	140
14	Comparison of FEM and practice test results	147
15	Conclusions and recommendations	149
15.1	Conclusions	149
15.2	Recommendations	152
16	References	157
Appendices		161
17	Appendix A: Volkersen	163
18	Appendix B: Goland and Reissner	167
18.1	Derivation of shear and peel formula	167
18.2	Derivation of h_0 , v_0 and m_0	171
19	Appendix C: Adhesive types	175
19.1	Chemical characterisation	175
19.2	Appearance	175
19.3	Number of components	175
19.4	Method of application	176
19.5	Method of curing	176
19.6	Pre-treatment	178
19.7	Additives	179
19.8	Overview of adhesive types	179
19.9	Testing	182
20	Appendix D: Design sketches	185
20.1	T-connections	185
20.2	L-connections	186
21	Appendix E: MatrixFrame calculation	187
21.1	Zero storeys	188
21.2	One storey	190
21.3	Two storeys	193
21.4	Three storeys	196
21.5	Four storeys	200
22	Appendix F: Element distribution of adhesive thickness	205
22.1	FEM model	205
22.2	Linear elements	206
22.3	Quadratic elements	209
22.4	Linear and quadratic elements	213
23	Appendix G: DIANA procedure for entire L-connection model	219
23.1	Input	219
23.2	Analysis	221

23.3	Output	222
24	Appendix H: FEM results of L-connection	223
24.1	Horizontal plane of the inner angle	223
24.2	Vertical plane of the inner angle	232
24.3	Horizontal plane of the outer angle	240
24.4	Vertical plane of the outer angle	252
24.5	Additional FEM Model	261
25	Appendix I: Elaboration of DE's for stress analysis of L-connection	271
25.1	Sign conventions	271
25.2	Rotation of the beam at the horizontal plane of inner angle	272
25.3	Uniform translation of the beam at the horizontal plane of inner angle	275
25.4	Moment on the vertical plane of inner angle	278
25.5	Point load on the vertical plane of inner angle	281
25.6	Shear deformation of the beam at the horizontal plane of outer angle	284
25.7	Uniform translation of the beam at the horizontal plane of outer angle	287
25.8	Rotation of the beam at the horizontal plane of outer angle	290
25.9	Rotation of the beam at the vertical plane of outer angle	293
25.10	Uniform translation of the beam at the vertical plane of outer angle	296
26	Appendix J: Design and calculation of bolted double strap	299
26.1	Mechanical properties	299
26.2	Measurements	299
26.3	Calculation	301
27	Appendix K: Double strap according to Volkersen	305
27.1	General solution for $0 \leq x \leq l_1$	306
27.2	General solution for $l_1 \leq x \leq l_1 + l_2$	308
27.3	General solution for $l_1 + l_2 \leq x \leq l_1 + l_2 + l_3$	310
27.4	Boundary and matching conditions	311
27.5	Solving the constants	312
28	Appendix L: DIANA procedure for double strap connection model	315
28.1	Input	315
28.2	Analysis	319
28.3	Output	320
29	Appendix M: FEM results of double strap connection	321
29.1	Shear stress of first adhesive layer at last load step	322
29.2	Peel stress of first adhesive layer at last load step	325
29.3	Equivalent stress of first adhesive layer at last load step	328
29.4	Equivalent strain of first adhesive layer at last load step	331
29.5	FEM results for comparison with DIC	334
30	Appendix N: Influence of adhesive thickness	341
30.1	Modelling and calculation	341
30.2	Results	341

30.3	Conclusion	346
31	Appendix O: Pictures of practice test	349
31.1	Location of pictures	349
31.2	Test 1	350
31.3	Test 2	353
31.4	Test 3	354
31.5	Test 4	356
31.6	Test 5	359
32	Appendix P: DIC results	361
32.1	Connection 2; DIC measurement of the front	362
32.2	Connection 4; DIC measurement of the side	365

1 List of symbols and abbreviations

1.1 Greek

α	angle	<i>rad</i>
	contact angle	<i>rad</i>
β	factor used for Goland and Reissner theory, see equation (18.22)	-
	factor used at appendix H, see equation (25.7)	<i>mm</i> ⁻¹
γ	safety factor	-
	(engineering) shear strain	-
δ	relative displacement	<i>mm</i>
ε	strain	<i>mm/mm</i>
θ	angle	<i>rad</i>
λ	factor used for Goland and Reissner theory, see equation (18.31)	-
μ	mean value	-
ν	Poisson's ratio or lateral contraction coefficient	-
	number of degrees of freedom of student's t distribution	-
ξ	reduction factor	-
σ	stress	<i>N/mm</i> ²
	standard deviation	-
τ	shear stress	<i>N/mm</i> ²
ψ	combination factor	-
	dilatancy angle	<i>rad</i>
ϕ	internal friction angle	<i>rad</i>
ω	factor used for Volkersen theory, see equation (17.20)	<i>mm</i> ⁻¹
Γ	gamma function, see equation (13.4)	-
Δ	difference	-
	factor used for Goland and Reissner theory, see equation (18.35)	-
Σ	sum	-

1.2 Latin

<i>A</i>	factor used for Goland and Reissner theory, see equation (18.12)	<i>N/mm</i>
	Area	<i>mm</i> ²
<i>C</i>	constant	<i>variable</i>
<i>D</i>	plate stiffness, see equation (18.9)	<i>Nmm</i>
	profile height	<i>mm</i>
<i>E</i>	Young's modulus or tensile modulus	<i>N/mm</i> ²
<i>F</i>	point load	<i>N</i> or <i>kN</i>
	force	<i>N</i> or <i>kN</i>

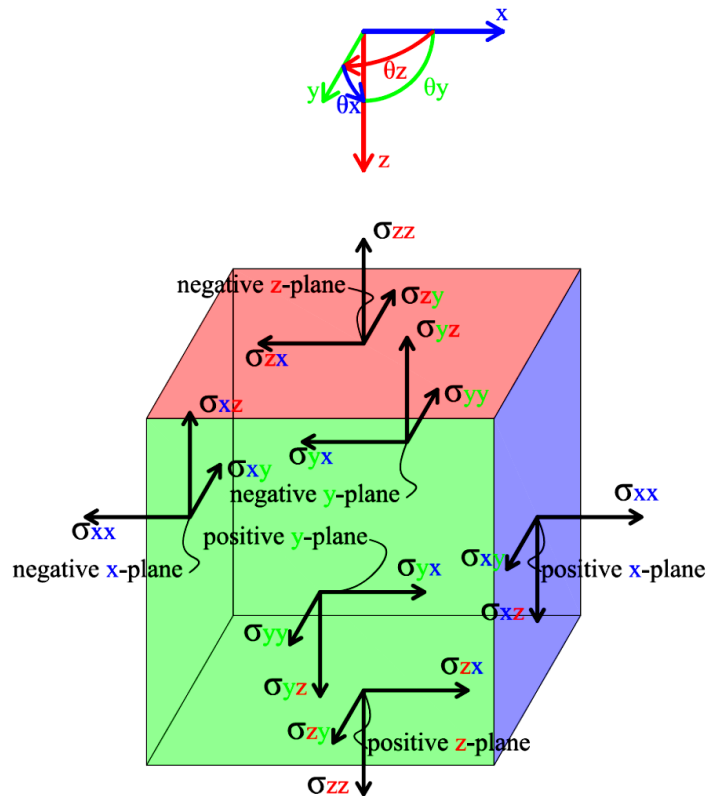
G	shear modulus	N/mm^2
G	fracture energy or strain energy release rate	J/mm^2
H	horizontal force	N or kN
I	second moment of area	mm^4
K	stress intensity factor	-
	factor used at Drucker-Prager criterion, see equation (28.6)/(28.11)	-
M	moment	Nmm or kNm
P	uniformly distributed load	N/mm^2 or kN/m^2
	cumulative distribution function	
T	temperature	$^{\circ}C$
V	shear force	N or kN
W	section modulus	mm^3
	prescribed displacement	mm
a	length of side	mm
b	(overlap) width	mm
	length of side	mm
c	half of overlap width	mm
	cohesion	N/mm^2
	coefficient	-
e	deviatoric strains (see (12.5))	mm/mm
f	strength	N/mm^2
	load per width	N/mm
h	height	mm
	distributed horizontal force	N/mm
k	bending moment factor	-
	reduction factor	-
	out-of-squareness	mm
	distributed spring stiffness	$N/mm^2/mm$
l	(overlap) length	mm
m	distributed moment	Nmm/mm
n	sample size	-
	number	-
p	probability density function	-
q	line load	N/mm or kN/m
	tolerance	mm
r	radius	mm
	factor used for Goland and Reissner theory see equation (18.36)	-
s	factor used in appendix H see equation (25.14) and (25.47)	mm
	deviatoric stresses (see (28.2))	N/mm^2
	sample standard deviation	-

t	time	s or h
	t-statistic of student's t-distribution	-
t_1, t_2	thickness of adherents	mm
t_a	thickness of adhesive (bondline thickness)	mm
u	longitudinal displacement	mm
	factor used for Goland and Reissner theory see equation (18.49)	mm^{-1}
v	distributed shear force	N/mm
w	transverse displacement	mm

1.3 Subscript

0	initial instantaneous 0 degrees with respect to the grain direction (timber)
1	element 1 principal direction 1
2	element 2 principal direction 2
3	principal direction 3
90	90 degrees with respect to the grain direction (timber)
95%	value which belongs to the 95% exceeding change
A	region A
B	region B
DP	Drucker-Prager
G	permanent
Q	variable
ST	stress free
T	temperature
VM	Von Mises
a	adhesive
ave	average
b	bottom
c	compression
d	design
dec	decomposition
$degr$	degradation
eq	equivalent
ess	essential
f	flange
fun	functional
g	glass transition

<i>i</i>	index number
<i>k</i>	characteristic
<i>l</i>	left
<i>m</i>	melting point
	material
max	maximal
min	minimal
<i>o</i>	operation
<i>pl</i>	plastic
<i>r</i>	rupture
	right
<i>ref</i>	reference
<i>rep</i>	representative
<i>s</i>	steel
<i>sh</i>	shear
<i>t</i>	top
	tension
<i>tot</i>	total
<i>u</i>	ultimate
<i>v</i>	shear
<i>v</i>	variance
<i>w</i>	web
<i>x</i>	x-direction
<i>xx</i>	x-direction on x-plane
<i>xy</i>	y-direction on x-plane
<i>y</i>	y-direction
	yield
<i>yy</i>	y-direction on x-plane
<i>yz</i>	z-direction on a y-plane
<i>z</i>	z-direction
<i>zz</i>	z-direction on z-plane
<i>zx</i>	x-direction on z-plane



1.4 Abbreviations

ABS	Acrylonitrile Butadiene Styrene
AN	Acrylonitrile
AUTOMA	Automatic solution method (solver of DIANA)
BL	Bilinear
CA	Cyanoacrylate
CFRP	Carbon Fibre Reinforced Polymers
CTE	Coefficient of Thermal Expansion
DASML	Delft Aerospace Structures and Materials Laboratory
DE	Differential Equation
DIC	Digital Image Correlation
DOF	Degree Of Freedom
DP	Drucker-Prager
DUT	Delft University of Technology
EB	Euler Bernoulli
EBC	Electron Beam Cured
EP	Elastic Plastic

FEM	Finite Element Modelling
FI	Flame cleaning
FRP	Fibre Reinforced Polymer
GB	Gigabyte
GENEL	Out-of-core direct solution method (solver of DIANA)
GUI	Graphic User Interface
HEA	European wide flange beams (type A)
HMA	Hot Melt Adhesive
HSFG	High Strength Friction Grip
HSS	High Strength Steel
IPE	European I beams
LE	Linear Elastic
LVDT	Linear Variable Differential Transformer
MS	Modified Silane
NDT	Non-Destructive Test
PA	Polyamide
PC	Polycarbonate
PE	Polyethylene
PF	Phenol Formaldehyde
PMMA	Polymethyl Methacrylate
POM	Polyoxymethylene
PP	Polypropylene
PS	Polystyrene
PSA	Pressure Sensitive Adhesive
PTFE	Polytetrafluorethylene
PU	Polyurethane
PVC	Polyvinyl Chloride
Qu	Quadratic
RAM	Random-Access Memory
RH	Relative humidity
RHS	Rectangular Hollow Section
Sa	Blast cleaning
SCF	Stress Concentration Factor
SIF	Stress Intensity Factor
SLS	Service Limit State
S-N	Stress amplitude versus Number of cycles
St	Hand and power tool cleaning
UF	Urea formaldehyde
UHPC	Ultra High Performance Concrete
ULS	Ultimate Limit State
UV	Ultra Violet
VM	Von Mises

2 Introduction

The first applications of adhesive bonding date back to at least 2000BC. These adhesives existed of organic materials. From the beginning of the 20th century the first synthetic adhesives were developed, but structural adhesive bonded steel-to-steel applications date back to only the Second World War. [1, 2]

A broad definition of adhesive is 'an intermediate layer which connects two materials in a durable way'. The two materials that are connected by the adhesive are called adherents or substrates. Out of coherence considerations the term adherent is preferred over substrate, because bonding between the adherent and adhesive particles is called adhesion. Bonding between adhesive particles itself is called cohesion.

2.1 Inducement

Many people (both structural engineers and laymen) are cautious about the structural use of adhesives. One thinks of badly sticking, nondurable and/or low strength tapes when adhesives are mentioned. But nowadays we trust structural adhesive bonds in our daily lives. Industries such as the automotive and aerospace industry use structural adhesive bonding as a fully fledged connection method. The use of adhesive in structural engineering seems to lag behind in comparison to other engineering sectors, due to several reasons such as the use of thick profiles, high tolerances, tailor made solutions and lack of knowledge. For instance, during the civil engineering master courses of the structural engineering track structural adhesive bonding is not taught at the Delft University of technology. In structural engineering adhesive bonding is rarely used, only for special cases such as carbon fibre reinforcement strengthening. Up to now only a few researches have focused on structural adhesive bonded applications for structural engineering. Because of this, there is a lack of knowledge and trust under structural engineers, architects and constructors.

A committee member which is involved with this thesis, professor Nijssen, was involved as engineer in a project where connections were calculated as structural adhesive bonds. Even tests were done to verify the calculations and ensure enough bearing capacity. But the contractor was not familiar with structural adhesive bonding which led to a lack of trust. In the end, the project is not carried out with structural adhesive bonds. Such a case shows that research is needed to increase the knowledge and trust in the civil and building industry.

2.2 Objective

The goal of this thesis is to investigate the possibilities and difficulties of structural adhesive bonding for structural engineering, especially for steel-to-steel connections. This thesis should give answers on questions like:

- What are the advantages of adhesive bonding?
- What are the disadvantages of adhesive bonding?
- What are adhesives exactly?
- How does adhesive bonding work?
- What are the mechanics behind adhesive bonding?
- What are points of attention during designing adhesive bonds?
- For which application are adhesive especially suitable?
- Can adhesives play a role in commonly used steel-to-steel connections?

2.3 Outline

The thesis is divided into two main sections. The first part consists of a literature study to obtain some basic knowledge about adhesive and adhesive bonding. In the second part a connection out of the structural engineering is chosen for further research. For this connection FEM calculations are made and practice tests are done to investigate the feasibility of adhesive bonds for structural engineering.

Part A: Theoretical backgrounds

3 Advantages and disadvantages

In structural engineering, the major part of all structural connections are bolted or welded. In most cases standardised details are used. Other types of connections, such as adhesive bonded connections, have to compete with these standardised details. It has to be proved that they are beneficial, this applies to every single detail.

For a good comparison between adhesive bonded, and bolted and welded connections, an overview of the advantages and disadvantages of adhesive bonded in comparison to bolted and welded connections is necessary. In this chapter an overview and short explanation of these advantages and disadvantages is provided.

3.1 Advantages

Adhesive bonded connections have the following advantages with respect to bolted and/or welded connections;

- Fewer and lower stress concentration;
- No significant heat input;
- Ability to avoid galvanic corrosion between dissimilar materials;
- Joining all kinds of materials and dissimilar materials;
- Small tolerances possible¹;
- Invisible connections possible;
- Good sealing properties with regard to gasses, moisture and chemicals;
- Good insulation properties with regard to heat, sound and electricity;
- No significant increase in weight;
- No influence on the straightness, cross sectional area of the elements;
- No introduction of large (residual) stress;
- Usable as gap-filler;
- Complex joint configurations possible.

With a good design and manufacturing process the following advantages can be added:

- Increase of stiffness;
- Increase of dynamic damping;
- Increase of fatigue life;
- Reduction of labour and capital costs.

3.1.1 Fewer and lower stress concentration

Adhesive bonded connections are nearly always plane connections, only the rarely used butt connections are an exception. The adhesive is spread over a plane by which the occurrence of high stress concentrations is prevented. Bolted connections are point connections and welded connections are line connections. Especially for bolted connections, high stress concentrations are unavoidable and of special interest.

Tough materials, which have a plastic strain behaviour, are capable of withstanding stress concentrations well, but brittle materials are less capable of doing so.

Thin materials may fail due to bearing failure when stress concentrations occur. Preventing high stress concentrations increases the failure load in that case.

So the reductions of stress concentrations, in number and height, improves the applicability of a connection type. [3]

¹ See also the disadvantages of small tolerances at section 3.2.6.

3.1.2 No significant heat input

During the curing process of adhesive bonded connections it may be required to heat up the adhesive to a certain temperature for some time. This temperature increase is rather low (in most heat cured case between 80 °C and 120 °C [4]) by which, in all likelihood, no significant negative effects take place in the steel.

On the other hand, welding goes hand in hand with significant heat input. This has some disadvantages;

- Heat input eliminates the advantages of heat treatment of structural steel, e.g. normalising, hardening, quenching and tempering partially or completely;
- Dissimilar metals melt at different temperatures, which may cause difficulty in welding;
- Heat can cause safety risks;
- Heated materials expand which can cause residual stresses.

3.1.3 Ability to avoid galvanic corrosion between dissimilar materials

The adhesive between the adherents acts as a separation through which the exchange of ions is prevented. Therefore, galvanic corrosion cannot take place in a proper designed adhesive bonded connection.

For bolted connections there are several solutions for preventing galvanic corrosion, e.g. stainless steel bolts, galvanised bolts and synthetic inlays, but those raise the costs and actions.

Galvanic corrosion limits the applicability of welding because there is no good solution available to prevent this. [3]

3.1.4 Joining all kinds of materials and dissimilar materials

For nearly all materials and material combinations there are adhesives available. The possibilities are practically endless.

Welding is only possible for metal to metal connections. Attention must be paid to the acceptability of heat input for both metals and galvanic corrosion.

Bolting is theoretically possible for all materials, but attention must be paid to stress concentrations and galvanic corrosion. [3]

3.1.5 Small tolerances possible

The bondline thickness of adhesives can be very small. In aerospace engineering a bondline thickness of 0.1 mm is not exceptional. This makes small tolerances possible.

For traditional bolted connections there are tolerances of 2 to 3 mm required to fit the bolt into the bolt hole [5]. This causes slip in the bolted connection, which should be taken into account in the design and applied tolerances.

Injection bolts solve the slip problem that traditional bolts have by injecting the bolt hole so no slip can take place.

Fitted bolts solve the slip problem that traditional bolts have by applying smaller tolerances for the bolt holes and making use of special bolts.

High Strength Friction Grip (HSFG) bolts are prestressed so that the load transfer takes places through friction. Slip will no longer take place, so smaller tolerances are possible.

Due to the heat input during welding metal will expand, which rises stress and/or strains, which should be taken into account in the design and applied tolerances. [3]

3.1.6 Invisible connections possible

Bondlines of adhesive bonded connections can be very thin, so connections can be made 'invisible', whereas in welded connections the weld remains visible. In bolted connections the bolts, nuts and washers remains visible. [3]

3.1.7 Good sealing properties with regard to gasses, moisture and chemicals

Adhesive bondlines work as a sealing, therefore gas-, moisture- and chemical-tight connections can be made.

Welds can also acts as a sealing.

Due to i.a. the bolts holes, tight connections are difficult to make with bolting. [3]

3.1.8 Good insulation properties with regard to heat, sound and electricity

Adhesives have good insulation properties with regard to heat (low thermal conductivity), sound (low acoustic conductivity¹) and electricity (electrically non-conductive). The adhesive prevents contact between the adherents so that good insulated connections can be made.

With plastic insulators the insulation properties of bolted connections can be improved. But ordinary bolted connections have bad insulation properties.

Due to metal-to-metal contact welds have bad insulation properties with regard to heat, sound and electricity. [3]

3.1.9 No significant increase in weight

Adhesives are light in comparison to most structural building materials. Welded and bolted connections are heavier due to the adding of metal.

3.1.10 No influence on the straightness and cross sectional area of the elements

In cold cured adhesive bonded connections the straightness and cross sectional area is not influenced. For hot cured adhesive bonded connections the straightness is affected due to the different coefficient of thermal expansion of the adhesive and adherent, see section 3.2.15.

During welding the heat input causes deformations and therefore a reduction of straightness. Because of this, welding, e.g. of internal stiffeners, is difficult.

For bolted connections bolt holes are made, which reduces the cross sectional area of the material. [3]

3.1.11 No introduction of high (residual) stress

During welding stresses will develop due to the expansion of the material. After the cooling down process not all of the stresses will disappear.

During the hardening process of the adhesive also heat may be used but at lower temperatures than for welding which results in lower stresses. Due to the low stiffness of the adhesive in comparison with steel, the residual stress will remain low.

Bolted connections do not give this kind of stress.

3.1.12 Adhesive can act as gap-filler

The adhesive can act as a gap-filler so that no additional gap-filler is required, which speeds up the preparation.

¹ The term 'acoustic conductivity' is not often used but the phenomenon is similar to heat and electrical conductivity. More commonly 'acoustic attenuation' is used, a large acoustic attenuation entails a low acoustic conductivity.

3.1.13 Complex joint configurations possible

The manufacturing of an adhesive bonded connection may be carried out without large pieces of equipment. Therefore complex joint configurations are possible because in the design process no manoeuvring space for equipment has to be taken into account. For instance, honeycomb panels are hard to make with bolts or welds. [3]

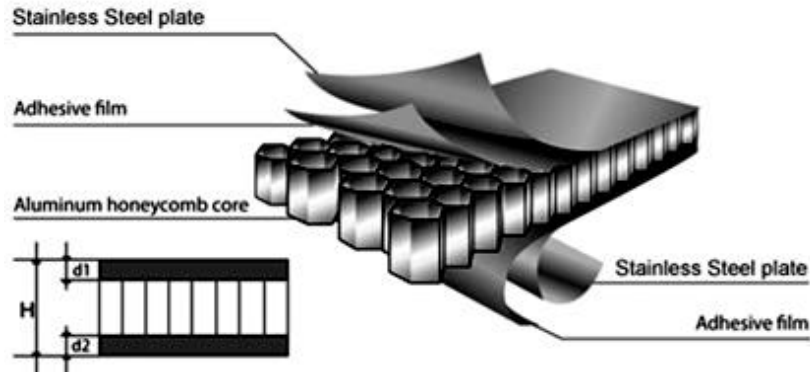


Figure 3.1: Adhesive bonded honeycomb panel [6]

3.1.14 Increase of stiffness

Adhesive bonded connections are plane connections, this can make the connection stiffer than welded (line) and bolted (point) connections. In the next picture stress distribution can be found for plane, line and point connections. The troughs in the stress distribution indicate a lower stiffness. Adhesive has a relative low stiffness in comparison to other building materials, so good designing is required to get a stiff connection. [3]

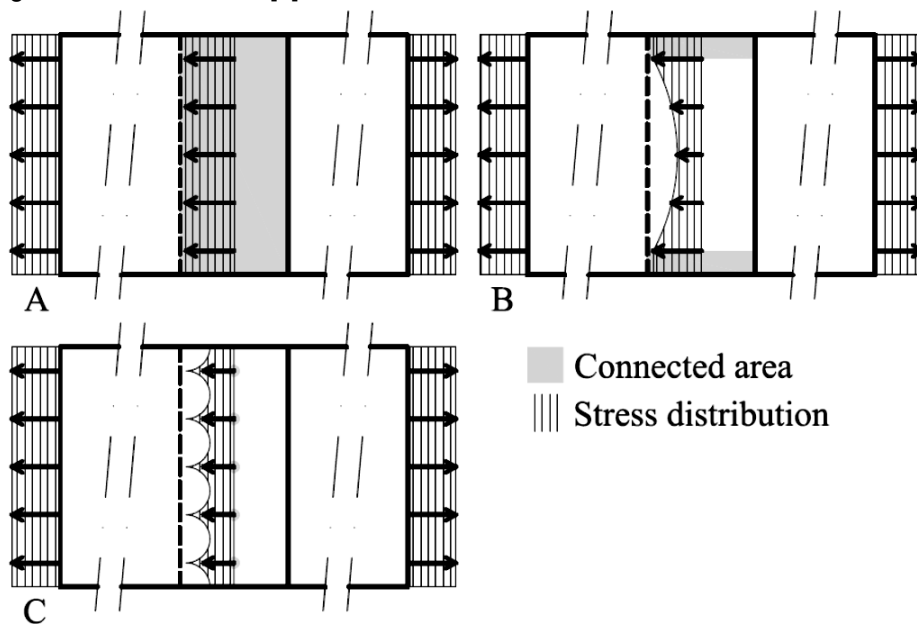


Figure 3.2: Stress distribution of a plane (A), a line (B) and a point (C) lap connection

3.1.15 Increase of the dynamic damping

Well designed structures with adhesive bonded connections have a higher structural damping than structures with welded or bolted connections, due to the better ability to dissipate kinetic energy (which is also responsible for good sound insulation, see section 3.1.8). [3]

The level of the effective damping depends on several factors, for instance the type of adhesive, adhesive thickness and temperature. In most cases adhesive layers are thin, consequently the damping of adhesive bonded structures is lower than those of the adhesive itself. [7]

According to [7] a damping ratio¹ between 0.04% and 0.95% can be expected for adhesive bonded structures. But the tests where these values are based on, are not representative for constructions in structural engineering. To compare the damping ratio of adhesive bonded structures some damping ratios mentioned in section 4.1.3 of [8] are depicted in the next table:

Type of structure	Damping ratio
Welded steel	0.02%
Bolted steel	0.04%
Prestressed concrete	0.02%
Reinforced concrete	0.05%

Table 3.1: Damping ratio Eurocode 8 [8]

3.1.16 Increase of the fatigue life

The fatigue life is generally calculated with a so called S-N or Wöhler curve and Palmer-Miner rule. These curves are based on the principle that high stress variations are more severe than low stress variations (logarithmic relation).

Adhesive bonded connections are less subjected to high stress peaks than welded and bolted connections, this increases the fatigue life.

Bolted connections are also subjected to prying/wiggle which can reduce the fatigue life drastically. [3]

3.1.17 Reduction of labour and capital costs

The manufacturing of some adhesive bonded connections can take place without specialised equipment, which reduces the capital costs. This depends on the required surface treatment of the adherents. Bolted connections are always made with several bolts, also welded connections are often made with several welds. Adhesive bonded connections have bond surfaces. The number of actions, and therefore the labour costs, for one surface can be less for that reason for adhesive bonded connections than bolted or welded connections. [3]

3.2 Disadvantages

Adhesive bonded connections have the following disadvantages with respect to bolted and/or welded connections:

- Complex manufacturing process;
- Fixing of the adherents during cure process is necessary;
- Significant influence of the environment on the durability;
- Environmental conditions affect the properties of the adhesive;
- Time dependent effects affect the properties of the adhesive;
- High strength bonding demands small tolerances;
- Possible toxicity and its effects on the environment and labour conditions;
- Difficulty to apply non-destructive test methods to control and check the bondline quality;
- Difficulty to dismantle the joint for repair or re-use of the materials;
- Stress levels in the bondline are hard to predict;
- No building codes available for calculation;
- Strong in shear and compression, but weak tension and peel;
- Specialised storing conditions may be required;

¹ The damping ratio is the ratio between the damping and the critical damping.

- Little practical experience among contractors and designers;
- Mismatch of coefficient of thermal expansion.

3.2.1 Complex manufacturing process

The manufacturing process of adhesive bonded connections is more complicated than for bolted and welded connections. Generally, a good adhesive bonding requires extensive preparation, e.g. cleaning of the surface and applying a primer. During curing the temperature, humidity, air and hardening pressure should be controlled to get the required quality. In some cases specialised equipment, that not every constructor has in store, is needed, e.g. an autoclave. Extensive preparation and the use of an autoclave will result in prefabrication in most cases. And last but not least skills are needed that are not common among construction workers. [3]

3.2.2 Fixing of the adherents during cure process is necessary

After curing the adhesive has its final strength. But in most cases the adhesive does not have enough strength to hold the adherents in place during curing. So the adherents should be fixed during curing. The length of the curing process is variable and depends i.a. on humidity and temperature. [3]

3.2.3 Significant influence of the environment on the durability

The environment, e.g. rain and frost, may have a negative effect on the durability of adhesives. Precautions should be made to limit the influences of the environment and so increase the life span of the connection. The application of a sealant or an insulation layer are possible precautions. During designing the exposed surface should be kept as small as possible so the influence of the environment is as small as possible. [3]

3.2.4 Environmental conditions affect the properties of the adhesive

The properties of adhesives, e.g. strength, stiffness and permeability are affected by temperature and humidity fluctuations of normal outside conditions. This should be taken into account in the design. Often this is done by applying reduction/knock down factors for the mechanical properties. [3]

3.2.5 Time dependent effects affect the properties of the adhesive

Adhesives are prone to creep and degradation which shortens the life span. Also fatigue can be seen as a time dependent phenomenon but in structural engineering this is mostly treated separately, because only constructions subjected to cyclic loads are prone to fatigue. [3]

3.2.6 High strength bonding demand small tolerances

Research has shown that a thin bondline results in high bond strength, see section 5.3.4.1. Small tolerances are often accompanied by high costs. In structural engineering mostly tolerances are used that are of a higher order than the optimal bondline thickness.

For welded and bolted connections high tolerances are allowable, which results in lower costs.

3.2.7 Possible toxicity and its effects on the environment and labour conditions

Some adhesives or aids used during manufacturing are toxic. This can have a bad influence on the environment and labour conditions. [3]

3.2.8 Difficult to apply non-destructive test methods to control the bondline quality

For adhesive bonded connections there are several specialised non-destructive test (NDT) methods. But it is hard to give a good evaluation of the properties. [3]

In section 19.9.2 a overview of the most important NDT methods can be found.

3.2.9 Difficult to dismantle the joint for repair or re-use of the materials

After the adhesive is cured it is difficult to dismantle the joint. At low temperatures most adhesive become brittle, this facilitates dismantling. At high temperatures some adhesives become viscous and for most adhesives the rupture strength drops significantly also this facilitates dismantling. [3]

3.2.10 Stress levels in the bondline are hard to predict

Several studies predict the stresses in the bondline incorrectly. In the end zone of the adhesive, where the stresses are highest, the predictions regularly do not match with the test results. Especially theories about the influence of the bondline thickness are contradictive. An optimal design is hard to make if the behaviour is not fully understood and cannot be predicted correctly. [1]

3.2.11 No building codes available for calculation

For adhesive bonded connections there are no building codes available yet. This means that for every single connection it has to be proved that it is safe and therefore a strategy for certification have to be made. This discourages the choice for adhesive bonded connections. The absence of codes is caused by the hard to predict stress levels as described in the preceding section.

3.2.12 Strong in shear and compression, but weak in tension and peel

Adhesive bonded connections are strong in shear and compression, but weak in tension and peel stresses. Specialised details are therefore necessary. Not every engineer has the expertise to do so.

3.2.13 Specialised storing conditions may be required

Some adhesive may require specialised storing conditions, such as a certain temperature, to ensure a certain shelf life. Not all constructors will have the equipment to create such conditions.[9]

3.2.14 Little practical experience among contractors

Structural adhesive bonded connections are not widely spread in the structural engineering, therefore there is little practical experience among contractors and designers. This may lead to errors.

3.2.15 Mismatch of coefficient of thermal expansion

Difference in coefficient of thermal expansion (CTE) gives rise to stresses at a temperature gradient. In general, the CTE's for adhesives and steel differ quite a lot. See also section 5.1.4.

4 Adhesive technology

To understand the adhesion process, knowledge about adhesive technology is required. This chapter provides a brief introduction in adhesive technology.

The properties of an adhesive bonded connection is determined by two factors, the adhesive and cohesive properties. For engineers the strength and stiffness are of most interest. The adhesive strength is the strength of the bonding of the adhesive layer to the adherent (bonding of different type of particles). The cohesive strength is the strength of the adhesive layer itself (bonding of same type of particles). The exact behaviour of interfaces is hard to predict, therefore most connections are designed so that the adhesion strength is the strongest link. Hence, failure will take place in the adherent or the adhesive. On the following pages the basics of cohesion and adhesion is provided.

4.1 Cohesion

There are a lot of adhesive types available nowadays. Most adhesives are organic or synthetic. The cohesion behaviour of those types can be described by what is known from the polymer technology.

4.1.1 Polymer structure

Polymers are macromolecules build up from smaller molecules called monomers. Polymers can be classified by their molecular structure. Polymer technology distinguishes four types; linear, branched, cross linked and network (see Figure 4.1).



Figure 4.1: Schematic illustration of a linear, (b) branched, (c) cross-linked and (d) network (3D) molecular structures [10]

The long chains of molecules of linear and branched structures are only bonded by weak physical bonds. The chains of cross linked and network structures are also bonded by stronger chemical bonds. Adhesives of all four types of structures are available, however most structural adhesives are cross linked or network polymers. [3]

4.1.2 Polymer behaviour

Instead of classifying polymers by structure, they can also be classified with respect to their behaviour, although this is practically the same. Three types are distinguished; elastomer (cross-linked), thermoset (network, also known as thermosetting) and thermoplastic (linear and branched). An elastomer has a low degree of cross linking which makes it capable of stretching to a high extension and recovering without permanent deformation. A thermoset has a higher degree of cross linking, so the monomers form a network, which makes a thermoset more rigid than an elastomer. Both latter types do not melt, but degrade above a certain temperature, T_{degr} . In contrast, a thermoplastic melt at a certain temperature, known as the melting temperature, T_m . A Thermoplastic is built of linear and branched polymers. Above the glass transition temperature, T_g , polymers soften. Especially thermoplastics exhibit this behaviour. They show a sort of ‘thermal plateau’ (see

Figure 4.2) between T_g and T_m , and become plastically deformable above the T_g and harden again if the temperature drops below T_g . For elastomer and thermoset polymers this behaviour is less clear, although they soften above T_g , they are not plastically deformable above T_g , therefore they are also known as thermohardening polymers. At a certain temperature, which is higher than T_m respectively T_{degr} , adhesive decompose, T_{dec} .

Adhesives can be classified into one of these three types, but for some adhesives distinguishing between elastomer and thermoset is difficult.[3]

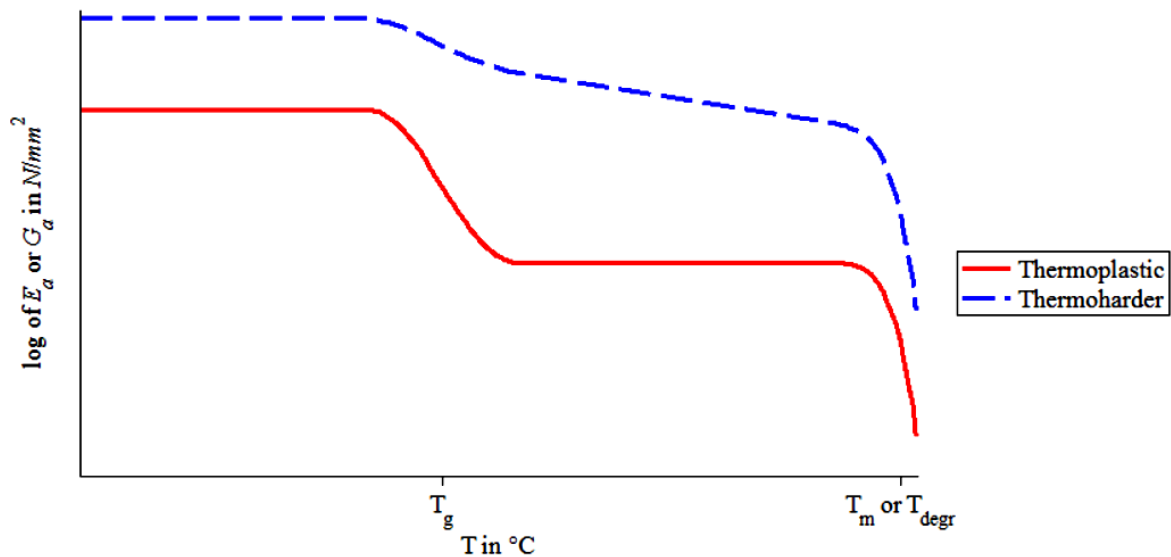


Figure 4.2: Qualitative influence of temperature on the elasticity of polymers

4.1.3 Additives

To influence the properties of the adhesive additives can be used. Fillers, plasticisers and stabilisers are the most important additives for the structural behaviour of adhesives. To improve properties like processability, strength, toughness, dimensional stability and thermal stability (coefficient of thermal expansion), fillers can be added, which do not interact with the adhesive. By increasing the distance between the polymer chains, a plasticiser influences the flexibility, ductility and toughness. To decrease deterioration of the polymer due to the environment, e.g. ultraviolet radiation and oxidation, stabilisers can be added. [3]

4.1.4 Service temperature

As mentioned before, the behaviour of polymers changes above a certain temperature, which is called the glass transition temperature, T_g . Below this temperature the adhesive is considered to be a (amorphous) solid. Above this temperature the adhesive becomes rubbery solid and at higher temperatures it becomes a viscous liquid or it disintegrates. The properties below and above the glass transition temperature may be completely different. The glass transition temperature can be in the range of the service temperature for some adhesive, which may cause problems. [3]

4.1.5 Ageing

Due to the polymers absorption uptake of liquids and gasses may take place. This causes an ageing effect. Ageing is a process in which the degree of polymerisation decreases during time due to environmental influences like contact with water, chemicals or ultraviolet radiation.

Ageing, which is a time-and-environmental-dependent effect, will influence the mechanical properties of the adhesive, and will be discussed more elaborately in chapter 6. [3]

4.2 Adhesion

There are two main types of adhesion, namely mechanical and specific adhesion. To discuss them all extensively is time-consuming and unnecessary, because as mentioned before, the cohesive strength is in most cases designed to be the weakest link. Besides that, an entirely conclusive theory is not available. Therefore only the basics of adhesion principles will be discussed. The adhesion strength depends on which of the mechanisms occur and on the surface over which adhesion takes place.

4.2.1 Mechanical adhesion

When an adhesive in a liquid state fills pores of the adherent, the adhesive and adherent are interlocked to each other after hardening, see Figure 4.3. This is called mechanical adhesion, mechanical anchorage or mechanical interlocking. [11]

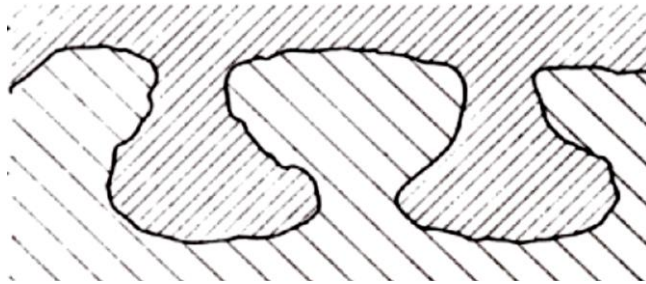


Figure 4.3: Mechanical adhesion [11]

4.2.2 Specific adhesion

Specific adhesion is adhesion through intermolecular forces, which can be divided into four types, namely chemical, dispersive, diffusive and electrostatic adhesion, which will be discussed later. Intermolecular forces have a small range of about $< 3 \cdot 10^{-6} \text{ mm}$. Surface treatments can smoothen the adherent surface. In mechanical machined surfaces the distance between peaks and troughs can be made as small as about $< 25 \cdot 10^{-6} \text{ mm}$. So the distance in mechanically treated surfaces is of a bigger order than the intermolecular forces. Hence, for achieving specific adhesion it is necessary that the adhesive wets the surface. How easy the adhesive can wet the surface depends on two major factors; the surface tension of the adhesive and the contact angle between the adhesive and adherent. [11]

4.2.2.1 Surface tension

Surface tension is the result of the attraction that liquid molecules encounter at the surface in the direction of the inner liquid mass, where the molecules are uniformly attracted to each other. As a result of this the liquid surface tends to make itself as small as possible. The surface free energy density for liquids is identical to the surface tension and is also often used. The surface tension depends strongly on the temperature. When the temperature is increased the surface tension will decrease. [11]

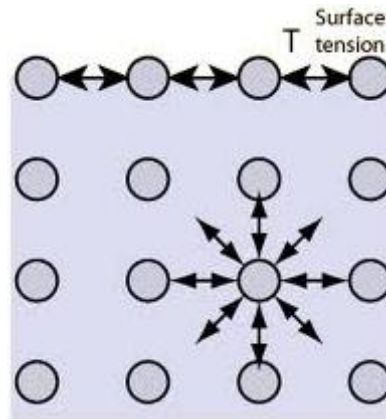


Figure 4.4: Surface tension [12]

4.2.2.2 Contact angle

The contact angle is the angle between the liquid and the surface which the liquid is in contact with. The contact angle is an interaction of the surface energy of the interface of adherent and adhesive, the surface energy of the interface of adherent and air and the free energy of the interface of adhesive and air. A small contact angle gives a big adhesion energy. [11, 13-15]

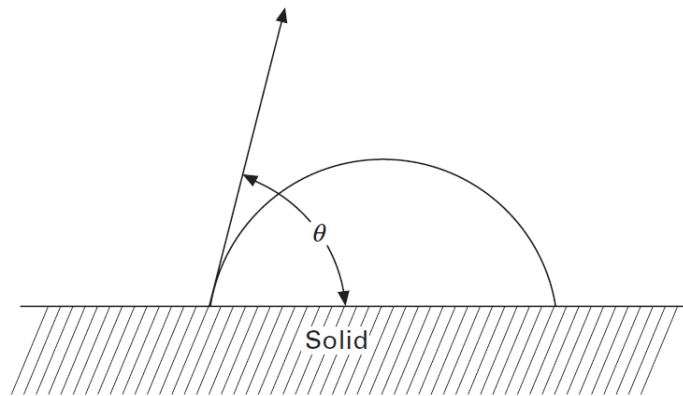


Figure 4.5: Liquid droplet on solid demonstrating the contact angle [13]

As mentioned before there are four types of specific adhesion, these are briefly discussed here.

4.2.2.3 Chemical adhesion

Chemical adhesion takes place at the molecular scale. At the interface of the adhesive and adherent a compound is formed. There are two appearances of chemical adhesion, namely ionic and covalent. Ionic bonding is based on the electrostatic attraction of two opposite charged ions. If two atoms share one or more electrons we speak of a covalent bond. [14]

4.2.2.4 Adsorptive adhesion/dispersive adhesion

Adsorptive adhesion is adhesion through van der Waals forces. Van der Waals forces are forces between dipoles. Dipoles are molecules that have an uneven distribution of electrons, this makes them charged negative on one side and positive on the other side. [16]

4.2.2.5 Diffusive adhesion

If two materials are soluble into one another, they form a solution. This way of bonding is called diffusive adhesion. Due to the solution there is no real interface between the adherent and adhesive anymore. The situation that the adherent and adhesive are soluble in one another is relative rare. [17]

4.2.2.6 Electrostatic adhesion

When two conductive materials (such as metals) are in contact to each other, electrons will be transferred from one to another. The interface layer of one conductive material will be charged positive and of the other material negative. Between those layer a force of attraction works. [14]

For a good specific adhesion a clean surface without pollution, such as water vapour, dust, oxide layer, and grease, is required. A good surface preparation can therefore increase the adhesion strength and so the failure load. Note that as mentioned before, the specific adhesion has only a small reach.

The roughness of the adherent is of influence on the adhesion energy. A rough adherent increases the contact surface but is also harder to clean and more sensitive to vapour inclusions. [11]

5 Mechanical behaviour

The mechanical behaviour of adhesive bonded connections is different from the traditional type of connections. This chapter provides the basic information needed to understand the mechanical behaviour of adhesive bonded connections. The mechanical material properties, elementary load cases and the calculation methods will be discussed. Due to the large number of different types of adhesives the properties are discussed qualitatively and not quantitatively; only some bandwidths are provided. Structural adhesives should be used below their glass transition temperature, therefore this chapter considers only the properties for structural adhesives that serve below their glass transition temperature.

5.1 Mechanical properties

The mechanical properties along with the geometrical properties, form the input data for calculations. Which properties should be known depends on the type of problem. For most cases information about the compression, tension and shear strength together with a yield criterion, the tensile modulus of elasticity and coefficient of lateral contraction is sufficient. In some cases the coefficient of thermal expansion should also be known. For calculations based on fracture mechanics, the fracture energy or strain energy release rate, G , is needed.

5.1.1 Stress-strain behaviour

For an adhesive bonded connection, the stress-strain behaviour of the adhesive has a major influence on the failure load. The stress-strain behaviour differs for the various types of adhesive. In general, adhesives exhibit an elastic behaviour up to a certain stress level (elastic limit). The tensile modulus of elasticity or Young's modulus, E , and the shear modulus of elasticity, G , describe the stiffness for this behaviour. After that, the adhesive fails (brittle behaviour) or the adhesive yields (plastic behaviour). The plastic behaviour can be of different types, namely: ideal plastic, strain hardening and strain softening. Strain softening is uncommon for structural adhesives. In all calculations the stress-strain behaviour is idealised, mostly with an elastic, elastic-plastic or bilinear model. [1, 14]

Plastic behaviour enables a material, especially those with a large deformation capacity (ductile), to spread the load over a bigger area, which increases the failure load. As a result of this behaviour, a material with a higher strength will not always have a higher failure load.

The temperature is of great influence on the stress-strain behaviour. In general if the temperature is below T_g , higher temperatures give a lower strength and stiffness, but a higher ductility.

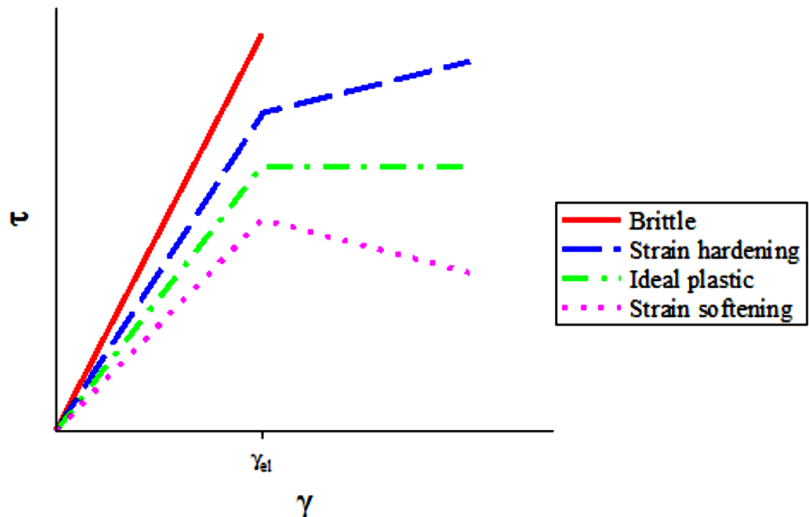


Figure 5.1: Types of material behaviour

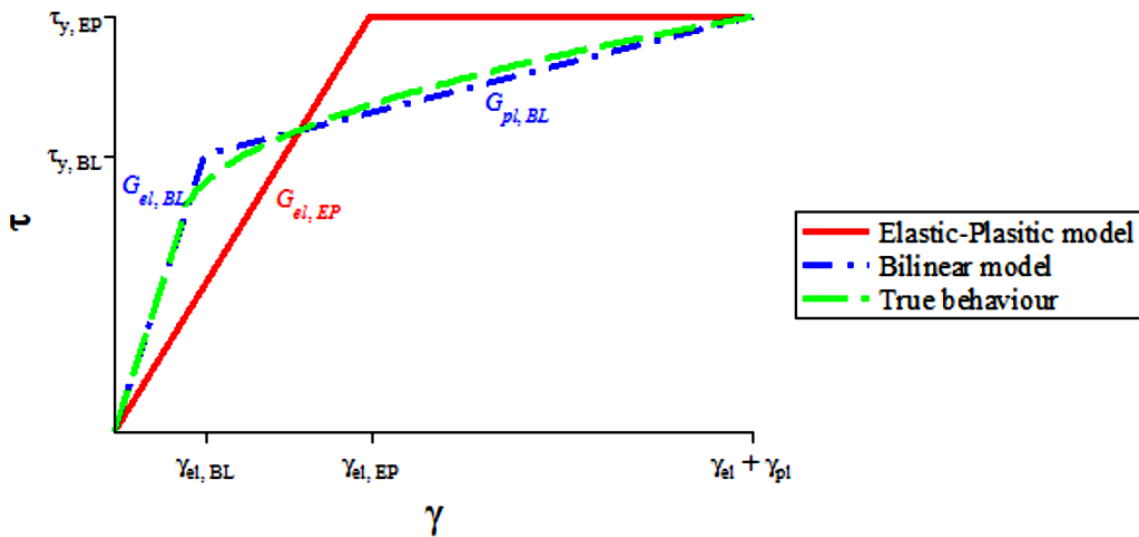


Figure 5.2: Stress-strain models for strain hardening

5.1.2 Coefficient of lateral contraction

The lateral contraction coefficient or Poisson's ratio, ν , describes the lateral contraction due to a uniaxial stress state. For polymers the lateral contraction coefficient lies between 0.33 (elastic) and 0.5 (plastic). [18]

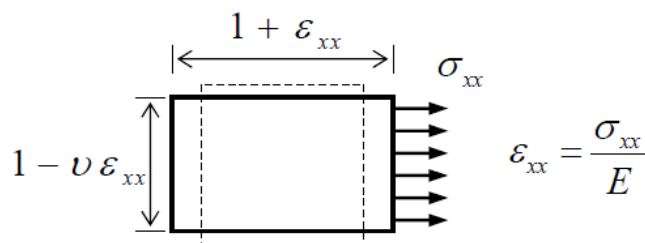


Figure 5.3: Lateral contraction principle [19]

The tensile modulus of elasticity, the shear modulus of elasticity and lateral contraction coefficient are related as shown in the following formula:

$$G = \frac{E}{2(1+\nu)} \tag{5.1}$$

5.1.3 Yield criterion

The standard stress-strain curves provide only information about one type of stress-strain behaviour, namely: tensile, compression or shear. In reality, a combination of stresses in different directions will occur and the elastic limit depends on the combination of stresses. Hence, the stress-strain behaviour of elastic-plastic materials is more complex than the stress-strain curves suggest. To take this effect into account so called yield criteria are used.

For different types of materials different types of yield criteria exist. Most criteria make use of principal stress, associated with principal planes. In every stress state, the axes can be chosen in such way, that for an infinite small element, the stresses on that element can be described with only normal stresses (tension and compression), so without shear stresses. The planes perpendicular to these stresses are the principal planes. Hence, for a three dimensional stress state there are three principal stresses. For practical reasons, the formula's of most criteria are also available for cases with shear stress, so the axes do not have to be transposed.

There is a wide variety of yield criteria. For adhesives, the Von Mises and Drucker-Prager yield criteria and modifications of these, such as the Raghava Yield Criterion, are often used. [18, 20-23] The fact that there is not one standard yield criterion indicates that there is some discrepancy between the models and reality.

Due to the great amount of computational work required to take account of the yield behaviour, yield criterions are particularly used for FEM calculations, see section 10.1.

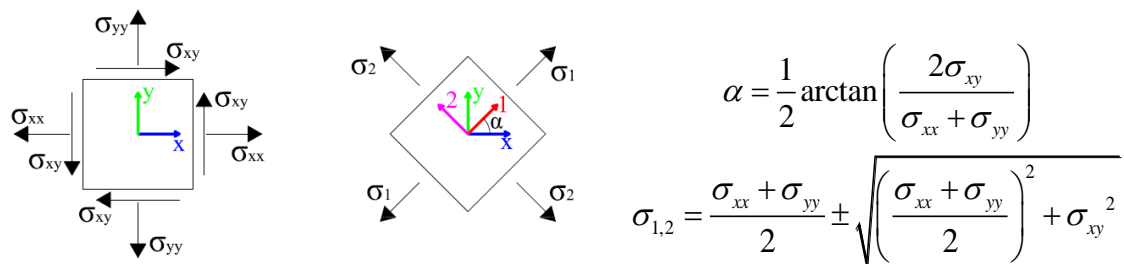


Figure 5.4: Transition of stress in an ordinary coordinate system to principal stresses

5.1.4 Coefficient of thermal expansion

The coefficient of thermal expansion (CTE) is the material property that describes the expansion due to a temperature difference, also known as temperature load. Differences in the CTE may cause stresses inside a construction. This holds especially when the service temperature has a large bandwidth and so the gradient can be large. For mild steel the CTE is $12 \cdot 10^{-6} / ^\circ\text{C}$. [24] For structural adhesive the smallest CTE is about $40 \cdot 10^{-6} / ^\circ\text{C}$. [18] Hence, the difference in thermal expansion between steel and an adhesive is at least a factor three. Therefore it is advisable to consider the effect of thermal expansion in adhesive bonded steel-to-steel connections when the service temperature has a large bandwidth. Some FEM programs are able to take the thermal expansion into account.

Due to the low stiffness of adhesive in comparison with steel the difference in CTE will not result in large stresses. The adhesive is not stiff enough to impose a significant displacement on the steel. The steel will restrain the expansion of the adhesive.

For instance, assume the CTE of the preceding paragraph ($12 \cdot 10^{-6} / ^\circ\text{C}$ and $40 \cdot 10^{-6} / ^\circ\text{C}$), a temperature difference of 10°C , a stiffness of 3000 N/mm^2 for the adhesive (quite stiff for adhesives) and only consider the expansion in x-direction.

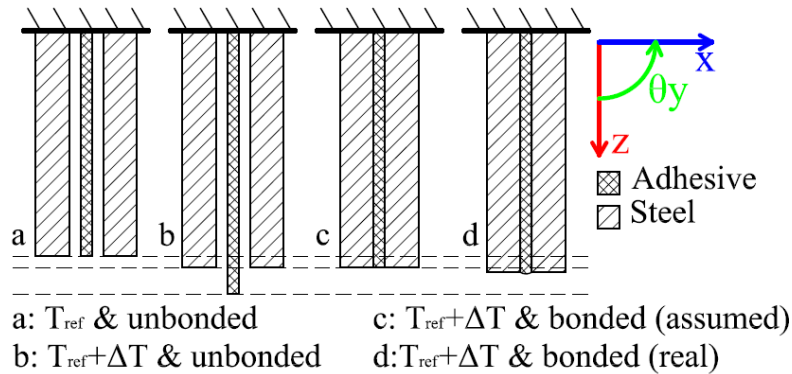


Figure 5.5: Temperature induced deformation

The differences in strain becomes:

$$\Delta \epsilon_T = \Delta CTE \cdot \Delta T = (40 \cdot 10^{-6} - 12 \cdot 10^{-6}) \cdot 10 = 28 \cdot 10^{-5}$$

If the total difference is taken by the adhesive¹ (Figure 5.5.c), the stress in the adhesive will be:

$$\sigma_a = \Delta \epsilon_T E = 28 \cdot 10^{-5} \cdot 3000 = 0.84 \text{ N/mm}^2$$

These stresses will be compressive stresses (expansion is restrained).

5.2 Calculation methods

There are different calculation methods available, all with their advantages and disadvantages. Basically, there are three main types; methods based on differential equations (DE's), fracture mechanics and finite element modelling (FEM). Methods that are based on DE's can, most of the time, be calculated by hand calculations and are suitable for simple problems. Fracture mechanics and FEM based calculations are mostly done by computers. With these methods complex problems can be solved. Quite often fracture mechanics and finite element modelling are used together. In structural engineering FEM methods are most commonly used for complex problems.

One of the main advantages of DE's is the closed form solution. In other words, an analytical expression, which results in short calculation time. The relation of each parameter can be read directly from the formula.

A disadvantage of DE's is that it is practically impossible to model physical non linear behaviour. Modelling of geometrical non linear behaviour is only possible for simple cases. And problems are nearly always simplified to 1D, or exceptionally 2D, problems. But the main disadvantage is that DE's can only be used for simple geometrical problems.

A fracture mechanics calculation is based on the stress that is needed to propagate a crack. Therefore the fracture energy or strain energy release rate, G , which is a material property, should be known. Also the stress intensity factor (SIF), K , which is a geometrical property, should be known. The SIF can be determined in several ways, e.g. by testing and by FEM. [1]

Finite element modelling is based on the equilibrium of finite elements and makes use of linear algebra (matrices). The matrix equations are solved numerical.

The main advantage of this method is the relatively easy modelling of complex problems. FEM programs often have a graphical user interface (GUI) that facilitates the data input. Generally, the results can be presented graphically and numerically.

¹ The reality is more complicated, both the steel and adhesive will take some of the strain difference which moreover depends on the support conditions. This example gives only an order of magnitude for the stresses due to ΔCTE

On the other hand, the interpretation and validation of the results can be difficult. The result precision and graphical presentation can be misleading. Due to the numerical process the calculations are slow.

	DE	Fracture mechanics	FEM
Closed form solution	yes	no	no
Calculation time	short	long	long
Physical non linear	no	yes	yes
Geometrical non linear	Only simple cases	yes	yes
1D, 2D or 3D	1D (exceptionally 2D)	2D and 3D	1D, 2D and 3D
Numerical errors	no	yes	yes

Table 5.1: Comparison of calculation methods

5.3 Theories

As mentioned before, connections in which the adhesive is loaded in shear are preferable. There are several ‘classic’ theories about such connections, which are often cited in literature. These theories will be treated in the next section.

5.3.1 Linear elastic adhesive with rigid adherents

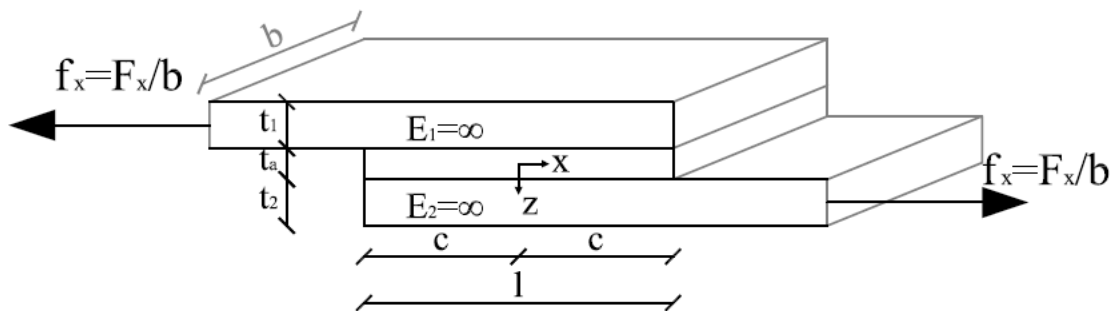


Figure 5.6: Single lap connection according to linear elastic theory

The most basic type of connection is the single lap connection, see Figure 5.6. Both adherents have the same geometrical and material properties. In the theoretical case with infinite stiff adherents, the shear stress distribution of the adhesive is constant over the width, overlap length and thickness, and is given by:

$$\tau_{x,a} = \frac{F_x}{bl} \tag{5.2}$$

The tensile stress in the adherent will decrease linearly to zero over the bond length and is assumed to be constant over the thickness and width.

In Figure 5.7 the shear stress distribution of (5.2), for the arbitrary constants; $F_x = 150 \cdot 10^3 N$, $l = 200 mm$ and $b = 100 mm$, can be found.

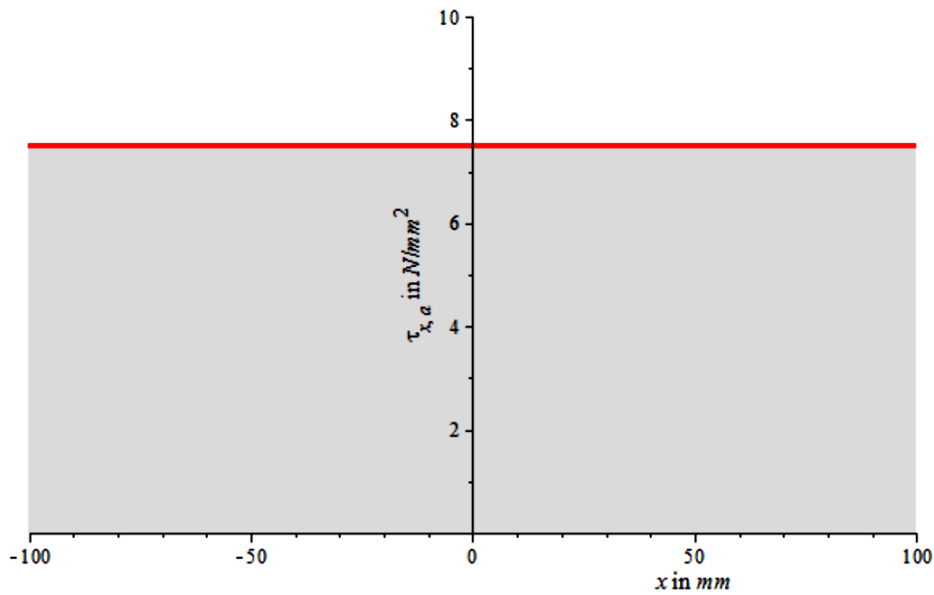


Figure 5.7: Shear stress distribution according to linear elastic theory (with aforementioned arbitrary constants)

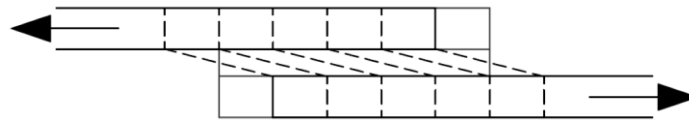


Figure 5.8: Schematisation of displacement according to linear elastic adhesive with rigid adherents theory

5.3.2 Volkersen (1938)

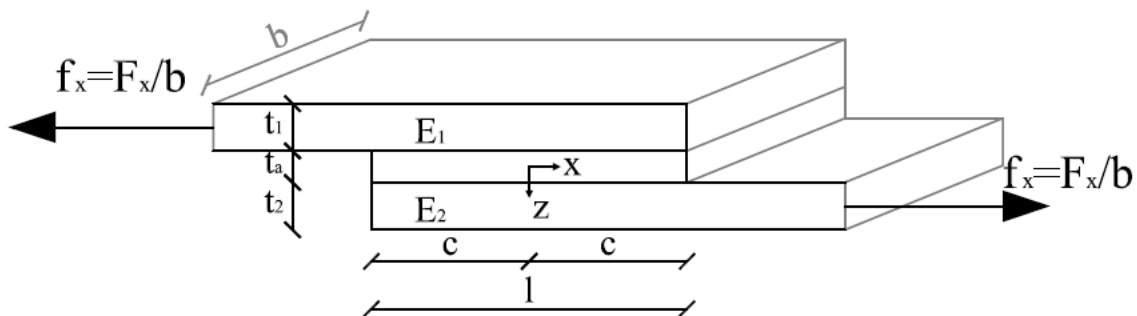


Figure 5.9: Single lap connection according to Volkersen

In the theory of Volkersen the adherents do not have infinite stiffness and will deform in the x direction (axial). The stress in the adherent decreases over the bond length, and so does the strain. A derivation of the Volkersen theory can be found in 'Appendix A: Volkersen'. The shear force distribution is given by equation (17.27):

$$\tau_{x;a}(x) = \frac{F_x \omega}{2b} \left\{ \frac{\cosh(\omega x)}{\sinh(\omega c)} + \frac{E_1 t_1 - E_2 t_2}{E_1 t_1 + E_2 t_2} \frac{\sinh(\omega x)}{\cosh(\omega c)} \right\}$$

In Figure 5.10 the shear stress distribution of (17.27) for the arbitrary constants; $F_x = 150 \cdot 10^3 \text{ N}$, $l = 200 \text{ mm}$, $b = 100 \text{ mm}$, $t_1 = t_2 = 5 \text{ mm}$, $E_1 = E_2 = 2.1 \cdot 10^5 \text{ N/mm}^2$ and $t_a = 1 \text{ mm}$, $G_a = 750 \text{ N/mm}^2$, can be found. This typical shear lag shape is also well known for (long) welded and (long) bolted connections.

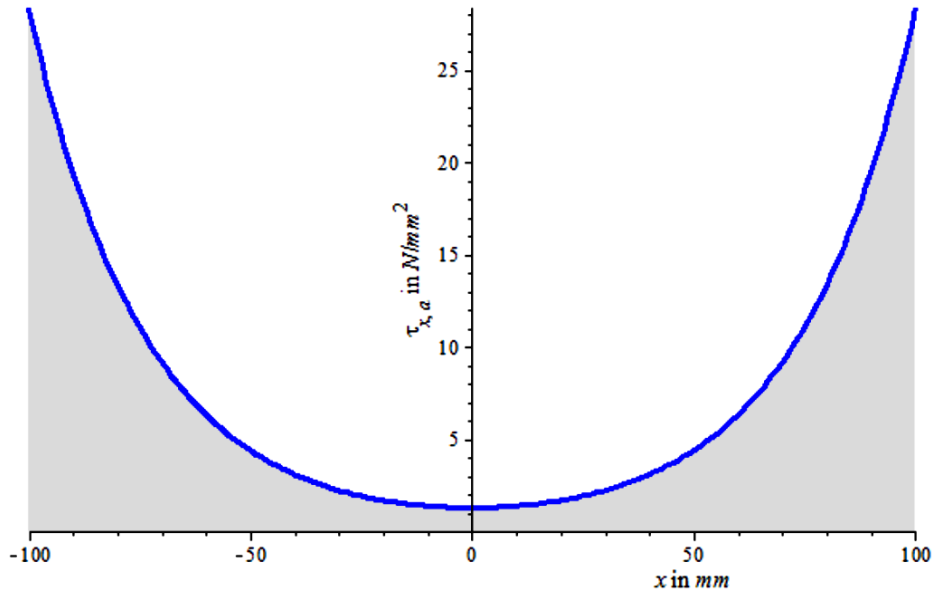


Figure 5.10: Shear stress distribution according to Volkersen (with aforementioned arbitrary constants)

In Figure 5.11 a schematisation of the displacement according to Volkersen can be found. Note the difference with the linear elastic theory, see Figure 5.8.

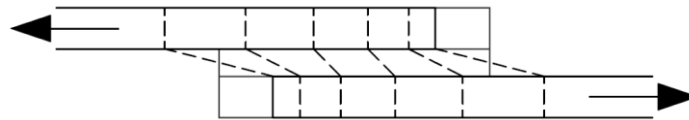


Figure 5.11: Schematisation of displacement according to Volkersen

5.3.3 Goland and Reissner (1944)

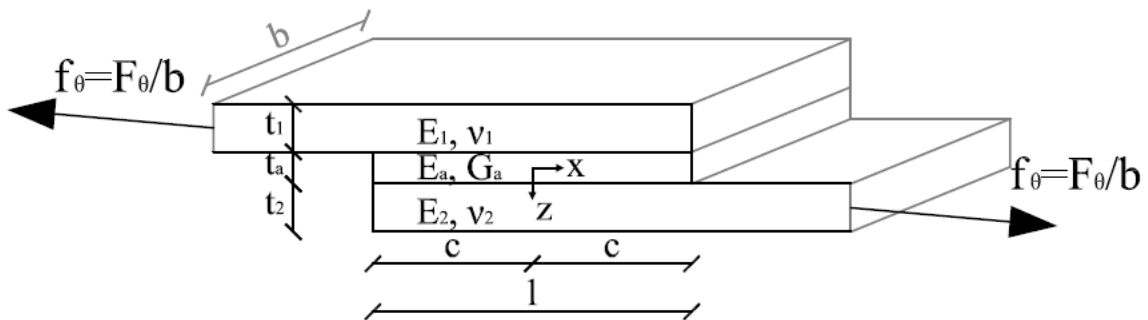


Figure 5.12: Single lap connection according to Goland and Reissner

The theory of Volkersen neglects the effect of the eccentricity of the applied loads. Due to this eccentricity, the connection is also loaded with a bending moment. This moment causes peel stresses in the adhesive and will rotate the adherents and adhesive. The theory of Goland and Reissner takes this effect into account.

A derivation of the Goland and Reissner theory can be found in ‘Appendix B: Goland and Reissner’. The shear force distribution is given by equation (18.27):

$$\tau_{x,a}(x) = \frac{t_1}{4t_1 + 3t_a} \frac{h_0}{2c} \left[1 + \frac{6m_0}{t_1 h_0} \frac{\beta}{\sinh(\beta)} \cosh\left(\frac{\beta}{c} x\right) + 3 \left(1 - \frac{2m_0}{t_1 h_0} + \frac{t_a}{t_1} \right) \right]$$

See the appendix for the definitions of β , m_0 and h_0 .

With the arbitrary constants; $F_x = 150 \cdot 10^3 N$, $b = 100 mm$, $l = 200 mm$, $t_1 = t_2 = 5 mm$, $E_1 = E_2 = 2.1 \cdot 10^5 N/mm^2$, $\nu_1 = \nu_2 = 0.3$, $t_a = 1 mm$, $G_a = 750 N/mm^2$, $h_0 = f_\theta$, $v_0 = 37.5 N/mm$, $m_0 = 1498.7 Nmm/mm$, formula (18.27) has the shape as depicted in the next figure:

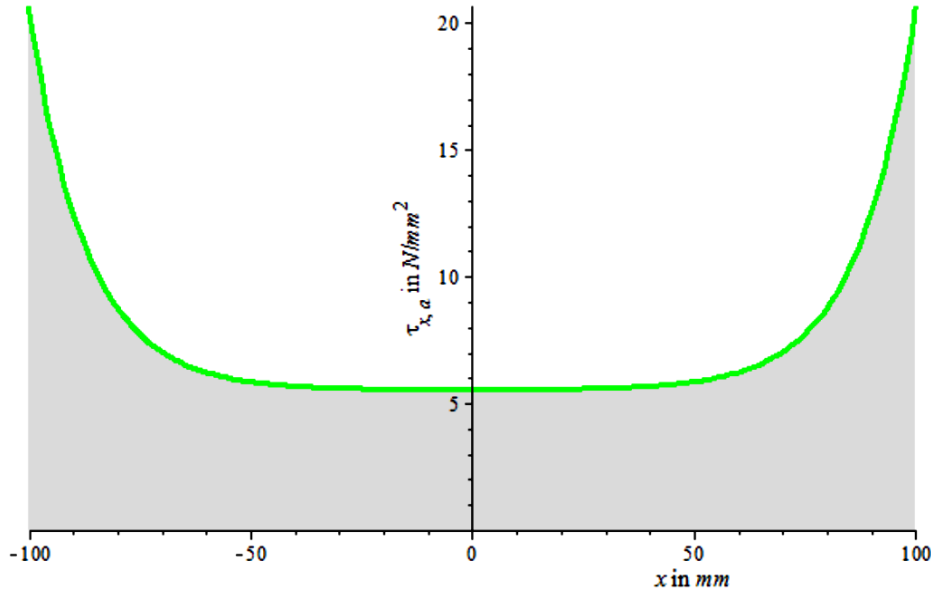


Figure 5.13: Shear stress distribution according to Goland and Reissner (with aforementioned arbitrary constants)

The peel force distribution is given by equation (18.34):

$$\sigma_{z,a}(x) = \frac{h_0}{t_1} \left[\frac{t_1}{c} \right]^2 \Delta \left[\left[\frac{r_1 \lambda^2 m_0}{t_1 h_0} + \frac{c v_0}{t_1 h_0} \sinh(\lambda) \sin(\lambda) \right] \sinh\left(\frac{\lambda x}{c}\right) \sin\left(\frac{\lambda x}{c}\right) + \dots \right. \\ \left. \dots + \left[\frac{r_2 \lambda^2 m_0}{t_1 h_0} + \frac{c v_0}{t_1 h_0} \cosh(\lambda) \cos(\lambda) \right] \cosh\left(\frac{\lambda x}{c}\right) \cos\left(\frac{\lambda x}{c}\right) \right]$$

See the appendix for the definitions of β , λ , r_1 , r_2 , m_0 , v_0 and h_0 .

With the arbitrary constants; $F_x = 150 \cdot 10^3 N$, $b = 100 mm$, $l = 200 mm$, $t_1 = t_2 = 5 mm$, $E_1 = E_2 = 2.1 \cdot 10^5 N/mm^2$, $\nu_1 = \nu_2 = 0.3$, $t_a = 1 mm$, $E_a = 2 \cdot 10^3 N/mm^2$, $G_a = 750 N/mm^2$, $h_0 = f_\theta$, $v_0 = 37.4 N/mm$, $m_0 = 1498.7 Nmm/mm$, formula (18.34) has the shape as depicted in Figure 5.14.

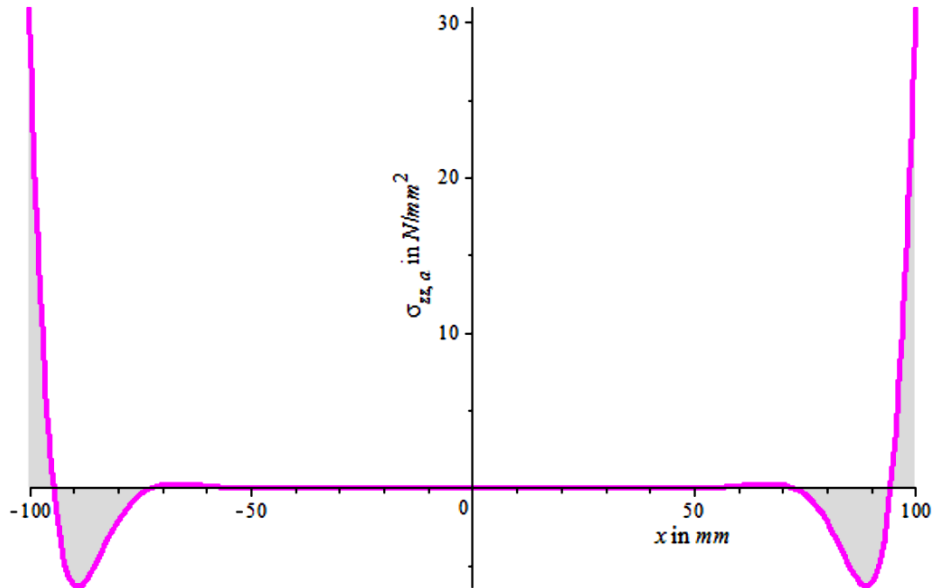


Figure 5.14: Peel stresses according to Goland and Reissner (with aforementioned arbitrary constants)

The derivation of h_0 , v_0 and m_0 can be found in 'Appendix B: Goland and Reissner'.

5.3.4 Other theories

The theories of Volkersen, and Goland and Reissner give a first insight in the behaviour of a lap joint. The shear and peel stresses are high in the end regions, see Figure 5.16. But due to some assumptions and simplification the real behaviour is different from what these two theories suppose. Some of the points that the theories of Volkersen, and Goland and Reissner don't take into account are [18]:

- No shear stress at edges;
- Lateral stresses due to lateral contraction (see Figure 5.15);
- Shear deformation of the adherents;
- Variable stress over the width;
- Variable stress over the thickness.

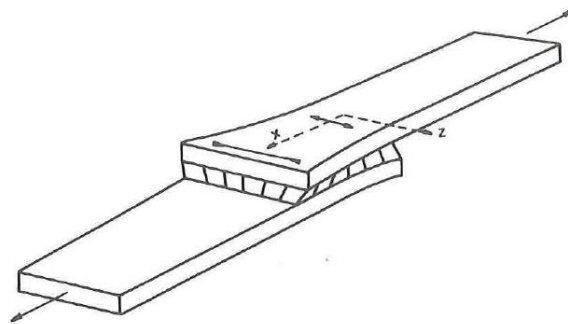


Figure 5.15: Deformation of single lap due to lateral contraction [18]

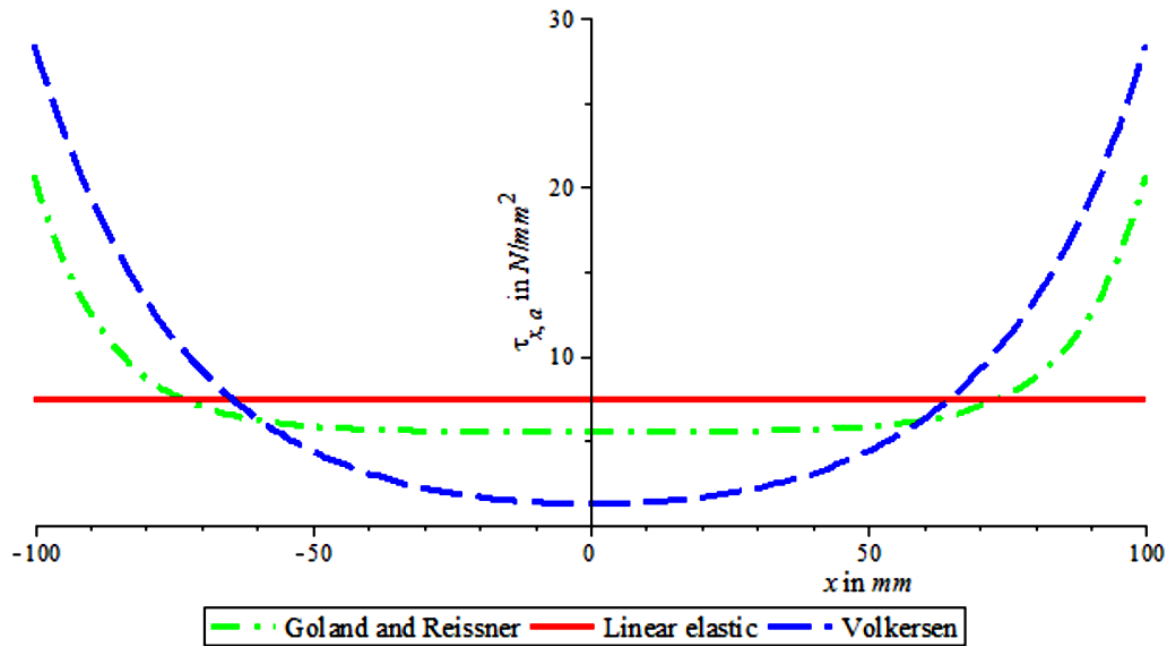


Figure 5.16: Comparison of shear stress distributions

In Table 5.2 an overview of other theories from 1938 to 2000, made by Gleich [1], can be found.

	Plasticity	Peel	Orthotropic adherents	Adherent shear	Free edge condition	Thermal affects	Stress variation over bondline	Closed form solution	Dissimilar adherents
Volkersen (1938)								✓	✓
Goland and Reissner (1944)		✓						✓	
Hart-Smith (1973a)	✓	✓	✓					✓	✓
Allman (1977)		✓	✓	✓	✓		✓	✓	
Renton and Vissen (1977)		✓	✓			✓		✓	
Ojalvo and Eidinoff (1978)		✓					✓	✓	
Yuceoglu and Updike (1981)		✓	✓	✓				✓	✓
Delale <i>et al.</i> (1991)		✓	✓	✓				✓	
Chen and Cheng (1983)		✓		✓	✓		✓	✓	
Bigwood and Crocombe (1989)		✓						✓	✓
Bigwood and Crocombe (1990)	✓	✓						✓	✓
Cheng <i>et al.</i> (1991)		✓		✓	✓		✓	✓	✓
Adams and Mallick (1992)	✓	✓	✓	✓	✓	✓	✓		✓
Tsai and Morton (1994)		✓	✓	✓				✓	✓
Yang and Pang (1996)		✓	✓	✓				✓	✓
Tsai <i>et al.</i> (1998)				✓				✓	
Sawa <i>et al.</i> (2000)		✓		✓			✓		✓

Table 5.2: Main features and assumptions of bonded joints analyses from 1938-2000 [1]

5.3.4.1 Bondline thickness

Research has shown that the bondline thickness has a different influence than some of the theories predict. Most theories predict that increasing the bondline thickness will lead to a higher failure load.

But that is not the case. There seems to be an optimal bondline thickness. The stress varies over the bondline thickness, so methods that consider this obtain a better result. Especially interface stresses seem to be important. [1]

5.3.5 Methods to reduce stress peaks

The occurrence of peak stresses will lower the efficiency of the connection. In the most ideal case the stress level is uniform. There are several ways to reduce the peak stresses and get a more uniform stress distribution, hence, increasing the efficiency of the connection. The most important methods are stated below.

5.3.5.1 Increasing the bond width

The most simple way to decrease the stress peaks is to increase the bond width. The stresses are spread over a greater width which decreases the stresses and stress peaks. The bandwidth and failure load have a nearly linear relation. [18]

5.3.5.2 Increasing the bond length

Increasing the bond length is less effective than increasing the bond width. Due to the shear lag effect the added length will cause a larger low stress area, see Figure 5.17. Above a certain bond length, increasing the length is therefore not effective. [18]

Cases with creep will be discussed in section 6.3.2.

With the arbitrary constants; $F = 1500 \text{ N/mm}$, $t_1 = t_2 = 5 \text{ mm}$, $E_1 = E_2 = 2.1 \cdot 10^5 \text{ N/mm}^2$, $\nu_1 = \nu_2 = 0.3$, $t_a = 1 \text{ mm}$, $G_a = 750 \text{ N/mm}^2$, $H_0 = F$, $V_0 = 37.4 \text{ N/mm}$, $M_0 = 1498.7 \text{ Nmm/mm}$, formula (18.27), the shear stress according to Goland and Reissner, has the shape as depicted in the next figure:

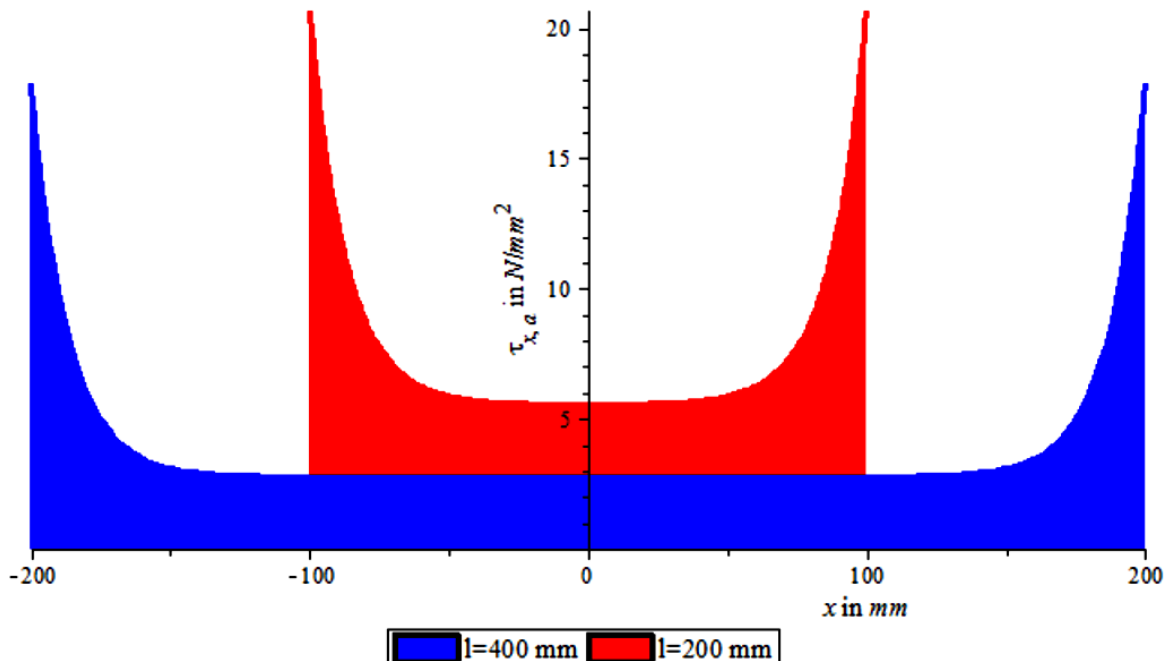


Figure 5.17: Shear stress distribution according to Goland and Reissner for different bond lengths

Note that the shaded red and blue sections have (necessarily) the same area.

5.3.5.3 Decreasing the adherent thickness

If the adherent thickness is decreased, the lever arm of the applied loads is decreased. For this reason the moment will be smaller and so the peel stresses will be smaller. But simply decreasing the adherent thickness will lead to a lower axial stiffness, which leads to higher shear stress peaks, see the next section.

5.3.5.4 Increasing the (axial) stiffness of the adherents

A stiffer adherent is capable of spreading the stresses better, which reduces the shear stress peaks due to a high contribution of the mid area. Increasing the axial stiffness by increasing the thickness will lead to high peel stresses, see latter section.

5.3.5.5 Decreasing the stiffness of the adhesive

An adhesive with a lower stiffness will give lower stresses at a certain strain than adhesives with a higher stiffness. Decreasing the stiffness of the adhesive will therefore decrease the stress peaks.

5.3.5.6 Double lap and double strap connections

Double lap and double strap connections are widely used. These types of connections have two major advantages above single lap connections:

- External force (moment) equilibrium
- Two shear planes instead of one (reduction of shear stress)

Theoretically they can be considered as two single lap connections, Figure 5.19. Due to the external force equilibrium the overlap itself will not rotate, but due to internal eccentricities peel stresses still occur. The outer adherents will still deform at the overlap, see Figure 5.18. [18]

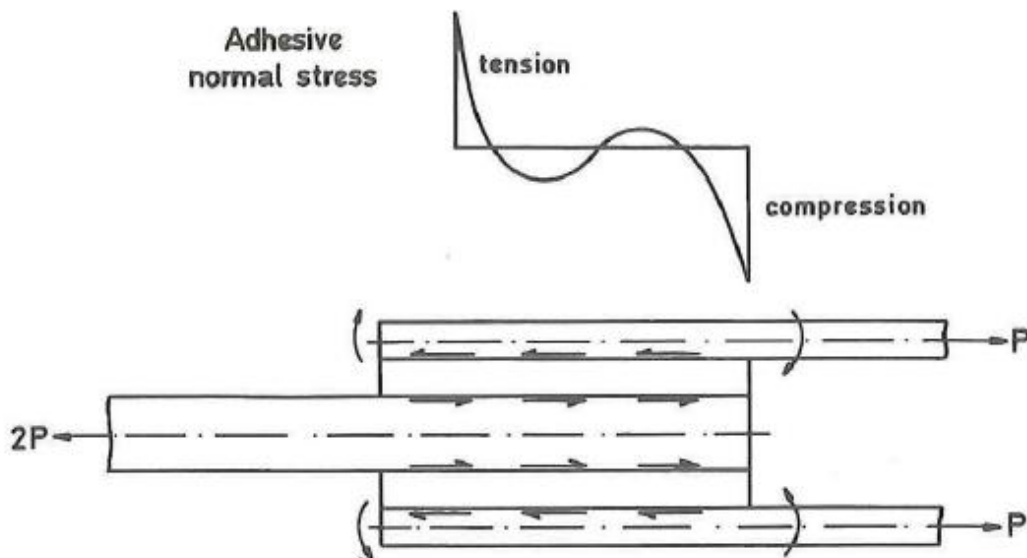


Figure 5.18: Peel stress in double lap due to internal moments [18]

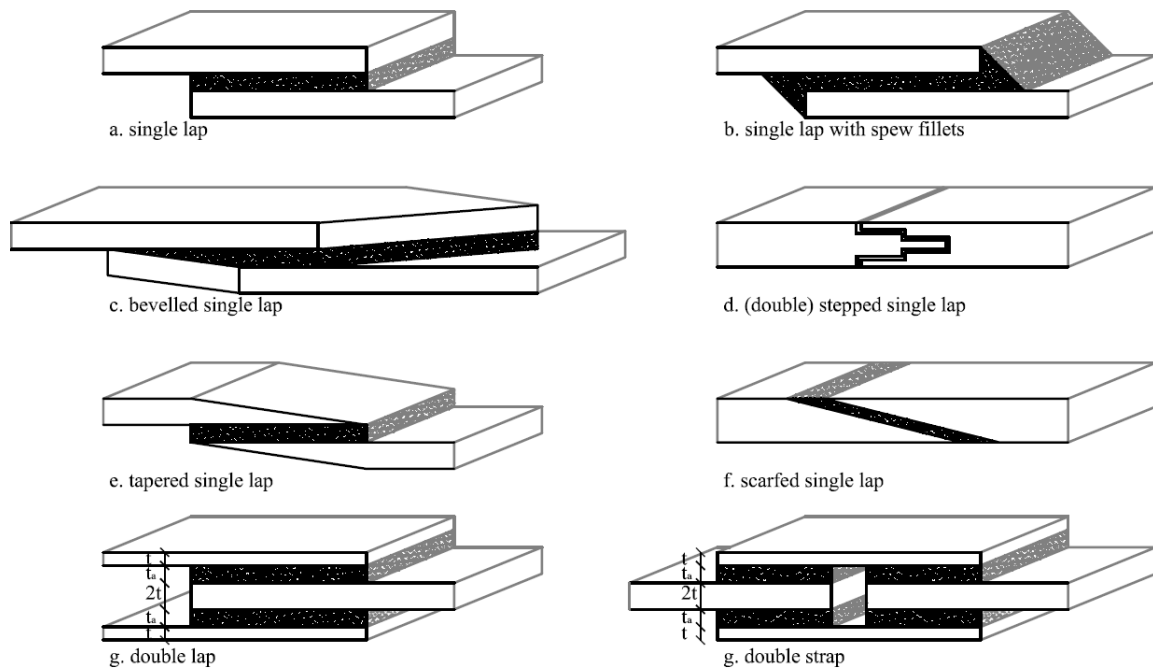


Figure 5.19: Basic configuration of adhesive bonded laps

5.3.5.7 Scarfed, tapered, bevelled and stepped adherents

To reduce the stress peaks at the ends of the adhesive the adherents can be modified from a continuous shape into a scarfed, tapered, bevelled or stepped adherent, see Figure 5.19. The stresses are introduced in a more gradual way which reduces the stress peaks. For the scarfed and tapered adherents also external force (moment) equilibrium is obtained by alignment of the centre lines, which reduces the peel stresses drastically. [18]

5.3.5.8 Spew fillets

Another method to reduce the stress peaks at the ends is by applying spew fillets, Figure 5.19. A spew fillet will introduce the stresses in a more gradual way and so reduce the stress peaks.

6 Time-and-environmental-dependent effects

Normally, a long service life is requested in structural engineering. The service life is mainly influenced by time-and-environmental-dependent effects. This chapter provides basic information about the time-and-environmental-dependent effects for adhesives.

6.1 Temperature

The effect of temperature on adhesive bonded connections can be distinguished in three main aspects, namely:

1. Shrinkage of the adhesive;
2. Differences in thermal expansion;
3. Temperature dependency of the mechanical properties.

6.1.1 Shrinkage of the adhesive

The curing process of the adhesive is accompanied by shrinkage of the adhesive. This shrinkage gives rise to internal stresses. Several studies show that the stress due to shrinkage has much less effect than those caused by differences in thermal expansion. Therefore the stress due to shrinkage often has a negligible effect on the total stress level. [13]

6.1.2 Differences in thermal expansion

The basic information about the influence of differences in thermal expansion can be found in section 5.1.4. Thermal stress builds up if the operating temperature, T_o , is different from the stress-free temperature, T_{SF} :

$$\Delta T = T_o - T_{SF} \quad (6.1)$$

For the T_{SF} it is reasonable to take the curing temperature if the T_o is always below the T_g . If the service temperature gets higher than the T_g , the thermal stresses are relaxed. If the temperature subsequently drops below the T_g , the adhesive turns hard again and the T_{SF} is equal to the T_g . [13]

6.1.3 Temperature dependency of the mechanical properties

As mentioned in section 5.1.1; in general, if the temperature is below T_g , higher temperatures give a lower strength and stiffness, but a higher ductility. The rate of change of the mechanical properties depends on the type of adhesive. Specialised adhesives are available for high and low temperatures. [13]

6.2 Moisture uptake

Moisture has a substantial influence on the properties of an adhesive. Hence, the uptake of moisture is an important factor to guarantee a sufficient service life. Water can enter the adhesive by diffusion. Normally, this will take place at free planes. But if water is able to enter the adherents, such as in wood, than diffusion will also take place at the bonded planes.

For systems where the adherent is not permeable, increasing the bond length and width increases the service life. Cracks on the outside can lead to deeper penetration of the water in the adhesives.

The permeability represents the rate of transport of moisture through the adhesives and therefore plays a key role in the diffusion behaviour. The permeability can be influenced by adding fillers to the adhesive and depends on temperature. The moisture uptake is a reversible process. [3, 18]

6.2.1 Swelling and plasticising

Due to the water uptake of the adhesive, the adhesive swells. This gives rise to stress. Moreover, the swelling increases the distance between the macromolecules of the adhesive. This has a negative influence on the strength and stiffness properties. The swelling may cause residual stress which might relax in some time due to creep. Due to the more open structure of the swollen adhesive, water works as a plasticiser. The swelling and plasticising are reversible phenomena. [3, 18, 25]

6.2.2 Displacement of the adhesive

In some cases, moisture can displace the adhesive from the interface with the adherent (on the molecular scale), this is also known as 'wicking'. This leads to less bond area, hence a lower failure load. Because the displacement of the adhesive is caused by moisture, the process starts at the planes which are exposed to moisture. Displacement of the adhesive at a metal adherent is often followed by corrosion of the metal. Therefore this process is irreversible for metal adhesive bonded connections. If no corrosion takes place this process is reversible. Primers do not corrode, hence a primer can be useful for metal adhesive bonded connections. [3, 18]

6.2.3 Influence on the T_g

The uptake of moisture lowers the T_g , which in general has a negative effect. A lower T_g means a smaller application range, and is often accompanied with lower strength and stiffness. This phenomenon is reversible. [18]

6.2.4 Hydrolysis

If water reacts chemically with the adhesive this is called hydrolysis. Hydrolysis lowers the strength and stiffness of the adhesive. This phenomenon is irreversible. [3, 18]

6.3 Creep and relaxation

Creep and relaxation are closely related phenomena. Both phenomena describe the stress-strain behaviour of the material after the instantaneous reaction for viscoelastic or viscoelastic-plastic materials. Both phenomena are well known in structural engineering; for concrete, timber and composites, it is common practice to take both phenomena into account. If the stress remains the same but the strain grows in time, it is called creep. If the strain remains the same and the stress decreases in time, it is called relaxation. The behaviour of the material on the molecular scale is the same for both phenomena. For engineers the creep behaviour below T_g (see 4.1.2) is of most interest, therefore this section focuses on the creep behaviour below T_g .

Temperature, stress, water content and time are the main parameters that determine the creep behaviour for adhesives. In general, a high stress, temperature, or humidity will increase the deformation due to creep in the same amount of time.

Adhesives with a high degree of cross linking are, in general, less sensitive to creep than those with a low degree of cross linking. A high degree of cross linking is accompanied with brittle behaviour and a high T_g (see 4.1.2). Curing at a high temperature can increase the degree of cross linking (and heightens the T_g), hence, lowering the sensibility to creep. [9]

6.3.1 Typical creep curve of bulk hardened adhesive specimen

Figure 6.1 shows a typical creep curve for a dead load tensile test of bulk hardened adhesive specimen. In such a test the load, humidity and temperature level are kept constant and the strain-time relation is measured. This is done for several load, humidity and temperature combinations.

After the instantaneous strain at $t = t_0$, ε_0 , three creep stages can be distinguished, namely the primary (or transient), secondary (or steady state) and tertiary stage. The instantaneous strain can be purely elastic, $\varepsilon_0 = \varepsilon_{el}$, or elastic-plastic, $\varepsilon_0 = \varepsilon_{el} + \varepsilon_{pl}$. After $t = t_0$ the strain behaviour is determined by the viscoelastic or viscoelastic-plastic properties of the adhesive. Often these properties are non-linear. In the tertiary state the strain rate of the adhesive increases. Failure due to creep is called creep failure and takes place in the tertiary stage.

If the load is released at a certain time, $t = t_1$, the strain follows the dashed line of Figure 6.1. A reversible part of the strain is 'recovered'. This recovery curve exists of an instantaneous part and a time-dependent part. The instantaneous part is equal to the ε_{el} component from ε_0 . The time-dependent part is the viscoelastic strain. The irreversible part of the strain that does not recover, is the viscoplastic strain. The proportion of recovery depends on the material and creep mechanism. A high degree of cross linking will increase the proportion of recovery. [13, 18]

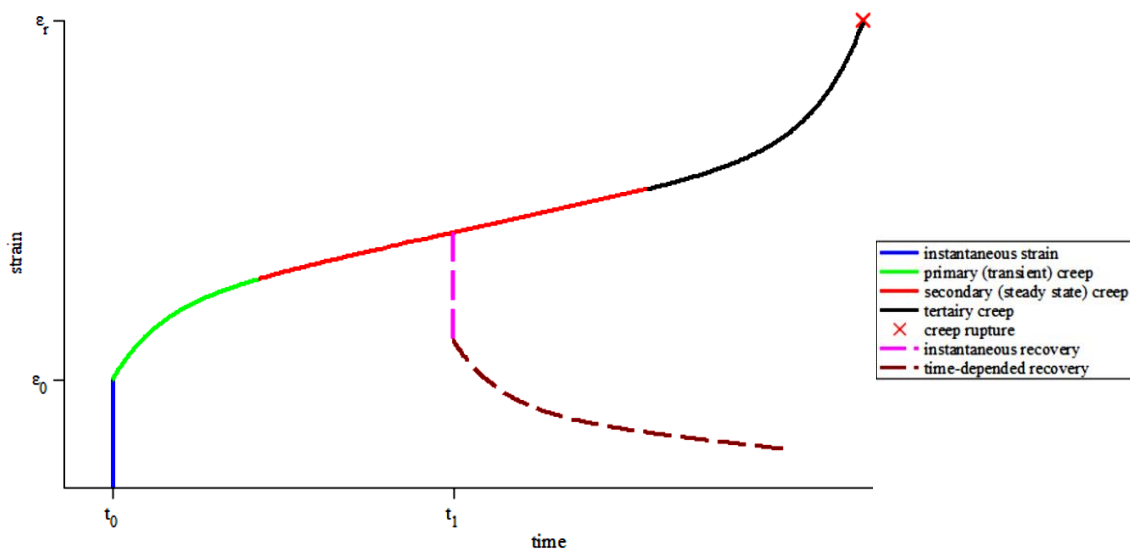


Figure 6.1: Typical creep curve for viscoelastic polymers

6.3.2 Creep behaviour of adhesives in connections

The creep behaviour of adhesives in connections is practically always different from that of bulk adhesives. The adherents affect the creep behaviour of the adhesive. Commonly, the adherents are stiffer than the adhesive and are less affected by creep. As a result of this, the adhesive is restrained by the adherent during the creep process. This effect is bigger in thin bondlines. [9]

The load in a creep test is an axial load, which causes nearly uniform tensile stresses. Adhesives are strong in shear and weak in tension. In a well designed connection the adhesive is loaded in shear. The shear stress distribution of such a connection is far from uniform as showed in section 5.3. Due to creep the distribution of shear stress will change. In Figure 6.2 a typical creep redistribution can be found. The peak stresses will decrease and the stresses in the middle will increase. Due to the equilibrium of forces in the x-direction the area of both curves is necessarily the same.

Due to the higher contribution of the mid area after creep, increasing the bond length is effective to deal with the creep phenomenon. This holds also for a large bond length, in contrast to section 5.3.5.2.

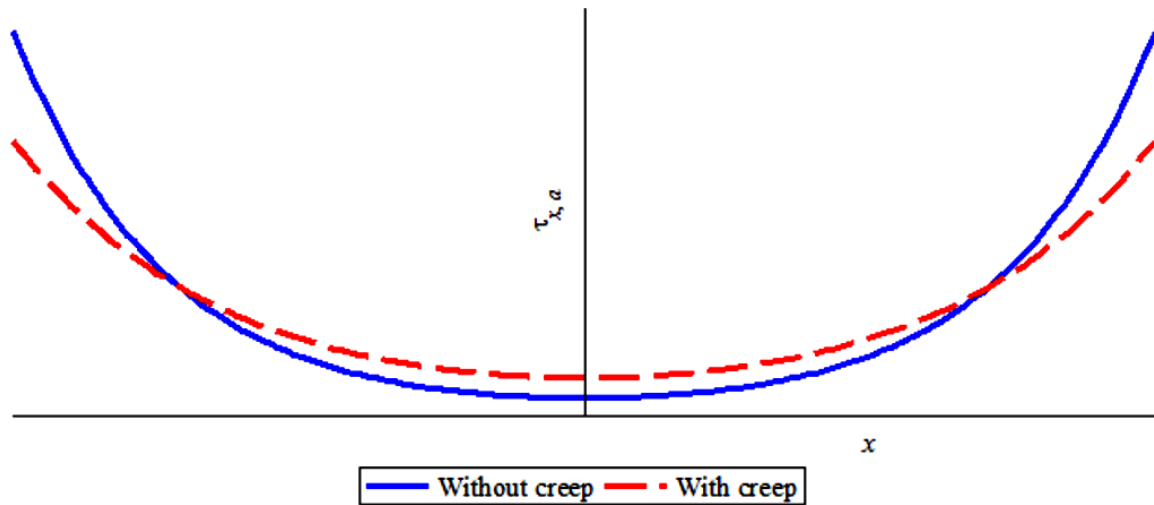


Figure 6.2: Redistribution of shear stresses due to creep in a lap connection

6.4 Crazeing

Crazeing is a phenomenon that can occur in thermoplastic polymers. Crazes are voids that are held together by highly drawn fibrils, see Figure 6.3, and can arise under stress. Due to the fibril the voids do not propagate and merge together. Fibrils are able to transfer stresses, this makes crazes different from normal cracks. Crazes result in brittle behaviour in normally ductile adhesives. [2, 13, 18]

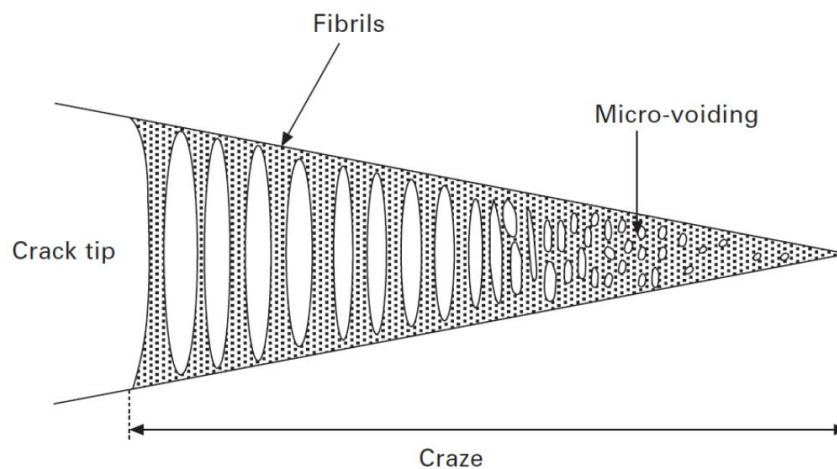


Figure 6.3: Schematisation of craze formation [13]

6.5 Oxidation

The majority of the polymers are susceptible to oxidation. The oxidation process is influenced by oxygen and/or moisture and for some adhesives heat must be present. Just like moisture, oxygen is able to diffuse into the adhesive. Light often works as a catalyst and chemicals can also influence the oxidation process. This phenomenon is irreversible. [3, 18]

6.6 Chemicals

Chemicals, such as organic solvents, acids and alkalis, can have an influence on the adhesive. Some effects correspond to the effects of moisture; swelling, plasticising, displacement of the

adhesive, decrease in strength, decrease of stiffness and lowering the T_g . But also chemical reactions and leaching of adhesive constituents can take place. Most structural adhesives are highly resistant to chemicals below their T_g . Moreover, the adhesive often has only a small plane that is subjected. [13]

6.7 UV radiation

When a polymer is subjected to UV radiation it will degrade. UV radiation will separate free radicals in the polymer, these free radicals initiate chain scission reactions. The radiation also creates heat. How harmful the radiation is and how deep it penetrates depends on the wavelength. Additives can improve the resistance to UV radiation. The UV radiation induced degradation is irreversible. [13]

6.8 High-energy radiation

High-energy radiation is the collection of a wide variety of manifestations of high-energy particulate and electromagnetic radiation. Among them are X-rays, gamma rays, neutrons, alpha particles and beta particles. Exposure to high-energy radiation induces the formation of free radicals or ions in the polymer, which results in chain scission or cross-linking reactions. This phenomenon is irreversible. [13]

6.9 Biological degradation

Polymers themselves are commonly not susceptible to biological degradation, but additives may be susceptible. Polymers that have good water and weather resistance properties have, in general, a good resistance to biological degradation. The resistance can be improved with antimicrobial additives. This phenomenon is irreversible. [13]

6.10 Calculation method

An exact calculation of the time-and-environmental-dependent effects is practically impossible. First of all the exact exposure conditions, such as stress and temperature, should be known for every moment. But moreover the time-and-environmental-dependent behaviour of the adhesive is complex, hard to describe and not yet fully understood. Therefore it is common practice to use a straight forward approximation with reduction factors, also known as i.a. knock down factors and k factors. There are reduction factors for strength and stiffness. These factors are determined by tests. Testing is mostly done by the supplier. The supplier provides the engineer graphs or empiric formulas for a specific type of adhesive. The engineer can then determine the reduction factors for the expected specific conditions. By simply multiplying or dividing the strength or stiffness parameters by the reduction factors, the time-and-environmental-depended effects are taken into account. Because the stress level and the stiffness are parameters in determining the reduction factors, the calculation can be iterative.

7 Applications and developments

Nowadays, structural adhesive bonds are used in many different applications for many different reasons. This chapter provides information about important and potential (structural) applications and developments for the construction industry.

7.1 Composite, hybrid and laminated structures

Composite, hybrid and laminated structures have the best of both worlds, therefore they are being increasingly applied. Adhesives are very suitable to make a shear connection between two components, because they are relatively strong in shear and are able to bond different materials.

7.1.1 Glulam

Glulam (glued laminated timber) is widely used in the building industry and one of the most well-known and proved applications of structural adhesive bonding. Due to the low tensile strength perpendicular to the grain ($f_{t,90}$) and the low shear strength ($f_{v,0}$) of timber, the adhesive is most likely not decisive for the strength.

7.1.2 Sandwich panels

For insulation sandwich panels, for instance with a foam core and outer steel or wooden panels, adhesive bonding is frequently used. With adhesive bonding problems due to too low bearing strength of the core or the thin panels are avoided. Moreover adhesives are light weight, so the total weight will remain low.

Due to their excellent weight-to-strength ratio, sandwich panels are not exclusively used for insulation, but also for light weight structures. Regularly, cores are made of honeycombs, foam or wood and panels are made of steel, aluminium, wood or FRP.

7.1.3 Bridge decks

The Gärtnerplatz Bridge in Kassel (Germany) is an example of usage of adhesive bonded ultra high performance concrete (UHPC), see Figure 7.1. [26, 27] A steel lattice girder with UHPC top chords is bonded to a UHPC slab. In general concrete has a low tensile and shear strength (especially in comparison to the compression strength), therefore the adhesive may not be decisive for shear connection with concrete. For instance, in Cur-aanbeveling 91 [28] the required adhesive strength, $\tau_1 \geq 12 \text{ N/mm}^2$ & $\sigma_1 \geq 15 \text{ N/mm}^2$, is chosen so that it will be higher than the concrete strength. Moreover adhesive bonded connections perform well in fatigue and are able to connect steel (girder) and concrete (deck). Nowadays shear connections are often made with a large amount of shear connectors. Adhesive bonds will reduce the amount of stress peaks, take away the necessity to pour concrete on the construction site and may reduce the labour costs. Hence adhesive bonded shear connections of bridges with concrete decks seem to be a potential market.

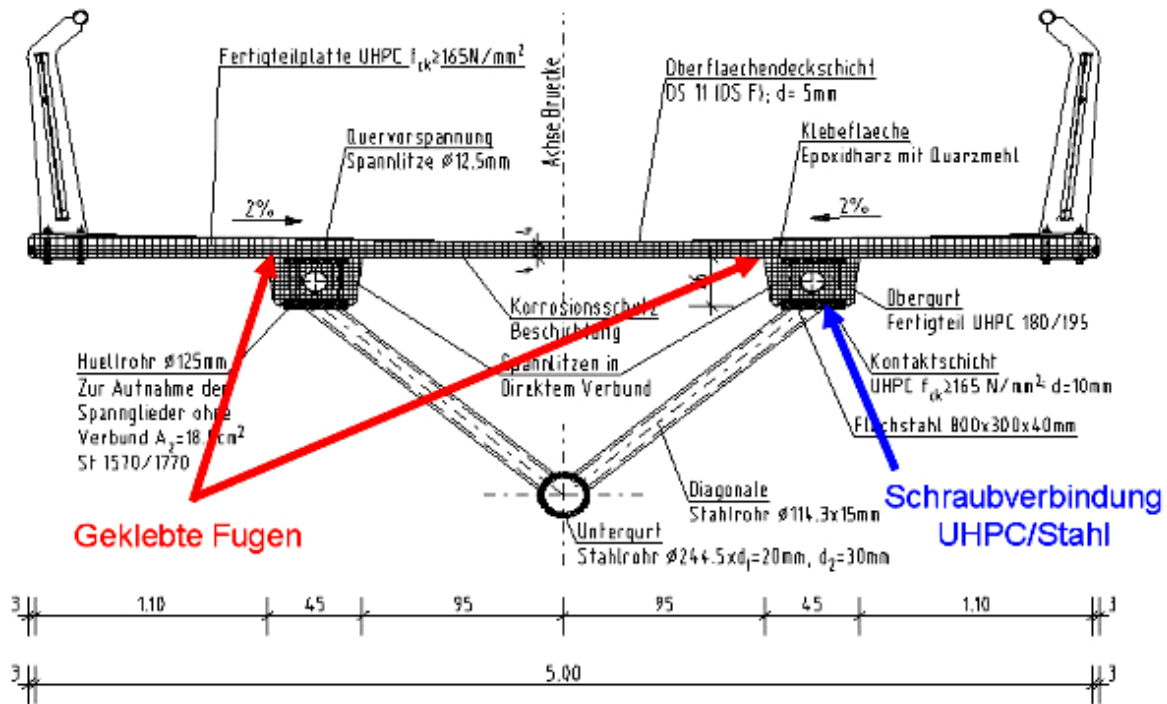


Figure 7.1: Cross section of the Gärtnerplatz Bridge in Kassel (Germany) [26]

7.1.4 Steel-concrete composite beams

Applications of adhesive bonded steel-concrete composite beams are nowadays not used in buildings. But adhesive bonding between a steel girder and prefab concrete floor elements may result in a lighter, faster and less labour intensive method, and so cheaper method than the traditional method. Traditionally all the concrete, or a large amount of concrete, is poured at the construction site. Note that both concrete and adhesive have to cure for some time, but poured concrete will be on the top (walking) surface and additional rebars have to be placed. Due to the high efficiency of steel-concrete composite beams, they have a large market share in multiple storey buildings, this makes the development of new solutions attractive.

7.1.5 FRP

FRP (fibre reinforced polymers) structures are increasingly applied. They are light weight and form free. Connections between different FRP elements or FRP and other materials can be made with adhesive bonds. Welding steel to FRP is not possible. Bolted FRP connections are possible but attention should be paid to the peak stresses (shear out, tension failure and cleavage tension failure) [29]. Adhesive match the nature of FRP well, the resin of FRP acts in fact also as an adhesive, therefore adhesive bonded connections seem to be the most logic choice for FRP structures.

7.1.6 Masonry

The cement mortar in masonry acts as an adhesive, therefore polymeric adhesive instead of cement mortar can be used. Adhesives are nowadays often used with gypsum blocks but also other stony materials are suitable. Masonry with adhesive performs better than those with cement mortar. [30]

7.1.7 Glass

Glass is increasingly used as a structural material. Due to its transparent character, glass is popular among architects. An example of a transparent glass structure is the Sonsbeek Pavilion (1986) of Bethem Crowwel Architects, which is depicted in Figure 7.2. The steel trusses seem to hover in the air. Nowadays glass can be used for practically everything such as beams, floors, columns, facades, walls and roofs. With adhesive bonds glass can be connected to steel and concrete in a transparent way, no bolts or clamps which reduce the transparency have to be applied. Moreover, adhesive bonded connections have less high stresses peaks than bolted connections, which is desirable for a brittle material such as glass. Adhesive also can be used for lamination of glass, which avoids brittle failure of glass structures. [31]



Figure 7.2: Sonsbeek Pavilion of Bethem Crowwel Architects

7.1.8 Aluminium

Aluminium is frequently used as building skin which protects the inner construction due to its impenetrable corrosion layer. Aluminium and steel contact should be avoided to prevent galvanic corrosion. Due to the difference of melting temperature welding of aluminium and steel is practically impossible. Welding of aluminium-to-aluminium itself requires special skills. For these reasons aluminium is most often connected to the inner construction with stainless steel bolts or normal bolts with special isolators. Adhesive bonded connections are a good alternative for those connections.

7.1.9 Strengthening and repair

Constructions are often reallocated, or the loads have changed or will change. Strengthening of those structures may be needed, because replacing is environment unfriendly, costly and time consuming. Today, many of the large (infra-) structures built after the second world war have reached their limits, which makes strengthening a hot topic. For concrete structures strengthening with bonded external carbon fibre reinforcement polymer (CFRP)¹ strips are frequently used. Enough documentation, such as the Dutch CUR-aanbeveling 91 [28], is available to make a proper design and calculation. Bonded external reinforcement has some major advantages in comparison to other methods. The most important advantage is without a doubt its relative ease of use. No

¹ Also other fibres or steel strips can be used but CFRP's are most often used

temporary support structures are needed, only temporary clamps may be needed to ensure enough pressure during hardening. If the CFRP strips are applied at the bottom most preparation, for instance the pre-treatment of the adherent, can take place when the structure is still (partially) in service. Before the bonding process starts, the variable load should be removed. After the adhesive is hardened the composite behaviour will take care of all the loads other than the permanent load (variable and accidental loads). Moreover the CFRP strips can be cut to the right size and some are flexible which make them easy to apply even for complex shapes, see Figure 7.3. Thereby adhesive bonded CFRP strips are light weight and small, so the increase in weight and cross section may be neglected.



Figure 7.3: Shear strengthening of a reinforced concrete bridge girder [32]

The good fatigue behaviour of adhesive bonded connections is a great advantage for bridges. For steel bridges several promising researches have been done to improve the fatigue life with adhesive bonded steel plates. [33, 34] Other steel structures are strengthened with adhesive bonds since the sixties. [28]

High strength steel (HSS) can lose its high strength when it is heated to high temperature, which is the case in welding. Strengthening with bolted plates is a bit contradictory, because the bolt holes weaken the original steel. For strengthening of HSS structures in particular, adhesive bonds may therefore be a good alternative.

7.1.10 Anchors and rebars in concrete

Structural adhesive bonded anchors and rebars in concrete are frequently used for many different reasons. For instance Hilti, a supplier of anchors, has several adhesive anchoring systems with corresponding calculation and design rules which are also integrated in special software.

7.2 Lengthening of steel beams

Due to transportation the length of beams or hollow sections, which are not made in situ, are limited. In some cases long beams may be desirable, such as for multiple span constructions or large span constructions. For the lengthening of RHS, H- or I-shaped sections, adhesive bonds can be used in its best possible way; in shear. Both the shear of the web(s) and the axial stresses in the flanges can be transferred through shear.

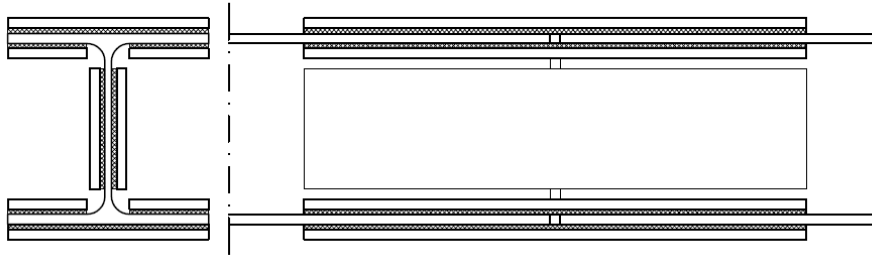


Figure 7.4: Principle detail of lengthening of an H-shaped steel section

7.3 Fatigue sensitive steel structures

In fatigue sensitive structures the most problematic areas are often the areas where stiffeners are welded to the steel profile. The stress concentrations around the welds limit the fatigue life. Adhesive bonded connections are more capable of spreading the stresses which increases the fatigue life. But in most cases adhesive bonded stiffeners will be made out of more material than welded stiffeners. Therefore research is needed to show which method of adhesive bonded stiffeners, welded stiffeners and heavier profiles, is most efficient for standard cases.

7.4 Aesthetics

Bolted connections are rather determinative for the appearance of a structure, especially on the detail level. For many material combinations bolting is the only possible structural connection technology which is nowadays frequently applied. Adhesive bonded connections are often 'smooth' connections, which are less determinative for the appearance of a structure. So for visible structural connections, adhesive bonding may be used for aesthetical reasons.

7.5 Thin elements

Thin elements, such as cold formed sections, are prone to bearing failure when they are bolted. Welding of thin elements may require special equipment and skills. Adhesive bonded thin elements do not suffer from these difficulties. Moreover the eccentricity of lap connections with thin elements are small which reduces the peel stresses.

7.6 Small tolerances

For structural adhesive bonding thin bondlines are required. In other words small tolerances are required. For structural engineering applications, these small tolerances will often lead to higher costs. But nowadays the amount of prefabricated elements on a construction site is high. In a fabrication shop small tolerances are easier and cheaper to achieve than on a construction site. Hence, when small tolerances are required, prefabricated adhesive bonds may form a good alternative.

7.7 Light weight structures

For some structures, such as movable bridges, high rise buildings and floating structures, weight is of special interest. The weight of a large amount of bolts can be significant. Due to the low weight of adhesives, for instance in comparison with steel a ratio of ± 4.0 , adhesive bonded connections may be suitable for light weight structures.

Note that light weight structures are often structures made out of different materials, for which adhesives are also suitable.

7.8 High strength steel (HSS)

HSS owes its high strength properties to special heat treatments. As mentioned before, due to high temperatures HSS loses its high strength. Welding of HSS is therefore problematic. During the adhesive bonding process only a small heat input occurs, which makes it suitable for HSS structures.

7.9 Journals

In the Dutch professional journal *Cement* several articles are published about repair and strengthening with adhesive bonds. Especially adhesive bonded carbon fibre reinforcement polymers (CFRP) is a popular topic with more than ten published articles. Adhesive suppliers, such as Henkel And Sika, have specialised adhesives for CFRP applications.

In the Dutch professional journal *Bouwen met Staal* (Building with Steel) only two articles are published about the use of adhesives [33, 35]. This indicates that adhesive bonding does not (yet) compete with the other connection methods such as welding and bolting. One article, [35], deals with the reason why adhesive bonding is not yet used on a large scale. Lack of regulation and legislation is given as the main reason for this.

In *Cement* three articles about glass are published in the period 2008-2010. At the Delft University of Technology the research group Glass & Transparency has done several tests with adhesive bonded glass structures. This indicates the increasing interest for adhesive bonded glass structures.

In international adhesive journals such as *International Journal of Adhesion and Adhesives* and *Journal of Adhesion Science and Technology* mainly 'fundamental' research is published. All kinds of articles about FEM modelling, fatigue behaviour, dynamic behaviour, impact behaviour, durability behaviour and all different kinds of lap and tensile tests are published in those journals. Most of those articles are for other (engineering) applications than structural engineering, nevertheless those articles also give structural engineers insight in the adhesive behaviour.

8 Key points of theoretical backgrounds

Section 3 to 7 form a brief introduction to the available literature about adhesive bonding. In this section this information will be summarised.

In section 3 an overview of advantages and disadvantages is presented. For structural engineering some advantages are of greater importance than others, but this will vary for different applications. In section 7 the most obvious structural engineering applications are discussed. The main advantages which allow the choice for adhesive bonding for a specific application can be found in the next table:

		Application								
		Composite, hybrid and laminated structures	Anchors and rebars in concrete	Lengthening of steel beams	Fatigue sensitive steel structures	Aesthetics	Thin elements	Small tolerances	Light weight structures	High strength steel (HSS)
Advantage	Fewer and lower stress concentration									
	No significant heat input									
	Ability to avoid galvanic corrosion between dissimilar materials									
	Joining all kinds of materials and dissimilar materials									
	Small tolerances possible									
	Invisible connection possible									
	Good sealing properties with regard to gasses, moisture and chemicals									
	Good insulation properties with regard to heat, sound and electricity									
	No significant increase in weight									
	No influence on the straightness and cross sectional area of the elements									
	No introduction of high (residual) stress									
	Adhesive can act as gap-filler									
	Complex joint configurations possible									
	Increase of stiffness									
	Increase of the dynamic damping									
	Increase of the fatigue life									
Reduction of labour and capital costs										

Table 8.1: Overview of main advantages for applications

Most disadvantages are a point of concern for every application. The main disadvantages can be found below:

1. Complex manufacturing process
2. Fixing of the adherents during cure process is necessary
3. Significant influence of the environment on the durability
4. Environmental conditions affect the properties of the adhesive
5. Time dependent effects affect the properties of the adhesive
6. High strength bonding demands small tolerances
7. Possible toxicity and its effects on the environment and labour conditions
8. Difficult to apply non-destructive test methods to control the bondline quality
9. Difficult to dismantle the joint for repair or re-use of the materials
10. Stress levels in the bondline are hard to predict
11. No building codes available for calculation

12. Strong in shear and compression, but weak in tension and peel
13. Specialised storing conditions may be required
14. Little practical experience among contractors
15. Mismatch of coefficient of thermal expansion

In section 4 a brief introduction to adhesive technology is presented. All of today's structural adhesives are polymers. For adhesive bonding two phenomena are of importance, cohesion and adhesion. In most cases cohesion is designed to be the decisive factor in strength.

The cohesion properties depend on the polymer structure, in other words, the degree of linking between the polymer chains. Four types are distinguished: linear, branched, cross-linked and network. Three types of polymer behaviour are distinguished, namely: elastomer, thermoset and thermoplastic. All adhesives soften above the glass transition temperature, the exact behaviour depends on the type of adhesive. For structural application the service temperature should remain below the glass transition temperature. With additives the behaviour of the adhesive can be influenced. Adhesives are prone to ageing which lowers the degree of polymerisation. Contact with water, chemical or ultraviolet radiation can accelerate the ageing process.

Two main types of adhesion are distinguished: mechanical adhesion and specific adhesion. Mechanical interlocking takes place through interlocking. Specific adhesion is based on intermolecular forces, which exist of four main types: chemical adhesion, adsorptive/dispersive adhesion, diffusive adhesion and electrostatic adhesion. Due to the small range of intermolecular forces, for good bonding it is important that the adhesive wets the adherent surface well. Key factors for wetting are the surface tension and contact angle. Contaminations will counteract good wetting. Therefore, surface treatments are a crucial factor in adhesive bonding.

In section 5 the mechanical behaviour is discussed. Due to the wide variety of types of adhesives a quantitative overview of the mechanical properties is impossible to give, but some qualitative relationship and bandwidth can be given. For structural application the service temperature should be lower than the glass transition temperature. Most adhesives exhibit an elastic-plastic behaviour. The temperature is of great influence on this behaviour. In general, a higher temperature results in a lower stiffness and strength, and a higher deformation capacity. For polymers, such as adhesive, the Drucker-Prager model (or a variant) describes the behaviour well. But also the Von Mises criterion is sometimes used. The Drucker-Prager model indicates that a material is stronger in compression than tension. The coefficient of lateral contraction varies from 0.33 (elastic) to 0.5 (plastic). The coefficient of thermal expansion of adhesive is at least $40 \cdot 10^{-6} / ^\circ C$, which is more than three times as high as that of mild steel. Therefore thermally induced stresses are inevitable for temperature differences.

Adhesive bonded connections are mostly overlap connections due to fact that adhesive are stronger in compression and shear than in tension. Many theory's, including the classical works of Volkersen (1938) and Goland and Reissner (1944), are developed to describe the behaviour of overlap connections. Important is the shear and peel distribution. Due to shear lag the shear distribution has a U-shape. Due to the internal lever arm peel stresses develop, especially at the ends of the overlap. The U-shape of the shear stresses limits the effectiveness of long overlaps; the majority of the load transfer takes place at the ends of the lap. Due to the low tension strength of adhesives, peel is known as the adhesive worst enemy. Research shows that there is an optimal bondline thickness with respect to strength, but many theory's predict that the strength increases with increasing bondline thickness.

There are several ways to reduce the stresses peaks at the end of laps. As mentioned before elongation of the lap has a limited effect. Increasing the bond width will lead to a pro rata increase of the failure load. Reducing the internal lever arm, e.g. through thinner or tapered adherents, will lead to lower peel stresses. Symmetric connections (e.g. double strap), with external moment equilibrium, have lower peel stresses than a asymmetric connection, with no external moment

equilibrium. Increasing the adherent stiffness over adhesive stiffness results in lower shear stresses. Spew filler reduces the peel and shear stresses.

In section 6 the time-and-environmental-dependent-effects are discussed. Temperature, moisture, oxidation, creep and relaxation are of most interest for structural engineering applications. Shrinkage and differences in thermal expansion effects are well known among structural engineers, but strong temperature dependency of the mechanical properties at room temperatures are less common for structural materials. Once again, the service temperature should be well below the T_g .

Exposure to moisture, e.g. high humidity, should be prevented. Moisture can lead to reversible processes like swelling, plasticising, lowering of the T_g and irreversible processes like displacement of the adhesive¹ and hydrolysis. All these processes have a negative influence on the adhesive and due to swelling stresses can develop.

Most adhesives are susceptible to oxidation, which is an irreversible process. Light and chemicals can influence the oxidation process.

The creep and relaxation behaviour of structural adhesives is viscoelastic-plastic of nature. Due to creep the U-shape of the shear distribution for lap connection will flatten.

Adhesives and/or it's additives can be affected by oxidation, chemicals, all sorts of radiation and biological degradation. Most effects are irreversible and should be prevented.

The rate of influence from harmful external factors depend on the geometry; a small as possible perimeter over volume ratio is recommendable. Also a sealing layer can be used to limit the exposure to harmful external factors.

The exact behaviour due to time-and-environmental-dependent-effects is not yet fully understood and a prediction of the exact exposure conditions of the entire service life is hard to make. Therefore an exact calculation is impossible; the calculation of time-and-environmental-dependent-effect is based on empirical research. Most suppliers provide reduction factors.

¹ For non corrosive materials displacement of the adhesive is reversible

Part B: Testing of a connection

9 Design study of L-connection

In structural engineering, many different types of structural steel-to-steel connections are used. When the Pareto principle, also known as the 80-20 rule, is used as an estimation, approximately 20% of the types of connections are used for 80% of the connections. Beam-to-column connections are, without a doubt, part of the 20% most often used types of steel-to-steel connections in structural engineering. Hence, if beam-to-column connections can be constructed as adhesive bonded connections there is a large potential market for those type of connections. To investigate the possibilities of structural adhesive bonded connections in structural engineering, beam-to-column connections seem to be a good starting point.

A FEM test and physical test can provide essential information about the mechanical feasibility, therefore these tests will be performed for one connection. If this connection is mechanically feasible, most likely more structural adhesive bonded connections are.

Before a good final design can be made this design study will be performed. The goal of this study is to come to a good adhesive bonded alternative for a specific traditionally bolted beam-to-column connection which can be tested.

9.1 Starting point

In structural engineering most steel beam-to-column connections are made with I-shaped sections. As a reference, connections from a utility building are taken because they are frequently used. There are two basic types of beam-to-column connections for single spans, at an intermediary place at the column (T-connection) and at the top of the column (L-connection). The intermediary one is used for floor details. The top one is used for roof details. In general use, the column of a T-connection is continuous and the beam is placed 'against' the column. For the T-connection either the beam on top or against the column is commonly used. For adhesive bonded connections the variant with the beam on top seems to be most suitable with regard to the transfer of forces.

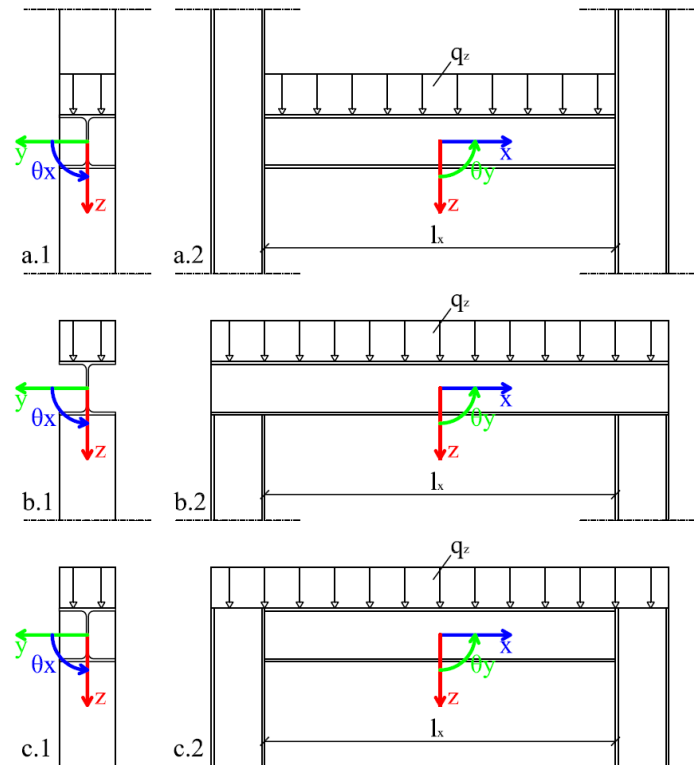


Figure 9.1: a: Typical beam-to-column floor layout¹, b&c: Typical beam-to-column roof layout¹

In this design study only the single span connection will be considered extensively. But for a comprehensive study also the multiple span connections are considered, but briefly. For multiple span floor and roof connections there are two basic types, which are depicted in the next figure. One with a continuous column and one with a continuous beam.

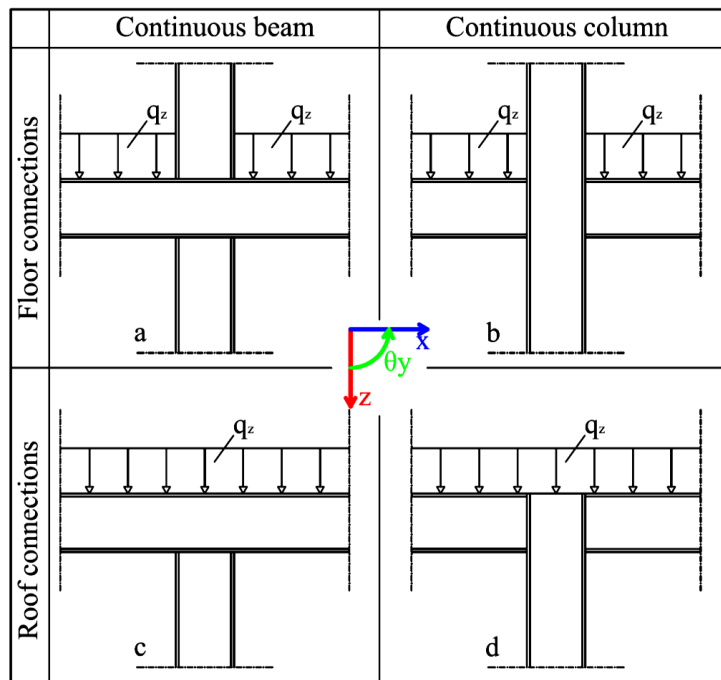


Figure 9.2: Multiple span beam-to-column connections²

In contrast of single span connections, continues beams are also commonly used for floor connections.

¹ Only the beams and columns are drawn; stiffeners, splice plates, angle cleat and similar elements may be needed.

² Only the beams and columns are drawn; stiffeners, splice plates, angle cleat and similar elements may be needed.

9.1.1 Profile shape

There are two widely applied I-shaped beam profiles, HEA- and IPE-profiles. The HEA has wider flanges than the IPE profile. This facilitates the placement of floor or roof elements. For instance a hollow core slab requires 70mm bearing length in standard cases. [36] The width is in most cases not of interest mechanically. Increasing the bond width is an effective method to generally increase the failure load, but this does not hold for this case. Because a wider flange means also a pro rata increase in the axial force in the flange for fully effective loaded profiles¹. Hence, the force per unit width will stay the same.

More important is the flange thickness. For a fully effective IPE profile the flange thickness will be smaller than for a fully effective HEA profile. A smaller thickness will result in a lower force per unit width which is an advantage.

The width can be of importance for a double lap connection. Due to tolerances and the non-linear relation of the web thickness and fillet radius with respect to the width, wider flanges can have a relative greater bond area at the internal sides of the flanges.

A fully effective IPE profile will have a greater height than a fully effective HEA profile if they are subjected to the same load. This means that the available bond area of the web is bigger for an IPE than for an HEA profile.

For columns, an HEA profile is more suitable due to the larger moment resistance in the 'weak' direction. This prevents buckling in the weak direction.

As a starting point an HEA-profile is taken. If the design study shows that an IPE-profile is beneficial, an IPE-profile will be taken.

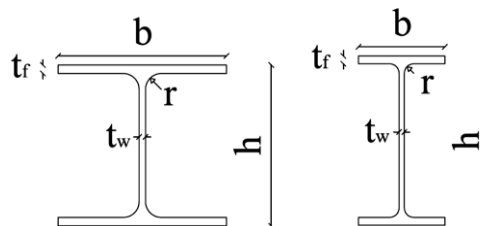


Figure 9.3: cross section of a HEA (right) and an IPE (left) profile

9.1.2 Moment resistance

Considering the characteristics of adhesive bonded connections, it is obvious to search for an alternative beam-to-column connection which can resist moments and shear forces. A frame with rigid connections is called a portal frame. A braced portal frame is depicted in the next figure.

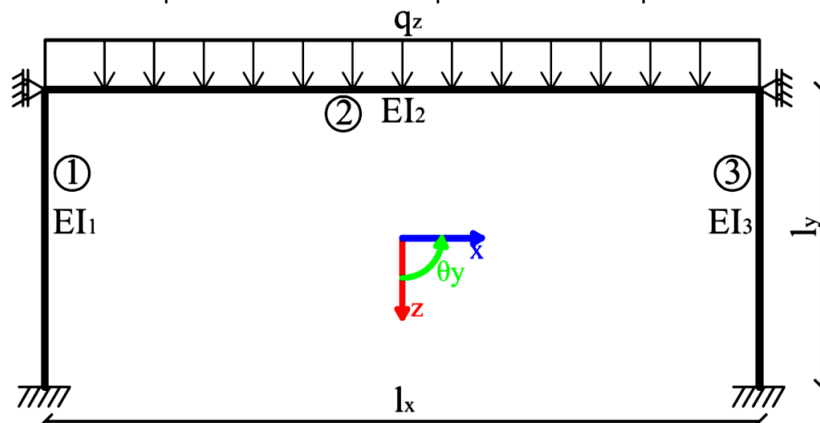


Figure 9.4: Braced portal frame

¹ In the flanges of a fully effective profile the yield stress will be reached if the beam is loaded with the maximum elastic bending moment.

9.2 Types of forces on the connection

In the limit case, where the columns have an infinite bending stiffness ($EI_1 = EI_3 = \infty$), according to the Euler-Bernoulli-beam-theory (EB-theory), the next diagrams apply when the beam is subjected to a uniform distributed load:

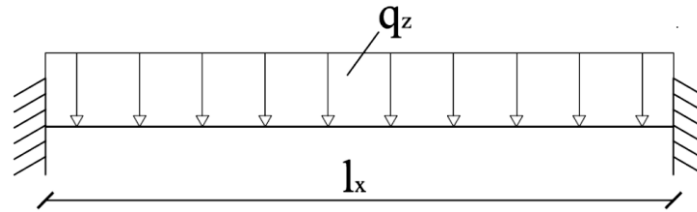


Figure 9.5: Mechanical schematisation of a clamped-clamped beam

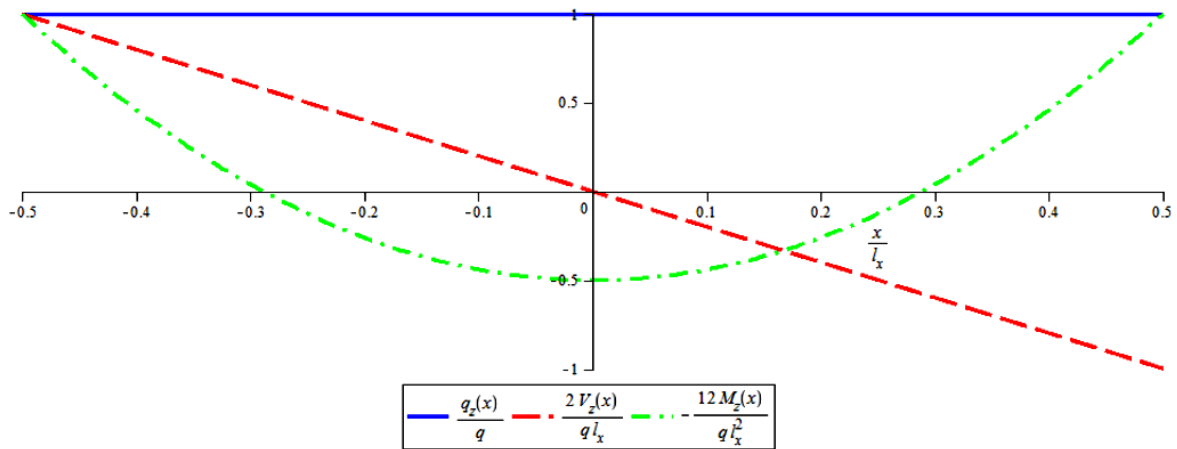


Figure 9.6: Normalised load, shear force and moment distribution of a clamped-clamped beam

In the other limit case where the column has zero bending stiffness ($EI_1 = EI_3 = 0$), according to the EB-theory the next diagrams apply when the beam is subjected to a uniform distributed load:

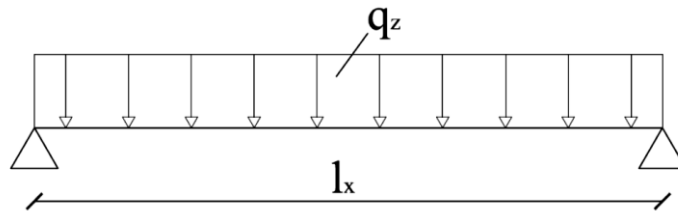


Figure 9.7: Mechanical schematisation of a hinged-hinged beam

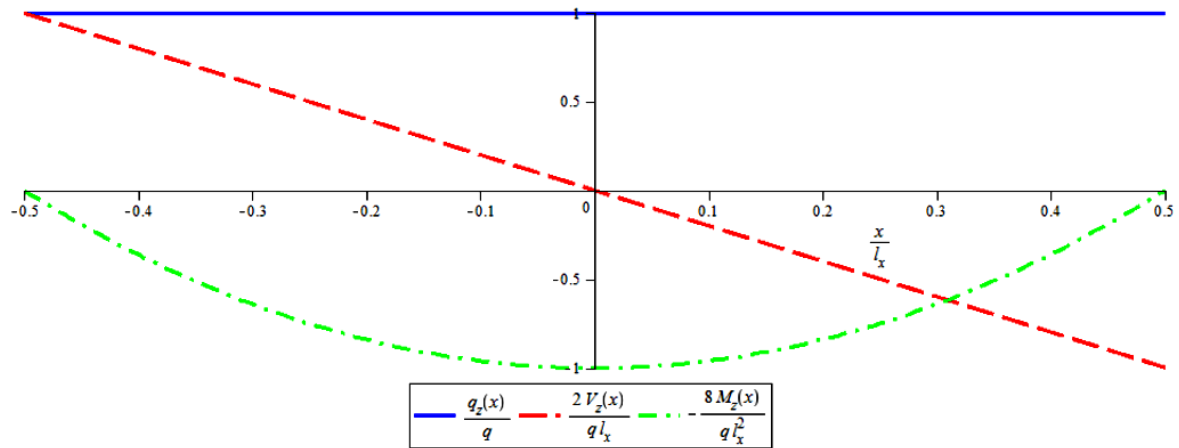


Figure 9.8: Normalised load, shear force and moment distribution of a hinged-hinged beam

The real force distributions will be somewhere in between those of Figure 9.6 and Figure 9.8, $0 \leq M_z \leq ql^2/12$ and $V_z = ql/2$. The connection should be able to transfer these forces from the beam to the column. Later, in section 9.7.3, a detailed calculation of the exact forces will be made.

The beams may also be loaded by the columns due to the frame action. However in most cases the load of the floors will be the most important.

In an unbraced frame wind loads cause forces on the moment resistant connections. Moments due to wind loads can be of opposite direction and bigger than those due to the load on the floor. Therefore tension and compression stresses can change direction in the connection. A proper designed connection takes this into account. This study will mainly focus on the forces due to the floor loads, because this is assumed to be the decisive factor in designing. But for high buildings the wind load causes high forces in the lower part of the portal frame. It is up to the designer to choose for bracings to lower the forces on the connections or to design strong connections which are capable of handling these forces. In this study the frame is assumed to be braced.

According to the EB-theory the contribution of the web of the beam is most important for the shear capacity of the beam. The flanges of the beam are most important for the moment capacity of the beam.

9.3 Analysis of a bolted T-connection

The following figure shows a typical moment-resistance-bolted beam-to-column-T-connection.

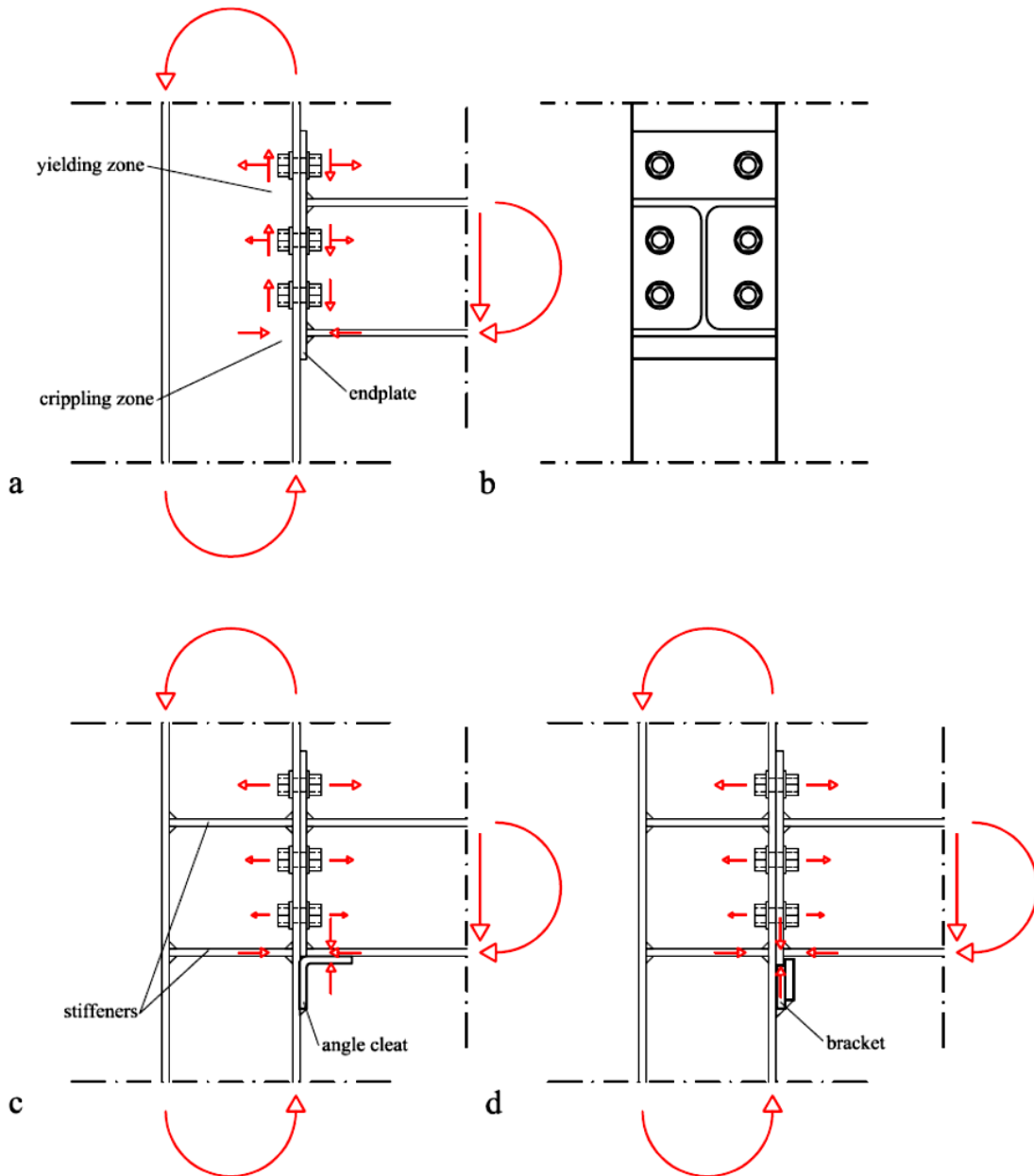


Figure 9.9: Typical bolted beam-to-column-T-connection

9.3.1 Transfer of force

In the fabrication shop endplates are welded to the beam. The upper bolt row is predominantly loaded in tension. The middle bolt row is loaded in tension and shear. The lower bolt row is predominantly loaded in shear. The lower flange of the beam is loaded in compression and will press to the column (rotation point). The combination of the tension in the two upper bolt rows and the pressure (compression) between the lower flange of the beam and the column allows this detail to resist moments. The resistance of the shaft of the bolt to shear allows this detail to resist shear forces.

To facilitate the erection an angle cleat can be used, see Figure 9.9.c. Such an angle cleat will transfer the shear force into the column. If the angle cleat is bolted to the beam also moments which cause tension in the bottom flange of the beam can be transferred, which can be needed to take up moments due to wind forces.

Also small brackets ('klufts' in Dutch) may be used, see Figure 9.9.d. A small piece of metal is welded to the column in the fabrication shop and acts in the same way as an angle cleat.

Due to the forces in the column, the column will deform which reduces the stiffness of the connection. Moreover, crippling at the bottom and yielding at the top in the column can occur, Figure 9.9.a. For both latter reasons it can be necessary to apply stiffeners in the column, Figure 9.9.c.

9.3.2 Converting the bolted into an adhesive bonded connection

Adhesives are strong in shear and weak in tension, therefore it is obvious to search for a detail where the adhesive is loaded in shear. For an unambiguous description the reference system of Figure 9.1 is used. In this reference system stresses in x-direction generate shear in a z-plane and a y-plane. Stresses in z-direction generate shear in a y-plane and an x-plane.

A moment around the y-axis, M_z , will generate normal stress on an x-plane in the x-direction in the beam. A shear force in the z-direction, V_z , will generate shear stresses on an x-plane in the z-direction.

The easiest way to convert the bolted detail depicted in Figure 9.9 into an adhesive bonded detail, is to put adhesive between the endplate of the beam and the flange of the column. Such a detail can resist a large V_z due to the x-bond plane. But it cannot resist a large M_z because this requires a z- or y-bond plane. Therefore an endplate is only useful to transfer shear forces in adhesive bonded column-to-beam connections.

For an adhesive bonded connection the compression in the lower beam flange can be transferred in the same way as for the bolted variant. For the tension in the upper flange probably another transmission mechanism is needed.

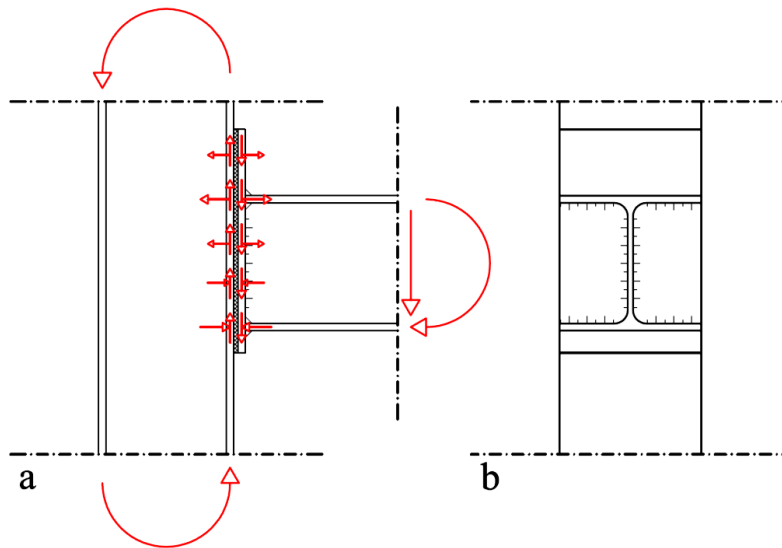


Figure 9.10: Adhesive bonded variant of Figure 9.9.a

9.3.3 Variant study for floor connection

In 'Appendix D: Design sketches', sketches of adhesive bonded connections can be found. One sketch, which is shown in Figure 9.11, seems to be the most feasible alternative of Figure 9.9.

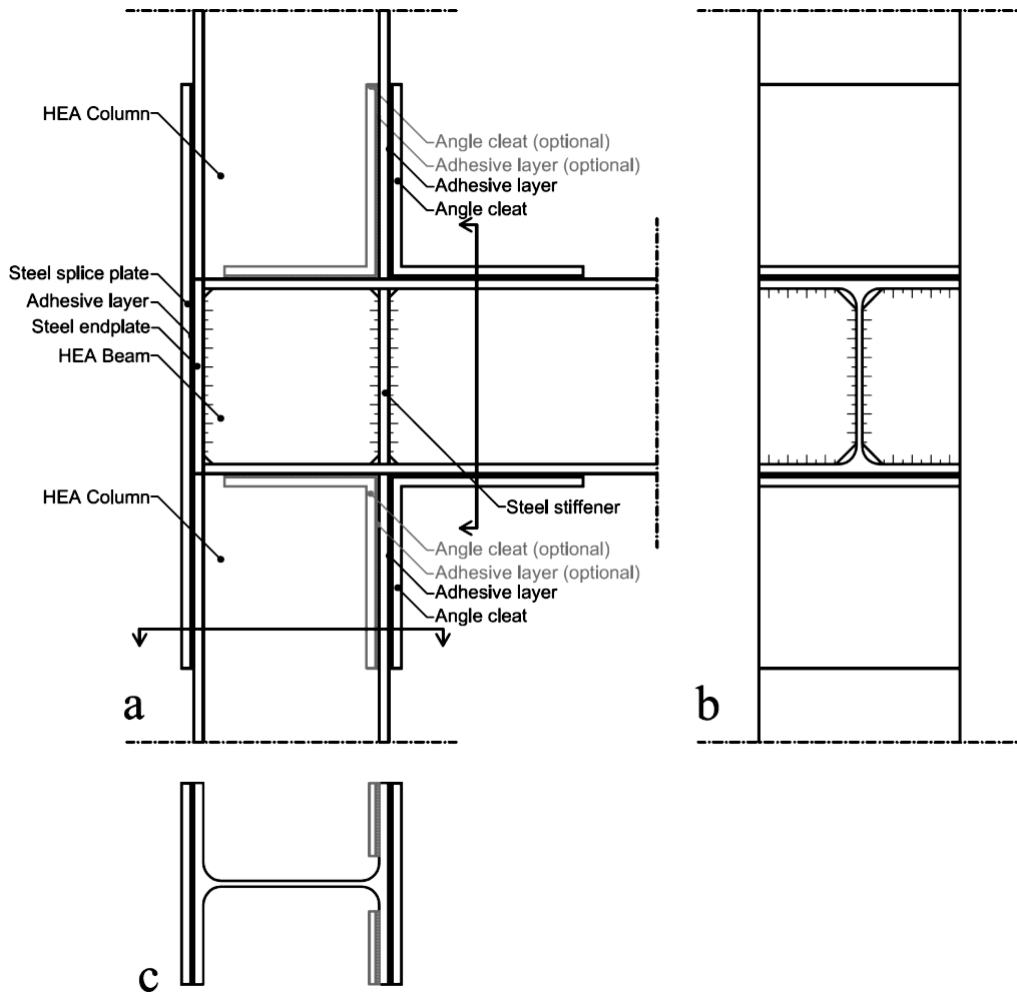


Figure 9.11: Most suitable (with respect to mechanical properties of adhesive) adhesive bonded T-connection

This T-connection has a continuous beam, instead of the usual continuous column, this solves the problem of the tension/peel stresses of the detail depicted in Figure 9.10.

The shear force of the beam is transferred via steel-to-steel contact to the lower column. The rotation point of the beam, the same place as where the resultant vector of the shear force engages, is approximately at the top of the right flange of the lower column. The counter clockwise moment of the beam generates shear stresses at the adhesive layer of the splice plate, which generates a clockwise moment on the beam. The downward vertical force of the upper column will generate a clockwise moment on the beam. The counter clockwise moments should make equilibrium with the clockwise moment. If the clockwise moment is too big, oversized profiles can be used so the bond area of the endplate of the beam increases and so a larger shear force can be transferred to the splice plate.

The horizontal forces of the upper column and/or beam in x-direction can be transferred by the angle cleats. Note that a movement in the negative x-direction, to the left, generates tensile/peel stresses in the x-bond plane of the angle cleats. Probably the optional angle cleats of Figure 9.11 are needed. In most cases the lower flange of the beam will only be loaded in compression, then the optional lower angle cleat is not needed. For frames, for instance the one depicted in the next figure, the upper column at the left clamp support may be loaded with a horizontal force in negative x-direction. If this is the case, the optional upper angle cleat is probably needed.

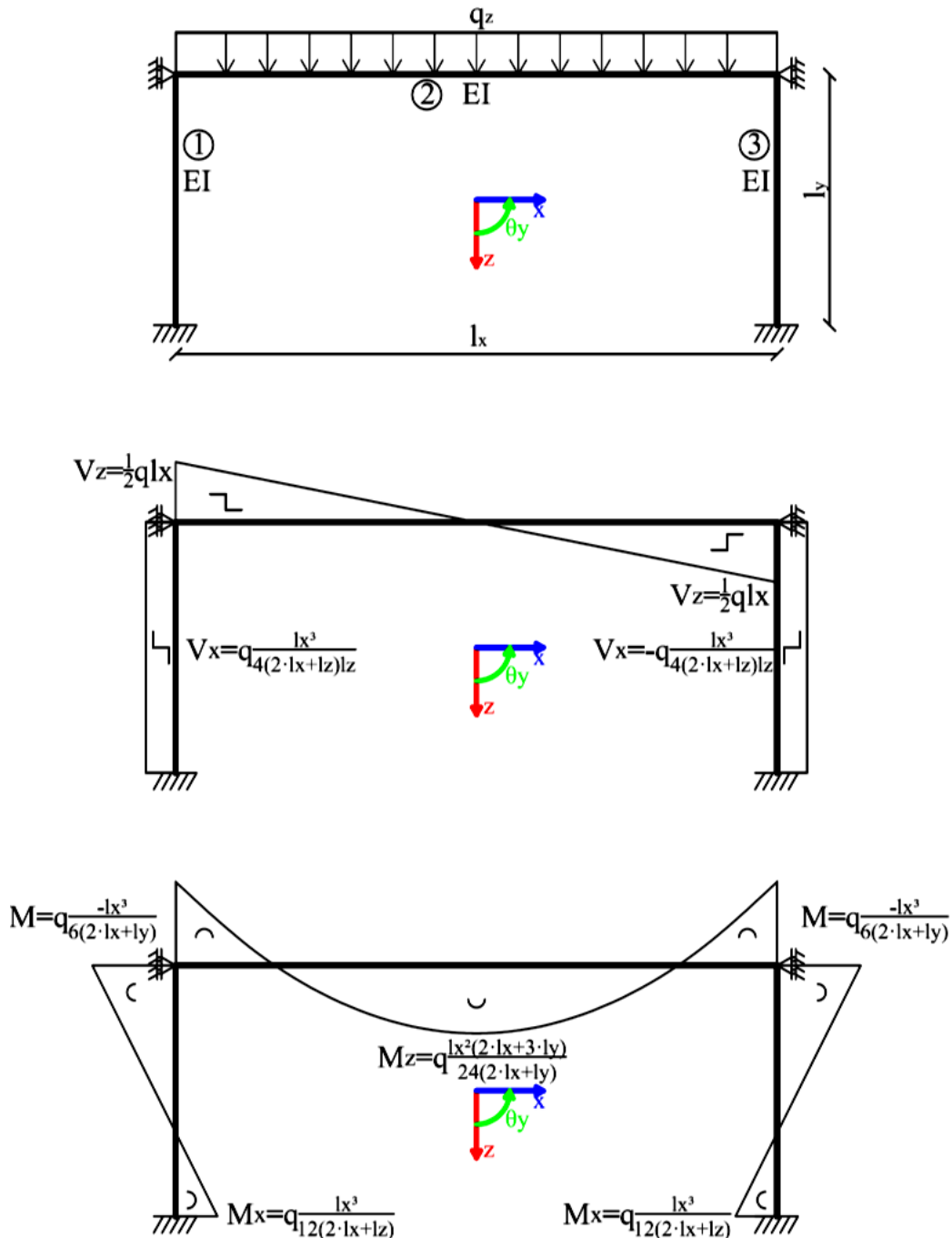


Figure 9.12: Standard (braced) portal frame

The upper column can be loaded with a moment by the beam at the top of the column. Most likely the resultant maximum moment is always in the counter clockwise direction at the connection. In that case, the right flange is loaded in tension. The tension in the right flange causes shear in the x-bond plane and tension/peel in the y-bond plane of the angle cleat. The optional angle cleat of Figure 9.11.b will lower the tension/peel stresses. Also an endplate welded to the column which is bonded by an adhesive layer to the beam will lower the peel stresses. If the tension/peel stresses stay too high, an oversized column can be used so the lever arm increases, which reduces the tensile force pro rata. Other adhesive bonded solutions are costly and/or labour-intensive.

The normal force of the upper column goes through the endplate, web and stiffener of the beam to the lower column. The stiffener and endplate are needed to prevent crippling and buckling of the web of the beam.

Setting the splice plate of Figure 9.11 can cause difficulties during the erection. With the splice plate three large members are connected to each other. Due to tolerances and temporary propping this is difficult. Therefore it can be beneficial to first make a good connection between the lower column and beam. Figure 9.13 shows a detail of how this can be done. The L-shaped splice plate will also increase the bending moment capacity of the connection, see also section 9.4.3.

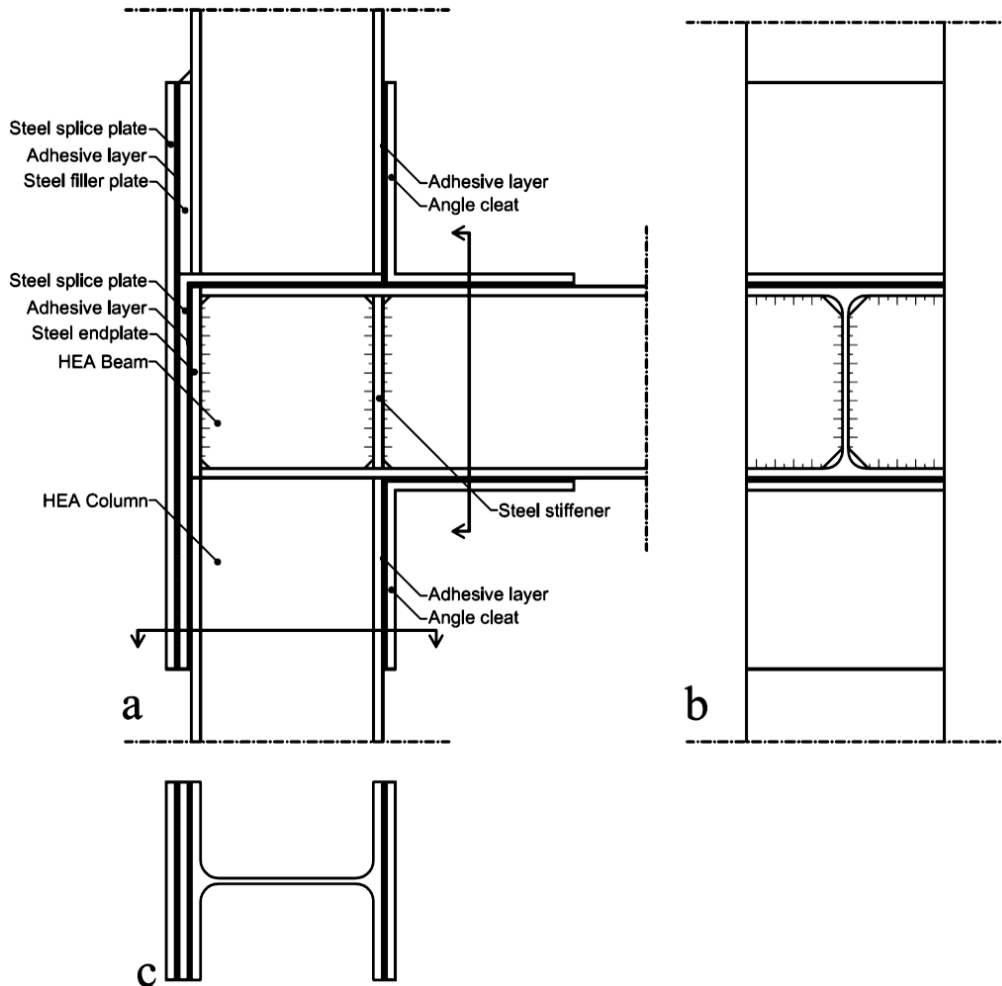


Figure 9.13: Better executable variant of Figure 9.11

9.4 Analysis of a bolted L-connection

The following figure shows a moment-resistance-beam-to-column-L-connection, a so called knee connection. The figure is based on Figure 17.10.2 of [37]. This type is the most feasible variant of a bolted knee connection to convert in a adhesive bonded one, due to the shear force transfer by steel contact.

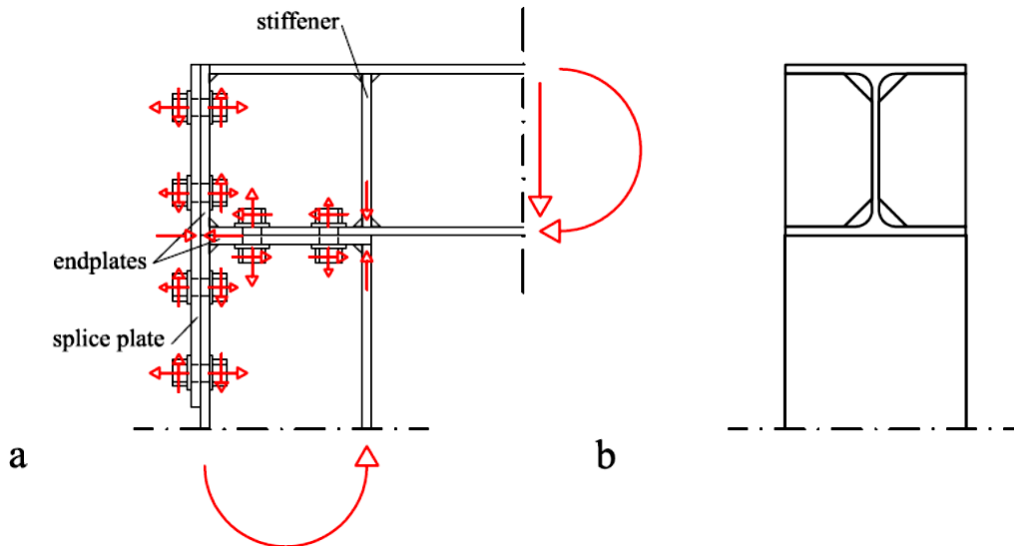


Figure 9.14: Most feasible bolted variant for converting into an adhesive bonded beam-to-column-L-connection

9.4.1 Analysis of a bolted L-connection

In the fabrication shop endplates are welded to the beam and column and a stiffener is welded inside the beam at the place of the inner flange of the column. On site a splice plate is bolted to the column flange and endplate of the beam.

The moment will generate tension and shear in the bolts of the endplate of the column, and tension and shear in the endplate of the beam. The shear force will generate compression at the stiffener (rotation point). The stiffener ensures, if required, that no crippling takes place at the web of the beam.

The shear forces will be transferred from the web of the beam to the web of the column by contact between the webs (compression).

9.4.2 Converting the bolted into an adhesive bonded connection

In section 9.3.2 is treated which forces give shear stresses at which specific plane. This should be known because adhesives are strong in shear and weak in tension.

The easiest way to convert the bolted detail depicted in Figure 9.14 into an adhesive detail, is to put adhesive between the endplate of the column and the lower flange of the beam, and between the splice plate and the endplate of the beam and the outer flange of the column. Such a detail can resist a large V_z because this is transferred through compression in the adhesive layer between the beam and column at the place of the stiffeners. This point will act as rotation point. The adhesive can be pressed out when the shear force is large. The moment, M_z , will cause, just like in the bolted connection, tension and shear at the endplate of the column, and tension and shear in the endplate of the beam. Note that although tension occurs in the adhesive layer this detail is capable of resist a rather high moment, because the bond plane at the endplate of the beam is rather large and therefore stiff. Hence the major part of the moment will be transferred trough shear.

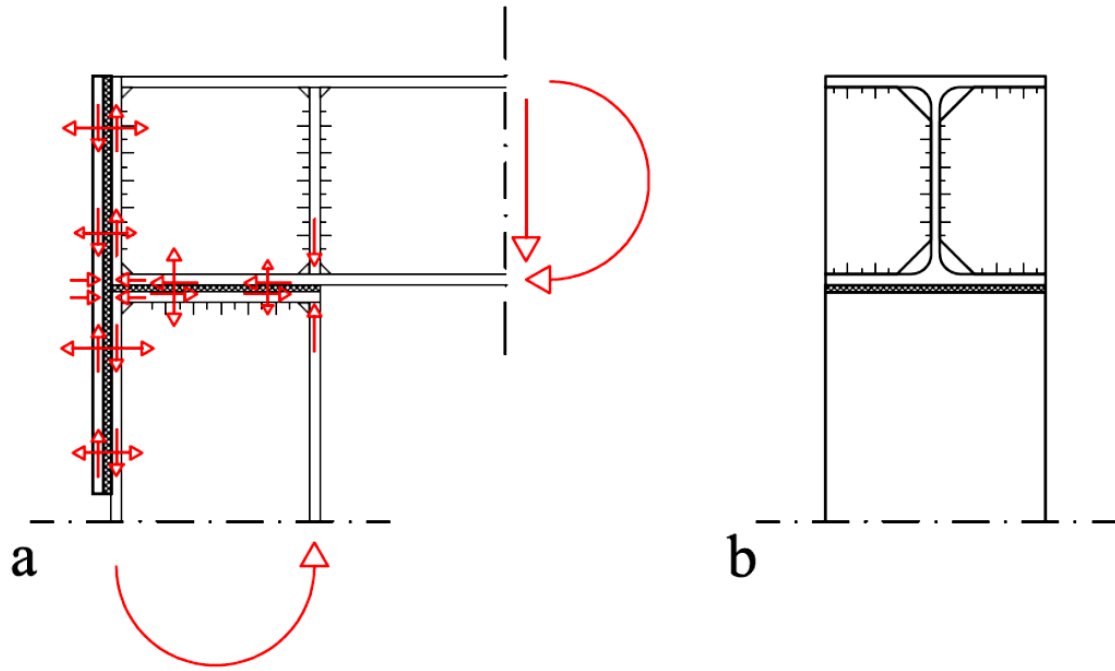


Figure 9.15: Adhesive bonded variant of Figure 9.14

9.4.3 Variant study for roof connection

In 'Appendix D: Design sketches', sketches of adhesive bonded connections can be found. One sketch, which is shown in Figure 9.16, seems to be the most feasible alternative of Figure 9.2.

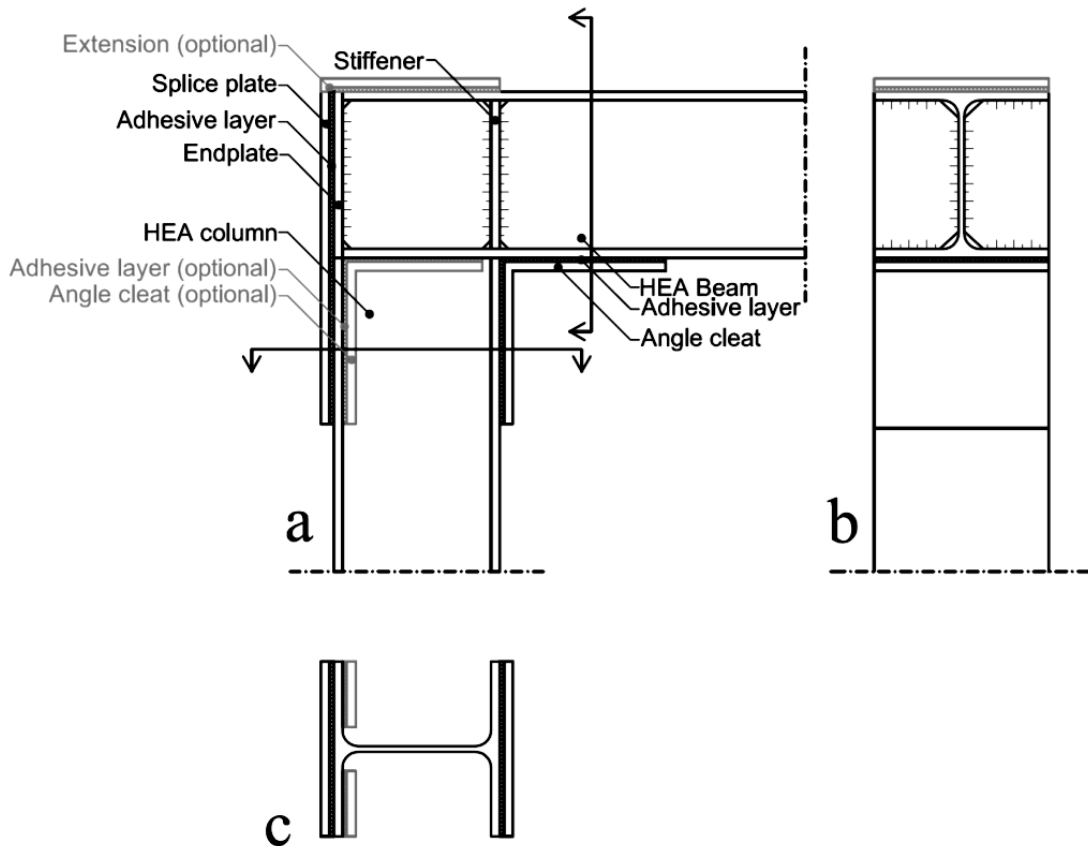


Figure 9.16: Adhesive bonded L-connection

The detail of Figure 9.16 looks a lot like the detail of Figure 9.15. Only Figure 9.16 has an angle cleat and no endplate on the column.

The shear force of the beam is transferred by contact of the beam and column at the place of the stiffeners. This place will act as the rotation centre.

The compression force of the lower flange of the beam is transferred to the column by the angle cleat. The z-plane of the angle cleat is loaded in shear and the x-plane is loaded in compression. If the capacity of the angle cleat is not enough, an additional angle cleat can be used, or an endplate on the column. An additional angle cleat, in comparison with an endplate, has as advantage that all bond planes can be made at the same time and that the adhesive cannot be pressed out near the stiffeners. Disadvantages are the higher amount of material usage and four instead of one extra bond planes.

Due to the rotation of the beam the adhesive layer between the column flange/endplate of the beam and the splice plate is loaded in shear. The bond area at the endplate of the beam is limited. If the shear stresses or peel stresses at the top become too high there are two possibilities.

As a first option, the splice can be extended with a part which is bonded to the top flange of the beam. This will lower the peel stresses, because the splice plate will follow the movement of the beam better by the more rigid bonding in x-direction. The shear stresses of the x-plane are lowered because the top flange of the beam will load the adhesive of the extension in compression.

As a second option the profiles can be chosen larger.

The most refined solution is the first.

9.5 Analysis of adhesive bonded X- and multiple-span-T-connections

For the X-connections (also known as crucifix connections) peel stresses are hard to avoid, without costly and/or labour-intensive solutions. Details with such solutions will not be made in practice. Therefore these solution are not considered. Only the moments due to the loads on the floors, which are negative, are considered. In the next figure details of adhesive bonded multiple span connections can be found.

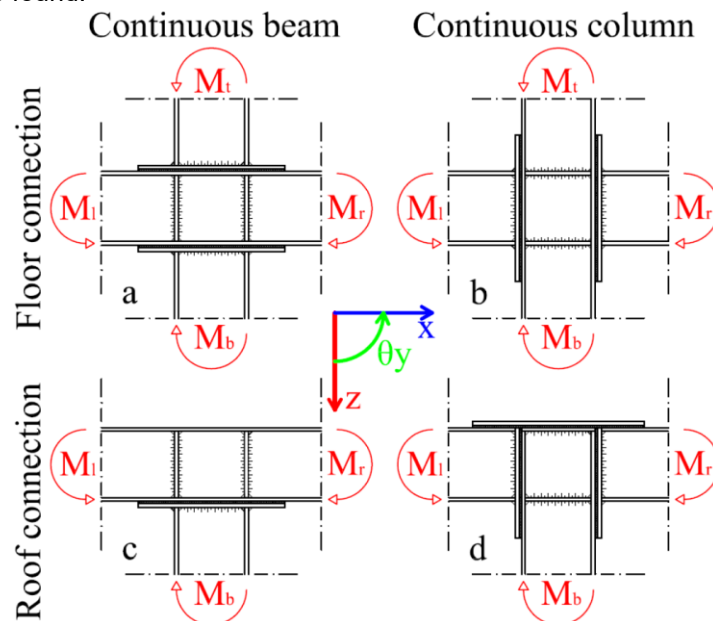


Figure 9.17: Adhesive bonded multiple span connections

If $M_l \neq M_r$, applies for the detail of Figure 9.17.a, this means also that $M_t \neq 0$ and $M_b \neq 0$, peel stresses occur in the adhesive layer. But due to the 'pre-stress' of the vertical force the tension/peel stresses in the bondline may be allowable.

If the geometric non-linear effects are not considered and $M_l = M_r$, $M_t = M_b = 0$ only shear stresses occur in the adhesive layer. This is the case at the centre of a symmetrical frame¹.

A shear force of a beam in positive z-direction causes compression in the lower bondline. Tension in the upper bondline is unlikely due to the downward vertical force in the upper column. Shear forces of the columns cause shear in the adhesive layer. Hence shear force will not lead to problems.

For the detail of Figure 9.17.b the same principle applies as for the detail of Figure 9.17.a, because their main difference between those two details is a 90 degree rotation. But now the 'pre-stress' cannot prevent tension in the bondline. Moreover the moments of the beams are most likely bigger than that of the columns. For x-connections the detail of Figure 9.17.a seems therefore to be the most feasible.

The shear forces of the beams cause shear stresses in the adhesive layer. The shear force of a column will cause compression in one and tension in the other adhesive layer. In a braced frame the shear force of the beam can be transmitted by the bracing and not by the adhesive.

If $M_l \neq M_r$ applies for the detail of Figure 9.17.c, this means $M_b \neq 0$, peel stresses occur in the adhesive layer. But due to the compression stress caused by the shear force of the beam the total stress in z-direction may be allowable. In the case that $M_l = M_r$, which also means $M_b = 0$, no peel stresses occur.

For the detail of Figure 9.17.d, the moments of the beams are transferred by pressure of the lower flange to the column and a plate which is bonded to the top flange. The bondline of this plate is loaded in shear. The shear force of the beam is transferred by shear in the bondline at the endplate. Tension stresses will occur at the top of the bondline of the endplate if the beam is loaded by a moment, but if the adhesive of the top plate is stiff these stresses will stay low.

9.6 Choice of connection

For the single span connections, the L-connection seems to be more feasible than the T-connection. The L-connection has no weak spots such as the T-connection (tension of the right flange of the column) and there are simple modifications possible to increase failure load. Moreover every utility building has a roof but not every utility building has multiple storeys. Therefore the L-connection is chosen over the T-connection.

9.7 Measurements and loads

An approximation of the measurements and loads is needed for a proper final design. As mentioned before the utility sector is taken as reference.

9.7.1 Modular dimensions

For utility buildings often prefabricated hollow core slabs (HCS) are used as floors. On these slabs a concrete topping is poured, typically with a thickness of 50mm. The standard width of the slabs is 1.2m. A beam length of 7.2m gives space to 6 HCS. The smallest slab, with a height of 150mm, has a maximum length of 8m. [36] A clearance of 2.4m and a construction height of +/- 0.6m gives a storey height of 3.0m. From the foregoing the next table can be deduced:

¹ For frames in most cases a chessboard or pattern load should be taken into account according to the Eurocode, in that case the frame and loads are not symmetric

Length	Magnitude	Unit
l_x	7.2	m
l_y	8.0	m
l_z	3.0	m

Table 9.1: modular dimensions

9.7.2 Loads

In the next table an overview of the expected loads for a utility building can be found.

Type	Magnitude	Unit
Hollow core slab (150mm)	2.63	kN/m^2
Concrete topping (50mm)	1.2 (= 24 · 0.05)	kN/m^2
Ceiling	0.1	kN/m^2
Steel roof plates (SAB 100R/825 t=0.88)	0.1	kN/m^2
Isolation & finishing for roof	0.3	kN/m^2
Floor beam (HE300A)	0.88	kN/m
Floor beam (HE200A)	0.42	kN/m
Variable load office building	2.5	kN/m^2
Variable load roof	1.0	kN/m^2

Table 9.2: loads on floor and roof beam

For utility buildings (consequence class 2 and risk class 2) the next table applies according to the Dutch Eurocode NEN-EN1990 [38].

Type	Magnitude	Symbol
Permanent loads	1.35	γ_g
Variable loads	1.5	γ_q
Reduction factor	0.89	ξ_G

Table 9.3: Safety factors

There are two sorts of load combinations (6.10a&6.10b of NEN-EN1990) that should be applied for structural failure¹:

$$\sum_{j \geq 1} (\gamma_{G,j} G_{k,j}) + \sum_{i \geq 1} (\gamma_{Q,i} \psi_{0,i} Q_{k,i}) \tag{9.1}$$

$$\sum_{j \geq 1} (\xi_j \gamma_{G,j} G_{k,j}) + \gamma_{Q,1} Q_{k,1} + \sum_{i > 1} (\gamma_{Q,i} \psi_{0,i} Q_{k,i}) \tag{9.2}$$

The first load case is generally not decisive for structures other than geotechnical structures (see appendix). The second load case simplifies for cases with one permanent and variable load to:

$$\xi \gamma_G G_k + \gamma_Q Q_k$$

To check the assumed profiles a simple hand calculation is made. As approximation, the force distributions of the limit cases derived in section 9.2 are used.

Check the steel profile for the roof beams:

¹ Abbreviated as STR in the Eurocode

$$\begin{aligned}
 \text{Loads :} \quad q_{G;rep;roof} &= (P_{steel\ roof\ plates} + P_{isolation\&\ finishing} + P_{ceiling})l_y + q_{Fbeam} = 4.42\text{ kN/m} \\
 q_{Q;rep;roof} &= P_Q l_y = 8\text{ kN/m} \\
 q_{d;roof} &= \xi \gamma_G q_{G;rep;roof} + \gamma_Q q_{Q;rep;roof} = 17.31\text{ kN/m} \\
 \text{Maximum forces :} \quad M_{d;roof} &= \frac{1}{12} q_{d;roof} l_x^2 = \frac{1}{12} 17.31 \cdot 7.2^2 = 74.78\text{ kNm} \\
 V_{d;roof} &= \frac{1}{2} q_{d;roof} l_x = \frac{1}{2} 17.31 \cdot 7.2 = 62.32\text{ kNm} \\
 \text{HE200A :} \quad M_u &= W_{z;el} \sigma_{s;yield} = (389 \cdot 10^3) \cdot 235 \cdot 10^{-6} = 91.42\text{ kNm} \\
 V_u &= t_w (h - 2t_f) \frac{\sigma_{s;yield}}{\sqrt{3}} \cdot 10^{-3} = 6.5(190 - 2 \cdot 10) \frac{235}{\sqrt{3}} \cdot 10^{-3} = 149.92\text{ kN}
 \end{aligned}$$

Check the steel profile for the floor beams:

$$\begin{aligned}
 \text{Loads :} \quad q_{G;rep;floor} &= (P_{HCS} + P_{topping} + P_{ceiling})l_y + q_{beam} = 32.32\text{ kN/m} \\
 q_{Q;rep;floor} &= P_Q l_y = 20.00\text{ kN/m} \\
 q_{d;floor} &= \xi \gamma_G q_{G;rep;floor} + \gamma_Q q_{Q;rep;floor} = 68.83\text{ kN/m} \\
 \text{Maximum forces :} \quad M_{d;floor} &= \frac{1}{12} q_{d;floor} l_x^2 = \frac{1}{12} 68.78 \cdot 7.2^2 = 297.15\text{ kNm} \\
 V_{d;floor} &= \frac{1}{2} q_{d;floor} l_x = \frac{1}{2} 68.78 \cdot 7.2 = 247.62\text{ kN} \\
 \text{HE300A :} \quad M_u &= W_{z;el} \sigma_{s;yield} = (1260 \cdot 10^3) \cdot 235 \cdot 10^{-6} = 296.10\text{ kNm} \\
 V_u &= t_w (h - 2t_f) \frac{\sigma_{s;yield}}{\sqrt{3}} \cdot 10^{-3} = 9(310 - 2 \cdot 15.5) \frac{235}{\sqrt{3}} \cdot 10^{-3} = 302.15\text{ kN}
 \end{aligned}$$

Note that an HE300A beam in the limit case will fail ($M_u < M_{d;floor}$). But the acting moment will be lower than the moments of the limit cases due to the frame action and the finite rotation stiffness's.

9.7.3 ULS forces

The exact forces on the connections depend on the number of storeys due to the frame action. The chance that all the storeys are loaded with an extreme load which has a five percent exceedance probability is so small that this does not have to be considered according to the Eurocode. The Eurocode prescribes that one storey should be loaded with an extreme load and the other with a reduced load. This reduced load is obtained by multiplying the extreme load with a combination factor, ψ_0 .

For utility buildings in the Netherlands [38]:

Type	Magnitude
Roofs	0
Snow loads	0
Office areas	0.5

Table 9.4: Reduction factors for combining variable load

For the ULS forces at the roof only frames with few storeys have to be considered. Increasing the numbers of floors will not give higher ULS forces, because they are less stiff than a fully clamped support and so will reduce the forces. Therefore only frames with a maximum of 4 storeys are considered.

In 'Appendix E: MatrixFrame calculation' a printout of several MatrixFrame calculation can be found. In this calculation the finite rotational stiffness of the connections is not taken into account, but this will lower the moments at the connections and increase the moments in the fields. The moments in the fields can increase with approximately a factor two before the HE200A profiles fail, this is unlikely to happen due to the finite rotational stiffness. The maximal force at the roof according to the MatrixFrame calculation occurs at a 1-storey-building, $V_{ULS,max,roof} = 62.29 kN$ and $M_{ULS,max,roof} = 64.43 kNm$. Both forces occur at the same load combination. Hence the connection should be able to resist a combination of $V_{ULS,max,roof} = 62.29 kN$ and $M_{ULS,max,roof} = 64.43 kNm$.

9.7.4 Estimation of overlap lengths

To estimate the dimensions of the splice plate and angle cleat the average stresses are estimated.

The next assumptions are made:

Maximum shear stress [39]:	18
Maximum tension stress:	23
Time-and-environmental losses:	60%
Stress concentration factor:	2

Hence the maximum allowable average shear stress is:

$$\sigma_{xz,max} = 0.40 \cdot \frac{18}{2} = 3.6 N/mm^2$$

With this maximum allowable average shear stress the overlap lengths can be estimated.

9.7.4.1 Vertical length of the splice (at column)

See Figure 9.18:

$$l_{v,splice;column} \approx \frac{M_{ULS,max,roof}}{\left(h_{HE200A} - \frac{1}{2} \cdot t_{f,HE200A}\right) \cdot b_{HE200A} \cdot \sigma_{xz,max}} = \frac{64.43 \cdot 10^6}{\left(190 - \frac{1}{2} \cdot 10\right) \cdot 200 \cdot 3.6} = 483.71 mm$$

As first try $l_{v,splice;column} = 500 mm$ will be used. Note that for such length probably a bevelled, tapered or stepped splice plate is needed to achieve an effective bond.

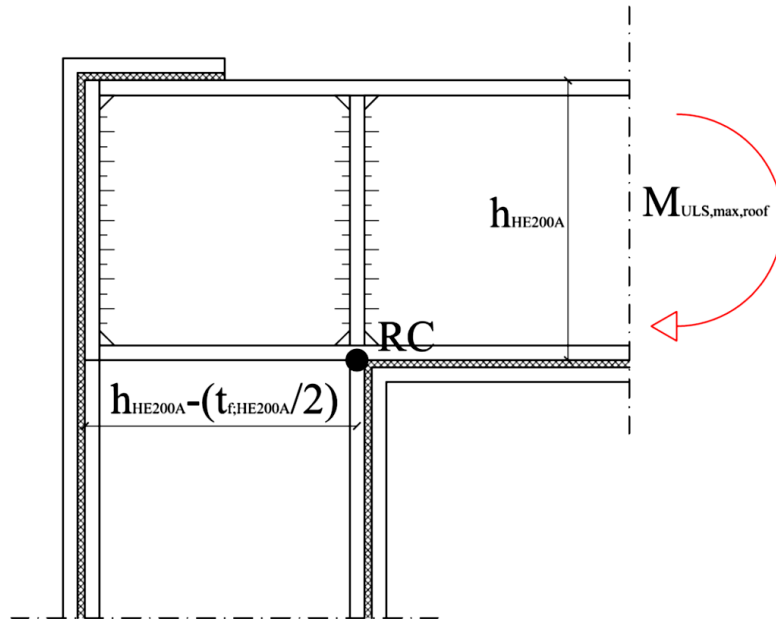


Figure 9.18: Lever arm for determining splice plate and angle cleat length

9.7.4.2 Horizontal length of splice

After the previous calculation it is clear that there is not enough bond area at the endplate of the beam. Therefore the splice should be extended with a horizontal part which is bonded on top of the beam. The length of this part is hard to estimate with a hand calculation therefore as a starting point $l_{h,splice} = \frac{1}{2} b_{HE200A} = 100\text{ mm}$ is taken. The calculation should make clear if this is too large or too small.

9.7.4.3 Horizontal length of the angle cleat

See Figure 9.18:

$$l_{v,angle} \approx \frac{M_{ULS,max,roof}}{h_{HE200A} \cdot b_{HE200A} \cdot \sigma_{xz,max}} = \frac{64.43 \cdot 10^6}{190 \cdot 200 \cdot 3.6} = 470.98\text{ mm}$$

As first try $l_{v,angle} = 500\text{ mm}$ will be used.

9.7.4.4 Vertical length of the angle cleat

The vertical bondline of the angle cleat is expected to be predominantly loaded in compression. Adhesives are strong in compression therefore a practical length of 200mm will be used.

9.8 Tolerances

The thickness of the bondline is of big influence on the failure load, therefore geometrical tolerances are important for the strength. In the next table a conventional division of tolerances and codes in the structural engineering for hot rolled sections can be found.

	Manufacturing tolerances	Erection tolerances
Essential tolerances	EN10034	EN1090-2 Annex D1
Functional tolerances	EN1090-2 Annex D2*	EN1090-2 Annex D2*
Special tolerances	Specified by client	

* Or imposed alternative

Table 9.5: Tolerances for hot rolled sections with corresponding norm [40]

Essential tolerances are necessary to satisfy the design assumptions for the structure in terms of mechanical resistance and stability. Functional tolerances are tolerances to meet functions other than mechanical resistance and stability, such as appearance and fit up. Special tolerances can be specified by the client if they are required.

In the case of structural adhesive bonded connections the tolerances should be kept as small as possible. This may be done by the use of special tolerances instead of (Euro)codes. For the functional tolerances EN1090 uses two classes, 1 and 2. Class 2 is more stringent than class 1 and is therefore most appropriate for adhesive bonded structures. As a first approach the codes specified in Table 9.5 are used.

Not all tolerances are of special interest. For instance, the height of the beam or column does not affect the thickness of the bondline if the interface with the bondline is taken as reference point. But an out-of-squareness deviation will affect the thickness of the bondline.

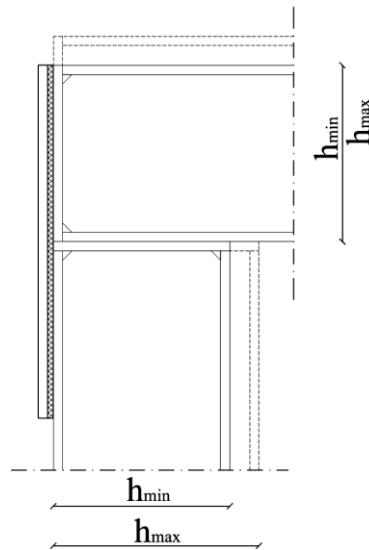


Figure 9.19: Influence of the height tolerances on the adhesive thickness

9.8.1 HE200A section

The EN10034 code gives an overview of the essential-manufacturing tolerances of hot rolled sections.

1. Section height
2. Flange width
3. Web thickness
4. Flange thickness
5. Out-of-squareness
6. Web off-centre
7. Straightness
8. Mass
9. Length

Although all of the points listed above affect the mechanical behaviour, only the out-of-squareness will affect the bondline thickness directly. The straightness can also affect the bondline thickness due to the angle of rotation of the beam, but this rotation ($\leq 0.002 \text{ rad}$) will be small enough to neglect his influence.

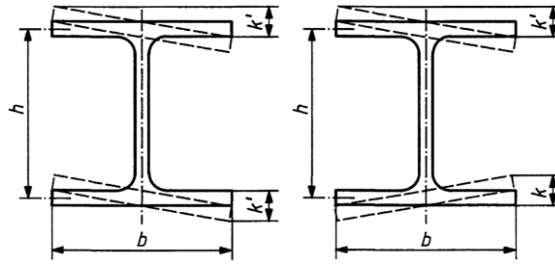


Figure 9.20: Out-of-squareness $k+k'$ [41]

For hot rolled sections with a flange width larger than 110mm the next tolerance applies according to EN10034:

$$k + k' \leq \min(0.02b, 6.5)$$

For an HE200A:

Width HE200A	0.02b	6.5
200	4	6.5

$$b = b_{HE200A} = 200 \text{ mm}$$

$$k + k' \leq \min(4, 6.5) = 4 \text{ mm}$$

Note that only the difference in rotation between both flanges is of interest, because the flanges can be kept parallel to the bond surface as much as possible. Then the 4 mm can be distributed between the two sides so the maximum difference in height for one flange is 2mm.

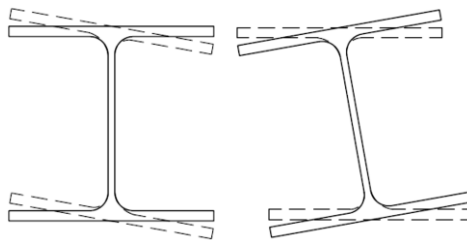


Figure 9.21: Distribution of out-of-squareness between the two flanges

In EN1090 Section D.2.1 the functional manufacturing tolerances of welded profiles can be found. An HEA profile is not a welded profile, but these tolerances give an order of magnitude of usual tolerances. There are two tolerances mentioned in the code, one for general cases and one for flange parts in contact with structural bearings.

Squareness of flanges: Flatness of flanges:

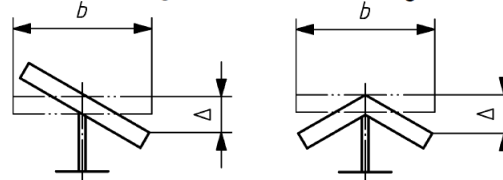


Figure 9.22: Tolerances of flanges of welded profiles

For flange parts in contact with structural bearings and functional class 2 the permitted Δ is:

$$|\Delta| \leq \frac{b}{400}$$

For an HE200A profile this reads:

$$b = b_{HE200A} = 200$$

$$|\Delta| \leq \frac{b}{400} = \frac{200}{400} = 0.5$$

Hence, the maximum difference in height between the highest and lowest side of the flanges is:

$$2 \cdot |\Delta| = 1 \text{ mm}$$

This is nearly a factor 2 smaller than the EN10034 prescribes.

With EN1090 section D.2.1 in mind the next permitted tolerance seems to be reasonable:

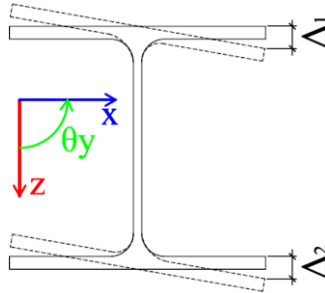


Figure 9.23: Special tolerance for out-of-squareness

$$|\Delta_1 - \Delta_2| \leq 2 \text{ and } |\Delta_1| \leq \min(0.02b, 6.5) \text{ and } |\Delta_2| \leq \min(0.02b, 6.5)$$

Hence the maximum difference in height for one flange is:

$$\frac{|\Delta_1 - \Delta_2|}{2} \leq \frac{2}{2} = 1 \text{ mm}$$

9.8.2 Welding deformations

Due to the welding of the stiffeners to the beam welding deformations will occur. In the applicable code, EN1090, there are two vertical tolerances specified for 'Stiffened plating'; the essential manufacturing tolerance in section D.1.6.3 and the functional manufacturing tolerance in section D.2.11.3. For both tolerances the next figure applies:

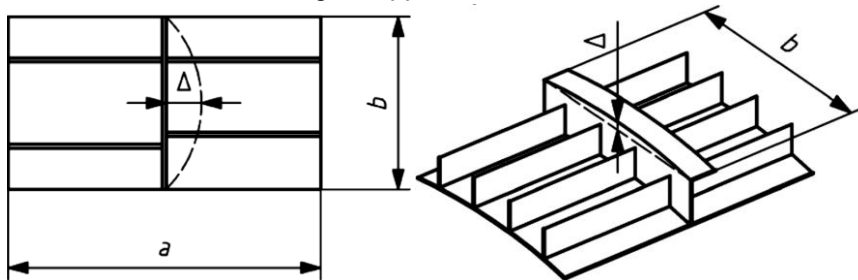


Figure 9.24: Tolerances of stiffened plating [42]

The equation for the permitted essential manufacturing tolerance is:

$$|\Delta_{ess}| \leq \min\left(\frac{a}{400}, \frac{b}{400}\right)$$

The equation for the permitted functional manufacturing tolerance (class 2) is:

$$|\Delta_{fun}| \leq \max\left(\min\left(\frac{a}{500}, \frac{b}{750}\right), 2\right)$$

The a and b of Figure 9.24 that should be applied are:

$$a = l_y = 7200$$

$$b = \frac{b_{HE200A} - t_{f,HE200A} - 2r_{HE200A}}{2} = \frac{190 - 10 - 2 \cdot 18}{2} = 72$$

Hence:

$$|\Delta_{ess}| \leq \min(18, 0.18) = 0.18 \text{ mm}$$

$$|\Delta_{fun}| \leq \max(\min(14.4, 0.10), 2) = 2 \text{ mm}$$

The most stringent tolerance is the essential tolerance ($2 \cdot 0.18 = 0.4 \text{ mm}$ in total), which will determine the actual allowable tolerance.

9.8.3 The end plate of the beam

At the endplate of the beam there are three tolerances of importance for the bondline thickness, namely the squareness of the beam ends, the squareness of the endplate and the length of the beam. There are no specific rules in the EN1090-2 for the squareness of the endplate, therefore the tolerance for the squareness of ends is applied for the endplate.

In section D.2.7.6 of [42], 'functional manufacturing tolerances – Components' the tolerances for the squareness of ends can be found.

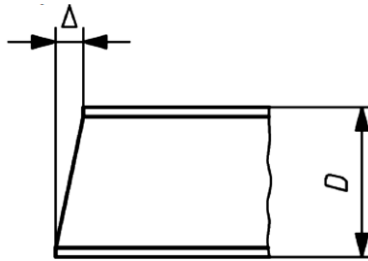


Figure 9.25: Tolerance of squareness of ends [42]

Two tolerances are mentioned, one for ends intended for full contact bearing and one for ends not intended for full contact bearing. The former one is applicable and the most stringent and reads for class 2:

$$|\Delta| \leq \frac{D}{1000}$$

For the detail of Figure 9.16:

$$D = h_{HE200A} = 190$$

$$|\Delta| \leq 0.19 \text{ mm}$$

Hence in total $2 \cdot 0.19 = 0.38 \text{ mm}$.

It is assumed that this value is valid for the squareness of ends in the height and the width direction. The combination of these two will twist the endplate. The most protruding corner will differ Δ from the most withdrawn corner, which is the corner at the other side of the diagonal. Note that this combination will not lead to a bigger longitudinal distance between the most protruding and withdrawn corner.

In section D.2.7.1 of [42], 'Functional manufacturing tolerances – Components' the tolerances for the length can be found.

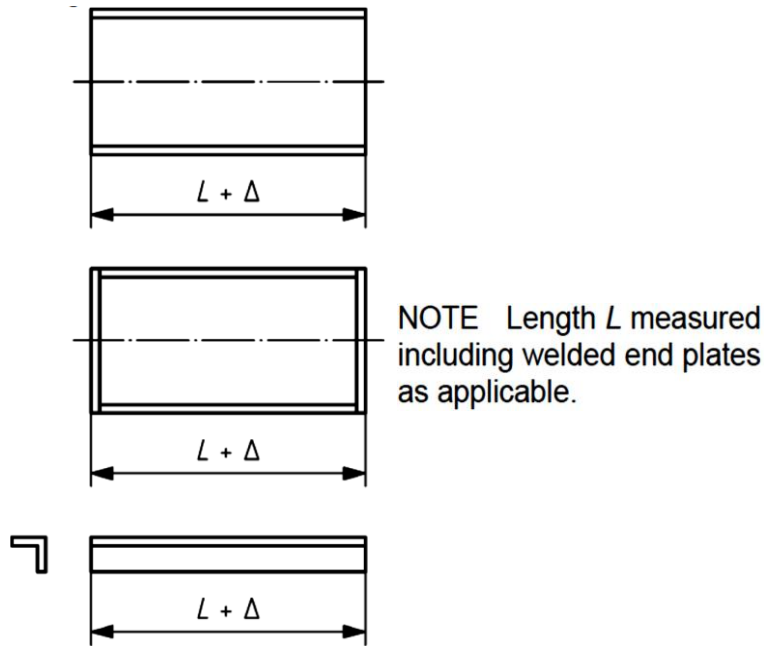


Figure 9.26: Tolerance of squareness of ends [42]

Two tolerances are mentioned, one for ends ready for full contact bearing and one for general cases. The former one is applicable and the most stringent and reads for class 2:

$$|\Delta| \leq 1\text{mm}$$

So the total tolerance bandwidth per side is 1mm.

Combining all the tolerances for the endplate of the beam will lead to an absolute bandwidth for the minimal and maximal tolerance of:

$$0.38+1=1.4\text{mm}$$

9.8.4 Column placement

During erection the alignment of the outer face of the flange of the column and the outer face of the endplate of the beam is important. Section D.2.22.5, Functional erection tolerances – Positions of columns, of the applicable code, [42], gives the tolerances for the alignment of the outer face of the flange of the column.

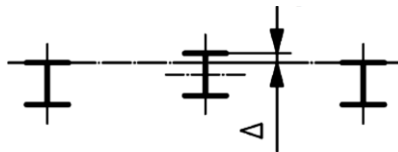


Figure 9.27: Perimeter column alignment [42]

For class 2 the permitted deviation is:

$$|\Delta| \leq 7$$

This tolerance is at the bottom of the column and the L-connection is at the top. For adhesive bonded structures the preceding tolerance is too big. For this reason an imposed special tolerance should be applied at the top of the column. For adhesive bonded structures the next stringent tolerance should be applied:

$$|\Delta| \leq 1$$

9.8.5 Adhesive thickness

When the maximum adhesive thickness is set to 4 mm, the minimum adhesive thickness is around 0.5 mm. Both are feasible with adhesive bonding. Hence:

$$0.5\text{ mm} \leq t_a \leq 4\text{ mm}$$

9.9 Fabrication

There are several methods to apply adhesives, see section: 19.4. For this study two are of most interest; the vacuum injection method and the application of an iron tool (rake, spatula, trowel) or hand pistol. Application with iron tools is easier, but with vacuum injection there is less risk of voids and large adhesive thicknesses can be achieved. The next table shows an overview of the different action for both methods.

Action	Vacuum injection	Iron tools
Drill holes	Yes	No
Clean the steel surfaces (apply primer)	Yes (May be required)	Yes (May be required)
Fix the spacers	Yes	Yes
Apply the adhesive (for iron tools/pistols)	No	Yes
Install clamps and apply slight pressure	Yes	Yes
Seal the outer perimeter	Yes	No
Apply the adhesive (for vacuum injection)	Yes	No
Heat the connection	May be required	May be required
Post processing	Yes	Yes

Table 9.6: Actions for vacuum injection and Iron tools

9.9.1 Drill holes

For the vacuum injection method at least two holes are needed; one for injection of the adhesive and one for creating the vacuum. To ensure a good spread of the adhesive more holes may be needed, this depends on the viscosity of the adhesive, placement of the holes and the form of the workpiece. Due to the non-uniform stress distribution around the holes, the holes should be located in low stress areas.

9.9.2 Clean the steel surfaces (apply primer)

To ensure a good adhesion between the adhesive and adherent the adherent surface should be clean. For steel structures usually the ISO 8501 standard is used to describe the rust and preparation grade. ISO 8501-1 describes three types of preparation: blast cleaning (Sa), hand and power tool cleaning (St), and flame cleaning (Fl); with gradations from 1 to 3. For new steel structures Sa 2½ is usual. [43] For most structural adhesive bonds this will be sufficient. [34, 39, 44-49]

To ensure a good bonding the application of a primer may be needed for some adhesives. Grid blasting in a fabrication shop is cheaper and easier than on a construction site. If the steel is grid blasted in the fabrication shop, a primer can be used to protect the clean surface if there is some time between grid blasting and application of the adhesive. On the construction site the primer is easier to clean than a steel surface with rust. For most epoxy adhesives no primer is needed for steel surfaces. [39, 44, 46-51]

9.9.3 Fix the spacers

To ensure a certain adhesive thickness spacers are used. Some suppliers have mixed their adhesives with glass beads which act as spacers. [45] In the other cases, separate spacers may be used or the contractor can mix the adhesive and glass beads. Due to the non-uniform stress distribution around the spacer, the spacer should be located in low stress areas. Glass beads will be distributed over the whole bond area, hence also in high stress areas. Therefore, separate spacers seems to be more suitable for structural bonding. Due to the relative thick (and so bending stiff) adherents only a few spacers are needed to ensure an evenly adhesive thickness.

9.9.4 Apply the adhesive (for iron tools/pistols)

The use of iron tools and pistols is simple and requires little explanation. For two component adhesives special pistols are available which can mix the adhesive itself. If the adhesive is on a vertical plane the adhesive should not drip off. This is the case for thixotropic adhesives. To prevent the formation of voids, more adhesive should be applied than the final bond volume. The surplus of adhesive will be pushed out during pressurising the clamps.

9.9.5 Install clamps and apply slight pressure

To get the intended adhesive thickness the clamps should be placed at the location of the spacers. Slight pressure should keep the angle cleat and splice plate at the same place during the application and hardening of the adhesive.

9.9.6 Seal the outer perimeter

In Figure 9.28 a diagram of the vacuum injection method can be found. After holes are drilled, the spacers installed and the clamps are tightened, the edges should be sealed airtight. The airtight sealing can be tested with a test vacuum.

9.9.7 Apply the adhesive (for vacuum injection)

The vacuum created by the pump will suck the adhesive through the workpiece. This is only possible for adhesives which have a low viscosity and are not thixotropic. Adhesives with substances which vaporise during the cure process are not suitable because these vapours cannot leave the adhesive, this cause voids and porosity. The adhesive trap prevents that adhesive will get in the vacuum pump. When the whole workpiece is filled with adhesive the valves are closed.

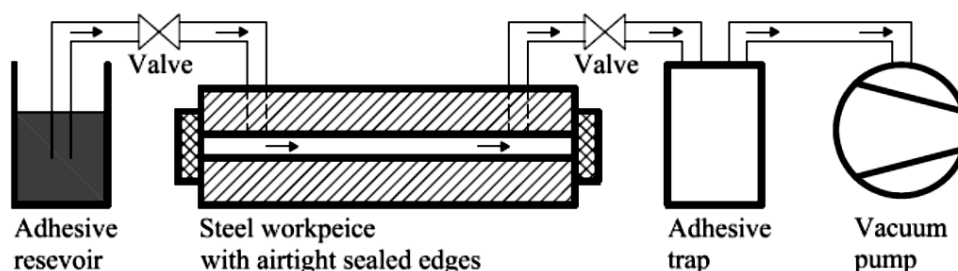


Figure 9.28: Application diagram of vacuum injection

9.9.8 Heat the connection

To gain high strength and good life span properties it can be required to heat the adhesive during the cure process. Heating will also shorten the curing process, for instance from seven to one day for the Sikadur®-30, which may be necessary in the construction process. Heating is often used for

buildings built with tunnel formwork to shorten curing, therefore for adhesive bonded structures it should also be allowed for the same reason.

Before heating the connection should be insulated. For instance, a tent or blanket can be used as insulation. Heating may be done by simple air-heaters. Most suppliers of adhesives have strength values for the adhesives cured at room temperature and at elevated temperatures. After the adhesive is heated for the required period and temperature the insulation can be removed.

9.9.9 Post processing

After the adhesive is cured the clamps, and if applied the sealing for vacuum injection, should be removed. If an iron tool or pistol is used the surplus of adhesive should be removed. The next points may be applied:

- NDT to check the quality of the adhesive cohesion and adhesion.
- A sealant to protect the adhesive (especially to moisture)
- An insulation layer to protect the adhesive during fire

For steel structures a paint or coating layer is always used to prevent corrosion. Also an insulation layer to protect the steel during fire is common. Therefore it is reasonable to demand such treatments for adhesive bonds. Note that a sealant and an insulation layer may be combined to one layer which lowers the labour and costs.

The most simple NDT is a visual check, which is often done for welds. For adhesive bonds this is less effective because only the outer perimeter can be seen. For adhesive bonds acoustic methods seem more suitable, such as tapping and ultrasonic methods.

9.10 Requirements for the adhesive and application

Out of the previous sections the requirements for the adhesive and application can be deduced. The requirements can have different natures, namely:

1. mechanically;
2. workability;
3. makeability
4. durability;
5. financially.

For utility buildings the following requirements are reasonable:

- Relative high strength in hardened state **(1)**
- Life span of 50 years at indoor conditions (10 – 35 °C and 15 – 85 % RH) **(4&5)**
- Applicable with as simple as possible pre treatments **(5)**
 - Degreasing, mechanical treatments and primers can be applied at the fabrication shop. Preparation grade Sa2.5, just as demanded for most new buildings, is allowable. [43]
 - On the building site the primer can be cleaned by simple processes (cloth or simple mechanical treatment).
 - No chemical or plasma treatments
- Applicable with simple/basic preparations **(5)**
 - Welding is only allowed in the fabrication shop and should be minimised. (It should be an adhesive bonded detail, not a bolted or welded detail with adhesive bonds)
 - Eventual coupling pieces may be bended or welded in the fabrication shop
 - Scarfed, bevelled, tapered or stepped adherents are allowable but not preferred
- Application should be simple **(5)**
 - In principle only application of adhesive; no cutting, welding, bolting on site.
 - Vacuum injection is not preferred but allowable if it scores high on other requirements

- Applicable without heat curing is preferred; curing at moderate outside conditions (10 – 35 °C and 15 – 85 % RH) **(3&5)**
- If other methods than vacuum injection are applied; sufficient high viscosity (thixotropic) in unhardened state if there are vertical bond planes; no dripping off during fabrication **(2&3)**
- If vacuum injection is applied no use of thixotropic adhesive **(2&3)**
- Pot life between 1 and 2 hours **(2&5)**
- Gain full strength (able to resist the stresses due to V_d and M_d) within a relative short period of time **(1&5)**
 - Avoid waiting time in the building process
 - Able to reuse clamps and suchlike for the same building
- Good gap filling properties; adhesive thickness will be 4mm **(3)**
- Adherent thicknesses should match to ensure an effective load transfer **(1)**
- Post processing should be simple **(5)**
 - Combine sealant and fire protection

There are no specific requirements concerning bond lengths. However, it must be noted that this can have consequences for the placement of floor and roof elements, if there are adhesive bonds on top of the flange of the beam. Without precautions the outer elements will no longer be in a horizontal position. Therefore support strips or blocks are applied for the outer element. The difference in height on top of the elements is levelled out by the concrete top or isolation layer.

9.11 Selection of the adhesive type

In the Netherlands Henkel en Sika play a major role in the supplier market of adhesive. Both have a wide variety of adhesive, some of them are suitable for application for a steel-to-steel beam-to-column connection. Sika and Henkel are asked to propose adhesive types. Sika proposed five adhesive types, two for vacuum injection [46, 51] and three for iron tools [47-49]. Henkel proposed two adhesive types both for iron tools or pistols [44, 45]. Also a self chosen adhesive of Henkel [50] is considered, because it has better sag properties. One adhesive of Tradecc is considered [39]. Due to this new field of application not all of the required information is available in the data sheets of the suppliers. Some of this information is known but not included in the data sheets and some of the information is simply not known by the suppliers. For similar adhesives most of the data will be similar. Therefore the available data is extrapolated to the unknown data.

Both the adhesives for vacuum injection of Sika are not specially suitable for steel. Along with the fact that vacuum injection is a more expensive application process, the vacuum injection adhesives are not further considered.

One adhesive of Henkel is a 2-component methacrylate, the rest of the adhesives are epoxy adhesives.

In the three data sheets of the epoxy adhesives of Sika a reduction of 20-25% for time-dependent behaviour is mentioned. All these adhesives probably have a high filler taking into account the good sag properties (maximum layer thickness of 30, 60 and 30 mm with no sag for respectively 3-5, 20 and 16 mm).

For the Loctite Hysol 9466 and Loctite Hysol 3425 of Henkel heat ageing test are done:

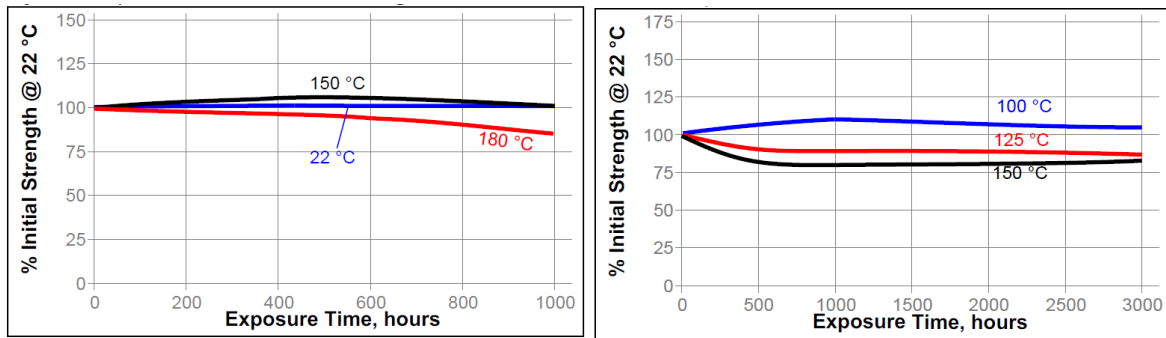


Figure 9.29: Heat ageing of Henkel Loctite 9466 (left) and Loctite 3425 (right)

Also here the maximum reduction is around 20%. The Loctite Hysol 3425 is mentioned as gap filling (can fill gaps up to 3mm), in contrast to the Loctite Hysol 9466. Therefore the 3425 should probably have a higher filler content. And the 9466 will probably not be able to fill the 4mm adhesive thickness. Therefore the 9466 is not suitable for this application.

The adhesive of Tradecc should probably also exhibit 20-25% reduction because it belongs to the same adhesive family.

For the Speedbonder® Product H3151 of Henkel no time-dependent information is available, due to the different types of adhesives no extrapolation can be used. This adhesive is specially made for the automotive industry. Life spans in the automotive industry are at least 50% shorter than in structural engineering.

The next figure shows the strength of the adhesives of Henkel under different temperatures.

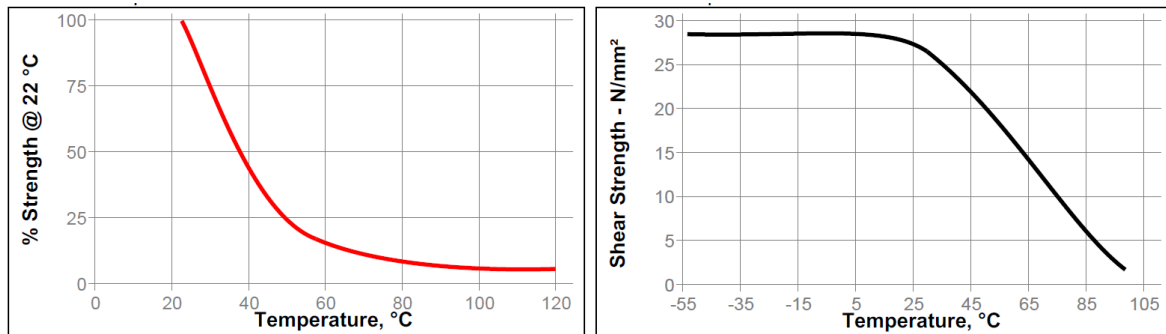


Figure 9.30: Hot Strength of Henkel Loctite 9466 (left) and Loctite 3425 (right)

Note that the left is an adhesive with probably less filler material than the right. In the right figure strength at 35°C is ±15% lower than the maximum strength. This is assumed to apply also for the three adhesives of Sika and the one of Tradecc.

For the Speedbonder® Product H3151 of Henkel such information is not available. This adhesive cannot be compared to the other adhesives due to lack of information, therefore this adhesive is not further considered.

For all the remaining adhesives curing at somewhat higher temperatures (30-40°C) than room temperature will result in faster curing and higher strengths. For instance, the Sikadur®-30 gains at least a compression strength of 80 N/mm² at 35°C in 12h and at least a compression strength of 70 N/mm² at 10°C in 7 days. The application of heating will probably pay back in the strength and building time. Note that heaters are also often used for concrete when tunnel shuttering is used, to speed up the hardening of the concrete.

In the next table an overview of the remaining adhesives can be found with scores on important point, the weight of the points and its total score. None of the adhesives require the use of a primer, and for all a preparation grade of Sa2,5 is sufficient.

Adhesive		Adhesive thickness of 4 mm without precautions possible			Working life			Shear Strength			Tension/Peel Strength			Durability			Total Score	
Supplier	Name	W	S	WS	W	S	WS	W	S	WS	W	S	WS	W	S	WS	S	RS
Sika	Sikadur®-30	9	10	90	9	10	90	4,9	6	29	4,2	6	25	8	10	80	7,49	10,00
Sika	Sikadur®-31 CF Normal	10	10	100	5,5	10	55	3	6	18	3,6	6	22	10	10	100	7,01	9,36
Sika	Sikadur®-41 CF Normal	10	10	100	6	10	60	3,5	6	21	3	6	18	9	10	90	6,88	9,19
Tradecc	PC® 5800/BL	10	10	100	4	10	40	7,5	6	45	4,8	6	29	8	10	80	7,00	9,34
Henkel	Loctite Hysol 3425	7	10	70	5,5	10	55	6,8	6	41	5,4	6	32	8	10	80	6,62	8,84

W=weight S=score WS=weighted score

Table 9.7: Selection matrix of adhesive

As can be seen, the Sikadur®-30 seems the most feasible adhesive for this application. The shear stiffness which Sika mentioned (11200 N/mm²) seems to be high. Out of tests done at the university at Bath [52] follow the next stiffnesses:

Young's Modulus 12800 N/mm²
 Shear Modulus 4273 N/mm²

This means a Poisson ratio of: $\frac{E}{2G} - 1 = 0.50$

These stiffnesses will be used in the FEM calculation.

The time-and-environmental-depended losses are estimated with:

$$k_{total\ time+environmental\ losses} = k_{time} k_{environmental} = 0.75 \cdot 0.85 = 0.64$$

Type of strength	Strength in N/mm ²	
	Initial	Long term
Compression	85	54
Tension	26	17
Shear	17	11

Table 9.8: Strength properties of Sikadur®-30

The material factor is estimated to be 1.5, hence:

Type of strength	Strength in N/mm ²	
	Initial	Long term
Compression	54	36
Tension	17	11
Shear	11	7

Table 9.9: Representative strength properties of Sikadur®-30

9.12 Final design of the connection

In the figure below the final design of the connection can be found.

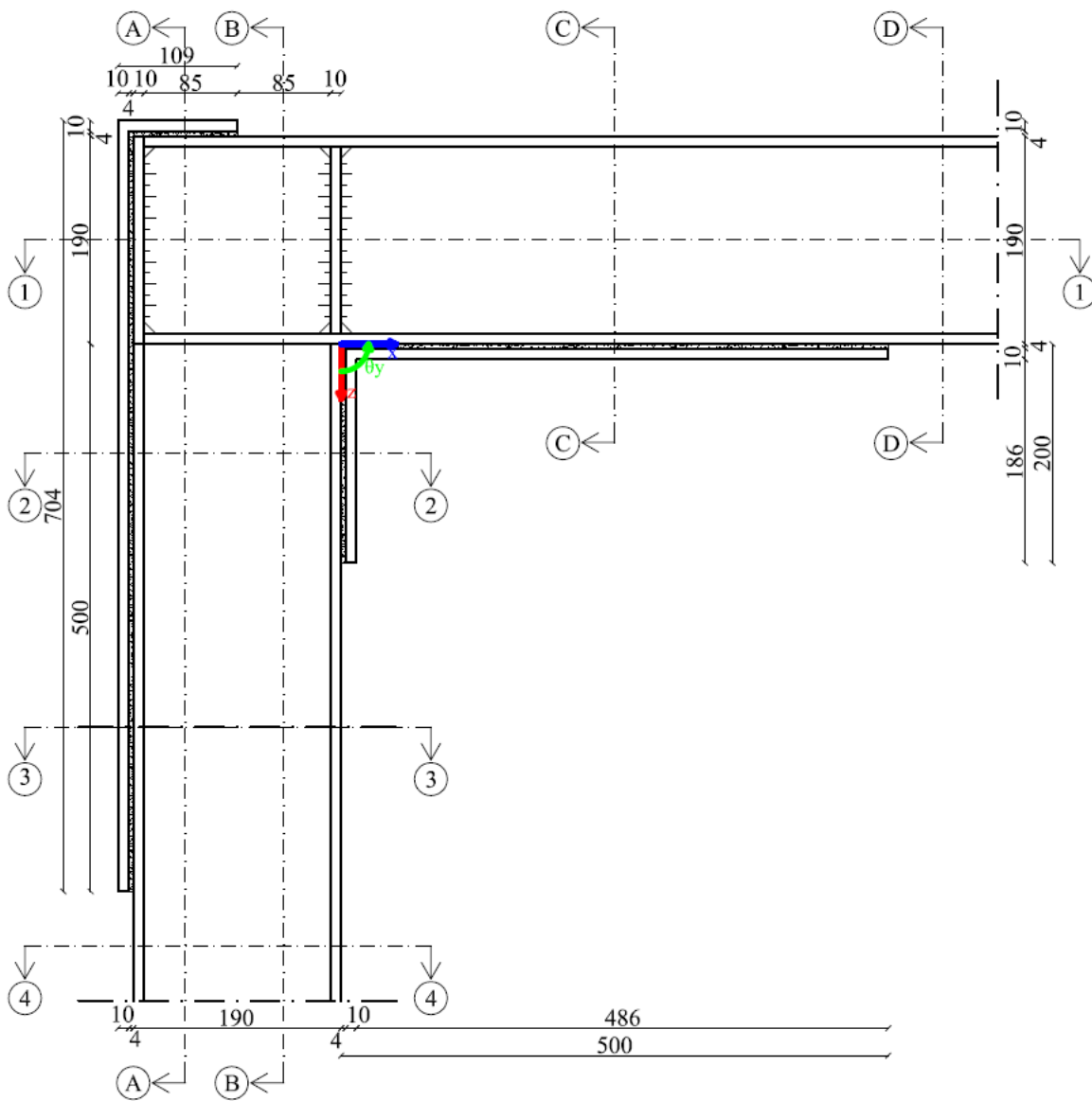


Figure 9.31: Design of connection after design study – front view of y-plane

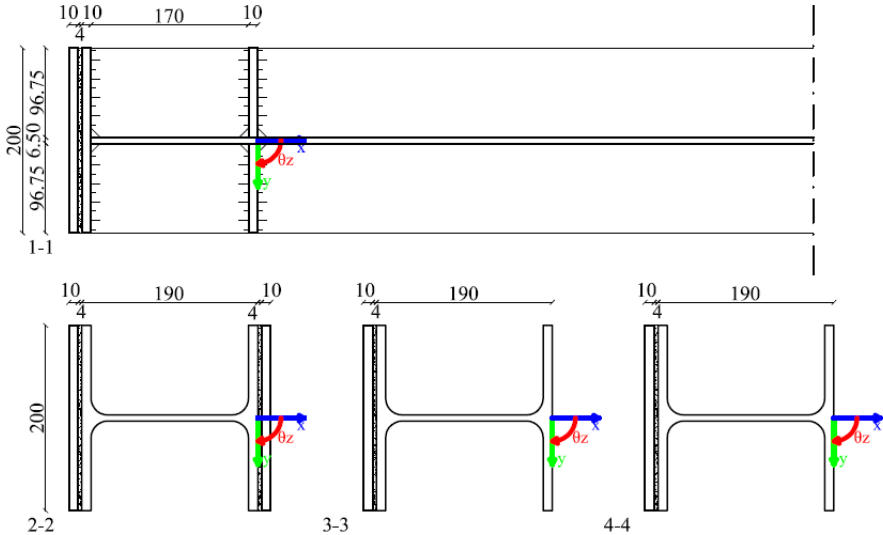


Figure 9.32: Design of connection after design study – cross sections of z-plane

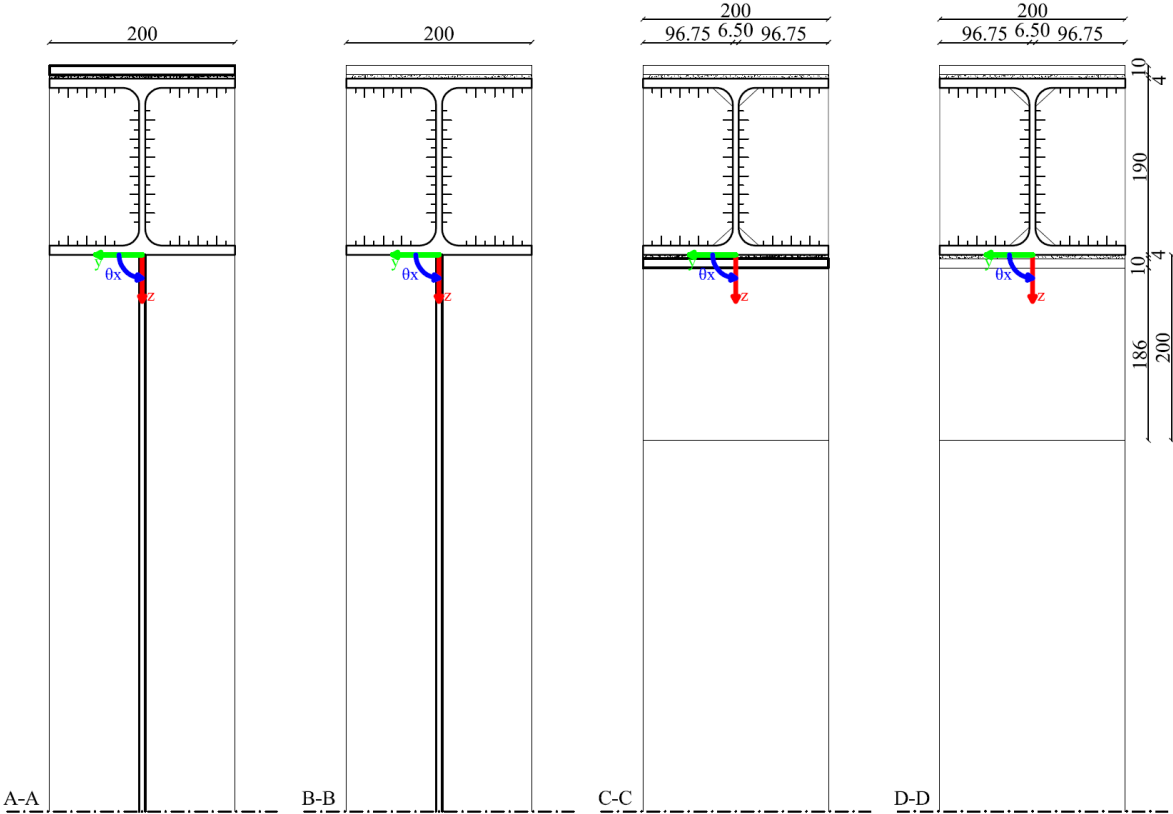


Figure 9.33: Design of connection after design study – cross sections of x-plane

10 FEM test of L-connection

The finite element method (FEM) is nowadays by far the most popular computer method to make detailed calculations of mechanical problems.

10.1 What is FEM?

The finite element method is a numerical method for which the structure is divided in small, so called, finite elements. These finite elements can have different shapes (e.g. rectangular, triangle) and different dimensions (0D/3D). Most important are the nodes and its DOF's (degree of freedom). The nodes are always located at the corners/ends of the elements and for some elements also at intermediate points. FEM programs only calculate stresses and strains at nodes, in between the nodes interpolation is used. For higher order interpolation intermediate nodes are needed. A FEM program compose a stiffness matrix. The stiffness matrix gives the relationships between the force and displacement of all the nodes. With this matrix together with the boundary conditions and loads the forces and displacements can be calculated.

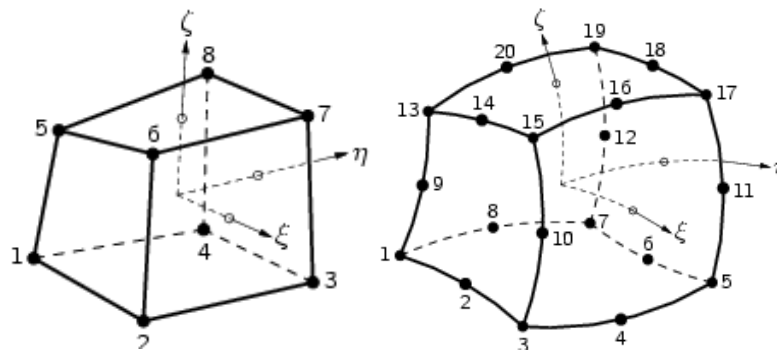


Figure 10.1: Linear (left) and quadratic (right) 3D elements [53]

The number and type of elements have a major influence on the results and calculation time. In FEM calculations different types of material behaviour can be assigned to the finite elements. Linear elastic models result in a relatively short calculation time, because the forces and displacements can be found at once. Non-linear material models result in a much longer calculation time, because the load is applied in increments. For every increment the forces and displacements have to be found. The number of applied increments depends on the model. Complex models require the use of more increments. Geometrical non linear calculations are needed when there are expected: large deformations, displacement depended loads and/or displacement depended stiffness. Also for geometrical non linear calculations increments are used which increase the calculation time drastically.

10.2 Cantilever length

A good model should represent the reality as well as needed in the simplest way or according to Albert Einstein: *'A scientific theory should be as simple as possible, but no simpler'*. So for investigating a connection from a frame, not the whole frame has to be modelled. For the L-connection the length of the beam and column should be large enough so that a stress distribution near the connection occurs that is nearly the same as in the real case. Only negligible differences are allowed. It is assumed that the edge effects will fade away in a length which is equal to 3 á 4 times the width (600mm and 800mm).

For testing also the type of load is of interest. In a laboratory distributed loads are mostly modelled with equivalent point loads, because presses are point loads. Important are similar stresses at the

connection. To ensure conformity the model of the FEM test should be done with the same type of loads as a practice test, hence with point loads.

If we take the MatrixFrame calculation as reference, see 'Appendix E: MatrixFrame calculation', the ultimate support reactions are:

$$\begin{aligned} V_{ULS,max,roof} &= 62.29 \text{ kN} \\ M_{ULS,max,roof} &= 64.43 \text{ kNm} \end{aligned} \quad (10.1)$$

For a cantilever beam with a point load at the end, the support reactions are:

$$\begin{aligned} V_F &= F \\ M_F &= Fl_F \end{aligned} \quad (10.2)$$

The point load and cantilever length can now be calculated:

$$V_{ULS,max,roof} = V_F \rightarrow F = V_{ULS,max,roof} = 62.29 \text{ kN} \quad (10.3)$$

$$M_{ULS,max,roof} = M_F \rightarrow l_F = \frac{M_{ULS,max,roof}}{F} = 1.03 \text{ m} \quad (10.4)$$

The length of (10.4) will not fulfil the 3 á 4 times free length requirement when the estimated lengths are applied. There the length should be at least:

$$l_F = \frac{1}{2} b_{HE200A} + l_{angle} + 3 \cdot b_{HE200A} = 1200 \text{ mm} \quad (10.5)$$

The length of (10.5) is based on the estimated length of the inner angle. Probably this length will change during the FEM calculations. Therefore in the beginning the length of the next figure will be used. After the dimensions are such that all the acting stresses are within the allowable stresses a final cantilever will be chosen and the model will be recalculated.

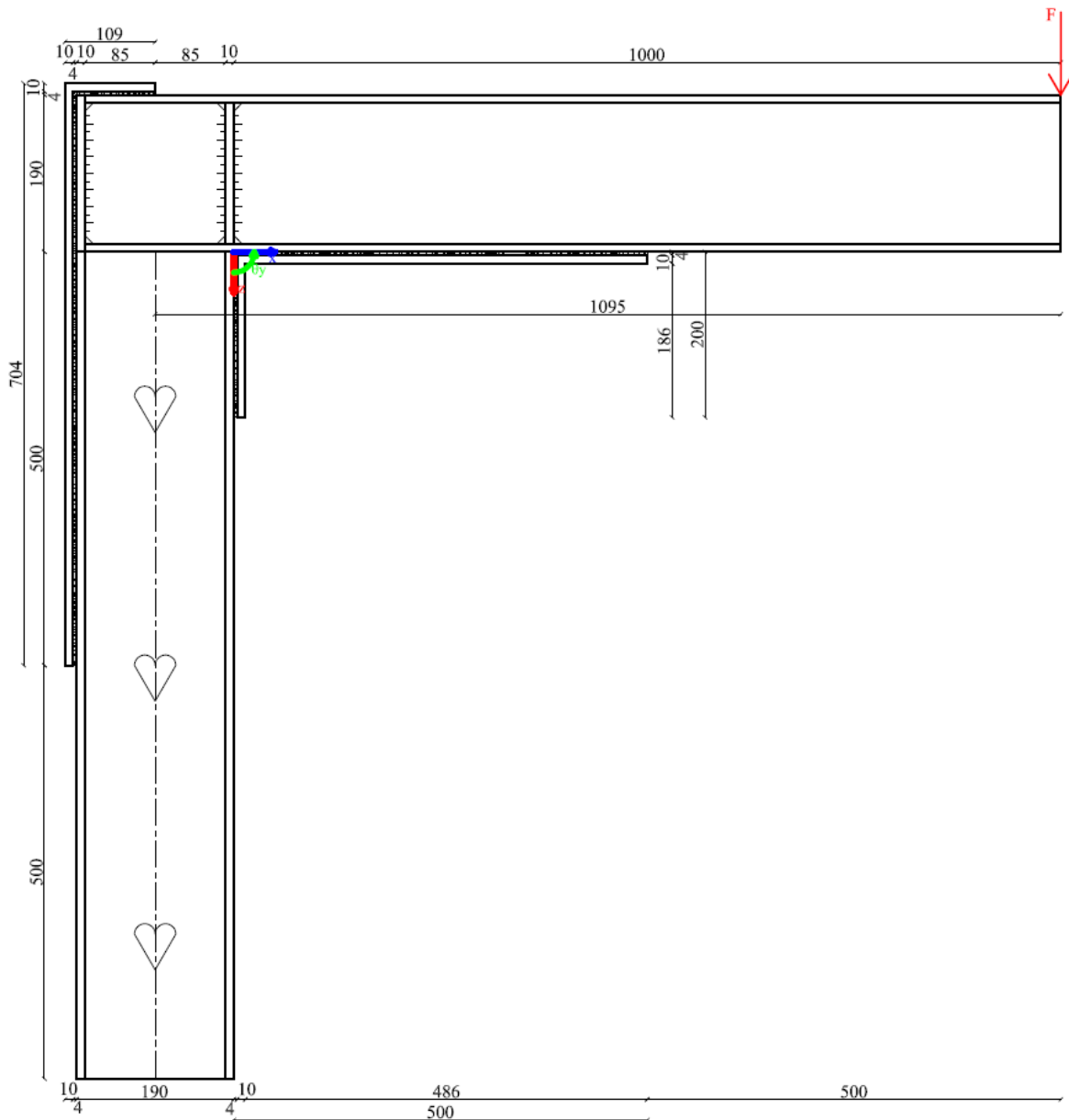


Figure 10.2: Initial FEM detail

10.3 Non linear calculation of the entire model

As a first attempt the entire model is calculated. The steel is modelled with elastic-plastic behaviour and the adhesive with linear elastic behaviour. Elements with linear elements are prone to shear locking¹, therefore quadratic elements are used. At the place where the beam and column make contact an interface is modelled. The interface is modelled with crack elements with a tensile strength of 0 N/mm^2 . This should give realistic and comprehensive stress distributions. At once the complete behaviour of the entire connection will be known. No composition of different models has to be done. Drawback is the large calculation time and sometimes the difficult interpretation of the results.

¹ The lines between the nodes of linear elements are straight. Therefore bending of a geometry with linear elements is achieved by shear deformations of the linear elements instead of actual bending. As a result of this geometries with linear elements have a higher bending stiffness than those with higher order elements, this error is called shear locking.

10.3.1 Findings

In the FEM program Abaqus of Simulia the entire connection is modelled. For the adhesive at least two elements should be modelled to get a good picture of the stresses, see 'Appendix F: Element distribution of adhesive thickness'. Several sizes of the other dimensions are used, but such calculation is not possible with Abaqus on the commercially available computer. The reason for this is the amount of available RAM on the computer (4GB). If the stiffness matrix, which Abaqus produces, is too big to handle, Abaqus give a warning and stops.

For this reason the calculation is also tried with FEM program DIANA with FX+ for DIANA both of TNO. With this program the same problem occurred. If the stiffness matrix is too big DIANA uses another solver¹ which probably would take days or weeks to calculate the problem and so DIANA is unsuitable to analyse this problem. [53] Even after an upgrade to 16GB RAM, which is very large for commercial computers and the maximum which Windows 7: Home Premium supports, these problems occurred. Also with linear elements and a coarse mesh, DIANA is not able to solve the stiffness matrix in a reasonable period of time.

10.3.2 Conclusion

The large amount of elements together with the physical non linear calculation results in a very large calculation time or in lack of RAM. The very large calculation time or the abortion of calculation makes it impossible to calculate the connection as a whole. The size of the stiffness matrix has a quadratic relationship with the number of nodes/elements. Therefore the problem should be calculated in a different way. Note that, contrary to what most people think, the available RAM is more important than the CPU power. CPU power will speed up a calculation but the RAM determines which possible solve strategy can be used, which has far more influence on the calculation time.

10.4 Redesign of the FEM model

For a FEM calculation the detail of Figure 10.2 can be modelled with only one half of the detail. The detail is symmetric with respect to a y -plane at $y=0$. Therefore the detail can be modelled with only the nodes with a positive y -coordinate, all the nodes at $y=0$ should be fixed in y -direction. Such a model can be calculated in DIANA with linear elastic and linear elements on the used computer² in roughly half an hour. With quadratic elements the calculation takes at least 36 hour, which makes such a model unsuitable for designing. Therefore the design calculations are performed with linear elements. Eventually, after designing a final calculation can be performed with quadratic elements.

In 'Appendix G: DIANA procedure for entire L-connection model', the input process is described extensively.

The next models are calculated:

¹ The default solver (*AUTOMA solver*) is initially based on Sparse Cholesky factorization and switches to the *GENEL solver* (out-of-core direct solution method based on Gauss decomposition) if there is not enough memory

² A computer with 16GB RAM and an Intel® Core™ i7-2630QM Processor



Figure 10.3: Initial FEM detail with additions with respect to the preceding model

10.5 Analysis of the results

In 'Appendix H: FEM results' the distributions of the stresses perpendicular to the face and xz-shear stresses can be found. In this section the shape of these distributions is analysed.

10.5.1 The horizontal plane at the inner steel angle

In this section the shape of the stress distributions at the horizontal plane at the inner steel angle is analysed.

10.5.1.1 General distribution of stresses perpendicular to the plane

The horizontal plane at the inner steel angle shows similarities with the more elementary Goland and Reissner case, discussed in section 5.3.3. But in this case the load is a compression force instead of a tensile force and applied on the opposite faces of the adherents. As a result of this the peel stress distribution becomes the mirror image of Figure 5.14. For the peel stresses this change is a great advantage. The tension stresses change into compression stresses which can be handled better by the adhesive.

The beam will rotate due to the load. This will influence the stresses in z-direction of the horizontal plane of the inner angle. The rotation centre will be somewhere at the top of the right flange of the column, which is close to the left side of the inner angle. The beam has a very large bending stiffness in comparison to the angle cleat. The horizontal plane of the angle has a rigid connection with the vertical plane of the angle. To investigate the qualitative behaviour due to the rotation of the beam, the case is simplified with the next assumptions:

- The bending stiffness of the beam is infinite, $EI_2 = \infty$, with respect to the angle.
- The adhesive layer can be modelled with translation springs in z-direction (no shear resistance).
- The vertical plane of the steel angle does not rotate and/or translate.
- Displacements occur only in z-direction.

These assumptions lead to the next structural diagrams:

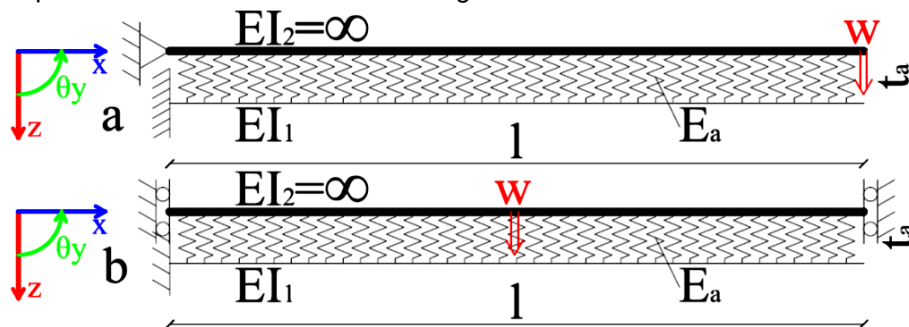


Figure 10.4: Structural diagrams per unit width for beam rotation (a) and translation (b)

In 'Appendix I: Elaboration of DE's for stress' the DE of these systems are derived and elaborated. The stress distribution can be found in Figure 25.5 and Figure 25.10.

The three elementary cases seem to be of most influence on the peel stress distributions which can be found in section 24.1.1/24.1.2. The high stresses perpendicular to the plane at the left side indicates that the inner angle plays a role in the transfer of the shear force of the beam to the column.

In section 24.1.1 there is a clear difference between the lines at $y=0$, $y=50$ and $y=100$. This difference is caused by the non-uniform stiffness in y-direction of the beam. As would be expected,

the stresses are highest at the stiffest part ($y=0$) and decrease towards the side. Moreover the internal lever arm for the Goland and Reissner case at $y=0$ is much larger to the web of the beam than at $y=50$ and $y=100$.

In section 24.1.1 there are only small differences between the lines at $z=0$, $z=2$ and $z=4$ near the ends. At the ends the stresses are higher so differences are amplified. The stresses at the interface of steel and adhesive are highest and lowest because the stiffness of the steel is much higher than the stiffness of the adhesive. Consequently, the stresses at $z=2$ fall in between of the stresses of $z=0$ and $z=4$.

In section 24.1.2 it can be seen that there is no significant difference between the tests.

10.5.1.2 General distribution of shear stresses

As mentioned in the previous section, the Goland and Reissner case shows similarities with the horizontal plane of the inner angle. For the shear stress distribution the direction of the load is of interest, not the type of load (compression or tension), see Figure 10.5. The load direction of the horizontal plane of the inner angle and Figure 5.12 are the same, therefore both will have a shear distribution of the shape depicted in Figure 5.13.

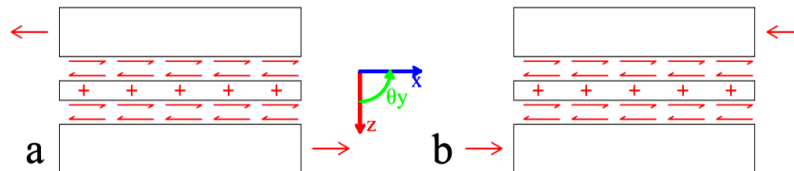


Figure 10.5: Load direction and shear stress

Figure 25.6 and Figure 25.11 show the moment distributions due to rotation and uniform translation of the beam. At the place of the left support high negative bending moments occur. This means that the stresses in the upper fibres of the steel inner angle are bigger than in the bottom fibres. For the case of Figure 10.5.b the steel inner angle is loaded in compression. The combined stresses at the top of the steel angle becomes positive and consequently the axial force changes direction. Therefore the shear stress becomes negative.

The steel inner angle, adhesive and beam form a sandwich construction. When a sandwich construction is subjected to a moment, the parts work together to take up the moment. The downwards point load on the right end of the beam will cause a negative moment which increases toward the point of engagement of the point load till zero. If the moment increases in positive direction the shear stress will be positive (see Figure 25.1 and Table 25.1). The adhesive layer is far away from the neutral axis. Therefore the shear stresses due to the sandwich behaviour in the adhesive will be relative low.

The positive shear due to the Goland and Reissner case and sandwich behaviour and the negative shear due to positive stresses at the top of the steel angle can explain the distributions of section 24.1.3/24.1.4 well.

In section 24.1.3 there is a small difference between the lines at $y=0$, $y=50$ and $y=100$. This difference is caused by the non-uniform stiffness in y -direction of the beam. Just as for the stresses perpendicular to the plane, the stresses are highest (or lowest) where the stiffness is highest.

In section 24.1.3 there are only clear differences between the lines at $z=0$, $z=2$ and $z=4$ near the ends, just as described for the stresses perpendicular to the plane.

In section 24.1.4 it can be seen that for the first part there are no significant differences between the tests.

10.5.1.3 No difference between the tests

As noticed, there are no significant differences between the tests for the stresses of the horizontal plane of the inner angle. If the length of other planes is of minor influence on this plane, this plane will be the plane which mainly transfers the force in negative x-direction of the beam.

10.5.2 The vertical plane of the inner angle

In this section the shape of the stress distributions at the vertical plane at the inner steel angle is analysed.

The top of the vertical plane is loaded by the horizontal plane by a clockwise moment (see moment distribution of section 25.2 and 25.3, and Figure 10.6), a force in negative x-direction and a force in z-direction (see shear force distribution of section 25.2 and 25.3).

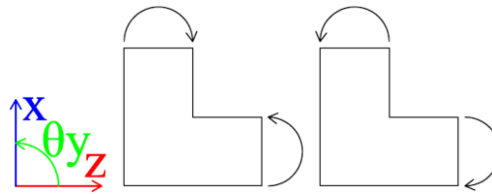


Figure 10.6: Relationship of moment of horizontal and vertical part.

10.5.2.1 General distribution of stresses perpendicular to the plane

The force in z-direction gives the same type of stress distribution as in the Goland and Reissner case with a compression load, just like for the horizontal part.

To investigate the qualitative behaviour due to the clockwise moment and force in negative x-direction, the case is simplified with the next assumptions:

- The bending stiffness of the column is infinite with respect to the angle.
- The column does not displace in x-direction.
- The adhesive layer can be modelled with translation springs in z-direction (no shear resistance).
- Displacements occur only in x-direction.

These assumptions lead to the next structural diagrams:

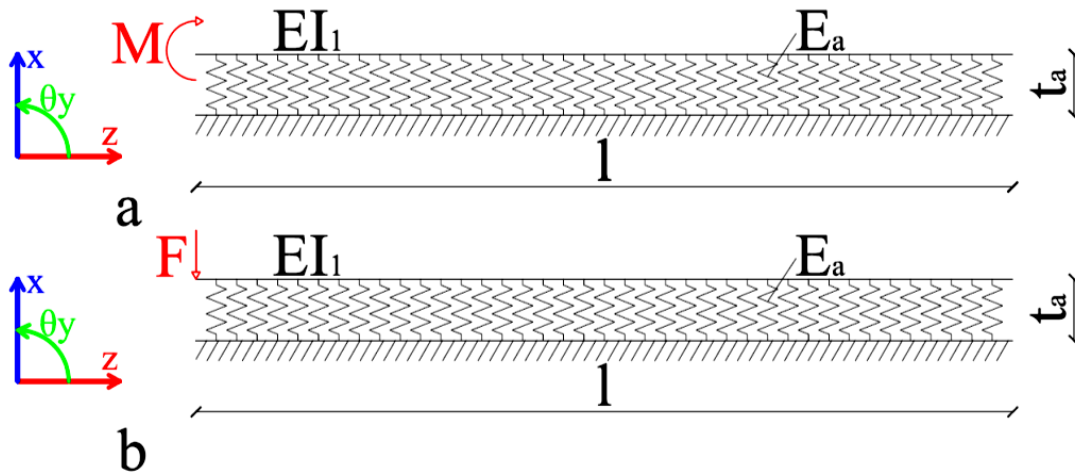


Figure 10.7: Structural diagrams per unit width of beam on elastic foundation with a moment load (a) and point load (b)

In 'Appendix I: Elaboration of DE's for stress' the DE's of these system are derived and elaborated. The stress distributions can be found in Figure 25.15 and Figure 25.20.

The combination of the Goland and Reissner, moment load and point load distributions can describe the distributions of section 24.2.1/24.2.2 well.

In section 24.2.1 there is a clear difference between the lines at $y=0$, $y=50$ and $y=100$. The same as mentioned in section 10.5.1.1 holds for this adhesive plane.

In section 24.2.1 there are only clear differences between the lines at $x=0$, $x=2$ and $x=4$ near the ends. Also the same as mentioned in section 10.5.1.1 holds for this adhesive plane.

In section 24.2.2 it can be seen that there is no significant difference between the tests for $x \lesssim 54$.

For $x \gtrsim 54$ the differences due to the lap length become visible. The result lines at $y=0$ show that if the plane becomes longer the line becomes less steep. When the same energy (area of the stress figure) is transferred, which is the case (no increase of the point load), this makes sense. But also the height of the peaks change a bit. Probably the longer and therefore stiffer lap will 'attract' more vertical load to itself, which leads to a higher stress peak. The increase in bond area and therefore decrease of the stress, and the higher load and therefore increase of the stress, will compensate each other for a part. For the mid length lap the stresses are highest, which indicates that the increase in stresses is dominant. This length is therefore not desirable.

For the lines at $y=50$ and $y=100$ there is no significant difference other than the length of the low stress part of the line.

10.5.2.2 General distribution of shear stresses

The force in z-direction causes positive shear in the adhesive, see Figure 10.8, with the Goland and Reissner shape (see Figure 5.13).

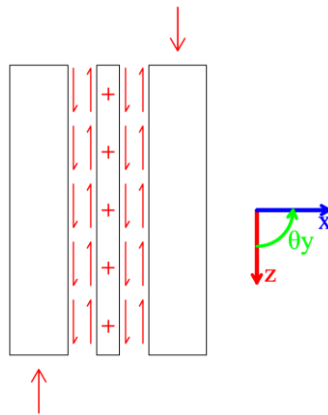


Figure 10.8: Shear stress direction of the vertical plane of the inner angle

Due to the clockwise moment at the top the shear stresses becomes positive (also described in section 10.5.2.1). Regarding the high negative shear stresses, the influence of (anticlockwise moment due to) the force in x-direction on the axial stresses seems to be small in comparison to the clockwise moment.

Just like the horizontal part, the vertical part of the steel angle is part of a sandwich construction, namely with the column and vertical part of the outer angle. The column is loaded by a negative moment due to shear of the vertical adhesive planes and by pressure of the beam on the top right flange. Due to the adhesive planes the negative moment becomes bigger in positive z-direction. Consequently the shear stresses due to the sandwich action will be negative (see Figure 25.1 and Table 25.2). The adhesive layer is far away from the neutral line of the sandwich construction, therefore the shear stresses due to the sandwich behaviour in the adhesive will be low.

The positive shear due to the Goland and Reissner case, the negative shear due to positive stresses at the left side of the steel angle and the negative shear due to the sandwich behaviour, can explain the distributions of section 24.2.3/24.2.4 well.

In section 24.1.3 there is a clear difference between the lines at $y=0$, $y=50$ and $y=100$. The same as mentioned in section 10.5.1.1 holds for this adhesive plane.

In section 24.2.3 there are only clear differences between the lines at $z=0$, $z=2$ and $z=4$, near the ends. Also the same as mentioned in section 10.5.1.1 holds for this adhesive plane.

In section 24.2.4 it can be seen that there is no significant difference between the tests for $x \lesssim 54$. For $x \gtrsim 54$ the differences due to the lap length become visible. For longer planes the lines are less steep, just like the stresses perpendicular to the plane. Also the peaks differ a bit in height, probably due to the same reason as described for the stresses perpendicular to the plane in the previous section. The length of other planes seems not to influence the shear stress lines.

10.5.2.3 No difference between the tests

As noticed, there are no significant differences between the tests for the stresses of the vertical plane of the inner angle due to the lengthening of other planes.

10.5.3 The horizontal plane of the outer angle

In this section the shape of the stress distributions at the horizontal plane at the outer steel angle is analysed.

10.5.3.1 General distribution of stresses perpendicular to the plane

Due to tension in the upper flange of the beam the positive Goland and Reissner distributions apply to this plane (see Figure 5.14). But due to the vertical part of the outer angle, which is bonded to the endplate, the peel effect at the left side will be negligible in all likelihood.

The end of the beam deforms due to shear stresses. The web is loaded in negative shear by the endplate, upper flange and stiffener, see Figure 10.9.a. The upper left corner of the web will 'open up' due to these stresses, see Figure 10.9.a.

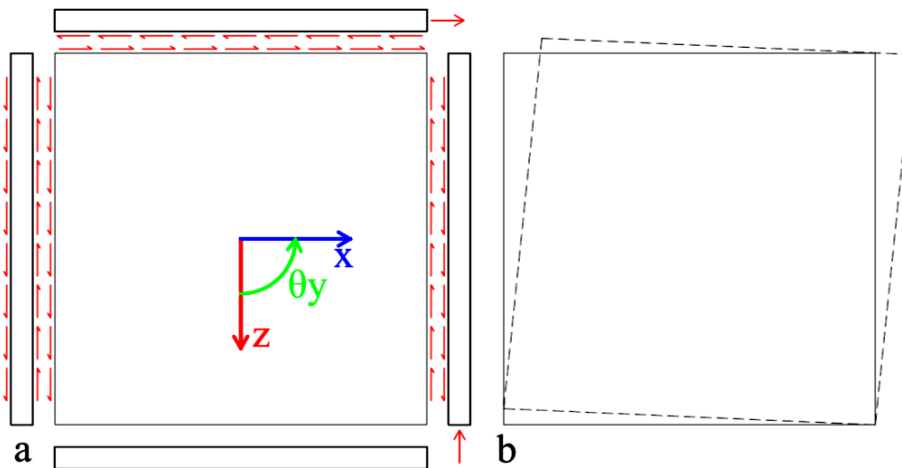


Figure 10.9: Shear deformation of the beam end

To investigate the qualitative behaviour due to the shear deformation of the beam, the case is simplified with the next assumptions:

- The bending stiffness of the beam is infinite, ($EI_2 = \infty$), with respect to the angle.
- The adhesive layer can be modelled with translation springs in z-direction (no shear resistance).
- The vertical plane of the steel angle does not rotate and/or translate.
- Displacements occur only in z-direction.

These assumptions lead to the next structural diagram:

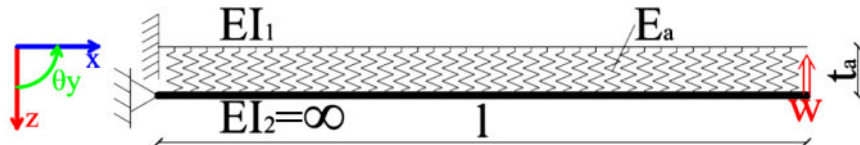


Figure 10.10: Structural diagram per unit width for shear deformation of the beam

In 'Appendix I: Elaboration of DE's for stress' the DE's of this system are derived and elaborated. The stress distribution can be found in Figure 25.25.

Due to the point load the beam will rotate in negative θ_y -direction and translate in negative z-direction at the left side of the rotation point. The upper vertical part of the outer angle is bonded to the endplate of the beam. Therefore the outer angle will follow the beam for the most part. The vertical force which is not transferred by shear of the bond plane at the endplate will be transferred by the horizontal bond plane. Note that due to failure and/or plasticity the capacity of the endplate bond plane is limited. To investigate the qualitative behaviour due to the rotation and translation for the horizontal bond plane, the case is simplified with the next assumptions:

- The bending stiffness of the beam is infinite, ($EI_2 = \infty$), with respect to the angle.
- The adhesive layer can be modelled with translation springs in z-direction (no shear resistance).
- The vertical plane of the steel angle does not rotate and/or translate.
- Displacements occur only in z-direction.

These assumptions lead to the next structural diagrams:

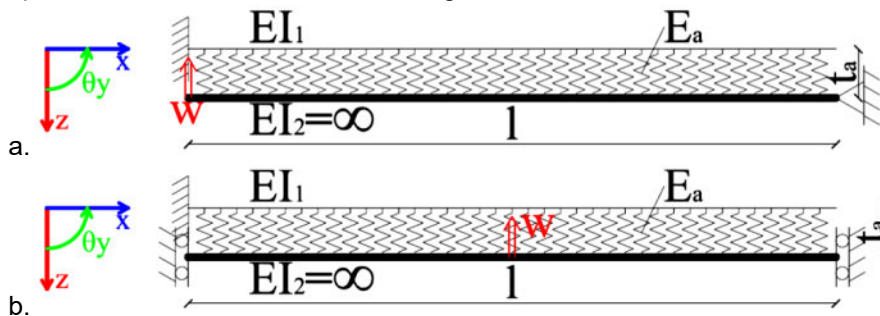


Figure 10.11: Structural diagrams per unit width of beam on elastic foundation which rotate (a) and translate (b)

In 'Appendix I: Elaboration of DE's for stress' the DE's of these systems are derived and elaborated. The stress distributions can be found in Figure 25.30 and Figure 25.35.

Combinations of stresses due to peel, shear deformation, and rotation and translation of the beam, will lead to high negative forces at the left side. In contrast to that, section 24.3.1 and 24.3.2 show mainly positive stresses at the left side.

The stresses due to shear deformation, rotation and translation of the beam at the right side of the lap are negligible, so only peel is of influence. The models with a 200mm lap exhibit a clear peel peak at the right side, in contrast of the models with a 100mm lap. The models with a 100mm lap exhibit negative stresses.

Another mechanism plays a role in the stress distributions of the horizontal part of the outer angle. In Figure 24.62 and Figure 24.63 counterplots can be found for a model with a short lap (100mm) and long lap (200mm). Both figures show a high positive stress area at the left side. The highest values are not located at the end or the middle of the flange as would be expected for the previously described mechanisms.

The stress distributions of the right side for a short and long lap show little similarity. For the long lap a clear peel distribution is shown, with the highest stresses at the place with the highest stiffness (at the web and fillet radius). For the short lap only at the outer side of the flange edge a significant change occurs. A negative peak occurs at this place. At the middle and intermediate area the stress becomes gradually more negative, but no distinct peak arises.

In order to determine the other mechanism a few additional FEM calculations are made. One of them shows great similarities with the behaviour. For the additional test the model IA300x500 OA100x500 and IA500x500 OA200x700 are taken as a starting point. Only the end part of the beam and the horizontal part of the outer angle of these models are considered. The other elements were deleted. The nodes at the right side of the beam are constrained (for all translation directions) and a displacement load in positive z-direction is applied to the most lower left nodes of the beam. In the next figure a layout of these additional FEM tests can be found:

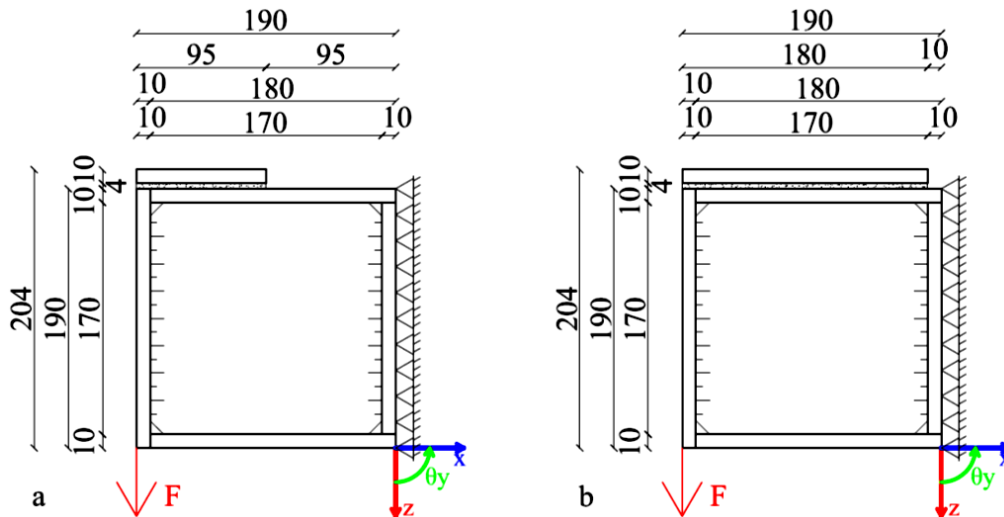


Figure 10.12: Layout additional FEM tests with a short lap (a) and a long lap (b)

In section 24.5 the results of the additional tests can be found. Note that the counterplots of the models with the short lap, Figure 24.62 and Figure 24.119, and the models with the long lap Figure 24.63 and Figure 24.120, show the same shapes. The additional models show the sandwich behaviour of the beam and outer angle. Note that the integral of the stresses in these adhesive layer should be zero out of equilibrium. This creates positive and negative peaks.

But the models of Figure 10.3 have an outer angle with a horizontal and vertical plane instead of only a horizontal plane. When the results of the additional models are considered the horizontal and vertical part seem not to transfer significant forces to each other. The stiffness of the vertical bond plane is probably so much stiffer than the horizontal bond plane that the force in the outer angle is nearly completely transferred by the vertical plane. Note that the used FEM calculation is linear elastic.

In section 24.3.1 there is a clear difference between the lines at $y = 0$, $y = 50$ and $y = 100$. The most significant differences are caused by the load cases of Figure 10.12.

In section 24.3.1 there are only clear differences between the lines at $x = 0$, $x = 2$ and $x = 4$ near the ends. Also the same as mentioned in section 10.5.1.1 holds for this adhesive plane.

Section 24.3.2 shows that there are no significant differences between the tests due to the change of length of other bond planes.

10.5.3.2 General distribution of shear stresses

Due to tension in the upper flange of the beam the positive Goland and Reissner shear distribution applies (see Figure 10.5.a and Figure 5.13). But due to the vertical part of the outer angle the left peak is likely to be small.

Positive moments occur on the left side due to shear deformation, rotation of the beam and translation of the beam (see Figure 25.26, Figure 25.31 and Figure 25.36). A positive moment in the steel outer angle results in tension stresses in the steel at the steel-adhesive interface. This results in higher positive shear stresses in the adhesive.

The steel outer angle, adhesive and beam form a sandwich construction. The rotation centre of the beam is assumed to be at the bottom of the stiffener. The vertical part of the steel outer angle is loaded with a force in positive z-direction. As a result of this, the left part of the beam is loaded with a negative moment which is zero at the left side and maximum at the right side. When a moment decreases in positive x-direction the shear stresses due to this moment will be negative (see Figure 25.1 and Table 25.1). The adhesive layer is far away from the neutral axis. Therefore the shear stresses due to the sandwich behaviour in the adhesive will be relatively low.

As noticed in the previous section the load cases of Figure 10.12 seem to have a large influence on the stress distribution for the stresses perpendicular to the plane. Most likely those load cases also have a large influence on the shear stress distributions. In section 24.5.3/24.5.4 the shear stress distributions can be found for those load cases.

When the shear stress distributions of the Goland and Reissner, the positive moment, the sandwich and the Figure 10.12 case are compared with those of section 24.3.3/24.3.4 it is clear that the cases of Figure 10.12 are of most influence. As described previously the shear stresses due to the sandwich behaviour are negative. The counterplots for Figure 10.12 show a large negative area near the web in the middle of the length. Near the web is the stiffest part for shear therefore it is not surprising that the shear stresses are negative here. The positive areas are located at places where the shear stiffness is lower.

In section 24.3.3 there is a clear difference between the lines at $y=0$, $y=50$ and $y=100$. The most significant differences are caused by the load cases of Figure 10.12.

In section 24.3.3 there are only clear differences between the lines at $x=0$, $x=2$ and $x=4$ near the ends. Also the same as mentioned in section 10.5.1.1 holds for this adhesive plane.

Section 24.3.4 shows that there are no significant differences between the tests due to the change of length of other bond planes.

10.5.3.3 No difference between the tests

As noticed, there are no significant differences between the tests for the stresses of the horizontal plane of the outer angle due to the lengthening of other planes.

10.5.4 The vertical plane of the outer angle

In this section the shape of the stress distributions at the vertical plane at the outer steel angle is analysed. The vertical bond plane of the outer angle actually consists of two adhesive bonded planes, one at the endplate of the beam and one at the column. The beam and column move with respect to each other.

10.5.4.1 General distribution of stresses perpendicular to the plane

As mentioned the beam and column will move with respect to each other. The beam will rotate in negative direction and translate in positive x-direction with respect to the beam. To investigate the qualitative behaviour due to the movement, the case is simplified with the next assumptions:

- The bending stiffnesses of the beam and column are infinite with respect to the angle.
- The column does not displace in x-direction.
- The adhesive layer can be modelled with translation springs in x-direction (no shear resistance).
- Displacements occur only in x-direction.

These assumptions lead to the next structural diagrams:

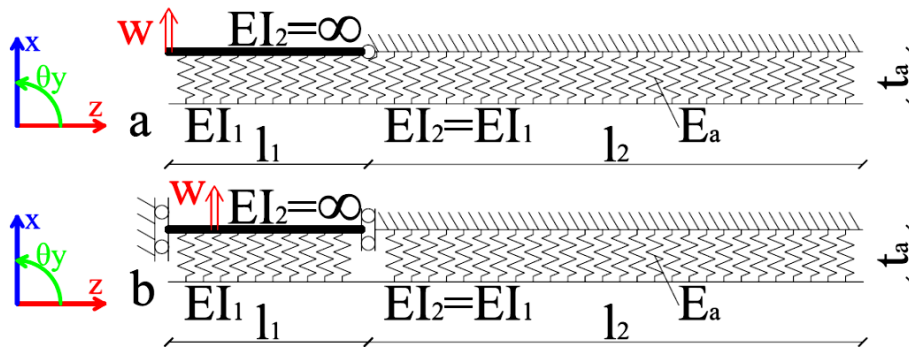


Figure 10.13: Structural diagrams per unit width for beam rotation (a) and translation (b)

In 'Appendix I: Elaboration of DE's for stress' the DE's of these systems are derived and elaborated. The stress distributions can be found in Figure 25.40 and Figure 25.45, where Figure 25.40 shows the symmetric and M-shaped stresses distribution of Figure 10.13.a and where Figure 25.45 shows the antisymmetric, Z-shaped stresses distribution of Figure 10.13.b.

Near the beam the angle and beam are loaded as in Figure 10.14.a. Near the column the angle and column are loaded as in Figure 10.14.b. If the adherents are loaded in tension, such as in these cases, the stresses perpendicular to the plane at the ends will be positive (Figure 5.14). At the transition between the beam and column this will lead to W-shaped distribution (two distributions as depicted in Figure 5.14 next to each other). The peel stresses at the top of the vertical part are expected to be small due to the horizontal part.

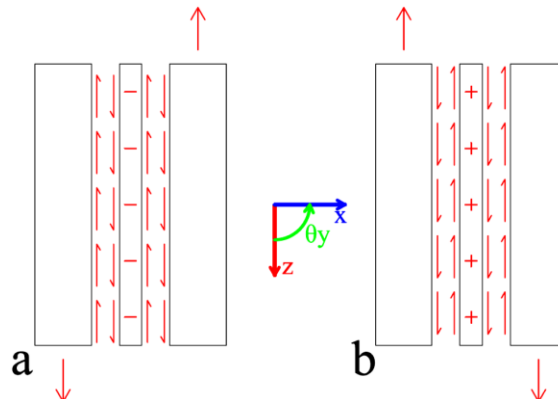


Figure 10.14: Shear stresses of vertical plane of outer angle at the beam (a) and at the column (b)

In section 10.5.3.1 the behaviour is analysed of the horizontal part of the outer angle. The horizontal part will load the vertical part at the top with a moment. Figure 25.26, Figure 25.31 and Figure 25.36 shows that this moment is positive (Figure 10.6), so the case of Figure 10.7.a applies which distribution is depicted in Figure 25.15. The axial force of the horizontal part will load the vertical part with a point load in positive x -direction. This will result in the case of Figure 25.18 only with the point load in another direction. The distributions are linear with respect to the load (note the constants of (25.62)). Hence the mirror case of Figure 25.20 applies.

Both the stresses due to the moment and point load should be small when the results of section 10.5.3.1, in particular the decisiveness of the case of Figure 10.12, are taken into consideration.

The combination of the Goland and Reissner, moment due to the horizontal part, rotation difference and translation difference distributions, can describe the distributions of section 24.4.1/24.4.2 well. Only the stresses at the top show some little deviations, especially at $y=0$. Most likely these deviations are caused by the case of Figure 10.12.

In section 24.4.1 there is a clear difference between the lines at $y=0$, $y=50$ and $y=100$. The same as mentioned in section 10.5.1.1 holds for this adhesive plane.

In section 24.4.1 there are only clear differences between the lines at $x=0$, $x=2$ and $x=4$ near the ends and at the beam/column transition. At the ends the stresses are higher so differences are amplified.

In section 24.4.2 it can be seen that the models with a longer outer horizontal part exhibit a somewhat lower peak at the top than those with a shorter part. Especially at $y=50$ and $y=100$ this effect is visible. At the bottom end the stresses for the longer plane are a bit lower but no significant differences are noticeable. At the beam/column transition the gradient of the stress distribution is high. This means that the differences between two result points are high and that the placement of those points is of great influence of the stress level. There are some differences between the models but it is hard to say if those differences occur due to different lengths or due to the exact placement of nodes/result points. In Table 10.1 the extreme values around the beam/column transition of the node can be found. Remarkable is that the minimal value for model IA15OA25 is higher than those values for the other models. But in general the values are relatively close to each other. Due to plasticity of the steel and adhesive the actual peaks will flatten out at a much lower level than the calculated peaks¹. For that reason the exact height of the peak is of less importance.

Model	IA15OA25	IA15OA35	IA25OA35	IA27OA35	IA27OA55
Minimum	-121,10	-133,83	-131,95	-131,90	-131,65
Maximum	187,03	184,71	181,66	181,66	181,15

Table 10.1: Extreme values of the stresses perpendicular to the plane for the outer angle at the beam/column transition

10.5.4.2 General distribution of shear stresses

Figure 10.14 shows the load cases of the vertical part of the outer angle. At the beam a negative and at the column a positive, Goland en Reissner shear stress distribution develop.

The sandwich behaviour at the beam will be negligible, because I_{xx} of the beam is practically infinite. At the column the sandwich behaviour is of influence. The shear stresses due to the sandwich behaviour are negative like for the vertical bond plane of the inner angle, which is described in section 10.5.2.2.

Due to the positive moment of the horizontal part of the steel outer angle, the top of the vertical part is loaded with a positive moment. This moment causes tension in the steel at the steel/adhesive interface, which lead to positive shear stresses.

The shear due to the Goland and Reissner case, the positive shear due to the moment on top and sandwich behaviour can explain the distributions of section 24.4.3/24.4.4 well.

In section 24.4.3 there is a clear difference between the lines at $y=0$, $y=50$ and $y=100$. At the beam the line of $y=100$ lays in between the lines of $y=0$ and $y=50$. As mentioned in section 10.5.1.1 the stresses at the stiffest parts are generally higher than those in less stiff parts. But the differences for $y=100$ and $y=50$ are relatively small. Probably the moments of the horizontal part due to the Figure 10.12 case causes these differences.

In section 24.4.3 there are only clear differences between the lines at $z=0$, $z=2$ and $z=4$, near the ends and at the beam/column transition. Also the same as mentioned in section 10.5.1.1 holds for this adhesive plane.

In section 24.4.4 it can be seen that there is no significant difference between the tests due to other planes, although the stresses for the longer plane are a bit lower than those of the shorter plane. Only at the beam/column transition some differences can be noticed, just as for the stresses perpendicular to the plane. In Table 10.2 an overview of the extreme shear stresses near the

¹ For narrow linear elastic peaks it is allowable to assume that plasticity can flatten out the peaks when the material has sufficient deformation capacity. Important is the area of the stress diagram. For narrow peaks the area is relatively small and so the development of a small plastic plateau is sufficient.

beam/column transition can be found. Remarkable is that the maximum value for model IA15OA25 is lower than those for other models. But in general the values are relatively close to each other. Possibly the exact placement of nodes/result points is of influence for the exact value, see the latter section.

Model	IA15OA25	IA15OA35	IA25OA35	IA27OA35	IA27OA55
Minimal	-59,26	-56,83	-55,74	-55,72	-55,59
Maximum	9,40	15,11	15,01	15,02	14,97

Table 10.2: Extreme values of the shear stresses for the outer angle at the beam/column transition

10.5.4.3 No difference between the tests

As noticed, there are no significant differences between the tests for the stresses of the vertical plane of the outer angle due to the lengthening of other planes.

10.5.5 Conclusion

Only for the outer horizontal bond plane significant differences for the extreme stresses are observed. For the vertical bond planes some small differences are observed and for the vertical inner bond plane no differences at all are observed. In general, the used lap lengths are rather big so that lengthening is of less influence, see section 5.3.5.2. With a plastic calculation this will probably not change. Plasticity will flatten out the peaks and spread them over a larger, but still relatively small, length. With a plastic calculation the maximum strain can be predicted much better because plastic behaviour of the adhesive seems to be inevitable.

Exploratory tests with bevelled and tapered inner and outer angles show that these are not very effective ways to reduce stress peaks, most likely due to the high stiffness of the beam and column. The ratio of the stiffnesses of the 10mm angle and the HE200A profile will not significantly change due to these methods.

Due to the linear elastic calculation the stiffness of the horizontal part of the outer angle is overestimated, so the outer horizontal part is practically 'deactivated'. With a plastic calculation the influence of the outer horizontal part will probably be better visible, because plasticity will limit the stiffness of the outer vertical part.

A plastic calculation only makes sense when the adhesive has some deformation capacity. The elastic limit for the shear strain, assuming the data of section 9.11, is:

$$\gamma_{el} = \frac{\tau}{G} = \frac{17}{4273} = 3.98 \cdot 10^{-3}$$

In table 14 of [54] an average ultimate shear strain of $8.77 \cdot 10^{-3}$ is found, which is roughly two times as big as the elastic limit. Such a difference allows the choice for a plastic calculation.

A plastic calculation for a model which is used for the elastic calculation is practically impossible with today's commercial computers. A plastic calculation of a part of the connection is therefore obvious if more detailed information is wanted of the acting stresses.

11 Design study of double strap connection

For the L-connection of the previous section, lengthening is not effective. An exact (plastic) calculation is practically impossible. Practice tests of the L-connection will only tell if it fails or not, but will give little insight in the real characteristics of adhesive bonds. Therefore a more fundamental connection will be investigated namely a double strap connection.

The bondline of adhesive bonded thick plates should transfer a rather big load, which is typical for civil structures. This demands a high failure load of the connection. Traditional lengthening appears, according to the previous section, to be ineffective to increase the failure load. Other methods should be used to increase the effectiveness. A tapered or stepped connection can increase the contribution of the middle part of the lap. But traditional tapered or stepped adherents are material intensive, due to the milling/cutting process, and therefore expensive. Therefore adherents can be combined to stepped straps by adhesive bonding, which is frequently done for aerospace applications. The bonded straps can be made in large quantities which lowers the costs. A double strap connection with stepped bonded straps seems therefore a good starting point to investigate the feasibility of structural adhesive bonding for civil structures.

In this section the materials and measurements are determined.

11.1 Materials

For the adhesive bonded double strap connection the steel grade and type of adhesive have to be chosen.

11.1.1 Steel

Due to the same modulus of elasticity for the different steel grades, the grade with the lowest strength, S235, is obviously a good starting point. A higher steel grade will result in a higher plastic capacity of the plate, for same steel thicknesses, and so the adhesive layer has to transfer a higher load. But the parameters which determine the capacity of the adhesive layer are not changed by a higher steel grade. Therefore a high steel grade is only profitable if the adhesive is not decisive for failure, which is probably not the case.

11.1.2 Adhesive

For the adhesive of the double strap connection only requirements with respect to tolerance and strength applies for testing. No time-and-environment-depended requirements apply which is not realistic for practical cases. Therefore the same adhesive as for the L-connection, Sikadur®-30, will be used. This adhesive type is chosen with consideration of the requirements for a practical case.

11.2 Dimensioning

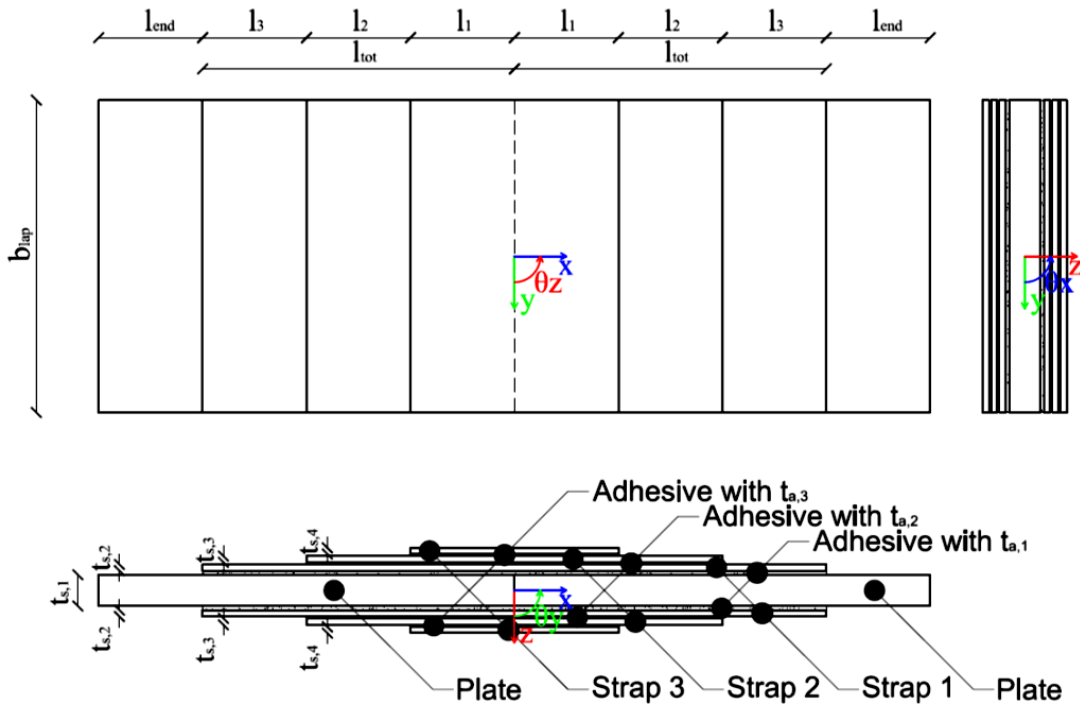


Figure 11.1: Typical adhesive bonded double strap connection

For designing the adhesive bonded double strap connection the next start assumptions are made:

- Width of the connection (b_{lap}) is 200mm
- Thickness of the plates ($t_{s,1}$) is 15mm
- Three straps per side
- Thickness of the straps is 3mm

Most obvious is to choose the sizes of the steel elements in agreement with standard sizes, otherwise the steel plate and/or straps have to be cut out of plates. For the assumed strap thickness the maximal standard width is 150mm [55]. Therefore the width is changed into 150mm.

A full strength connection should be able to resist the ultimate load of the plates. Due to shear lag and limited deformation capacity of the adhesive, the ultimate strength of the adhesive is not the shear strength times area. Therefore the maximal ideal plastic capacity divided by the nominal plastic capacity of the plate should be greater than one. With a lap length of 100mm the ratio is 1.45:

$$\frac{(l_{lap1} + l_{lap2} + l_{lap3}) \sigma_{a,sh} b_{lap}}{t_{s,1} f_{s,y} b_{lap}} = \frac{(100 + 100 + 100) \cdot 17 \cdot 150}{15 \cdot 235 \cdot 150} = 1.45 \quad (11.1)$$

This ratio is assumed to be large enough.

11.2.1 Tolerances

For the adhesive thickness, the tolerances of the plates and straps are of influence. In the NEN-EN10058 [56], the tolerances of hot rolled flat bars are specified. Five tolerances on dimension and shape are specified in [56], namely:

1. Thickness
2. Width
3. Length

4. Straightness
5. Out-of-section

Only the tolerances on the thickness and straightness will affect the thickness of the adhesive.
For the thickness the next tolerance applies:

$$\Delta_{thickness} \leq \pm 0.5 \text{ mm} \quad \text{for} \quad t \leq 20 \text{ mm} \quad (11.2)$$

For the straightness the next table applies:

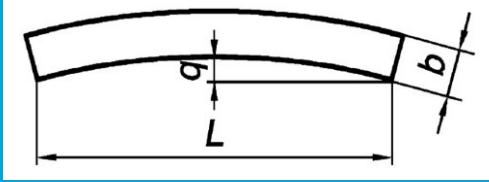
	Nominal cross section	Tolerance in the plane of b
	< 1000 mm ²	$q \leq 0.4\% \text{ of } L$
$\geq 1000 \text{ mm}^2$	$q \leq 0.25\% \text{ of } L$	

Table 11.1: Straightness of hot rolled flat bar [56]

The nominal cross section of the plates and straps are:

$$A_{s,1} = t_{s,1} b_{lap} = 15 \cdot 150 = 2250 \text{ mm}^2 \quad (11.3)$$

$$A_{s,2} = A_{s,3} = A_{s,4} = t_{s,2} b_{lap} = 3 \cdot 150 = 450 \text{ mm}^2 \quad (11.4)$$

As mentioned before $l_{lap1} = l_{lap2} = l_{lap3} = 100 \text{ mm}$ is assumed.

$$q_{plate} \leq 3 \cdot 100 \cdot 0.4 \cdot 10^{-2} = 1.2 \text{ mm} \quad (11.5)$$

$$q_{strap} \leq 4 \cdot 100 \cdot 0.25 \cdot 10^{-2} = 1 \text{ mm} \quad (11.6)$$

The difference in thickness of the plates is maximally 1mm, which can be spread over two bondlines. The thickness of the straps is not of influence on the adhesive thickness. The tolerances due to straightness cannot be spread over two bondlines. In total the minimal adhesive thickness, for the first adhesive layer, should be:

$$t_{a,1} \geq \frac{|\Delta_{thickness}|}{2} + q_{plate} + q_{strap} = 2.45 \text{ mm} \quad (11.7)$$

For the other two layers the straightness tolerances of the straps are decisive:

$$t_{a,2} = t_{a,3} \geq q_{strap} + q_{strap} = 2.0 \text{ mm} \quad (11.8)$$

Note that these minimal adhesive thicknesses are very or even too large for structural adhesive bonding. For plates of the same batch the thickness differences are negligible. The distance between the plates due to curvature can be minimised by placing the plates in such a way that for all plates the convex sides are upwards (or are all downwards). The straps are probably from the same batch, and so the curvature will be more or less the same, therefore a reduction of 50% is assumed. The plate and strap cannot come from the same batch so only a reduction of 20% is assumed.

$$t_{a,1} \geq (q_{plate} + q_{strap}) 0.8 = 1.56 \text{ mm} \quad (11.9)$$

$$t_{a,2} = t_{a,3} \geq (q_{strap} + q_{strap}) 0.5 = 1.0 \text{ mm} \quad (11.10)$$

To ensure filling of the bondline and out of practical reasons the next adhesive thicknesses are chosen:

$$t_{a,1} = 1.7 \text{ mm} \quad (11.11)$$

$$t_{a,2} = t_{a,3} = 1.0 \text{ mm} \quad (11.12)$$

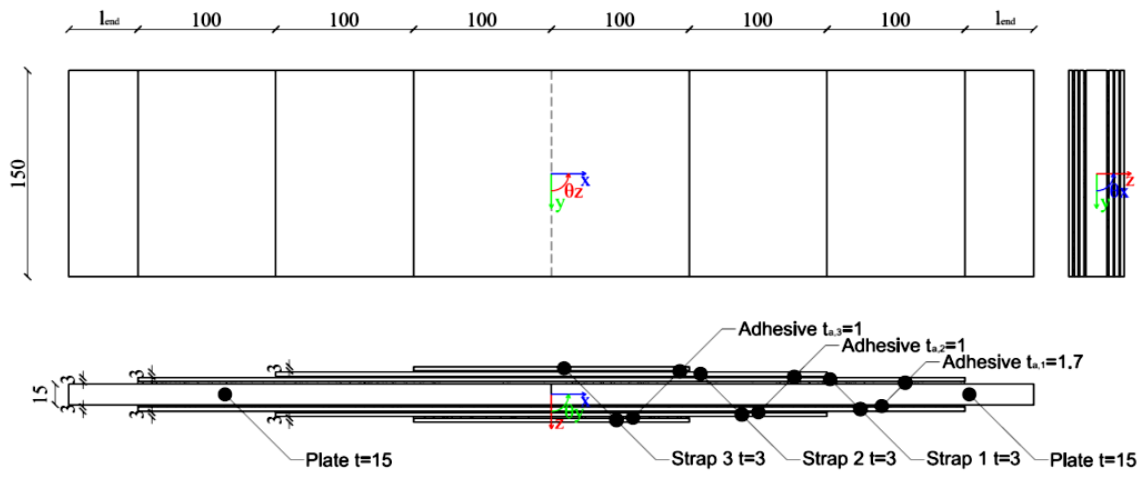


Figure 11.2: Adhesive bonded double strap connection with chosen measurements

12 FEM test of double strap connection

To determine the dimensions for the practice test and to verify the practice test several FEM calculations will be made. In this section the FEM tests and outcomes are described.

12.1 Modelling

Due to symmetry in three directions, only $1/8$ ($=1/2^3$) of the connection has to be modelled. The end length has to be long enough to ensure a uniform stress distribution at the beginning of the adhesive. It is assumed that $l_{end} = 100\text{mm}$ fulfils this requirement.

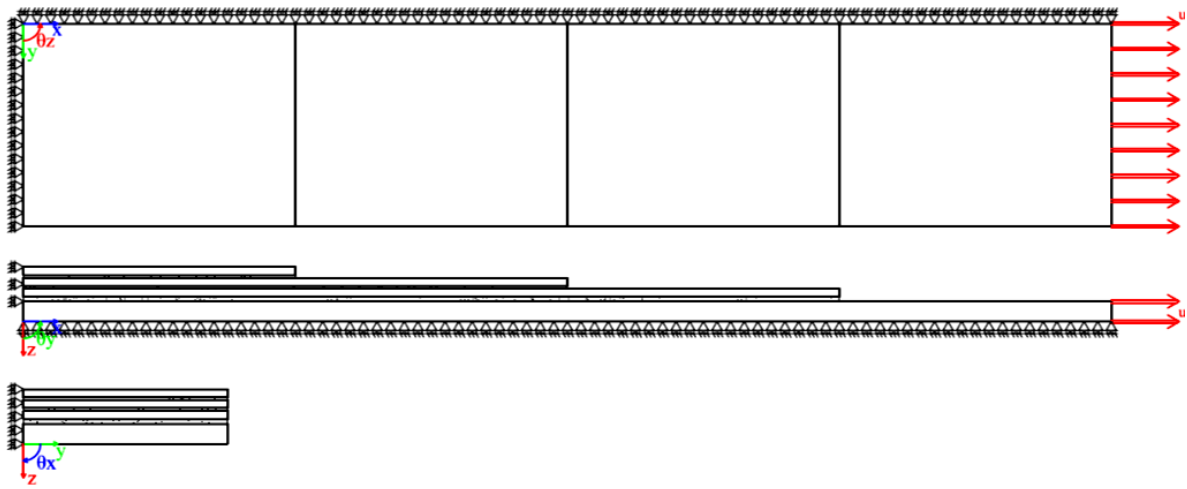


Figure 12.1: Element division in x- and y-direction and supports of double strap FEM models

In the 'Appendix L: DIANA procedure for double strap connection model' the DIANA procedure for the double strap is provided.

12.2 Calculation

Several FEM models will be made to calculate the double strap connection. This double lap model is a lot smaller than those of the entire L-connection described in section 12. Due to the smaller size of the model, non-linear calculations with quadratic elements are possible. As a starting point calculations with linear elements are made. After the lap length is chosen calculations with quadratic elements will be made.

To get some basic insight in the stepped characteristics, the connection is also analysed according to the theory of Volkersen, see 'Appendix K: Double strap according to Volkersen'. The activation of the middle part due to the stepped adherents can be clearly seen in Figure 27.5.

To get some insight in the influence of the adhesive thickness some calculations with different adhesive thicknesses are executed, see 'Appendix N: Influence of adhesive thickness'.

12.2.1 FEM Models

In total nine FEM models are calculated. In the next table an overview of the parameters is given:

		Model													
		3 LE 300	8 LE 300	3-3-3 LE 300	3-3-3 LE Butt 300	3-3-3 VM Butt 300	3-3-3 VM 300	3-3-3 VM 375	3-3-3 VM 450	3-3-3 DP 300	3-3-3 DP 375	3-3-3 DP 450	3-3-3 LE 300 Qu	3-3-3 VM 300 Qu	3-3-3 DP 300 Qu
Parameters (see Figure 11.1)	l_1	300	300	100	100	100	100	125	150	100	125	150	100	100	100
	l_2	0	0	100	100	100	100	125	150	100	125	150	100	100	100
	l_3	0	0	100	100	100	100	125	150	100	125	150	100	100	100
	l_{end}	100	100	100	100	100	100	100	100	100	100	100	100	100	100
	$t_{s,1}$	3	8	3	3	3	3	3	3	3	3	3	3	3	3
	$t_{s,2}$	0	0	3	3	3	3	3	3	3	3	3	3	3	3
	$t_{s,3}$	0	0	3	3	3	3	3	3	3	3	3	3	3	3
	$t_{a,1}$	1.7	1.7	1.7	1.7	1.7	1.7	1.7	1.7	1.7	1.7	1.7	1.7	1.7	1.7
	$t_{a,2}$	1	1	1	1	1	1	1	1	1	1	1	1	1	1
	$t_{a,3}$	1	1	1	1	1	1	1	1	1	1	1	1	1	1
	Material model adhesive	LE	LE	LE	LE	VM	VM	VM	VM	DP	DP	DP	VM	VM	DP
	Material model steel	LE	LE	LE	LE	VM	VM	VM	VM	VM	VM	VM	VM	VM	VM
	Linear or quadratic elements	Lin	Lin	Lin	Lin	Lin	Lin	Lin	Lin	Lin	Lin	Lin	Qu	Qu	Qu
	2mm butt	No	No	No	Yes	Yes	No	No	No	No	No	No	No	No	No

Figure 12.2: Overview characteristics double strap FEM models

12.2.2 Failure strain

To determine when a material with physical non linear behaviour fails, often the failure strain is taken as criterion. In [54] a shear stress-strain diagram and table of the applied adhesive can be found:

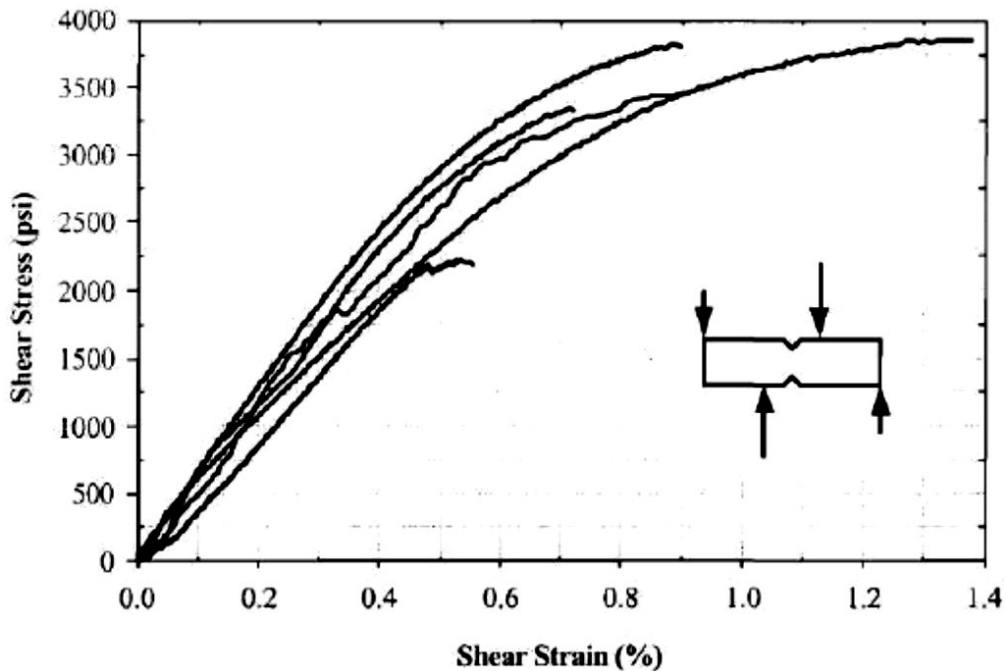


Figure 12.3: Stress-strain diagram of shear tests of Sikadur®-30 epoxy [54]

Coupon Number	Width (in)	Thickness (in)	Ultimate Strain (%)	Ultimate Load (lb)	Strength (psi)
1	0.464	0.081	0.713	125.6	3343
2	0.443	0.078	0.532	76.8	2224
3	0.439	0.081	1.322	1.322	3854
4	0.447	0.079	0.885	0.885	3823
5	0.460	0.078	0.934	0.934	3492
Average	0.451	0.079	0.877	121.2	3347
C.O.V.(%)	2.4	1.9	33.6	20.8	19.8

Table 12.1: Shear test results of Sikadur®-30 epoxy [54]

From Table 12.1 follows for the shear strain that $\bar{\gamma} = 8.77 \cdot 10^{-3} \text{ mm/mm}$ and for the sample size that $n = 5$. The sample standard deviation for the shear strain can be calculated with the coefficient of variance:

$$s = c_v \cdot \bar{\gamma} = 33.6 \cdot 10^2 \cdot 8.87 \cdot 10^{-3} = 2.95 \cdot 10^{-3} \text{ mm/mm} \quad (12.1)$$

With the student's t-test the critical value, which will be exceeded in 95% of the cases, can be calculated. The t-value for this critical value for a student's t-distribution with $n - 1 (= 4)$ degrees of freedom is:

$$t_{4,95\%} = 2.132 \quad (12.2)$$

The critical value follows from:

$$\gamma_{95\%} = \bar{\gamma} - t_{n,95\%} \frac{s}{\sqrt{n}} = 5.96 \cdot 10^{-3} \text{ mm/mm} \quad (12.3)$$

It's assumed that the adhesive will fail due to a certain Von Mises strain. DIANA uses the next formula to calculate the Von Mises strain¹ ([53]):

$$\varepsilon_{eq} = \sqrt{\frac{3}{2}(e_{xx}^2 + e_{yy}^2 + e_{zz}^2) + \frac{3}{4}(\gamma_{xy}^2 + \gamma_{yz}^2 + \gamma_{zx}^2)} \quad (12.4)$$

With:

$$\begin{aligned} e_{xx} &= \frac{2}{3}\varepsilon_{xx} - \frac{1}{3}\varepsilon_{yy} - \frac{1}{3}\varepsilon_{zz} \\ e_{yy} &= -\frac{1}{3}\varepsilon_{xx} + \frac{2}{3}\varepsilon_{yy} - \frac{1}{3}\varepsilon_{zz} \\ e_{zz} &= -\frac{1}{3}\varepsilon_{xx} - \frac{1}{3}\varepsilon_{yy} + \frac{2}{3}\varepsilon_{zz} \end{aligned} \quad (12.5)$$

For the pure shear case this formula simplifies to:

$$\varepsilon_{eq} = \frac{\sqrt{3}}{2} \gamma \quad (12.6)$$

Hence:

$$\varepsilon_{eq,95\%} = \frac{\sqrt{3}}{2} \gamma_{95\%} = 5.16 \cdot 10^{-3} \text{ mm/mm} \quad (12.7)$$

If the FEM calculations are a good representation of the reality, the Von Mises strain should not exceed $5.16 \cdot 10^{-3} \text{ mm/mm}$ to ensure a sufficient capacity in 95% of the cases.

The expected value for failure of the Von Mises strain is:

$$\varepsilon_{eq,expected} = \frac{\sqrt{3}}{2} \bar{\gamma} = 7.60 \cdot 10^{-3} \text{ mm/mm} \quad (12.8)$$

¹ The Von Mises strain is denoted as equivalent strain in DIANA

12.2.1 Stress distribution

In 'Appendix M: FEM results of double strap connection', section 29.1/29.4 some distributions of the first adhesive layer can be found for the last load step of the FEM models with stepped straps and 3x100mm lap length.

In section 29.1 the uplift of the shear stress distribution due to the stepped adherent is visible. For the models with the Von Mises material model a clear plastic plateau is visible. The models with the Drucker Prager material model are comparable with the linear elastic models.

In the peel stress distributions in section 29.2, the effect of the stepped adherent is visible. The peel distribution of the Von Mises models without quadratic elements (3-3-3 VM 300 and 3-3-3 butt VM 300) are remarkable, no reason for this is found.

For the Von Mises models a clear plastic plateau is visible for the equivalent stress in section 29.3. Just as for the shear stress, the Drucker Prager and linear elastic distributions are close to each other.

The equivalent strains of the models with non-linear material behaviour are larger than the models with linear model behaviour, see section 29.4.

12.2.2 Results

In the next figure the load-displacement behaviour of the models can be found. The displacement is measured in the middle and on the face of the plate, between the restrained nodes at x=0 and at 50mm from the end of the strap (times two to account for symmetry). This is the same place as the LVDT's will measure the displacement during the practice test. Note that the longer lap models are less stiff than the shorter lap models in the figure (less steep slope). This can be explained by the length of the model, $k = F/EA l$. In practice longer laps will give stiffer connections when the same measure length is used.

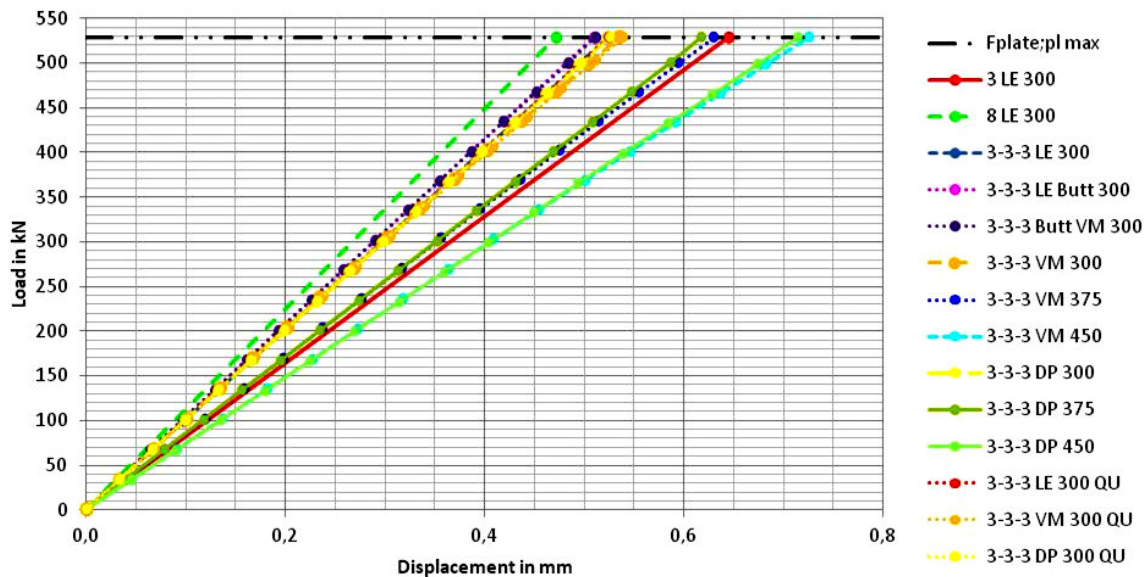


Figure 12.4: Load-displacement curves of FEM calculation of double strap

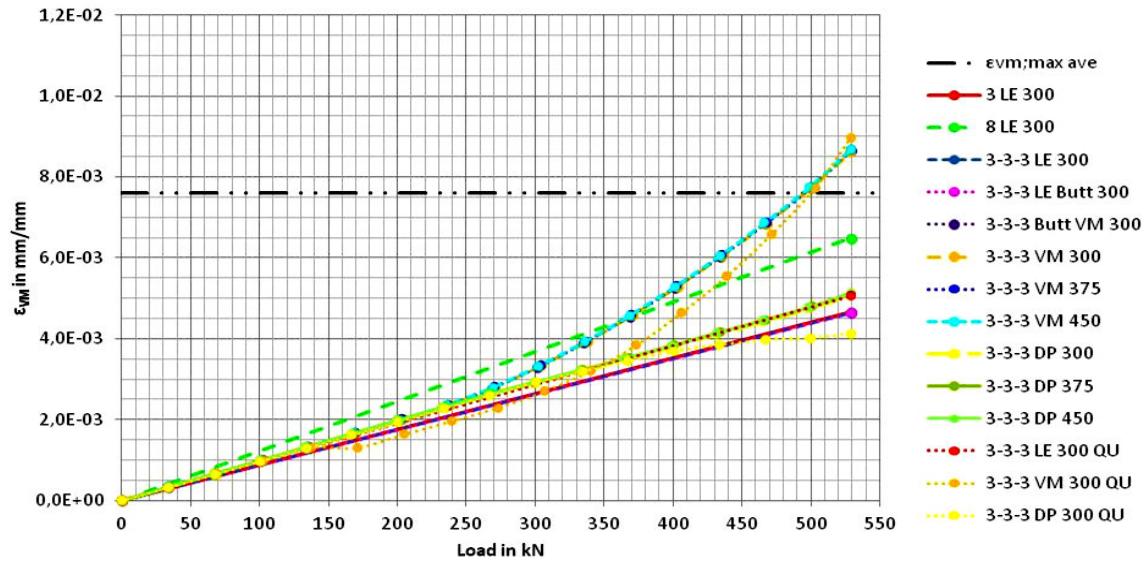


Figure 12.5: Strain-load diagram for the top point at $y=75$ and $x=l_{tot}$

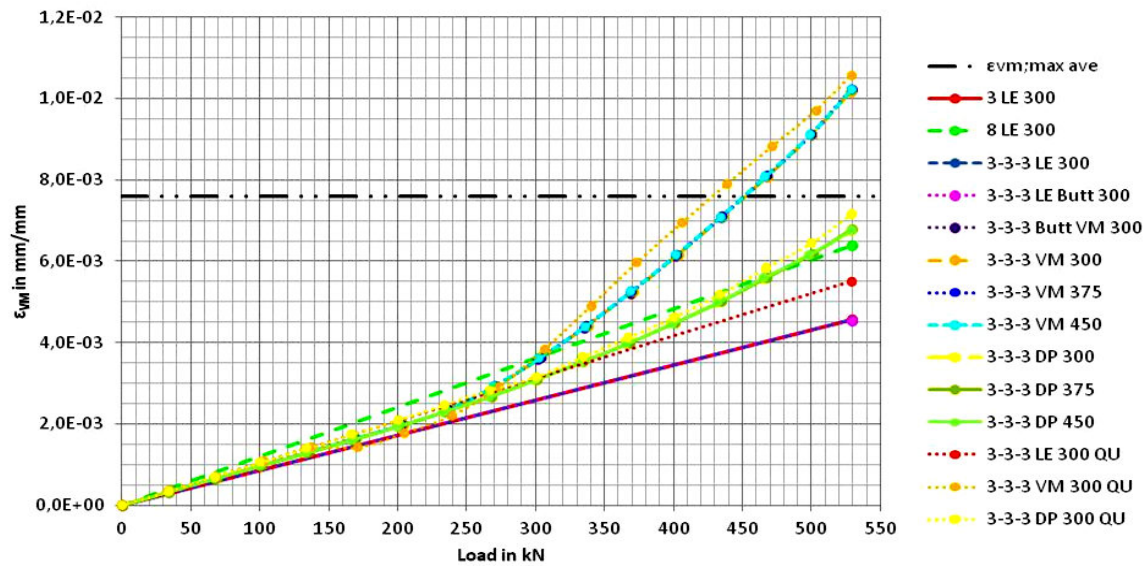


Figure 12.6: Strain-load diagram for the midpoint at $y=75$ and $x=l_{tot}$

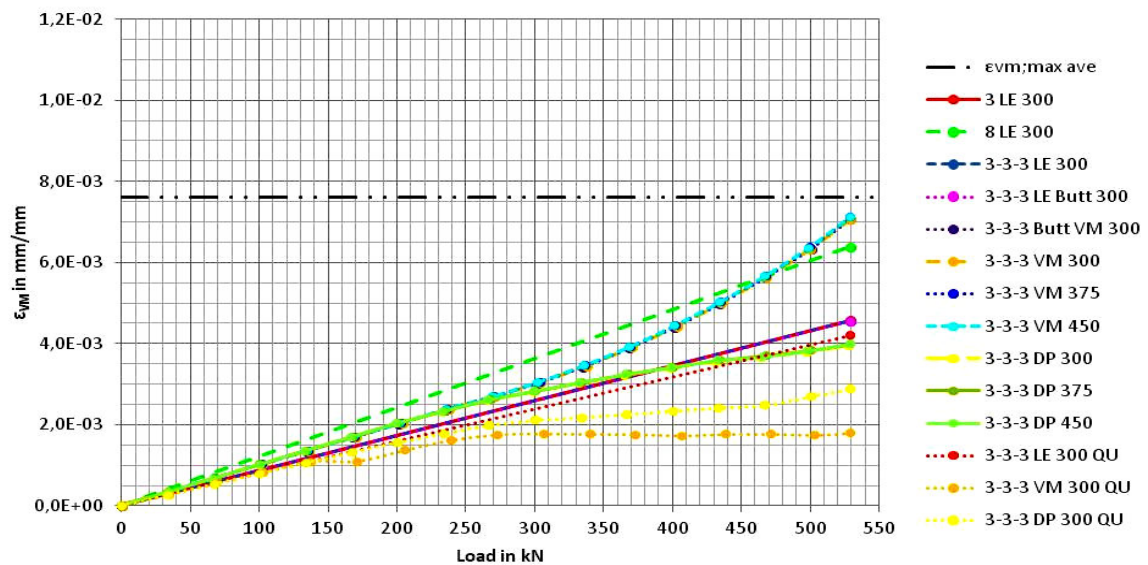


Figure 12.7: Strain-load diagram for the bottom point at $y=75$ and $x=l_{tot}$

12.3 Conclusion

According to Figure 12.4 the load-displacement behaviour is practically linear for all models. Assuming a uniform stress distribution for the first adhesive layer (rigid adherents) and Von Mises plasticity for the adhesive, the maximal plastic capacity is:

$$2 \cdot \tau_{VM} \cdot b \cdot l_{lap} = 2 \cdot \frac{\sigma_{VM}}{\sqrt{3}} \cdot b \cdot l_{lap} = 2 \cdot \frac{26}{\sqrt{3}} \cdot 150 \cdot 300 = 1351.00 \cdot 10^3 N \quad (12.9)$$

This is far larger than the plastic capacity of the plates. Therefore the load-displacement curve will flatten due to plastic behaviour of the plates and not due to plastic behaviour of the adhesive. For this reason the behaviour until the plastic capacity of the plates is practically linear.

Figure 12.5/Figure 12.7 show that elongation of the lap has no significant influence on the Von Mises strains at the decisive point. Therefore a longer lap will not result in a higher failure load. The most economical lap is the shortest lap ($l_{lap1} = l_{lap2} = l_{lap3} = 100 \text{ mm}$), hence that will be chosen.

The Drucker Prager criterion results in a higher failure load than the Von Mises criterion. Based on the FEM results the expected failure load is minimal 400 kN, which is 75% of the nominal plastic capacity of the plate.

13 Practice test of double strap connection

To verify the FEM calculations practice tests are performed. A sample size of five is assumed to be a proper balance between uncertainty (size of sample standard deviation) and economics. Therefore five identical double strap connections are tested. The first test piece is made as a trial, so that errors in the process will not lead to problems for all pieces. In this section all matters concerning the practice tests are described.

13.1 Design of test connection

The adhesive bonded double strap connection will be tested with a tensile test machine. This machine has a clamp which is 80mm wide and 90mm long. The width of the clamp is smaller than the test piece, therefore there is a 150mm free space between the clamp and the beginning of the lap. The space is assumed to be enough to spread the stresses and give a uniform stress state at the beginning of the lap.

To measure the displacement LVDT's are used. These LVDT's are placed at 50mm of the beginning and end of the lap, in the middle of the width. With the LVDT and the information of the tensile machine a load-displacement curve will be made.

For a detailed analysis digital image correlation (DIC) will be used. DIC will not be used for the trial piece. The trial piece provides some useful information to set the DIC equipment. The DIC method requires no special requirements concerning the design of the connection.

Taking the previous points into consideration the test connection is defined as the following figure.

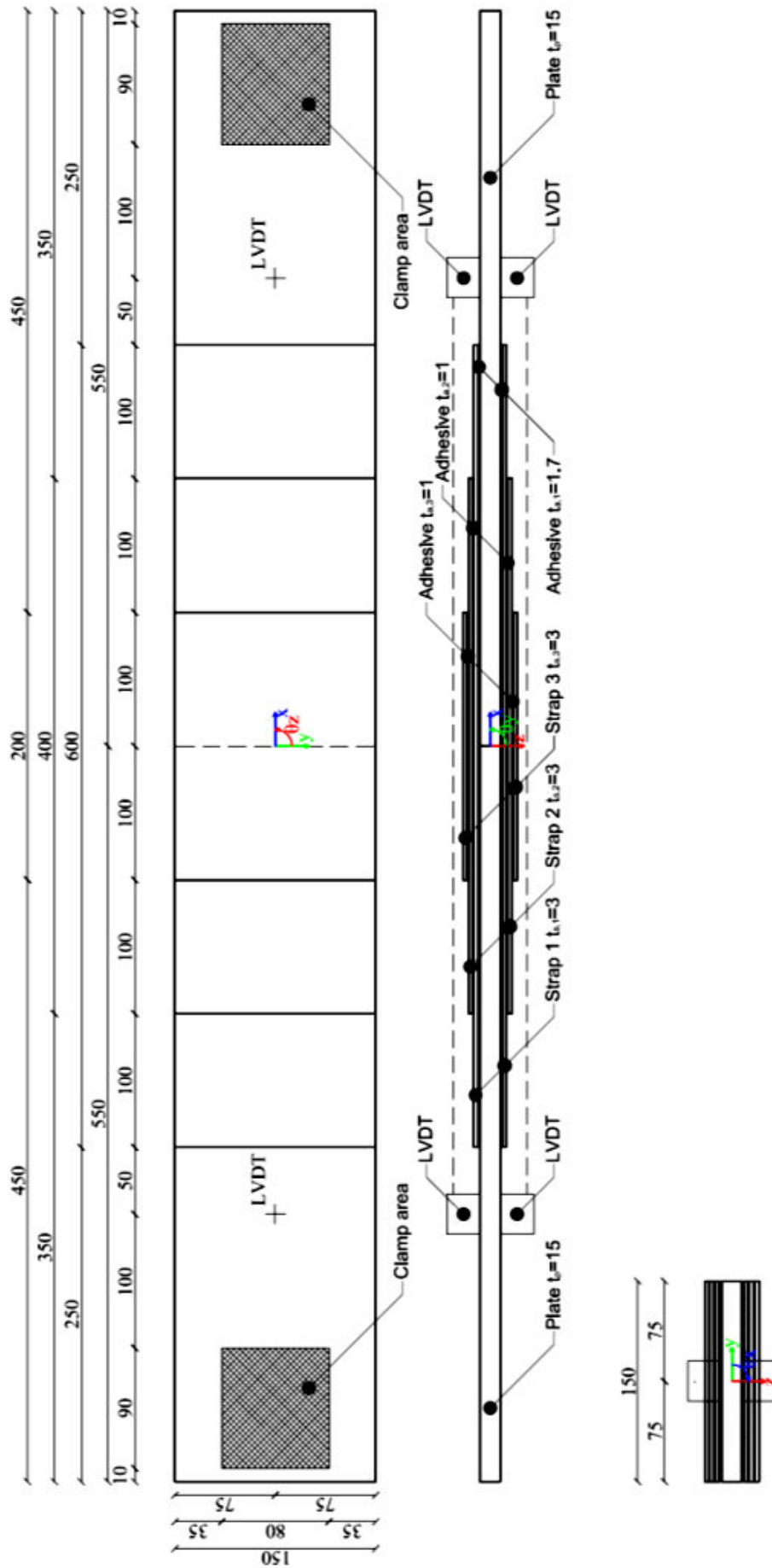


Figure 13.1: Design of test connection

13.2 Materials

The test detail exists of three types of material: adhesive, steel and spacers.

13.2.1 Adhesive

For the test the adhesive Sikadur®-30 (2 component, thixotropic, epoxy adhesive) is used.

$n_{\text{per detail}}$	n_{tests}	b in mm	l in mm	t_a in mm	$n_{\text{per detail}} n_{\text{tests}} b l t_a$ in L
2	5	150	600	1.7	1,53
2	5	150	400	1	0,60
2	5	150	200	1	0,30
Total					2,43

Table 13.1: overview of adhesive volume

Two sets of 6kg Sikadur®-30 are sponsored by Sika, which is good for $\pm 7,27$ litres. Note that to ensure proper filling of the adhesive layer, more adhesive should be applied than the volume of the adhesive layer. After producing the trial connection a ratio of 1.8 is set for the applied adhesive volume over the net adhesive layer volume ratio.

13.2.2 Steel

For the test detail steel grade S235 is used.

Grade	b in mm	t in mm	$n_{\text{per detail}}$	n_{tests}	l in mm
S235	150	15	2	5	550
		3	2	5	600
					400
					200

Table 13.2: Overview of steel measurements

13.2.3 Spacers

The spacers are made of stainless steel welding wire. Welding wire is available in a wide variety of measurements, cheap and available in each workshop. This makes welding wire a good pragmatic solution for spacers. The welding wire will run through the entire adhesive layer from one side to the other side.

t in mm	$n_{\text{per detail}}$	n_{tests}	$n_{\text{per detail}} n_{\text{tests}}$
1.7	4	5	20
1	8	5	40

Table 13.3: Overview of number of spacers

The total weight of one test piece is $\pm 28,5$ kg.

13.3 Equipment

Two types of equipment are used, fabrication and measuring equipment.

13.3.1 Fabrication equipment

1. Mould and stamps
2. Teflon foil
3. Separating foil
4. Clamps (8 for manufacturing of the straps and 8 for bonding the straps to the plates)
5. Mixing equipment
 - a. Weighing equipment to determine the right volume of adhesive component
 - b. Measuring cup
 - c. Mixing sticks
6. Rake to apply the adhesive

13.3.2 Measuring equipment

1. 2 LVDT's
2. DIC equipment
 - a. 2 cameras
 - b. Spackle spray
3. Load displacement controlled tensile machine
4. Computer to register measurements

13.4 Fabrication

The fabrication was carried out in the Delft Aerospace Structures and Materials Laboratory (DASML).

The actual bonding process consists of two major steps. First two straps are made. Then these straps are bonded to two plates. During the bonding process of the straps, the steel straps can 'float' on the adhesive which can cause misalignment and so a weaker connection. Therefore the steel will be 'locked' in a mould during the bonding process.

During the bonding process of the straps to the plate, floating is of less importance due to the vertical placement of the adhesive layer in combination with the heavier components.

In order to ensure no bonding of the mould and worktable, the contact surface will be covered with Teflon foil. Teflon foil is impermeable and does not bond to the adhesive. To ensure that the clamps and stamps are not bonded by or contaminated with the adhesive, the clamps and stamps are separated from the connection with separating foil.

As rake, an aluminium plate is used. The plate is cut out of waste material which is in stock in the DASML.

During the bonding process some of the adhesive between the steel is squeezed out. This surplus of adhesive is removed at the side because it has no function. At the end of the steel the surplus of adhesive helps to lower the peel stresses and is known as spew fillet (see section 5.3.5.8). Therefore the surplus of adhesive at the ends is not removed.

Hardening of the first connection took place in the hall of the Construction Laboratory of the Macromechanic laboratory, hardening of the other four connections took place in the hall of the DASML lab. At both halls moderate conditions applied (room temperature).

The fabrication can be divided in 7 steps:

1. Cutting of steel to right length (already done by the steel supplier)
2. Blasting of the steel to Sa2,5 (already done by the steel supplier)
3. Manufacturing of the mould and stamps
4. Manufacturing of the straps
5. Bonding of the straps to the plates
6. Abrasion of DIC side
7. Application of spackle pattern

13.4.1 Cutting of steel to right length

See Table 13.2 for measurements. The cutting was already done by the steel supplier.

13.4.2 Blasting of the steel to Sa2,5

To ensure good bonding the surface of the steel should have no contaminations, therefore the steel should be blasted to Sa2,5 by the steel supplier. The description according to table 1 of NEN-EN-ISO 8501-1-EN is: *'When viewed without magnification, the surface shall be free from visible oil, grease and dirt, and from mill scale, rust, paint coatings and foreign matter. Any remaining traces of contamination shall show only as slight stains in the form of spots or stripes.'* [57]

Due to the blasting process, the 3mm thick steel for the straps were deformed. With a manual roller the curves are straightened as much as possible. Twisted plates are straightened as much as possible with a vice and some hand power.

13.4.3 Manufacturing of the mould and stamps

The mould is made of timber. In the mould two straps can be made simultaneously next to each other. With more straps next to each other a uniform pressure by the clamps is harder to obtain.

The next figure shows the design of the mould:

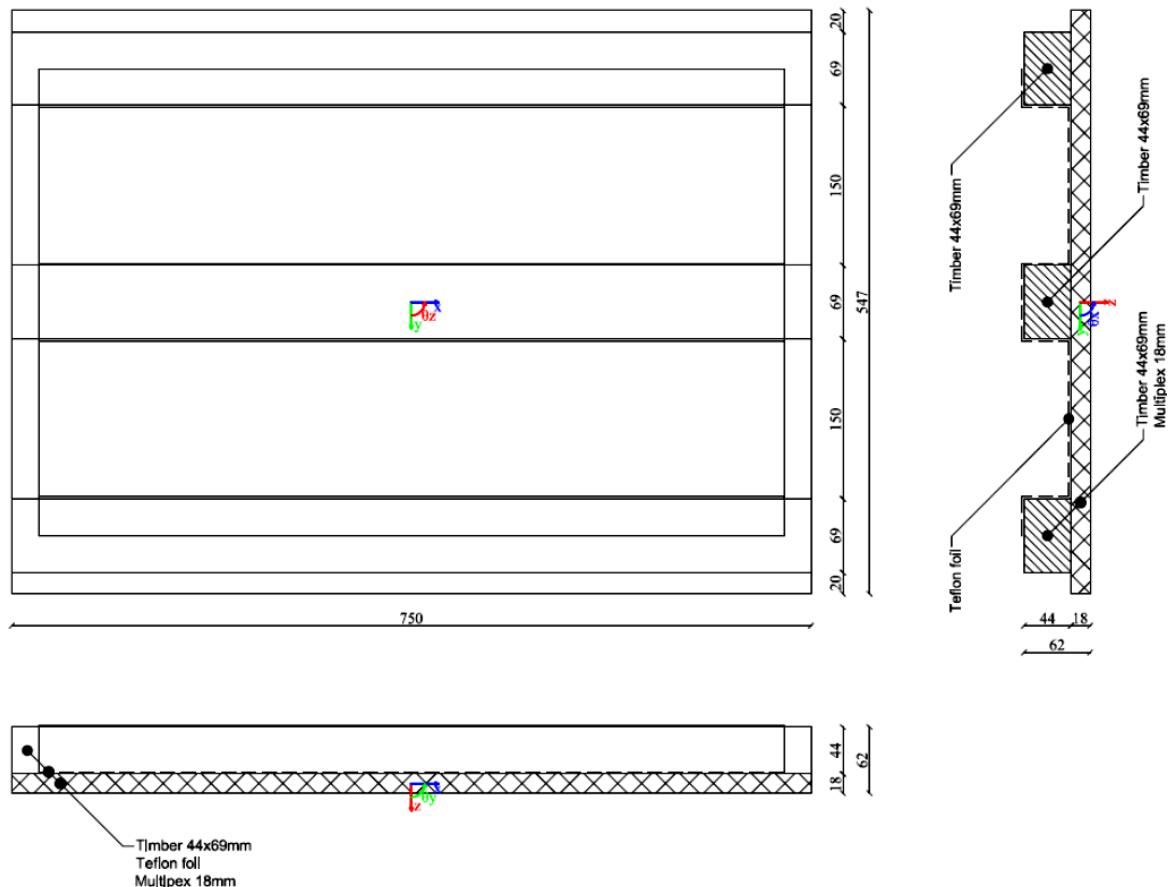


Figure 13.2: Design of mould

To be able to use the clamps properly, stamps were used. For manufacturing the straps, eight blocks and four beams are made out of the same type of timber beam as for the guiding beam of the mould. The blocks are made in such a way they fit in between the guiding beams of the mould ($l_{stampblock} \leq 150\text{ mm}$). The blocks are placed with their wide side on the straps so the clamp pressure of the beam can spread out. The beams are longer than the width of the mould

($l_{stampbeam} \geq 547 \text{ mm}$) for an easy placement of the clamps. These beams are placed on the blocks with their narrow side, so the beams are used in the stiffest way. In Figure 13.5 and Figure 13.6 the arrangement of the clamps and stamps for manufacturing the straps can be found.

For bonding the straps to the plates twelve blocks are made out of the same type of beam as for the other blocks and beams. The blocks are placed on the straps with their narrow side so the clamp pressure can spread out.

13.4.4 Manufacturing of the straps

The straps are made of three adhesive bonded steel plates. The next chronological steps are taken to manufacture the straps:

1. Covering of the mould in Teflon foil.
2. Degreasing of the steel, spacers and rake (for degreasing PF-QD Quick Drying Cleaning Solvent of Paint Services Group Ltd with a cloth is used).
3. Placement of the spacers of second adhesive layer at first steel strap ($y=30$ and $y=-30$, see Figure 13.3) with tape.
4. Placement of the spacers of third adhesive layer at second steel strap ($y=30$ and $y=-30$, see Figure 13.4) with tape.
5. Placement of the first steel strap in the mould.
6. Mixing of the two components of the adhesive (536g in total, 134g of component A and 402g of component B). The two components are thoroughly mixed by hand with a mixing stick in a plastic measuring cup.
7. Application of the second adhesive layer with a rake. The upper surface of the first and the lower surface of the second straps are smeared with adhesive.
8. Placement of the second steel strap on the first steel strap.
9. Application of the third adhesive layer with a rake. The upper surface of the second and the lower surface of the third straps are smeared with adhesive.
10. Placement of the third steel strap on the second steel strap in the mould.
11. Removing of the tape which holds the spacers.
12. Placement of the separating foil to ensure no bonding of the clamps and stamps.
13. Placement of the stamps and tightening of the clamps (see Figure 13.5 and Figure 13.6).
14. Removing the clamps when the adhesive has some strength (one day).
15. Removing the surplus of adhesive at the sides (y -plane) by abrasion.
16. Removing the surplus of spacers.

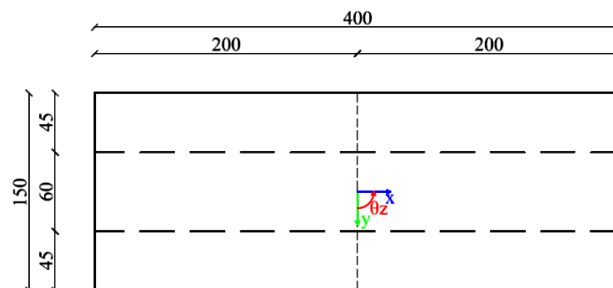


Figure 13.3: Placement of spacers at adhesive layer 2

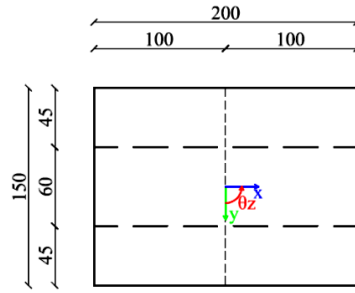


Figure 13.4: Placement of spacers at adhesive layer 3

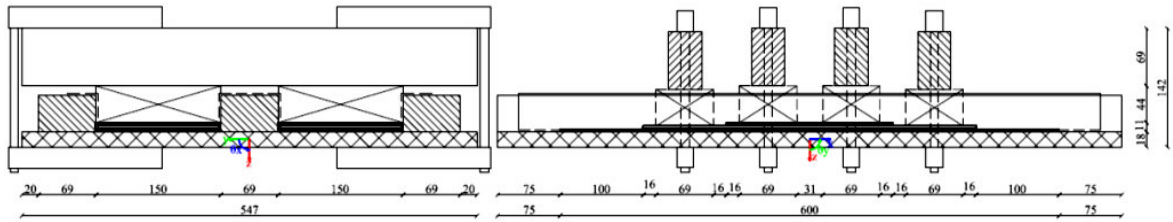


Figure 13.5: Bonding of straps (sections)

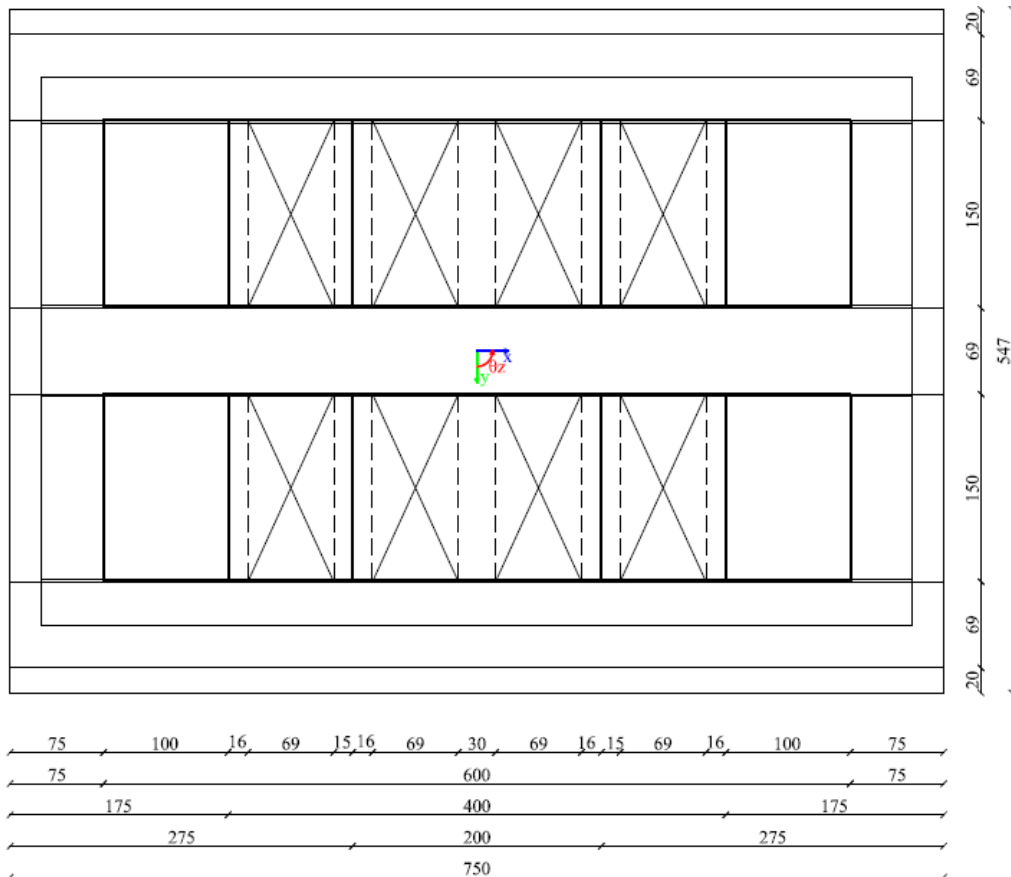


Figure 13.6: Bonding of straps (top view)



Figure 13.7: Pictures of the manufacturing of the straps; application of spacer with tape, outflow of the adhesive after tightening the clamps and mould with straps during hardening

13.4.5 Bonding of the straps to the plates

The next chronological steps are taken to bond the straps to the plates:

1. Placement of Teflon foil on the worktable to ensure no bonding between the connection and worktable.
2. Degreasing of the steel, spacers and rake (for degreasing PF-QD Quick Drying Cleaning Solvent of Paint Services Group Ltd with a cloth is used).
3. Placement of spacers at both steel straps ($y=30$ and $y=-30$, see Figure 13.8). The spacers are bent around the straps and fixed with tape.
4. Placement of the plates on the Teflon foil, aligning them and tightening clamps on the ends to prevent the plates from tipping over.
5. Mixing of the two components of the adhesive (912g, 228g of component A and 684g of component B). The two components are thoroughly mixed by hand with a mixing stick in a plastic measuring cup.
6. Application of the adhesive for both first adhesive layers with a rake. The straps contact surface and both of the plate surfaces are smeared with adhesive.
7. Placement of the straps against the plates.
8. Removing the tape which holds the spacers.
9. Placement of the separating foil to ensure no bonding of the clamps and stamps.
10. Placement of the stamps and tightening of the clamps (see Figure 13.9).
11. Removing the clamps when the adhesive has some strength (one day).
12. Removing the surplus of adhesive at the sides (y -plane) by abrasion.
13. Removing the surplus of spacers.

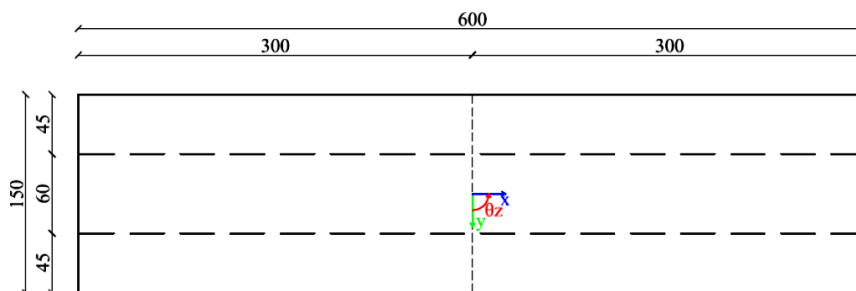


Figure 13.8: Placement of spacer at adhesive layer 1

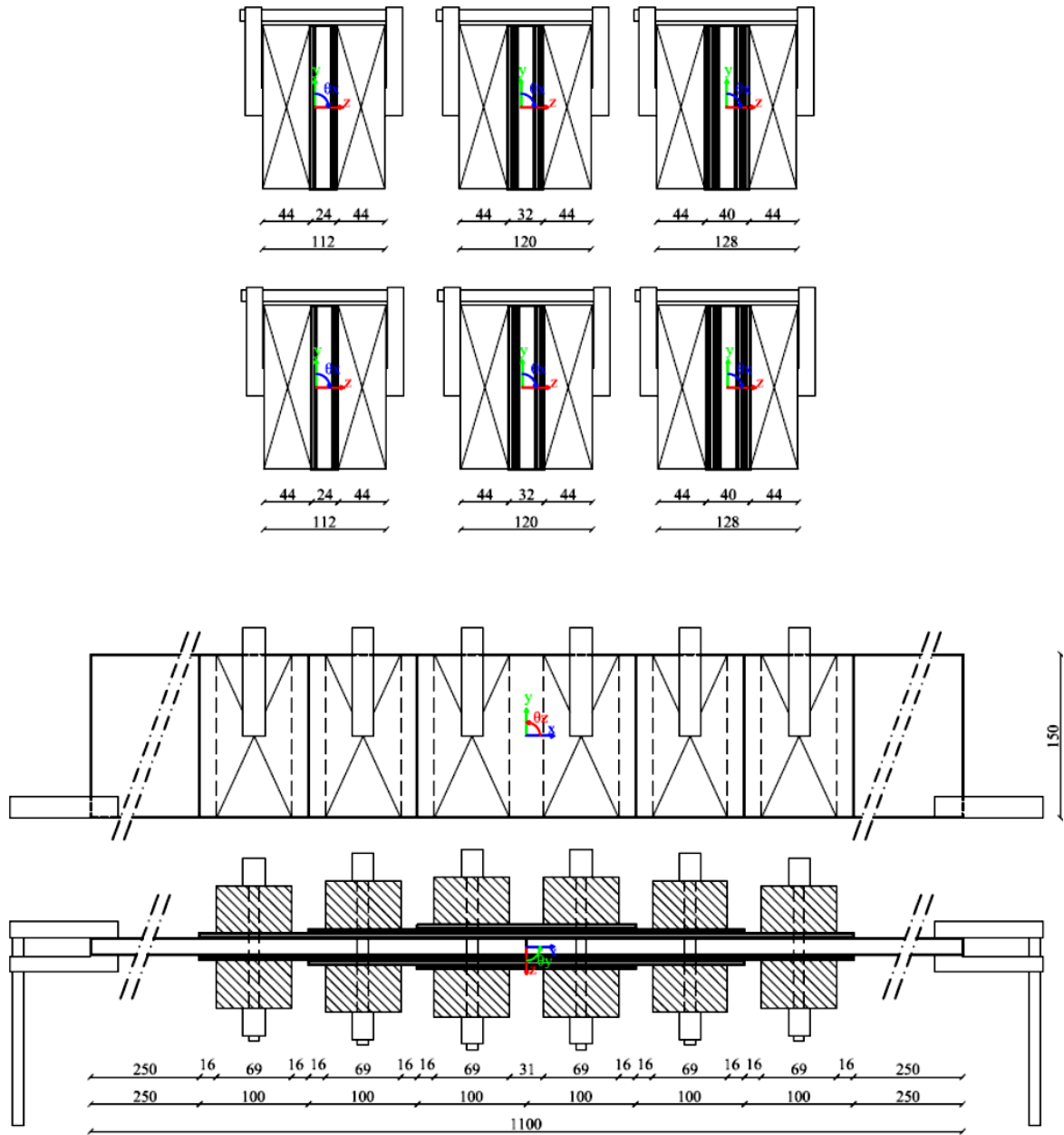


Figure 13.9: Bonding of straps to plates; front view, side view and top view



Figure 13.10: Pictures of the bonding of the straps to the plates; application of spacer with tape, outflow of the adhesive after tightening the clamps and connection during hardening

13.4.6 Abrasion of DIC side (at L&R)

To ensure a flat surface for the spackle pattern, the side at which the spackle spray is applied is abraded.

13.4.7 Application of spackle pattern (at L&R)

The spackle pattern is applied by a spray.

13.5 Practice test

In total 5 test are performed. For all tests LVDT's are used. For two tests DIC is also used. DIC is used at a side (y-plane) of one connection and at the top (z-plane) of another connection. All test are executed at room temperature.

13.5.1 DIC

The DIC method compares the spackle pattern of pictures made during testing. These pictures are made at a fixed interval. To ensure a clear image of the movement of the spackle pattern two camera's are used. DIC (Digital Image Correlation) will be used to measure the displacements and strains. With the used DIC equipment an area with a maximum of 500x500mm can be observed. Below $\pm 90\%$ of the failure load the behaviour of the symmetric parts will be almost the same. Failure will probably take place at a discontinuity in the adhesive; the exact place is hard to predict. Therefore the exact place and the related local displacements and strains of failure are of less interest. A complete picture of the entire connection is not needed to get a clear picture of the behaviour of the connection. An area of 500x500mm is enough to get an image of the half of the lap at one side of a test piece. Therefore the DIC measurement are taken at one half of the lap.

13.5.2 Test setup

A 600 kN hydraulic press made by Schenck PCX is used for testing. [58]

For the LVDT's docking stations are used. In between the docking stations and the plate a sandpaper is placed according to the placement of Figure 13.1. Then the two docking stations are connected so the sandpaper is compressed between the docking station and plate. The sandpaper ensures that the docking station follows the movement of the connection at the desired place.

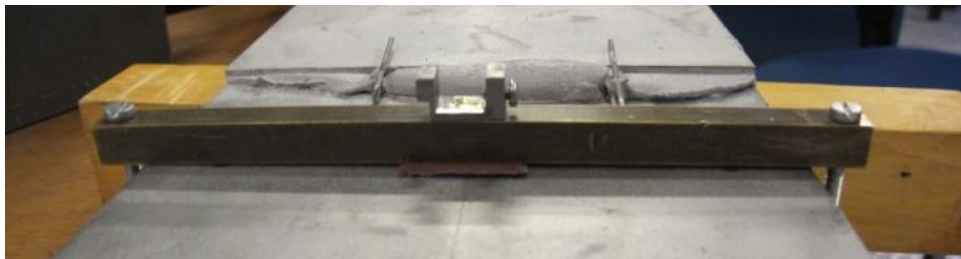


Figure 13.11: Placement of docking station for LVDT

After the connection is placed in the clamps of the tensile testing machine the actual LVDT's are placed. The measuring unit (the actual LVDT) is placed at the upper docking station. A steel rod with a sleeve is placed in the lower docking station. The LVDT is placed inside the sleeve of the rod. The sleeve is now adjusted in such a way that the LVDT is completely compressed. During testing the sleeve moves away from the LVDT. The LVDT measures this movement.



Figure 13.12: Placement of LVDT and steel rod with sleeve

A computer combines the data of the LVDT and the tensile machine in a table.

For test 2 and 4 also DIC is used for measuring. Before testing a white paint layer is sprayed on the measuring area, after that a (irregular) spackle pattern is sprayed on top of the white layer. After the connection is placed in the tensile test machine lamps are placed to ensure proper lighting. Two camera's are placed on a tripod. After aligning and adjusting the camera's they are calibrated. The computer which registers the camera images also register the LVDT and load.

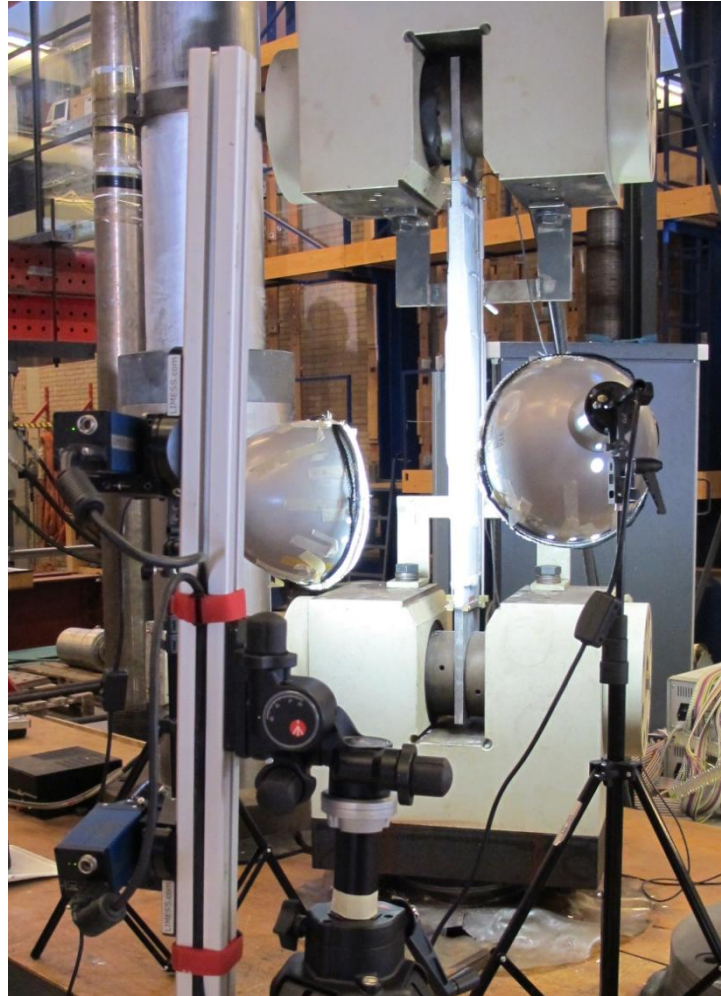


Figure 13.13: Picture of DIC equipment at test 4 (camera in the left front and two lamps)

In the table below an overview of the fabrication and testing dates can be found:

Connection	Manufacturing of straps	Bonding of straps to plate	Execution of test
1	31-1-2014 + 3-2-2014	5-2-2014	17-2-2014
2	19-2-2014	21-2-2014	16-4-2014
3	20-2-2014	24-2-2014	16-4-2014
4	24-2-2014	26-2-2014	16-4-2014
5	25-2-2014	27-2-2014	16-4-2014

Table 13.4: Dates of fabrication and testing

13.6 Test results

The test results can be divided in two parts, the observation and the measurements. Both can be found in this section.

13.6.1 Observations

Observations made during and after the tests are important for a proper conclusion. For each test the observations are written down below.

13.6.1.1 Test 1

Test 1 is executed with a displacement load of $1 \cdot 10^{-3} \text{ mm/s}$. Until failure, no crack development was visually or auditively observed. After roughly an hour the connection fails with an extremely loud bang. After failure, at one side the outer steel plates of the straps is completely torn of the rest of the connections, at the other side two of the outer steel plates of the straps are completely torn of the rest but are still bonded to each other. In all adhesive layers cracks arose, see section 31.3 for pictures.

During the test, the rolling door of the lab has been open for a short period of time. During that period cold air ($\pm 6^\circ\text{C}$) entered the lab. Due to the cold air, the steel rod of the LVDT shortens which is registered by the LVDT. The influence can be seen in the load-displacement curve, see Figure 13.14 at $(0.25, 255)$ and $(0.35, 330)$.

In Figure 13.14 can be seen that the two LVDT's measure about the same values up to point $(0.59, 475)$. After that LVDT 2 measures a bigger elongation of the lab than LVDT 1.

13.6.1.2 Test 2

Test 2 is executed with a displacement load of $2 \cdot 10^{-3} \text{ mm/s}$. During testing DIC is used at the front of the connection. Until failure, no crack development was visually observed. Small cracking sounds where observed around 322kN, but no differences in the load-displacement curve occurred. After roughly half an hour the connection fails with an extremely loud bang. After failure the most outer plate of a strap is completely torn of the rest of the connection. In the other adhesive layers cracks and/or delamination arose, see section 31.3 for pictures.

13.6.1.3 Test 3

Test 3 is executed with a displacement load of $2 \cdot 10^{-3} \text{ mm/s}$. Until failure, no crack development was visually observed. Small cracking sounds where observed around 281kN, but no differences in the load-displacement curve occurred. After roughly a half an hour the connection fails with an extremely loud bang. During failure complete delamination arose of the strap-plate interface at one side of one plate and at the other side of the other plate, in Z-shape so to speak. In the rest of the adhesive layers cracks and/or delamination arose, see section 31.3 for pictures.

13.6.1.4 Test 4

Test 4 is executed with a displacement load of $2 \cdot 10^{-3} \text{ mm/s}$. During testing DIC is used at one side of the connection. Until failure, no crack development was visually or auditively observed. After roughly half an hour the connection fails with an extremely loud bang. After failure the most outer plate of a strap is completely torn of the rest of the connection and a large Z-shape crack arose just as for test 3. In the rest of the adhesive layers cracks and/or delamination arose, see section 31.3 for pictures.

13.6.1.5 Test 5

Test 5 is executed with a displacement load of $2 \cdot 10^{-3} \text{ mm/s}$. Until failure, no crack development was visually or auditively observed. After roughly half an hour the connection fails with an extremely loud bang. During failure complete delamination arose of the strap-plate interface at one side of one plate and at the other side of the other plate, in Z-shape so to speak. In the rest of the adhesive layers only small cracks arose, see section 31.3 for pictures.

13.6.2 Overview of test results

In the figure below the load-displacement curves of the tests out of the data from the LVDT and tensile test machine can be found:

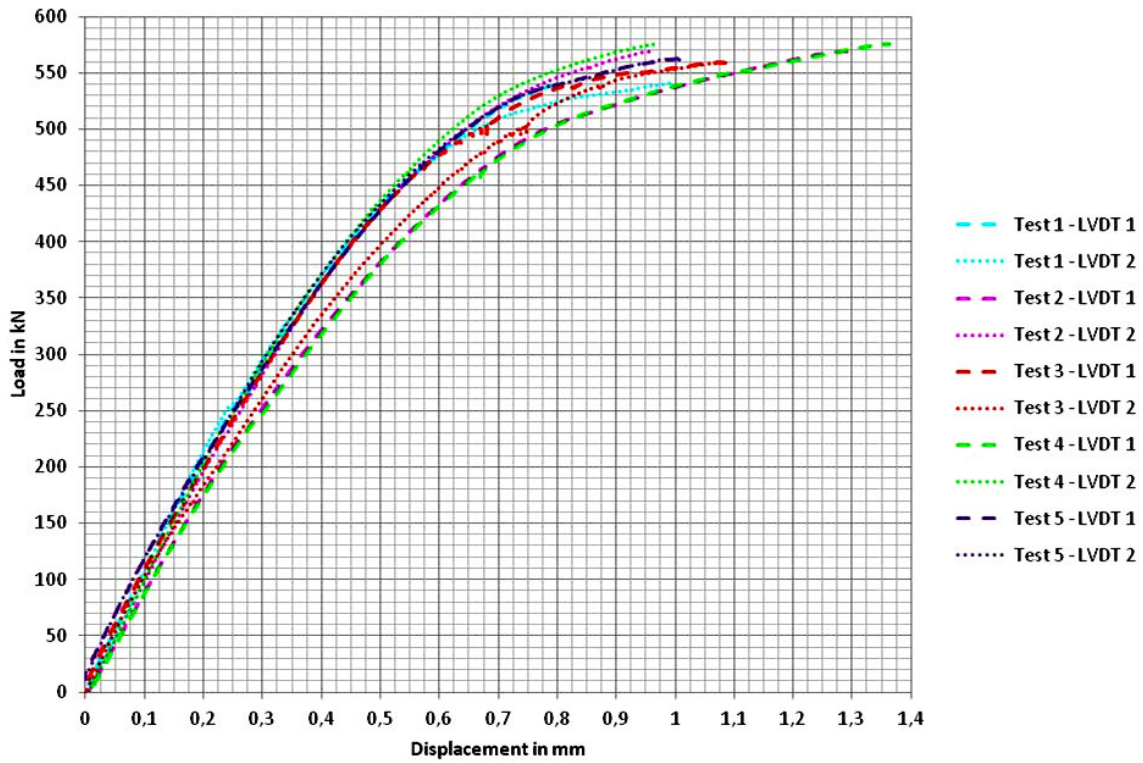


Figure 13.14: Load-displacement curves of practice tests

In the next table the results of the tensile test machine and LVDT's can be found.

i	$F_{u,i}$ in kN	$u_{u,LVDT1,i}$ in mm	$u_{u,LVDT2,i}$ in mm	$u_{u,ave,i}$ in mm
1	541.559554	0.806169	0.997661	0.901915
2	568.586243	1.299306	0.959567	1.129437
3	575.869227	1.87274	1.081413	1.477077
4	559.027432	1.362616	0.968408	1.165512
5	561.970058	1.012115	1.007777	1.009946

Table 13.5: Overview of test data of tensile test machine and LVDT's

13.6.3 DIC results

In 'Appendix P: DIC results' an overview of DIC images can be found. To compare the DIC images similar FEM images are made of the 3-3-3 DP 300 model, see section 29.5.

In Table 32.1 and Table 29.1 the strains in lateral direction of the front view can be found. A real distinctive pattern is not observed with DIC but the last image looks a bit like the FEM pattern (positive peaks near the corner of the lap end and negative peaks near the corner of the step above).

In Table 32.2 and Table 29.2 the strains in axial direction of the front view can be found. The DIC images show only a clear difference for the last three images. The strain rises near the end of the laps, especially near the end of the first lap and near the middle of the third lap (transition of thick plates).

In Table 32.3 and Table 29.3 the shear strains of the front view can be found. A real distinctive pattern is not observed with DIC.

In Table 32.4 and Table 29.4 the strains in lateral direction of the side view can be found. The DIC images show some small increase near the lap ends, and at the last two images a clear hot spot near the end of the first strap is visible. Although a crack arises at this hot spot, this is not the place of main failure. In Figure 31.45 two pictures of this location can be found. Complete delamination took place at the other adhesive layer.

In Table 32.5 and Table 29.5 the strains in axial direction of the side view can be found. The DIC images show a clear pattern. The strains are large where the axial area is small and near the end of a lap there is a small hot spot. Also the development of the crack can be observed.

In Table 32.6 and Table 29.6 the shear strains of the side view can be found. Also here the DIC images show the same pattern as for the axial and lateral strains.

13.6.4 Statistical analysis

With the data of Table 13.5 the probability density function and cumulative density function can be deduced. First it is assumed that the student's t-distribution applies, which applies for normally distributed data with a small sample size and unknown standard deviation. Five tensile tests are executed so the sample size is 5:

$$n = 5 \quad (13.1)$$

The standardised probability density function of the student's t-distribution is given by:

$$p_\nu(x) = \frac{\Gamma\left(\frac{\nu+1}{2}\right)}{\sqrt{\nu\pi}\Gamma\left(\frac{\nu}{2}\right)} \left(1 + \frac{x^2}{\nu}\right)^{-\frac{\nu+1}{2}} \quad (13.2)$$

Where ν is the number of degrees of freedom, defined by:

$$\nu = n - 1 \quad (13.3)$$

And where $\Gamma(x)$ is the gamma function which is defined by:

$$\Gamma(x) = \int_0^{\infty} e^{-z} z^{x-1} dz \quad (13.4)$$

For the domain of interest ($x > 0 \in \mathbb{R}$), the gamma function simplifies to:

$$\Gamma(x) = (x-1)! \quad (13.5)$$

Instead of the standardised student's t-distribution, the non-standardised student's t-distribution can be used. The values of the probability density function and cumulative density function then no longer need to be converted. The non-standardised probability density function of the student's t-distribution is given by:

$$p_{\nu,\mu,\sigma}(x) = \frac{\Gamma\left(\frac{\nu+1}{2}\right)}{\Gamma\left(\frac{\nu}{2}\right)\sigma\sqrt{\nu\pi}} \left(1 + \left(\frac{x-\mu}{\sigma\sqrt{\nu}}\right)^2\right)^{-\frac{\nu+1}{2}} \quad (13.6)$$

Where μ is a location parameter given by the mean value:

$$\mu = \bar{x} = \frac{1}{n} \sum_{i=1}^n x_i \quad (13.7)$$

Where σ is a scaling parameter given by:

$$\sigma = \frac{s}{\sqrt{n}} \quad (13.8)$$

With the sample standard deviation:

$$s = \sqrt{\frac{1}{n-1} \sum_{i=1}^n (x_i - \bar{x})^2} \quad (13.9)$$

In the case of a sample size of five the non-standardised probability density function becomes:

$$p_{5,\mu,s}(x) = \frac{3\sqrt{5}}{8s} \left(1 + \frac{5}{4} \left(\frac{x-\mu}{s} \right)^2 \right)^{-\frac{5}{2}} \quad (13.10)$$

Where is made use of:

$$\Gamma\left(\frac{\nu+1}{2}\right) = \Gamma\left(\frac{5}{2}\right) = \frac{3}{4}\sqrt{\pi} \quad (13.11)$$

$$\Gamma\left(\frac{\nu}{2}\right) = \Gamma(2) = 1 \quad (13.12)$$

For the exact determination of the probability density function now only the mean value and sample standard deviation of the data have to be computed.

$$\bar{x}_F = \bar{F}_u = \frac{1}{n} \sum_{i=1}^n F_{u,i} = 561.402503 \text{ kN} \quad (13.13)$$

$$s_F = \sqrt{\frac{1}{n-1} \sum_{i=1}^n (F_{u,i} - \bar{F})^2} = 12.851050 \text{ kN} \quad (13.14)$$

$$\bar{x}_u = \bar{u}_{u,ave} = \frac{1}{n} \sum_{i=1}^n u_{u,ave,i} = 1.136777 \text{ mm} \quad (13.15)$$

$$s_u = \sqrt{\frac{1}{n-1} \sum_{i=1}^n (u_{u,ave,i} - \bar{u}_{u,ave})^2} = 0.216754 \text{ mm} \quad (13.16)$$

Sometimes the coefficient of variance instead of the sample standard deviation is used as measure of scatter. The coefficient of variance for sample data is given by:

$$c_v = \frac{s}{\bar{x}} \quad (13.17)$$

Hence:

$$c_{v,F} = \frac{s_F}{\bar{F}} = 0.022891 \quad (13.18)$$

$$c_{v,u} = \frac{s_u}{\bar{u}_{u,ave}} = 0.190674 \quad (13.19)$$

In general the cumulative density function is given by:

$$P(x) = \int_{-\infty}^x p(u) du \quad (13.20)$$

The next figures follow from (13.10) and (13.20) with (13.13)/(13.16).

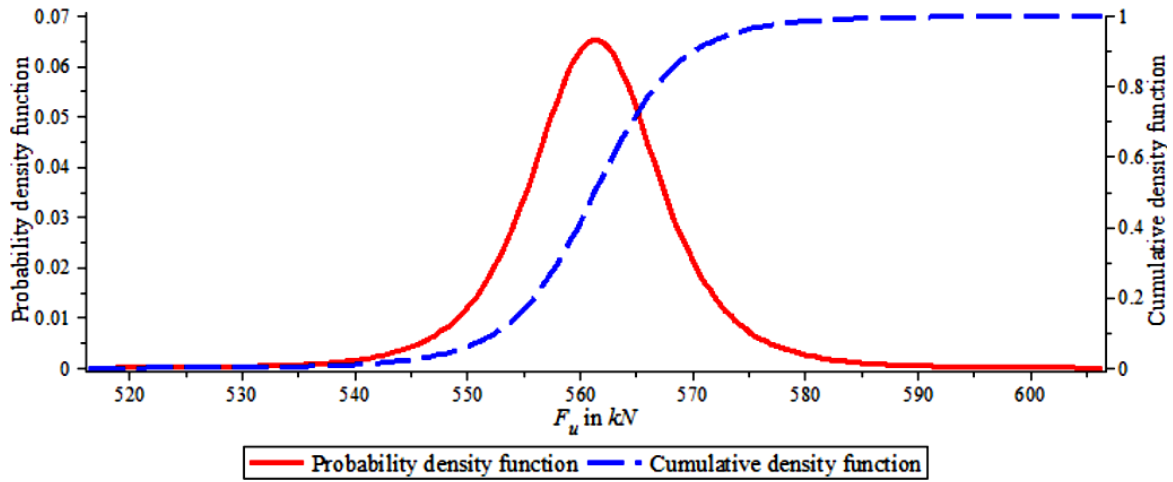


Figure 13.15: Probability density function and cumulative density function of the force

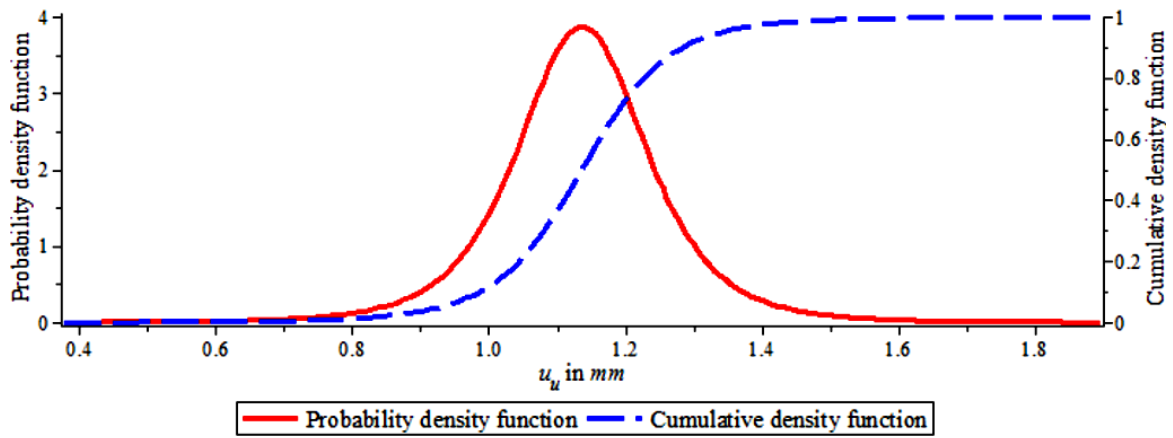


Figure 13.16: Probability density function and cumulative density function of the displacement

To find the exact force and displacement which belongs to the 5th-percentile, the next equations have to be solved:

$$F_{v,\mu_F,\sigma_F}(x_F) = 0.05 \rightarrow x_F = 549.149761 \text{ kN} \quad (13.21)$$

$$F_{v,\mu_u,\sigma_u}(x_u) = 0.05 \rightarrow x_u = 0.930125 \text{ mm} \quad (13.22)$$

The value of the cumulative density function which belongs to the nominal plastic capacity of the plates is:

$$F_{v,\mu_F,\sigma_F}(x_F = F_{d,pl,plate} = 528.75) = 0.002369 \quad (13.23)$$

In the next table an overview of important statistical values can be found:

	Ultimate load	Ultimate strain
average	561.402503	1.136777
s	12.851050	0.216754
c_v	0.022891	0.190674
5th percentile	549.149761	0.930125

Table 13.6: Overview of statistical values

13.6.5 Conclusion

No significant differences are observed during testing. The failure load of the five tested connections are relative close to each other (34.3kN or 6%) and relative high (549.15kN for the 5th percentile). From this it may be concluded that the design, material choice and fabrication was good.

Failure for all connections is imposed by adhesion failure (failure of the adhesive adherent interface). For most adhesive layers after failure, cracks where observed at the end of the lap and propagate further towards the middle of the lap. Three of the five tested connections fail with a clear Z-shape, but this is not sufficient evidence to conclude that this is the main failure behaviour. Especially due to the brittle behaviour of the adhesive.

The stiffness behaviour of the connection, see Figure 13.14, is best described by a bilinear model.

Based on (13.23) in $(1 - 0.002369) \cdot 100 = 99.7631\%$ of the connections will fail at a higher load than the nominal plastic capacity of the plates.

14 Comparison of FEM and practice test results

In the next figure the load-displacement curves of the FEM and practice tests can be found:

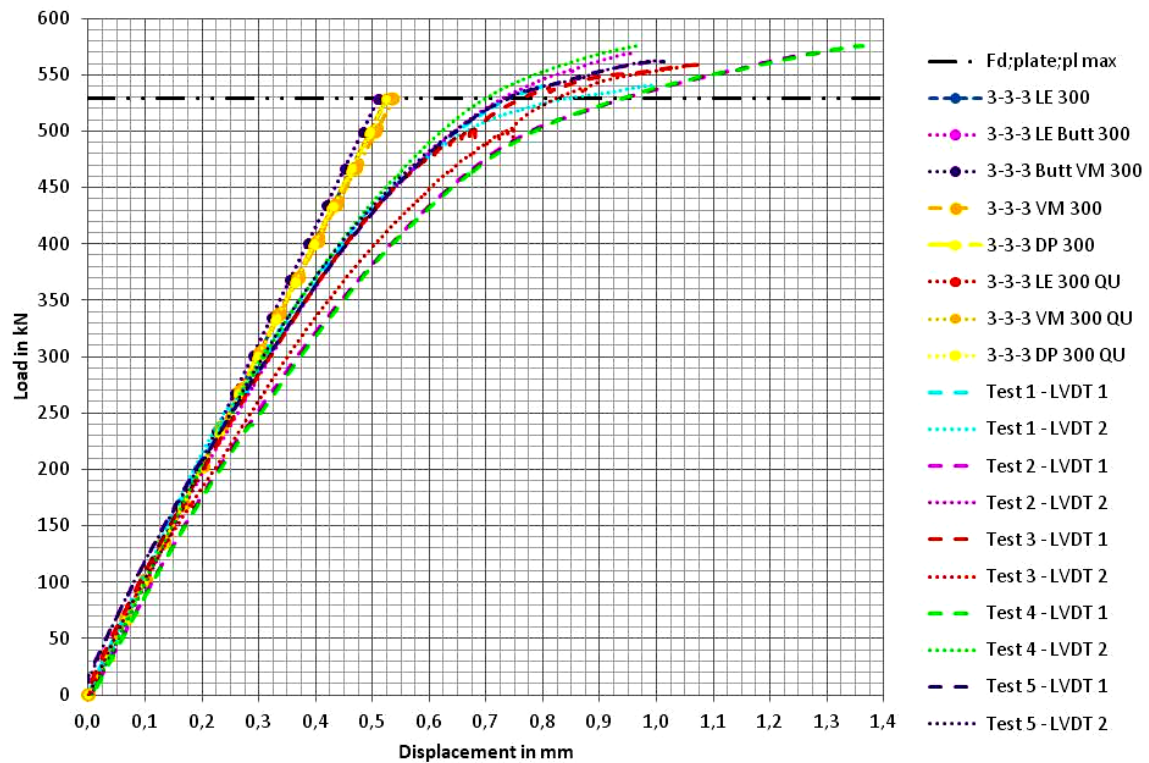


Figure 14.1: Load-displacement curve of FEM and practise test

Based on the figure above, it can be said that the FEM calculations predict the onset of the load-displacement curve well. With the chosen parameters on material models, the FEM calculation fails to predict the rest of the load-displacement curve accurately. The Von Mises material model describes the behaviour of steel very well. For adhesives there is no consensus about the best material model. Therefore most likely the behaviour of the adhesive is not modelled well or the parameters are chosen incorrectly.

15 Conclusions and recommendations

The goal of this research is to investigate the possibilities and difficulties for structural adhesive bonding in structural engineering. A literature study, FEM calculations and five practice tests are executed to achieve this. All the research questions can now be answered based on this research:

- The advantages and disadvantages of special interest for structural engineering are listed on the next page.
- Structural adhesives are polymers, additives to influence the properties may be used.
- Adhesive bonding takes place through mechanical adhesion (interlocking) or specific adhesion (chemical, adsorptive, diffusive and electrostatic).
- Lap connections transfer the load through shear. Long laps are prone to shear lag. Due to eccentricity of the line of work, peel stresses develop at the end of a lap.
- In the recommendations section the points of attention for designing structural engineering applications are listed.
- Adhesive bonded connections are especially suitable for:
 - Composite, hybrid and laminated structures;
 - Lengthening of steel beams;
 - Fatigue sensitive steel structures;
 - Aesthetics;
 - Thin elements;
 - Small tolerances;
 - Light weight structures;
 - High strength steel (HSS).
- The executed tests show that adhesive bonding have a good potency to play a role in commonly used steel-to-steel connections.

15.1 Conclusions

From this research several conclusions can be drawn. They can be divided in the more general conclusions drawn from the literature review (Part A), the conclusions drawn from the research on the L-connection and the conclusions drawn from the research on the double strap connection.

15.1.1 General for structural engineering

There is little information about adhesive bonded structural engineering applications in general. The information that is available mostly focuses on specific applications, which is in line with the practical applications. The reasons for the few and specific applications can be found in the advantages and disadvantages of structural adhesive bonded connections. The most important advantages for existing structural engineering applications are (as mentioned before) the ability to bond all kinds of materials, the ability to bond different kinds of materials and the increase of the fatigue life.

For the civil field of work a number of disadvantages are of special interest. Maybe the most important disadvantage is the lack of knowledge. Today no design rules, codes or directives exist for structural adhesive bonded connections for structural engineering applications. Moreover, the stress levels in the adhesive are hard to predict, especially at the decisive adherent-adhesive interface. Both facts make it hard for an engineer to prove the strength of a connection. In addition, there is little or no experience among contractors and engineers, which is a breeding ground for stick-in-the-muds. Then, the choice for a different type of connection will be made easily.

Structural engineering applications are characterised by large profiles. Firstly, large profiles have large tolerances. High strength adhesive bonding requires a thin adhesive layer. These two points are hard to combine. Secondly, large profiles lead to rather large internal eccentricities for lap

connections. Which leads to high peel stresses. Adhesives are stronger in shear and compression than in tension. Therefore, tension stresses should be as low as possible for adhesive bonded connections. Thirdly, large profiles lead to a high axial load per unit width for lap connections. Due to shear lag it is hard to transfer such high loads.

Most structural engineering applications are designed for a service life of 50 or 100 years. The time-and-environment depended effects are of special interest then. But for such long time spans, an exact calculation/estimation of the time-and-environment depended effect is not yet possible. However, the properties of most adhesives are strongly time-and-environment depended. In general, the decrease in strength of adhesives used for structural engineering applications will be substantial. Especially extreme conditions, such as fire, require more attention than for steel and concrete. But it should be noted that adhesive bonding is widely used in the aerospace industry with more extreme service conditions than those for civil industry.

In general, structural adhesive bonding requires a pre-treatment of the adherents. The adherents should be as clean as possible to ensure bonding of the actual adherent instead of bonding the contaminated layer. Pre-treating at a construction site is inconvenient. But nowadays, the actual construction increasingly takes place at the workshop instead of at the construction site. Therefore pre-treatments become easier to realise.

Most adhesives exhibit a substantial curing time under normal indoor conditions which extends the building time on the construction site. But concrete also exhibits a substantial curing time. For concrete and most adhesives the curing time can be shortened drastically by elevated temperatures, frequently used for the tunnel form construction method. Moreover, optimal curing conditions provides a higher adhesive final strength.

Although there are countless types of adhesives available, only a few are tailored/suitable for structural engineering. This is a matter of supply and demand. If adhesives prove themselves by further research the adhesive suppliers probably will tailor adhesives for structural engineering.

Summarised, the advantages of adhesive bonds which are of special interest for structural engineering are:

- Ability to bond all kinds of materials;
- Ability to bond different kinds of materials;
- Increase of the fatigue live.

Summarised, the next points specifically for structural engineering, complicates the use of adhesive bonding:

- Lack of knowledge and regulations tailored for structural engineering;
- Large profiles with the associated large tolerance;
- Long life spans of structures;
- Pre-treatments are required;
- Cure time of adhesive.

15.1.2 L-connection

Tension stresses are hard to avoid for column-to-beam connections. For floor X- and T-connections and roof T-connections a continuous floor/roof beam is beneficial with respect to tension stresses. Accurate FEM calculations of entire beam-to-column connections with commercial computers available nowadays is practically impossible. The maximal possible RAM is insufficient for a small mesh which is required to calculate exact stress and strain levels. Obtaining exact stress distributions is therefore impossible.

From calculations of an L-connection with a coarse mesh follows that lengthening of the laps is insufficient, due to shear lag, and that load transfer mainly takes place near the webs as one would expect. The shape of these stress distributions can be explained well by some differential equations. Exploratory FEM calculations showed no significant benefits of bevelled and tapered

angle cleats. The difference in axial stiffness of the angle cleat and H-profile near the web is very large. A change in the axial stiffness of the angle cleat as a result of bevelling or tapering shows not to be sufficient enough to reduce the shear lag effect. To find an efficient way to transfer the loads seems to be the biggest challenge.

Summarised:

- For floor X- and T-connections and roof T-connections a continuous floor/roof beam is beneficial with respect to tension stresses.
- Accurate FEM calculations of entire beam-to-column connections require a very large RAM.
- Load transfer mainly takes place near the ends (due to shear lag) and near the web (due to locally higher axial stiffness).

15.1.3 Double strap connection

According to the test results a double stepped strap connection is an effective way to transfer tensile loads. Out of five tensile tests a 5th percentile ultimate failure load of 549.15 kN is achieved. For comparison the nominal load of the plates is $15 \cdot 150 \cdot 235 \cdot 10^{-3} = 528.75 \text{ kN}$.

But some remarks should be made. The test is performed at moderate indoor conditions, with a short-time load case and relatively short after fabrication. These are ideal conditions. In a practical situation time-and-environmental dependent effects will influence the ultimate failure load of the connection. The supplier of the adhesive mentioned that, generally due to creep a 20-25% lower failure load should be assumed. [49] Due to environmental effects most adhesives exhibit at least a 15% smaller failure load. So the maximum for the design load is: $0.8 \cdot 0.85 \cdot 549.15 = 373.42 \text{ kN}$.

But also now some remarks should be made. Due to creep the effectiveness of the mid part of the lap will increase, so longer laps will be more effective. Longer laps can be designed to compensate the effects due to creep. Also a higher steel grade for the plate can be chosen. A 10mm thick plate of S355 has nearly the same capacity as a 15mm thick plate of S235:

$$\left. \begin{array}{l} t = 15 \text{ \& } S235 \\ t = 10 \text{ \& } S355 \end{array} \right\} \rightarrow F_{nom pl} = t \cdot b \cdot f_y \rightarrow \begin{cases} 15 \cdot 150 \cdot 235 = 528.75 \cdot 10^3 \text{ N} \\ 10 \cdot 150 \cdot 355 = 532.50 \cdot 10^3 \text{ N} \end{cases} \quad (15.1)$$

But a 10mm plate has smaller tolerances which results in a smaller adhesive thickness. Moreover the axial stiffness differences will increase which increases the effectiveness of the outer steel straps. Both are beneficial for the failure load.

Failure of the connections is induced by adhesion failure/delamination (failure of adhesive adherent interface). This is in accordance with other research results, which show that the interface is the place with the highest stress levels. It can be concluded that the adhesion strength of the adhesive to the steel is lower than the cohesive strength. Otherwise the adhesive close by the interface should have failed and a thin adhesive residue layer should be visible on the steel. Which is not the case. With a better/other pre-treatment and/or the use of a primer, the adhesion strength and so the failure load may be increased.

The load-displacement behaviour of the connection, see the figure below, is best described by a bilinear model. The FEM models only succeed to describe the behaviour up to around 50% of the failure load. After that the load-displacement curve of the practice test slowly flattens out.

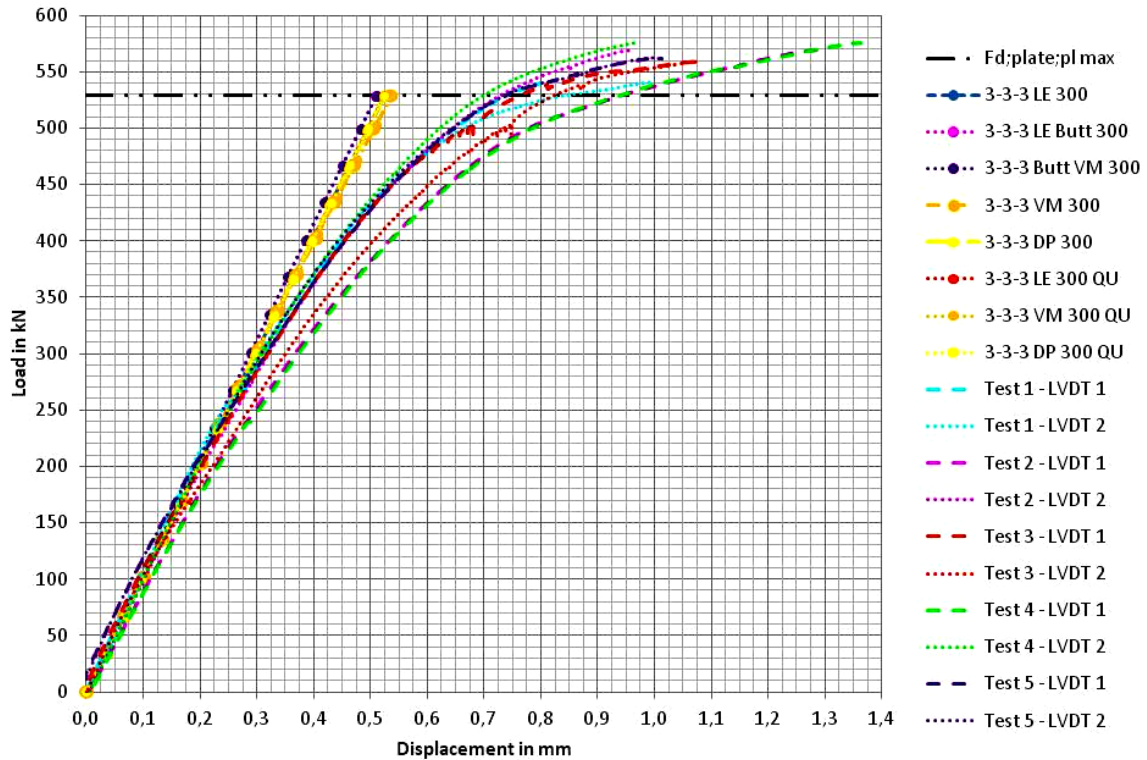


Figure 15.1: Load-displacement curves of practice tests

Summarised:

- Out of the practice tests a 5th percentile ultimate failure load of 549.15 kN is achieved.
- The design load will be lower due to time-and-environmental depended effects.
- A higher steel grade for the plates probably results in a higher failure load.
- Better or other surface treatment and/or a primer may increase the failure load.
- The load-displacement behaviour of the connection is best described by a bilinear model and is in accordance with the FEM calculations up to around 50% of the failure load.

15.2 Recommendations

Just as for the conclusion the recommendations can be divided in the more general conclusions drawn from the literature review (Part A), the conclusions drawn from the research on the L-connection and the conclusions drawn from the research on the double strap connection.

15.2.1 General for structural engineering

Based on part A of this thesis, some general recommendations are made with respect to design, production and further research.

15.2.1.1 Design

- Design adhesive bonded connections in such a way that they are predominantly loaded in shear and avoid tension stresses, such as peel stresses, as much as possible.
- Apply the most stringent requirements with respect to the essential, functional, manufacturing and erection tolerances. Requiring special tolerances is worth considering and may be cost efficient.
- Apply the smallest as possible adhesive thickness.

- Apply thin plates instead of thick plates for lap connections. A higher strength grade and/or widening of plates can be used.
- To increase the failure load of a lap connection, apply widening instead of lengthening.
- Make sure the service temperature of the adhesive is (well) below its glass transition temperature.

15.2.1.2 Production

- Wear suitable clothing. Every adhesive supplier provides information about the specific health risks and prescribed clothing.
- Work in a clean, dust free space and use plastic gloves to avoid grease contaminations.
- Clean the adherent surface sufficiently.
 - For steel adherents, blasting is required.
 - For all adherents, degreasing is required.
 - Application of a primer may be required.
- Replace plastic gloves, degreasing cloth and suchlike regularly to avoid cross-contaminations.
- Apply the adhesive as soon as possible after the cleaning of the adherents.
- Use a suitable waste disposal. Adhesive suppliers provide information about the toxicity of the adhesive.

15.2.1.3 Further research

- Set up codes and directives.
- Perform further research on:
 - Connections with thick steel plates/profiles.
 - How many steps of a stepped connection is most effective?
 - How to deal with the large stress concentration near webs?
 - How to deal with the less effectiveness of bevelled and stepped plate-to-profile connections?
 - Connections with thick adhesive layers.
 - What is the exact influence of large adhesive thicknesses and what is the optimal adhesive thickness for thick plates?
 - Is the use of filler plates an economical and effective solution to reduce the adhesive thickness?
 - Typical structural engineering connections in fire conditions.
 - How much insulation is needed to ensure sufficient protection?
 - What is the relationship between the temperature and strength of connections?
 - Time-and-environmental behaviour of typical structural engineering connections.
 - Which type of sealant should be applied?
 - What is the decrease in strength at 50 and 100 years for different exposure conditions?
 - Adhesive types which are suitable for structural engineering applications.

15.2.2 L-connection

Based on this research, some recommendations are made with respect to design and further research.

15.2.2.1 Design

- Design connections with continuous beams instead of continuous columns.
- If FEM calculations are made for research purpose:
 - Perform FEM calculations of a beam-to-column connection on a computer with lots of RAM.

- Divide the adhesive thickness in at least two finite elements for FEM calculations.

15.2.2.2 Further research

- Perform further research on:
 - FEM models of beam-to-column connections with non-linear material behaviour.
 - The rotational stiffness of adhesive bonded beam to column connections.
 - Thick steel plate-to-profile connections.
 - How to deal with the large stress concentration near webs?
 - How to deal with the less effectiveness of bevelled and stepped (see figure below) plate-to-profile connections?

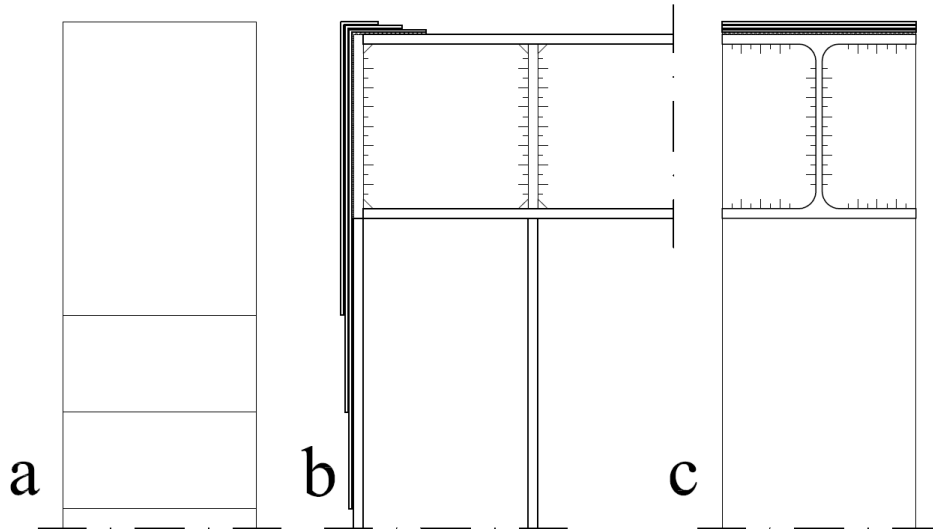


Figure 15.2: L-connection with stepped plates; a front view, b longitudinal cross section, c transverse cross section

15.2.3 Double strap connection

Based on this research, some recommendations are made with respect to design and further research.

15.2.3.1 Design

- Substitute the 15mm thick S235 with a 10mm thick S355 plate.

15.2.3.2 Production

- Use spacers which are not present over the whole length. For instance, a small piece of welding wire can be welded to the steel, this also prevents the welding wire from turning.
- Use a vacuum as clamp for uniform clamp pressure.

15.2.3.3 Further research

- Perform further research on:
 - The material model and parameters for FEM calculations with adhesives.
 - Behaviour of the interface of adhesive and steel.
 - How high are the stress levels near the interface?
 - How to model the interface?
 - More types of load and load combinations.
 - What is the influence of compression loads and moments?
 - A connection with 10mm thick S355 plates.

- Influence of time-and-environmental effects.
 - What is the creep behaviour of the connection?
 - What is the relationship between the temperature and strength of connections?
- More accurate FEM models to predict the load-displacement behaviour.
- An effective way to use stepped straps for connections with I-shaped profiles.
 - Is the connection depicted in Figure 15.2 an effective way for L-connections with I-shaped profiles?
 - Is the connection depicted in Figure 15.3 an effective way for lengthening I-shaped profiles?
 - Should the thickness of the stepped splice plates of the connections depicted in Figure 15.2 and Figure 15.3 also increase towards the end of the width for an effective load transfer?

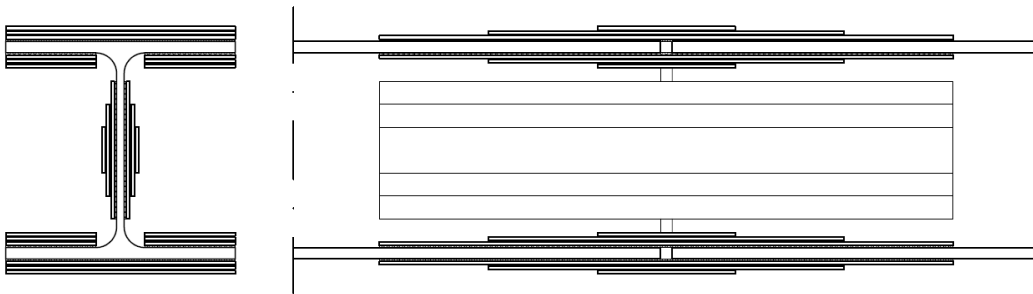


Figure 15.3: Lengthening of I-shaped profile with stepped plates

16 References

1. Gleich, D., *Stress Analysis of Structural Bonded Joints*, 2002, Delft University of Technology: Delft.
2. Hechtingsinstituut, *Lijmen is een kunst voor iedereen*, 2004, Hechtingsinstituut: Delft.
3. van Straalen, I.J., *Development of Design Rules for Structural Adhesive Bonded Joints - A Systematic Approach*, in *Civil Engineering and Geosciences 2001*, Delft University of Technology: Delft.
4. Vereniging FME-CWM, *VM 86 Lijmen algemeen*, 2008, Vereniging FME-CWM: Zoetermeer.
5. ESDEP Society. *Lecture 3.2.2. Erection II*. ESDEP-European Steel Design Education Programme 2012 [cited 2012 20-10-2013]; Available from: <http://www.fgg.uni-lj.si/kmk/esdep/master/wg03/t0220.htm>.
6. Ningbo Jay & Min Industry co. *JAY & MIN*. 2013 [cited 2013 27-1-2013]; Available from: <http://www.jaymin-international.com/steel-honeycomb-panel.html>.
7. da Silva, L.F.M., A. Öchsner, and R.D. Adams, *Handbook of Adhesion Technology* 2011, Berlin: Springer-Verlag Berlin Heidelberg.
8. Normalisation, C.-C.E.d., *NEN-EN 1998-2 Eurocode 8: Design of structures for earthquake resistance - Part 2: Bridges*, 2006, Nederlands Normalisatie-instituut: Delft.
9. Mossallam, A.S., *Design Guide for FRP Composite Connections* ASCE Manuals and Reports on Engineering Practice 2011, Reston: American Society of Civil Engineers.
10. Salvador, P. *Materials in Engineering - Understanding Polymeric Materials, their Structure and Properties*. 2000 [cited 2012 1-9-2012]; Available from: http://neon.mems.cmu.edu/cramb/27-100/lab/S00_lab2/lab2.html.
11. Schliekelmann, R.J., *Gelijmde metalen constructies* 1970, Amsteram: Agon Elsevier.
12. Agrawal, A. *Introduction to Surface Tension*. Fundamentals of Surface Tension/Wettability [cited 2013 8-8-2013]; Available from: <http://web.mit.edu/nmf/education/wettability/intro.html>.
13. Dillard, D.A., *Advances in structural adhesive bonding* 2010, Cambridge: Woodhead Publishing Limited.
14. Adams, R.D., J. Comyn, and W.C. Wake, *Structural Adhesive Joints in Engineering* 2th ed 1997, London: Chapman & Hall.
15. Mays, G.C. and A.R. Hutchinson, *Adhesives in Civil Engineering* 1st ed 1992, Cambridge: Press Syndicate of the University of Cambridge.
16. Differencebetween. *Difference Between Adhesion and Cohesion*. Nov 1st, 2011 [cited 2012 8-10-2012]; Available from: <http://www.differencebetween.com/difference-between-adhesion-and-vs-cohesion/#ixzz1y90ZFKSa>.
17. Pocius, A.V., *Adhesion and adhesives technology: an introduction* 2th ed 2002, München: Carl Hanser Verlag.
18. Adams, R.D. and W.C. Wake, *Structural Adhesive Joints in Engineering* 1985, Essex: Elsevier Applied Science Publishers LTD.
19. Blaauwendraad, J., *Plate analysis, theory and application; Volume 1, Theory* 2006, Delft: Delft University of Technology.
20. Charalambides, M.N. and G.D. Dean, *Constitutive models and their data requirements for use in Finite Element Analysis of adhesives under impact loading.*, in *Project PAJ2 Dynamic Performance of Adhesively Bonded Joints* 1997, Centre for Materials Measurement and & Technology; National Physical Laboratory: Teddington.
21. Ignjatovic, M., P. Chalkley, and C. Wang, *The Yield Behaviour of a Structural Adhesive under Complex Loading*, 1998: Melbourne.
22. Broughton, W.R., L.E. Crocker, and J.M. Urquhart, *Strength of Adhesive Joints: A Parametric Study*, 2001, NPL Materials Centre: Teddington.
23. Cassino, C.D., *Characterization and Development of General Material Models for use in Modeling Structures Bonded with Ductile Adhesives*, in *Mechanical Engineering* 2005, Virginia Polytechnic Institute and State University: Blacksburg.
24. CEN - Comité Européen de Normalisation, *NEN-EN 1993-1-1 - Eurocode 3: Design of steel structures - Part 1-1: General rules and rules for buildings (includes C1:2006)* 2006, Nederlands Normalisatie-instituut: Delft.
25. Verhulst, R.P., et al., *Properties of Pressure Sensitive Adhesives Found in Paper Recycling Operations in 2006 TAPPI Engineering, Pulping & Environmental* 2004, TAPPI: Atlanta.

26. Germany - Land of Ideas. *Gaertnerplatz bruecke*. 2013 [cited 2013 2-3-2013]; Available from: <http://www.gaertnerplatzbruecke.de/>.
27. Sika Services AG, *Gärtnerplatz Bridge in Kassel, Germany*, in *Sika at Work*, Sika Services AG, Editor 2007, Sika Services AG: Pfäffikon.
28. CUR BOUW & INFRA, *Aanbeveling 91 (tweede, herziene uitgave)*, in *Versterken van gewapendbetonconstructies met uitwendig gelijmde koolstofvezelwapening 2007*, Stichting CURNET: Gouda.
29. Kolstein, M.H., *Fibre reinforced Polymer (FRP) Structures 2008*, Delft: TU Delft.
30. Martens, D.R.W., *Lijmwerk in de gevel*. Cement, 2001. **8**.
31. Nijssse, R., *Glass in Structures 2003*, Basel: Birkhäuser - Publisher for Architecture.
32. Busel, J.P. and D. Richards. *Prefabricated Bridge Elements and Systems*. 2013 [cited 2013 3-2-2013]; Available from: http://www.fhwa.dot.gov/everydaycounts/technology/bridges/pbeswebinartraining/s3_m9.cfm.
33. Labordus, M. and W.H.M. Souren, *Verlijmen tegen vermoeien*. Bouwen met Staal, 2009. **211**.
34. Teixeira De Freitas, S., *Steel plate reinforcement of orthotropic bridge decks*, in *Faculty of Civil Engineering and Geosciences 2012*, Delft University of Technology: Delft.
35. Fuchs, H., *Lijmen van metalen in de bouw - Op zoek naar richtlijnen en rekenregels*. Bouwen met Staal, 2000. **152**.
36. BetonSon, *Kanaalplaatvloer*, Beton Son B.V., Editor 2012, Beton Son B.V.: Son
37. Bijlaard, F.S.K. and A.M. Gresnigt, *Dictaat CT3121 - Staalconstructies 2 2006*, Delft: Delft University of Technology.
38. CEN - Comité Européen de Normalisation, *NEN-EN 1990 - Basis of structural design.*, in 2002, Nederlands Normalisatie-instituut: Delft.
39. TRADECC nv, *Technical Data - PC@ 5800/BL*, 2009, TRADECC nv: Wilrijk.
40. Meekels, P. *Studiedag EN1090*. in *Studiedag EN1090*. 2012. Edegem: Infosteel.
41. CEN - Comité Européen de Normalisation, *NEN-EN 10034 - I- en H-profielen van constructiestaal. Toleranties op vorm en afmetingen.*, 1994, Nederlands Normalisatie-instituut: Delft.
42. CEN - Comité Européen de Normalisation, *NEN-EN 1090-2+A1 - Execution of steel structures and aluminium structures - Part 2: Technical requirements for steel structures.*, 2011, Nederlands Normalisatie-instituut: Delft.
43. Verburg, W.H., *Basisboek*. 4th ed. (Over)spannend staal 2004, Zoetermeer Bouwen met Staal.
44. Henkel Loctite Europe, *Loctite - Technical Data Sheet - Hysol® 9466™* 2006, Henkel Corporation.
45. Loctite Corporation, *Loctite - Product Description Sheet - Speedbonder® Product H3151* 2002, Loctite Corporation.
46. Sika Nederland B.V., *Productinformatieblad - Sikadur®-52 Injection Type N en LP*, 2010, Sika Nederland B.V.: Utrecht.
47. Sika Nederland B.V., *Productinformatieblad - Sikadur®-31 CF Normal*, 2011, Sika Nederland B.V.: Utrecht.
48. Sika Nederland B.V., *Productinformatieblad - Sikadur®-41 CF Normal*, 2011, Sika Nederland B.V.: Utrecht.
49. Sika Nederland B.V., *Productinformatieblad - Sikadur® -30*, 2012, Sika Nederland B.V.: Utrecht.
50. Henkel Corporation, *Technical Data Sheet - Hysol® 3425™*, 2012, Henkel Corporation.,
51. Sika Nederland B.V., *Sika® Injection-451*, 2010, Sika Nederland B.V.: Utrecht.
52. Isaac, P.M., *Effect of Adhesive Stiffness on FRP Anchorage Strengthening of Steel*, in *Department of Architecture and Civil Engineering 2009*, University of Bath: Bath.
53. TNO. *DIANA Finite Element Analysis - User's Manual - Release 9.3*. 2009 [cited 2013 2-3-2013]; Available from: <https://support.tnodiana.com/manuals/d93/Diana.html>.
54. Zureick, A., L.F. Kahn, and Y.S. Kim, *Strengthening of Reinforced Concrete Bridge Deck Slabs with Shop-Manufactured Carbon Composite Plates*, 2002, Georgia Institute for Technology: Atlanta.
55. Eldik, C.H.v. and Bouwen met Staal, *Wegwijzer Constructiestaal 2006*, Zoetermeer: Bouwen met Staal

56. CEN - Comité Européen de Normalisation, *NEN-EN 10058 - Hot rolled flat steel bars for general purposes - Dimensions and tolerances on shape and dimensions*, 2003, Nederlands Normalisatie-instituut: Delft.
57. CEN - Comité Européen de Normalisation, *NEN-EN-ISO 8501-1 - Preparation of steel substrates before application of paints and related products - Visual assessment of surface cleanliness - Part 1: Rust grades and preparation grades of uncoated steel substrates and of steel substrates after overall removal of previous coatings (ISO 8501-1:2007, IDT) 2007*, Nederlands Normalisatie-instituut: Delft.
58. TU Delft. *Hydraulic press 600 kN*. 2014 [cited 2014 18-2-2014]; Available from: <http://www.labs.tudelft.nl/index.php?action=instrument&id=170>.
59. Vereniging FME-CWM, *VM 87 Lijmen van metalen*, 2008, Vereniging FME-CWM: Zoetermeer.
60. Adhesive toolkit. *Adhesive toolkit*. 2012 [cited 2012 8-10-2012]; Available from: <http://www.adhesivestoolkit.com>.
61. CEN - Comité Européen de Normalisation, *NEN-EN 1993-1-8 - Eurocode 3: Design of steel structures - Part 1-8: Design of joints (includes C1:2006)* 2006, Nederlands Normalisatie-instituut: Delft.
62. CEN - Comité Européen de Normalisation, *National Annex to NEN-EN 1993-1-1 - Eurocode 3: Design of steel structures - Part 1-1: General rules and rules for buildings (includes C1:2006)* 2006, Nederlands Normalisatie-instituut: Delft.
63. SIMULIA, *Abaqus Analysis User's Manual*, in *Abaqus 6.11* 2011, SIMULIA: Rising Sun Mills.

Appendices

17 Appendix A: Volkersen

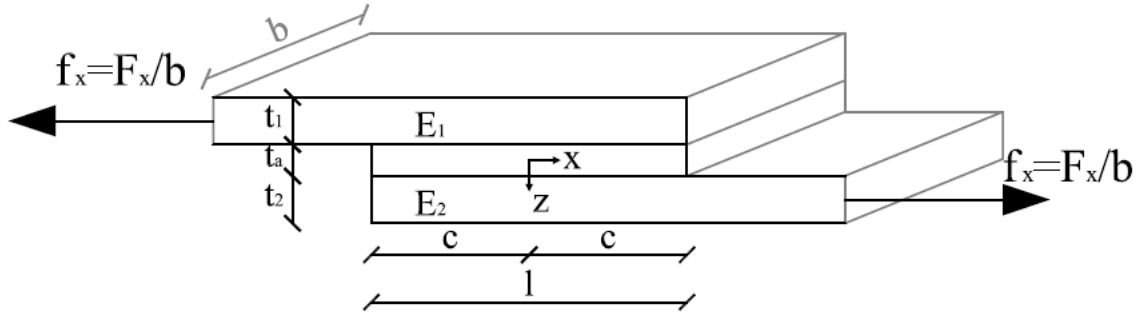


Figure 17.1: Single lap connection according to Volkersen

In the theory of Volkersen the adherents do not have infinite stiffness and will deform in the x direction (axial). The stress in the adherent decreases over the bond length, and so does the strain.

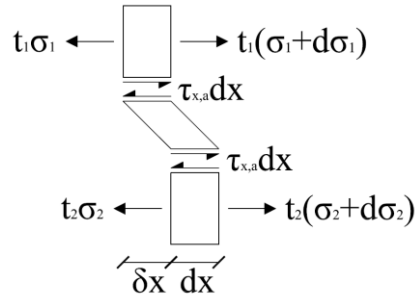


Figure 17.2: Section of displaced unit width according to Volkersen

The relative displacement for a unit width of the adherents, Figure 17.2, is:

$$\delta_x(x) = -u_1(x) + u_2(x) \quad (17.1)$$

The relative displacement of the adherents cause a shear stress in the adhesive which is given by:

$$\tau_{x;a}(x) = \gamma_x(x) G_a = \frac{\delta_x(x)}{t_a} G_a = \frac{u_2(x) - u_1(x)}{t_a} G_a \quad (17.2)$$

The axial strain of the adherents is given by kinematic relations:

$$u_1(x) = \int_{-c}^x \varepsilon_1(x) dx \quad (17.3)$$

$$u_2(x) = \int_{-c}^x \varepsilon_2(x) dx \quad (17.4)$$

For the upper and lower adherent the next equilibrium equations hold (see Figure 17.2):

$$\frac{d\sigma_1(x)}{dx} = -\frac{\tau_{x;a}(x)}{t_1} \quad (17.5)$$

$$\frac{d\sigma_2(x)}{dx} = \frac{\tau_{x;a}(x)}{t_2} \quad (17.6)$$

Integration of (17.5) and (17.6) with respect to x gives:

$$\sigma_1(x) = -\int_{-c}^x \frac{\tau_{x;a}(x)}{t_1} dx + C_1 \quad (17.7)$$

$$\sigma_2(x) = \int_{-c}^x \frac{\tau_{x;a}(x)}{t_2} dx + C_2 \quad (17.8)$$

The constants of (17.7) and (17.8) can be solved by the boundary conditions at $x = -c$:

$$\sigma_1(-c) = \frac{F_x}{bt_1} = -\int_{-c}^{-c} \frac{\tau_{x;a}(x)}{t_1} dx + C_1 \rightarrow C_1 = \frac{F_x}{bt_1} \quad (17.9)$$

$$\sigma_2(-c) = 0 = \int_{-c}^{-c} \frac{\tau_{x;a}(x)}{t_2} dx + C_2 \rightarrow C_2 = 0 \quad (17.10)$$

Hence:

$$\sigma_1(x) = \frac{F_x}{bt_1} - \int_{-c}^x \frac{\tau_{x;a}(x)}{t_1} dx \quad (17.11)$$

$$\sigma_2(x) = \int_{-c}^x \frac{\tau_{x;a}(x)}{t_2} dx \quad (17.12)$$

The relationship between stresses and strains is given by the constitutive equations:

$$\varepsilon_1(x) = \frac{\sigma_1(x)}{E_1} \quad (17.13)$$

$$\varepsilon_2(x) = \frac{\sigma_2(x)}{E_2} \quad (17.14)$$

Combining (17.3), (17.13) and (17.11) gives:

$$u_1(x) = \int_{-c}^x \frac{F_x}{bE_1t_1} dx - \int_{-c}^x \int_{-c}^x \frac{\tau_{x;a}(x)}{E_1t_1} dx dx \quad (17.15)$$

Combining (17.4), (17.14) and (17.12) gives:

$$u_2(x) = \int_{-c}^x \int_{-c}^x \frac{\tau_{x;a}(x)}{E_2t_2} dx dx \quad (17.16)$$

Substituting (17.15) and (17.16) in (17.2) gives:

$$\tau_{x;a}(x) = \left(\int_{-c}^x \int_{-c}^x \frac{\tau_{x;a}(x)}{E_2t_2} dx dx - \int_{-c}^x \frac{F_x}{bE_1t_1} dx + \int_{-c}^x \int_{-c}^x \frac{\tau_{x;a}(x)}{E_1t_1} dx dx \right) \frac{G_a}{t_a} \quad (17.17)$$

Differentiating (17.17) twice with respect to x gives:

$$\frac{d^2 \tau_{x;a}(x)}{dx^2} = \left(\frac{\tau_{x;a}(x)}{E_2t_2} + \frac{\tau_{x;a}(x)}{E_1t_1} \right) \frac{G_a}{t_a} \quad (17.18)$$

Rearranging (17.18) gives:

$$\frac{d^2 \tau_{x;a}(x)}{dx^2} - \frac{E_1t_1 + E_2t_2}{E_1t_1E_2t_2} \frac{G_a}{t_a} \tau_{x;a}(x) = 0 \quad (17.19)$$

To elegantly solve this second order, linear, homogeneous, DE the next factor is introduced:

$$\omega = \sqrt{\frac{E_1t_1 + E_2t_2}{E_1t_1E_2t_2} \frac{G_a}{t_a}} \quad (17.20)$$

Which gives:

$$\frac{d^2 \tau_{x;a}(x)}{dx^2} - \omega^2 \tau_{x;a}(x) = 0 \quad (17.21)$$

Such an equation can be solved with a general solution of the next form:

$$\tau_{x;a}(x) = A \sinh(\omega x) + B \cosh(\omega x) \quad (17.22)$$

Due to equilibrium the next conditions apply:

$$\int_{-c}^c \tau_{x;a}(x) dx = \frac{F_x}{b} \quad (17.23)$$

With this equation and (17.22) constant B can be solved:

$$\frac{2B}{\omega} \sinh(\omega c) = \frac{F_x}{b} \rightarrow B = \frac{F_x \omega}{2b} \frac{1}{\sinh(\omega c)} \quad (17.24)$$

Substituting (17.22) and (17.24) in (17.17) and differentiating with respect to x gives:

$$A\omega \cosh(\omega x) + \frac{F_x \omega^2 \sinh(\omega x)}{2b \sinh(\omega c)} = \left(\int_{-c}^x \frac{\tau_{x;a}(x)}{E_2 t_2} dx - \frac{F_x}{b E_1 t_1} - \int_{-c}^x \frac{\tau_{x;a}(x)}{E_1 t_1} dx \right) \frac{G_a}{t_a} \quad (17.25)$$

A can now be solved by evaluating this equation at $x = -c$.

$$A = \left(\frac{E_1 t_1 - E_2 t_2}{E_1 t_1 + E_2 t_2} \right) \frac{F_x \omega}{2b} \frac{1}{\cosh(\omega c)} \quad (17.26)$$

Combining (17.22), (17.24) and (17.26) gives:

$$\tau_{x;a}(x) = \frac{F_x \omega}{2b} \left\{ \frac{\cosh(\omega x)}{\sinh(\omega c)} + \frac{E_1 t_1 - E_2 t_2}{E_1 t_1 + E_2 t_2} \frac{\sinh(\omega x)}{\cosh(\omega c)} \right\} \quad (17.27)$$

18 Appendix B: Goland and Reissner

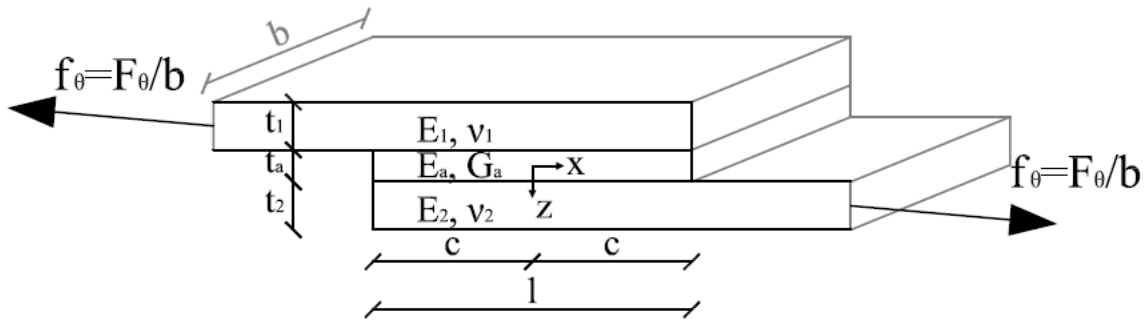


Figure 18.1: single lap connection according to Goland and Reissner

18.1 Derivation of shear and peel formula

The single lap connection is divided in two parts. One part consists of the upper adherent and upper half of the adhesive, and one part consists of the lower half of the adhesive and the lower adherent. The adherents are assumed to have the same thickness and stiffness properties, $t_1 = t_2$, $\nu_1 = \nu_2$ and $E_1 = E_2$.

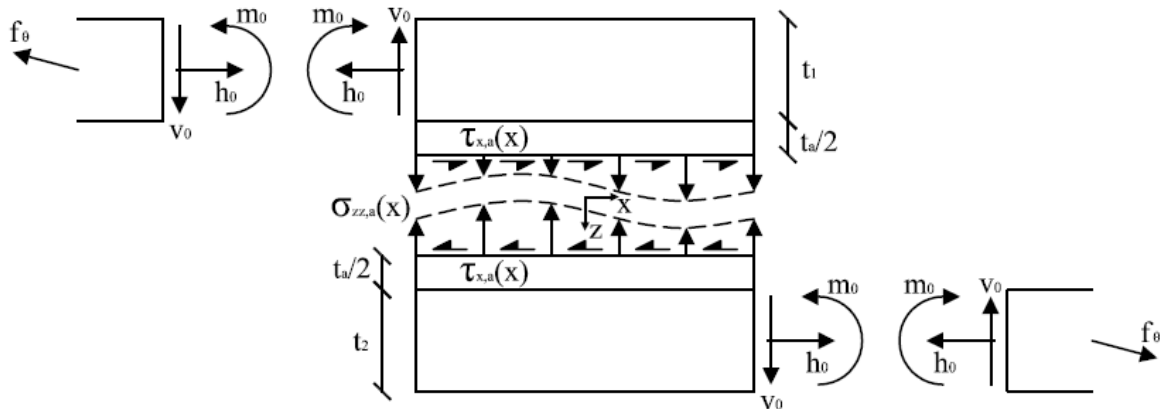


Figure 18.2: Internal forces according to Goland and Reissner

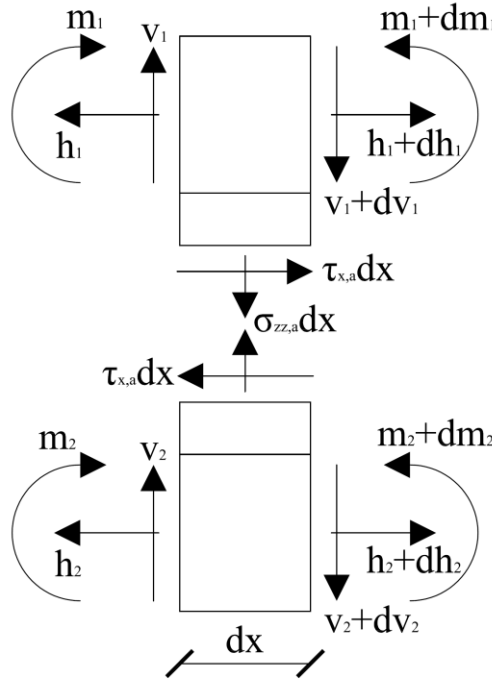


Figure 18.3: Unit width at bond region according to Goland and Reissner

First the horizontal, vertical and moment equilibrium equations are composed:

$$\frac{dh_1(x)}{dx} + \tau_{x;a}(x) = 0 \quad (18.1)$$

$$\frac{dh_2(x)}{dx} - \tau_{x;a}(x) = 0 \quad (18.2)$$

$$\frac{dv_1(x)}{dx} + \sigma_{zz;a}(x) = 0 \quad (18.3)$$

$$\frac{dv_2(x)}{dx} - \sigma_{zz;a}(x) = 0 \quad (18.4)$$

$$\frac{dm_1(x)}{dx} - v_1(x) + \tau_{x;a}(x) \left[\frac{t_a + t_1}{2} \right] = 0 \quad (18.5)$$

$$\frac{dm_2(x)}{dx} - v_2(x) + \tau_{x;a}(x) \left[\frac{t_a + t_1}{2} \right] = 0 \quad (18.6)$$

It is assumed that the deflection of the adherents can be described by the simple bending plate theory:

$$\frac{d^2 w_1(x)}{dx^2} + \frac{m_1(x)}{D} = 0 \quad (18.7)$$

$$\frac{d^2 w_2(x)}{dx^2} + \frac{m_2(x)}{D} = 0 \quad (18.8)$$

Where D is the plate stiffness given by:

$$D = \frac{E_1 t_1^3}{12(1 - \nu_1^2)} \quad (18.9)$$

The influence of the adhesive to the flexural stiffness is not considered. The shear deformation of the adhesive is assumed to be small compared to the flexural deformation and is neglected.

The strain in x direction of the adherents is given by:

$$\varepsilon_{xx;1}(x) = \frac{h_1(x)}{A} + \frac{t_1}{2} \frac{m_1(x)}{D} \quad (18.10)$$

$$\varepsilon_{xx;2}(x) = \frac{h_2(x)}{A} - \frac{t_1}{2} \frac{m_2(x)}{D} \quad (18.11)$$

Where A is:

$$A = \frac{E_1 t_1}{(1 - \nu_1^2)} \quad (18.12)$$

Kinematic relationship for strain and displacement reads:

$$\varepsilon_{xx;1}(x) = \frac{du_{x;1}(x)}{dx} \quad (18.13)$$

$$\varepsilon_{xx;2}(x) = \frac{du_{x;2}(x)}{dx} \quad (18.14)$$

The shear and normal stress are assumed to be constant over the thickness of the adhesive. Hence:

$$\frac{\tau_{x;a}(x)}{G_a} = \frac{u_2(x) - u_1(x)}{t_a} \quad (18.15)$$

$$\frac{\sigma_{zz;a}(x)}{E_a} = \frac{w_2(x) - w_1(x)}{t_a} \quad (18.16)$$

The forces on adherents on the left and right are given by:

$$h_2(-c) = v_2(-c) = m_2(-c) = 0 \quad (18.17)$$

$$h_1(-c) = h_0, v_1(-c) = v_0, m_1(-c) = m_0$$

$$h_1(c) = v_1(c) = m_1(c) = 0 \quad (18.18)$$

$$h_2(c) = h_0, v_2(c) = v_0, m_2(c) = -m_0$$

18.1.1 Shear formula

Differentiating (18.15) once, and combining this with (18.10) / (18.14) gives:

$$\frac{d\tau_{x;a}(x)}{dx} = G_a \left[\frac{1}{At_a} [h_2(x) - h_1(x)] - \frac{t_1}{2Dt_a} [m_2(x) + m_1(x)] \right] \quad (18.19)$$

Differentiating (18.19) once and combining this with (18.1), (18.2), (18.5) and (18.6) gives:

$$\frac{d^2\tau_{x;a}(x)}{dx^2} \frac{1}{G_a} = \tau_{x;a}(x) \left[\frac{2}{At_a} + \frac{t_1[t_a + t_1]}{2Dt_a} \right] - \frac{t_1}{2Dt_a} [v_2(x) + v_1(x)] \quad (18.20)$$

Differentiating (18.20) once and combining this with (18.3) and (18.4) gives:

$$\frac{d^3\tau_{x;a}(x)}{dx^3} = \frac{d\tau_{x;a}(x)}{dx} G_a \left[\frac{2}{At_a} + \frac{t_1[t_a + t_1]}{2Dt_a} \right] \quad (18.21)$$

Now a parameter is introduced to keep the formulas manageable:

$$\beta = c \sqrt{G_a \left[\frac{2}{At_a} + \frac{t_1[t_a + t_1]}{2Dt_a} \right]} = c \sqrt{\frac{G_a(1 - \nu_1^2)}{t_a E_1 t_1^2} (8t_1 + 6t_a)} \quad (18.22)$$

Which gives:

$$\frac{d^3 \tau_{x;a}(x)}{dx^3} - \left[\frac{\beta}{c} \right]^2 \frac{d\tau_{x;a}(x)}{dx} = 0 \quad (18.23)$$

To solve the third order, linear, homogeneous, DE, (18.23), three boundary conditions should be provided. Substituting (18.17) and (18.18) into (18.19) gives:

$$\left. \frac{d\tau_{x;a}(x)}{dx} \right|_{-c} = - \frac{G_a(1-\nu_1^2)}{t_a E_1 t_1} \left[h_0 + \frac{6}{t_1} m_0 \right] \quad (18.24)$$

$$\left. \frac{d\tau_{x;a}(x)}{dx} \right|_c = \frac{G_a(1-\nu^2)}{t_a E_1 t_1} \left[h_0 + \frac{6}{t_1} m_0 \right] \quad (18.25)$$

As the third condition, the equilibrium of external force is used:

$$\int_{-c}^c \tau_{x;a}(x) dx = h_0 \quad (18.26)$$

With (18.24) / (18.26) the solution of (18.23) is:

$$\tau_{x;a}(x) = \frac{t_1}{4t_1 + 3t_a} \frac{h_0}{2c} \left[1 + \frac{6m_0}{t_1 h_0} \frac{\beta}{\sinh(\beta)} \cosh\left(\frac{\beta}{c} x\right) + 3 \left(1 - \frac{2m_0}{t_1 h_0} + \frac{t_a}{t_1} \right) \right] \quad (18.27)$$

18.1.2 Peel formula

Differentiating (18.16) twice, and combining this with (18.7) and (18.8) gives:

$$\frac{d^2 \sigma_{zz;a}(x)}{dx^2} \frac{1}{E_a} = \frac{m_1(x) - m_2(x)}{Dt_a} \quad (18.28)$$

Differentiating (18.28) once, and combining this with (18.5) and (18.6) gives:

$$\frac{d^3 \sigma_{zz;a}(x)}{dx^3} \frac{1}{E_a} = \frac{v_1(x) - v_2(x)}{Dt_a} \quad (18.29)$$

Differentiating (18.29) once, and combining this with (18.3) and (18.4) gives:

$$\frac{d^4 \sigma_{zz;a}(x)}{dx^4} + 4 \frac{\lambda^4}{c^4} \sigma_{zz;a}(x) = 0 \quad (18.30)$$

With:

$$\lambda = c^4 \sqrt{\frac{E_a}{2t_a D}} \quad (18.31)$$

To solve the fourth order, linear, homogeneous, DE, (18.30), four boundary conditions should be provided. Substituting (18.17) and (18.18) into (18.28) gives:

$$\left. \frac{d^2 \sigma_{zz;a}(x)}{dx^2} \right|_{-c} = \left. \frac{d^2 \sigma_{zz;a}(x)}{dx^2} \right|_c = \frac{E_a m_0}{Dt_a} \quad (18.32)$$

Substituting (18.17) and (18.18) into (18.29) gives:

$$\left. \frac{d^3 \sigma_{zz;a}(x)}{dx^3} \right|_{-c} = - \left. \frac{d^3 \sigma_{zz;a}(x)}{dx^3} \right|_c = \frac{E_a v_0}{Dt_a} \quad (18.33)$$

With (18.32) and (18.33) the solution of (18.30) is:

$$\sigma_{zz,a}(x) = \frac{h_0}{t_1} \left[\frac{t_1}{c} \right]^2 \Delta \left[\left[\frac{r_1 \lambda^2 m_0}{t_1 h_0} + \frac{c v_0}{t_1 h_0} \sinh(\lambda) \sin(\lambda) \right] \sinh\left(\frac{\lambda x}{c}\right) \sin\left(\frac{\lambda x}{c}\right) + \dots \right. \\ \left. \dots + \left[\frac{r_2 \lambda^2 m_0}{t_1 h_0} + \frac{c v_0}{t_1 h_0} \cosh(\lambda) \cos(\lambda) \right] \cosh\left(\frac{\lambda x}{c}\right) \cos\left(\frac{\lambda x}{c}\right) \right] \quad (18.34)$$

With:

$$\Delta = \frac{2}{\sin(2\lambda) + \sinh(2\lambda)} \quad (18.35)$$

$$r_1 = \sinh(\lambda) \cos(\lambda) + \cosh(\lambda) \sin(\lambda) \quad (18.36)$$

$$r_2 = \sinh(\lambda) \cos(\lambda) - \cosh(\lambda) \sin(\lambda)$$

18.2 Derivation of h_0 , v_0 and m_0

With (18.27) and the shear stresses and can be determined if h_0 , v_0 and m_0 are known. How these values can be determined is explained in this section.

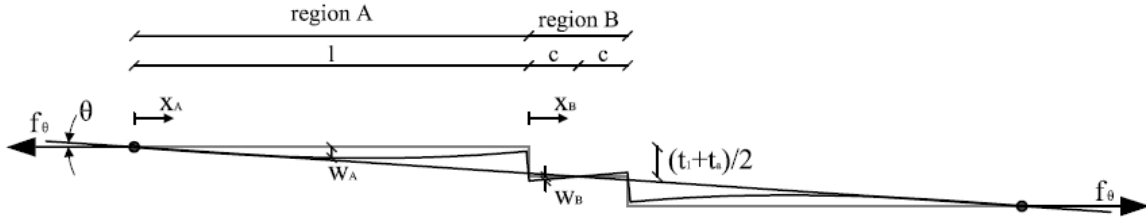


Figure 18.4: Deformation of the neutral axis according to Goland and Reissner

The horizontal force in adherent is given by:

$$h_0 = f_\theta \cos(\theta) \quad (18.37)$$

With:

$$\cos(\theta) = \frac{l + c}{\sqrt{[l + c]^2 + \left[\frac{t_1 + t_a}{2} \right]^2}}$$

The moment in the upper adherent of domain A en B due to the applied force F on the left end is:

$$m_A(x_A) = f_\theta \cos(\theta) [x_A \tan(\theta) - w_A(x_A)] \quad (18.38)$$

$$m_B(x_B) = f_\theta \cos(\theta) [(x_B - c) \tan(\theta) - w_B(x_B)] \quad (18.39)$$

With:

$$\tan(\theta) = \frac{\left[\frac{t_1 + t_a}{2} \right]}{l + c}$$

The influence of the stiffness of the adhesive is neglected. The bending stiffness of region B is assumed to be the summation of the upper and lower adherent, hence:

$$D_B = \frac{E_1 [2t_1]^3}{12(1-\nu_1^2)} = 8 \frac{E_1 t_1^3}{12(1-\nu_1^2)} = 8D \quad (18.40)$$

Now the equation (18.7) is used here:

$$\frac{d^2 w_A(x_A)}{dx^2} = -\frac{m_A(x_A)}{D} = -\frac{f_\theta \cos(\theta) [x_A \tan(\theta) - w_A(x_A)]}{D} \quad (18.41)$$

$$\frac{d^2 w_B(x_B)}{dx^2} = -\frac{m_B(x_B)}{D_B} = -\frac{f_\theta \cos(\theta) [[x_B - c] \tan(\theta) - w_B(x_B)]}{8D} \quad (18.42)$$

From symmetry and continuity the next conditions can be composed:

$$w_A(0) = 0 \quad (18.43)$$

$$w_B(c) = 0 \quad (18.44)$$

$$w_A(l) = w_B(0) \quad (18.45)$$

$$\left. \frac{dw_A(x_A)}{dx} \right|_{x_A=l} = \left. \frac{dw_B(x_B)}{dx} \right|_{x_B=0} \quad (18.46)$$

The set of two second order linear inhomogeneous DE's, (18.41) and (18.42), can be solved with the conditions (18.43) / (18.46):

$$w_A(x_A) = \frac{2\sqrt{2} \tan(\theta) \sinh(u_2 c) \cosh(u_1 l) x_A}{\left[2\sqrt{2} \sinh(u_2 c) \cosh(u_1 l) + \sinh(u_1 l) \cosh(u_2 c) \right]} + \dots \quad (18.47)$$

$$\dots + \frac{-\tan(\theta) \cosh(u_2 c) [[c+l] \sinh(u_1 x_A) - \sinh(u_1 l) x_A]}{\left[2\sqrt{2} \sinh(u_2 c) \cosh(u_1 l) + \sinh(u_1 l) \cosh(u_2 c) \right]}$$

$$w_B(x_B) = \frac{\sqrt{2} [c+l] [\cosh(u_1 l) \cosh(u_2 x_B) - 2 \cosh(u_1 l) \cosh(u_2 c) \sinh(u_2 x_B)]}{\cos(\theta) \left[2\sqrt{2} \sinh(u_2 c) \cosh(u_1 l) + \sinh(u_1 l) \cosh(u_2 c) \right]} + \dots \quad (18.48)$$

$$\dots + \frac{\left[\sinh(u_1 l) \cosh(u_2 c) + \sqrt{2} \sinh(u_2 c) \cosh(u_1 l) \sin(\theta) \right] [x_B - c]}{\cos(\theta) \left[2\sqrt{2} \sinh(u_2 c) \cosh(u_1 l) + \sinh(u_1 l) \cosh(u_2 c) \right]}$$

With:

$$u_1 = \sqrt{\frac{f_\theta \cos(\theta)}{D}} \quad (18.49)$$

$$u_2 = \sqrt{\frac{f_\theta \cos(\theta)}{8D}}$$

Now the moment at the transition from A to B, m_0 , can be calculated with equation (18.41) and (18.47):

$$m_0 = -D \left. \frac{d^2 w_A(x_A)}{dx^2} \right|_{x_A=l} = \frac{\tanh(u_1 l)}{\tanh(u_1 l) + 2\sqrt{2} \tanh(u_2 c)} \cos(\theta) f_\theta \frac{[t_1 + t_a]}{2} \quad (18.50)$$

Now the shear force at the transition from A to B, v_0 , can be calculated with the general relation (18.51):

$$v_A(x_A) = \frac{dm_A(x_A)}{dx} = -D \frac{d^3 w_A(x_A)}{dx^3} \quad (18.51)$$

$$v_0 = -D \left. \frac{d^3 w_A(x_A)}{dx^3} \right|_{x_A=l} = \frac{u_1}{\tanh(u_1 l) + 2\sqrt{2} \tanh(u_2 c)} \cos(\theta) f_\theta \frac{[t_1 + t_a]}{2} \quad (18.52)$$

When $l \rightarrow \infty$:

$$\lim_{l \rightarrow \infty} f_0 = \lim_{l \rightarrow \infty} f_\theta \cos(\theta) = f_\theta \quad (18.53)$$

$$\begin{aligned} \lim_{l \rightarrow \infty} v_0 &= \lim_{l \rightarrow \infty} \frac{u_1}{\tanh(u_1 l) + 2\sqrt{2} \tanh(u_2 c)} \cos(\theta) f_\theta \frac{[t_1 + t_a]}{2} = \dots \\ &= \frac{u_1}{1 + 2\sqrt{2} \tanh(u_2 c)} f_\theta \frac{[t_1 + t_a]}{2} \end{aligned} \quad (18.54)$$

$$\begin{aligned} \lim_{l \rightarrow \infty} m_0 &= \lim_{l \rightarrow \infty} \frac{\tanh(u_1 l)}{\tanh(u_1 l) + 2\sqrt{2} \tanh(u_2 c)} \cos(\theta) f_\theta \frac{[t_1 + t_a]}{2} = \dots \\ &= \frac{1}{1 + 2\sqrt{2} \tanh(u_2 c)} f_\theta \frac{[t_1 + t_a]}{2} \end{aligned} \quad (18.55)$$

With:

$$\begin{aligned} \lim_{l \rightarrow \infty} u_1 &= \lim_{l \rightarrow \infty} \sqrt{\frac{f_\theta \cos(\theta)}{D}} = \sqrt{\frac{f_\theta}{D}} \\ \lim_{l \rightarrow \infty} u_2 &= \lim_{l \rightarrow \infty} \sqrt{\frac{f_\theta \cos(\theta)}{8D}} = \sqrt{\frac{f_\theta}{8D}} \end{aligned}$$

For the bending moment, the first part of (18.55) is often collected into one term, the so called bending moment factor k , which takes the stiffness into account:

$$k = \frac{1}{1 + 2\sqrt{2} \tanh\left(\sqrt{\frac{f_\theta}{8D}} c\right)} \quad (18.56)$$

For infinite stiff adherents $k = 1$, for all other cases $k < 1$.

19 Appendix C: Adhesive types

There is a wide variety of different types of adhesives available. These can be distinguished in different ways, for instance:

1. natural versus synthetic adhesives;
2. function;
3. physical characterisation;
4. chemical characterisation;
5. number of components;
6. method of application;
7. method of curing;
8. appearance.

This thesis focuses on structural adhesives. Adhesives for other functions, such as non-structural, conductive, locking and sealing adhesives, will not be discussed extensively. Structural adhesives are in general synthetic adhesives, hence natural adhesives will also not be discussed extensively. The physical characterisation is discussed in section 4.1.2; three types can be distinguished; elastomer, thermoset and thermoplastic. [4, 59]

This chapter provides basic information about the different types of adhesives.

19.1 Chemical characterisation

Most structural adhesives are based on the main components listed below. [4, 59, 60]

- epoxy;
- polyurethane;
- silicone;
- cyanoacrylate;
- acrylic;
- phenolic;
- MS polymer.

Some adhesives, hybrid adhesives, are composed out of several main components.

19.2 Appearance

Adhesives in uncured state can have the following appearances [4, 59]:

- liquid
- paste
- solid
 - film
 - powder
 - bar
 - pill

19.3 Number of components

If an adhesive exists of several components, usually one of them is a resin and another one is the starter liquid. In practice the number of components is especially important for the difference between adhesives for those that are mixed before application and those that are not. Some adhesives have more components but these components are not mixed. For example the 'no-mix' acrylic adhesive, where the resin is applied on one adherent and the starter liquid on the other

adherent. Some phenolic adhesives have a powdery hardener, which has to be strewed on the adhesive before the adhesive can be cured under heat and pressure.

Adhesives with one component are non-reactive adhesives. Adhesives with multiple components are reactive adhesives. [4, 59]

19.4 Method of application

The method of application depends on several factors [4, 59]:

- Adherents:
 - size;
 - quantity;
 - quality requirements.
- Appearance of the adhesive:
 - liquid;
 - paste;
 - solid (film, bar, pill or powder,);
 - one-component, multi-component.
- Environmental requirements/norms.

Adhesives which are liquid can be applied through [4, 59];

- brushes;
- iron tools (rake, spatula, trowel);
- casting;
- dipping;
- pressures;
- using hand-or air actuated cartridge pistols;
- automatic high-pressure guns;
- rollers;
- spraying;
- use of mixing and/or dosing equipment;
- injection (vacuum injection).

Adhesive films are normally enclosed by protection foil. After removing the foil the film can be applied on the adherent. [4, 59]

Adhesives in bar, pill or powder form are heated before application, these are also known as hot melt adhesives (HMA). [4, 59]

19.5 Method of curing

For curing three main aspects are of importance:

- curing temperature;
- curing pressure;
- curing time.

Some adhesives may require additional conditions. As mentioned before in section 19.3 there are reactive and non-reactive adhesives. Reactive adhesives cure due to a chemical reaction between the components. Non-reactive adhesives cure due to different reasons and can be distinguished in:

- drying adhesives;
- pressure sensitive adhesives (PSA);
- contact adhesives;
- hot melt adhesives (HMA);
- anaerobic adhesives;

- radiation-cured adhesives;
- moisture curing adhesives.

19.5.1 Curing pressure

To ensure that the adherents and adhesive stay in contact with each other pressure may be required. The pressure level depends on the viscosity of the adhesive. Adhesives with a low viscosity can easily be squeezed out when the pressure level is high. But an adhesive with a high viscosity requires a high pressure to ensure bonding at a rough adherent.

During curing of some adhesives a condensation reaction takes place. This reaction releases water in the form of steam. In those cases the curing pressure should be higher than the steam pressure. Otherwise, voids filled with water can be formed, which lower the failure load and service life. [4, 59]

Pressure can be applied through:

- weights;
- clamps;
- press pressure;
- air pressure (autoclave).

19.5.2 Curing temperature

Two types of adhesives can be distinguished with respect to the curing temperature:

- cold-curing adhesives;
- hot-curing adhesives.

For cold-curing adhesives the curing process can take place at room temperature. For hot-curing adhesives heating, commonly between 80 °C and 120 °C, should take place for the curing process. [4, 59]

Heating can be applied through;

- Radiant heat;
- An oven (autoclave);
- a resistance element which is clamped between the adherent and adhesive;
- a resistance wire embedded in adhesive;
- inductive, respectively, high-frequency heating;
- pressing plates or moulds which are heated by steam, water, oil or an electric element.

19.5.3 Curing time

The curing time is defined as the time period in which the curing temperature is maintained. Commonly the curing time is kept longer than strictly necessary. [4, 59]

19.5.4 Drying adhesives

There are two types of drying adhesives, solvent based adhesives and dispersion adhesives. [4, 59]

19.5.4.1 Solvent based adhesives

Adhesives that are solved in a solvent are solvent based adhesives. In the curing process the solvent disappears, mostly by evaporating, and the adhesive hardened. [4, 59, 60]

19.5.4.2 Dispersion adhesives

Dispersion adhesives harden due to the emigration of water out of the adhesive. Therefore in principle one of the adhesives should be able to take up water. [4, 59]

19.5.5 Pressure sensitive adhesives (PSA)

For pressure sensitive adhesives moderate pressure alone is sufficient for hardening. [4, 59, 60]

19.5.6 Contact adhesives

Contact adhesive are applied on each adherent. After a certain period the two adherent with the adhesive are pressed together. [4, 59]

19.5.7 Hot melt adhesives (HMA)

As mentioned in section 19.4 hot melt adhesives have a solid form in the uncured state. After heating the adhesive hardens again and obtains its final strength. [4, 59, 60]

19.5.8 Anaerobic adhesives

Anaerobic adhesives cure in absence of oxygen. [4, 59, 60]

19.5.9 Radiation-cured adhesives

Some adhesives cure when they are radiated. Usually this is done by UV-radiation (UV adhesives) but also electron radiation (electron beam cured (EBC) adhesives), low- or high frequency waves (microwave) or a laser can be required. [4, 59, 60]

19.5.10 Moisture curing adhesives

Some adhesives cure under influence of moisture, these are called moisture curing adhesives. [4, 59]

19.6 Pre-treatment

Pre-treatments are meant to improve bonding and durability. Degreasing, chemical treatments and mechanical treatments are examples of surface treatments. A good pre-treatment will lead to [4, 59, 60]:

- improvement of mechanical properties;
- improvement of durability;
- improvement of service life;
- ability to bond difficult adherents

19.6.1 Degreasing

Degreasing is the most basic form of a surface treatment. In most cases degreasing is required to obtain sufficient strength. [4, 59]

19.6.2 Chemical treatment

Some adherents demand chemical treatments to ensure sufficient bonding and chemical resistance. The main types of chemical treatments are [4, 59]:

- etching;
- pickling;
- anodising.

19.6.3 Mechanical treatment

Mechanical treatments are applied for two reasons [4, 59]:

- Removing contaminations;
- Roughening to increase the surface for better (mechanical or specific) adhesion.

There are four main types of mechanical treatments [4, 59]:

- blasting;
- grinding;
- abrading;
- brushing;

19.6.4 Plasma treatment

Plasma can be used for different purposes [4, 59]:

- cleaning and etching;
- UV/ozone cleaning;
- polymerisation of a primer to a substrate surface;
- ion-implantation.

19.6.5 Primers

Primers form a thin layer on the adherent. They are applied for different reasons:

- increase wettability of adherent/primer by adhesive;
- increase the application range of an adhesive;
- increase durability;
- increase flexibility of production process.

Primers with a low surface energy are better wettable than adhesive with a high surface energy, see section 4.2.2.1 and 4.2.2.2.

Adhesives and adherent combinations that have bad bond qualities can sometimes be improved by the intermediary of a primer. This increases the application range of an adhesive.

Primers can form a layer which has good bond qualities to the adherent and adhesive.

As mentioned in section 6.2.2, primers can prevent the adherent from corroding when the adhesive is displaced under influence of moisture, which increases the durability.

This property also increases the flexibility of the production process. The time between surface treatments and application of the adhesive can be longer. Moreover, the surface of a primer is generally easier to clean than the surface of an adherent. [4, 59]

19.7 Additives

Additives are discussed in section 4.1.3.

19.8 Overview of adhesive types

The next two tables present an overview of the adhesive types. These two tables do not include all types and are general. The tables are a translation of table 5.1 and 5.2 of reference [4].

	Metal	Wood	Glass, ceramics	Textile	Thermoset	Cellulosic plastics	ABS	PVC, hard	PVC, soft	PA	PC	Saturated polyester	PF	PF	PMMA	POM	PP	PS	PTFE	PS	PTFE	PU	Natural rubber	Neoprene	AN rubber	Silicone rubber	Foam, PVC	Foam, PS	Foam, PU
Metal	2,3,5,6, 8/11,13	1/3,5,7, 9,10,11, 12	3,5,7/10, 10,13	1/3,5,9, 10,13	3,5,6, 9/11,13	3,9, 10	3,4,9, 10	3,6, 8/10	3, 10	3,4,7, 8/10	3,4,6, 8/10	3,6,9, 3,9,1	6,9, 0	11	4,6,9, 9/11	3,6, 9/11	3,9, 10	1/3, 10	3,6, 9/11,14	1/3,6,7, 9,10	3,6, 9/11,14	3, 9/11	1/3,8, 10,11	3, 8/11	3,8/11	14	3,9,1 3,9,10	3,7,10	
Wood		1/3,7,9/ 10,14	3,7,9, 10,14	1/3,10,14	1,9/12, 9/12	1/3, 10	1/4,9, 10	10	10	2,3,9, 3,9,10	3,7,9, 3,6,7, 10	1/3, 9	10	11,12	3,9,10, 9/11,13	1/3, 10	1/3, 10	1/3, 10	1/4,7,9, 10	1/4,7,9, 10	6,9	1/3, 9/11	1/3, 10,11	2,3, 9/11	14	1/3, 10	2,3,7,10		
Glass, ceramics		3,7,9,10, 13,14	3,7,9, 10,14	1,9,10, 14	7,9,14	3,7, 10	3,9, 10	14	14	3,9,14	3,6,9, 3,7, 14	3,14, 14	14	14	3,6,9, 14	3,14, 10	3,14, 10	3,14, 10	3,7,9, 10	3,7,9, 10	6,9,14	9,10	8,10, 11	9,9,14	14	3,9,1 3,9	3,7,10, 14		
Textile		1/3,10	1/3,10	1,9/12	1,9/12	1/3, 10	1/4, 10	3,9	3	2,3,9, 10	3,9, 10	3,7,9, 10	10	10	3,4,6, 10,11	2,3,10	10,13, 14	1/3,7,9, 10	1/3,7,9, 10	1/3,7,9, 10	1,3,10	2,3, 10	1/3, 10	3,10	14	1/3, 10	2,3		
Thermoset					6/11	3,6,7, 9/11	3,4,9, 10	3,9	3	3,9,10	6,9, 10	3,6,7, 10	3,10	7,9	3,6,7, 9	3,6,9, 10	3,10	3,4,9, 10	3,4,7,9, 10	3,4,7,9, 10	3,6,9, 10	3,10	3,2,3, 10	3, 10	1/3,9, 10	1/3,9,10	3,7		
Cellulosic plastics						1/4,7, 9,10	1/4,9, 10	3,9	3	3,9,10	3,6,9, 10	3,6,7, 10	3,10	11	3,9, 10	3,9, 10	3,10	3,7,9, 10	3,7,9, 10	3,7,9, 10	3,9,11	3,9, 10	2,3, 10	2,3, 10	14	3,9,1 3,10	3,7		
ABS						4,9, 10	4,9, 10	11	11	3,4,6, 10	3,9, 10	3,7, 10	3	11	3,4,6, 9,10	3,9/11	3,10	3,9,10	3,9,10	3,9,10	3,9	2,3,9, 10	2,3, 10	2,3, 10	14	2,3,9, 10	1/3,9,10		
PVC, hard								8/10	8/10	2,4,6, 9,10	3,4, 6/10	3,6,7, 9	3,10	3	3,9	3,6,9, 10	3,9, 10	3,4, 8/10,14	3,4, 8/10,14	3,4, 8/10,14	3,9,10	2,3,9, 10	2,3, 10	2,3, 10	14	2,3,9, 10	3,9,10		
PVC, soft																													
PA																													
PC																													
Saturated polyester																													
PE																													
PF																													
PMMA																													
POM																													
PP																													
PS																													
PTFE																													
PU																													
Natural rubber																													
Neoprene																													
AN rubber																													
Silicone rubber																													
Foam, PVC																													
Foam, PS																													
Foam, PU																													

Table 19.1: Overview of different adhesives and adherent combinations [4]

19.9 Testing

Testing can be done on bulk adhesives, to determine material properties, and on connections, to detect defects in the bondline or determine the failure load. To determine material properties and failure loads, commonly destructive tests are applied. To detect defects non-destructive testing is applied. In Figure 19.1 the most important defects can be found. A defect forms a discontinuity in the bondline which causes peak stresses, hence lowering the failure load. [4, 18, 59]

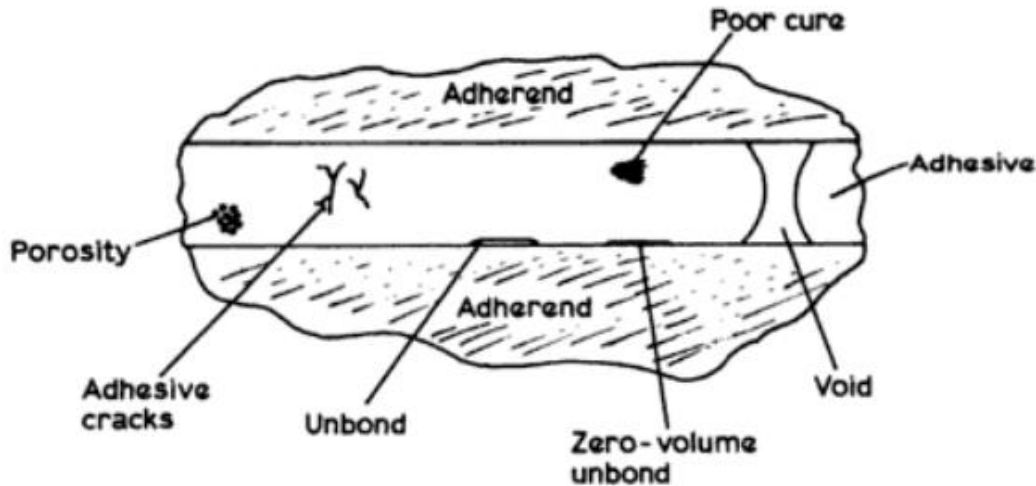


Figure 19.1: Typical defects in an adhesive bondline [18]

Volatiles and air can cause porosity. Adhesive cracks are caused by stresses or curing problems. Unbond is a special form of a void and is often caused by application of the adhesive on one adherend only and unevenly. Poor cure is caused by poor mixing, poor formulation or insufficient heating. When the adherend and adhesive are in contact but they do not have significant strength it is called zero-volume unbond. This can be caused by, for instance, poor surface treatment. Voids are caused by air that is trapped or the lack of applied adhesive. [4, 18, 59]

19.9.1 Destructive testing

Destructive tests are always mechanical test. There is a wide variety of different types, either for determining the bulk properties or for the failure loads. Most important are the properties with respect to: [4, 59, 60]

- shear;
- tensile;
- peel;
- cleavage;
- creep;
- fatigue;
- durability.

19.9.2 Non-destructive testing (NDT)

There is a wide variety of different types of non-destructive testing, the most important ones are listed below: [4, 18, 59, 60]

- visual inspection;
- tapping;
- thermal inspection;
- ultrasonic inspection;

- acoustic inspection;
- optical holography;
- radiography;
- capacity measuring;
- electromagnetic inspection;

Visual inspection will give some information about the mixing quality (consistent colour), application of enough adhesive (squeeze out some of the adhesive) and large debond areas. This method is especially useful to investigate if further testing is needed. A larger perimeter-area-ratio makes this method more effective.

With tapping debonds and delamination can be detected.

With thermal inspection large areas can be checked for voids at the surface.

With the ultrasonic method planar defects as small as 0.3 mm such as debonding and delamination but also voids and porosity can be detected. Due to the low acoustic conductivity (see section 3.1.8) of adhesives the depth of inspection is limited to 40-50mm.

With acoustic inspection all kinds of differences in material changes can be found.

With optical holography small surface deformation (0.5 μ m) caused by defects can be found, but not the defect itself. This method is especially effective for thin substrates.

Radiography is, due to the large difference in density of steel and adhesives, not suitable for adhesive bonded metal connections

Capacity measuring is not suitable for large areas, which makes this method not suitable for adhesive bonds in structural engineering.

Electromagnetic methods can detect all kind of differences in material changes i.e. conductivity. Defects parallel to the magnetic current cannot be detected. The achievable inspection depth depends on the conductivity of the material. Adhesives have a low conductivity which limits the inspection depth. Therefore this method seems more suitable for inspecting adherents.

20 Appendix D: Design sketches

In this appendix design sketches can be found made during the design study. The next abbreviations and colours are used:

s	shear	Red	prefabricated welds
p	peel	Blue	steel plates
t	tension	Green	adhesive
c	compression		

20.1 T-connections

① + Simple Profiles
- Peel

② + Simple
- Peel

③ + Simple Profiles
- MANY welds
+ Shear

④ + Shear & Compression
- Laborios

⑤ + Simple
- Tension

⑥ + Simple
- Peel
- MANY Pieces
+ Double Lap

⑦ + Double Lap
- Tension
- Laborios
- Tolerances

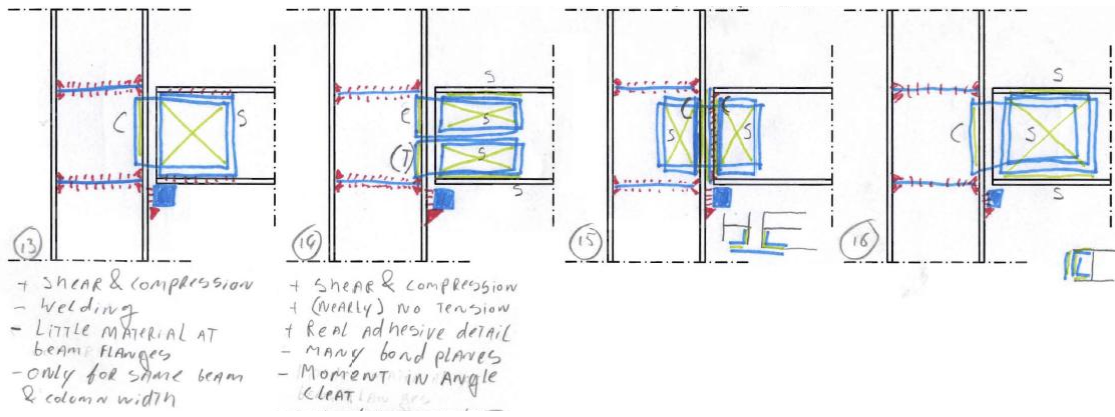
⑧ + (NEARLY) no Tension
- MAKEABILITY inner welds
- Place for stiffeners
- Placement floor element
- only for same beam & column width

⑨ + Shear
+ Easy bondplanes
- inner welds
- MANY welds
- only for same beam & column width

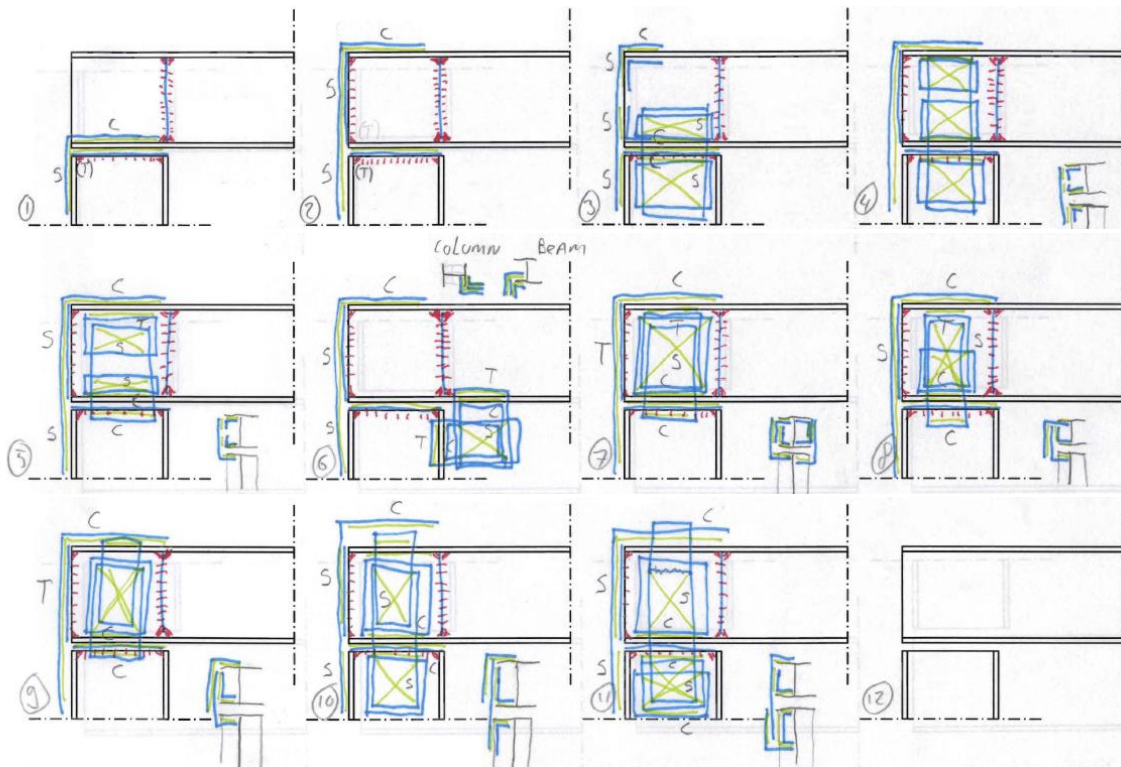
⑩ + Shear
+ Easy bondplanes
- many welds
- only for same beam & column width

⑪ + Shear & Compression
+ NEARLY no Tension
+ Double Lap
- Many bondplanes
- only for same beam & column width
- Moment in angle cleat

⑫ Same as ⑪



20.2 L-connections

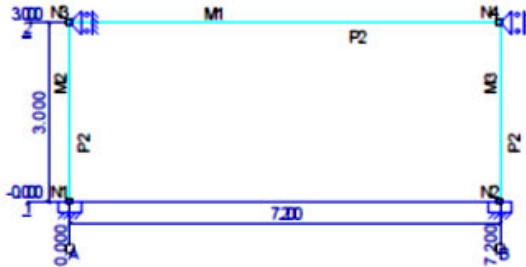


21 Appendix E: MatrixFrame calculation

On the next pages a printout of MatrixFrame calculations can be found.

21.1 Zero storeys

Graduation		Frame of utility building		0 storeys	
Design calculation of frame of utility building					
Job Name	Graduation	Job Number	0 storeys		
Part Description	Frame of utility building	Structural Engineer	JHJ Floor		
Client	4050614	Units	m, kN, kNm		
File	D:\TU Delft\Graduation\Products\MatrixFrame\HE200-300A\0Storey.mxe				



Pic. Geometry: Frame

Sections

Section	Section Name	Area	ly Material	Angle
P2	HE200A	5.3831e-03	3.8622e-05 S235	0
-	-	m ²	m ⁴	°

Materials

Material Name	Density	Youngs mod.	Lin. Exp.
S235	78.50	2.1000e+08	12.0000e-06
-	kN/m ³	kN/m ²	C/m

Members

Member	Node B	Node E	Section	X-B	Z-B	X-E	Z-E	Length
M1	N3	N4	P2	0,000	-3,000	7,200	-3,000	7,200
M2	N3	N1	P2	0,000	-3,000	0,000	0,000	3,000
M3	N4	N2	P2	7,200	-3,000	7,200	0,000	3,000
-	-	-	-	m	m	m	m	m

Supports

Support	Node	X	Z	Yr	AngleYr
S1	N1	fixed	fixed	fixed	0
S2	N2	fixed	fixed	fixed	0
S3	N3	fixed	free	free	0
S4	N4	fixed	free	free	0
-	-	kN/m	kN/m	kNm/rad	°

Loads Cases

Type	Value Begin	Value End	Dist. Begin	Dist. End	Direction Member/Node
LC1: G_roof					
q	4,42	4,42	0,000	7,200(L)	Z M1
Sum of loads	X:	0,00	kN Z:	31,82	kN
LC2: Q_roof					
q	8,00	8,00	0,000	7,200(L)	Z M1
Sum of loads	X:	0,00	kN Z:	57,60	kN
-	-	-	m	m	- -

Persistent Loads Combinations

L.C.	Description	Pe.C.1	Pe.C.2
LC1	G_roof	1.20	1.35
LC2	Q_roof	1.50	-

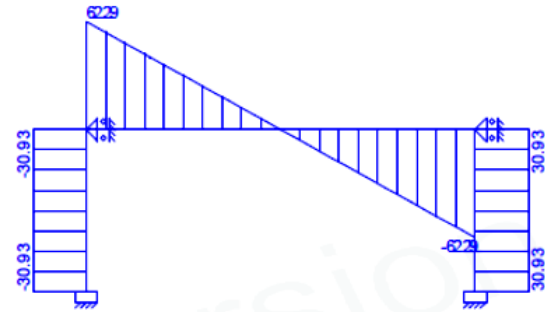
Analysis Assumptions

Linear Elastic Analysis performed

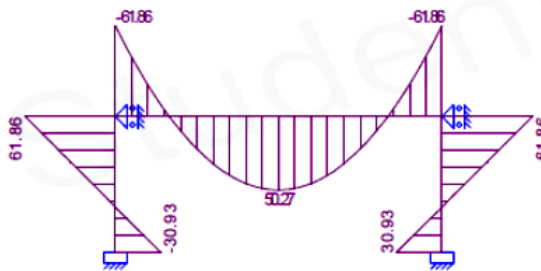
Graduation	Frame of utility building	0 storeys
------------	---------------------------	-----------



Pic. Pe.C. Normal force (Nx) Envelope



Pic. Pe.C. Shear force (Vz) Envelope



Pic. Pe.C. Moments (My) Envelope



Pic. Pe.C. Support reactions Envelope

Pe.C. Extreme Support Reactions

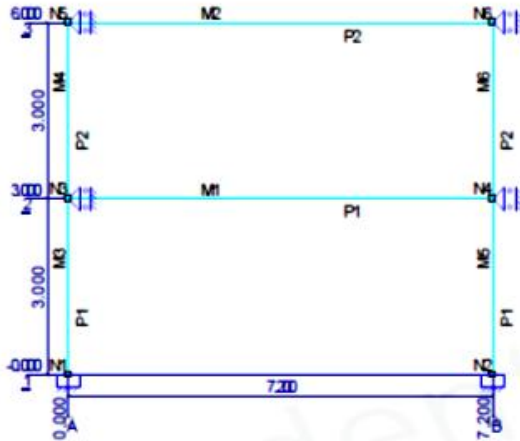
Support	Node	LComb	Xmax	Z	My	LComb	X	Zmax	My	LComb	X	Z	Mymax
S1	N1	Pe.C.1	30.93	-62.29	-30.93								
S1	N1				Pe.C.1	30.93	-62.29	-30.93	Pe.C.1	30.93	-62.29	-30.93	
S2	N2					Pe.C.1	-30.93	-62.29	30.93	Pe.C.1	-30.93	-62.29	30.93
S2	N2	Pe.C.1	-30.93	-62.29	30.93	Pe.C.1	-30.93	-62.29	30.93				
S3	N3	Pe.C.1	-30.93	0.00	0.00								
S4	N4	Pe.C.1	30.93	0.00	0.00								
Global extreme values													
S4	N4	Pe.C.1	30.93	0.00	0.00								
S3	N3	Pe.C.1	-30.93	0.00	0.00								
S2	N2				Pe.C.1	-30.93	-62.29	30.93					
S2	N2					Pe.C.1	30.93	-62.29	-30.93				
S1	N1					Pe.C.1	30.93	-62.29	-30.93				
-	-	-											
			kN	kN	kNm		kN	kN	kNm		kN	kN	kNm

Pe.C. Envelope

Member	Nx Minus	Nx Plus	Vz Minus	Vz Plus	My Minus	My Plus
M1	0.00	0.00	-62.29	62.29	-61.86	50.27
M2	-62.29	0.00	-30.93	0.00	-30.93	61.86
M3	-62.29	0.00	0.00	30.93	-61.86	30.93
-	kN	kN	kN	kN	kNm	kNm

21.2 One storey

Graduation		Frame of utility building		1 storeys	
Design calculation of frame of utility building					
Job Name	Graduation	Job Number	1 storeys		
Part Description	Frame of utility building	Structural Engineer	JHJ Floor		
Client	4050614	Units	m, kN, kNm		
File	D:\TU Delft\Graduation\Products\MatrixFrame\HE200-300A\1Storey200-300.mxe				



Pic. Geometry: Frame

Sections

Section	Section Name	Area	Iy Material	Angle
P1	HE300A	1.1253e-02	1.8263e-04 S235	0
P2	HE200A	5.3831e-03	3.6922e-05 S235	0
-	-	m2	m4 -	°

Materials

Material Name	Density	Youngs mod.	Lin. Exp.
S235	78.50	2.1000e+08	12.0000e-06
-	kN/m3	kN/m2	C/m

Members

Member	Node B	Node E	Section	X-B	Z-B	X-E	Z-E	Length
M1	N3	N4	P1	0,000	-3,000	7,200	-3,000	7,200
M2	N5	N6	P2	0,000	-6,000	7,200	-6,000	7,200
M3	N3	N1	P1	0,000	-3,000	0,000	0,000	3,000
M4	N5	N3	P2	0,000	-6,000	0,000	-3,000	3,000
M5	N4	N2	P1	7,200	-3,000	7,200	0,000	3,000
M6	N6	N4	P2	7,200	-6,000	7,200	-3,000	3,000
-	-	-	-	m	m	m	m	m

Supports

Support	Node	X	Z	Yr	AngleYr
S1	N1	fixed	fixed	fixed	0
S2	N2	fixed	fixed	fixed	0
S3	N3	fixed	free	free	0
S4	N4	fixed	free	free	0
S5	N5	fixed	free	free	0
S6	N6	fixed	free	free	0
-	-	kN/m	kN/m	kNmrad	°

Loads Cases

Type	Value Begin	Value End	Dist. Begin	Dist. End	Direction Member/Node
LC1: G_roof					
q	4,42	4,42	0,000	7,200(L)	Z' M2
Sum of loads	X:	0,00 kN	Z:	31,82 kN	
LC2: Q_roof					
q	8,00	8,00	0,000	7,200(L)	Z' M2

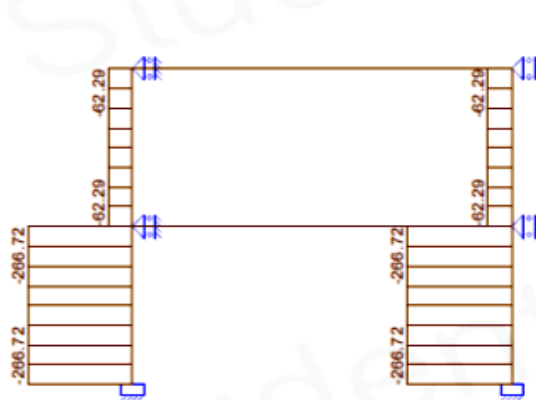
Graduation		Frame of utility building		1 storeys	
Type	Value Begin	Value End	Dist. Begin	Dist. End	Direction Member/Node
Sum of loads	X: 0,00	kN Z: 57,60			
LC3: G_storey_A	q	32,32	0,00	7,200(L)	Z' M1
Sum of loads	X: 0,00	kN Z: 232,70			
LC4: Q_storey_A	q	20,00	0,00	7,200(L)	Z' M1
Sum of loads	X: 0,00	kN Z: 144,00			
-	-	-	m	m	- -

Persistent Loads Combinations

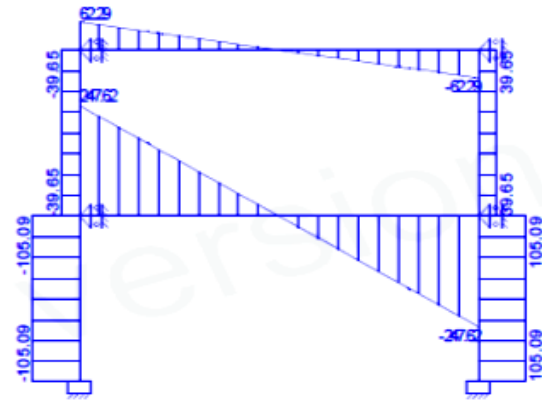
L.C.	Description	Pe.C.1	Pe.C.2	Pe.C.3
LC1	G_roof	1.20	1.20	1.35
LC2	Q_roof	1.50	-	-
LC3	G_storey_A	1.20	1.20	1.35
LC4	Q_storey_A	0.75	1.50	0.75

Analysis Assumptions

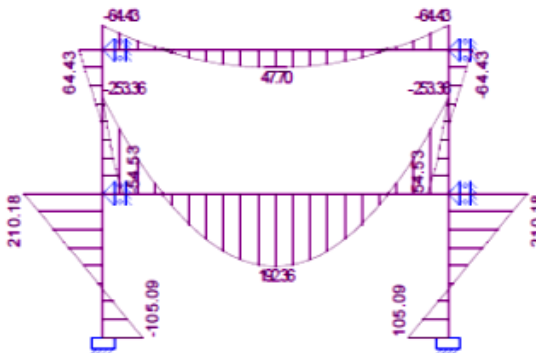
Linear Elastic Analysis performed



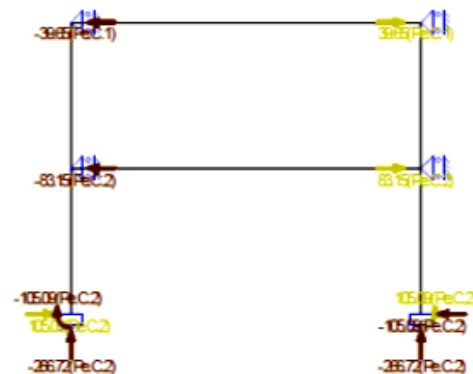
Pic. Pe.C. Normal force (Nx) Envelope



Pic. Pe.C. Shear force (Vz) Envelope



Pic. Pe.C. Moments (My) Envelope



Pic. Pe.C. Support reactions Envelope

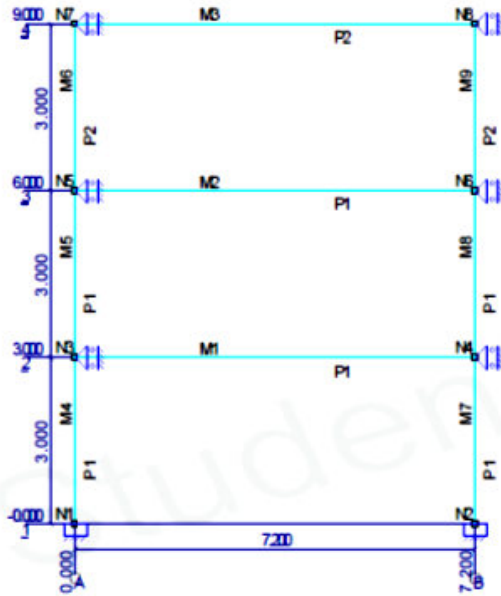
Pe.C. Extreme Support Reactions

Support	Node	LComb	Xmax	Z	My LComb	X	Zmax	My LComb	X	Z	Mymax	
S1	N1	Pe.C.2	105.09	-266.72	-105.09							
S1	N1				Pe.C.2	105.09	-266.72	-105.09	Pe.C.2	105.09	-266.72	-105.09
S2	N2				Pe.C.2	-105.09	-266.72	105.09				
S2	N2	Pe.C.2	-105.09	-266.72	105.09	Pe.C.2	-105.09	-266.72	105.09		105.09	

Graduation			Frame of utility building				1 storeys						
Support	Node	LComb	Xmax	Z	My	LComb	X	Zmax	My	LComb	X	Z	Mymax
S3	N3	Pe.C.2	-83.15	0.00	0.00								
S4	N4	Pe.C.2	83.15	0.00	0.00								
S5	N5	Pe.C.1	-39.65	0.00	0.00								
S6	N6	Pe.C.1	39.65	0.00	0.00								
Global extreme values													
S1	N1	Pe.C.2	105.09	-266.72	-105.09								
S2	N2	Pe.C.2	-105.09	-266.72	105.09								
S2	N2					Pe.C.2	-105.09	-266.72	105.09				
S2	N2									Pe.C.2	-105.09	-266.72	105.09
S1	N1									Pe.C.2	105.09	-266.72	-105.09
-	-	-	kN	kN	kNm	-	kN	kN	kNm		kN	kN	kNm
Pe.C. Envelope													
Member	Nx Minus	Nx Plus	Vz Minus	Vz Plus	My Minus	My Plus							
M1	0.00	0.00	-247.62	247.62	-253.36	182.36							
M2	0.00	0.00	-62.29	62.29	-64.43	47.70							
M3	-266.72	0.00	-105.09	0.00	-105.09	210.18							
M4	-62.29	0.00	-39.65	0.00	-54.53	64.43							
M5	-266.72	0.00	0.00	105.09	-210.18	105.09							
M6	-62.29	0.00	0.00	39.65	-64.43	54.53							
-	kN	kN	kN	kN	kNm	kNm							

21.3 Two storeys

Graduation		Frame of utility building		2 storeys	
Design calculation of frame of utility building					
Job Name	Graduation	Job Number	2 storeys		
Part Description	Frame of utility building	Structural Engineer	JHJ Floor		
Client	4050614	Units	m, kN, kNm		
File	D:\TU Delft\Graduation\Products\MatrixFrame\HE200-300A\2Storey200-300.mxe				



Pic. Geometry: Frame

Sections

Section	Section Name	Area	Iy Material	Angle
P1	HE300A	1.1253e-02	1.8263e-04 S235	0
P2	HE200A	5.3831e-03	3.6922e-05 S235	0
-	-	m ²	m ⁴	°

Materials

Material Name	Density	Youngs mod.	Lin. Exp.
S235	78.50	2.1000e+08	12.0000e-06
-	kN/m ³	kN/m ²	C/m

Members

Member	Node B	Node E	Section	X-B	Z-B	X-E	Z-E	Length
M1	N3	N4	P1	0.000	-3.000	7.200	-3.000	7.200
M2	N5	N6	P1	0.000	-6.000	7.200	-6.000	7.200
M3	N7	N8	P2	0.000	-9.000	7.200	-9.000	7.200
M4	N3	N1	P1	0.000	-3.000	0.000	0.000	3.000
M5	N5	N3	P1	0.000	-6.000	0.000	-3.000	3.000
M6	N7	N5	P2	0.000	-9.000	0.000	-6.000	3.000
M7	N4	N2	P1	7.200	-3.000	7.200	0.000	3.000
M8	N6	N4	P1	7.200	-6.000	7.200	-3.000	3.000
M9	N8	N6	P2	7.200	-9.000	7.200	-6.000	3.000
-	-	-	-	m	m	m	m	m

Supports

Support	Node	X	Z	Yr	AngleYr
S1	N1	fixed	fixed	fixed	0
S2	N2	fixed	fixed	fixed	0
S3	N3	fixed	free	free	0
S4	N4	fixed	free	free	0
S5	N5	fixed	free	free	0
S6	N6	fixed	free	free	0

Graduation	Frame of utility building	2 storeys
------------	---------------------------	-----------

Support	Node	X	Z	Yr	AngleYr
S7	N7	fixed	free	free	0
S8	N8	fixed	free	free	0
-	-	kN/m	kN/m	kNmrad	°

Loads Cases

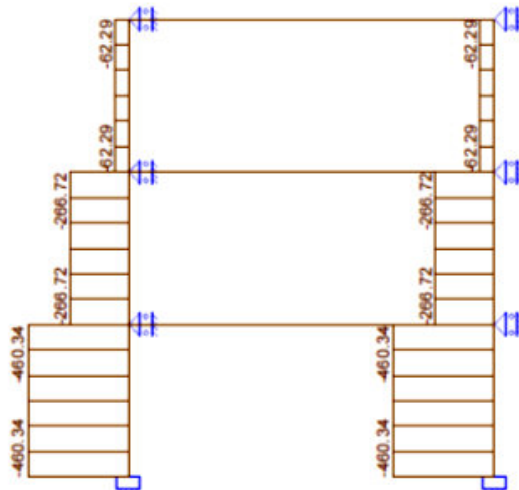
Type	Value Begin	Value End	Dist. Begin	Dist. End	Direction Member/Node
LC1: G_roof					
q	4.42	4.42	0.000	7.200(L)	Z' M3
Sum of loads	X: 0,00	kN Z: 31,82	kN		
LC2: Q_roof					
q	8.00	8.00	0.000	7.200(L)	Z' M3
Sum of loads	X: 0,00	kN Z: 57,60	kN		
LC3: G_storey_A					
q	32.32	32.32	0.000	7.200(L)	Z' M2
Sum of loads	X: 0,00	kN Z: 232,70	kN		
LC4: Q_storey_A					
q	20.00	20.00	0.000	7.200(L)	Z' M2
Sum of loads	X: 0,00	kN Z: 144,00	kN		
LC5: Q_storey_B					
q	32.32	32.32	0.000	7.200(L)	Z' M1
Sum of loads	X: 0,00	kN Z: 232,70	kN		
LC6: Q_storey_B					
q	20.00	20.00	0.000	7.200(L)	Z' M1
Sum of loads	X: 0,00	kN Z: 144,00	kN		
-	-	-	m	m	--

Persistent Loads Combinations

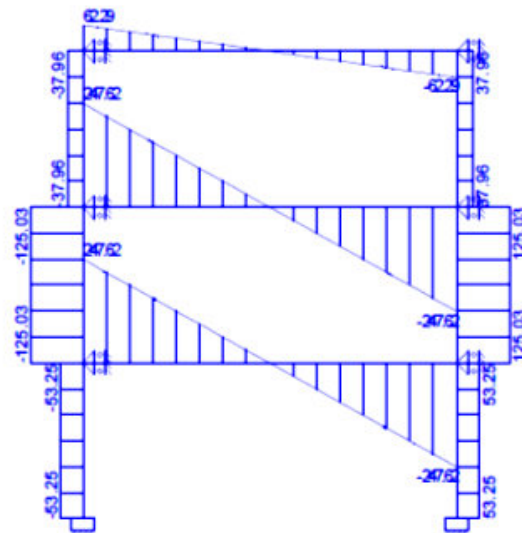
LC	Description	Pe.C.1	Pe.C.2	Pe.C.3	Pe.C.4
LC1	G_roof	1.20	1.20	1.20	1.35
LC2	Q_roof	1.50	-	-	-
LC3	G_storey_A	1.20	1.20	1.20	1.35
LC4	Q_storey_A	0.75	1.50	0.75	0.75
LC5	Q_storey_B	1.20	1.20	1.20	1.35
LC6	Q_storey_B	0.75	0.75	1.50	0.75

Analysis Assumptions

Linear Elastic Analysis performed

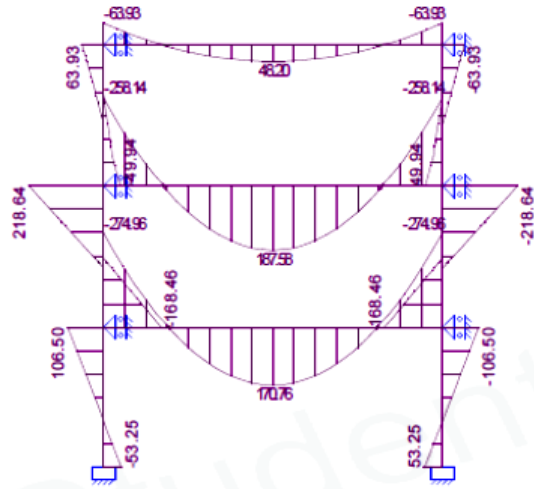


Pic. Pe.C. Normal force (Nx) Envelope

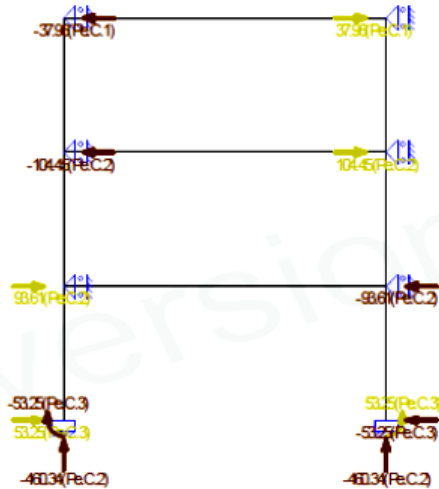


Pic. Pe.C. Shear force (Vz) Envelope

Graduation	Frame of utility building	2 storeys
------------	---------------------------	-----------



Pic. Pe.C. Moments (My) Envelope



Pic. Pe.C. Support reactions Envelope

Pe.C. Extreme Support Reactions

Support	Node	LComb	Xmax	Z	My	LComb	X	Zmax	My	LComb	X	Z	Mymax
S1	N1	Pe.C.3	53.25	-460.34	-53.25								
S1	N1					Pe.C.2	31.41	-460.34	-31.41	Pe.C.3	53.25	-460.34	-53.25
S2	N2									Pe.C.3	-53.25	-460.34	53.25
S2	N2	Pe.C.3	-53.25	-460.34	53.25	Pe.C.2	-31.41	-460.34	31.41				
S3	N3	Pe.C.2	93.61	0.00	0.00								
S4	N4	Pe.C.2	-93.61	0.00	0.00								
S5	N5	Pe.C.2	-104.45	0.00	0.00								
S6	N6	Pe.C.2	104.45	0.00	0.00								
S7	N7	Pe.C.1	-37.96	0.00	0.00								
S8	N8	Pe.C.1	37.96	0.00	0.00								
Global extreme values													
S6	N6	Pe.C.2	104.45	0.00	0.00								
S5	N5	Pe.C.2	-104.45	0.00	0.00								
S2	N2					Pe.C.2	-31.41	-460.34	31.41				
S2	N2									Pe.C.3	-53.25	-460.34	53.25
S1	N1									Pe.C.3	53.25	-460.34	-53.25
-	-	-	kN	kN	kNm	-	kN	kN	kNm		kN	kN	kNm

Pe.C. Envelope

Member	Nx Minus	Nx Plus	Vz Minus	Vz Plus	My Minus	My Plus
M1	0.00	0.00	-247.62	247.62	-274.96	170.76
M2	0.00	0.00	-247.62	247.62	-258.14	187.58
M3	0.00	0.00	-62.29	62.29	-63.93	48.20
M4	-460.34	0.00	-53.25	0.00	-53.25	106.50
M5	-266.72	0.00	-125.03	0.00	-168.46	218.64
M6	-62.29	0.00	-37.96	0.00	-49.94	63.93
M7	-460.34	0.00	0.00	53.25	-106.50	53.25
M8	-266.72	0.00	0.00	125.03	-218.64	168.46
M9	-62.29	0.00	0.00	37.96	-63.93	49.94
-	kN	kN	kN	kN	kNm	kNm

21.4 Three storeys

Graduation		Frame of utility building		3 storeys	
Design calculation of frame of utility building					
Job Name	Graduation	Job Number	3 storeys		
Part Description	Frame of utility building	Structural Engineer	JHJ Floor		
Client	4050614	Units	m, kN, kNm		
File	D:\TU Delft\Graduation\Products\MatrixFrame\HE200-300A\3Storey200-300.mxe				



Pic. Geometry: Frame

Sections

Section	Section Name	Area	Iy Material	Angle
P1	HE300A	1.1259e-02	1.8263e-04 S235	0
P2	HE200A	5.3831e-03	3.6922e-05 S235	0
-	-	m2	m4 -	°

Materials

Material Name	Density	Youngs mod.	Lin. Exp.
S235	78.50	2.1000e+08	12.0000e-08
-	kN/m3	kN/m2	C/m

Members

Member	Node B	Node E	Section	X-B	Z-B	X-E	Z-E	Length
M1	N4	N5	P1	0,000	-3,000	7,200	-3,000	7,200
M2	N8	N7	P1	0,000	-6,000	7,200	-6,000	7,200
M3	N8	N9	P1	0,000	-9,000	7,200	-9,000	7,200
M4	N10	N11	P2	0,000	-12,000	7,200	-12,000	7,200
M5	N4	N2	P1	0,000	-3,000	0,000	0,000	3,000
M6	N8	N4	P1	0,000	-6,000	0,000	-3,000	3,000
M7	N8	N6	P1	0,000	-9,000	0,000	-6,000	3,000
M8	N10	N8	P2	0,000	-12,000	0,000	-9,000	3,000
M9	N5	N3	P1	7,200	-3,000	7,200	0,000	3,000
M10	N7	N5	P1	7,200	-6,000	7,200	-3,000	3,000
M11	N9	N7	P1	7,200	-9,000	7,200	-6,000	3,000
M12	N11	N9	P2	7,200	-12,000	7,200	-9,000	3,000
-	-	-	-	m	m	m	m	m

Graduation	Frame of utility building	3 storeys
------------	---------------------------	-----------

Supports

Support	Node	X	Z	Yr	AngleYr
S3	N10	fixed	free	free	0
S4	N8	fixed	free	free	0
S5	N6	fixed	free	free	0
S6	N4	fixed	free	free	0
S7	N2	fixed	fixed	fixed	0
S8	N3	fixed	fixed	fixed	0
S9	N5	fixed	free	free	0
S10	N7	fixed	free	free	0
S11	N9	fixed	free	free	0
S12	N11	fixed	free	free	0
-	-	kN/m	kN/m	kNmrad	°

Loads Cases

Type	Value Begin	Value End	Dist. Begin	Dist. End	Direction Member/Node
LC1: G_roof q	4,42	4,42	0,000	7,200(L)	Z' M4
Sum of loads	X: 0,00	kN Z: 31,82	kN		
LC2: Q_roof q	8,00	8,00	0,000	7,200(L)	Z' M4
Sum of loads	X: 0,00	kN Z: 57,60	kN		
LC3: G_storey_A q	32,32	32,32	0,000	7,200(L)	Z' M3
Sum of loads	X: 0,00	kN Z: 232,70	kN		
LC4: Q_storey_A q	20,00	20,00	0,000	7,200(L)	Z' M3
Sum of loads	X: 0,00	kN Z: 144,00	kN		
LC5: Q_storey_B q	32,32	32,32	0,000	7,200(L)	Z' M2
Sum of loads	X: 0,00	kN Z: 232,70	kN		
LC6: Q_storey_B q	20,00	20,00	0,000	7,200(L)	Z' M2
Sum of loads	X: 0,00	kN Z: 144,00	kN		
LC7: G_storey_C q	32,32	32,32	0,000	7,200(L)	Z' M1
Sum of loads	X: 0,00	kN Z: 232,70	kN		
LC8: Q_storey_C q	20,00	20,00	0,000	7,200(L)	Z' M1
Sum of loads	X: 0,00	kN Z: 144,00	kN		
-	-	-	m	m	- -

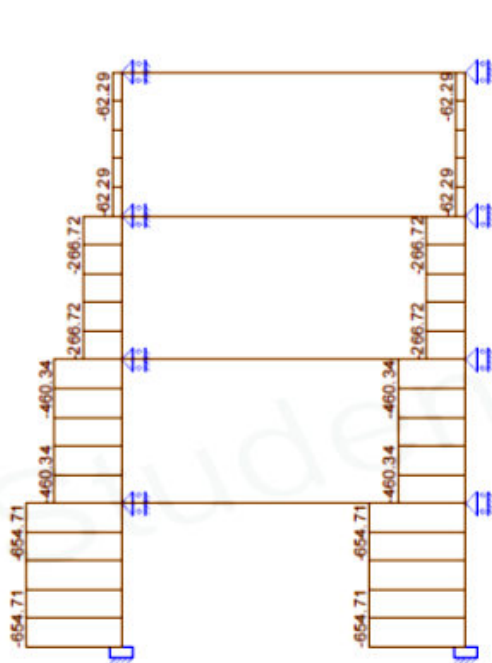
Persistent Loads Combinations

LC.	Description	Pe.C.1	Pe.C.2	Pe.C.3	Pe.C.4	Pe.C.5
LC1	G_roof	1.20	1.20	1.20	1.20	1.35
LC2	Q_roof	1.50	-	-	-	-
LC3	G_storey_A	1.20	1.20	1.20	1.20	1.35
LC4	Q_storey_A	0.75	1.50	0.75	0.75	0.75
LC5	Q_storey_B	1.20	1.20	1.20	1.20	1.35
LC6	Q_storey_B	0.75	0.75	1.50	0.75	0.75
LC7	G_storey_C	1.20	1.20	1.20	1.20	1.35
LC8	Q_storey_C	0.75	0.75	0.75	1.50	0.75

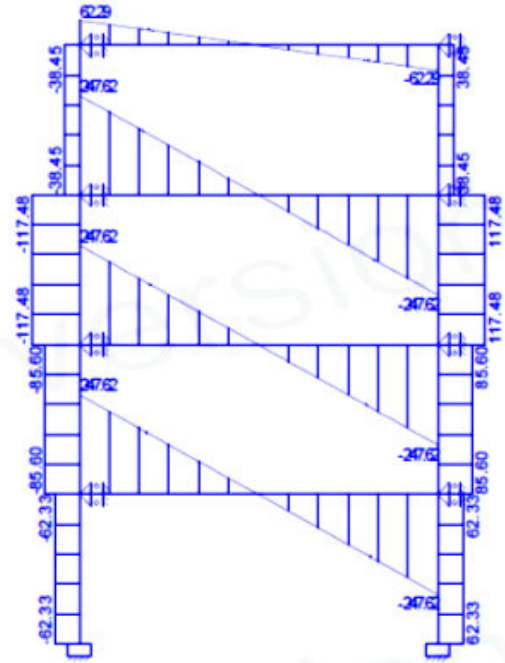
Analysis Assumptions

Linear Elastic Analysis performed

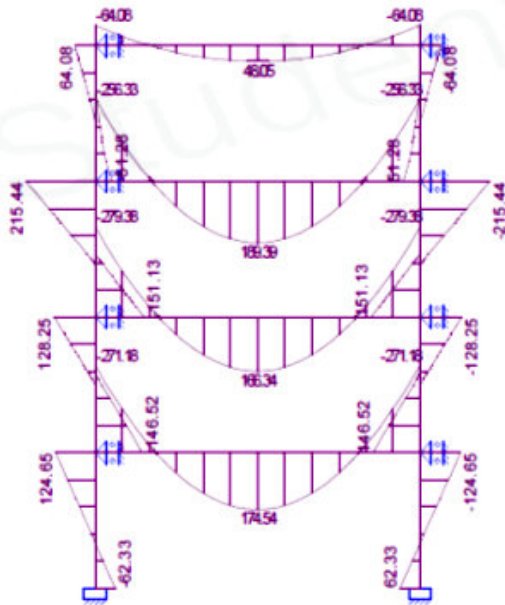
Graduation	Frame of utility building	3 storeys
------------	---------------------------	-----------



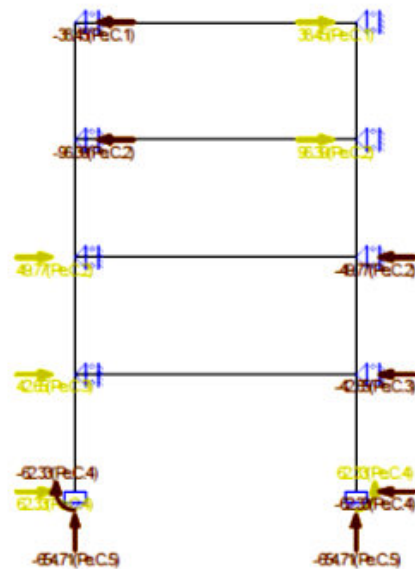
Pic. Pe.C. Normal force (Nx) Envelope



Pic. Pe.C. Shear force (Vz) Envelope



Pic. Pe.C. Moments (My) Envelope



Pic. Pe.C. Support reactions Envelope

Pe.C. Extreme Support Reactions

Support	Node	LComb	Xmax	Z	My LComb	X	Zmax	My LComb	X	Z	Mymax
S3	N10	Pe.C.1	-38.45	0.00	0.00						
S4	N6	Pe.C.2	-96.39	0.00	0.00						

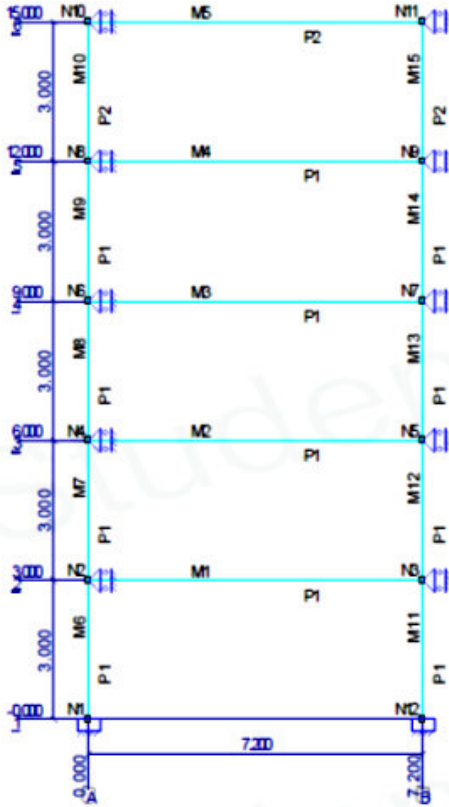
Graduation			Frame of utility building				3 storeys						
Support	Node	LComb	Xmax	Z	My	LComb	X	Zmax	My	LComb	X	Z	Mymax
S5	N8	Pe.C.2	49.77	0.00	0.00								
S6	N4	Pe.C.3	42.65	0.00	0.00								
S7	N2	Pe.C.4	62.33	-653.96	-62.33								
S7	N2				Pe.C.5	51.00	-654.71	-51.00	Pe.C.4	62.33	-653.96	-62.33	
S8	N3								Pe.C.4	-62.33	-653.96	62.33	
S8	N3	Pe.C.4	-62.33	-653.96	62.33	Pe.C.5	-51.00	-654.71	51.00				62.33
S9	N5	Pe.C.3	-42.65	0.00	0.00								
S10	N7	Pe.C.2	-49.77	0.00	0.00								
S11	N9	Pe.C.2	96.39	0.00	0.00								
S12	N11	Pe.C.1	38.45	0.00	0.00								
Global extreme values													
S11	N9	Pe.C.2	96.39	0.00	0.00								
S4	N8	Pe.C.2	-96.39	0.00	0.00								
S7	N2				Pe.C.5	51.00	-654.71	-51.00					
S8	N3								Pe.C.4	-62.33	-653.96	62.33	
S7	N2								Pe.C.4	62.33	-653.96	-62.33	
-	-	-	kN	kN	kNm	-	kN	kN	kNm		kN	kN	kNm

Pe.C. Envelope

Member	Nx Minus	Nx Plus	Vz Minus	Vz Plus	My Minus	My Plus
M1	0.00	0.00	-247.62	247.62	-271.18	174.54
M2	0.00	0.00	-247.62	247.62	-279.38	166.34
M3	0.00	0.00	-247.62	247.62	-256.33	189.39
M4	0.00	0.00	-62.29	62.29	-64.08	48.05
M5	-654.71	0.00	-62.33	0.00	-62.33	124.85
M6	-460.34	0.00	-85.60	0.00	-146.52	128.25
M7	-266.72	0.00	-117.48	0.00	-151.13	215.44
M8	-62.29	0.00	-38.45	0.00	-51.28	64.08
M9	-654.71	0.00	0.00	62.33	-124.85	62.33
M10	-460.34	0.00	0.00	85.60	-128.25	146.52
M11	-266.72	0.00	0.00	117.48	-215.44	151.13
M12	-62.29	0.00	0.00	38.45	-64.08	51.28
-	kN	kN	kN	kN	kNm	kNm

21.5 Four storeys

Graduation		Frame of utility building		4 storeys	
Design calculation of frame of utility building					
Job Name	Graduation	Job Number	4 storeys		
Part Description	Frame of utility building		Structural Engineer	JHJ Floor	
Client	4050614	Units	m, kN, kNm		
File	D:\TU Delft\Graduation\Products\MatrixFrame\HE200-300A\4Storey200-300.mxe				



Pic. Geometry: Frame

Sections

Section	Section Name	Area	Iy Material	Angle
P1	HE300A	1.1253e-02	1.8263e-04 S235	0
P2	HE200A	5.3831e-03	3.6922e-05 S235	0
-	-	m2	m4 -	°

Materials

Material Name	Density	Youngs mod.	Lin. Exp.
S235	78.50	2.1000e+08	12.0000e-06
-	kN/m3	kN/m2	C/m

Members

Member	Node B	Node E	Section	X-B	Z-B	X-E	Z-E	Length
M1	N2	N3	P1	0.000	-3.000	7.200	-3.000	7.200
M2	N4	N5	P1	0.000	-6.000	7.200	-6.000	7.200
M3	N6	N7	P1	0.000	-9.000	7.200	-9.000	7.200
M4	N8	N9	P1	0.000	-12.000	7.200	-12.000	7.200
M5	N10	N11	P2	0.000	-15.000	7.200	-15.000	7.200
M6	N2	N1	P1	0.000	-3.000	0.000	0.000	3.000
M7	N4	N2	P1	0.000	-6.000	0.000	-3.000	3.000
M8	N6	N4	P1	0.000	-9.000	0.000	-6.000	3.000
M9	N8	N6	P1	0.000	-12.000	0.000	-9.000	3.000

Graduation	Frame of utility building	4 storeys
------------	---------------------------	-----------

Member	Node B	B	Release E	Node E	Section	X-B	Z-B	X-E	Z-E	Length
M10	N10	NVM	NVM	N8	P2	0,000	-15,000	0,000	-12,000	3,000
M11	N3	NVM	NVM	N12	P1	7,200	-3,000	7,200	0,000	3,000
M12	N5	NVM	NVM	N3	P1	7,200	-6,000	7,200	-3,000	3,000
M13	N7	NVM	NVM	N5	P1	7,200	-9,000	7,200	-6,000	3,000
M14	N9	NVM	NVM	N7	P1	7,200	-12,000	7,200	-9,000	3,000
M15	N11	NVM	NVM	N9	P2	7,200	-15,000	7,200	-12,000	3,000
-	-	-	-	-	-	m	m	m	m	m

Supports

Support	Node	X	Z	Yr	AngleYr
S1	N1	fixed	fixed	fixed	0
S2	N12	fixed	fixed	fixed	0
S3	N10	fixed	free	free	0
S4	N8	fixed	free	free	0
S5	N6	fixed	free	free	0
S6	N4	fixed	free	free	0
S7	N2	fixed	free	free	0
S8	N3	fixed	free	free	0
S9	N5	fixed	free	free	0
S10	N7	fixed	free	free	0
S11	N9	fixed	free	free	0
S12	N11	fixed	free	free	0
-	-	kN/m	kN/m	kNmrad	°

Loads Cases

Type	Value Begin	Value End	Dist. Begin	Dist. End	Direction Member/Node
LC1: G_roof					
q	4,42	4,42	0,000	7,200(L)	Z' M5
Sum of loads	X:	0,00 kN	Z:	31,82 kN	
LC2: Q_roof					
q	8,00	8,00	0,000	7,200(L)	Z' M5
Sum of loads	X:	0,00 kN	Z:	57,60 kN	
LC3: G_storey_A					
q	32,32	32,32	0,000	7,200(L)	Z' M4
Sum of loads	X:	0,00 kN	Z:	232,70 kN	
LC4: Q_storey_A					
q	20,00	20,00	0,000	7,200(L)	Z' M4
Sum of loads	X:	0,00 kN	Z:	144,00 kN	
LC5: Q_storey_B					
q	32,32	32,32	0,000	7,200(L)	Z' M3
Sum of loads	X:	0,00 kN	Z:	232,70 kN	
LC6: Q_storey_B					
q	20,00	20,00	0,000	7,200(L)	Z' M3
Sum of loads	X:	0,00 kN	Z:	144,00 kN	
LC7: G_storey_C					
q	32,32	32,32	0,000	7,200(L)	Z' M2
Sum of loads	X:	0,00 kN	Z:	232,70 kN	
LC8: Q_storey_C					
q	20,00	20,00	0,000	7,200(L)	Z' M2
Sum of loads	X:	0,00 kN	Z:	144,00 kN	
LC9: G_storey_D					
q	32,32	32,32	0,000	7,200(L)	Z' M1
Sum of loads	X:	0,00 kN	Z:	232,70 kN	
LC10: Q_storey_D					
q	20,00	20,00	0,000	7,200(L)	Z' M1
Sum of loads	X:	0,00 kN	Z:	144,00 kN	
-	-	-	m	m	- -

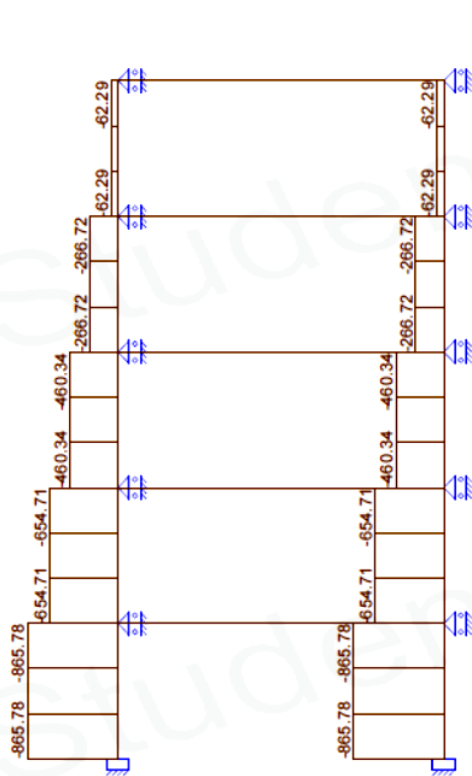
Persistent Loads Combinations

LC	Description	Pe.C.1	Pe.C.2	Pe.C.3	Pe.C.4	Pe.C.5	Pe.C.6
LC1	G_roof	1.20	1.20	1.20	1.20	1.20	1.35
LC2	Q_roof	1.50	-	-	-	-	-
LC3	G_storey_A	1.20	1.20	1.20	1.20	1.20	1.35
LC4	Q_storey_A	0.75	1.50	0.75	0.75	0.75	0.75
LC5	Q_storey_B	1.20	1.20	1.20	1.20	1.20	1.35
LC6	Q_storey_B	0.75	0.75	1.50	0.75	0.75	0.75

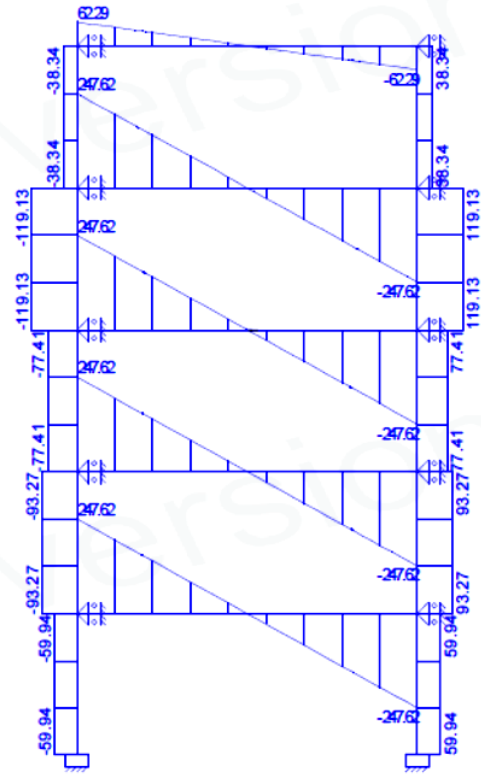
Graduation		Frame of utility building				4 storeys	
LC7	G_storey_C	1.20	1.20	1.20	1.20	1.20	1.35
LC8	Q_storey_C	0.75	0.75	0.75	1.50	0.75	0.75
LC9	G_storey_D	1.20	1.20	1.20	1.20	1.20	1.35
LC10	Q_storey_D	0.75	0.75	0.75	0.75	1.50	0.75

Analysis Assumptions

Linear Elastic Analysis performed

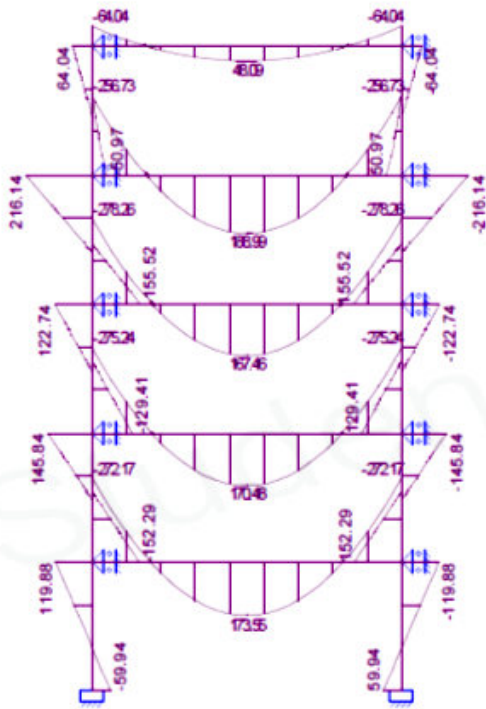


Pic. Pe.C. Normal force (Nx) Envelope

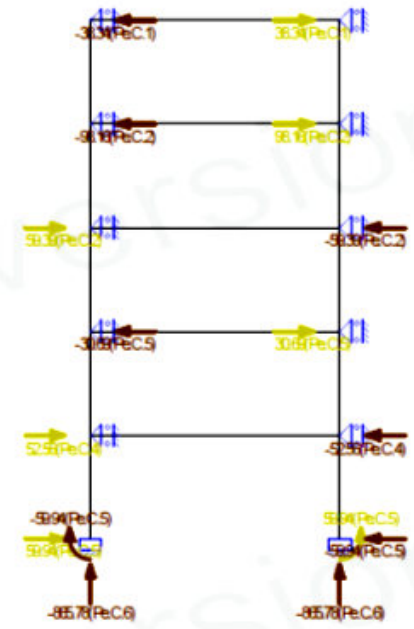


Pic. Pe.C. Shear force (Vz) Envelope

Graduation	Frame of utility building	4 storeys
------------	---------------------------	-----------



Pic. Pe.C. Moments (My) Envelope



Pic. Pe.C. Support reactions Envelope

Pe.C. Extreme Support Reactions

Support	Node	LComb	Xmax	Z	My LComb	X	Zmax	My LComb	X	Z	Mymax	
S1	N1	Pe.C.5	59.94	-847.58	-59.94							
S1	N1				Pe.C.6	48.43	-865.78	-48.43	Pe.C.5	59.94	-847.58	
S2	N12				Pe.C.5	-59.94	-847.58	59.94			59.94	
S2	N12	Pe.C.5	-59.94	-847.58	59.94	Pe.C.6	-48.43	-865.78	48.43			
S3	N10	Pe.C.1	-38.34	0.00	0.00							
S4	N8	Pe.C.2	-98.16	0.00	0.00							
S5	N6	Pe.C.2	59.39	0.00	0.00							
S6	N4	Pe.C.5	-30.69	0.00	0.00							
S7	N2	Pe.C.4	52.56	0.00	0.00							
S8	N3	Pe.C.4	-52.56	0.00	0.00							
S9	N5	Pe.C.5	30.69	0.00	0.00							
S10	N7	Pe.C.2	-59.39	0.00	0.00							
S11	N9	Pe.C.2	98.16	0.00	0.00							
S12	N11	Pe.C.1	38.34	0.00	0.00							
Global extreme values												
S11	N9	Pe.C.2	98.16	0.00	0.00							
S4	N8	Pe.C.2	-98.16	0.00	0.00							
S1	N1				Pe.C.6	48.43	-865.78	-48.43				
S2	N12				Pe.C.5	-59.94	-847.58	59.94			59.94	
S1	N1				Pe.C.5	59.94	-847.58	-59.94			-59.94	
-	-	-	kN	kN	kNm	-	kN	kN	kNm	kN	kN	kNm

Pe.C. Envelope

Member	Nx Minus	Nx Plus	Vz Minus	Vz Plus	My Minus	My Plus
M1	0.00	0.00	-247.62	247.62	-272.17	173.55
M2	0.00	0.00	-247.62	247.62	-275.24	170.48
M3	0.00	0.00	-247.62	247.62	-278.26	167.46
M4	0.00	0.00	-247.62	247.62	-256.73	188.99
M5	0.00	0.00	-82.29	82.29	-64.04	48.09

	Graduation		Frame of utility building			4 storeys
Member	Nx Minus	Nx Plus	Vz Minus	Vz Plus	My Minus	My Plus
M6	-865.78	0.00	-59.94	0.00	-59.94	119.88
M7	-654.71	0.00	-93.27	0.00	-152.29	145.84
M8	-460.34	0.00	-77.41	0.00	-129.41	122.74
M9	-266.72	0.00	-119.13	0.00	-155.52	216.14
M10	-62.29	0.00	-38.34	0.00	-50.97	64.04
M11	-865.78	0.00	0.00	59.94	-119.88	59.94
M12	-654.71	0.00	0.00	93.27	-145.84	152.29
M13	-460.34	0.00	0.00	77.41	-122.74	129.41
M14	-266.72	0.00	0.00	119.13	-216.14	155.52
M15	-62.29	0.00	0.00	38.34	-64.04	50.97
-	kN	kN	kN	kN	kNm	kNm

22 Appendix F: Element distribution of adhesive thickness

For the FEM-calculation the adhesive thickness has to be divided in a number of elements. Small elements will increase the calculation time but also may increase the accuracy. However, too small elements may increase stress peaks drastically to unrealistic values. No explicit rules exist for this division therefore a few FEM-calculations are performed. A simple lap test should give sufficient information about the effect of the number of elements. Because shear and peel stresses are of most interest, only these stresses will be compared to each other.

22.1 FEM model

In the next figure the measurements, coordinate system, load and boundary conditions can be found.

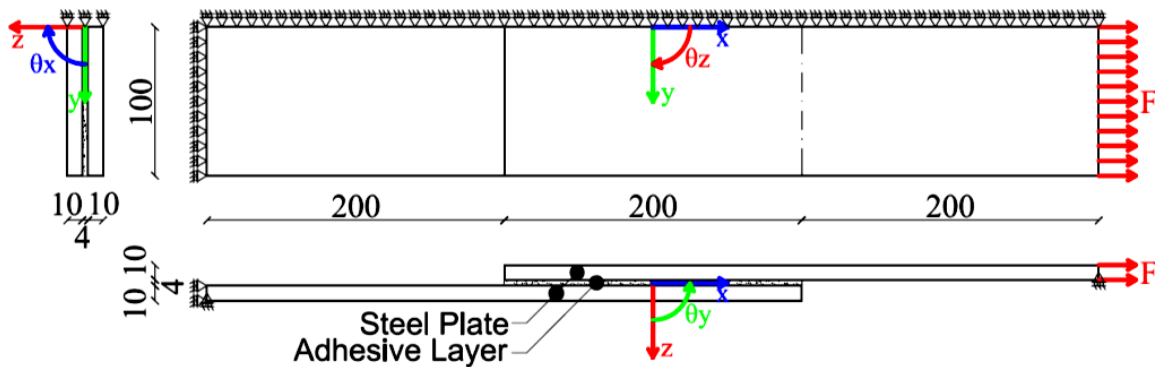


Figure 22.1: Detail for FEM calculation

22.1.1.1 Load and boundary conditions

For all calculations a displacement load in x-direction of 0.1mm is used for all the nodes of the positive x-plane of the upper steel plate.

All the nodes at $y=0$ are constrained in y-direction to model the symmetry condition. The nodes at $x=-300\text{mm}$ are constrained in x-direction. At the lines $(x, z) = (-300, 7)$ and $(x, z) = (300, -7)$ the nodes are constrained in z-direction.

22.1.1.2 Material and properties

The material and properties can be found in the next table:

Name	Type	Property	Value	Unit	Model Type
Steel	Isotropic	E	210000	N/mm ²	Elastic
		ν	0.33		
Adhesive	Isotropic	E	12800	N/mm ²	Elastic
		G	4273	N/mm ²	

Table 22.1: Material of solids for elements division adhesive thickness test

Name	Type	Sub-Type		Material
Steel	3D	Solid	Regular	Steel
Adhesive	3D	Solid	Regular	Adhesive

Table 22.2: Properties for solids for elements division adhesive thickness test

22.1.2 Mesh

The steel is divided in two elements (of 5mm) over the thickness (z-direction), the width (y-direction) is divided in 25 elements (of 4mm) and the length (x-direction) is divided in 3 x 50 elements (of 4mm). Obviously the element division of the adhesive thickness varies per test, from one up to five. The calculations should show if a calculation should be made with more than five elements.

22.2 Linear elements

In this section the peel and shear stresses out of FEM calculations with linear elements can be found. Only results for lines at z=-2 and z=0 are included, because the results of z=2 are a mirror image of those of z=-2. For all the figures below the next colours are used to indicate the number of applied elements: **1** (red) **2** (green) **3** (magenta) **4** (purple) **5** (blue).

22.2.1 Peel stresses

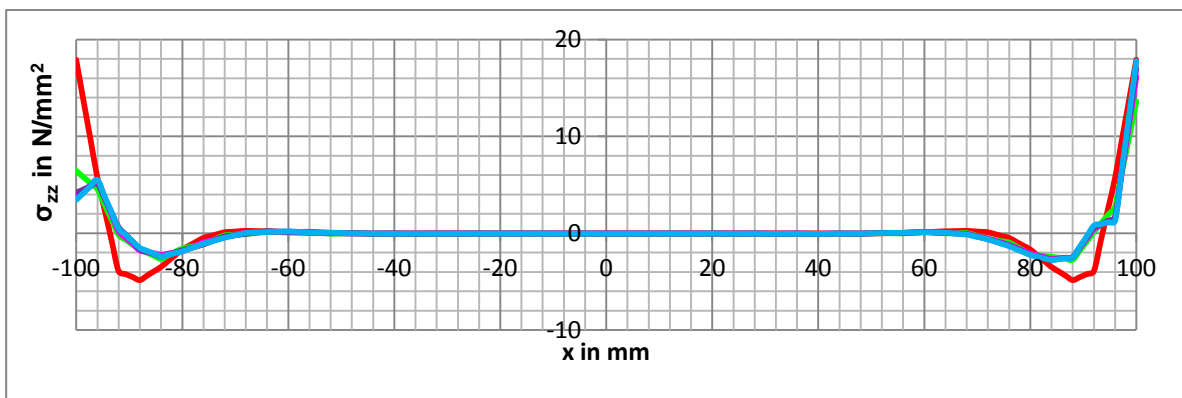


Figure 22.2: Peel stresses of FEM lap tests with linear elements at Y=0 & Z=-2

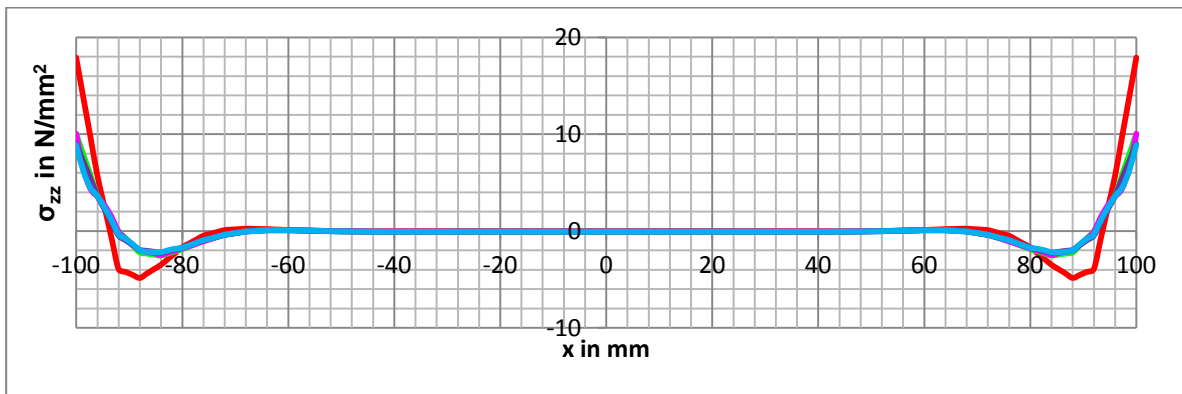


Figure 22.3: Peel stresses of FEM lap tests with linear elements at Y=0 & Z=0

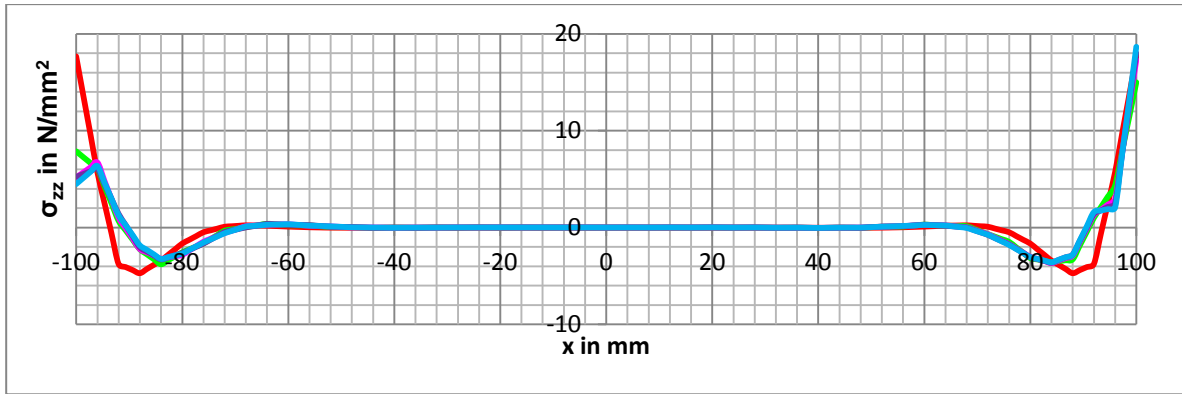


Figure 22.4: Peel stresses of FEM lap tests with linear elements at Y=50 & Z=-2

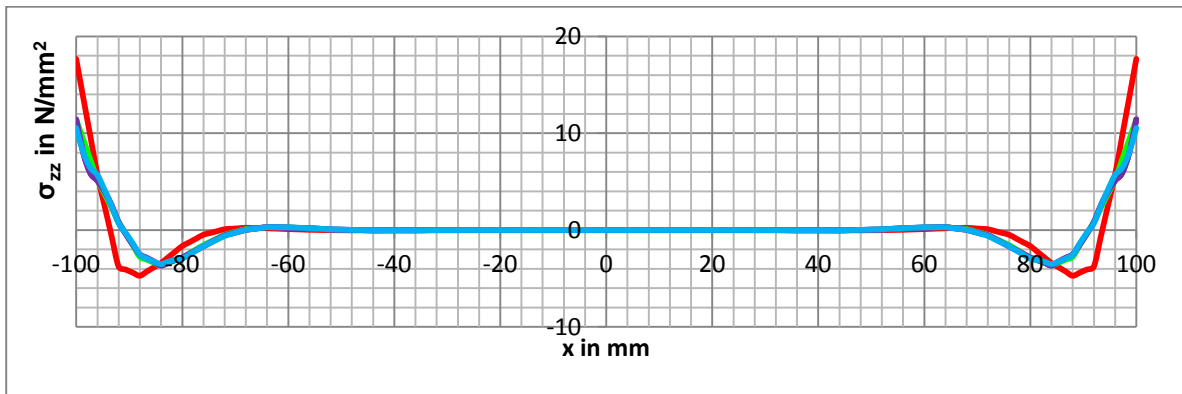


Figure 22.5: Peel stresses of FEM lap tests with linear elements at Y=50 & Z=0

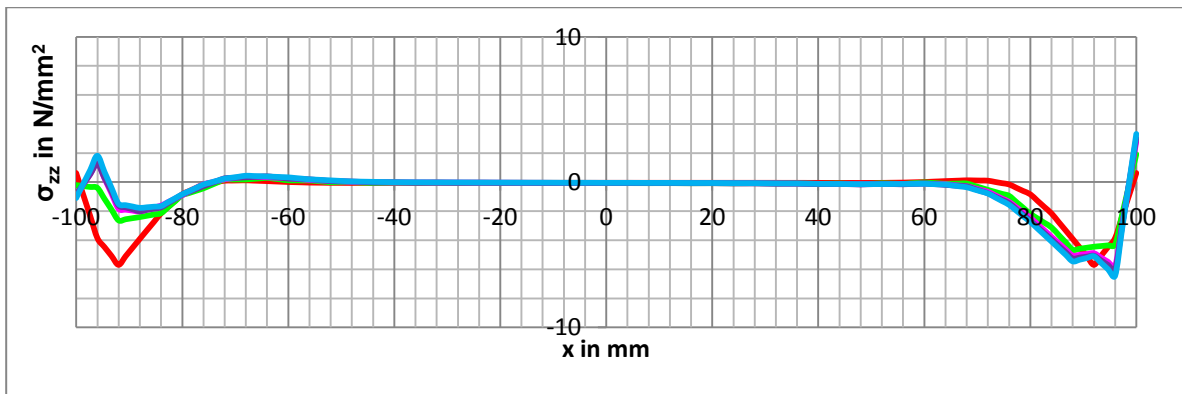


Figure 22.6: Peel stresses of FEM lap tests with linear elements at Y=100 & Z=-2

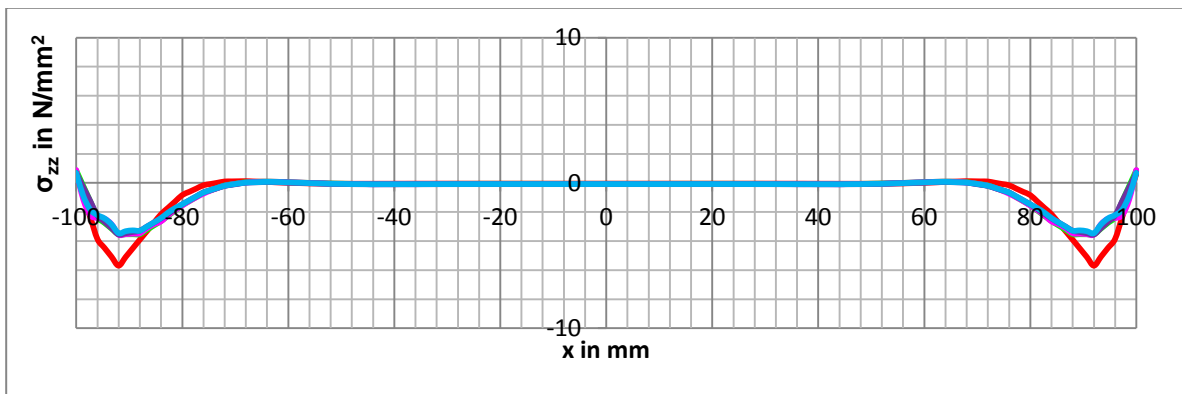


Figure 22.7: Peel stresses of FEM lap tests with linear elements at Y=100 & Z=0

22.2.2 Shear stresses

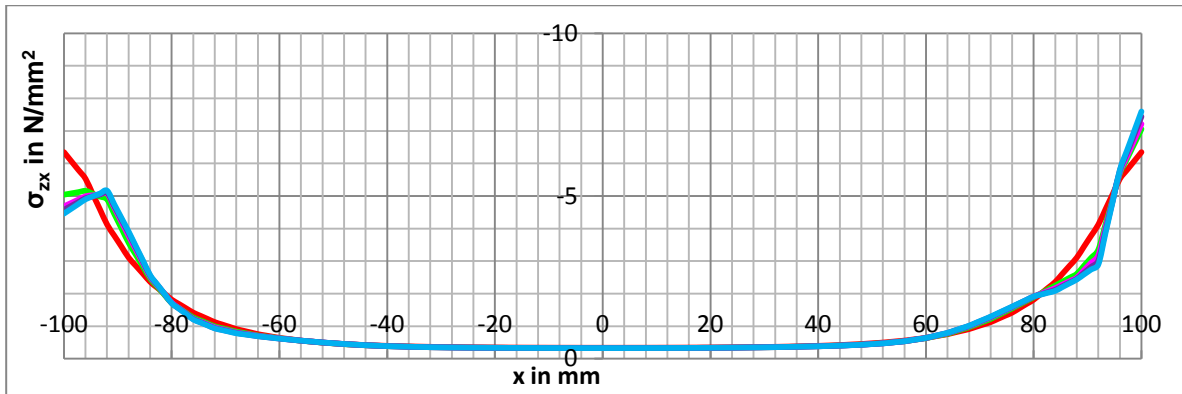


Figure 22.8: Shear stresses of FEM lap tests with linear elements at Y=0 & Z=-2

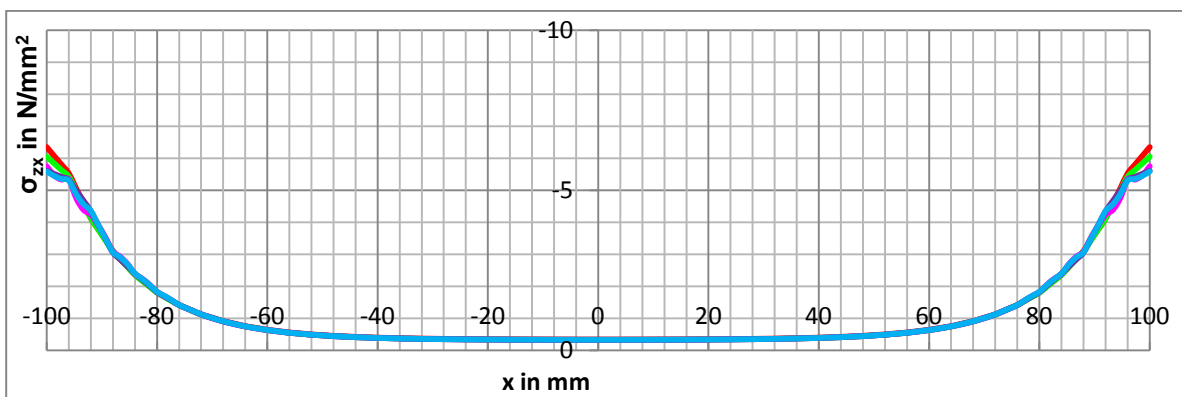


Figure 22.9: Shear stresses of FEM lap tests with linear elements at Y=0 & Z=0

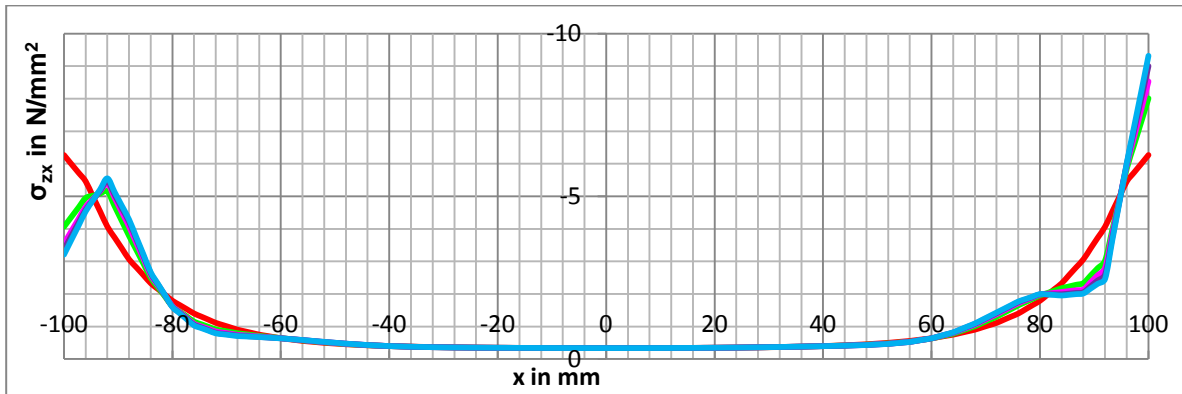


Figure 22.10: Shear stresses of FEM lap tests with linear elements at Y=50 & Z=-2

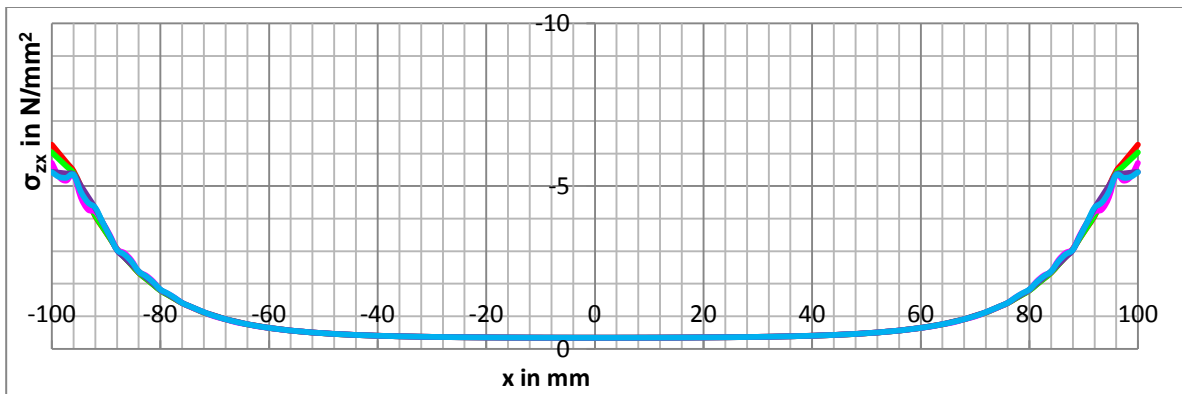


Figure 22.11: Shear stresses of FEM lap tests with linear elements at Y=0 & Z=0

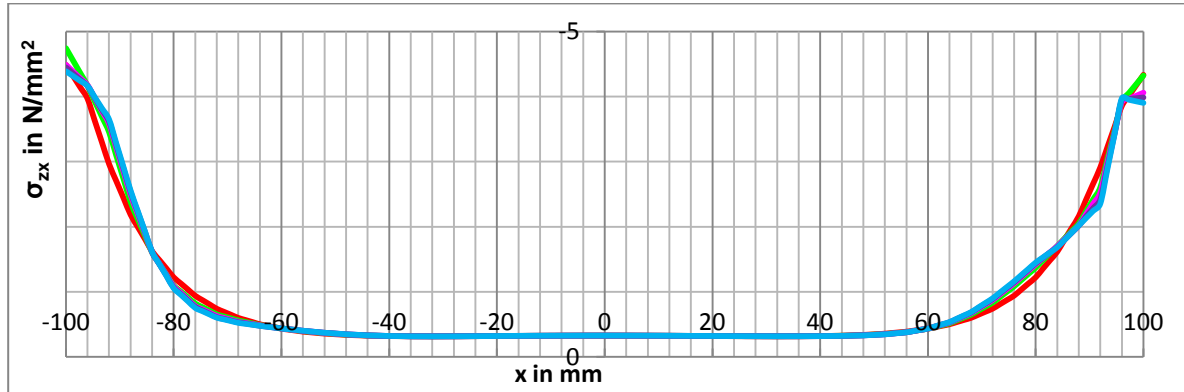


Figure 22.12: Shear stresses of FEM lap tests with linear elements at Y=100 & Z=-2

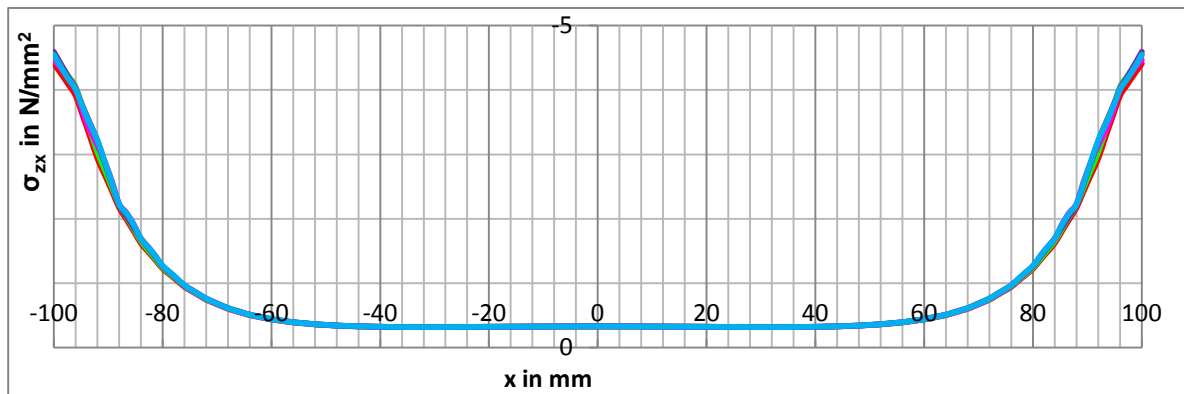


Figure 22.13: Shear stresses of FEM lap tests with linear elements at Y=0 & Z=0

22.2.3 Conclusion

In Figure 22.2/Figure 22.13 the differences between three, four and five elements are negligible. The line belonging to two elements deviates just a little from the lines of three, four and five elements at Figure 22.2, Figure 22.4, Figure 22.6, Figure 22.8, Figure 22.9, Figure 22.10, Figure 22.11 and Figure 22.12. The line belonging to one element deviates quite a lot in some figures. One element seems therefore not be the best choice. The differences for two, three, four and five elements are relatively small. Increasing the number of elements will lead to longer calculations. Therefore a calculation with two elements will be a proper choice. Calculations with more than five elements is not necessary.

22.3 Quadratic elements

In this section the peel and shear stresses out of FEM calculations with quadratic elements can be found. Only results for lines at z=-2 and z=0 are included, because the results of z=2 are a mirror image of those of z=-2. For all the figures below the next colours are used to indicate the number of applied elements: **1** (red) **2** (green) **3** (magenta) **4** (purple) **5** (blue).

22.3.1 Peel stresses

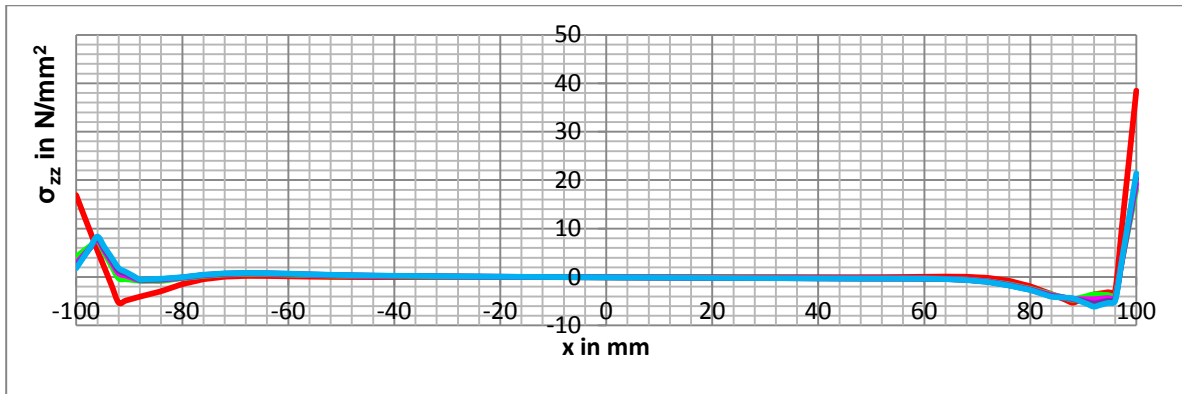


Figure 22.14: Peel stresses of FEM lap tests with quadratic elements at Y=0 & Z=-2

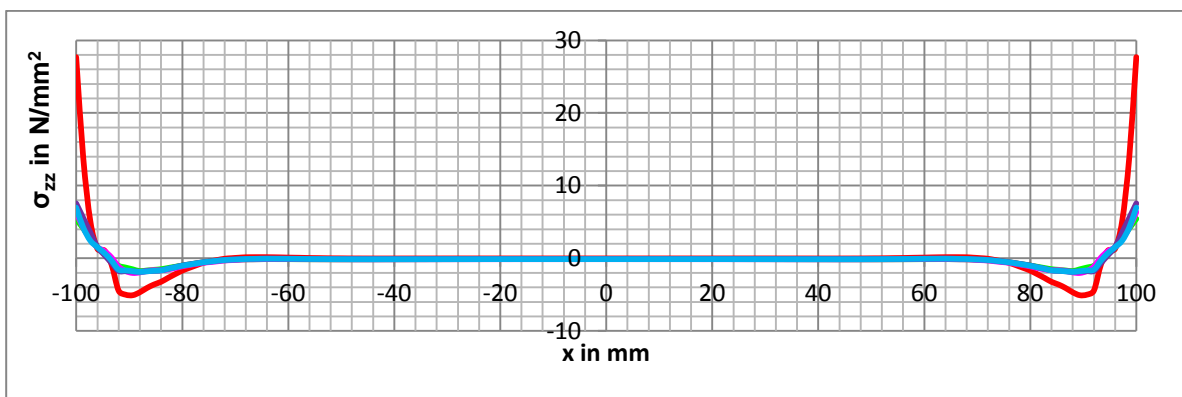


Figure 22.15: Peel stresses of FEM lap tests with quadratic elements at Y=0 & Z=0

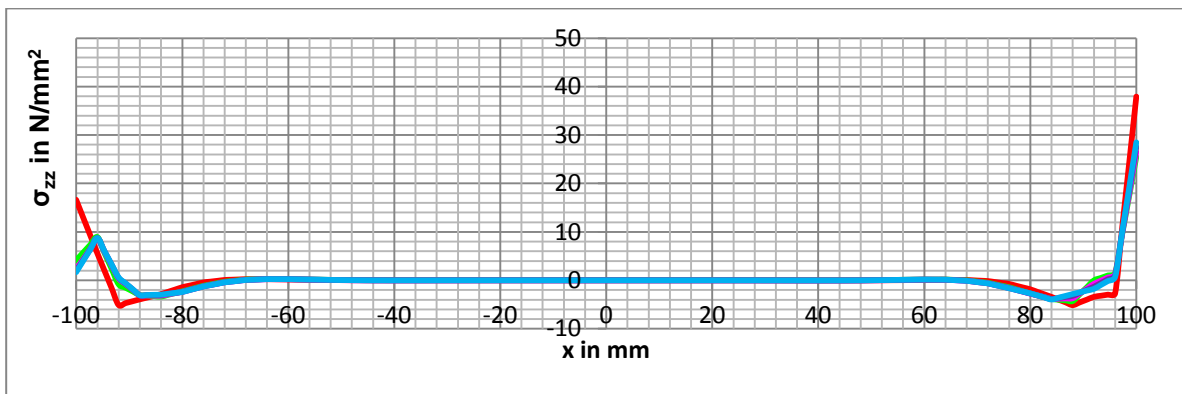


Figure 22.16: Peel stresses of FEM lap tests with quadratic elements at Y=50 & Z=-2

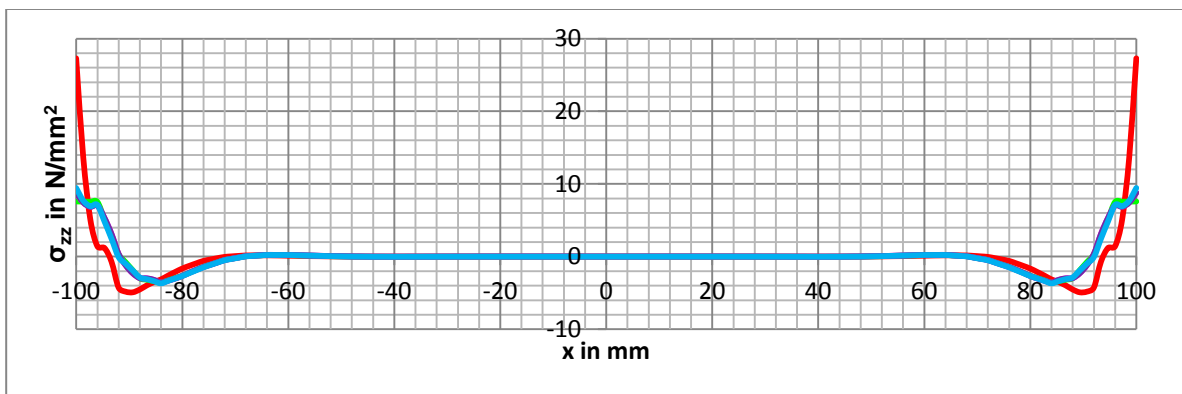


Figure 22.17: Peel stresses of FEM lap tests with quadratic elements at Y=50 & Z=0

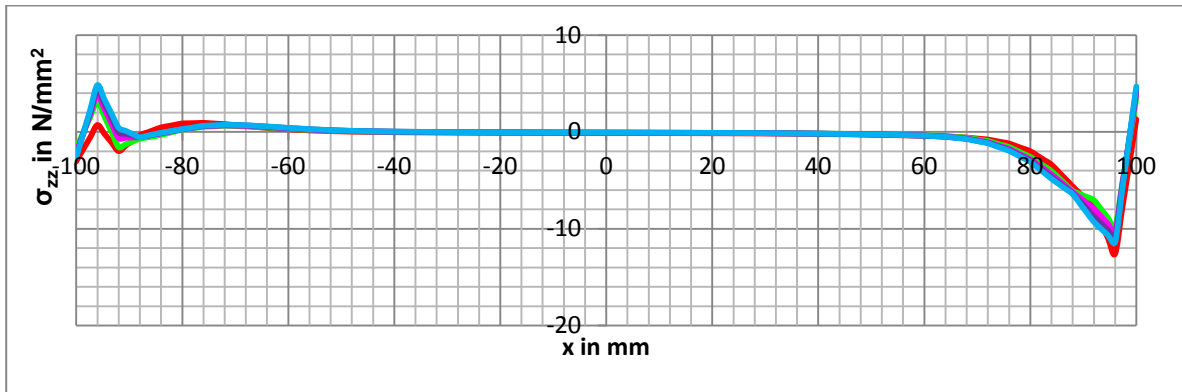


Figure 22.18: Peel stresses of FEM lap tests with quadratic elements at $Y=100$ & $Z=-2$

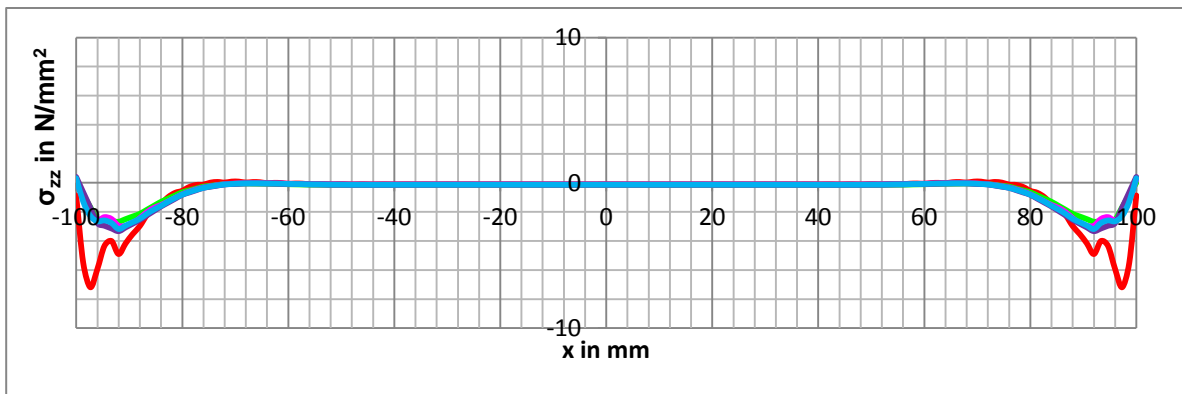


Figure 22.19: Peel stresses of FEM lap tests with quadratic elements at $Y=100$ & $Z=0$

22.3.2 Shear stresses

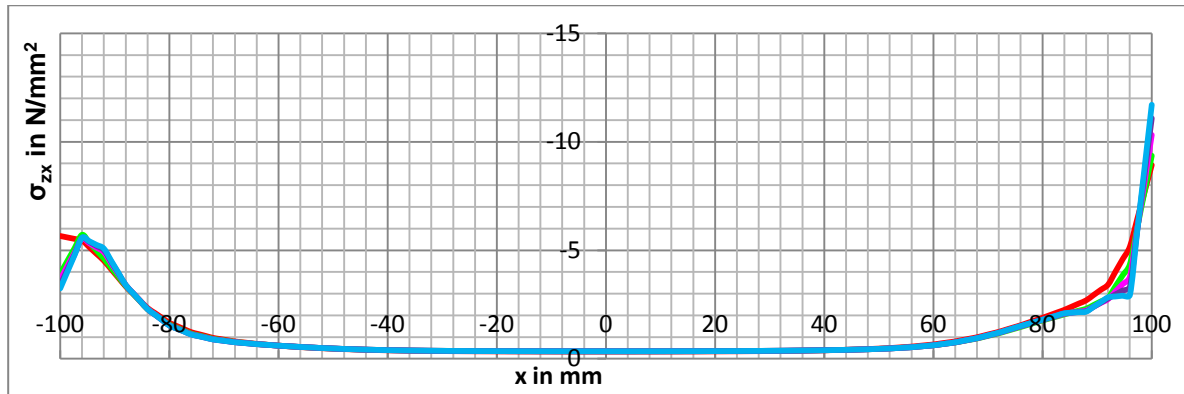


Figure 22.20: Shear stresses of FEM lap tests with quadratic elements at Y=0 & Z=-2

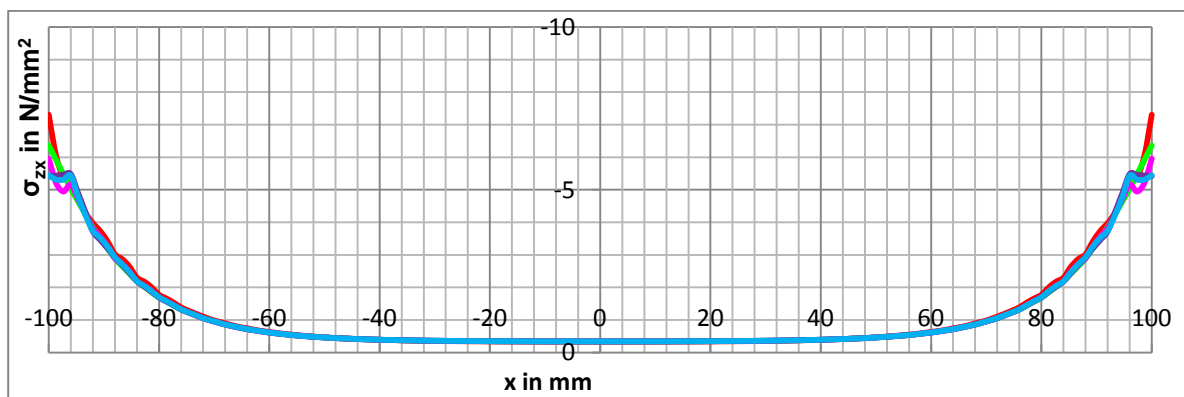


Figure 22.21: Shear stresses of FEM lap tests with quadratic elements at Y=0 & Z=0

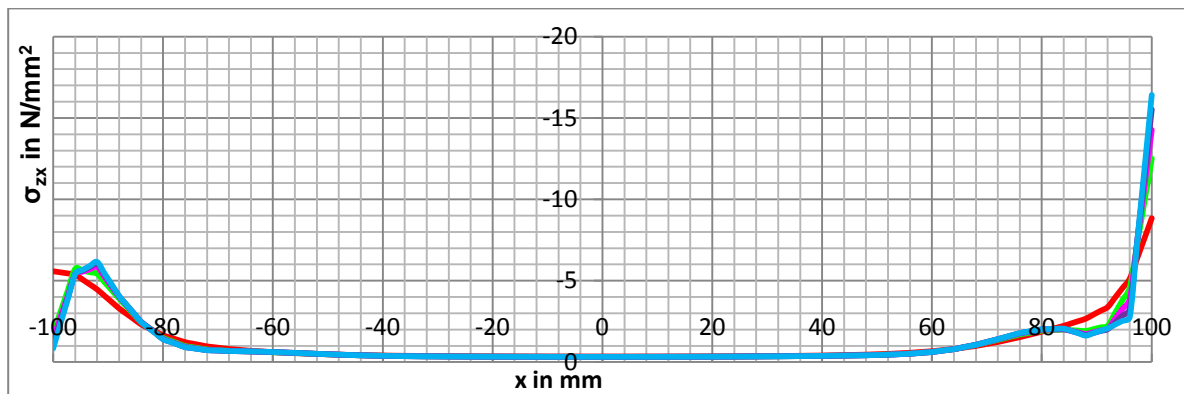


Figure 22.22: Shear stresses of FEM lap tests with quadratic elements at Y=50 & Z=-2

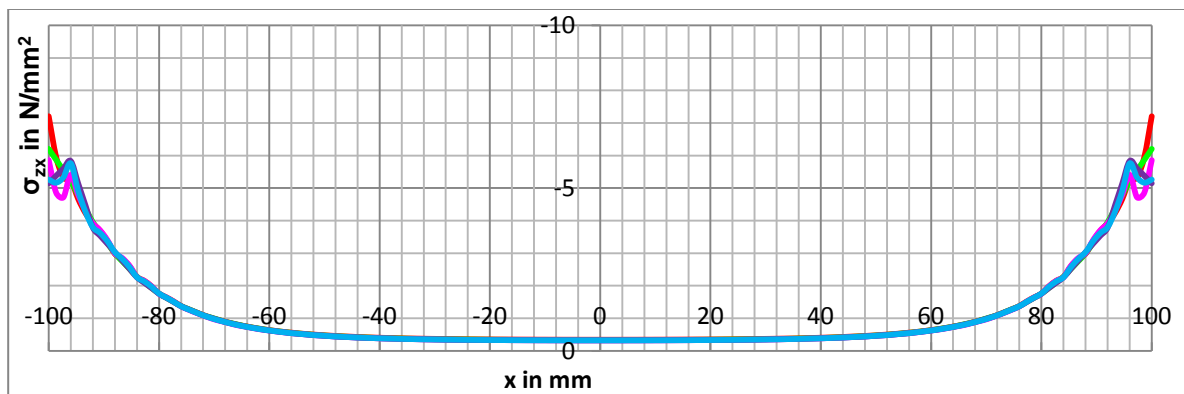


Figure 22.23: Shear stresses of FEM lap tests with quadratic elements at Y=50 & Z=0

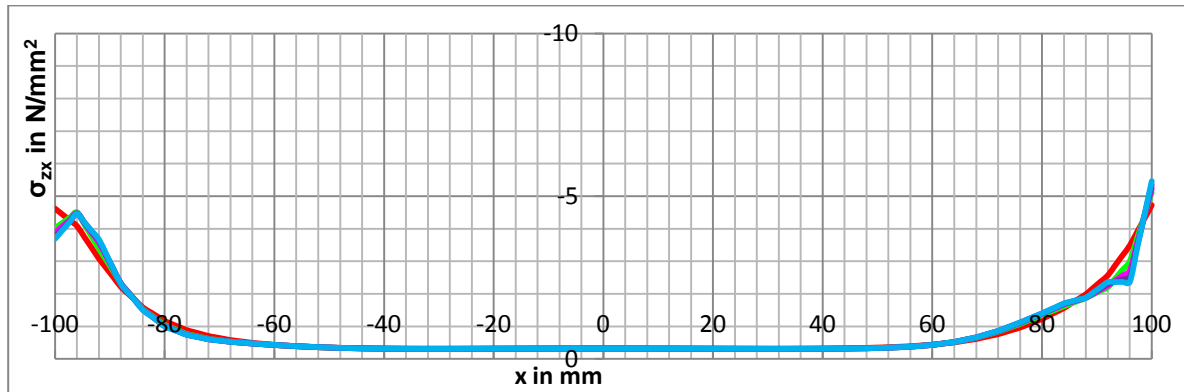


Figure 22.24: Shear stresses of FEM lap tests with quadratic elements at Y=100 & Z=-2

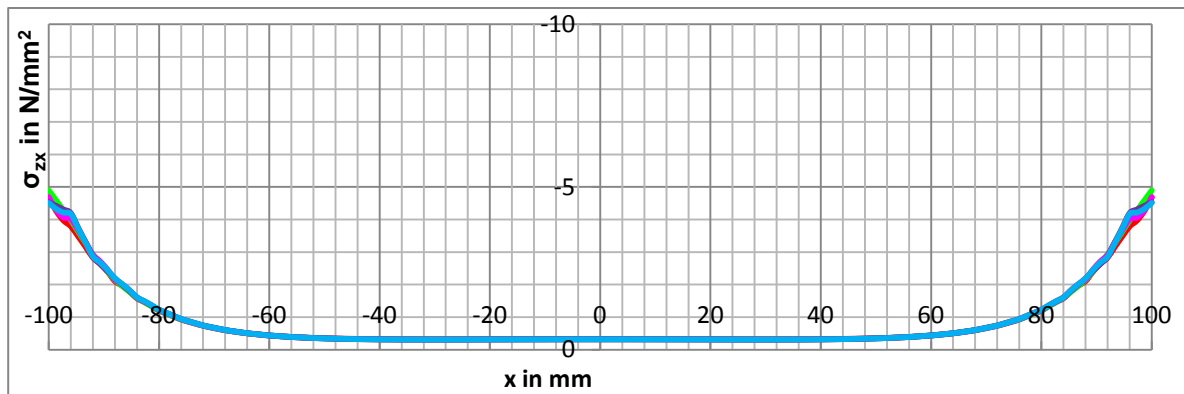


Figure 22.25: Shear stresses of FEM lap tests with quadratic elements at Y=0 & Z=100

22.3.3 Conclusion

In Figure 22.14/Figure 22.25 the differences between two, three, four and five elements are negligible. Only at the ends of the shear stress distribution some differences occur, in some cases more elements lead to higher stresses and in some cases vice versa. The line belonging to one element deviates quite a lot from the other lines, especially for the peel stress distributions. The minimum of applied elements should therefore be two. Calculations with more than five elements is not necessary.

22.4 Linear and quadratic elements

As mentioned in section 22.2.3 and 22.3.3 at least two linear or quadratic elements are needed for a proper calculation. In this section the two element linear and quadratic calculations are compared to each other. Only results for lines at $z=-2$ and $z=0$ are included, because the results of $z=2$ are a mirror image of those of $z=-2$. For all the figures below the next colours are used to indicate the order of applied elements: — Linear — Quadratic.

22.4.1 Peel stresses

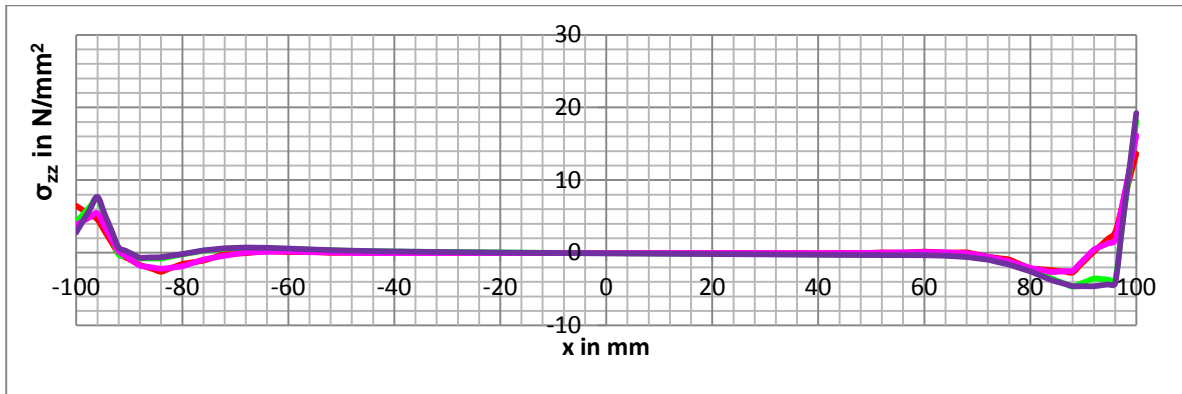


Figure 22.26: Peel stresses of FEM lap tests with 2 linear or 2 quadratic elements at Y=0 & Z=-2

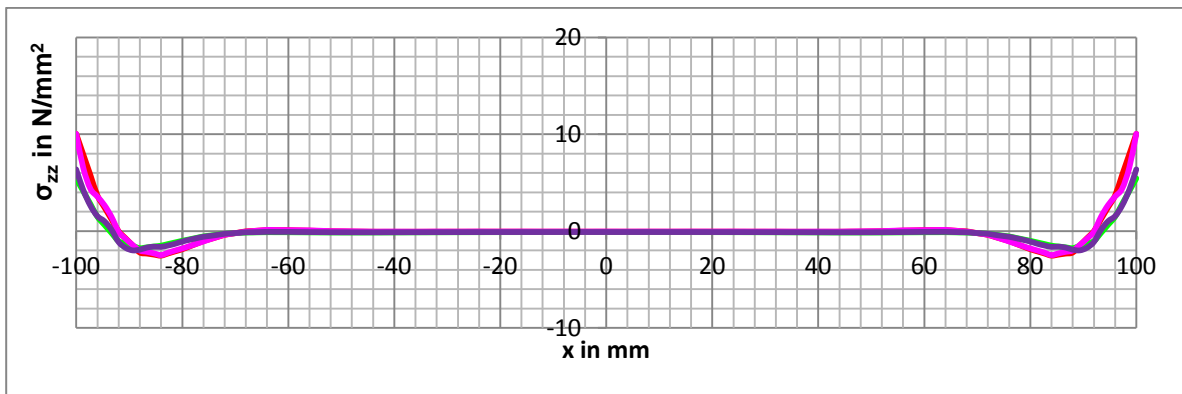


Figure 22.27: Peel stresses of FEM lap tests with 2 linear or 2 quadratic elements at Y=0 & Z=0

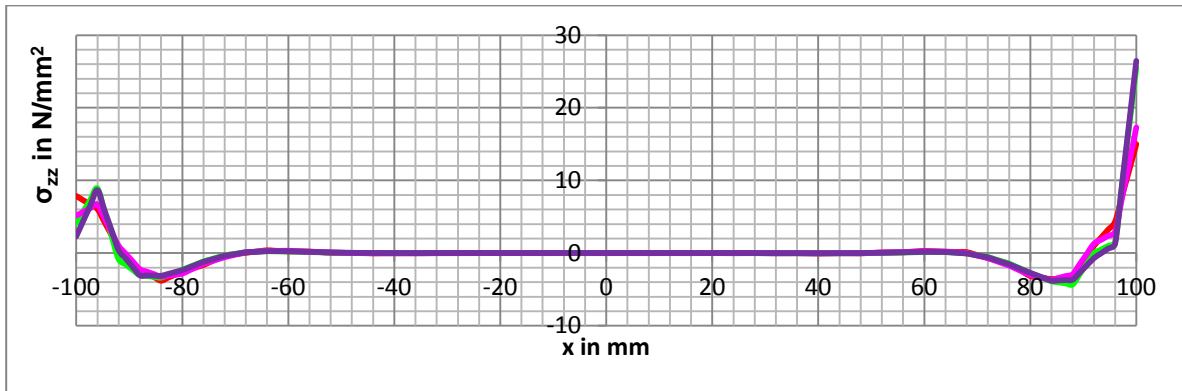


Figure 22.28: Peel stresses of FEM lap tests with 2 linear or 2 quadratic elements at Y=50 & Z=-2

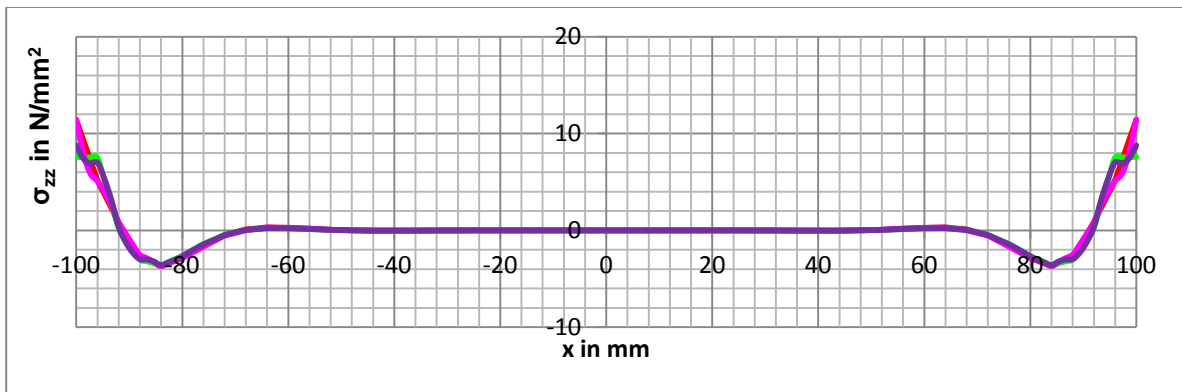


Figure 22.29: Peel stresses of FEM lap tests with 2 linear or 2 quadratic elements at Y=50 & Z=0

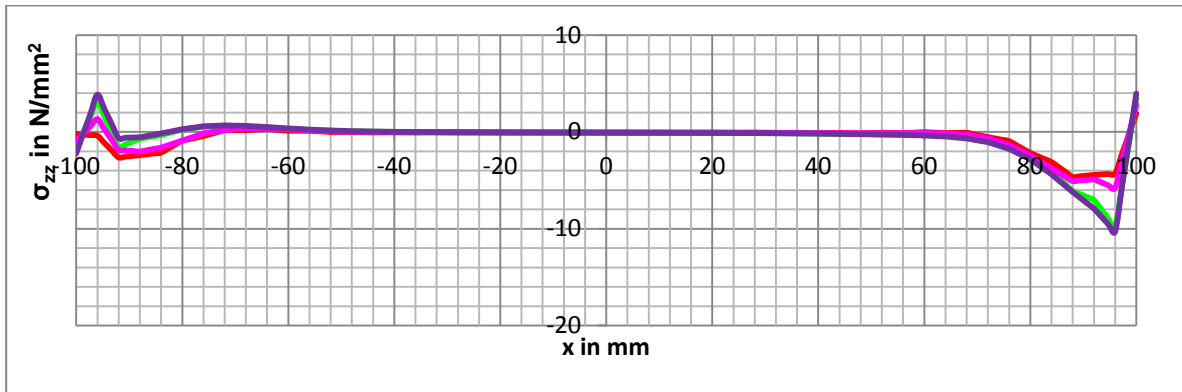


Figure 22.30: Peel stresses of FEM lap tests with 2 linear or 2 quadratic elements at $Y=100$ & $Z=-2$

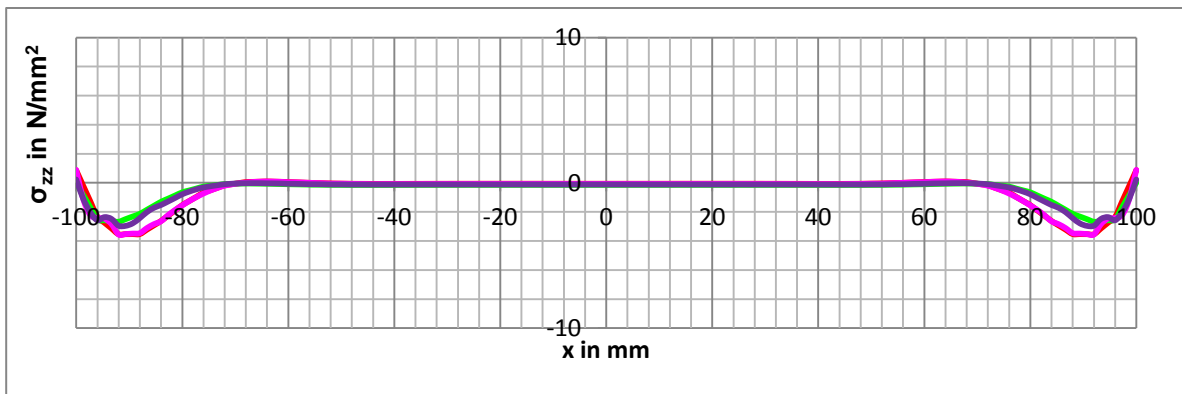


Figure 22.31: Peel stresses of FEM lap tests with 2 linear or 2 quadratic elements at $Y=100$ & $Z=-2$

22.4.2 Shear stresses

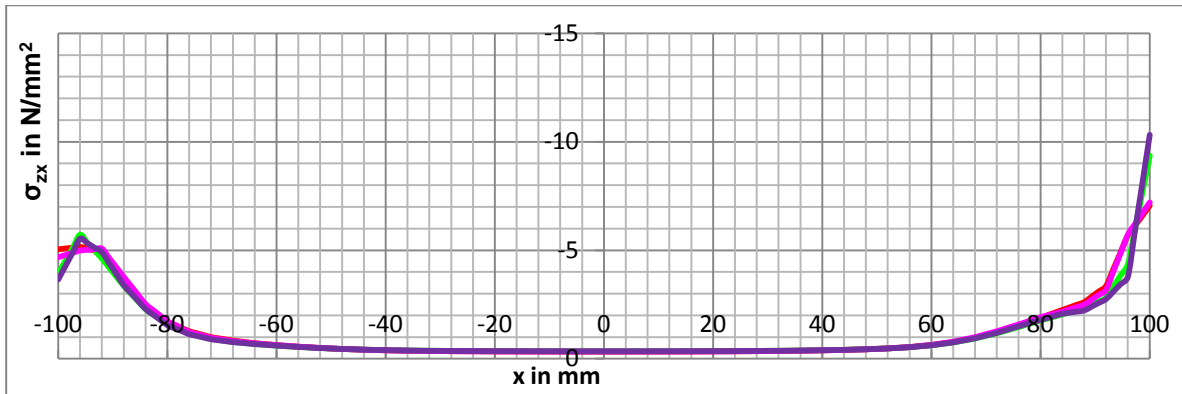


Figure 22.32: Shear stresses of FEM lap tests with 2 linear or 2 quadratic elements at Y=0 & Z=-2

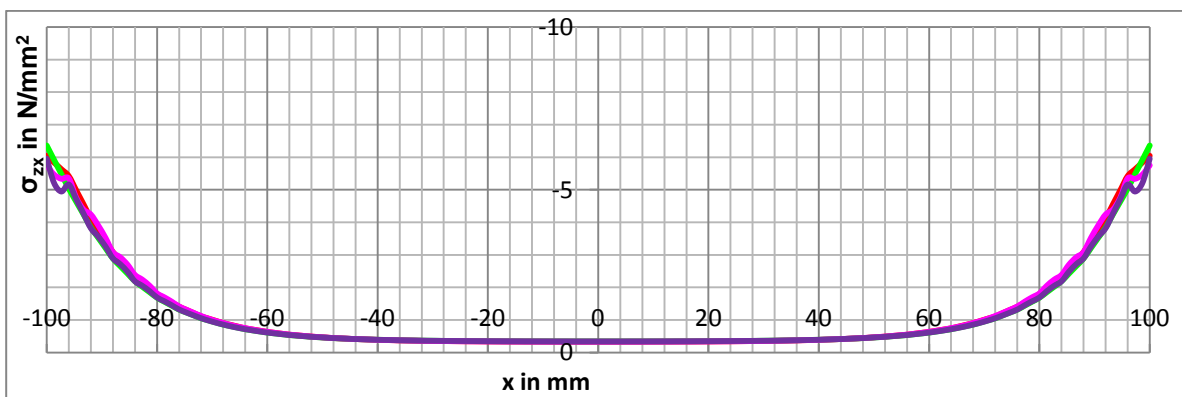


Figure 22.33: Shear stresses of FEM lap tests with 2 linear or 2 quadratic elements at Y=0 & Z=0

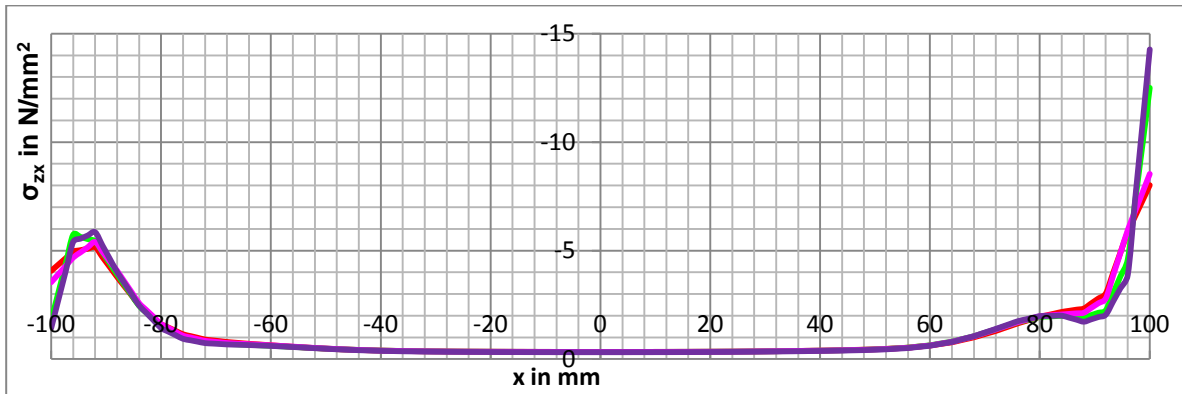


Figure 22.34: Shear stresses of FEM lap tests with 2 linear or 2 quadratic elements at Y=50 & Z=-2

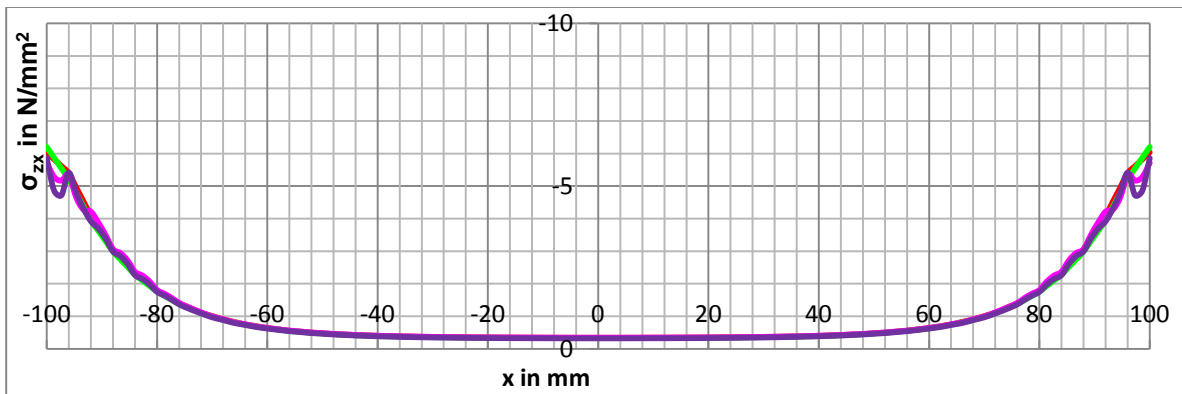


Figure 22.35: Shear stresses of FEM lap tests with 2 linear or 2 quadratic elements at Y=50 & Z=0

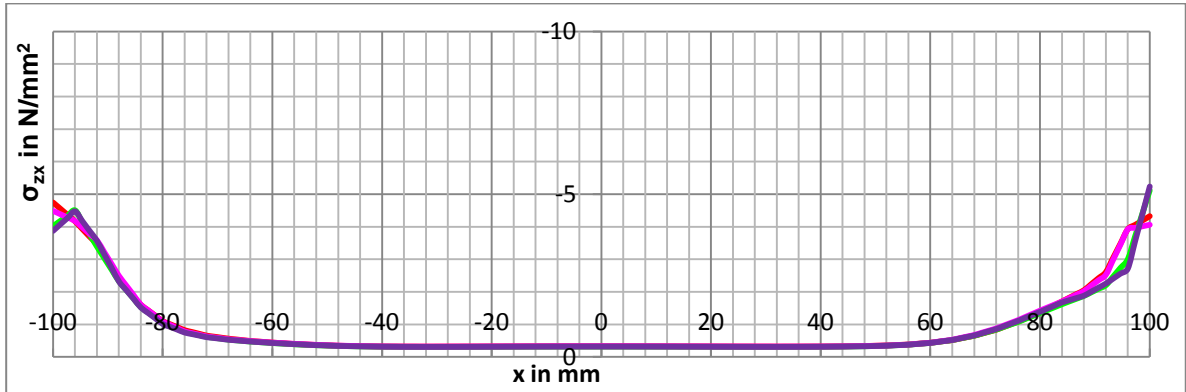


Figure 22.36: Shear stresses of FEM lap tests with 2 linear or 2 quadratic elements at Y=100 & Z=-2

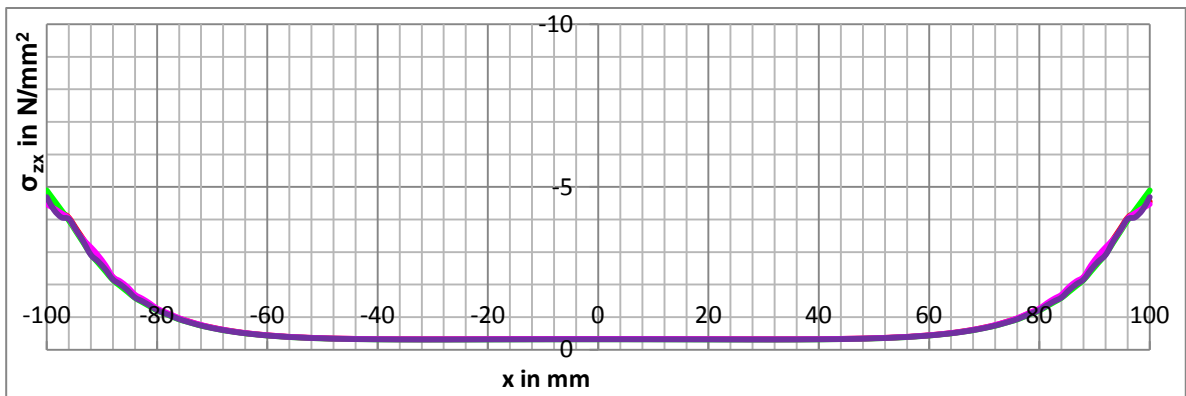


Figure 22.37: Shear stresses of FEM lap tests with 2 linear or 2 quadratic elements at Y=100 & Z=0

22.4.3 Conclusion

For most figures, the results of the linear and quadric calculations differ. However, the shear stresses at the lines at $z=0$ are nearly similar. Hence to get an accurate view of the stresses a calculation with quadratic elements should be applied.

23 Appendix G: DIANA procedure for entire L-connection model

For this thesis TNO DIANA version 9.4.4 and FX+ for DIANA version 3.1.0 is used.

23.1 Input

The input of data for FEM programs needs to be done in a proper way. Bad modelling results in inaccurate and unreliable results, or as often said: 'Rubbish in is rubbish out'.

23.1.1 Solids

3D geometries in FX+ for DIANA are modelled with solids. There are several ways to make the desired solids in FX+ for DIANA. Which way is used will not influence the final result, therefore this will not be considered extensively. To ensure a proper mesh in a later phase, the geometries/profiles are divided in a few solids. The division of the HE200A cross section is showed in the next figure. The solid division for the other geometries are directly derived from the HE200A division. Except for solids at the fillet radius, all the solids will be rectangular cuboids.

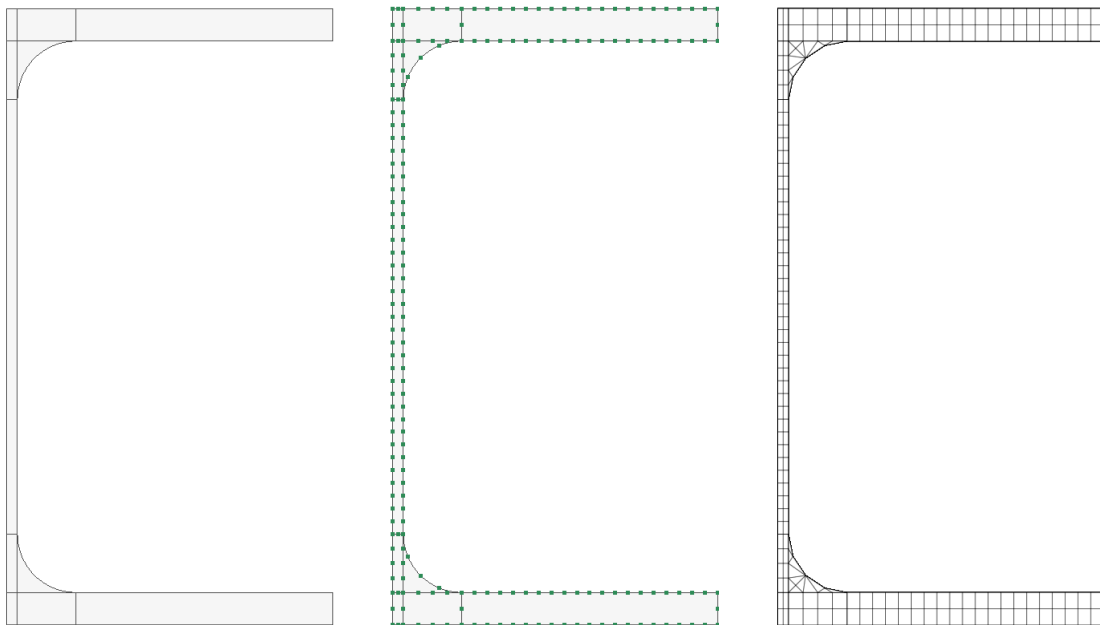


Figure 23.1: Solid division, seed division and FEM division of HE200A profile

23.1.2 Seeds

Seeds are points which will later, during the mesh generation, be turned into nodes. In Figure 23.1 this is shown for an HE200A profile. In the table below the division which is used can be found.

Member	Dimension in mm
Web thickness	1.63
Adhesive thickness	2
Flange thickness	5
Angle thickness	5
Width at fillet radius	4.5
Height at fillet radius	4.5
Curve of fillet radius	7.07
Web height	3.94
Flange width	3.94

Table 23.1: General applied seed division of L-connection

The length of the elements will not be the same at the whole length of the solid, otherwise some elements will not be able to connect to the elements of other solids. As base value 4mm (the same as the adhesive thickness) is used for the length, other lengths will follow from the thickness of other elements. For the inner corner this will lead for instance to a mesh as depicted in the following figure.

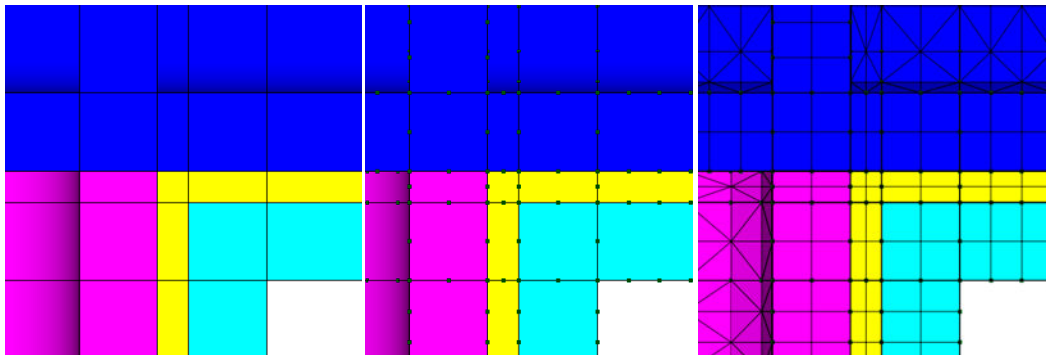


Figure 23.2: Element division at inner angle (dark blue=beam, magenta=column, yellow=adhesive, light blue=angle)

23.1.3 Material and properties

The material and properties used for the solids can be found in the next tables.

Name	Type	Property	Value	Unit	Model Type
Steel	Isotropic	E	210000	N/mm ²	Elastic
		v	0.33		
Adhesive	Isotropic	E	12800	N/mm ²	Elastic
		G	4273	N/mm ²	

Table 23.2: Material of solids

Name	Type	Sub-Type		Material
Steel	3D	Solid	Regular	Steel
Adhesive	3D	Solid	Regular	Adhesive

Table 23.3: Properties for solids

The material and properties used for the interface can be found in the next tables.

Material	Type	Property	Value	Unit	Interface Nonlinearities
Interface	Interface	Kn	21000000	N/mm ²	Linear
		Kt	1	N/mm ²	

Table 23.4: Material of interface

Name	Type	Sub-Type	Material	Orientation
Interface	2D	Surface Interface	Interface	1,0,0

Table 23.5: Properties for interfaces

23.1.4 Mesh

There are a few ways to make a mesh in FX+ for DIANA. For the solids which are rectangular cuboids the *Map-Mesh k-Edge Volume* command is used. These solid will be divided in small rectangular cuboid shaped elements. For the solids at the fillet radius the *Auto-Mesh Solid* command is used. These solids will be divided in tetrahedron shaped elements. During meshing the nodes of the elements of adjacent solids will automatically be merged with the elements of the to be meshed solid. Only at the interface of the beam and column this is unwanted. Therefore for that part this function is turned off. Later the nodes that should be merged are merged with the *Merge Node* command. The nodes of the adhesive at the beam-column interface are merged with the beam but not with the column. When these adhesive nodes are also merged with the column, the column nodes are also merged with the beam nodes, which is not the actual case.

After the solids are meshed the interface elements between the column web and beam stiffener are made with the *Create Interface Element* command and the *From Free-Face* method.

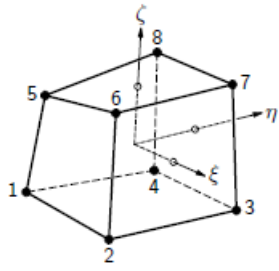
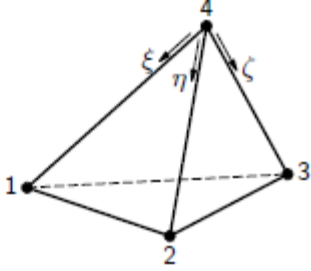
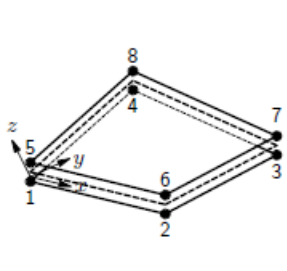
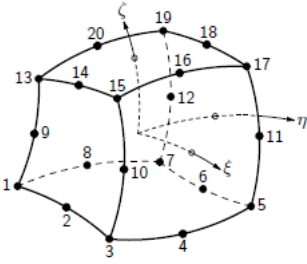
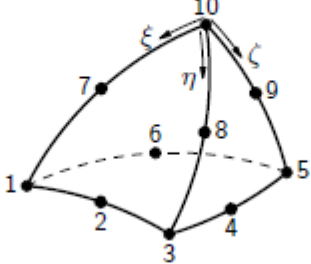
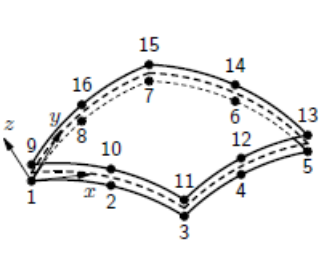
	Rectangular cuboids	Tetrahedron	Interface
Linear finite elements	HX24L Brick 8 nodes	TE12L Pyramid 3 sides 4 nodes	Q24IF Plane quadrilateral 3-D 4+4 nodes
			
Quadratic finite elements	CHX60 Brick 20 nodes	CTE30 pyramid, 3 sides 10 nodes	CQ48I, Plane quadrilateral 3-D 8+8 nodes
			

Table 23.6: Used finite elements

23.1.5 Loads and boundary conditions

For the load a displacement load is used. In general such a load leads to a more stable calculation than a force load. The load is applied at the most upper nodes of the beam end at the positive x-direction near the web and fillet radius.

As symmetry condition all the nodes at $y=0$ are restrained in y-direction. All the nodes at the bottom of the column are restrained in z-direction. The nodes at the bottom in positive x-direction are also restrained in x-direction.

23.2 Analysis

With the command *Edit model with Diana mesh-editor* the mesh editor of DIANA itself can be launched. The mesh editor makes a Filos File (with the extension .ff). The Filos file can be read by

DIANA in contrast to the files made by FX+ for DIANA. In the DIANA mesh-editor, DIANA can be launched by the *Analysis/Run...* command.

In DIANA the analysis type should be chosen. For a linear elastic calculation *Structural linear static* analysis is used, for physical and/or geometrical nonlinear calculation the *Structural nonlinear* analysis should be used.

23.3 Output

After the analysis is done the result file (*Post Result* file with extension .dpg) can be imported in FX+ for DIANA. This can be done by the *File/Import/Post-Neutral (DPB)...* command.

Extracting all results from a calculation is labour intensive, therefore only a few results are extracted. With the command *Post/On-Curve Diagram...* a line can be made on which the desired results are shown. Six lines are made for all adhesive planes. For the two steel/adhesive interfaces and the middle of the adhesive thickness lines are made at the symmetry axis ($y=0$), at the middle of the width ($y=50$) and at the end of the width ($y=100$). For those lines a division has to be specified for the points for which values will be generated. As baseline a division with a 3/10 ratio is used. With this ratio for practically each finite element, with a base length of 4mm, a value is generated. Increasing the number of points will also increase the time to produce these lines. A higher ratio will be used if it is shown to be necessary.

24 Appendix H: FEM results of L-connection

In this section the results of the FEM calculations of the entire model can be found. A description of the y-values used for the result lines can be found in the next table:

y-value	Description
0	At the middle of the beam width
50	Right in between the mid and outside of the beam width
100	At the outside of the beam width

Table 24.1: Values of y for the horizontal plane of the inner angle

24.1 Horizontal plane of the inner angle

A description of the z-values used for the result lines can be found in the next table:

z-value	Description
0	Interface of beam and adhesive
2	At the middle of the adhesive
4	Interface of adhesive and steel angle

Table 24.2: Values of z for the horizontal plane of the inner angle

For the horizontal part of the inner angle there are a few specific point, listed below:

x-value	Description
0	Interface of adhesive (inner angle) and column
4	Left side of vertical part of the inner angle
14	Right side of the vertical plane of the inner angle

Table 24.3: Specific points for horizontal plane of the inner angle

24.1.1 Stresses perpendicular to the plane per test

For all the figures below the next colours are used to indicate the place of the result lines:

— Y=0 Z=0 — Y=0 Z=2 — Y=0 Z=4 — Y=50 Z=0 — Y=50 Z=2 — Y=50 Z=4 — Y=100 Z=0 — Y=100 Z=2 — Y=100 Z=4

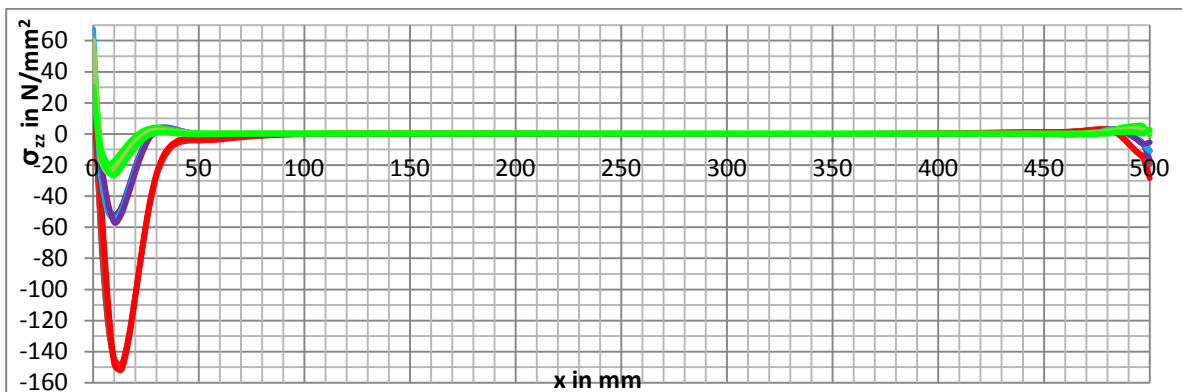


Figure 24.1: Stresses perpendicular to the horizontal plane of the inner angle of test IA200x500 OA100x500

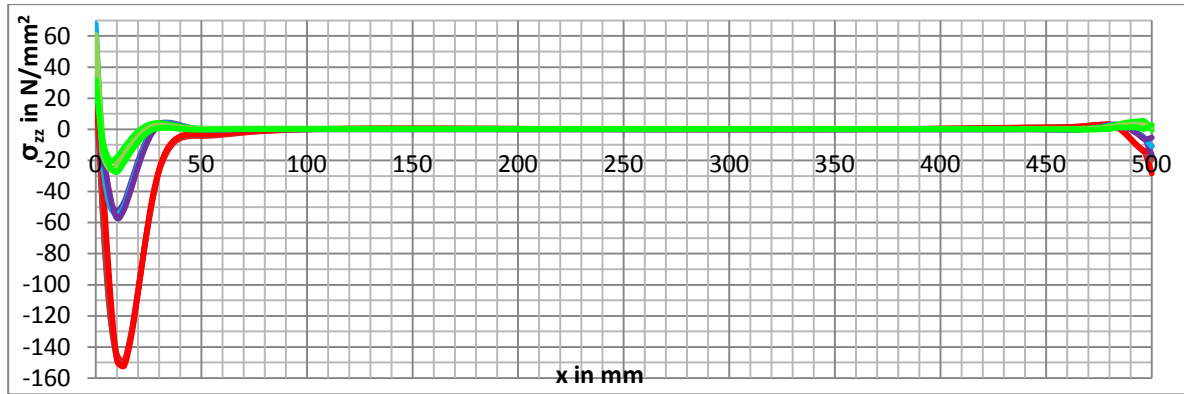


Figure 24.2: Stresses perpendicular to the horizontal plane of the inner angle of test IA300x500 OA100x500

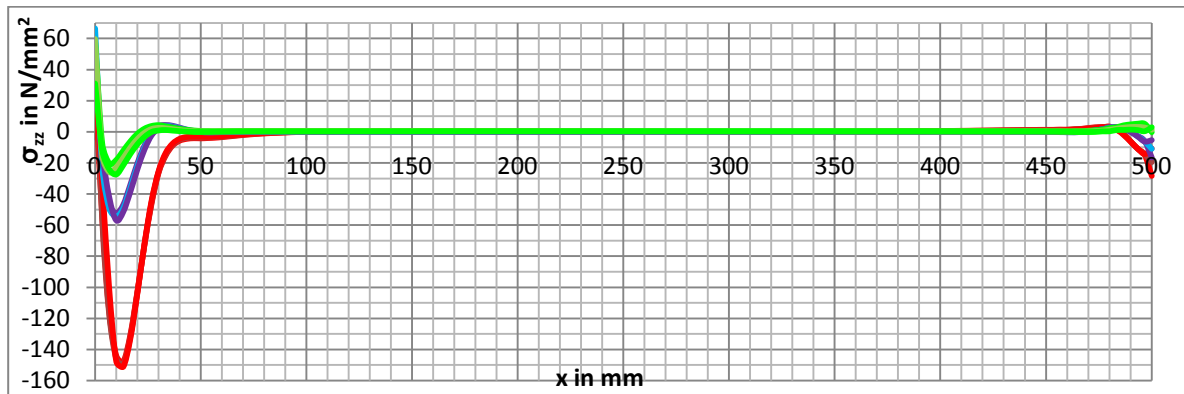


Figure 24.3: Stresses perpendicular to the horizontal plane of the inner angle of test IA300x500 OA200x500

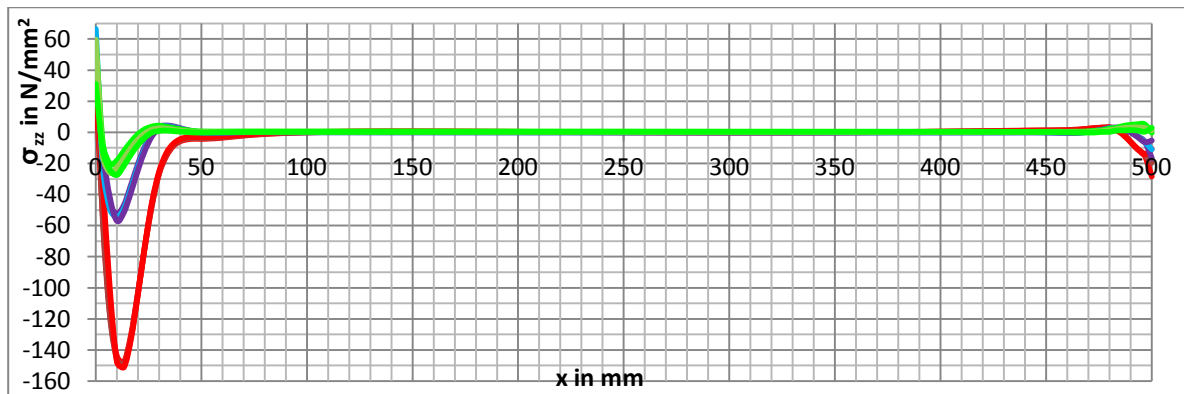


Figure 24.4: Stresses perpendicular to the horizontal plane of the inner angle of test IA300x500 OA200x700

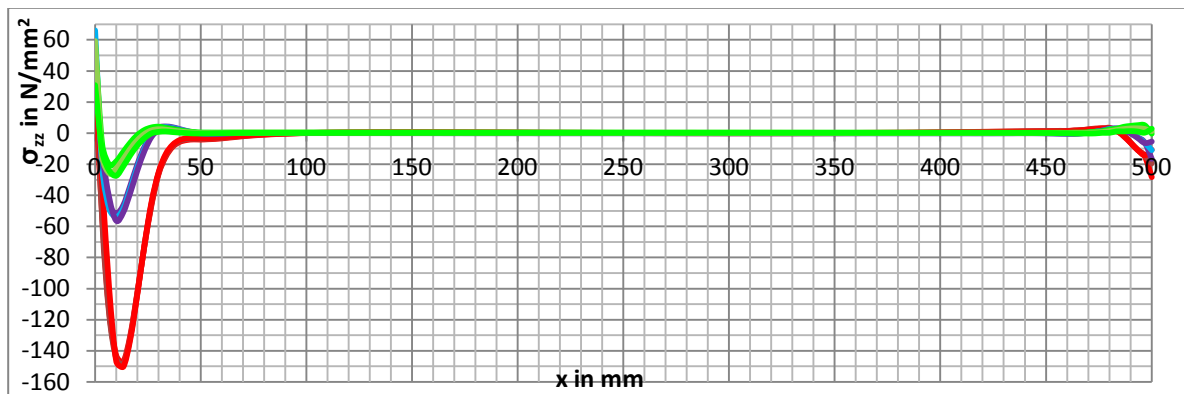


Figure 24.5: Stresses perpendicular to the horizontal plane of the inner angle of test IA500x500 OA200x700

24.1.2 Stresses perpendicular to the plane per result line

For all the figures below the next colours are used to indicate the models:

— IA200x500 OA100x500
 - - - IA300x500 OA100x500
 - - - IA300x500 OA200x500
 - - - IA300x500 OA200x700
 - - - IA500x500 OA200x700

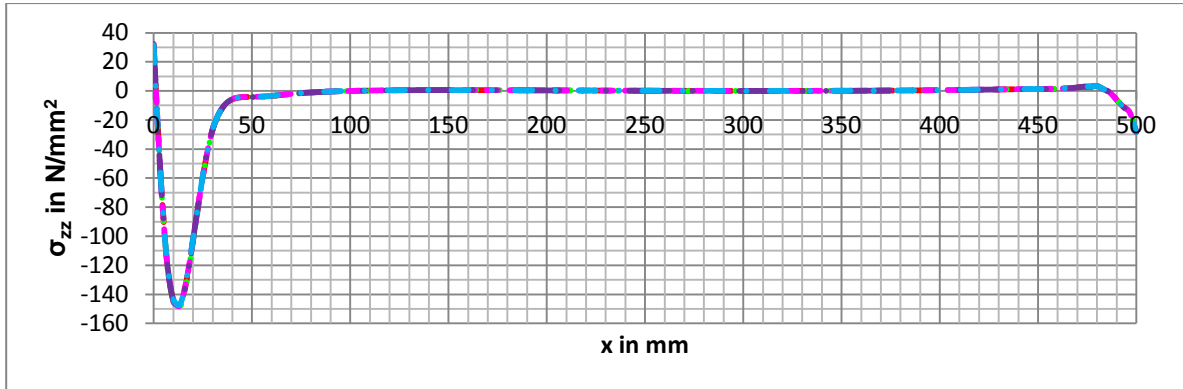


Figure 24.6: Comparison of stresses perpendicular to the horizontal plane of the inner angle at $y=0$ $z=0$

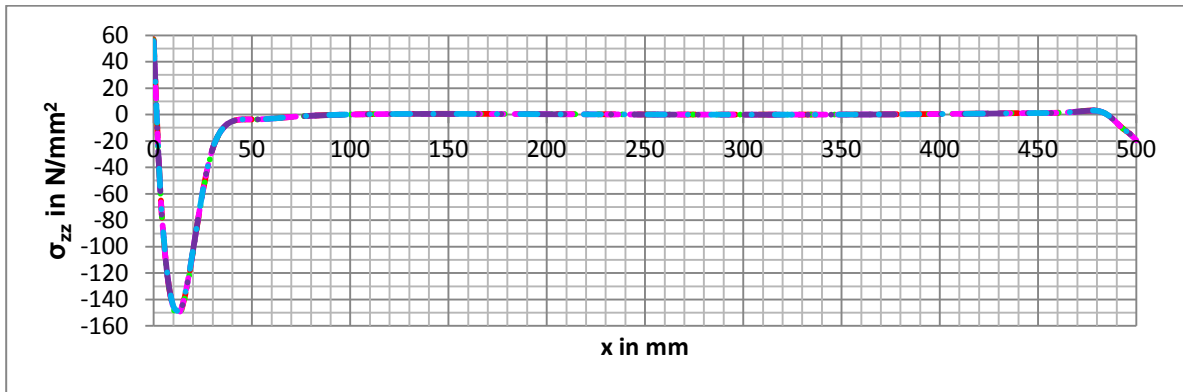


Figure 24.7: Comparison of stresses perpendicular to the horizontal plane of the inner angle at $y=0$ $z=2$

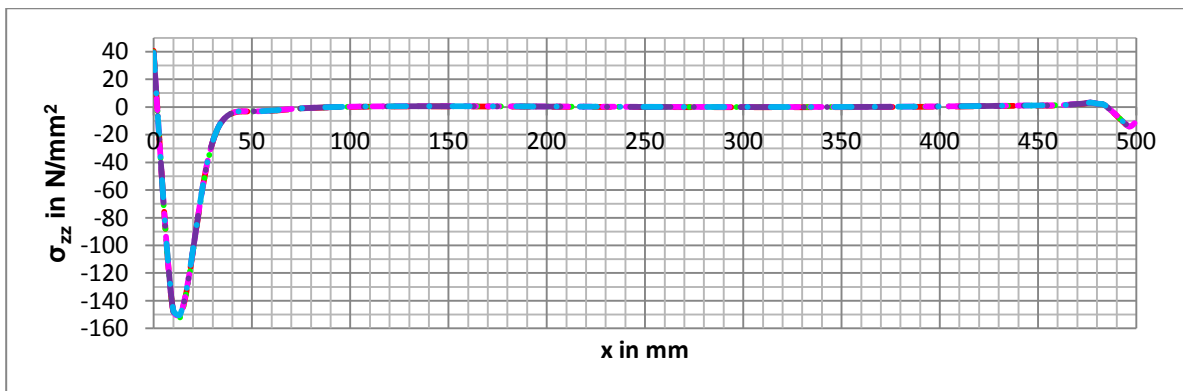


Figure 24.8: Comparison of stresses perpendicular to the horizontal plane of the inner angle at $y=0$ $z=4$

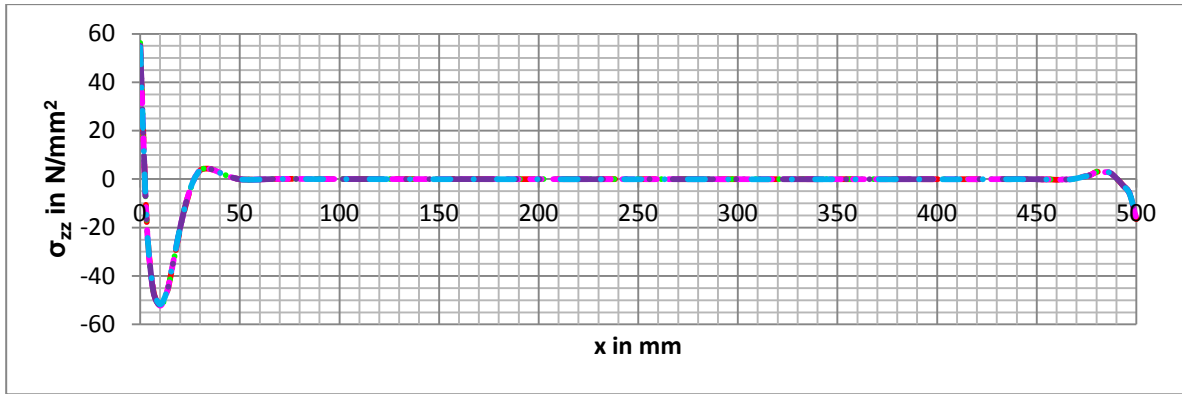


Figure 24.9: Comparison of stresses perpendicular to the horizontal plane of the inner angle at $y=50$ $z=0$

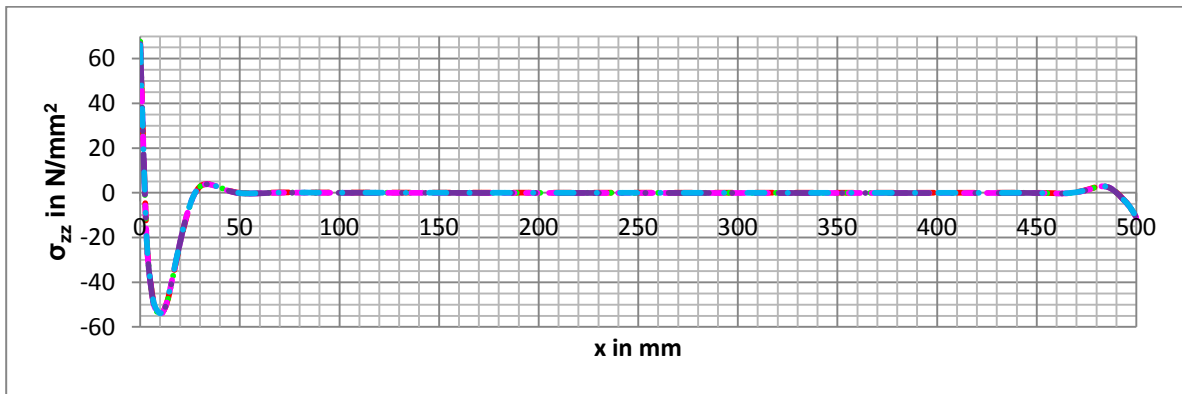


Figure 24.10: Comparison of stresses perpendicular to the horizontal plane of the inner angle at $y=50$ $z=2$

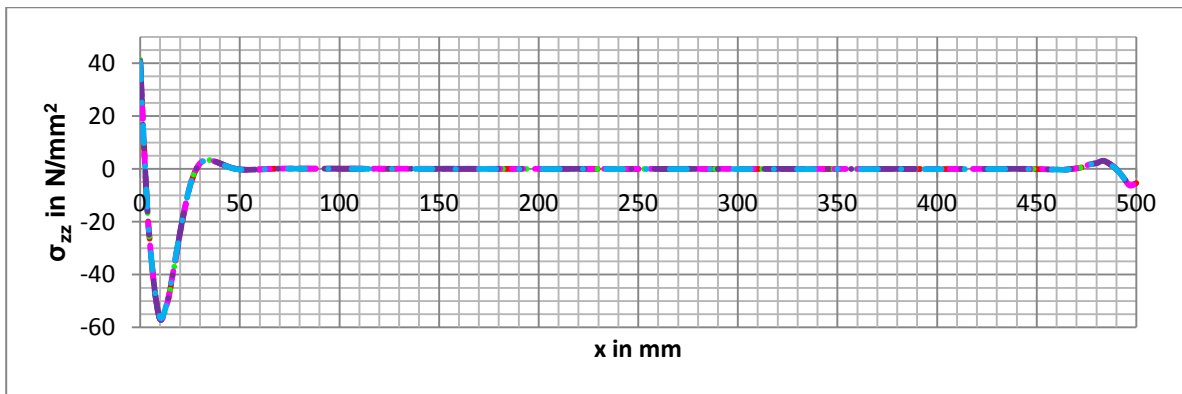


Figure 24.11: Comparison of stresses perpendicular to the horizontal plane of the inner angle at $y=50$ $z=4$

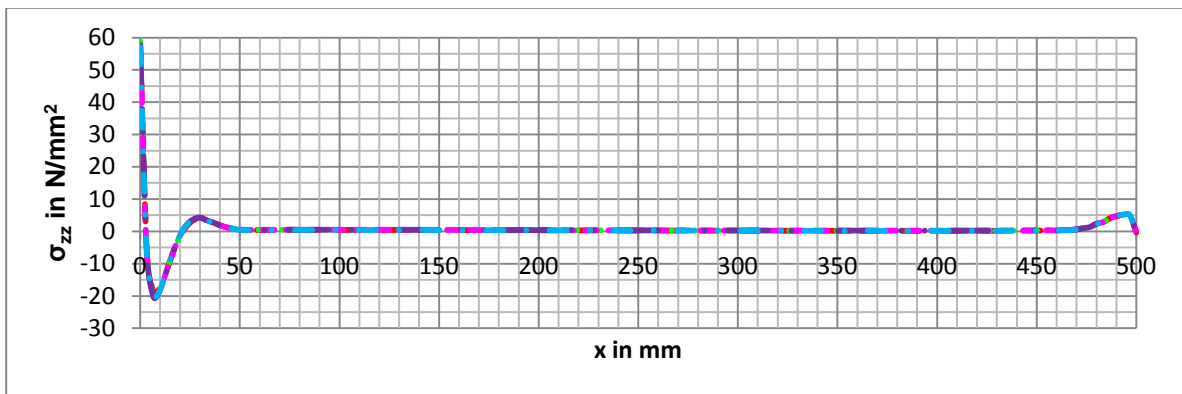


Figure 24.12: Comparison of stresses perpendicular to the horizontal plane of the inner angle at $y=100$ $z=0$

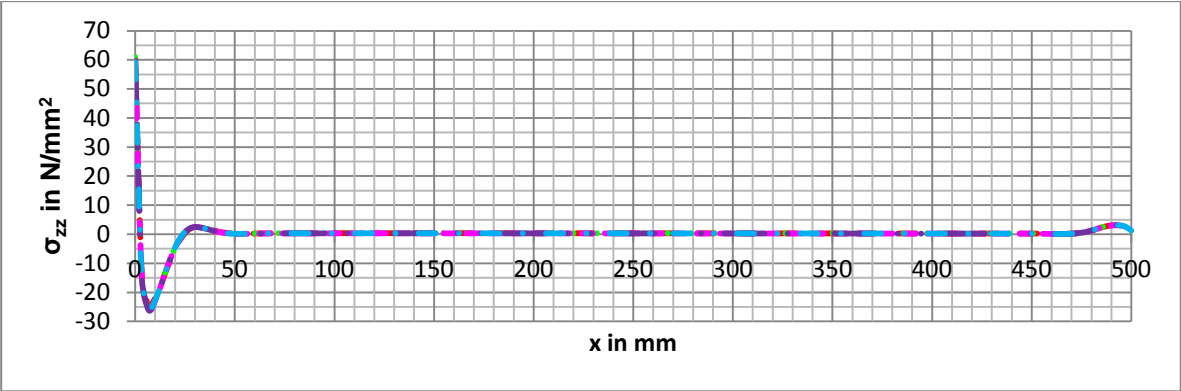


Figure 24.13: Comparison of stresses perpendicular to the horizontal plane of the inner angle at $y=100$ $z=2$

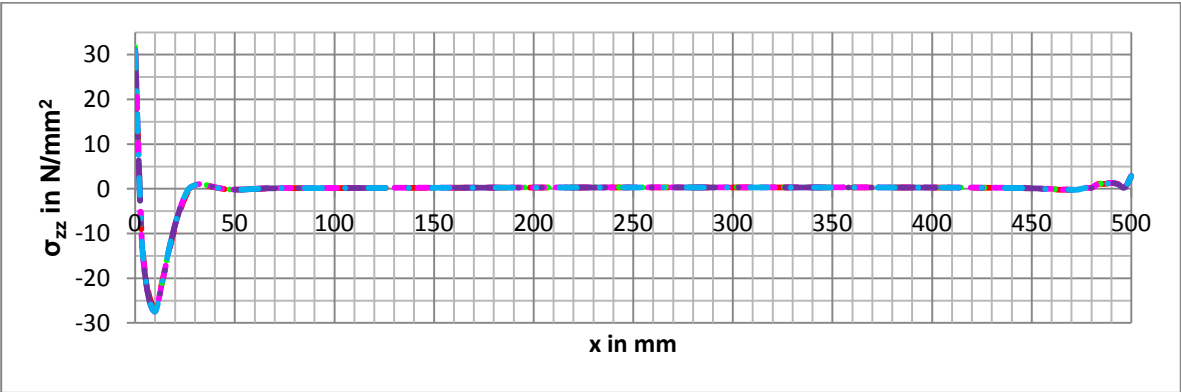


Figure 24.14: Comparison of stresses perpendicular to the horizontal plane of the inner angle at $y=100$ $z=4$

24.1.3 Shear stresses (zx-direction) per test

For all the figures below the next colours are used to indicate the place of the result lines:

— Y=0 Z=0 — Y=0 Z=2 — Y=0 Z=4 — Y=50 Z=0 — Y=50 Z=2 — Y=50 Z=4 — Y=100 Z=0 — Y=100 Z=2 — Y=100 Z=4

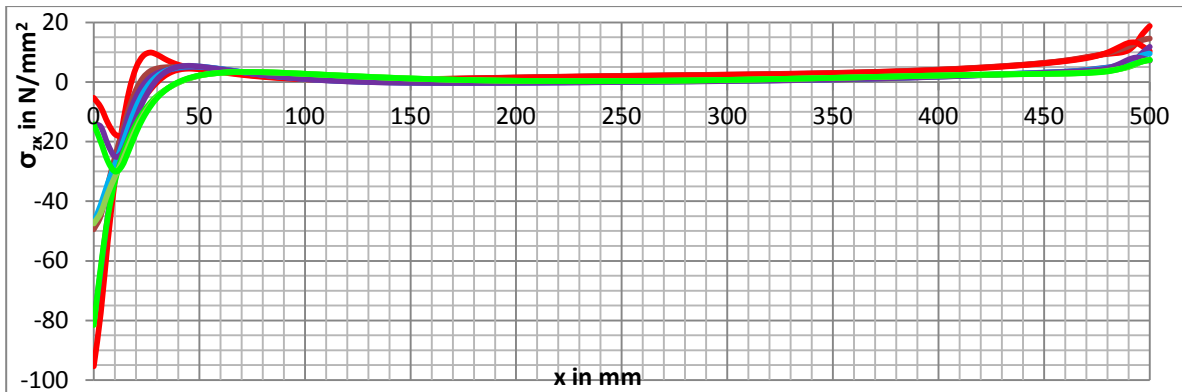


Figure 24.15: Shear stresses in zx-direction of the horizontal plane of the inner angle of test IA200x500 OA100x500

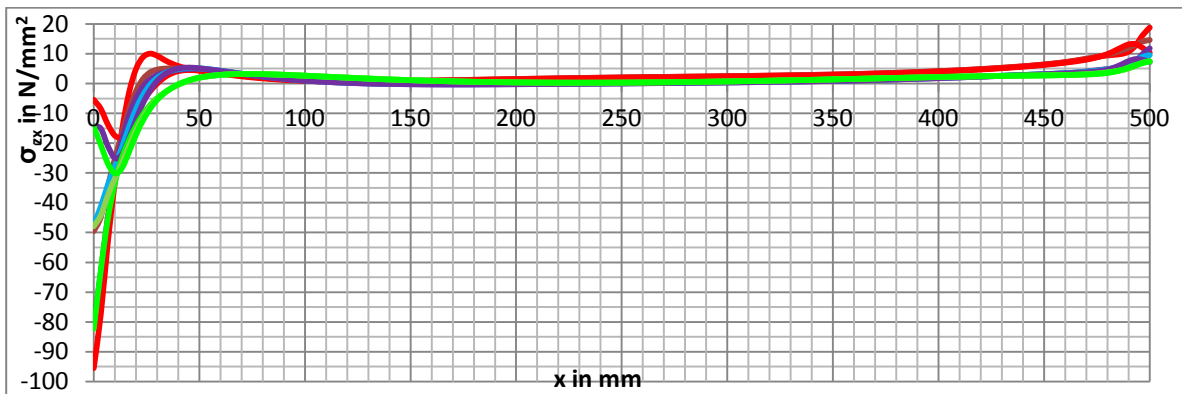


Figure 24.16: Shear stresses in zx-direction of the horizontal plane of the inner angle of test IA300x500 OA100x500

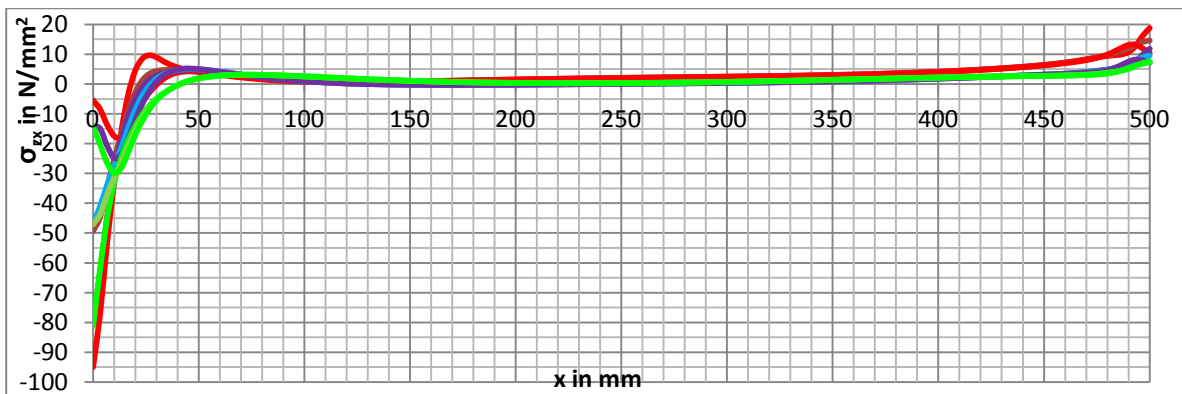


Figure 24.17: Shear stresses in zx-direction of the horizontal plane of the inner angle of test IA300x500 OA200x500

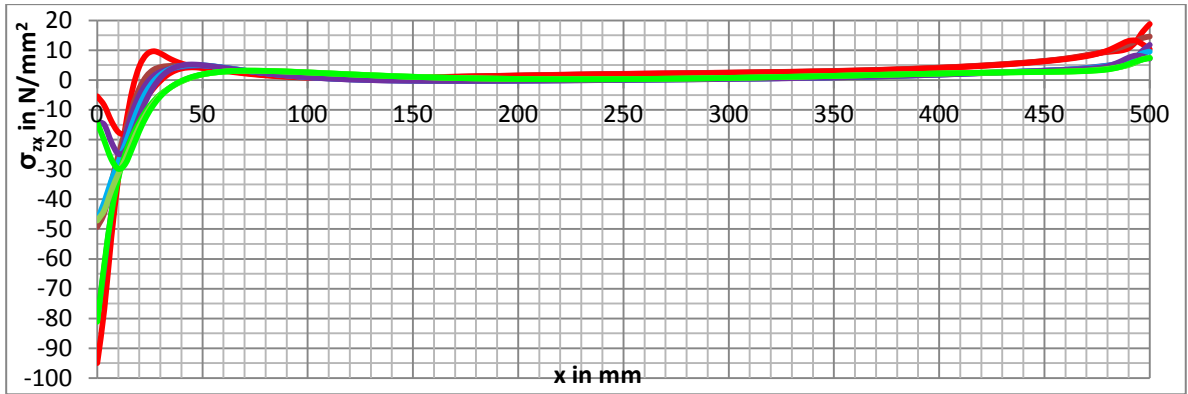


Figure 24.18: Shear stresses in zx-direction of the horizontal plane of the inner angle of test IA300x500 OA200x700

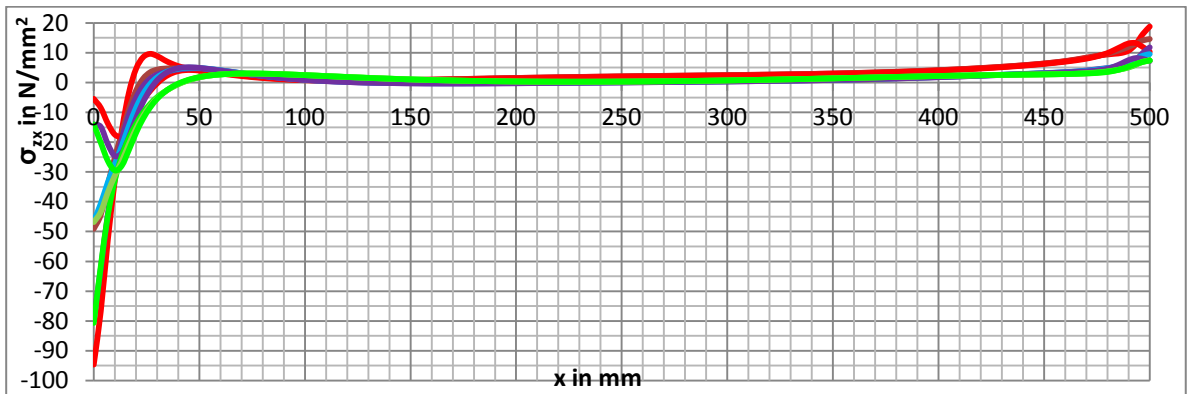


Figure 24.19: Shear stresses in zx-direction of the horizontal plane of the inner angle of test IA500x500 OA200x700

24.1.4 Shear stresses (zx-direction) per result line

For all the figures below the next colours are used to indicate the models:

— IA200x500 OA100x500
 - - - IA300x500 OA100x500
 - - - IA300x500 OA200x500
 - - - IA300x500 OA200x700
 - - - IA500x500 OA200x700

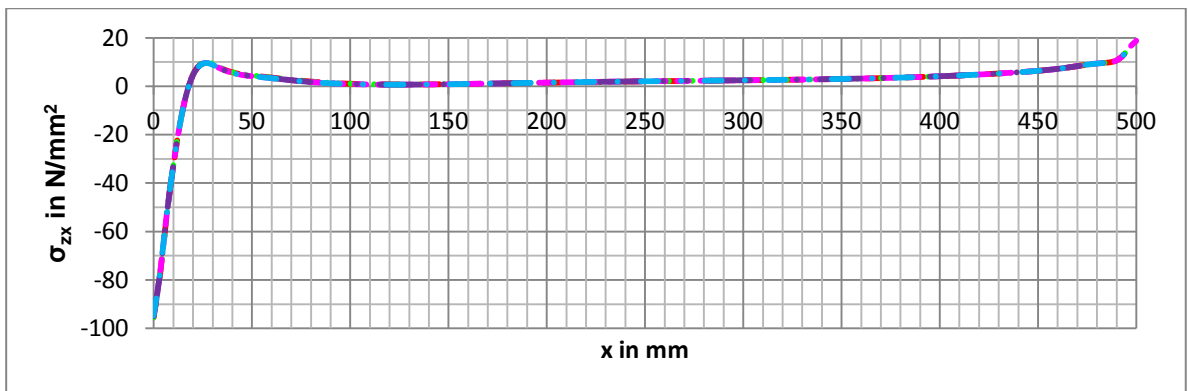


Figure 24.20: Comparison of shear stresses in zx-direction of the horizontal plane of the inner angle at y=0 z=0

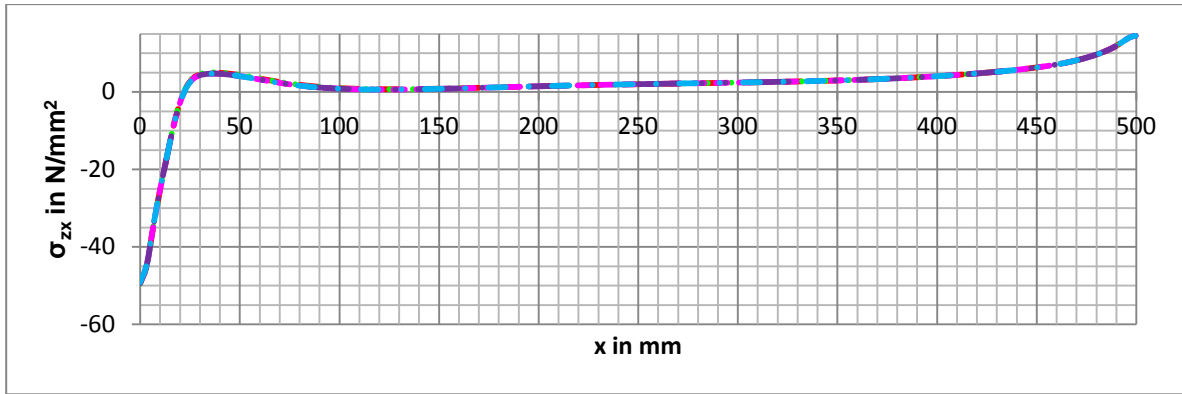


Figure 24.21: Comparison of shear stresses in zx-direction of the horizontal plane of the inner angle at $y=0$ $z=2$

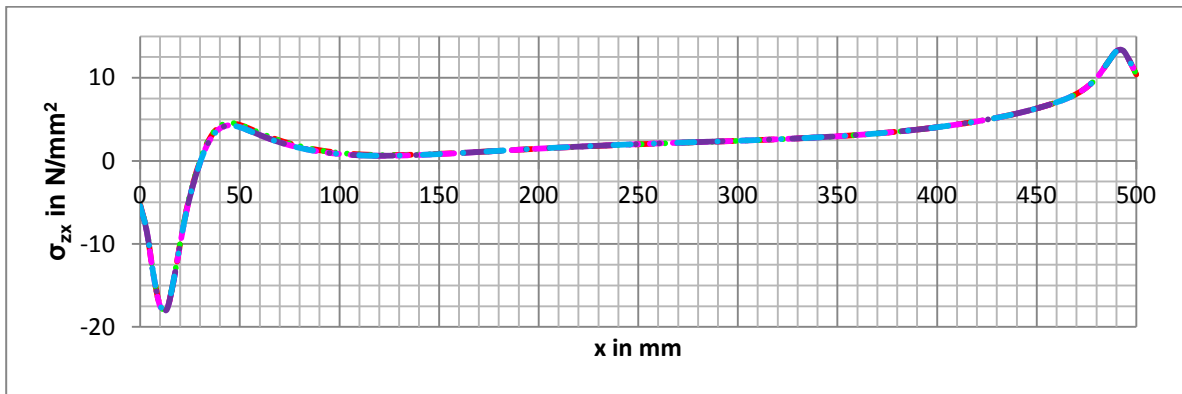


Figure 24.22: Comparison of shear stresses in zx-direction of the horizontal plane of the inner angle at $y=0$ $z=4$

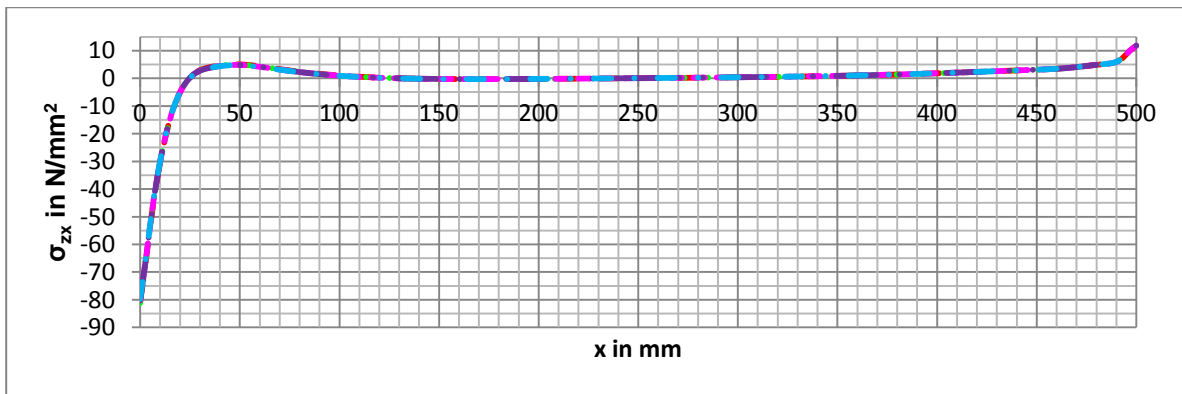


Figure 24.23: Comparison of shear stresses in zx-direction of the horizontal plane of the inner angle at $y=50$ $z=0$

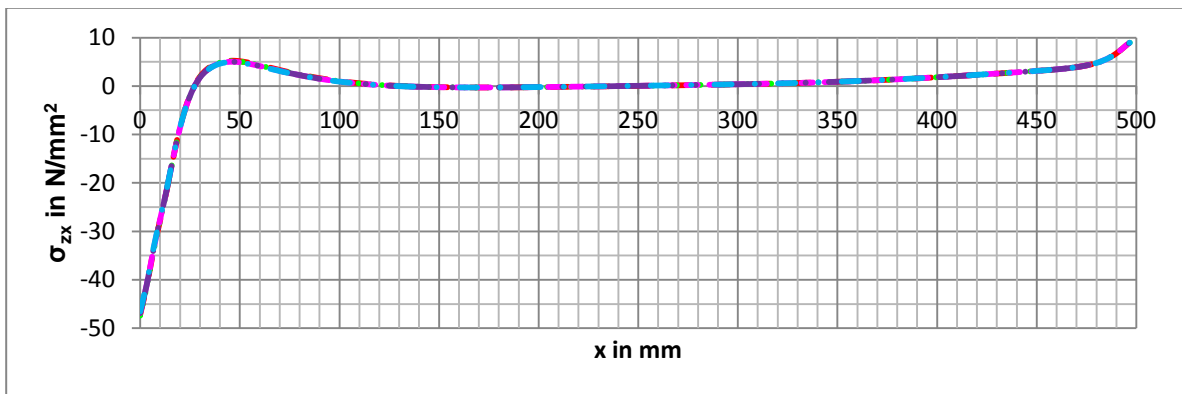


Figure 24.24: Comparison of shear stresses in zx-direction of the horizontal plane of the inner angle at $y=50$ $z=2$

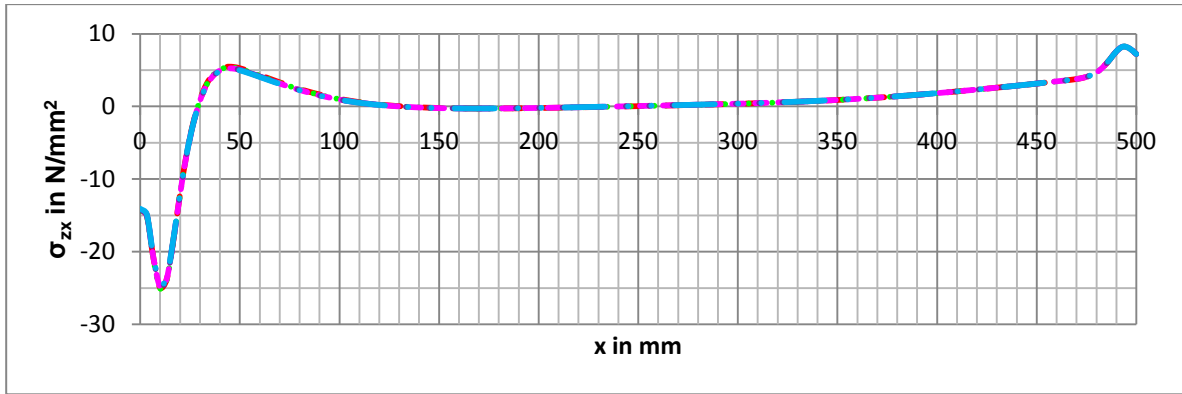


Figure 24.25: Comparison of shear stresses in zx-direction of the horizontal plane of the inner angle at y=50 z=4

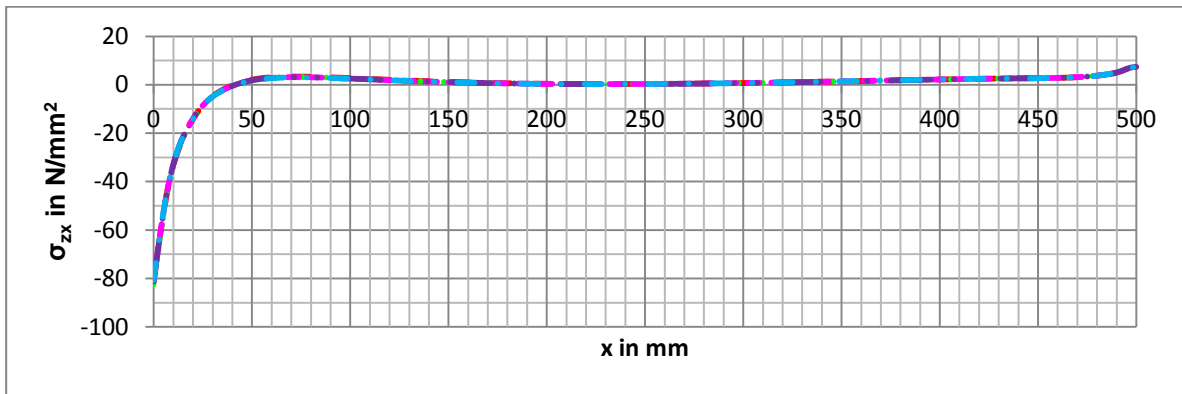


Figure 24.26: Comparison of shear stresses in zx-direction of the horizontal plane of the inner angle at y=100 z=0

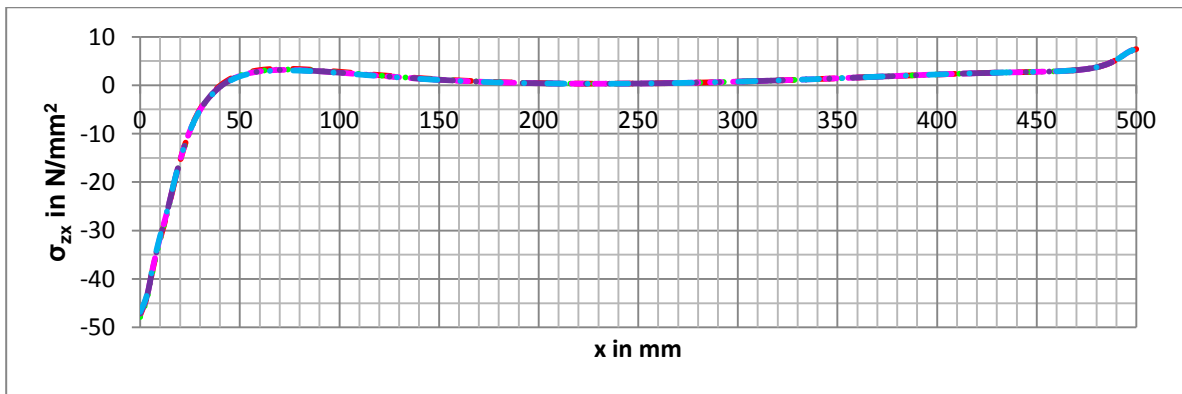


Figure 24.27: Comparison of shear stresses in zx-direction of the horizontal plane of the inner angle at y=100 z=2

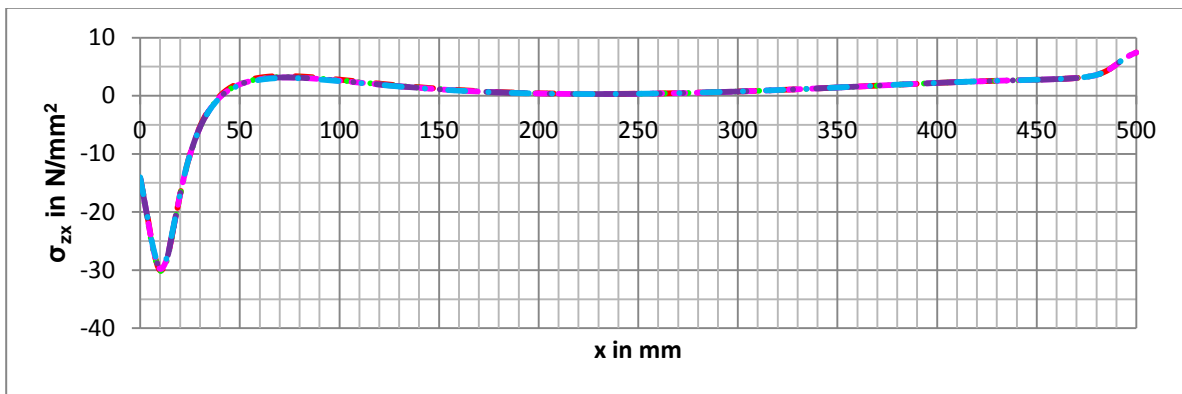


Figure 24.28: Comparison of shear stresses in zx-direction of the horizontal plane of the inner angle at y=100 z=4

24.2 Vertical plane of the inner angle

A description of the x-values used for the result lines can be found in the next table:

x-value	Description
0	Interface of column and adhesive
2	At the middle of the adhesive
4	Interface of adhesive and steel angle

Table 24.4: Values of z for the horizontal plane of the inner angle

For the vertical part of the inner angle there are a few specific points, listed below:

z-value	description
0	Interface of adhesive and beam
4	Top of the horizontal part of the inner angle
14	bottom of the horizontal part of the inner angle

Table 24.5: Specific points for horizontal plane of the inner angle

24.2.1 Stresses perpendicular to the plane per test

For all the figures below the next colours are used to indicate the place of the result lines:

— X=0 Y=0 — X=2 Y=0 — X=4 Y=0 — X=0 Y=50 — X=2 Y=50 — X=4 Y=50 — X=0 Y=100 — X=2 Y=100 — X=4 Y=100

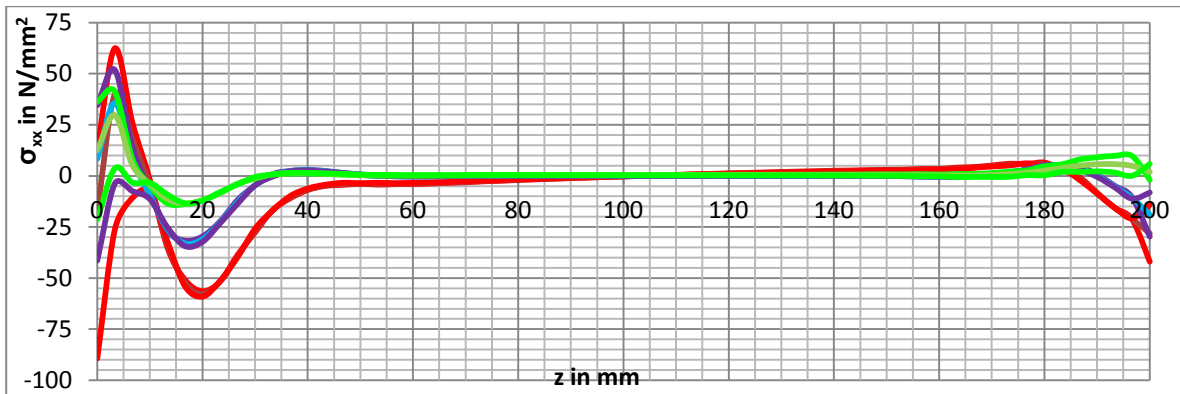


Figure 24.29: Stresses perpendicular to the horizontal plane of the inner angle of test IA200x500 OA100x500

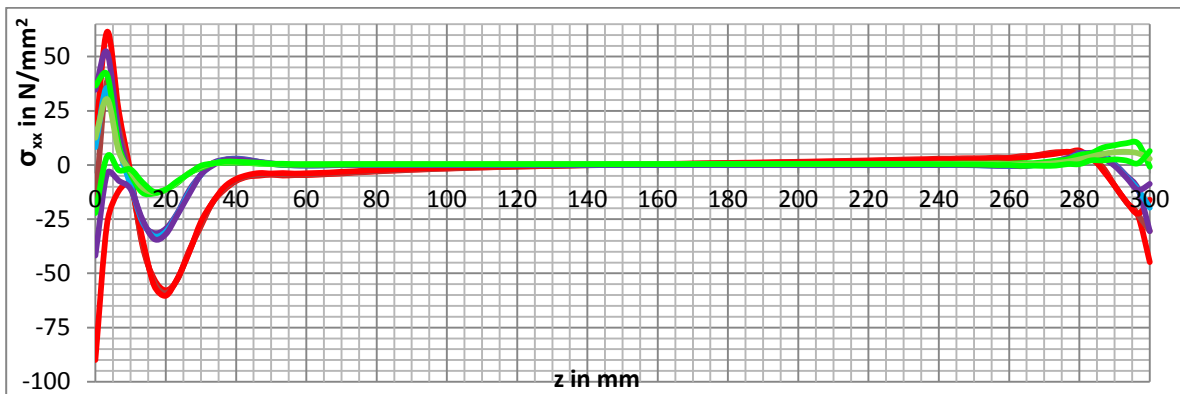


Figure 24.30: Stresses perpendicular to the horizontal plane of the inner angle of test IA300x500 OA100x500

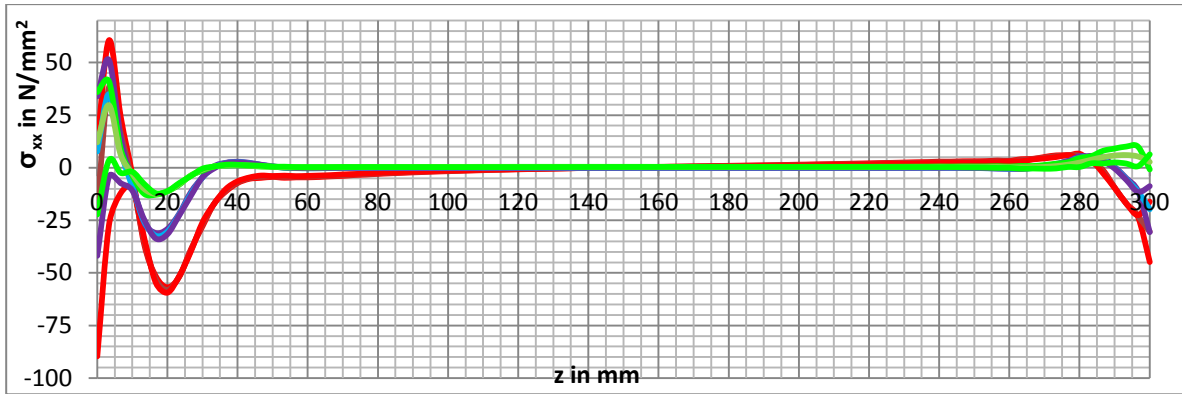


Figure 24.31: Stresses perpendicular to the horizontal plane of the inner angle of test IA300x500 OA200x500

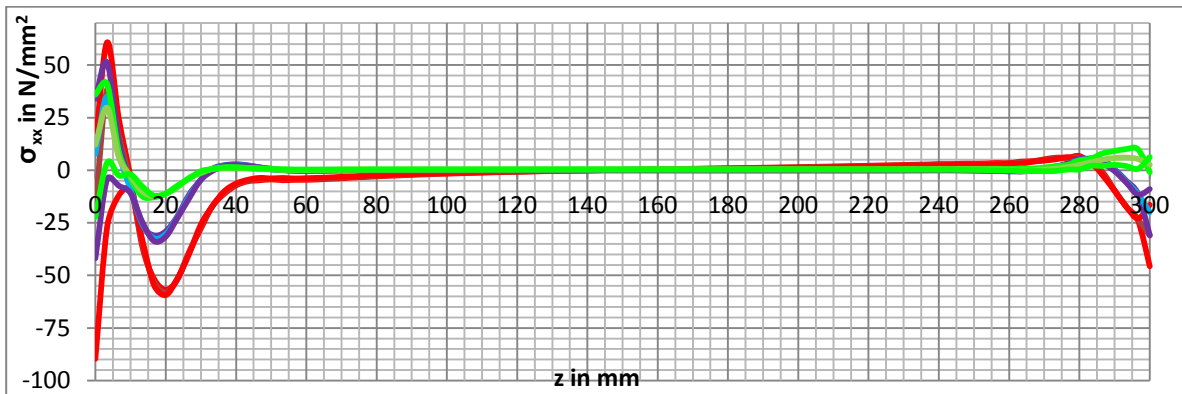


Figure 24.32: Stresses perpendicular to the horizontal plane of the inner angle of test IA300x500 OA200x700

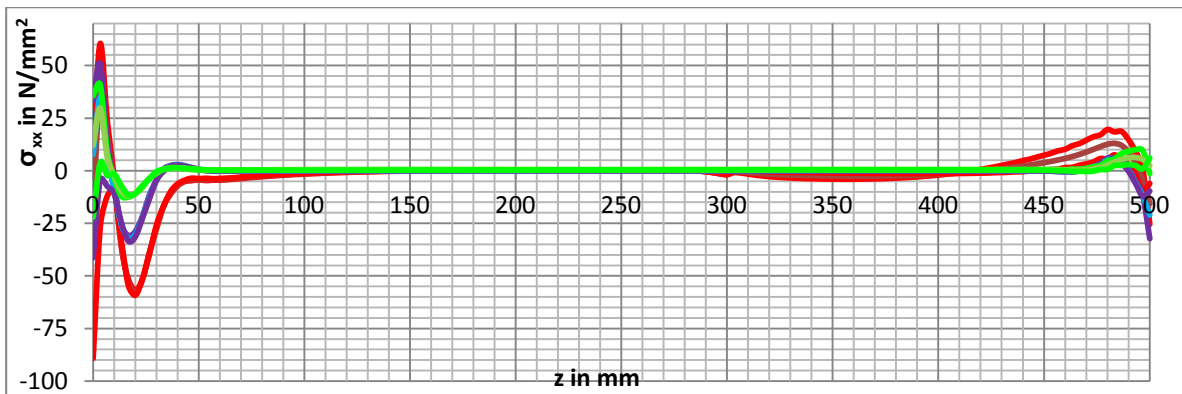


Figure 24.33: Stresses perpendicular to the horizontal plane of the inner angle of test IA300x500 OA500x700

24.2.2 Stresses perpendicular to the plane per result line

For all the figures below the next colours are used to indicate the models:

- IA200x500 OA100x500
- - - IA300x500 OA100x500
- - - IA300x500 OA200x500
- - - IA300x500 OA200x700
- - - IA500x500 OA200x700

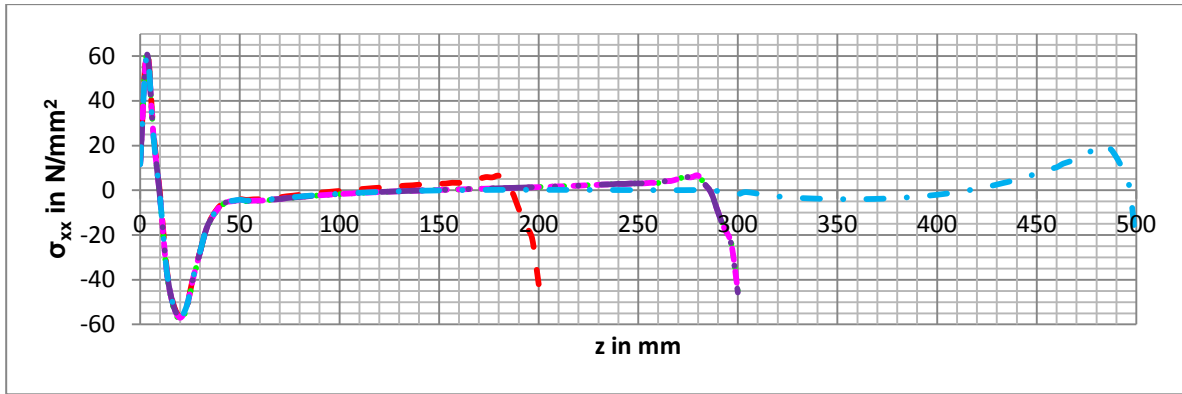


Figure 24.34: Comparison of stresses perpendicular to the vertical plane of the inner angle at $y=0$ $x=0$

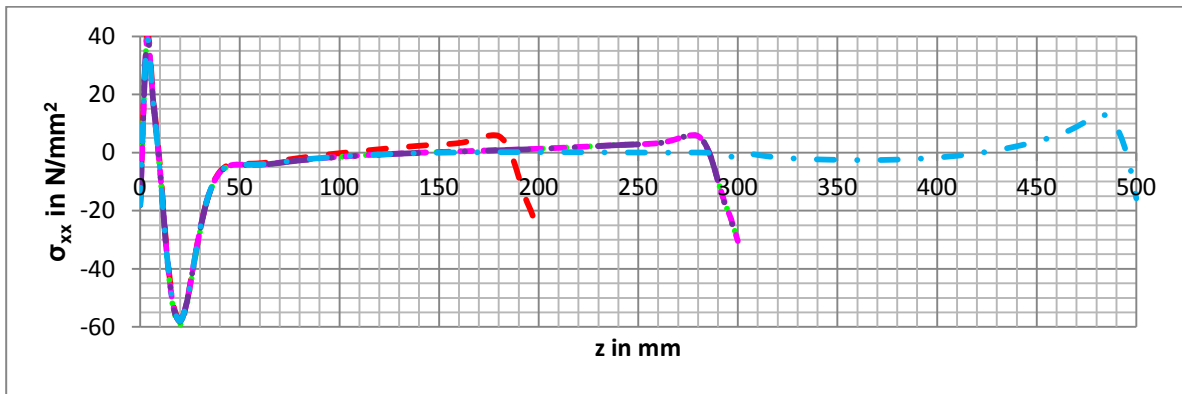


Figure 24.35: Comparison of stresses perpendicular to the vertical plane of the inner angle at $y=0$ $x=2$

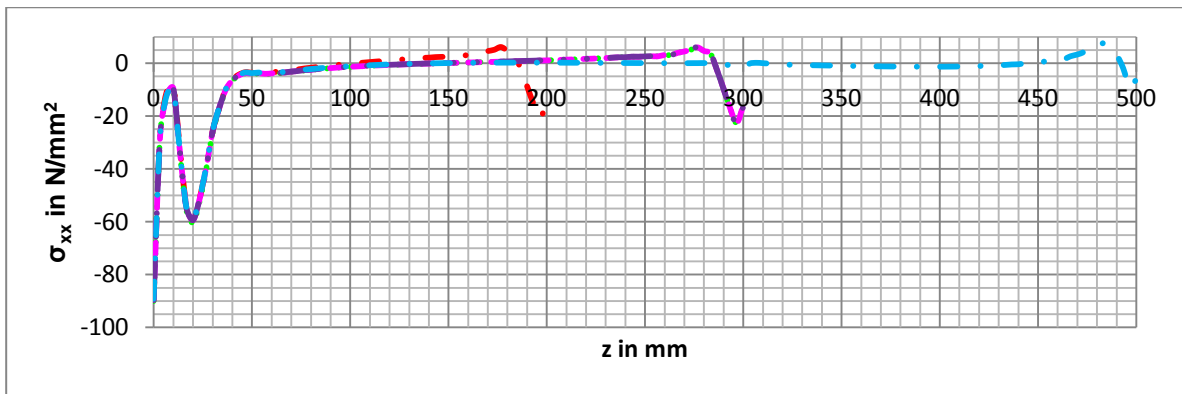


Figure 24.36: Comparison of stresses perpendicular to the vertical plane of the inner angle at $y=0$ $x=4$

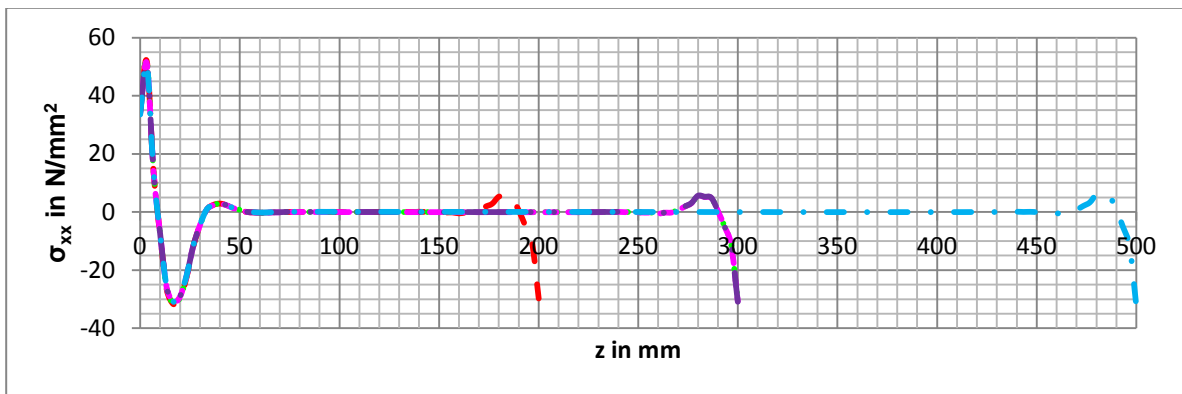


Figure 24.37: Comparison of stresses perpendicular to the vertical plane of the inner angle at $y=50$ $x=0$

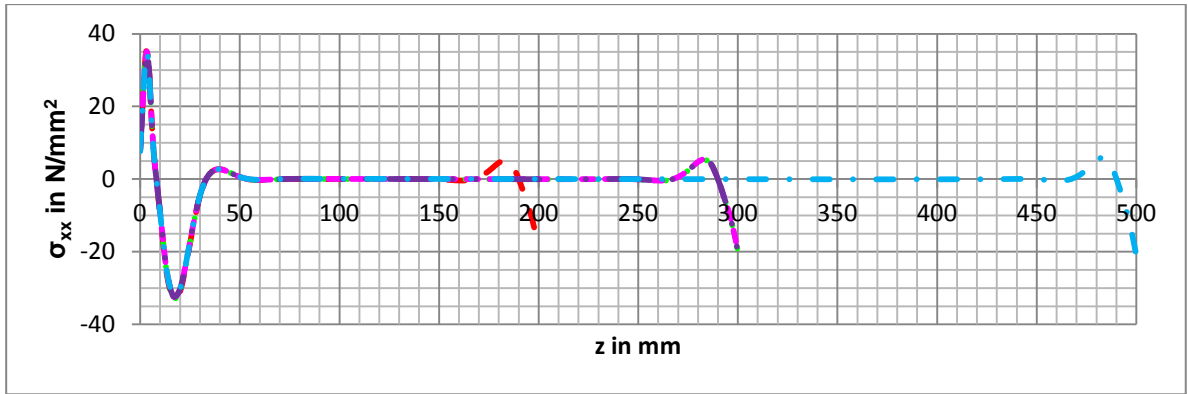


Figure 24.38: Comparison of stresses perpendicular to the vertical plane of the inner angle at $y=50$ $x=2$

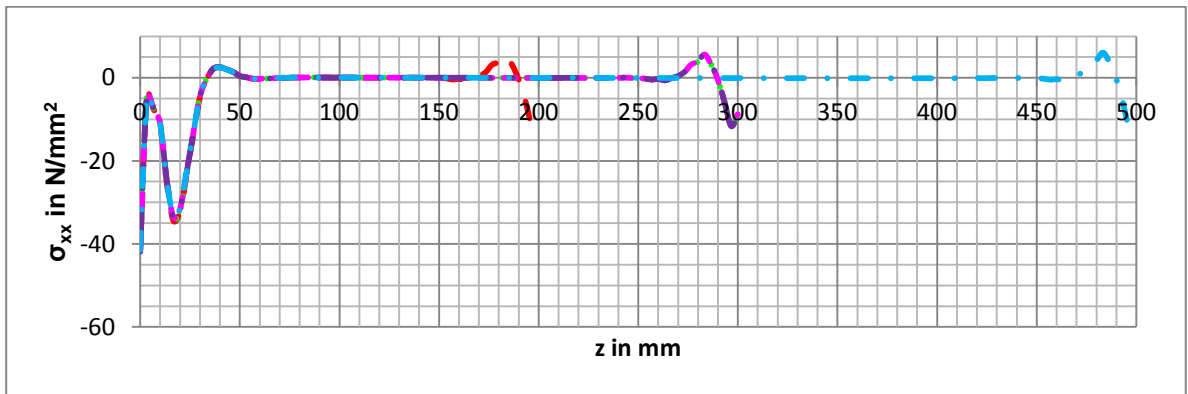


Figure 24.39: Comparison of stresses perpendicular to the vertical plane of the inner angle at $y=50$ $x=4$

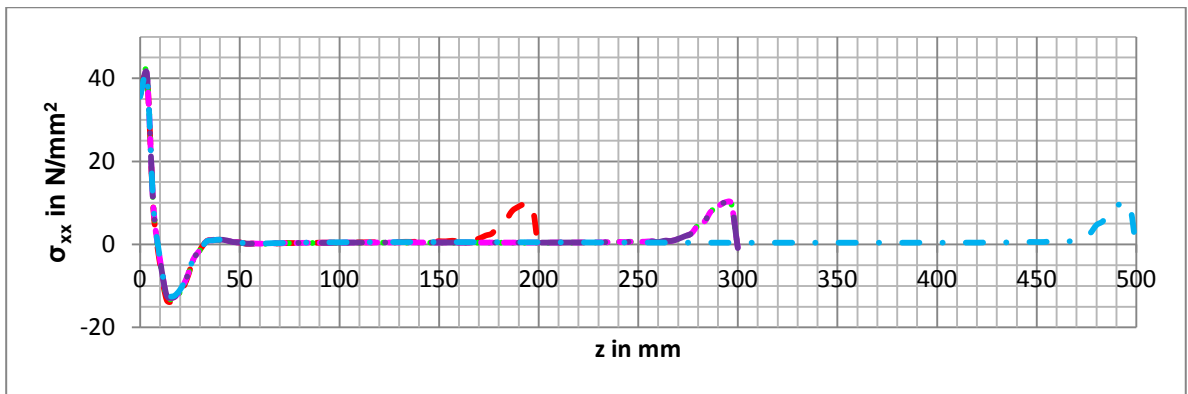


Figure 24.40: Comparison of stresses perpendicular to the vertical plane of the inner angle at $y=100$ $x=0$

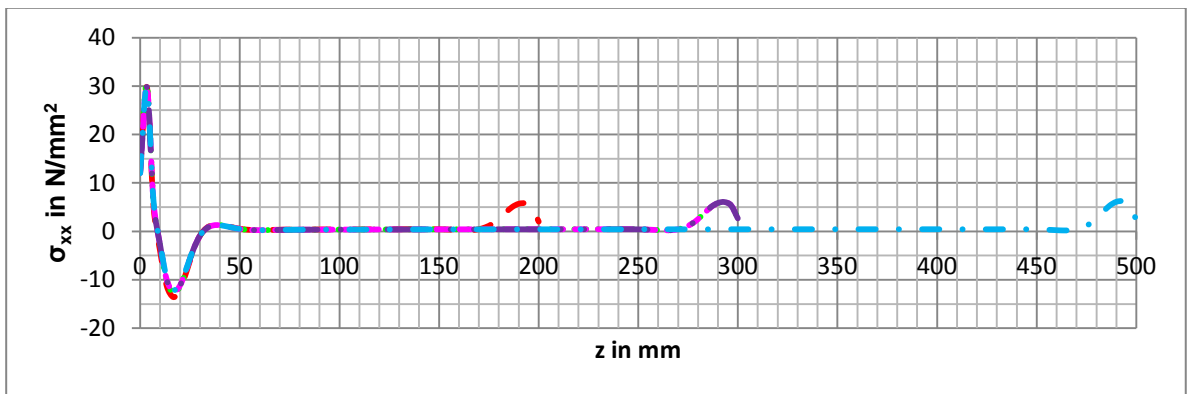


Figure 24.41: Comparison of stresses perpendicular to the vertical plane of the inner angle at $y=100$ $x=2$

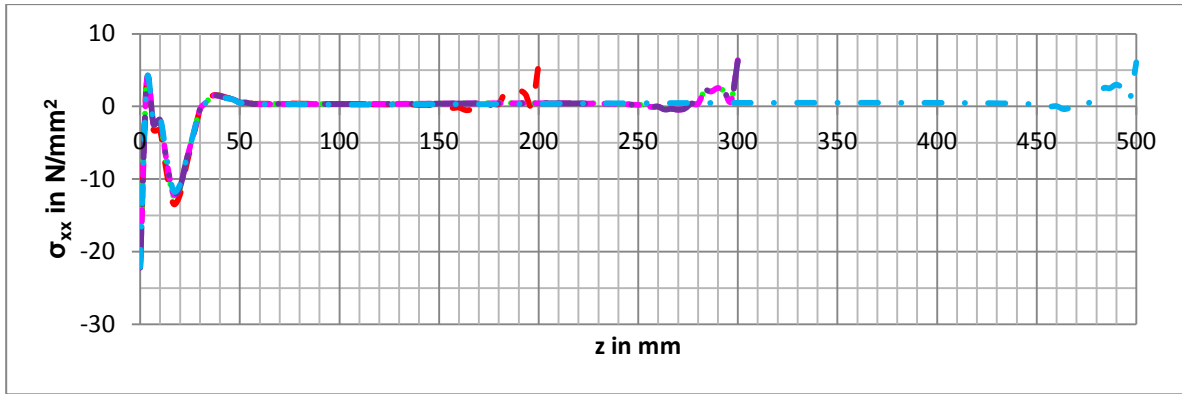


Figure 24.42: Comparison of stresses perpendicular to the vertical plane of the inner angle at $y=100$ $x=4$

24.2.3 Shear stresses (zx-direction) per test

For all the figures below the next colours are used to indicate the place of the result lines:

— $X=0$ $Y=0$ — $X=2$ $Y=0$ — $X=4$ $Y=0$ — $X=0$ $Y=50$ — $X=2$ $Y=50$ — $X=4$ $Y=50$ — $X=0$ $Y=100$ — $X=2$ $Y=100$ — $X=4$ $Y=100$

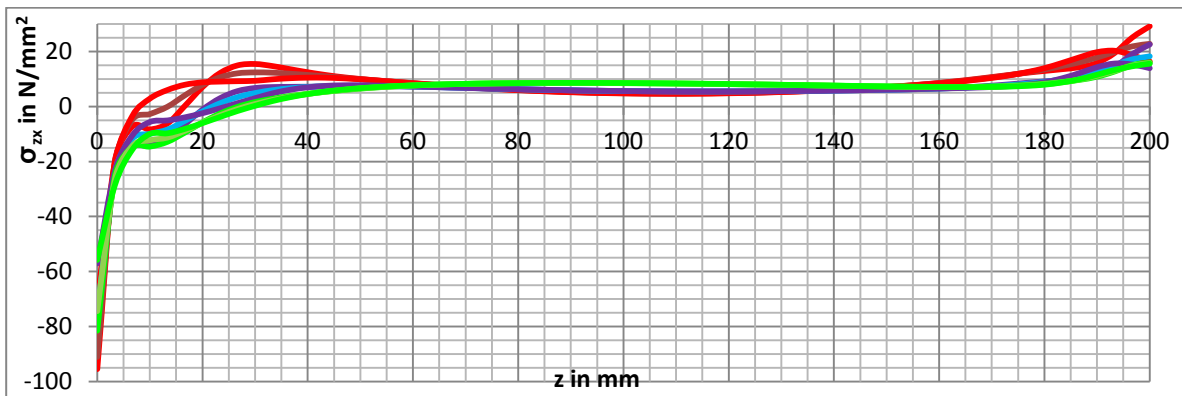


Figure 24.43: Shear stresses in zx -direction of the vertical plane of the inner angle of test IA200x500 OA100x500

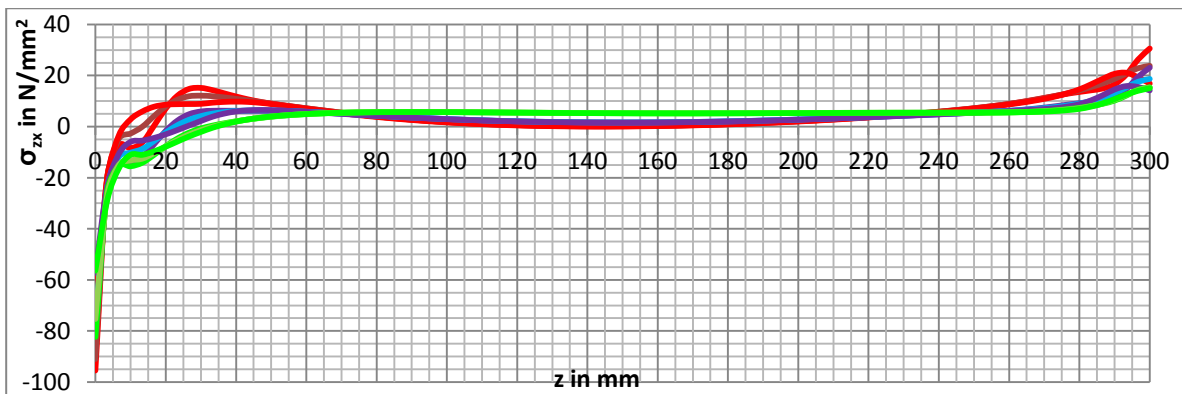


Figure 24.44: Shear stresses in zx -direction of the vertical plane of the inner angle of test IA300x500 OA100x500

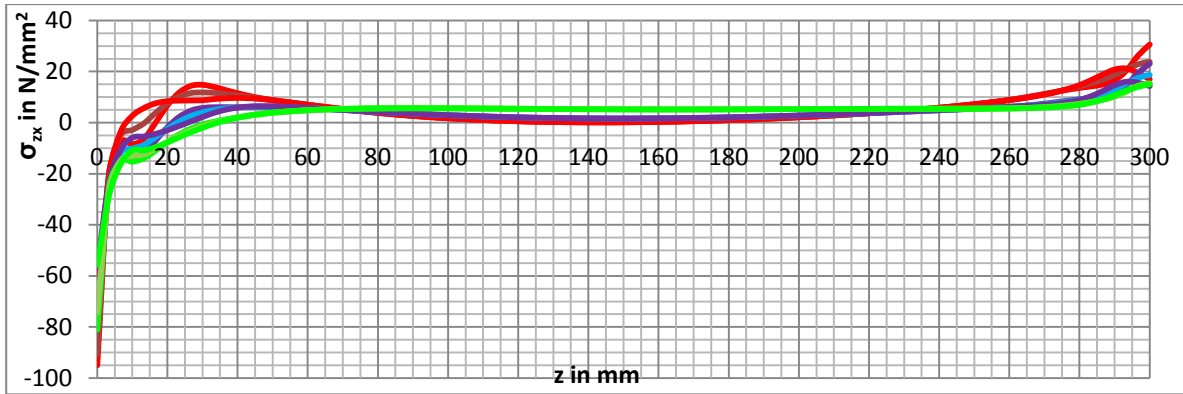


Figure 24.45: Shear stresses in zx-direction of the vertical plane of the inner angle of test IA300x500 OA200x500

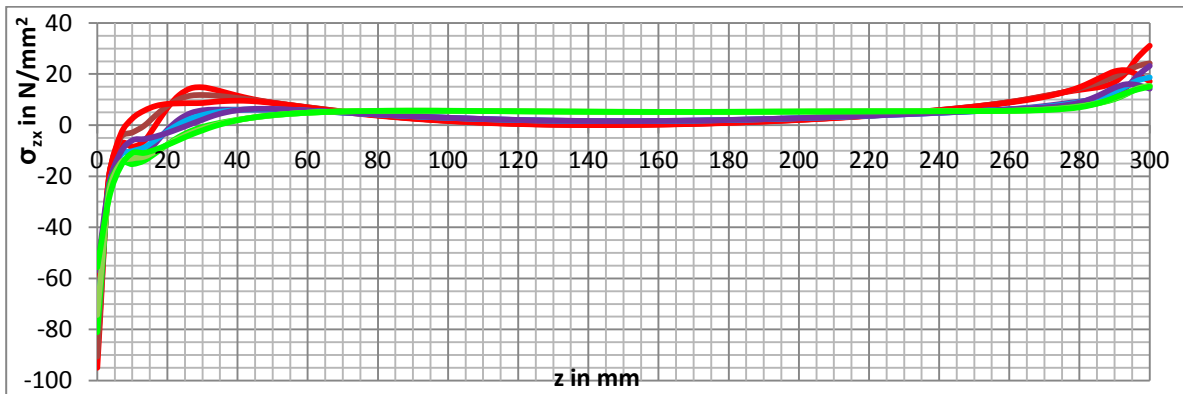


Figure 24.46: Shear stresses in zx-direction of the vertical plane of the inner angle of test IA300x500 OA200x700

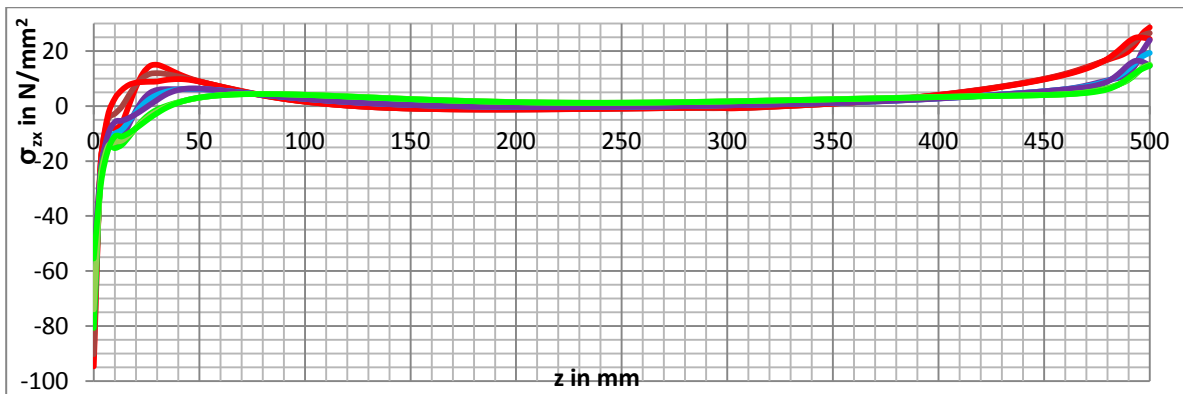


Figure 24.47: Shear stresses in zx-direction of the vertical plane of the inner angle of test IA500x500 OA200x700

24.2.4 Shear stresses (zx-direction) per result line

For all the figures below the next colours are used to indicate the models:

— IA200x500 OA100x500
 - - - IA300x500 OA100x500
 - - - IA300x500 OA200x500
 - - - IA300x500 OA200x700
 - - - IA500x500 OA200x700

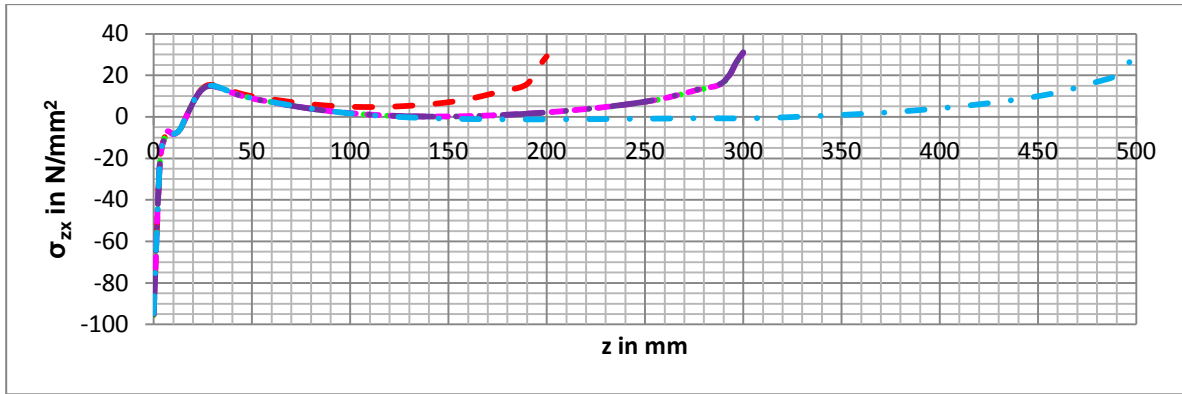


Figure 24.48: Comparison of shear stresses in zx-direction of the vertical plane of the inner angle at $y=0$ $x=0$

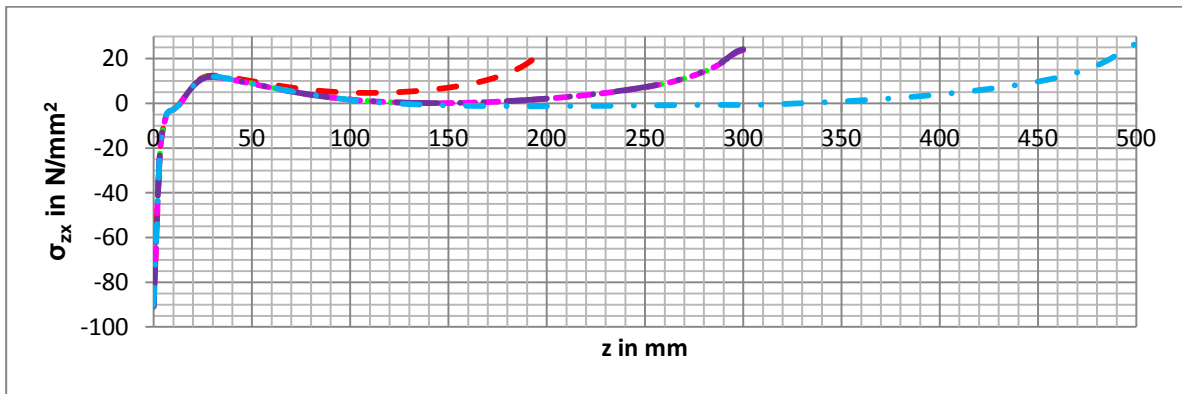


Figure 24.49: Comparison of shear stresses in zx-direction of the vertical plane of the inner angle at $y=0$ $x=2$

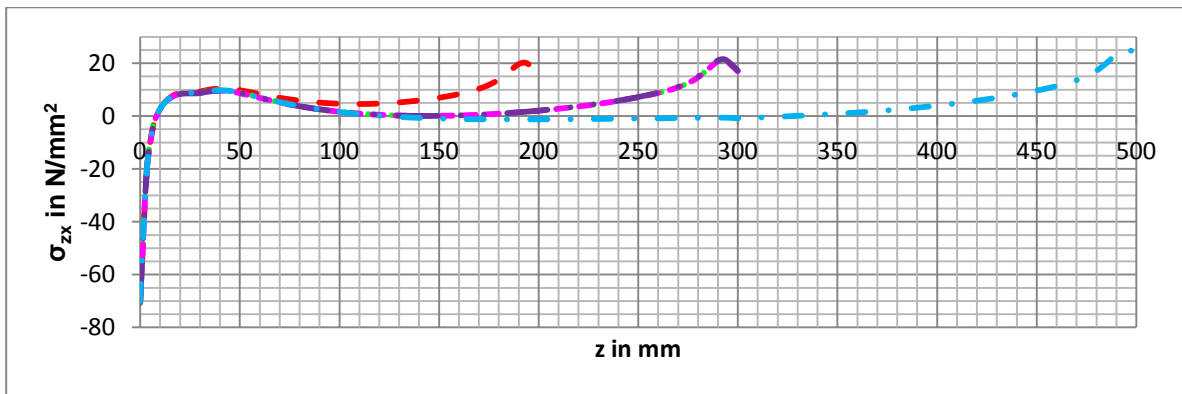


Figure 24.50: Comparison of shear stresses in zx-direction of the vertical plane of the inner angle at $y=0$ $x=4$

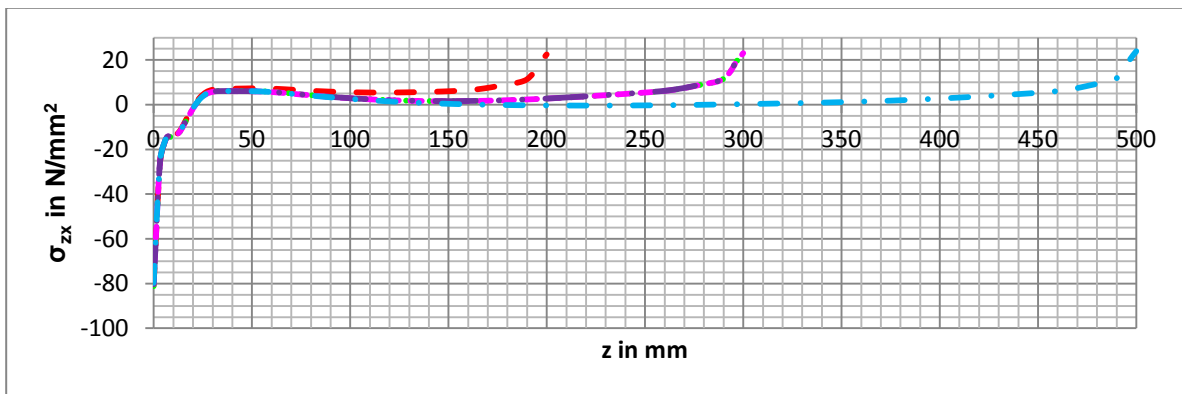


Figure 24.51: Comparison of shear stresses in zx-direction of the vertical plane of the inner angle at $y=50$ $x=0$

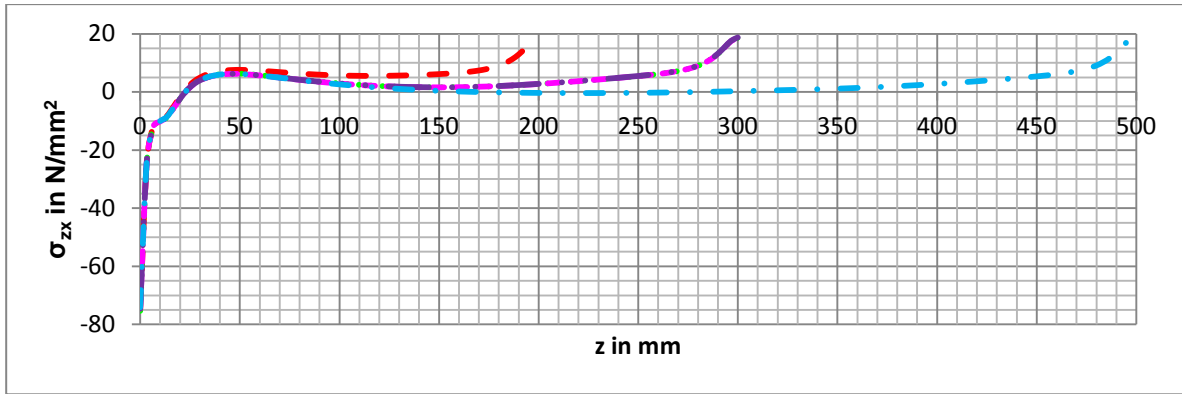


Figure 24.52: Comparison of shear stresses in zx-direction of the vertical plane of the inner angle at y=50 x=2

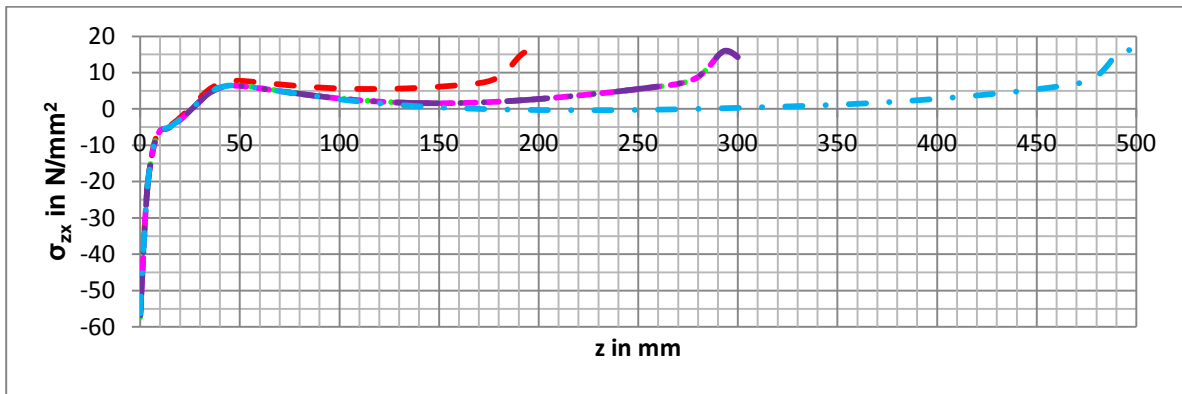


Figure 24.53: Comparison of shear stresses in zx-direction of the vertical plane of the inner angle at y=50 x=4

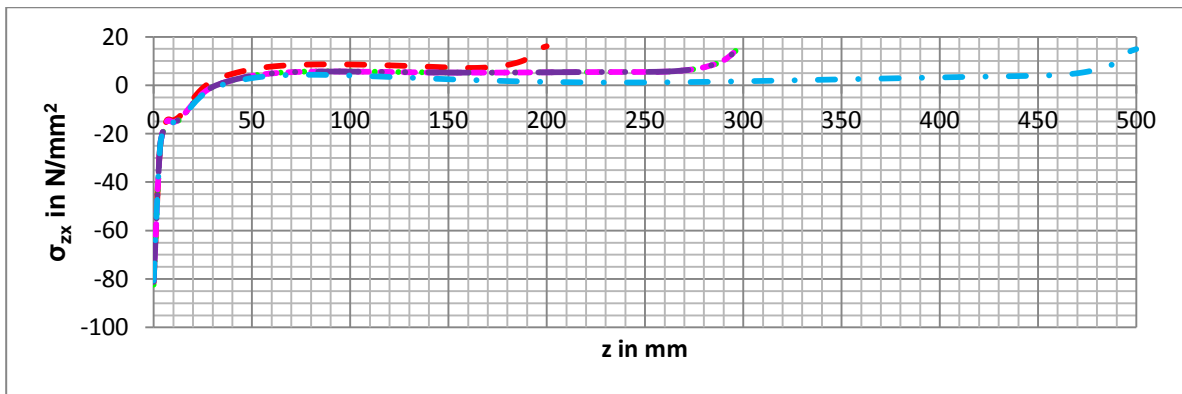


Figure 24.54: Comparison of shear stresses in zx-direction of the vertical plane of the inner angle at y=100 x=0

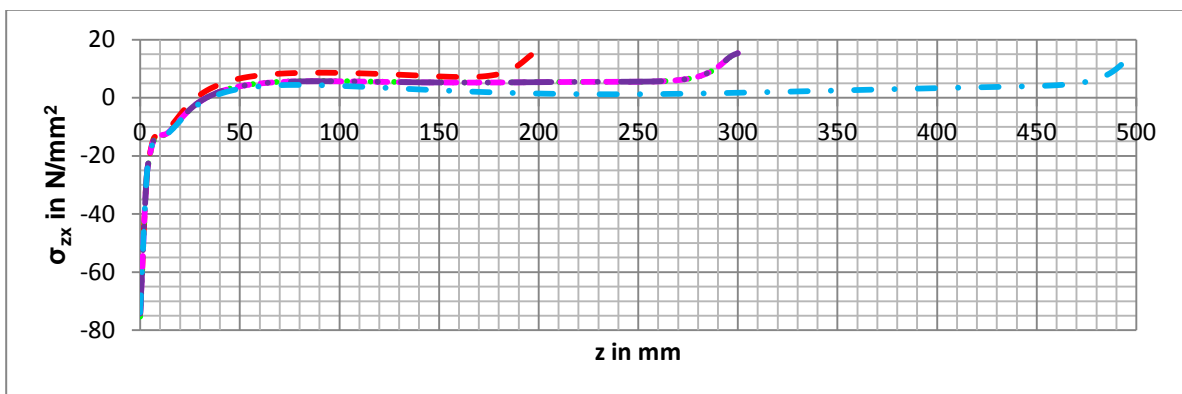


Figure 24.55: Comparison of shear stresses in zx-direction of the vertical plane of the inner angle at y=100 x=2

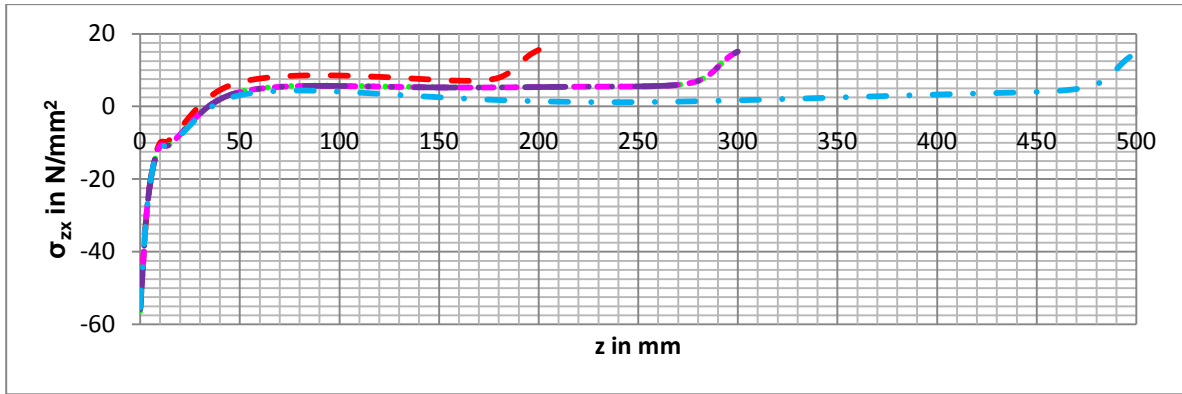


Figure 24.56: Comparison of shear stresses in zx-direction of the vertical plane of the inner angle at y=100 x=4

24.3 Horizontal plane of the outer angle

A description of the z-values used for the result lines can be found in the next table:

z-value	Description
-194	Interface of steel angle and adhesive
-192	At the middle of the adhesive
-190	Interface of adhesive and beam

Table 24.6: Values of z for the horizontal plane of the inner angle

For the horizontal part of the outer angle there are a few specific points, listed below:

x-value	description
-194	Interface of adhesive and the outer angle
-190	Interface a adhesive and endplate
-180	Right side of endplate

Table 24.7: Specific points for horizontal plane of the outer angle

24.3.1 Stresses perpendicular to the plane per test

For all the figures below the next colours are used to indicate the place of the result lines:

— Y=0 Z=-194 — Y=0 Z=-192 — Y=0 Z=-190 — Y=50 Z=-194 — Y=50 Z=-192 — Y=50 Z=-190 — Y=100 Z=-194 — Y=100 Z=-192 — Y=100 Z=-190

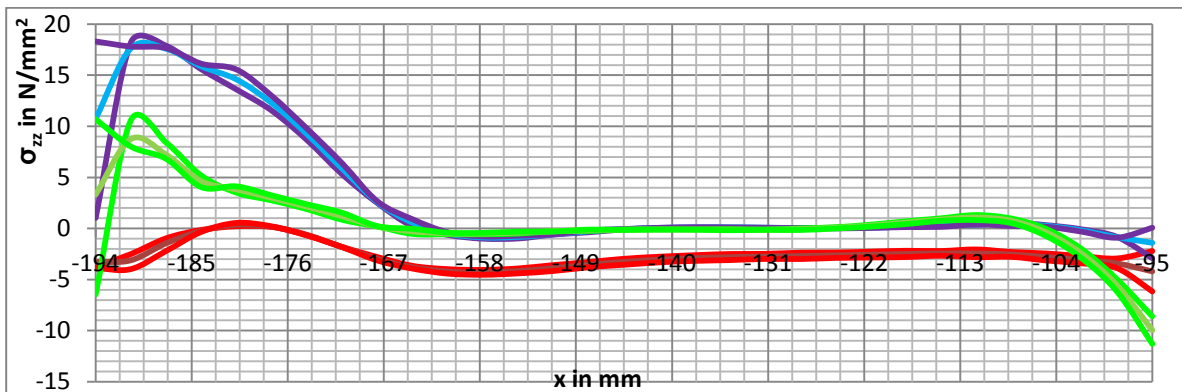


Figure 24.57: Stresses perpendicular to the horizontal plane of the outer angle of test IA200x500 OA100x500

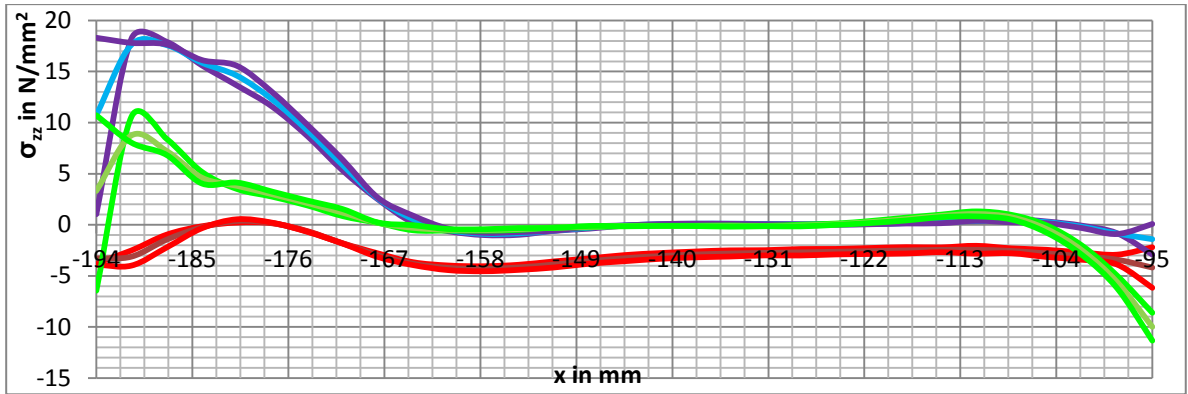


Figure 24.58: Stresses perpendicular to the horizontal plane of the outer angle of test IA300x500 OA100x500

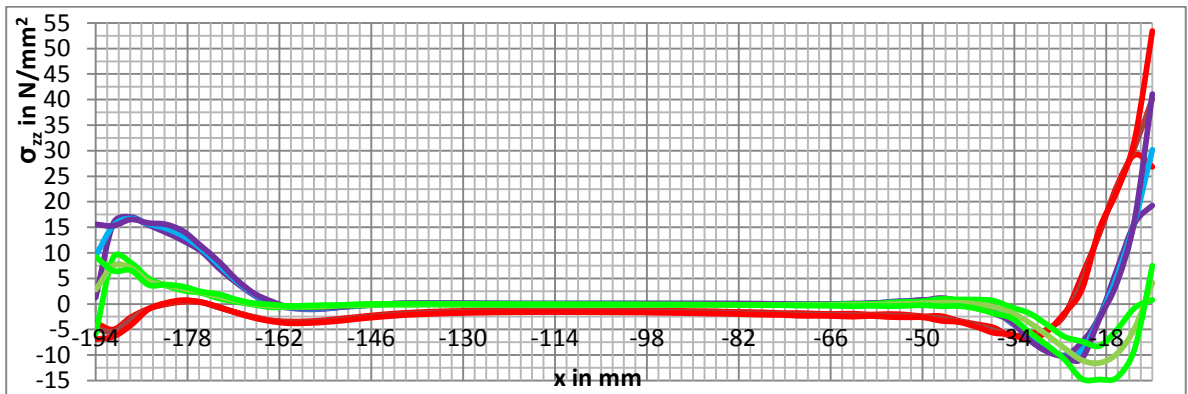


Figure 24.59: Stresses perpendicular to the horizontal plane of the outer angle of test IA300x500 OA200x500

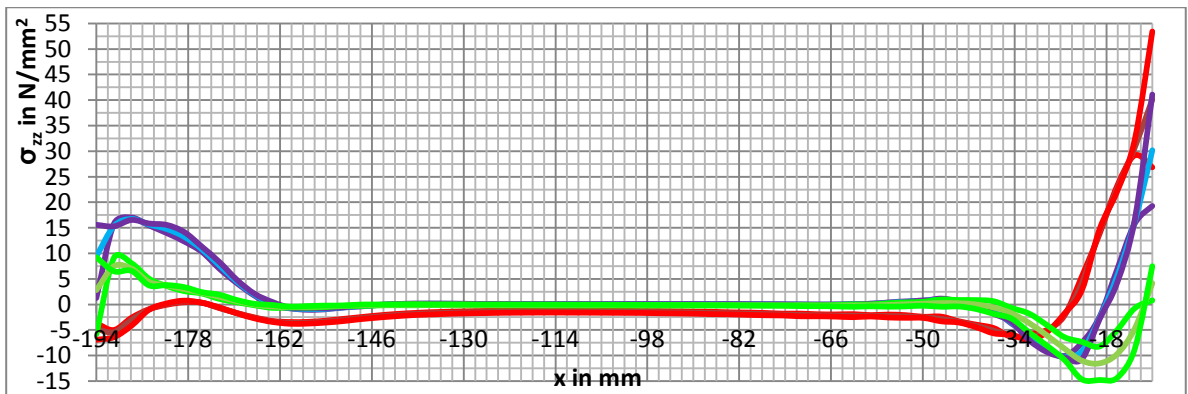


Figure 24.60: Stresses perpendicular to the horizontal plane of the outer angle of test IA300x500 OA200x700

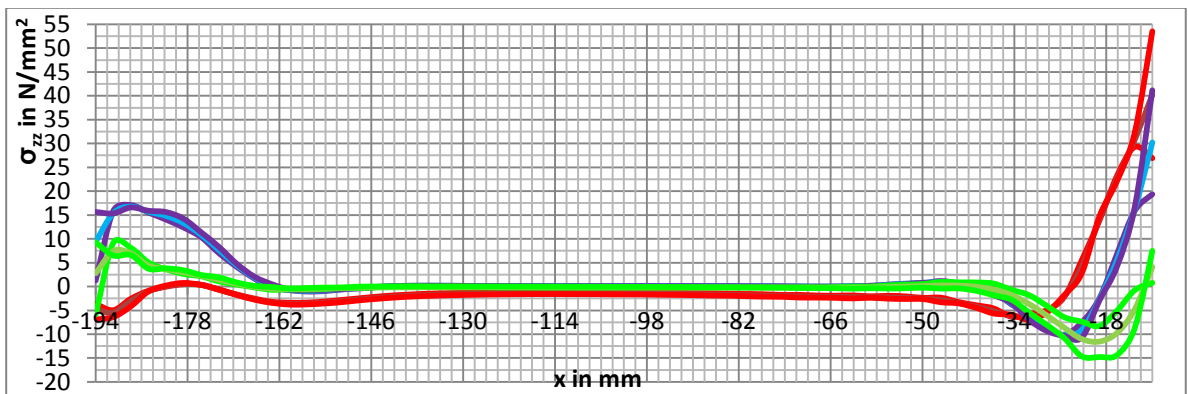


Figure 24.61: Stresses perpendicular to the horizontal plane of the outer angle of test IA500x500 OA200x700

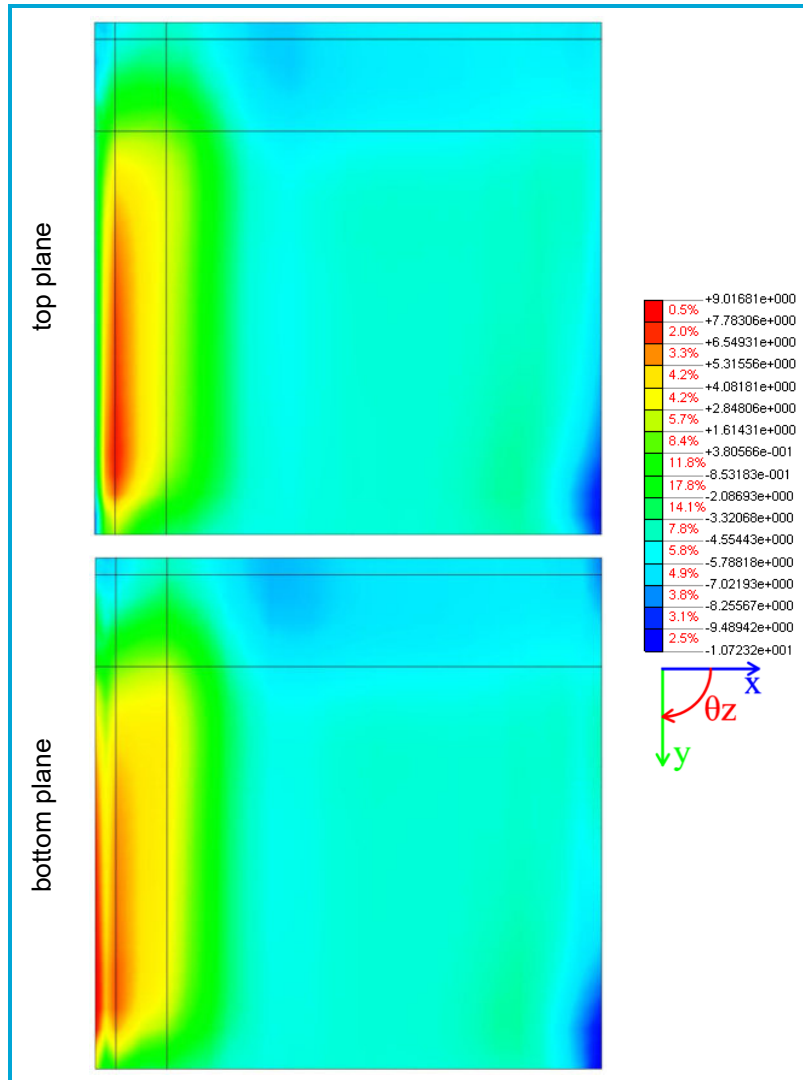


Figure 24.62: Counterplot of stresses perpendicular to the horizontal plane of the outer angle of test IA300x500 OA100x500

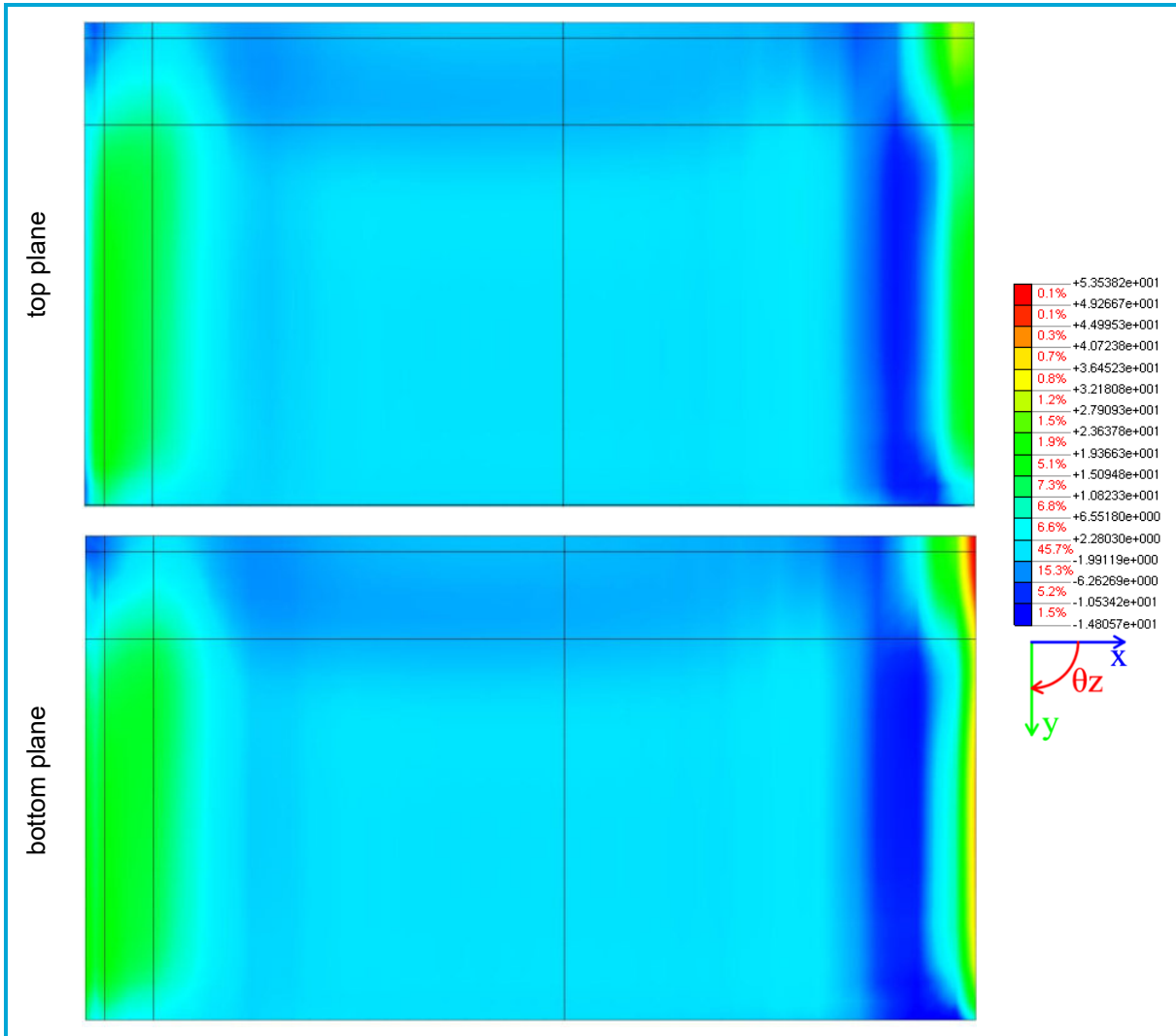


Figure 24.63: Counterplot of stresses perpendicular to the horizontal plane of the outer angle of test IA500x500 OA200x700

24.3.2 Stresses perpendicular to the plane per result line

For all the figures below the next colours are used to indicate the models:

--- IA200x500 OA100x500
 -.-.- IA300x500 OA100x500
 -.-.- IA300x500 OA200x500
 --- IA300x500 OA200x700
 -.-.- IA500x500 OA200x700

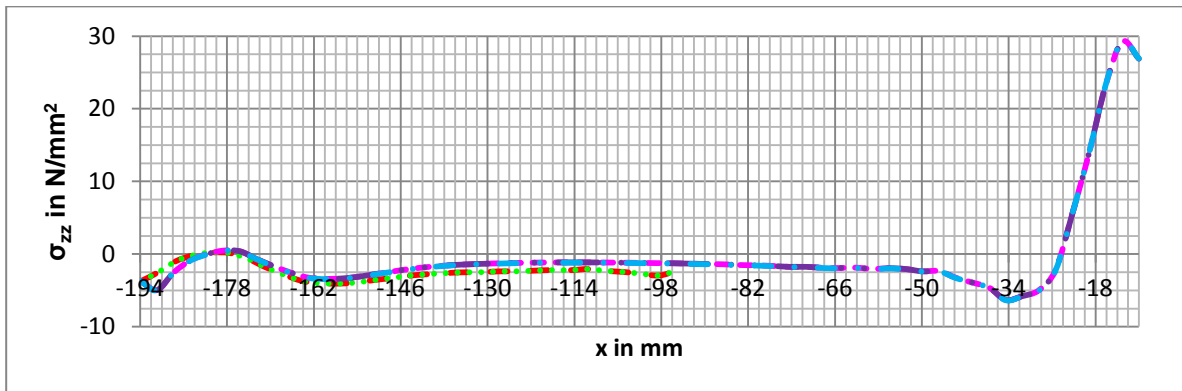


Figure 24.64: Comparison of stresses perpendicular to the horizontal plane of the outer angle at $y=0$ $x=-194$

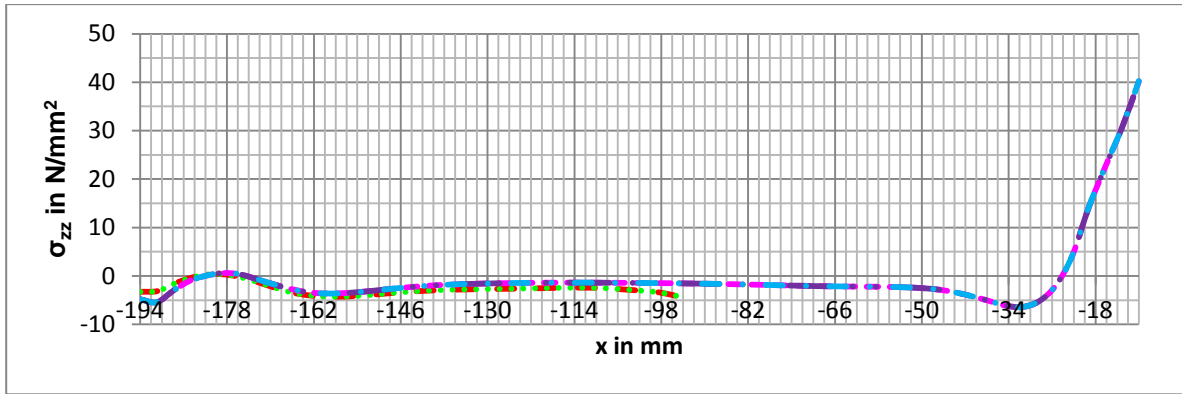


Figure 24.65: Comparison of stresses perpendicular to the horizontal plane of the outer angle at $y=0$ $x=-192$

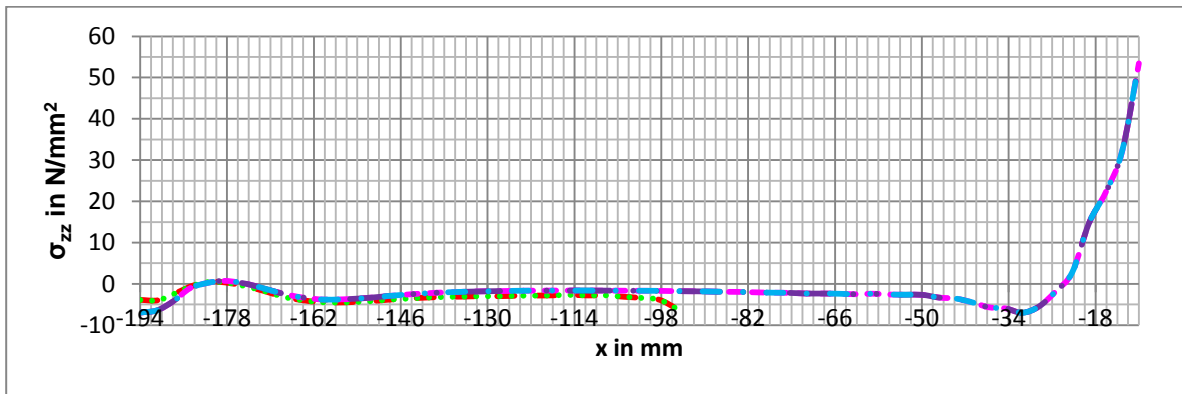


Figure 24.66: Comparison of stresses perpendicular to the horizontal plane of the outer angle at $y=0$ $x=-190$

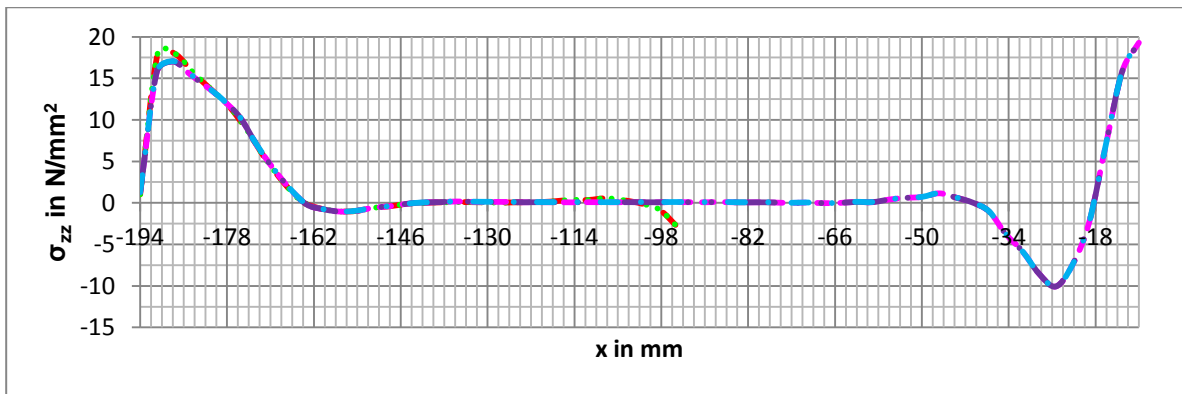


Figure 24.67: Comparison of stresses perpendicular to the horizontal plane of the outer angle at $y=50$ $x=-194$

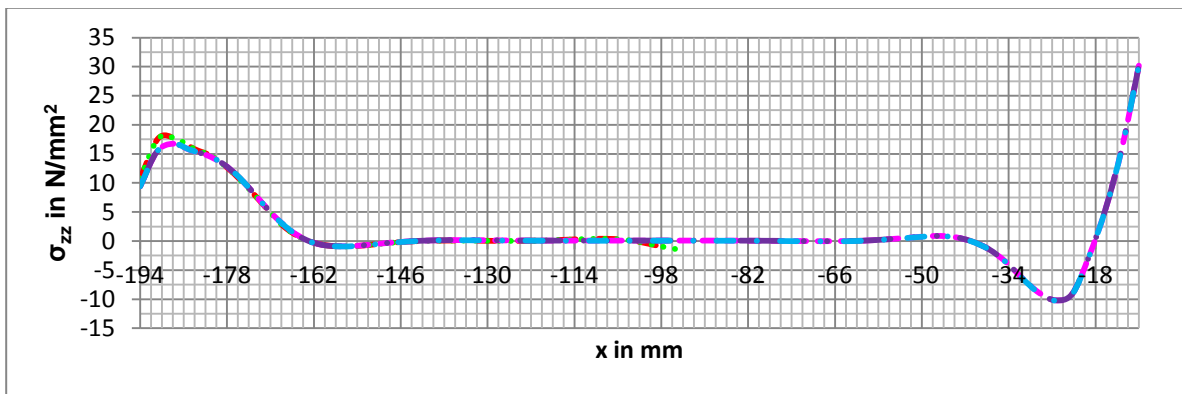


Figure 24.68: Comparison of stresses perpendicular to the horizontal plane of the outer angle at $y=50$ $x=-192$

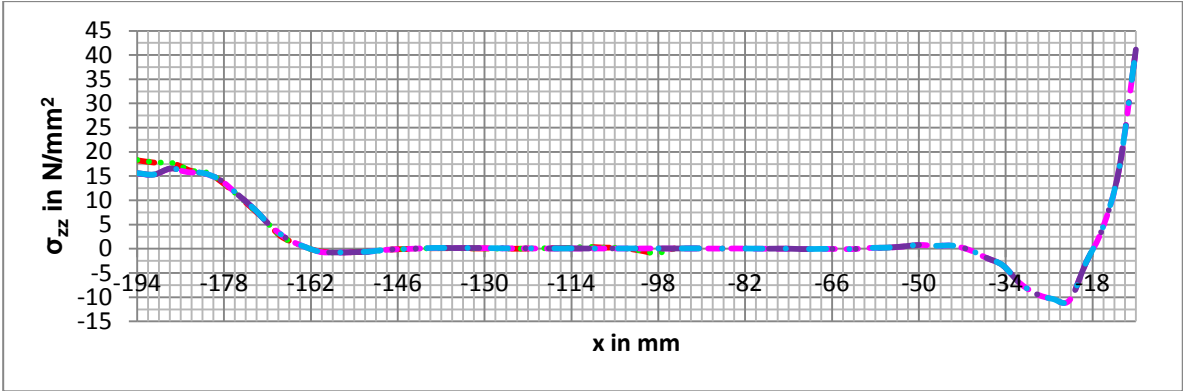


Figure 24.69: Comparison of stresses perpendicular to the horizontal plane of the outer angle at y=50 x=-190

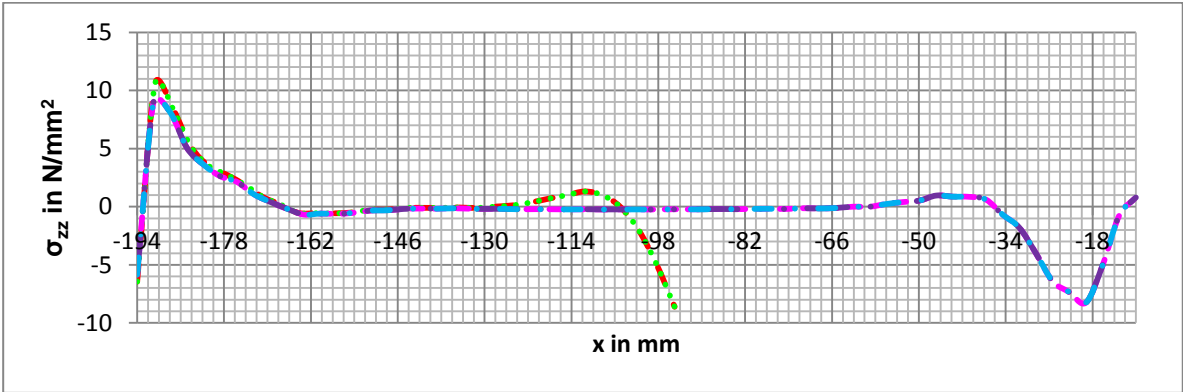


Figure 24.70: Comparison of stresses perpendicular to the horizontal plane of the outer angle at y=100 x=-194

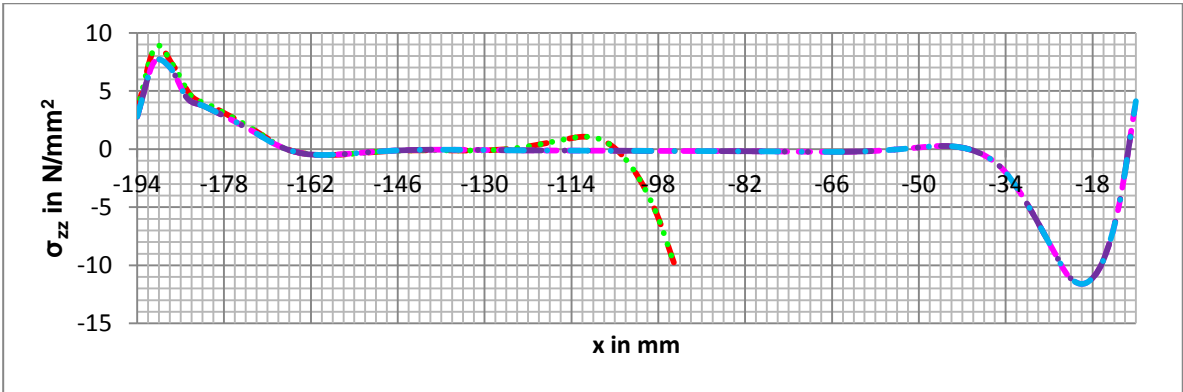


Figure 24.71: Comparison of stresses perpendicular to the horizontal plane of the outer angle at y=100 x=-192

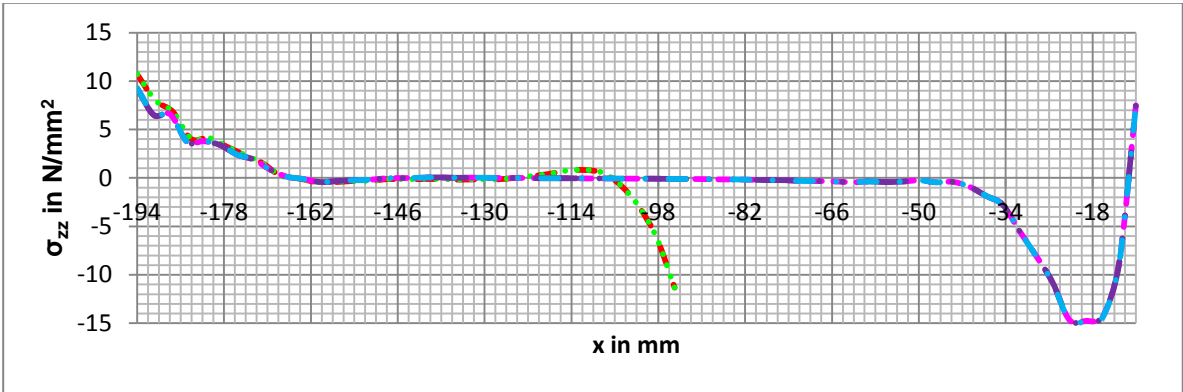


Figure 24.72: Comparison of stresses perpendicular to the horizontal plane of the outer angle at y=100 x=-190

24.3.3 Shear stresses (zx-direction) per test

For all the figures below the next colours are used to indicate the place of the result lines:

— Y=0 Z=-194 — Y=0 Z=-192 — Y=0 Z=-190 — Y=50 Z=-194 — Y=50 Z=-192 — Y=50 Z=-190 — Y=100 Z=-194 — Y=100 Z=-192 — Y=100 Z=-190

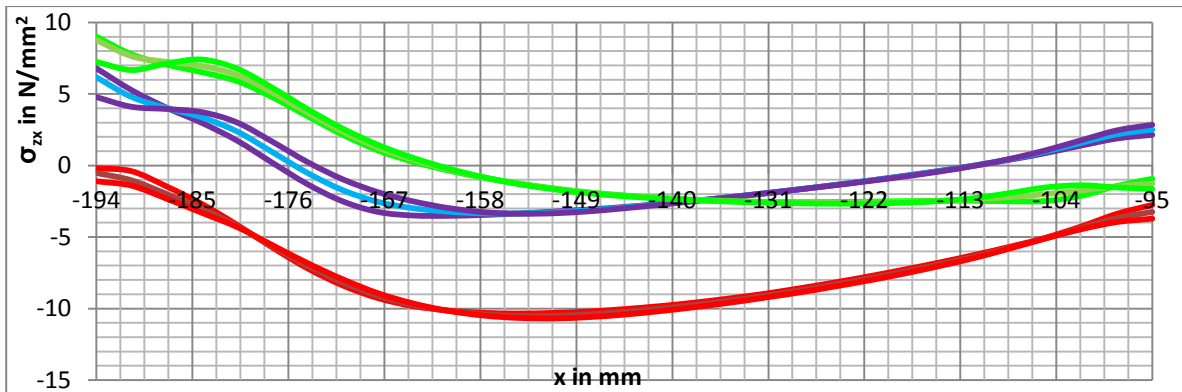


Figure 24.73: Shear stresses in zx-direction of the horizontal plane of the outer angle of test IA200x500 OA100x500

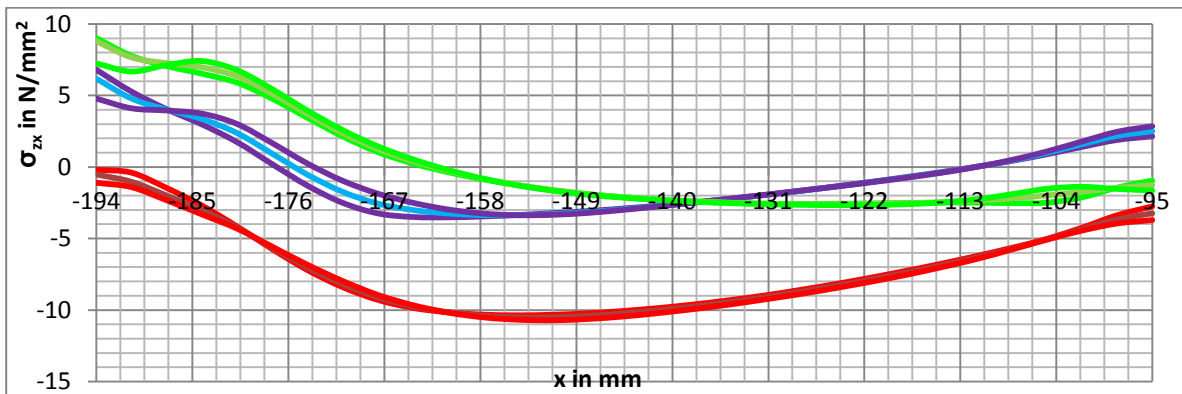


Figure 24.74: Shear stresses in zx-direction of the horizontal plane of the outer angle of test IA300x500 OA100x500

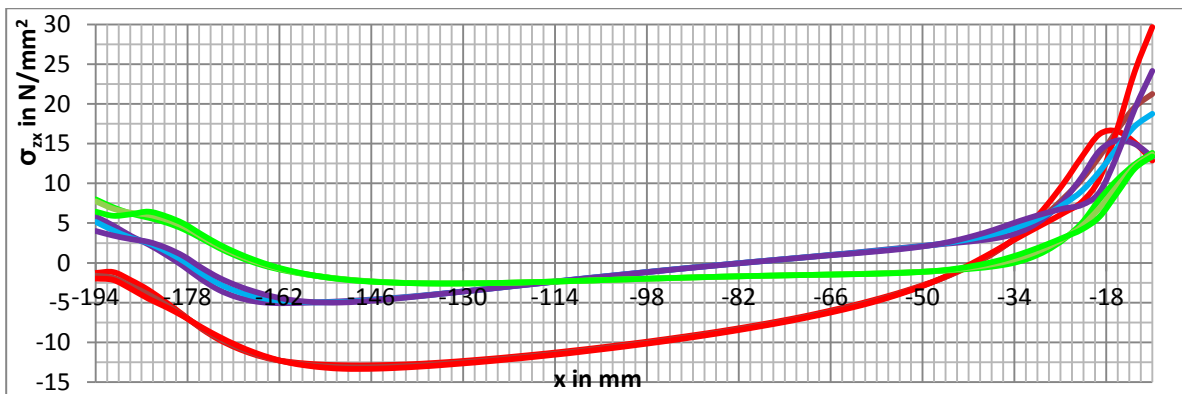


Figure 24.75: Shear stresses in zx-direction of the horizontal plane of the outer angle of test IA300x500 OA200x500

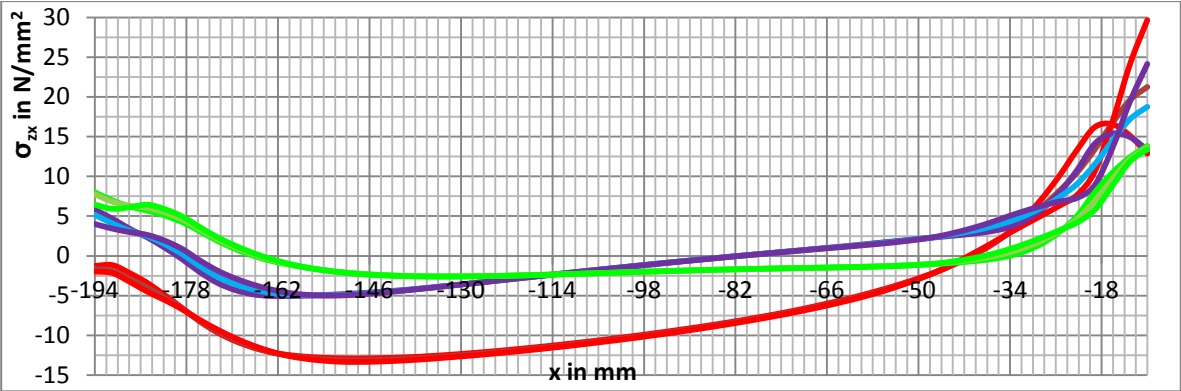


Figure 24.76: Shear stresses in zx-direction of the horizontal plane of the outer angle of test IA300x500 OA200x700

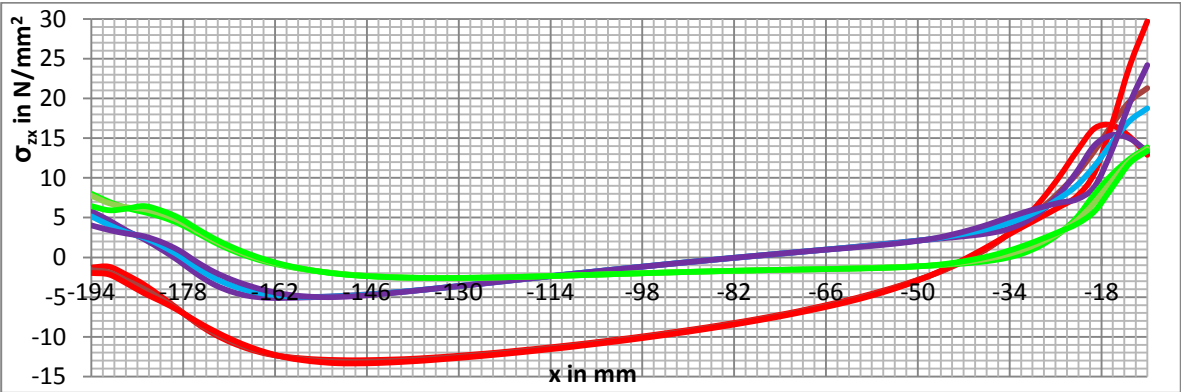


Figure 24.77: Shear stresses in zx-direction of the horizontal plane of the outer angle of test IA500x500 OA200x700

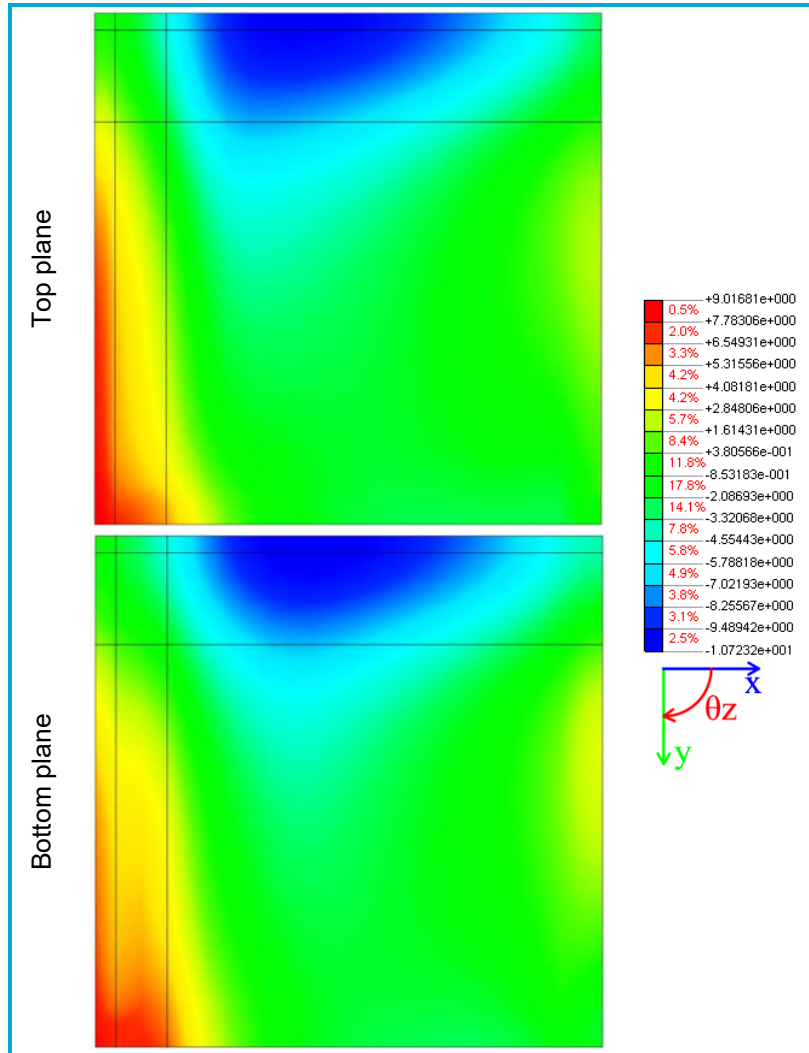


Figure 24.78: Counterplot of shear stresses in zx-direction of the horizontal plane of the outer angle of test IA300x500 OA100x500

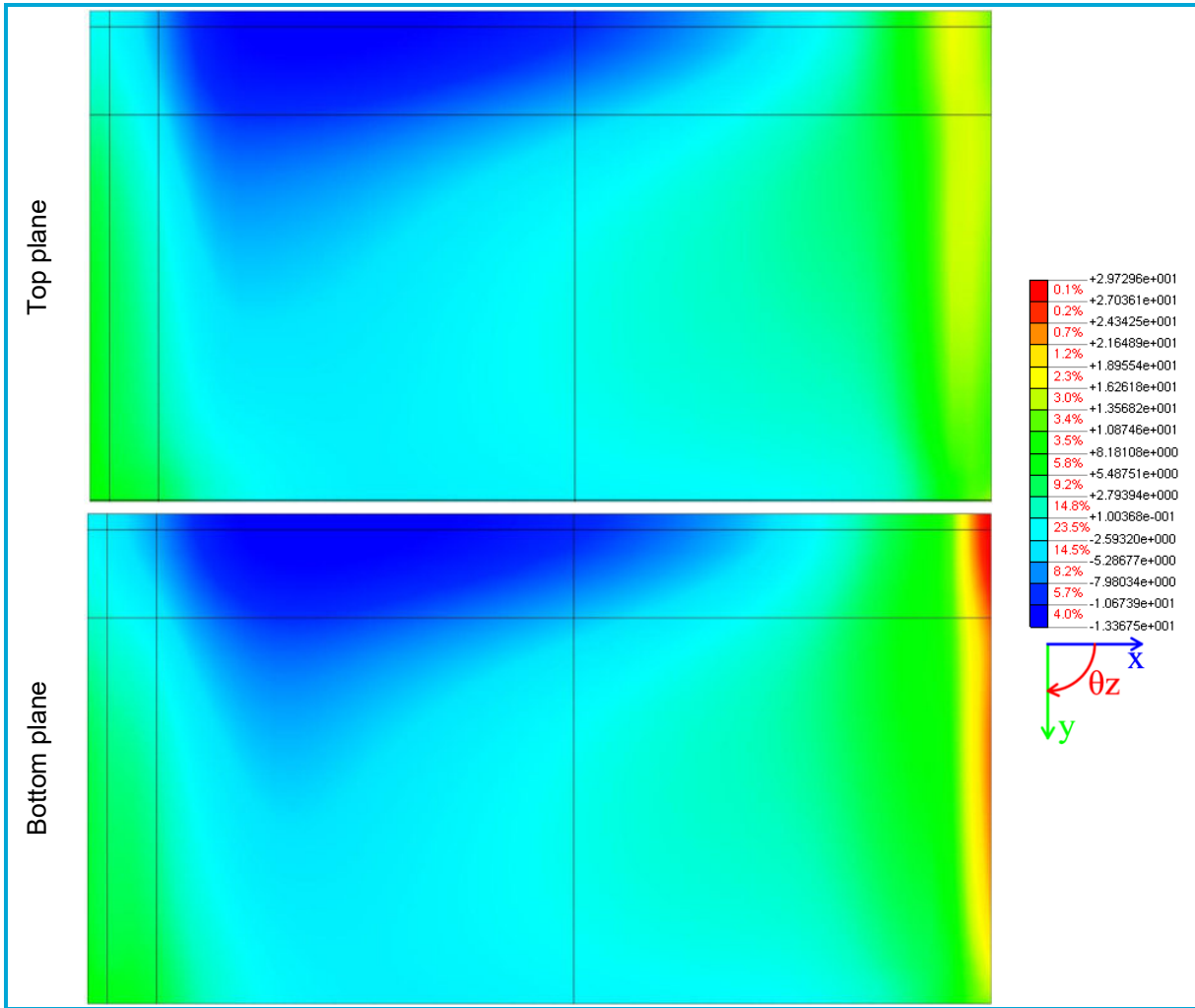


Figure 24.79: Counterplot of shear stresses in zx-direction of the horizontal plane of the outer angle of test IA500x500 OA200x700

24.3.4 Shear stresses (zx-direction) per result line

For all the figures below the next colours are used to indicate the models:

- - IA200x500 OA100x500
- - IA300x500 OA100x500
- - IA300x500 OA200x500
- - IA300x500 OA200x700
- - IA500x500 OA200x700

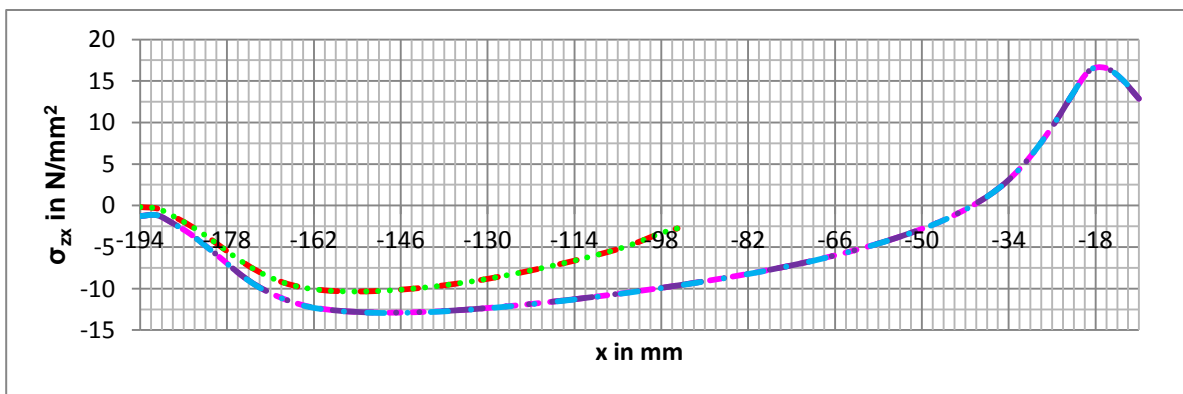


Figure 24.80: Comparison of shear stresses in zx-direction of the horizontal plane of the outer angle at $y=0$ $x=-194$

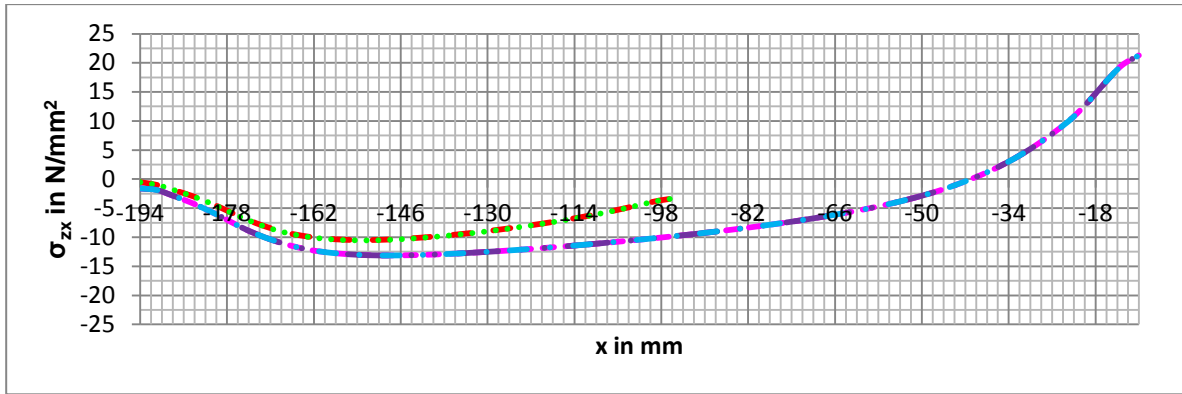


Figure 24.81: Comparison of shear stresses in zx-direction of the horizontal plane of the outer angle at $y=0$ $x=-192$

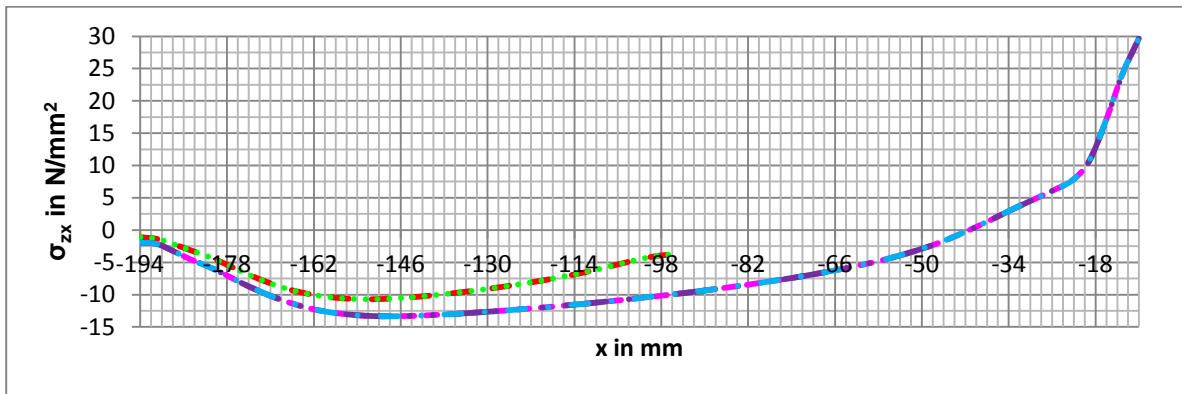


Figure 24.82: Comparison of shear stresses in zx-direction of the horizontal plane of the outer angle at $y=0$ $x=-190$

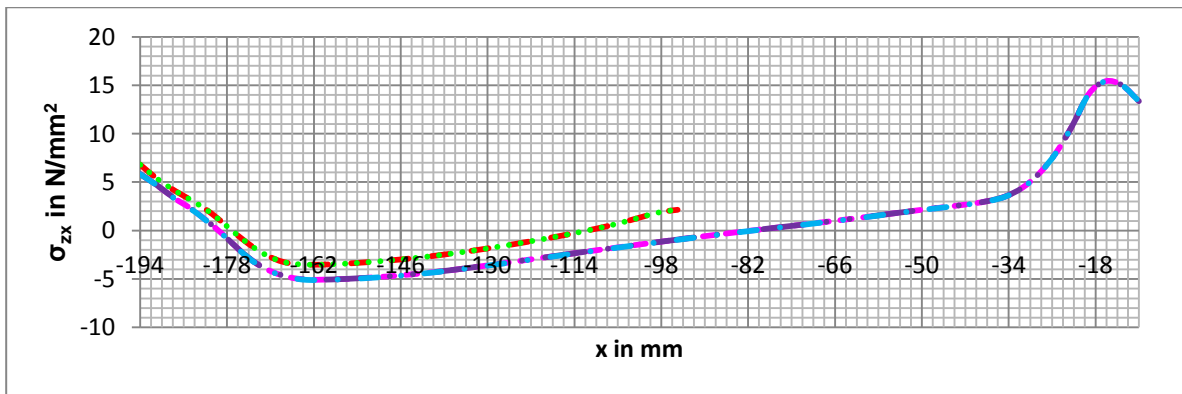


Figure 24.83: Comparison of shear stresses in zx-direction of the horizontal plane of the outer angle at $y=50$ $x=-194$

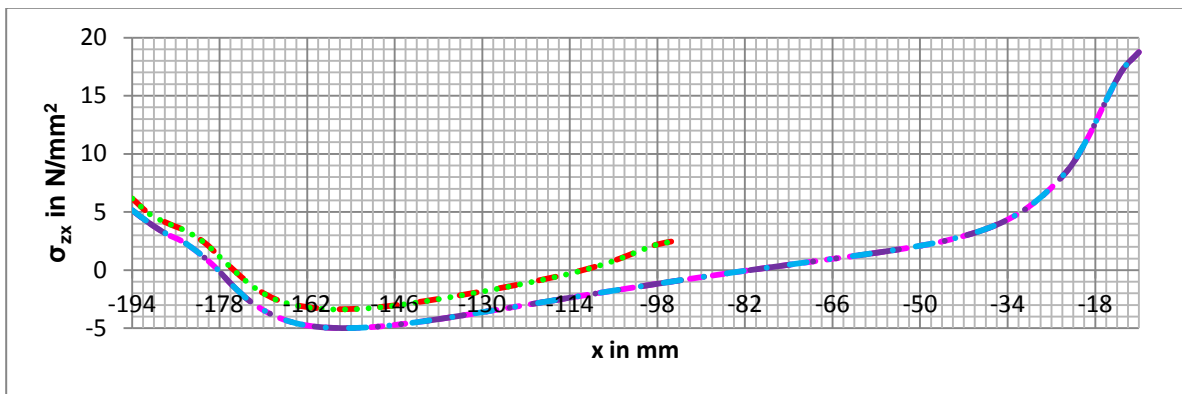


Figure 24.84: Comparison of shear stresses in zx-direction of the horizontal plane of the outer angle at $y=50$ $x=-192$

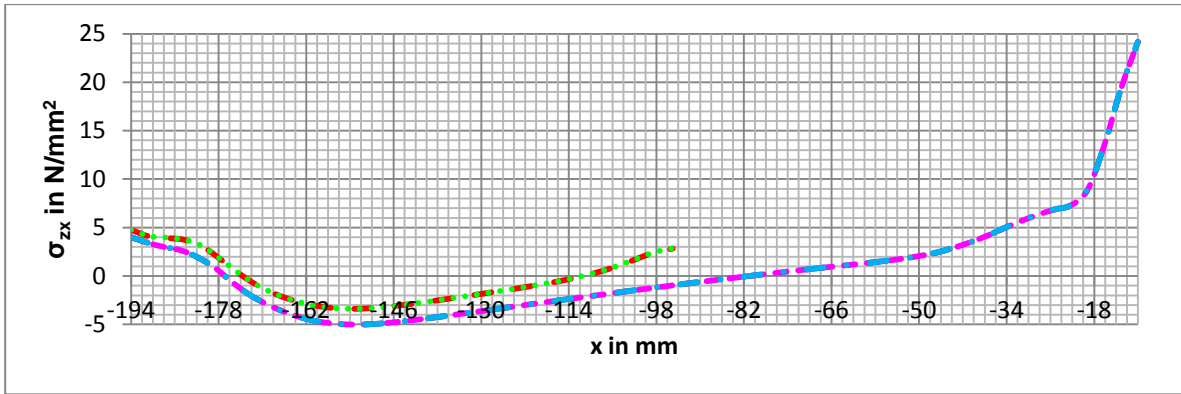


Figure 24.85: Comparison of shear stresses in zx-direction of the horizontal plane of the outer angle at y=50 x=-190

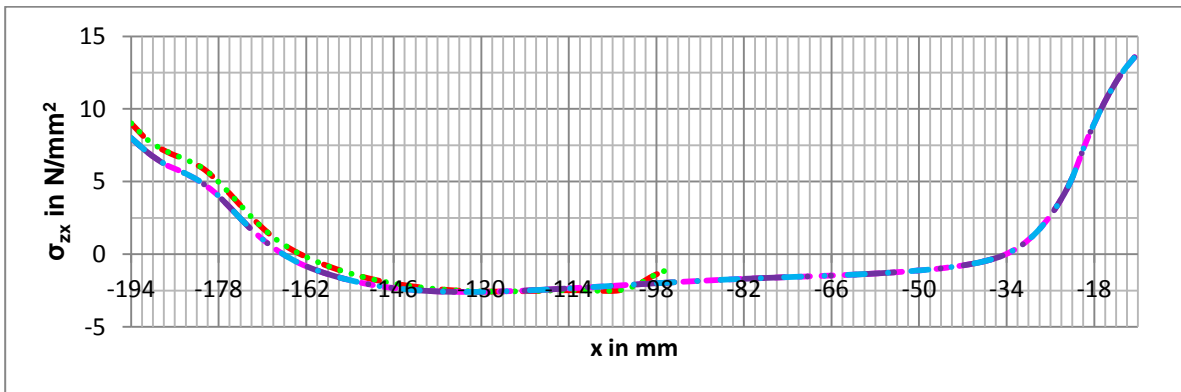


Figure 24.86: Comparison of shear stresses in zx-direction of the horizontal plane of the outer angle at y=100 x=-194

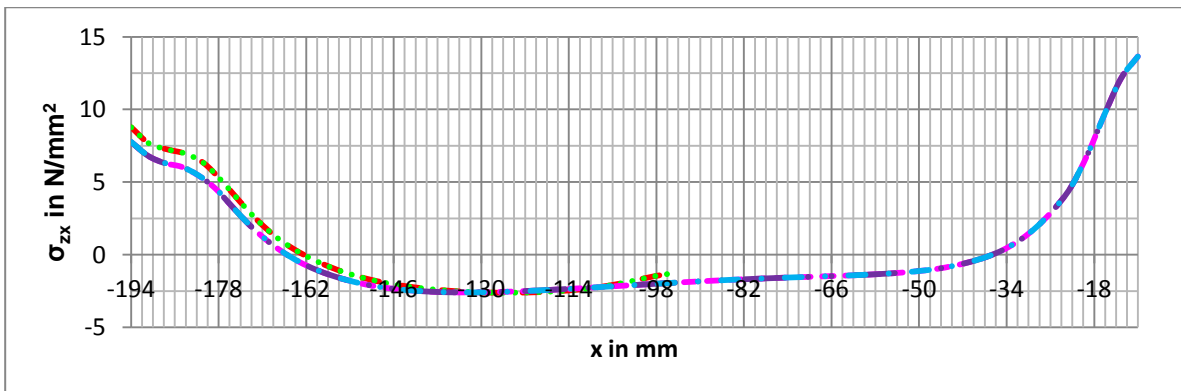


Figure 24.87: Comparison of shear stresses in zx-direction of the horizontal plane of the outer angle at y=100 x=-192

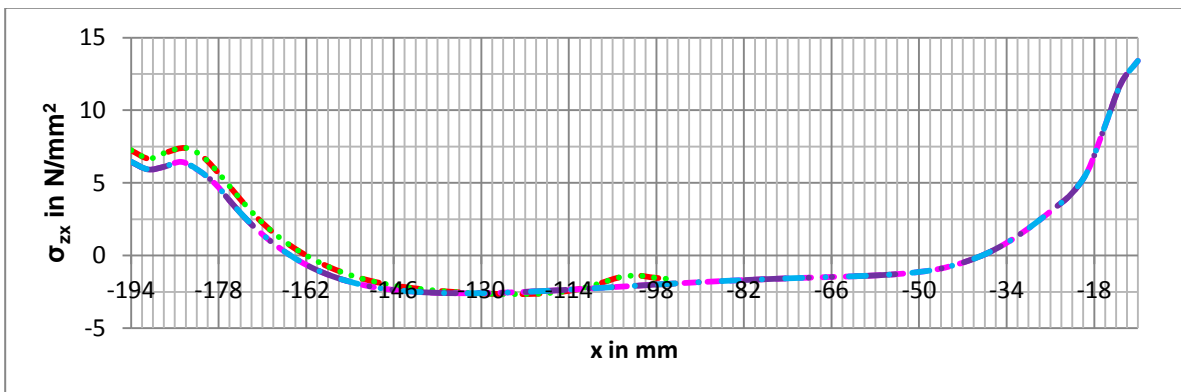


Figure 24.88: Comparison of shear stresses in zx-direction of the horizontal plane of the outer angle at y=100 x=-190

24.4 Vertical plane of the outer angle

A description of the x-values used for the result lines can be found in the next table:

x-value	Description
-194	Interface of steel angle and adhesive
-192	At the middle of the adhesive
-190	Interface of adhesive and column or beam

Table 24.8: Values of z for the horizontal plane of the inner angle

For the vertical part of the outer angle there are a few specific points, listed below:

z-value	description
-194	Interface of adhesive and the outer angle
-190	Top of the beam
-180	Bottom of the top flange of the beam
-10	Top of the bottom flange of the beam
0	Interface of beam and column

Table 24.9: Specific points for horizontal plane of the inner angle

24.4.1 Stresses perpendicular to the plane per test

For all the figures below the next colours are used to indicate the place of the result lines:

— X=-194 Y=0 — X=-192 Y=0 — X=-190 Y=0 — X=-194 Y=50 — X=-192 Y=50 — X=-190 Y=50 — X=-194 Y=100 — X=-192 Y=100 — X=-190 Y=100

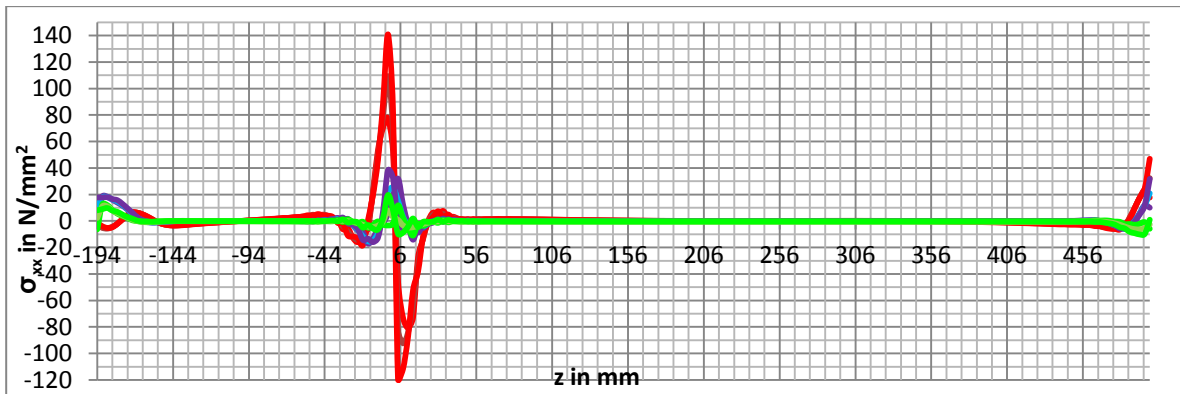


Figure 24.89: Stresses perpendicular to the vertical plane of the outer angle of test IA200x500 OA100x500

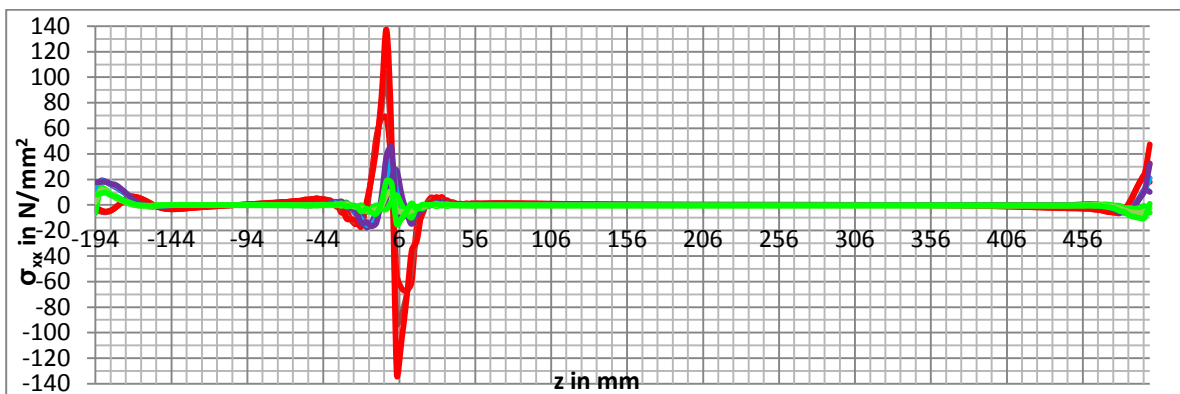


Figure 24.90: Stresses perpendicular to the vertical plane of the outer angle of test IA300x500 OA100x500

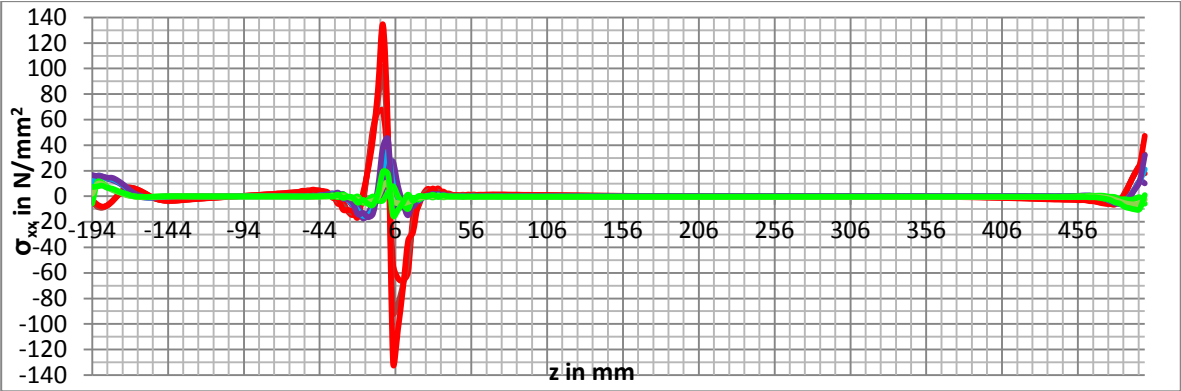


Figure 24.91: Stresses perpendicular to the vertical plane of the outer angle of test IA300x500 OA200x500

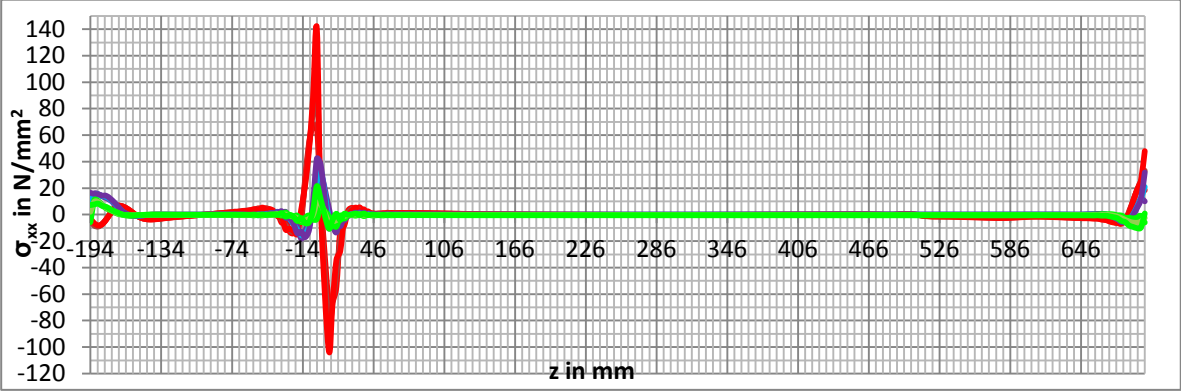


Figure 24.92: Stresses perpendicular to the vertical plane of the outer angle of test IA300x500 OA200x700

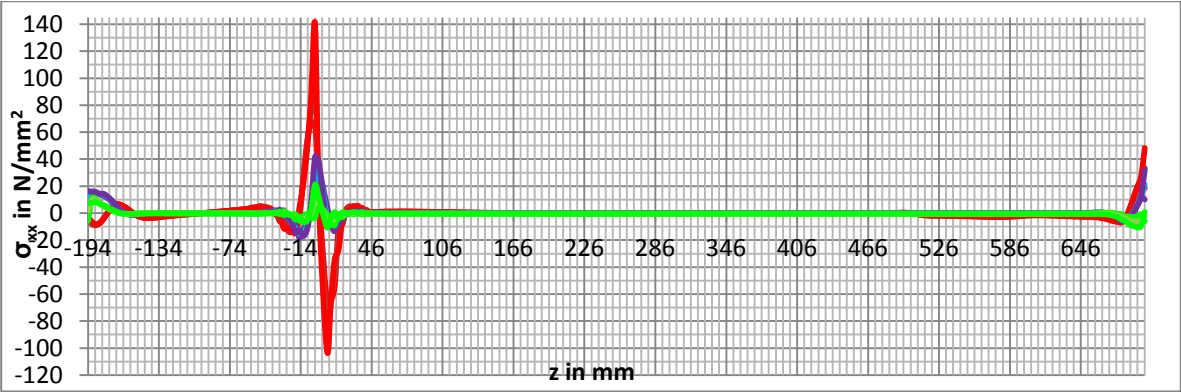


Figure 24.93: Stresses perpendicular to the vertical plane of the outer angle of test IA300x500 OA500x700

24.4.2 Stresses perpendicular to the plane per result line

For all the figures below the next colours are used to indicate the models:

— IA200x500 OA100x500
 - - - IA300x500 OA100x500
 - - - IA300x500 OA200x500
 - - - IA300x500 OA200x700
 - - - IA500x500 OA200x700

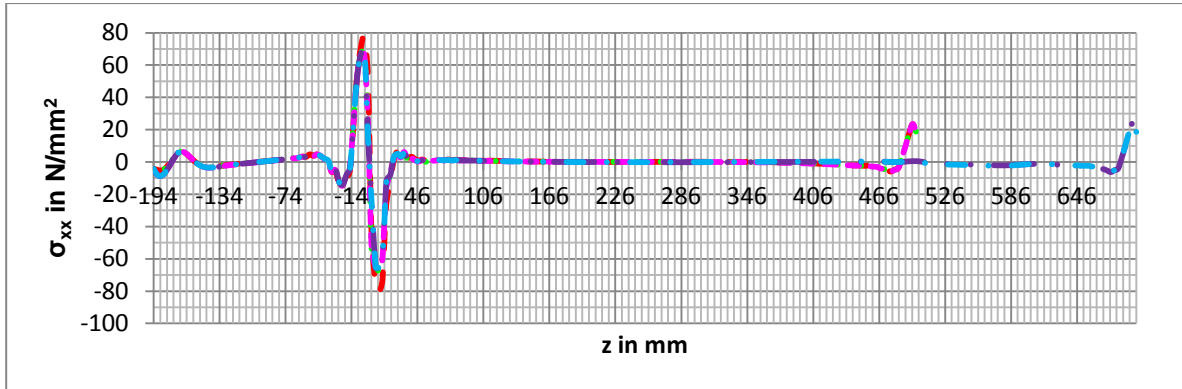


Figure 24.94: Comparison of stresses perpendicular to the vertical plane of the outer angle at y=0 z=-194

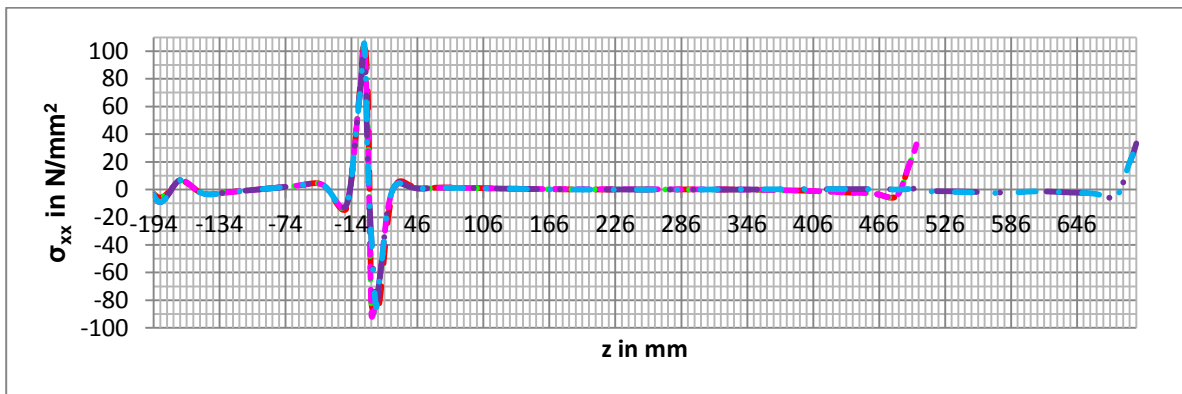


Figure 24.95: Comparison of stresses perpendicular to the vertical plane of the outer angle at y=0 z=-192

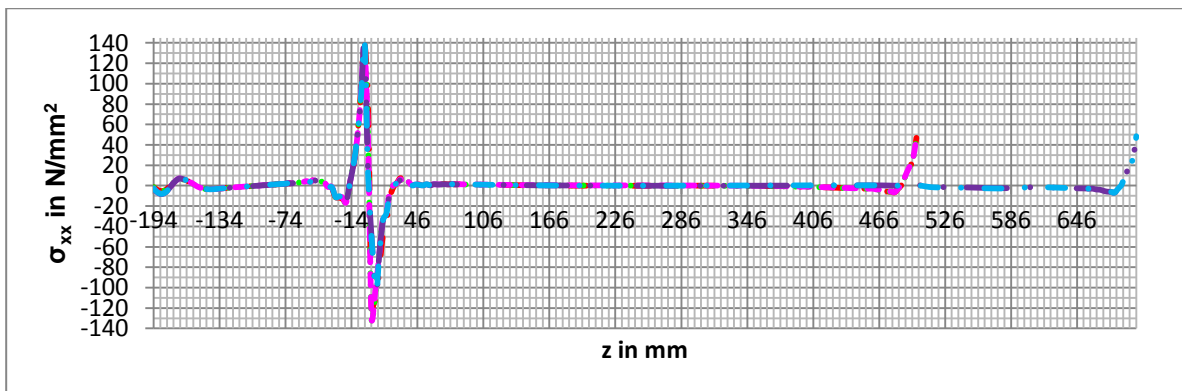


Figure 24.96: Comparison of stresses perpendicular to the vertical plane of the outer angle at y=0 z=-190

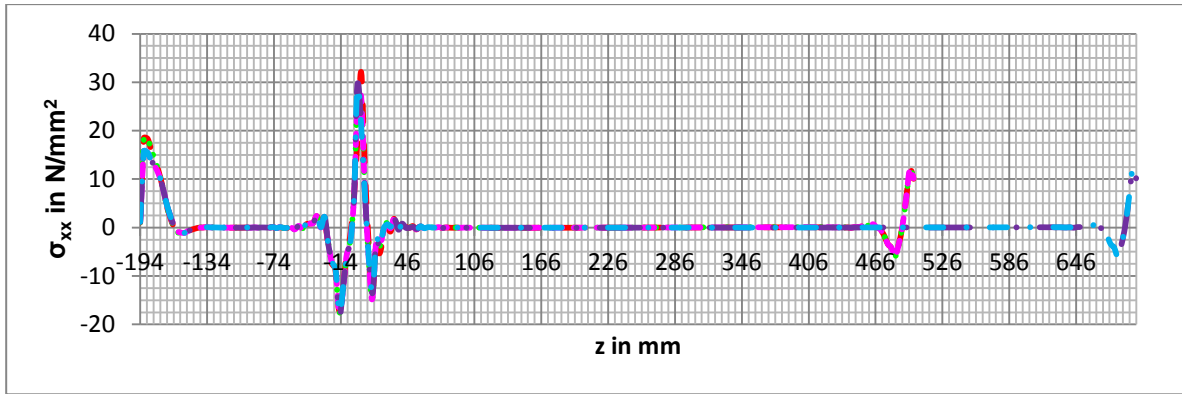


Figure 24.97: Comparison of stresses perpendicular the vertical plane of the outer angle at $y=50$ $z=-194$

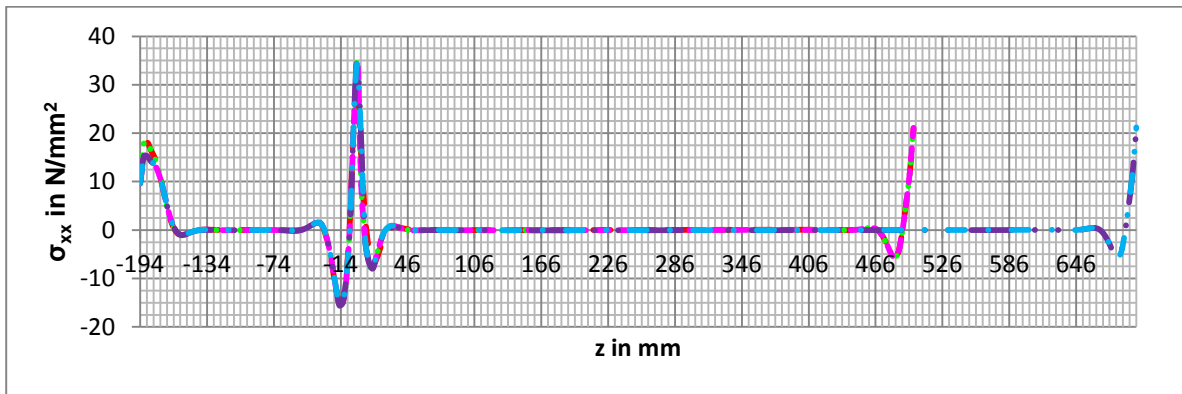


Figure 24.98: Comparison of stresses perpendicular to the vertical plane of the outer angle at $y=50$ $z=-192$

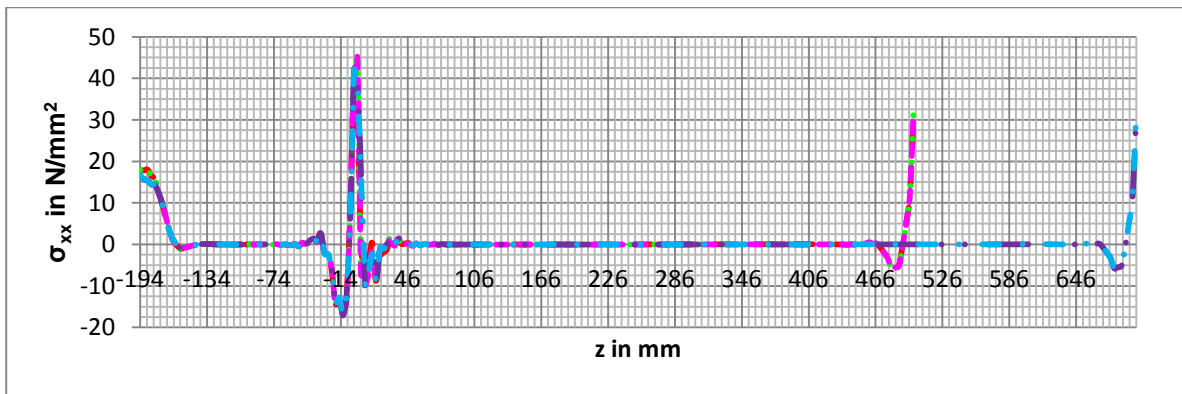


Figure 24.99: Comparison of stresses perpendicular to the vertical plane of the outer angle at $y=50$ $z=-190$

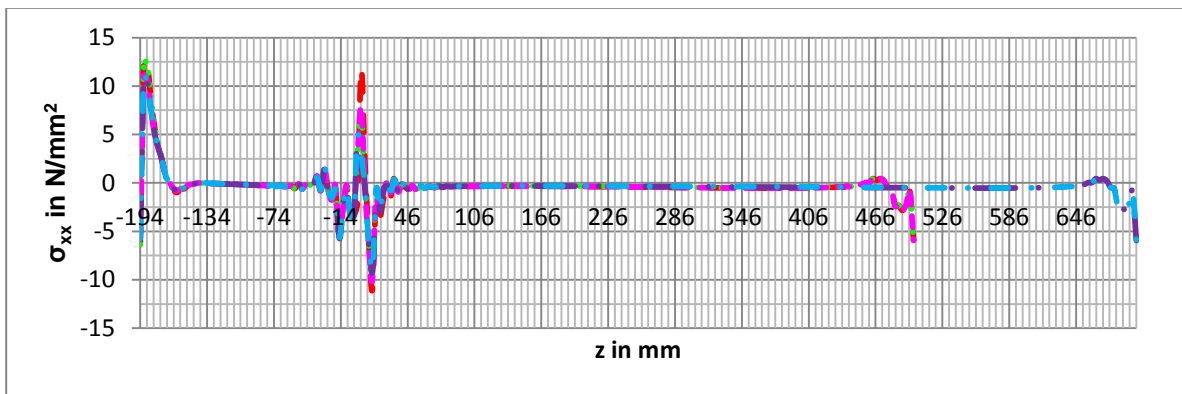


Figure 24.100: Comparison of stresses perpendicular to the vertical plane of the outer angle at $y=100$ $z=-194$

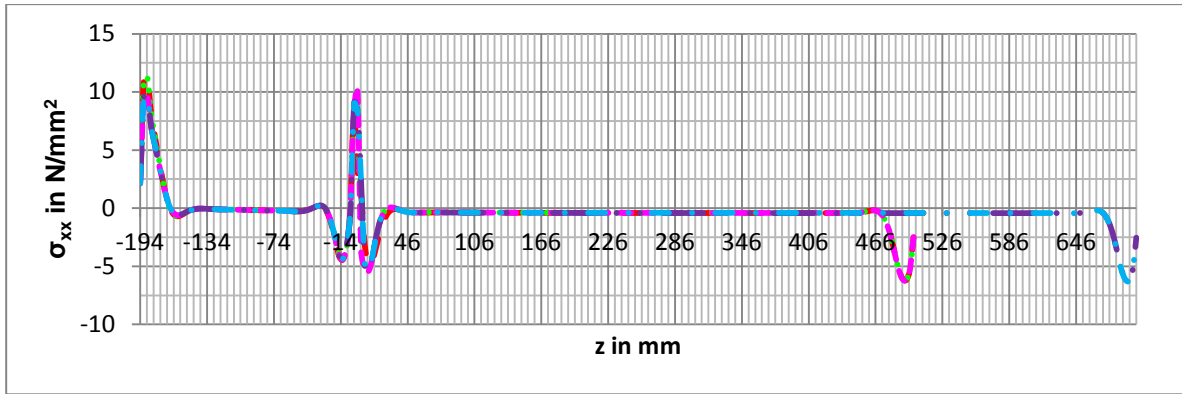


Figure 24.101: Comparison of stresses perpendicular to the vertical plane of the outer angle at y=100 z=-192

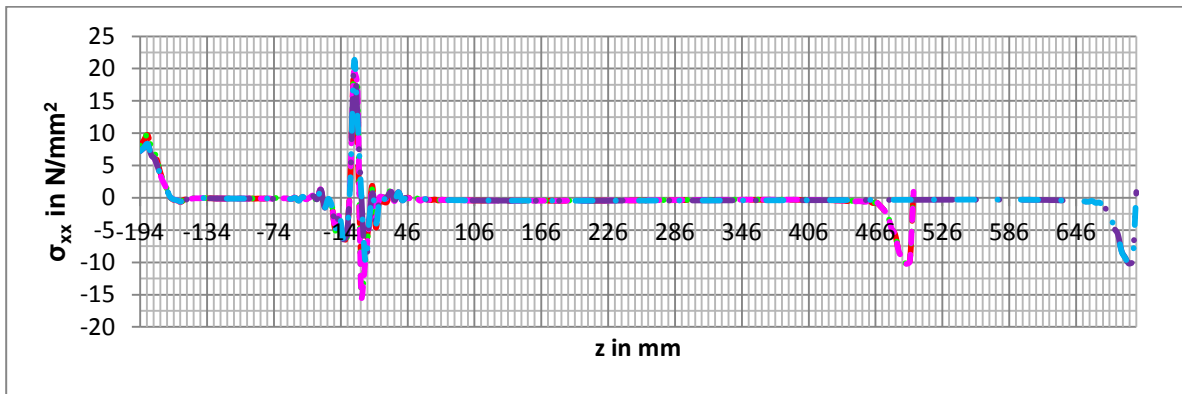


Figure 24.102: Comparison of stresses perpendicular to the vertical plane of the outer angle at y=100 z=-190

24.4.3 Shear stresses (zx-direction) per test

For all the figures below the next colours are used to indicate the place of the result lines:

— X=0 Y=0 — X=2 Y=0 — X=4 Y=0 — X=0 Y=50 — X=2 Y=50 — X=4 Y=50 — X=0 Y=100 — X=2 Y=100 — X=4 Y=100

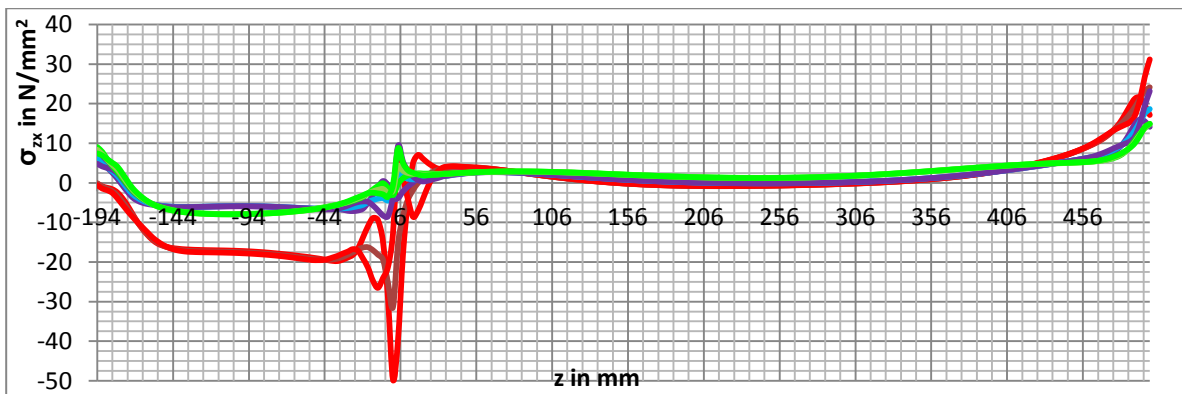


Figure 24.103: Shear stresses in zx-direction of the vertical plane of the outer angle of test IA200x500 OA100x500

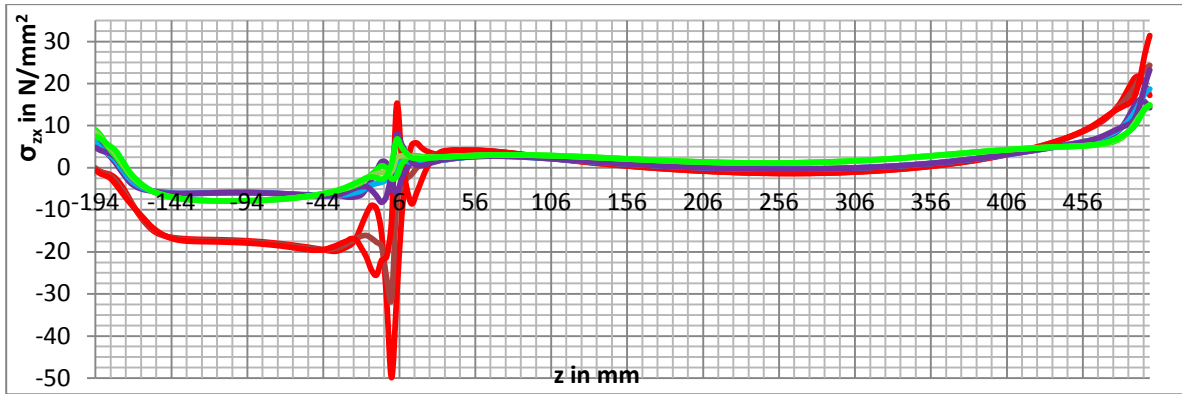


Figure 24.104: Shear stresses in zx-direction of the vertical plane of the outer angle of test IA300x500 OA100x500

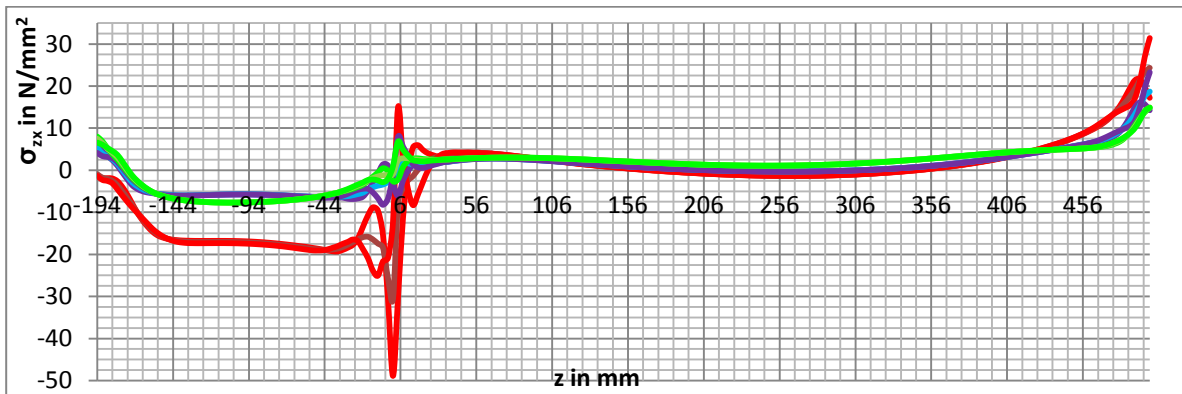


Figure 24.105: Shear stresses in zx-direction of the vertical plane of the outer angle of test IA300x500 OA200x500

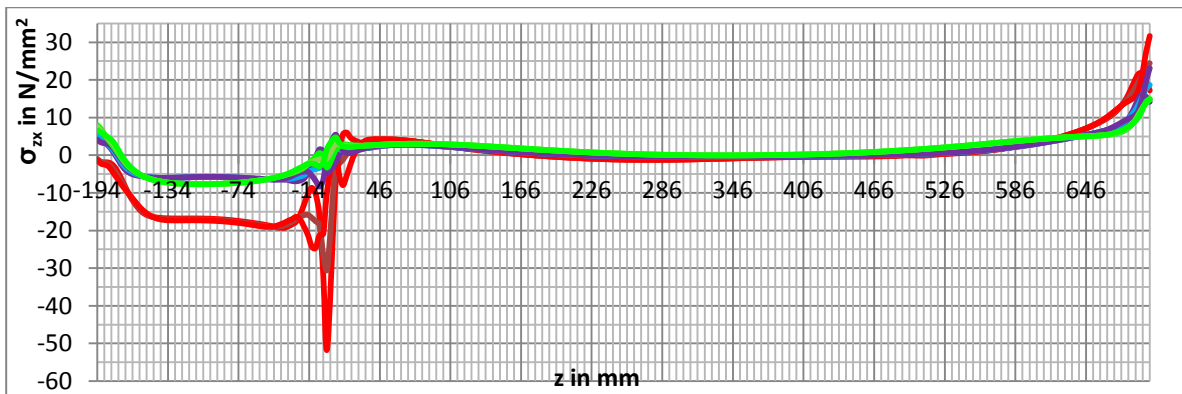


Figure 24.106: Shear stresses in zx-direction of the vertical plane of the outer angle of test IA300x500 OA200x700

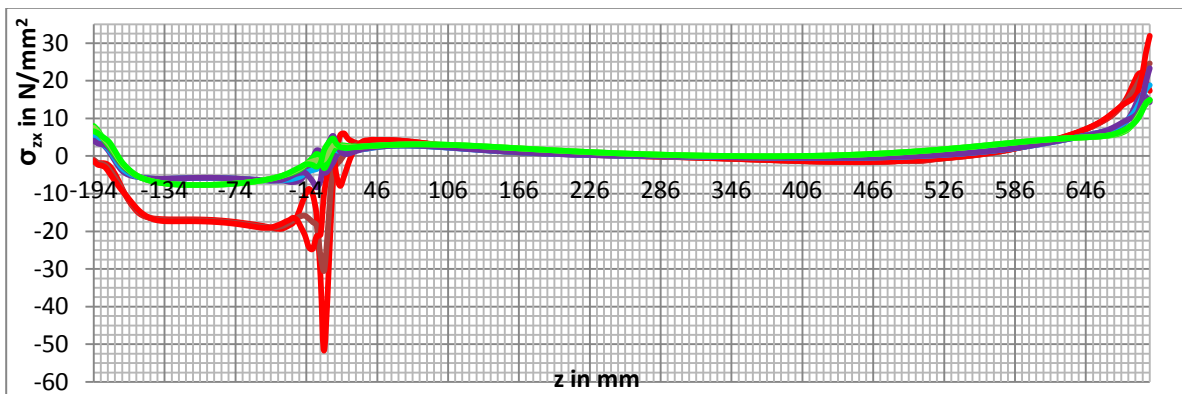


Figure 24.107: Shear stresses in zx-direction of the vertical plane of the outer angle of test IA500x500 OA200x700

24.4.4 Shear stresses (zx-direction) per result line

For all the figures below the next colours are used to indicate the models:

— IA200x500 OA100x500
 - - - IA300x500 OA100x500
 - - - IA300x500 OA200X500
 - - - IA300x500 OA200X700
 - - - IA500x500 OA200X700

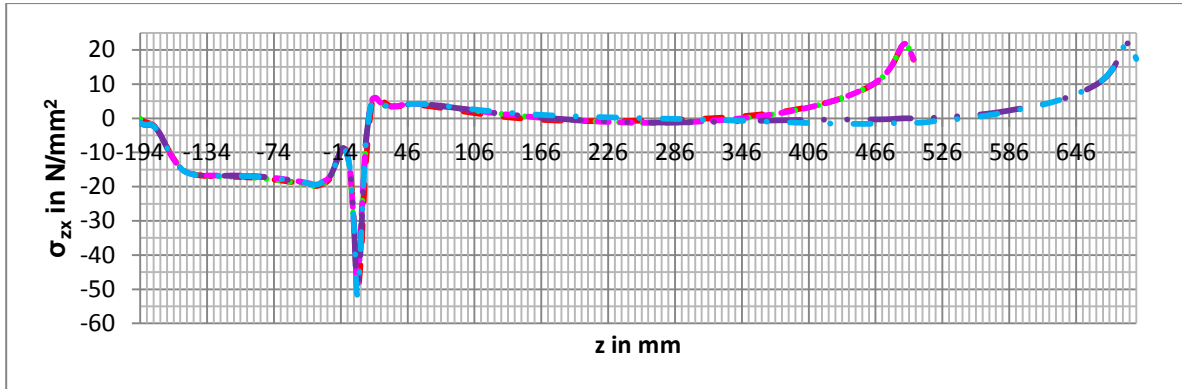


Figure 24.108: Comparison of shear stresses in zx-direction of the vertical plane of the outer angle at y=0 z=-194

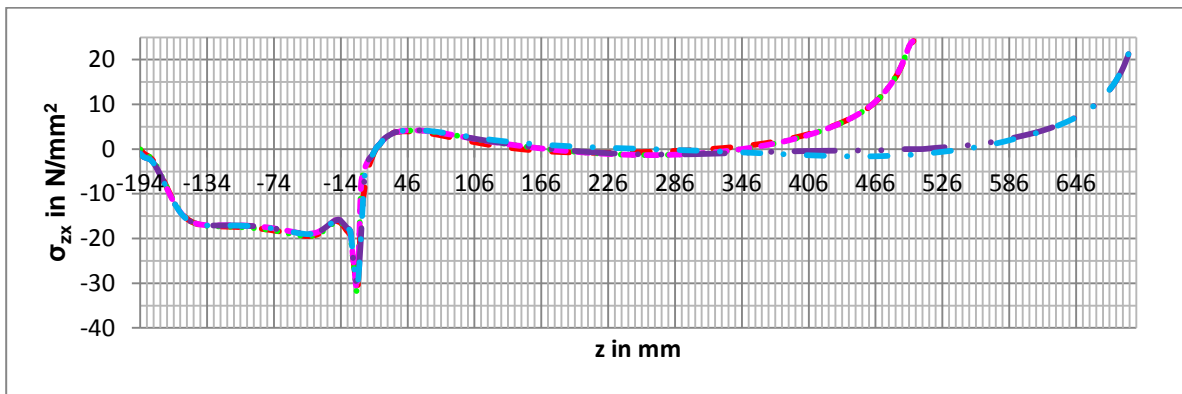


Figure 24.109: Comparison of shear stresses in zx-direction of the vertical plane of the outer angle at y=0 z=-192

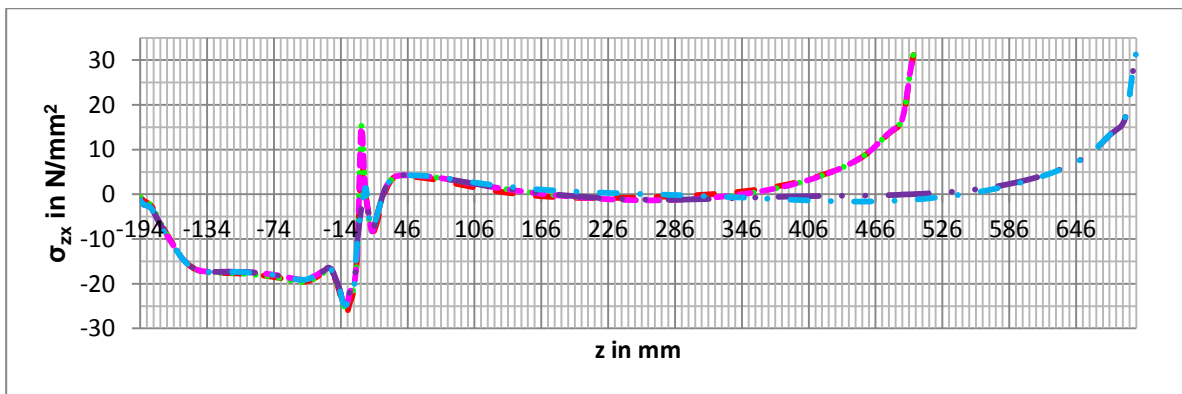


Figure 24.110: Comparison of shear stresses in zx-direction of the vertical plane of the outer angle at y=0 z=-190

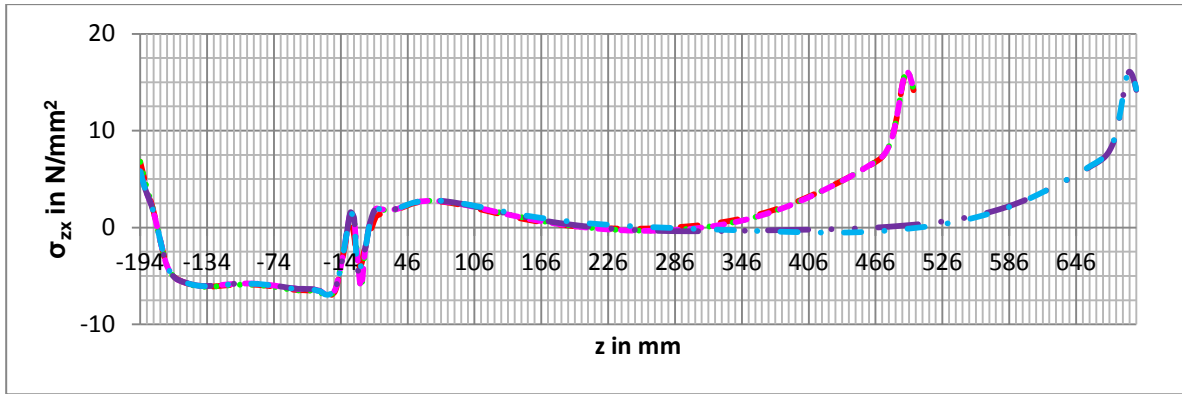


Figure 24.111: Comparison of shear stresses in zx-direction of the vertical plane of the outer angle at $y=50$ $z=-194$

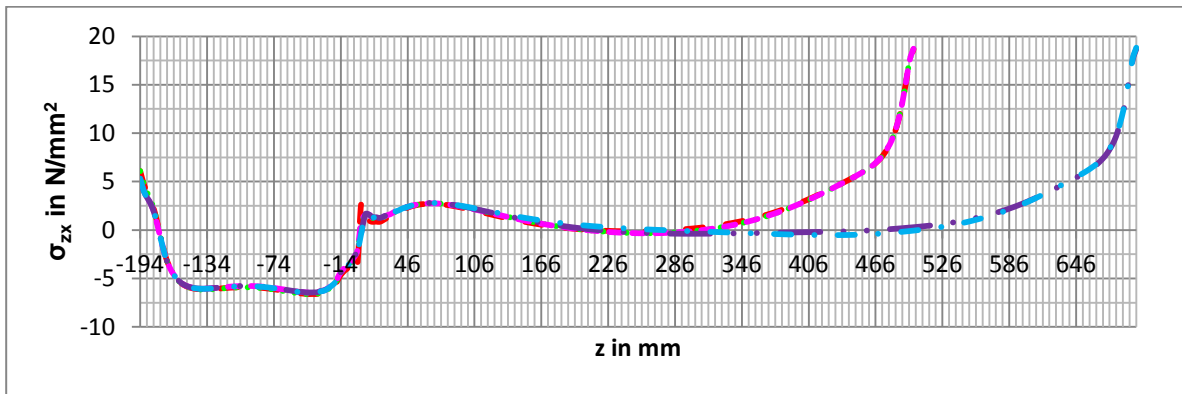


Figure 24.112: Comparison of shear stresses in zx-direction of the vertical plane of the outer angle at $y=50$ $z=-192$

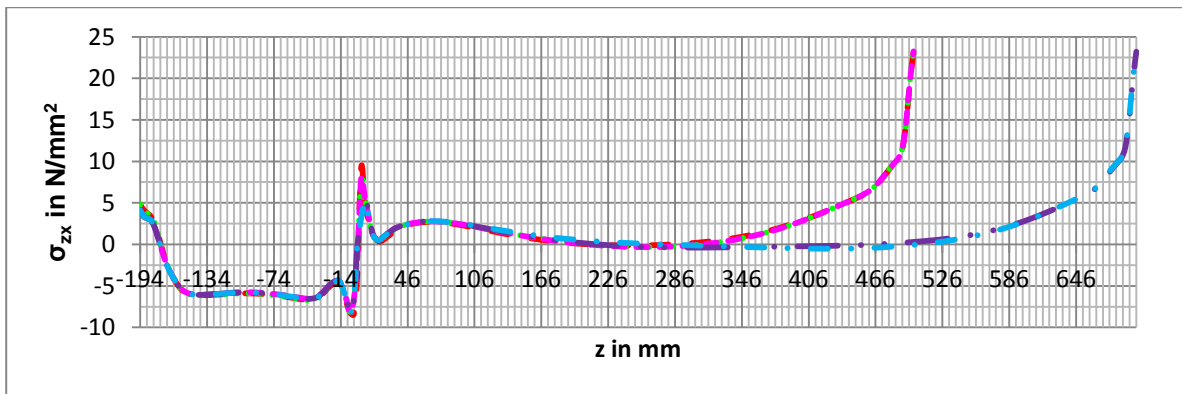


Figure 24.113: Comparison of shear stresses in zx-direction of the vertical plane of the outer angle at $y=50$ $z=-190$

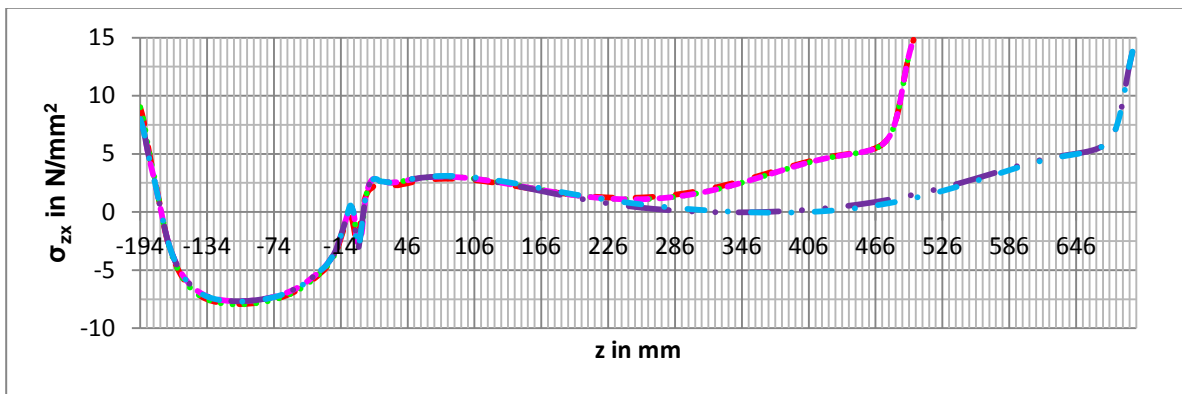


Figure 24.114: Comparison of shear stresses in zx-direction of the vertical plane of the outer angle at $y=100$ $z=-194$

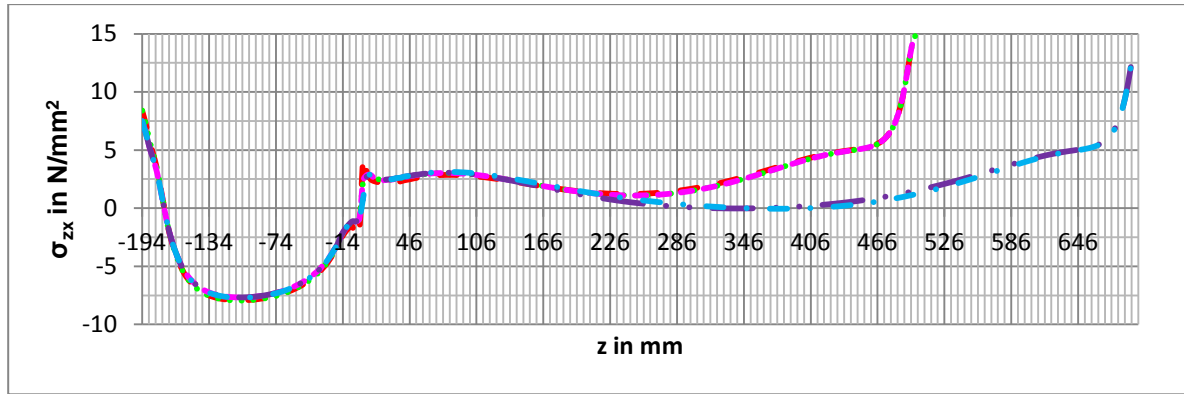


Figure 24.115: Comparison of shear stresses in zx-direction of the vertical plane of the outer angle at $y=100$ $z=-192$

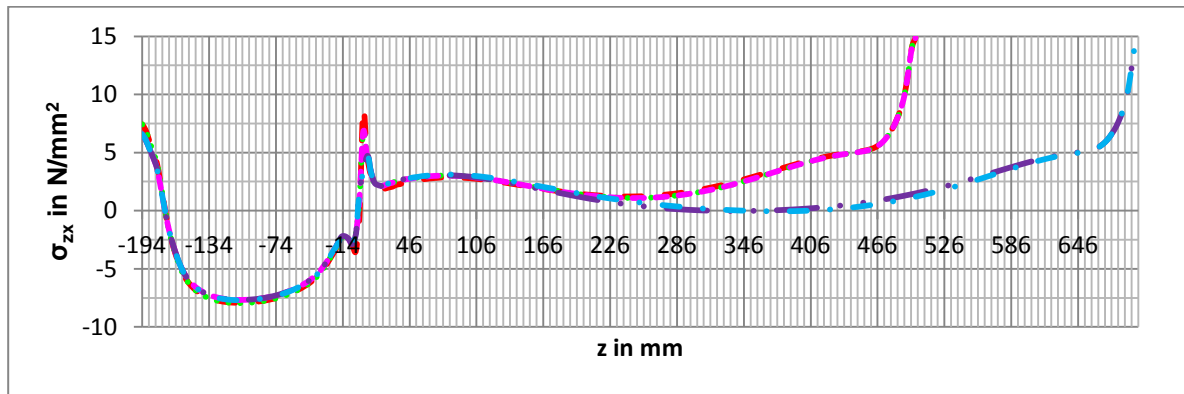


Figure 24.116: Comparison of shear stresses in zx-direction of the vertical plane of the outer angle at $y=100$ $z=-190$

24.5 Additional FEM Model

A description of the z-values used for the result lines can be found in the next table:

z-value	Description
-194	Interface of steel plate and adhesive
-192	At the middle of the adhesive
-190	Interface of adhesive and beam

Table 24.10: Values of z for the horizontal plane of the inner angle

For the horizontal part of the outer angle there are a few specific points, listed below:

x-value	description
-190	Left side of endplate and stiffener
-180	Right side of endplate
-95	Right side of short lap
-10	Right side of long lap and left side of stiffener
0	Right side of stiffener

Table 24.11: Specific points for horizontal plane of the outer angle

24.5.1 Stresses perpendicular to the plane per test

For all the figures below the next colours are used to indicate the place of the result lines:

— Y=0 Z=-194 — Y=0 Z=-192 — Y=0 Z=-190 — Y=50 Z=-194 — Y=50 Z=-192 — Y=50 Z=-190 — Y=100 Z=-194 — Y=100 Z=-192 — Y=100 Z=-190

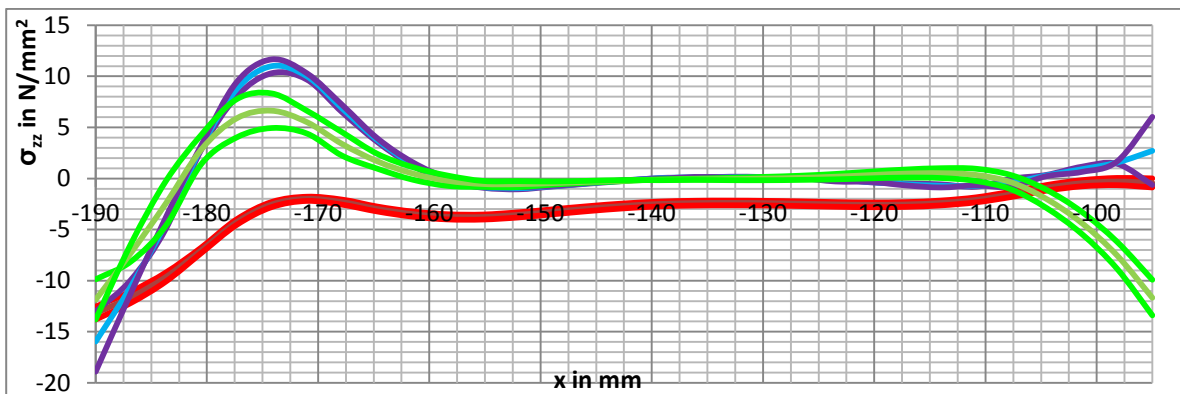


Figure 24.117: Stresses perpendicular to the horizontal plane of the additional model with short lap

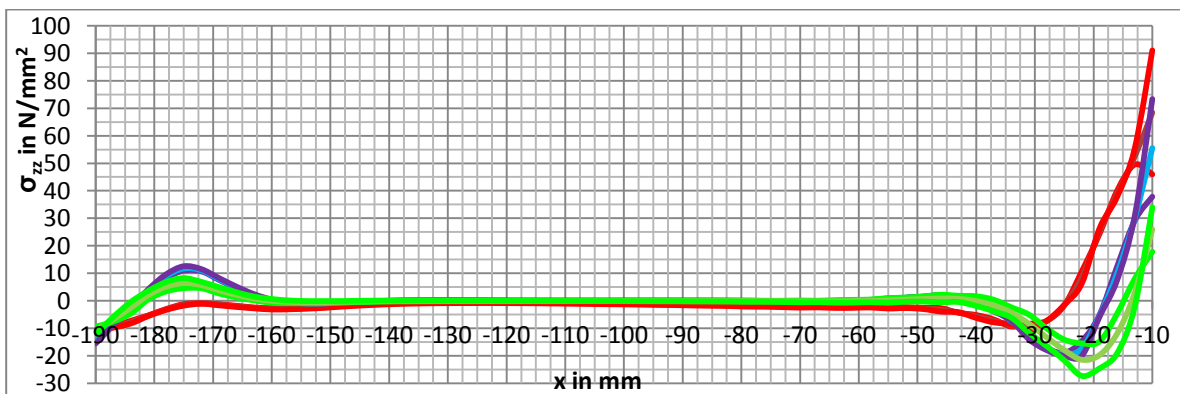


Figure 24.118: Stresses perpendicular to the horizontal plane of the additional model with long lap

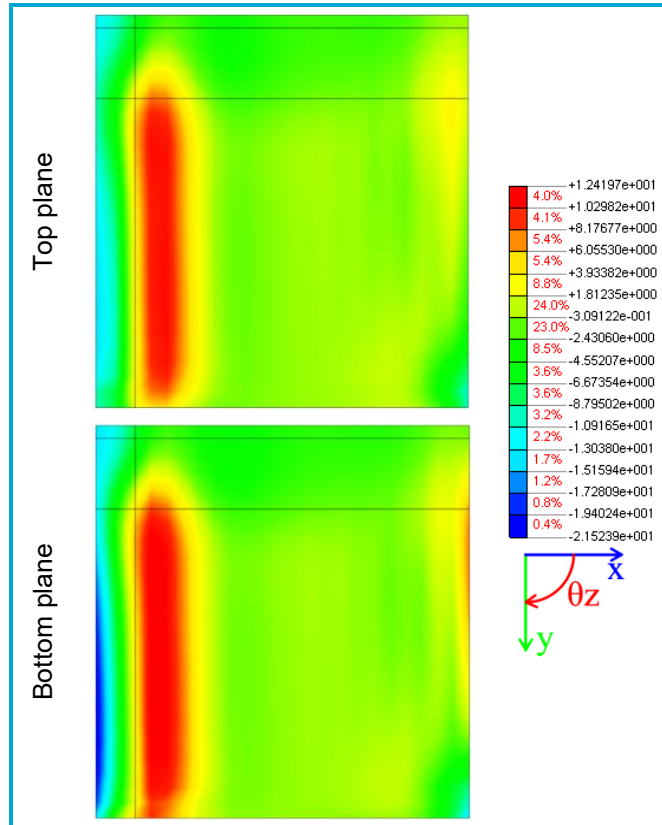


Figure 24.119: Counterplot of stresses perpendicular to the horizontal plane of the additional model with short lap

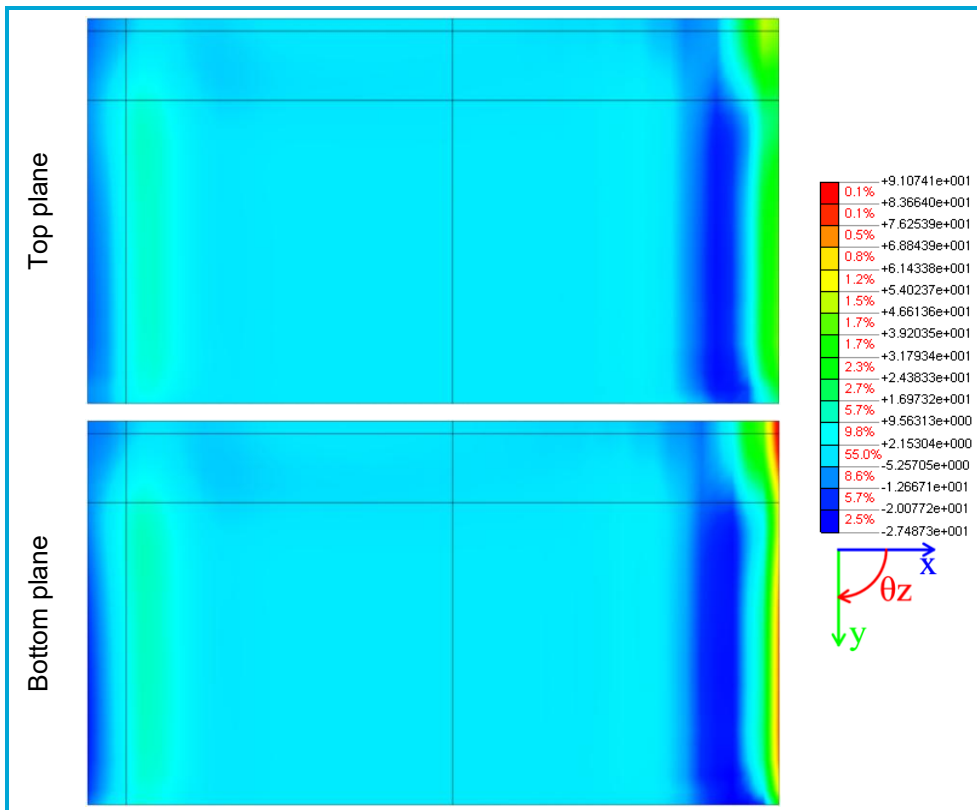


Figure 24.120: Counterplot of stresses perpendicular to the horizontal plane of the additional model with long lap

24.5.2 Stresses perpendicular to the plane per result line

For all the figures below the next colours are used to indicate the models: - - Short Lap - - - Long Lap.

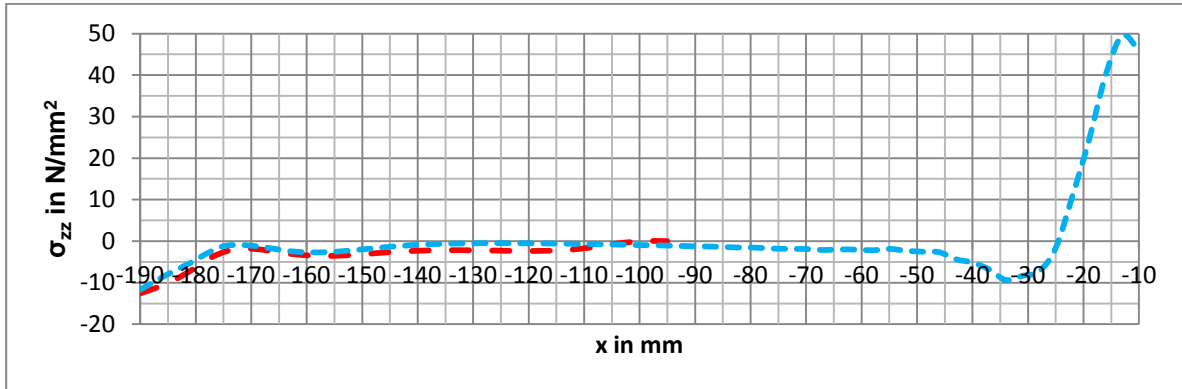


Figure 24.121: Comparison of stresses perpendicular to the horizontal plane of the outer angle at $y=0$ $z=-194$

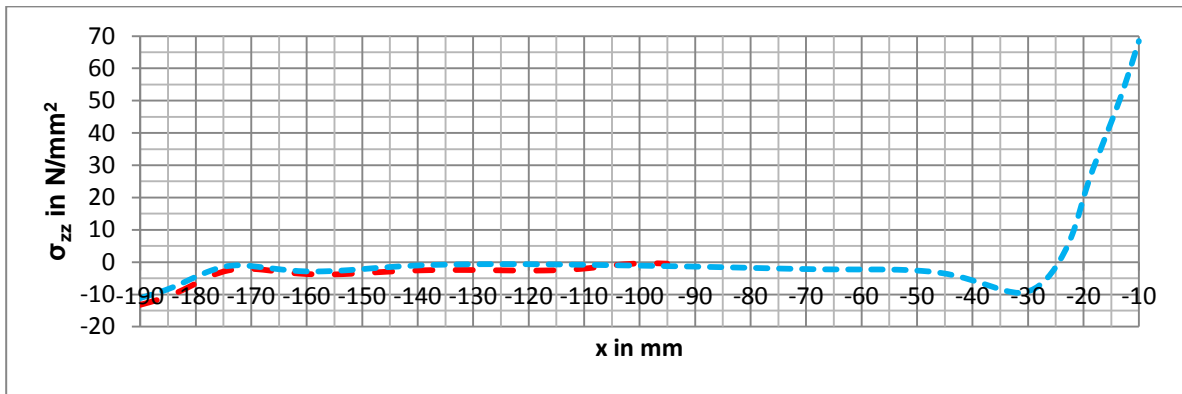


Figure 24.122: Comparison of stresses perpendicular to the horizontal plane of the outer angle at $y=0$ $z=-192$

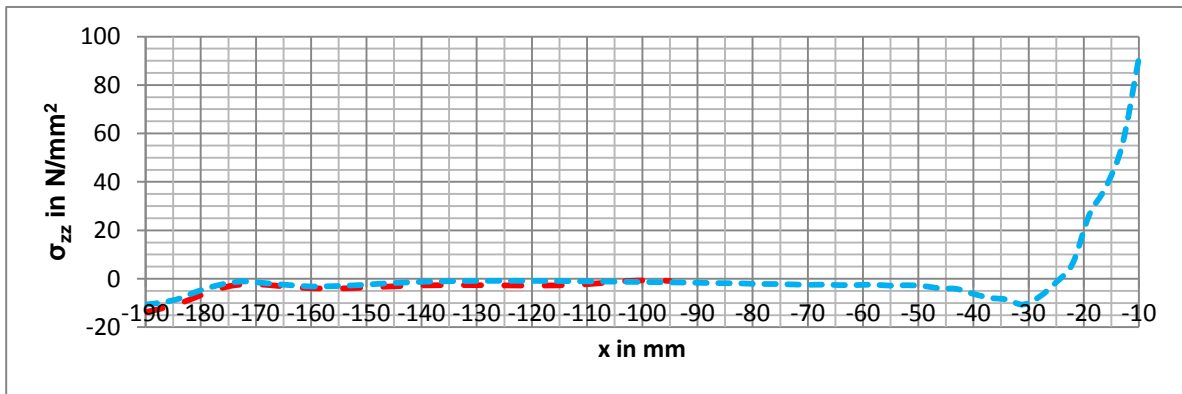


Figure 24.123: Comparison of stresses perpendicular to the horizontal plane of the outer angle at $y=0$ $z=-190$

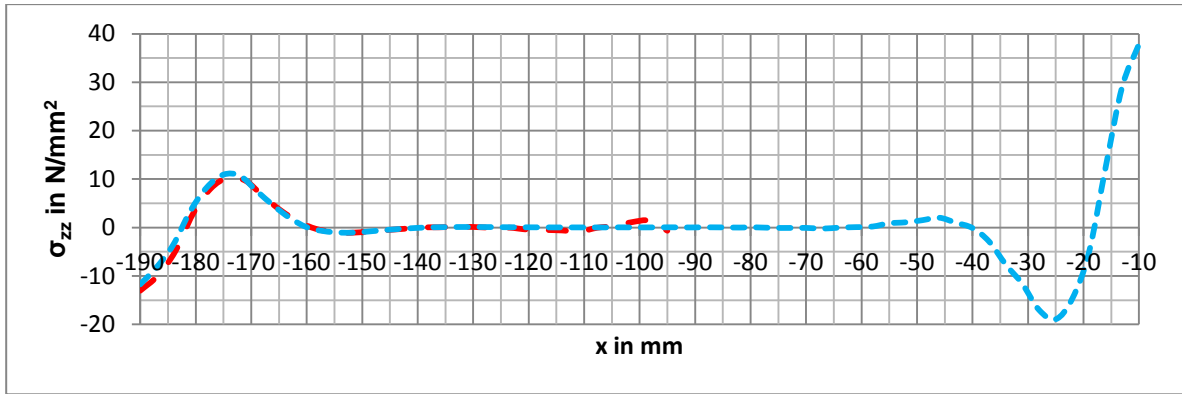


Figure 24.124: Comparison of stresses perpendicular to the horizontal plane of the outer angle at $y=50$ $z=-194$

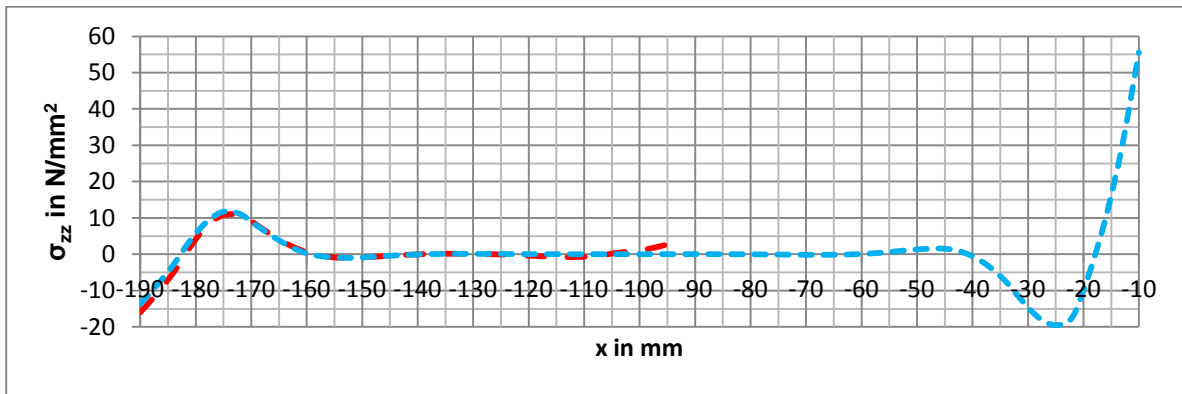


Figure 24.125: Comparison of stresses perpendicular to the horizontal plane of the outer angle at $y=50$ $z=-192$

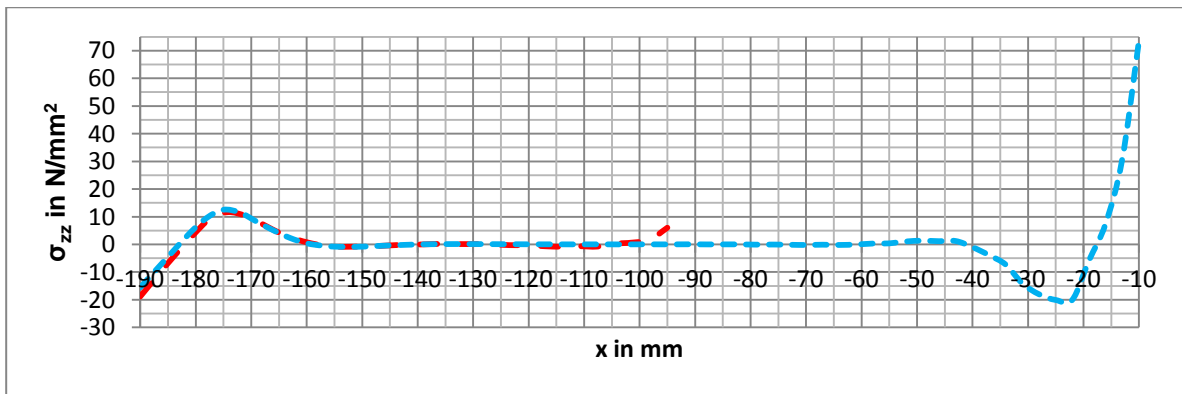


Figure 24.126: Comparison of stresses perpendicular to the horizontal plane of the outer angle at $y=50$ $z=-190$

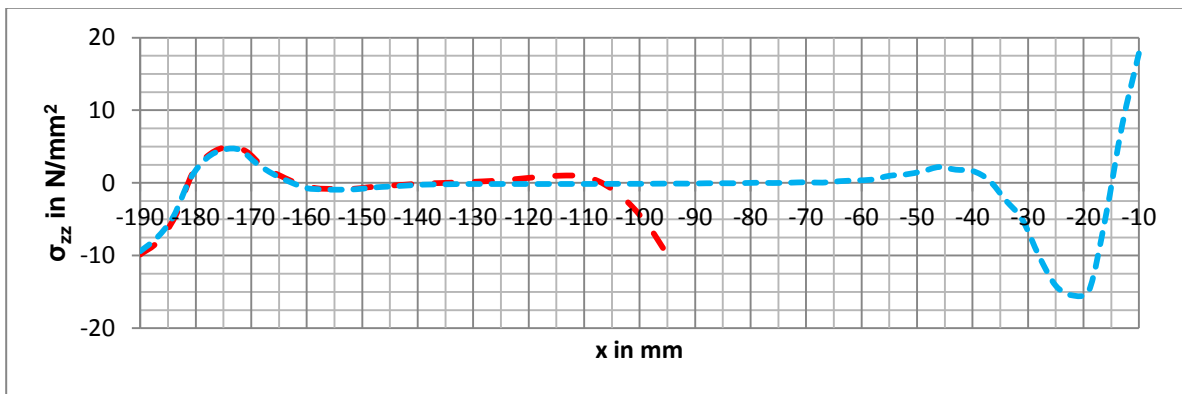


Figure 24.127: Comparison of stresses perpendicular to the horizontal plane of the outer angle at $y=100$ $z=-194$

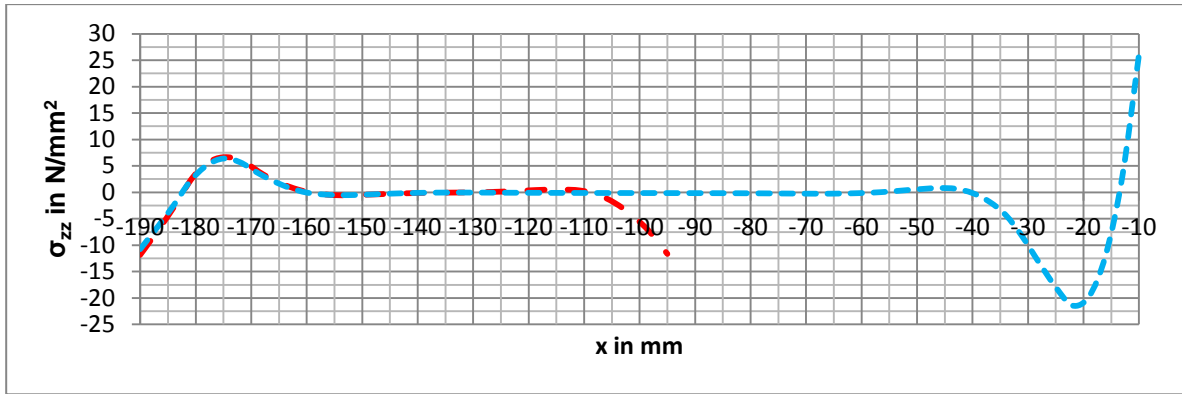


Figure 24.128: Comparison of stresses perpendicular to the horizontal plane of the outer angle at y=100 z=-192

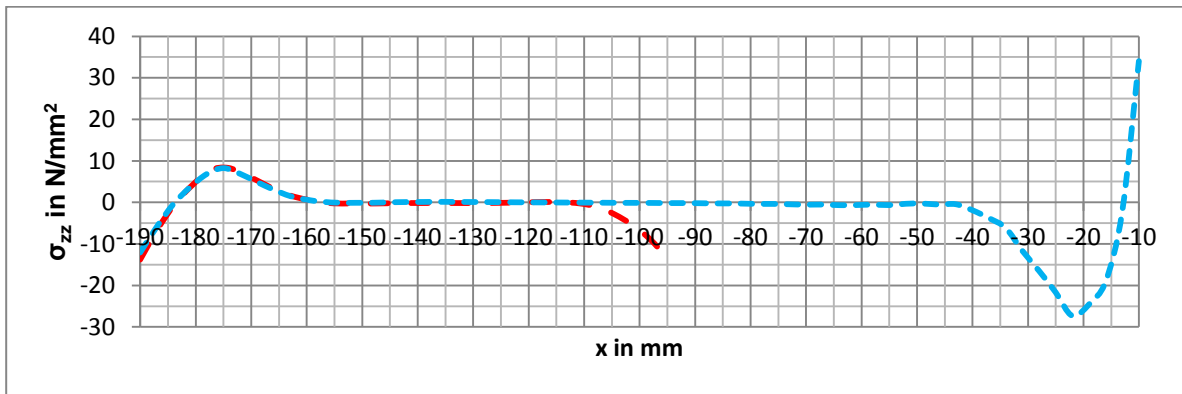


Figure 24.129: Comparison of stresses perpendicular to the horizontal plane of the outer angle at y=100 z=-190

24.5.3 Shear stresses (zx-direction) per test

For all the figures below the next colours are used to indicate the place of the result lines:

— Y=0 Z=-194 — Y=0 Z=-192 — Y=0 Z=-190 — Y=50 Z=-194 — Y=50 Z=-192 — Y=50 Z=-190 — Y=100 Z=-194 — Y=100 Z=-192 — Y=100 Z=-190

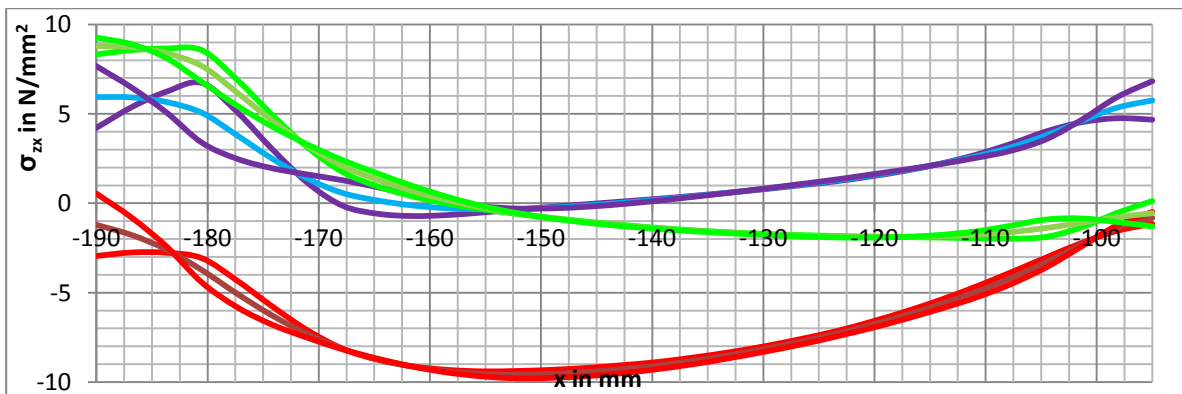


Figure 24.130: Stresses perpendicular to the horizontal plane of the additional model with short lap

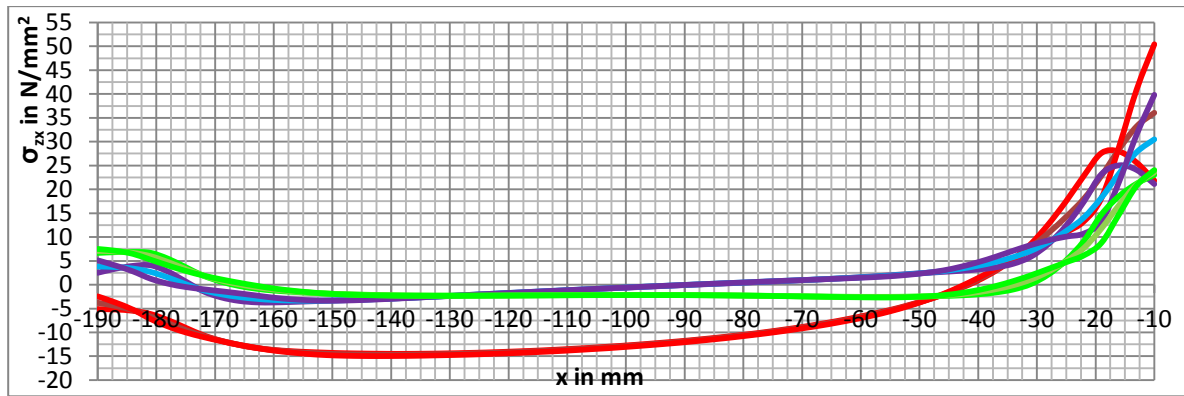


Figure 24.131: Stresses perpendicular to the horizontal plane of the additional model with long lap

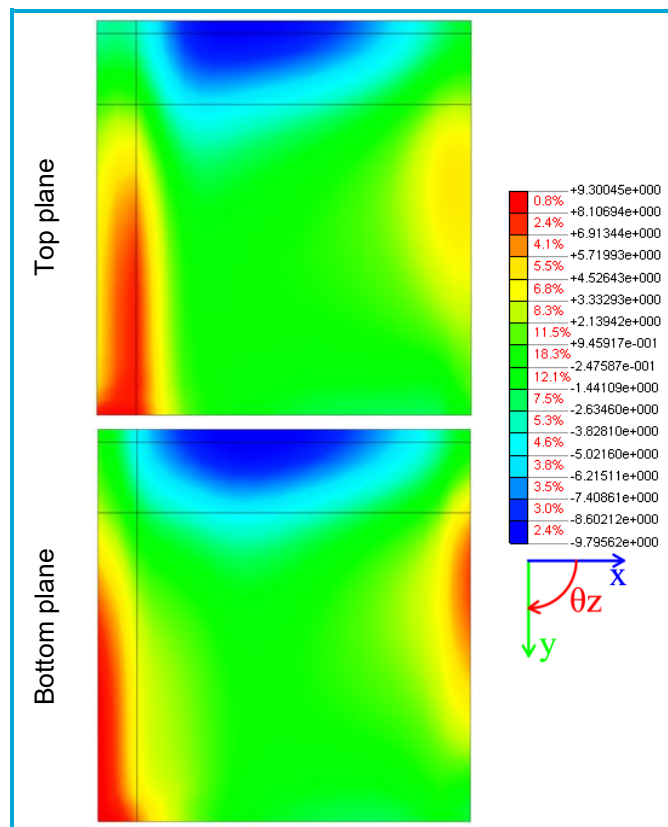


Figure 24.132: Counterplot of shear stresses of the horizontal plane of the additional model with short lap

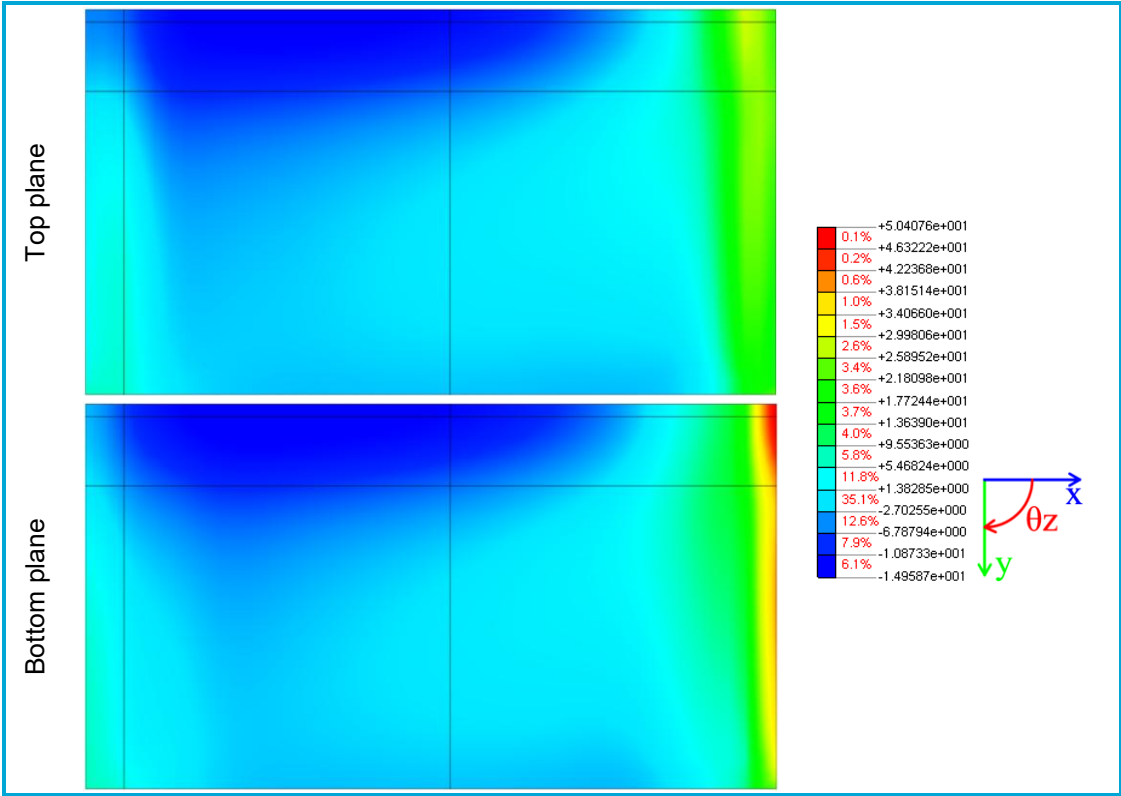


Figure 24.133: Counterplot of shear stresses of the horizontal plane of the additional model with long lap

24.5.4 Shear stresses (zx-direction) per result line

For all the figures below the next colours are used to indicate the models: - - Short Lap - - - Long Lap.

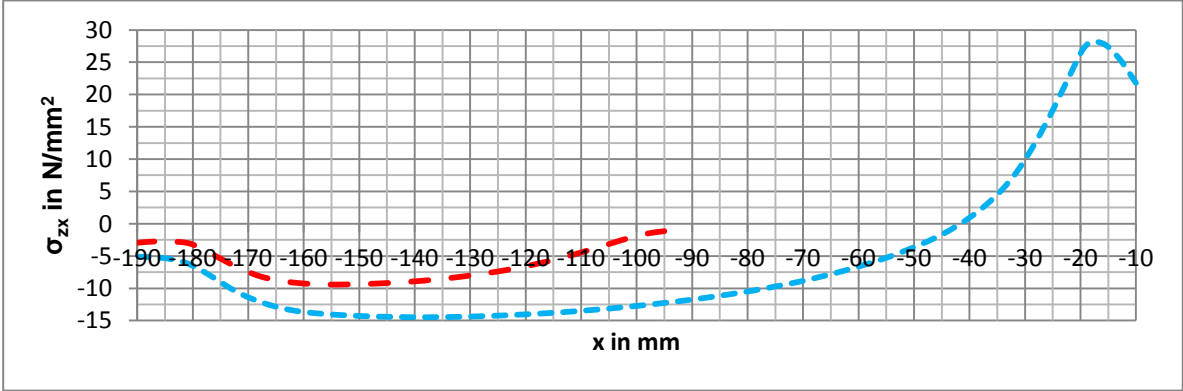


Figure 24.134: Comparison of shear stresses in zx-direction of the horizontal plane of the outer angle at $y=0$ $x=-194$

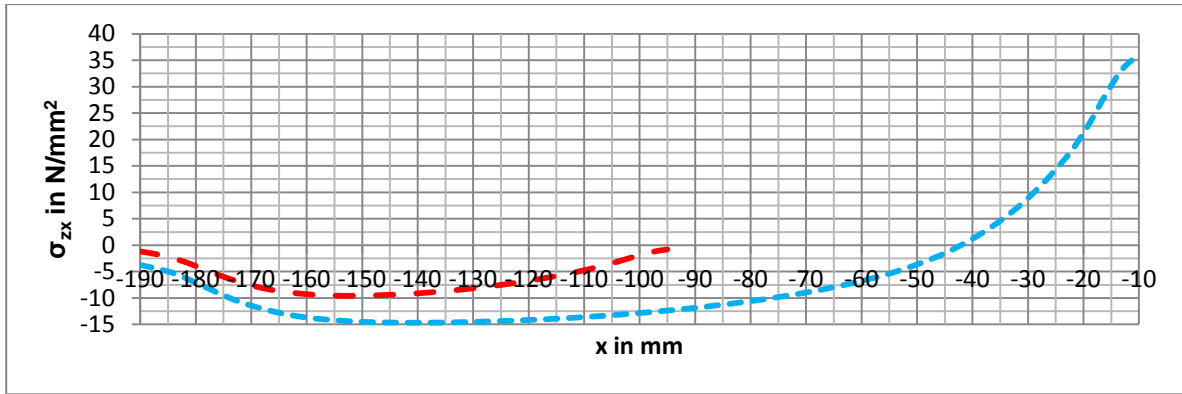


Figure 24.135: Comparison of shear stresses in zx-direction of the horizontal plane of the outer angle at $y=0$ $x=-192$

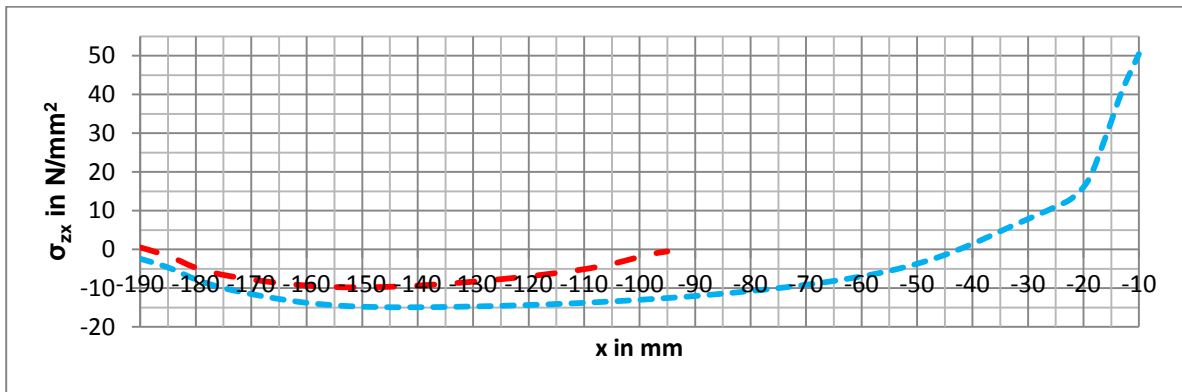


Figure 24.136: Comparison of shear stresses in zx-direction of the horizontal plane of the outer angle at $y=0$ $x=-190$

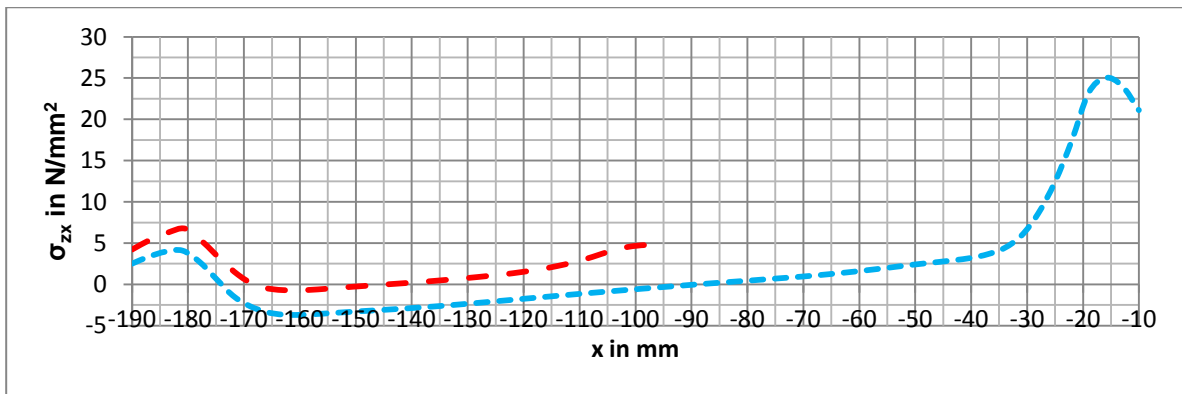


Figure 24.137: Comparison of shear stresses in zx-direction of the horizontal plane of the outer angle at $y=50$ $x=-194$

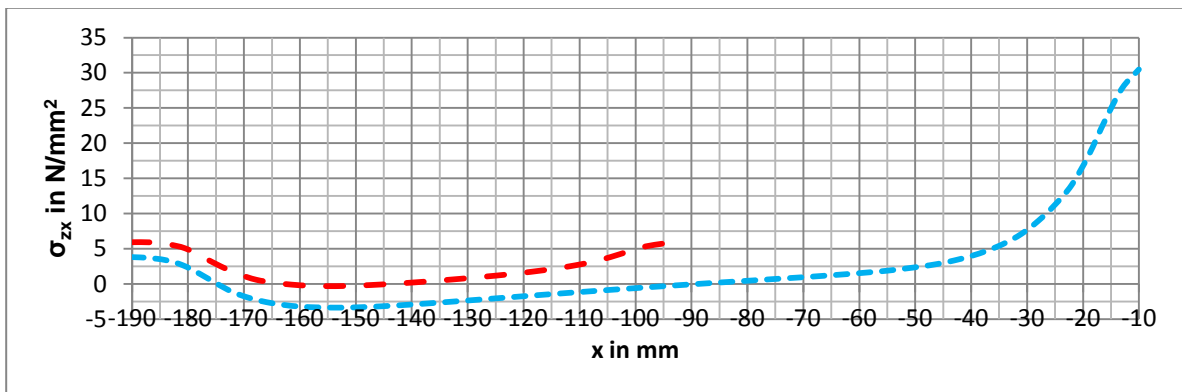


Figure 24.138: Comparison of shear stresses in zx-direction of the horizontal plane of the outer angle at $y=50$ $x=-192$

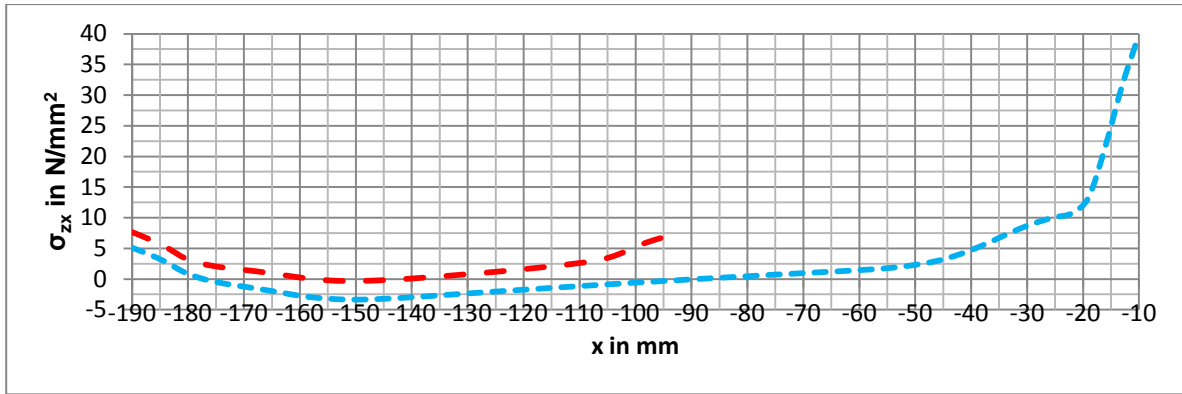


Figure 24.139: Comparison of shear stresses in zx-direction of the horizontal plane of the outer angle at y=50 x=-190

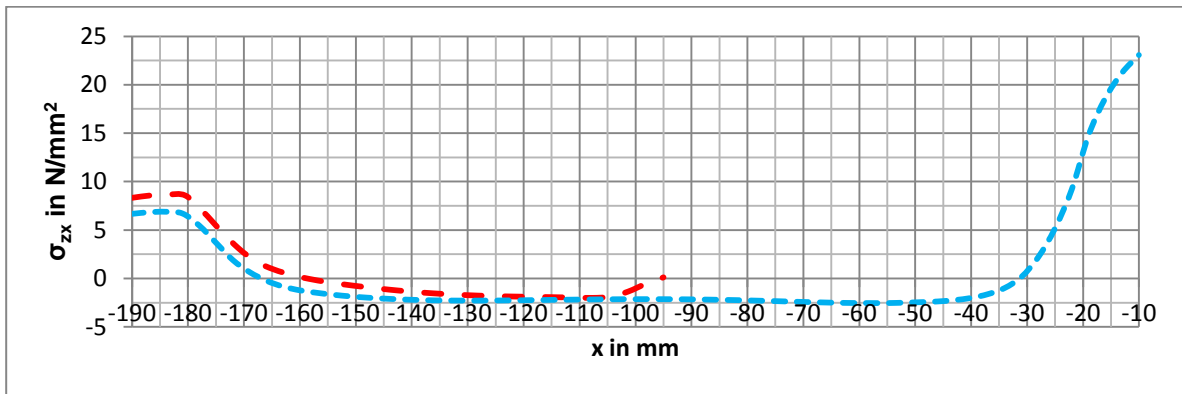


Figure 24.140: Comparison of shear stresses in zx-direction of the horizontal plane of the outer angle at y=100 x=-194

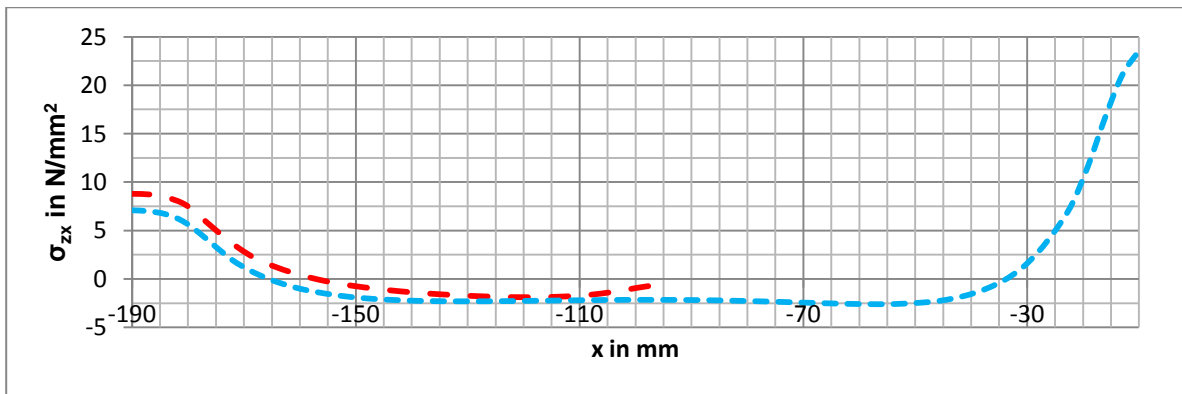


Figure 24.141: Comparison of shear stresses in zx-direction of the horizontal plane of the outer angle at y=100 x=-192

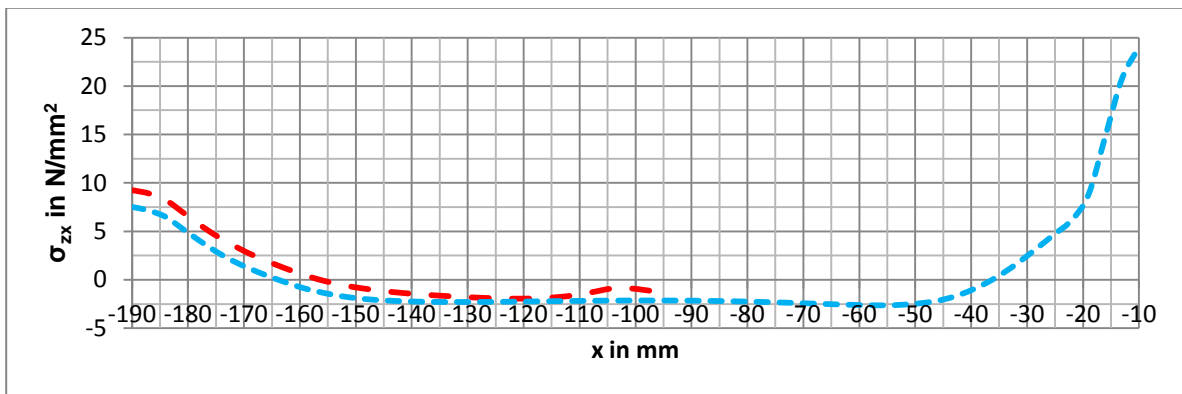


Figure 24.142: Comparison of shear stresses in zx-direction of the horizontal plane of the outer angle at y=100 x=-190

25 Appendix I: Elaboration of DE's for stress analysis of L-connection

In this appendix several DE's can be found which are derived from the analysis of stresses.

25.1 Sign conventions

For all axes systems the next conventions are used:

- Angular rotation, curvature and shear angle are positive for positive rotation of axes system;
- Positive moment creates tension at positive direction of axes system;
- Shear force, with force in positive direction on positive plane of axes system, is positive;
- Positive load is in positive direction of axes system.

25.1.1 Conventions for bending DE's in y-plane and x as variable

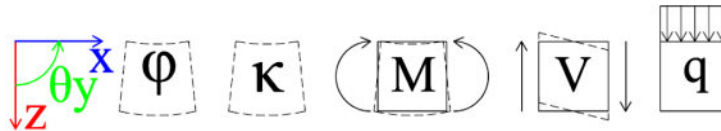


Figure 25.1: Conventions for bending DE's in y-plane and x as variable

Kinematic	Constitutive	Static
$\varphi(x) = -\frac{dw(x)}{dx}$	$M(x) = EI\kappa(x)$	$V(x) = \frac{dM(x)}{dx}$
$\kappa(x) = \frac{d\varphi(x)}{dx}$		$q(x) = -\frac{dV(x)}{dx}$

Table 25.1: Relationship for bending DE's in y-plane and x as variable

The relationship of Table 25.1 will lead to the following system:

$$q(x) = EI \frac{d^4 w(x)}{dx^4} \quad V(x) = -EI \frac{d^3 w(x)}{dx^3} \quad M(x) = -EI \frac{d^2 w(x)}{dx^2} \quad \varphi(x) = -\frac{dw(x)}{dx}$$

25.1.2 Conventions for bending DE's in y-plane and z as variable



Figure 25.2: Conventions for bending system DE's in y-plane and z as variable

Kinematic	Constitutive	Static
$\varphi(z) = \frac{dw(z)}{dz}$	$M(z) = -EI\kappa(z)$	$V(z) = \frac{dM(z)}{dz}$
$\kappa(z) = \frac{d\varphi(z)}{dz}$		$q(z) = -\frac{dV(z)}{dz}$

Table 25.2: Relationship for bending DE's in y-plane and z as variable

The relationship of Table 25.2 will lead to the following system:

$$q(z) = EI \frac{d^4 w(z)}{dz^4} \quad V(z) = -EI \frac{d^3 w(z)}{dz^3} \quad M(z) = -EI \frac{d^2 w(z)}{dz^2} \quad \varphi(z) = \frac{dw(z)}{dz}$$

25.2 Rotation of the beam at the horizontal plane of inner angle

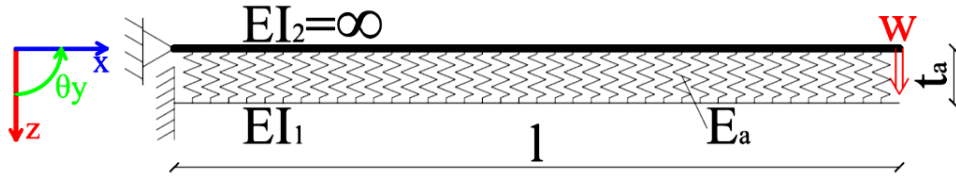


Figure 25.3: Structural diagram per unit width

For the displacement of the upper beam the next equation applies:

$$w_2(x) = \frac{W}{l}x \quad (25.1)$$

For the lower beam the fourth order, linear DE of the Euler Bernoulli theory is assumed:

$$E_1 I_1 \frac{d^4 w_1(x)}{dx^4} = q_z(x) \quad (25.2)$$

Where the second moment of area for a unit width is given by:

$$I_1 = \frac{bt_1^3}{12} = \frac{t_1^3}{12} \quad (25.3)$$

The load is given by:

$$q_z(x) = k_a (w_2(x) - w_1(x)) \quad (25.4)$$

With the distributed spring stiffness:

$$k_a = \frac{E_a}{t_a} \quad (25.5)$$

Combining (25.1), (25.2) and (25.4), and rearranging gives:

$$\frac{d^4 w_1(x)}{dx^4} + 4\beta^4 w_1(x) = 4\beta^4 \frac{W}{l}x \quad (25.6)$$

With:

$$\beta = \sqrt[4]{\frac{k_a}{4E_1 I_1}} \quad (25.7)$$

The general solution of (25.6) can be written in the form:

$$w_1(z) = e^{\beta z} (C_1 \sin(\beta z) + C_2 \cos(\beta z)) + e^{-\beta z} (C_3 \sin(\beta z) + C_4 \cos(\beta z)) + \frac{W}{l}x \quad (25.8)$$

To solve the integration constants four boundary conditions are necessary. At the left end ($x=0$) the displacement and rotation are zero, at the right end ($z=l$) the moment and shear force are zero, consequently:

$$w_1(0) = 0 \quad (25.9)$$

$$\left. \frac{dw_1(x)}{dx} \right|_{x=0} = 0 \quad (25.10)$$

$$\left. \frac{d^2 w_1(x)}{dx^2} \right|_{x=l} = 0 \quad (25.11)$$

$$\left. \frac{d^3 w_1(x)}{dx^3} \right|_{x=l} = 0 \quad (25.12)$$

This gives:

$$\begin{aligned}
 C_1 &= -\frac{W}{\beta l} s_1 (e^{-2\beta l} + 2 \sin(\beta l) \cos(\beta l) + 1) \\
 C_2 &= -\frac{W}{\beta l} s_1 2 \cos^2(\beta l) \\
 C_3 &= -\frac{W}{\beta l} s_1 (e^{2\beta l} - 2 \sin(\beta l) \cos(\beta l) + 1) \\
 C_4 &= -C_2
 \end{aligned} \tag{25.13}$$

With:

$$s_1 = \frac{1}{(e^{2\beta l} + e^{-2\beta l} + 4 \cos^2(\beta l) + 2)} \tag{25.14}$$

The strain in the adhesive is given by:

$$\varepsilon_{a,zz}(x) = \frac{w_1(x) - w_2(x)}{t_a} \tag{25.15}$$

For the stress in the adhesive Hooke's law is used:

$$\sigma_{a,zz}(x) = E_a \varepsilon_{a,zz}(x) \tag{25.16}$$

Hence:

$$\sigma_{a,zz}(x) = \frac{E_a}{t_a} (w_1(x) - w_2(x)) \tag{25.17}$$

The distributions of $w_1(x)$, $w_2(x)$, $\sigma_{a,zz}(x)$, $M(x)$, $V(x)$ for the constants $t_a = 4 \text{ mm}$, $E_a = 12800 \text{ mm}$, $W = 1 \text{ mm}$, $l = 500 \text{ mm}$, $E_1 = 2.1 \cdot 10^5 \text{ N/mm}^2$ and $t_1 = 10 \text{ mm}$, can be found in the next figures:

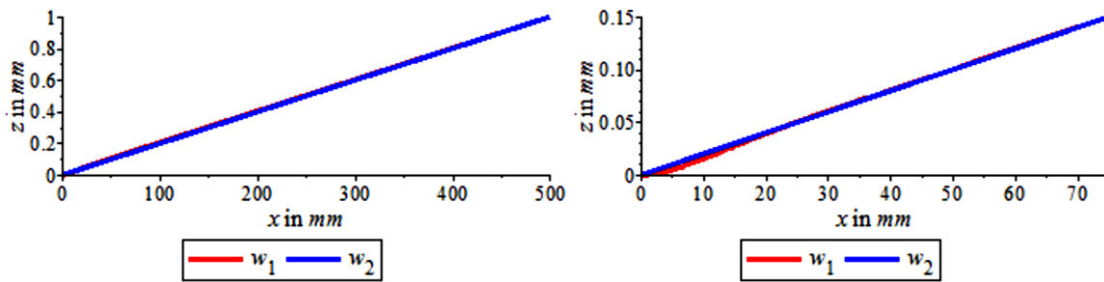


Figure 25.4: Displacement due to rotation of the beam

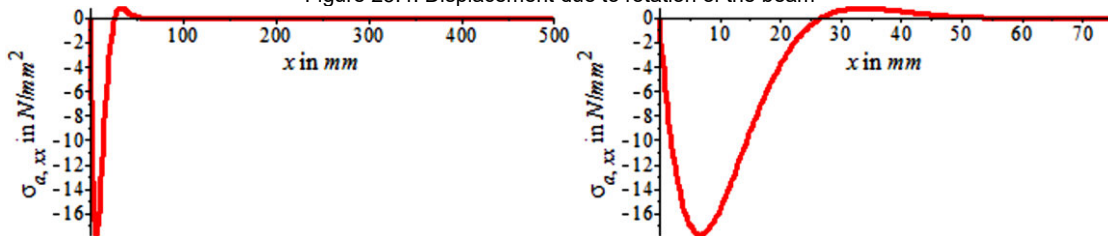


Figure 25.5: Adhesive stress in z-direction due to rotation of the beam

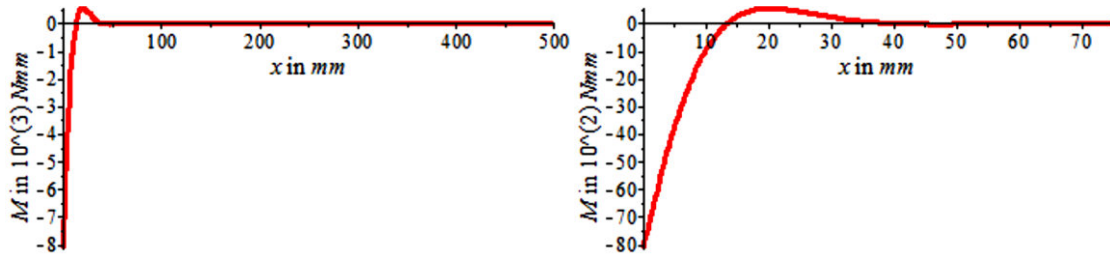


Figure 25.6: Moment due to rotation of the beam

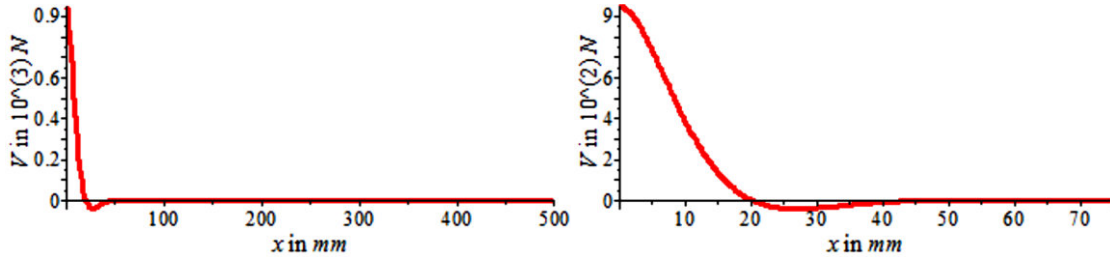


Figure 25.7: Shear force due to rotation of the beam

Figure 25.4, Figure 25.5, Figure 25.6 and Figure 25.7 show that for the used constants for $x > 2\pi/\beta \approx 54\text{ mm}^1$, $w_1(x) \approx w_2(x)$, which results in $\sigma_{a,zz}(x) \approx 0$. Note that the system is linear with respect to the load. Hence when the load is increased the stresses at $x > 2\pi/\beta \approx 54\text{ mm}$ will stay small and are negligible with respect to the stresses at $0 \leq x < 2\pi/\beta$.

¹ $1/\beta$ is also known as the characteristic length

25.3 Uniform translation of the beam at the horizontal plane of inner angle

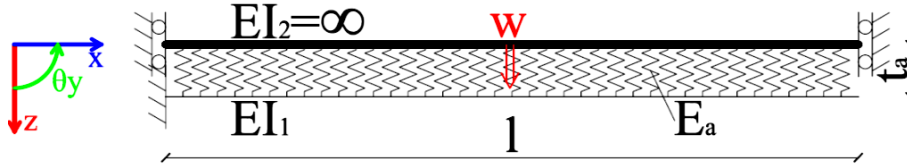


Figure 25.8: Structural diagram per unit width

For the displacement of the upper beam the next equation applies:

$$w_2(x) = W \quad (25.18)$$

For the lower beam the fourth order, linear DE of the Euler Bernoulli theory is assumed:

$$E_1 I_1 \frac{d^4 w_1(x)}{dx^4} = q_z(x) \quad (25.19)$$

Where the second moment of area for a unit width is given by:

$$I_1 = \frac{bt_1^3}{12} = \frac{t_1^3}{12} \quad (25.20)$$

The load is given by:

$$q_z(x) = k_a (w_2(x) - w_1(x)) \quad (25.21)$$

With the distributed spring stiffness:

$$k_a = \frac{E_a}{t_a} \quad (25.22)$$

Combining (25.18), (25.19) and (25.21), and rearranging gives:

$$\frac{d^4 w_1(x)}{dx^4} + 4\beta^4 w_1(x) = 4\beta^4 \frac{W}{l} x \quad (25.23)$$

With:

$$\beta = \sqrt[4]{\frac{k_a}{4E_1 I_1}} \quad (25.24)$$

The general solution of (25.23) can be written in the form:

$$w_1(z) = e^{\beta z} (C_1 \sin(\beta z) + C_2 \cos(\beta z)) + e^{-\beta z} (C_3 \sin(\beta z) + C_4 \cos(\beta z)) + \frac{W}{l} x \quad (25.25)$$

To solve the integration constants four boundary conditions are necessary. At the left end ($x=0$) the displacement and rotation are zero, at the right end ($x=l$) the moment and shear force are zero, consequently:

$$w_1(0) = 0 \quad (25.26)$$

$$\left. \frac{dw_1(x)}{dx} \right|_{x=0} = 0 \quad (25.27)$$

$$\left. \frac{d^2 w_1(x)}{dx^2} \right|_{x=l} = 0 \quad (25.28)$$

$$\left. \frac{d^3 w_1(x)}{dx^3} \right|_{x=l} = 0 \quad (25.29)$$

This gives:

$$\begin{aligned}
 C_1 &= Ws_1 \left(e^{-2\beta l} - 2 \sin(\beta l) \cos(\beta l) - 2 \cos^2(\beta l) + 1 \right) \\
 C_2 &= -Ws_1 \left(e^{-2\beta l} - 2 \sin(\beta l) \cos(\beta l) + 2 \cos^2(\beta l) + 1 \right) \\
 C_3 &= -Ws_1 \left(e^{2\beta l} + 2 \sin(\beta l) \cos(\beta l) - 2 \cos^2(\beta l) + 1 \right) \\
 C_4 &= -Ws_1 \left(e^{2\beta l} + 2 \sin(\beta l) \cos(\beta l) + 2 \cos^2(\beta l) + 1 \right)
 \end{aligned}
 \tag{25.30}$$

With:

$$s_1 = \frac{1}{\left(e^{2\beta l} + e^{-2\beta l} + 4 \cos^2(\beta l) + 2 \right)}
 \tag{25.31}$$

The strain in the adhesive is given by:

$$\varepsilon_{a,zz}(x) = \frac{w_1(x) - w_2(x)}{t_a}
 \tag{25.32}$$

For the stress in the adhesive Hooke's law is used:

$$\sigma_{a,zz}(x) = E_a \varepsilon_{a,zz}(x)
 \tag{25.33}$$

Hence:

$$\sigma_{a,zz}(x) = \frac{E_a}{t_a} \left(w_1(x) - w_2(x) \right)
 \tag{25.34}$$

The distributions of $w_1(x)$, $w_2(x)$, $\sigma_{a,zz}(x)$, $M(x)$, $V(x)$ for the constants $t_a = 4mm$, $E_a = 12800mm$, $W = 1mm$, $l = 500mm$, $E_1 = 2.1 \cdot 10^5 N/mm^2$ and $t_1 = 10mm$, can be found in the next figures:

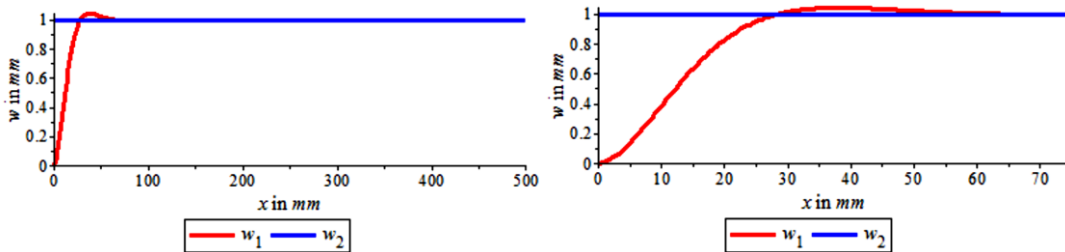


Figure 25.9: Displacement due to uniform translation of the beam

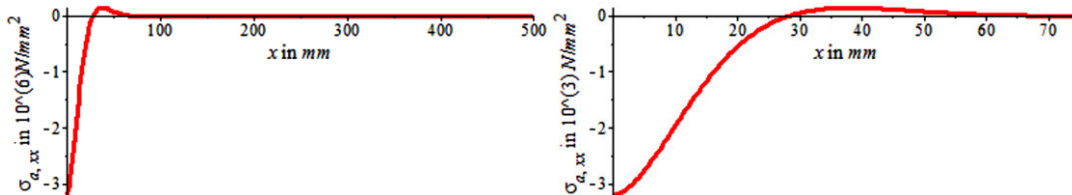


Figure 25.10: Adhesive stress in z-direction due to translation of the beam

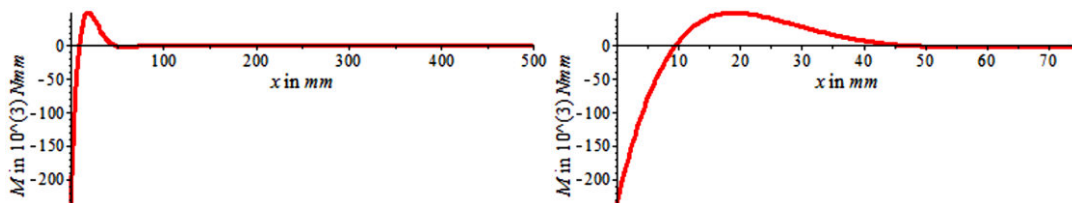


Figure 25.11: Moment due to uniform translation of the beam

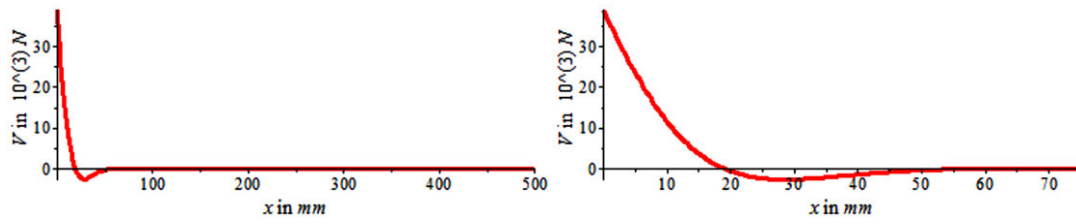


Figure 25.12: Shear force due to uniform translation of the beam

Note that the stress fades out before $x = 2\pi/\beta \approx 54 \text{ mm}$, just as for the latter sections.

25.4 Moment on the vertical plane of inner angle

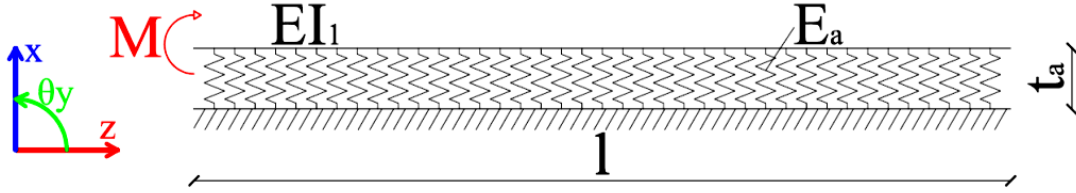


Figure 25.13: Structural diagram per unit width of beam on elastic foundation with a moment load

For the beam the fourth order, linear DE of the Euler Bernoulli theory is assumed:

$$E_1 I_1 \frac{d^4 w_1(z)}{dz^4} = q_x(z) \quad (25.35)$$

Where the second moment of area for a unit width is given by equation (25.3):

$$I_1 = \frac{b t_1^3}{12} = \frac{t_1^3}{12} \quad (25.36)$$

The load is given by:

$$q_x(z) = -k_a w_1(z) \quad (25.37)$$

With the distributed spring stiffness:

$$k_a = \frac{E_a}{t_a} \quad (25.38)$$

Combining and rearranging (25.35) and (25.37) gives:

$$\frac{d^4 w_1(z)}{dz^4} + 4\beta^4 w_1(z) = 0 \quad (25.39)$$

With:

$$\beta = \sqrt[4]{\frac{k_a}{4E_1 I_1}} \quad (25.40)$$

The general solution of (25.39) can be written in the form:

$$w_1(z) = e^{\beta z} (C_1 \sin(\beta z) + C_2 \cos(\beta z)) + e^{-\beta z} (C_3 \sin(\beta z) + C_4 \cos(\beta z)) \quad (25.41)$$

To solve the integration constants four boundary conditions are necessary. At the right end ($z = 0$) the shear force is zero and a moment M acts, at the left end ($z = l$) the shear force and moment are zero, consequently:

$$\left. \frac{d^3 w_1(z)}{dz^3} \right|_{z=0} = 0 \quad (25.42)$$

$$-E_1 I_1 \left. \frac{d^2 w_1(z)}{dz^2} \right|_{z=0} = -M \quad (25.43)$$

$$\left. \frac{d^3 w_1(z)}{dz^3} \right|_{z=l} = 0 \quad (25.44)$$

$$\left. \frac{d^2 w_1(z)}{dz^2} \right|_{z=l} = 0 \quad (25.45)$$

This gives:

$$\begin{aligned}
 C_1 &= \frac{M}{E_2 I_2 \beta^2} \frac{s_2}{2} (e^{-2\beta l} + 2 \cos^2(\beta l) - 2 \sin(\beta l) \cos(\beta l) - 3) \\
 C_2 &= \frac{M}{E_2 I_2 \beta^2} \frac{s_2}{2} (e^{-2\beta l} - 2 \cos^2(\beta l) - 2 \sin(\beta l) \cos(\beta l) + 1) \\
 C_3 &= \frac{M}{E_2 I_2 \beta^2} \frac{s_2}{2} (-e^{2\beta l} - 2 \cos^2(\beta l) - 2 \sin(\beta l) \cos(\beta l) + 3) \\
 C_4 &= \frac{M}{E_2 I_2 \beta^2} \frac{s_2}{2} (e^{2\beta l} - 2 \cos^2(\beta l) + 2 \sin(\beta l) \cos(\beta l) + 1)
 \end{aligned} \tag{25.46}$$

With:

$$s_2 = \frac{1}{(e^{2\beta l} + e^{-2\beta l} + 4 \cos^2(\beta l) - 6)} \tag{25.47}$$

The strain in the adhesive is given by:

$$\varepsilon_{a,xx}(z) = \frac{w_1(z)}{t_a} \tag{25.48}$$

For the stress in the adhesive Hooke's law is used:

$$\sigma_{a,xx}(z) = E_a \varepsilon_{a,xx}(z) \tag{25.49}$$

Hence:

$$\sigma_{a,xx}(z) = \frac{E_a}{t_a} w_1(z) \tag{25.50}$$

The distribution of $\sigma_{a,xx}(z)$ for the constants $t_a = 4 \text{ mm}$, $E_a = 12800 \text{ mm}$, $M = 1 \text{ Nmm}$, $l = 200 \text{ mm}$, $E_1 = 2.1 \cdot 10^5 \text{ N/mm}^2$ and $t_1 = 10 \text{ mm}$, can be found in the next figure:

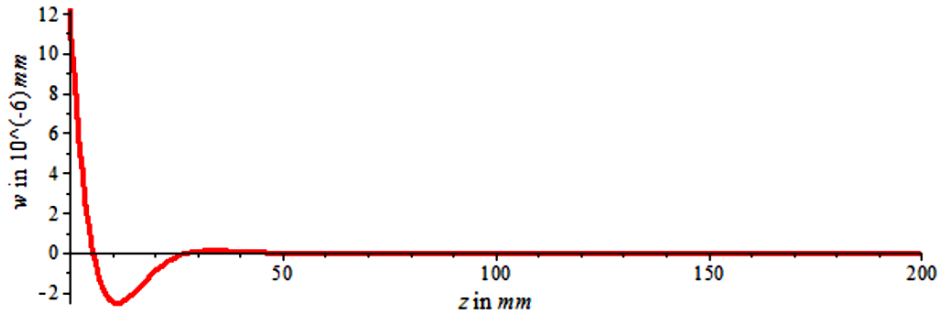


Figure 25.14: Displacement due to a moment

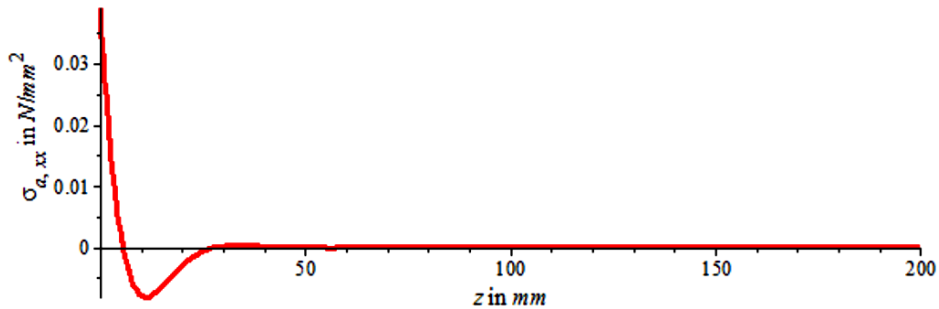


Figure 25.15: Adhesive stress in x-direction due to a moment

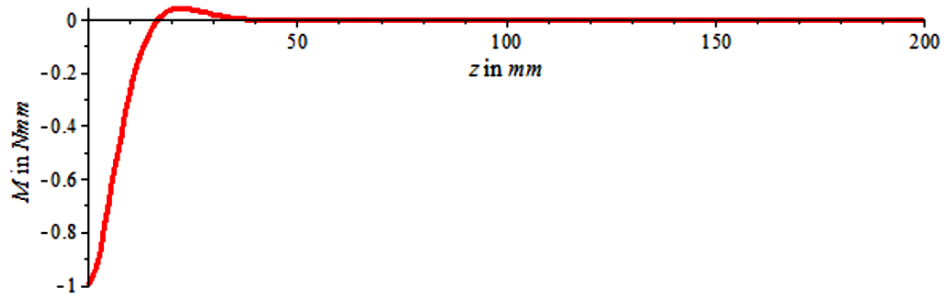


Figure 25.16: Moment due to a moment

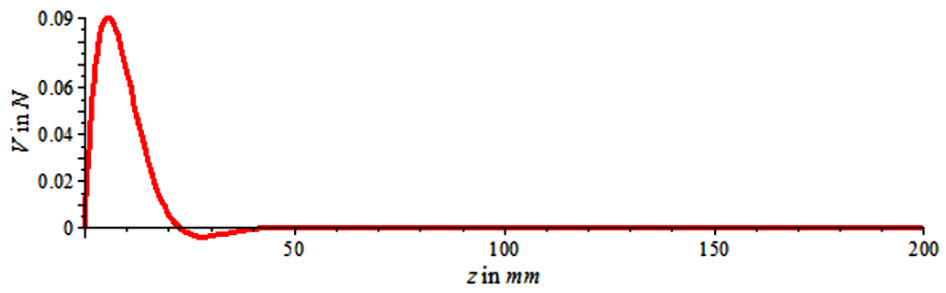


Figure 25.17: Shear force due to a moment

Note that the stress fades out before $x = 2\pi/\beta \approx 54\text{ mm}$, just as for the latter sections.

25.5 Point load on the vertical plane of inner angle

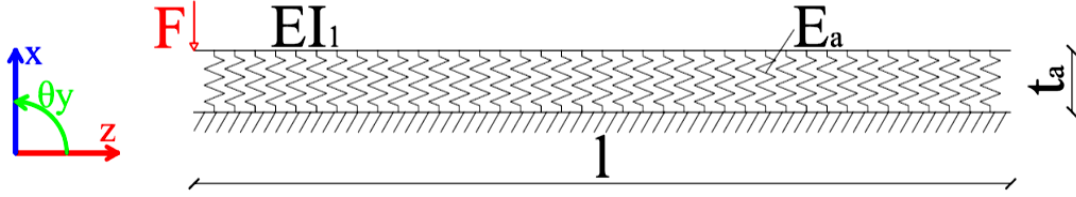


Figure 25.18: Structural diagram per unit width of beam on elastic foundation with a point load

For the beam the fourth order, linear DE of the Euler Bernoulli theory is assumed:

$$E_1 I_1 \frac{d^4 w_1(z)}{dz^4} = q_x(z) \quad (25.51)$$

Where the second moment of area for a unit width is given by equation (25.3):

$$I_1 = \frac{b t_1^3}{12} = \frac{t_1^3}{12} \quad (25.52)$$

The load is given by:

$$q_x(z) = -k_a w_1(z) \quad (25.53)$$

With the distributed spring stiffness:

$$k_a = \frac{E_a}{t_a} \quad (25.54)$$

Combining and rearranging (25.35) and (25.37) gives:

$$\frac{d^4 w_1(z)}{dz^4} + 4\beta^4 w_1(z) = 0 \quad (25.55)$$

With:

$$\beta = \sqrt[4]{\frac{k_a}{4E_1 I_1}} \quad (25.56)$$

The general solution of (25.39) can be written in the form:

$$w_1(z) = e^{\beta z} (C_1 \sin(\beta z) + C_2 \cos(\beta z)) + e^{-\beta z} (C_3 \sin(\beta z) + C_4 \cos(\beta z)) \quad (25.57)$$

To solve the integration constants four boundary conditions are necessary. At the right end ($z=0$) the moment is zero and a shear force F acts, at the left end ($z=l$) the displacement and moment are zero, consequently:

$$\left. \frac{d^2 w_1(z)}{dz^2} \right|_{z=0} = 0 \quad (25.58)$$

$$-E_1 I_1 \left. \frac{d^3 w_1(z)}{dz^3} \right|_{z=0} = F \quad (25.59)$$

$$\left. \frac{d^2 w_1(z)}{dz^2} \right|_{z=l} = 0 \quad (25.60)$$

$$\left. \frac{d^3 w_1(z)}{dz^3} \right|_{z=l} = 0 \quad (25.61)$$

This gives:

$$\begin{aligned}
 C_1 &= \frac{F}{E_2 I_2 \beta^3} \frac{s_2}{2} (-2 \cos^2(\beta l) + 2) \\
 C_2 &= \frac{F}{E_2 I_2 \beta^3} \frac{s_2}{2} (e^{-2\beta l} + 2 \cos(\beta l) \sin(\beta l) - 1) \\
 C_3 &= C_1 \\
 C_4 &= \frac{F}{E_2 I_2 \beta^3} \frac{s_2}{2} (-e^{-2\beta l} + 2 \cos(\beta l) \sin(\beta l) + 1)
 \end{aligned}
 \tag{25.62}$$

With:

$$s_2 = \frac{1}{(e^{2\beta l} + e^{-2\beta l} + 4 \cos^2(\beta l) - 6)}
 \tag{25.63}$$

The distribution of $\sigma_{a,xx}(z)$ for the constants $t_a = 4 \text{ mm}$, $E_a = 12800 \text{ mm}$, $F = 1 \text{ N}$, $l = 200 \text{ mm}$, $E_1 = 2.1 \cdot 10^5 \text{ N/mm}^2$ and $t_1 = 10 \text{ mm}$, can be found in the next figure:

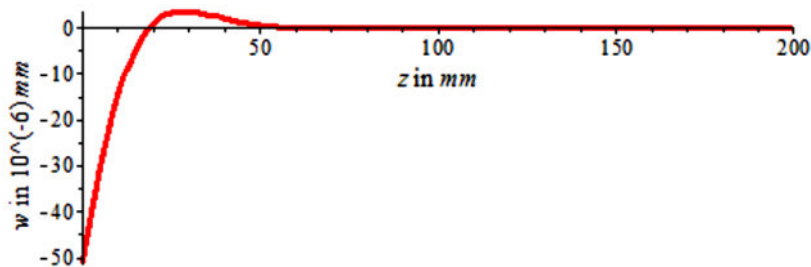


Figure 25.19: Displacement due to a point load

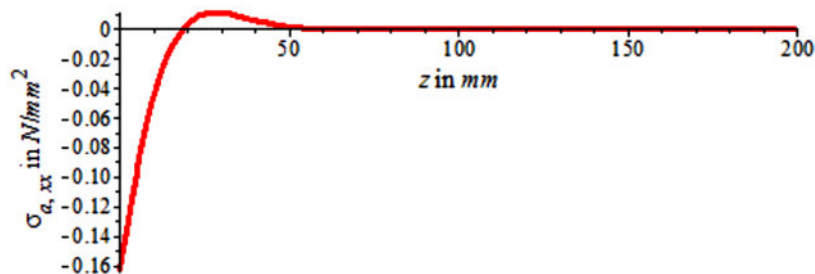


Figure 25.20: Adhesive stress in x-direction due to a point load

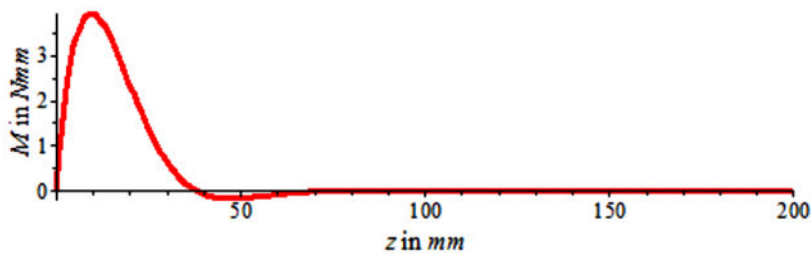


Figure 25.21: Moment due to a point load

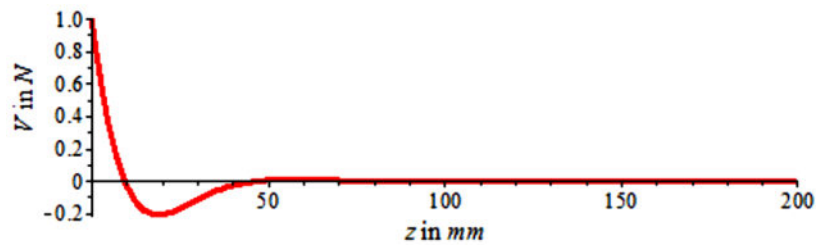


Figure 25.22: Shear force due to a point load

Note that the stress fades out before $x = 2\pi/\beta \approx 54 \text{ mm}$, just as for the latter sections.

25.6 Shear deformation of the beam at the horizontal plane of outer angle

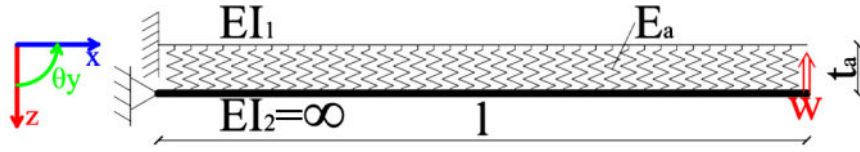


Figure 25.23: Structural diagram per unit width

For the displacement of the upper beam the next equation applies:

$$w_2(x) = -W \frac{x}{l} \quad (25.64)$$

For the lower beam the fourth order, linear DE of the Euler Bernoulli theory is assumed:

$$E_1 I_1 \frac{d^4 w_1(x)}{dx^4} = q_z(x) \quad (25.65)$$

Where the second moment of area for a unit width is given by:

$$I_1 = \frac{bt_1^3}{12} = \frac{t_1^3}{12} \quad (25.66)$$

The load is given by:

$$q_z(x) = k_a (w_2(x) - w_1(x)) \quad (25.67)$$

With the distributed spring stiffness:

$$k_a = \frac{E_a}{t_a} \quad (25.68)$$

Combining (25.64), (25.65) and (25.67), and rearranging gives:

$$\frac{d^4 w_1(x)}{dx^4} + 4\beta^4 w_1(x) = -4\beta^4 W \frac{x}{l} \quad (25.69)$$

With:

$$\beta = \sqrt[4]{\frac{k_a}{4E_1 I_1}} \quad (25.70)$$

The general solution of (25.69) can be written in the form:

$$w_1(z) = e^{\beta z} (C_1 \sin(\beta z) + C_2 \cos(\beta z)) + e^{-\beta z} (C_3 \sin(\beta z) + C_4 \cos(\beta z)) + \dots \quad (25.71)$$

$$\dots - W \frac{x}{l}$$

To solve the integration constants four boundary conditions are necessary. At the left end ($x = 0$) the displacement and rotation are zero, at the right end ($z = l$) the moment and shear force are zero, consequently:

$$w_1(0) = 0 \quad (25.72)$$

$$\left. \frac{dw_1(x)}{dx} \right|_{x=0} = 0 \quad (25.73)$$

$$\left. \frac{d^2 w_1(x)}{dx^2} \right|_{x=l} = 0 \quad (25.74)$$

$$\left. \frac{d^3 w_1(x)}{dx^3} \right|_{x=l} = 0 \quad (25.75)$$

This gives:

$$\begin{aligned}
 C_1 &= \frac{W}{\beta l} s_1 (e^{-2\beta l} + 2 \sin(\beta l) \cos(\beta l) + 1) \\
 C_2 &= \frac{W}{\beta l} s_1 (2 \cos^2(\beta l)) \\
 C_3 &= \frac{W}{\beta l} s_1 (e^{2\beta l} - 2 \sin(\beta l) \cos(\beta l) + 1) \\
 C_4 &= -C_2
 \end{aligned} \tag{25.76}$$

With:

$$s_1 = \frac{1}{(e^{2\beta l} + e^{-2\beta l} + 4 \cos^2(\beta l) + 2)} \tag{25.77}$$

The strain in the adhesive is given by:

$$\varepsilon_{a,zz}(x) = \frac{w_2(x) - w_1(x)}{t_a} \tag{25.78}$$

For the stress in the adhesive Hooke's law is used:

$$\sigma_{a,zz}(x) = E_a \varepsilon_{a,zz}(x) \tag{25.79}$$

Hence:

$$\sigma_{a,zz}(x) = \frac{E_a}{t_a} (w_2(x) - w_1(x)) \tag{25.80}$$

The distributions of $w_1(x)$, $w_2(x)$, $\sigma_{a,zz}(x)$, $M(x)$, $V(x)$ for the constants $t_a = 4 \text{ mm}$, $E_a = 12800 \text{ mm}$, $W = 1 \text{ mm}$, $l = 100 \text{ mm}$, $E_1 = 2.1 \cdot 10^5 \text{ N/mm}^2$ and $t_1 = 10 \text{ mm}$, can be found in the next figures:

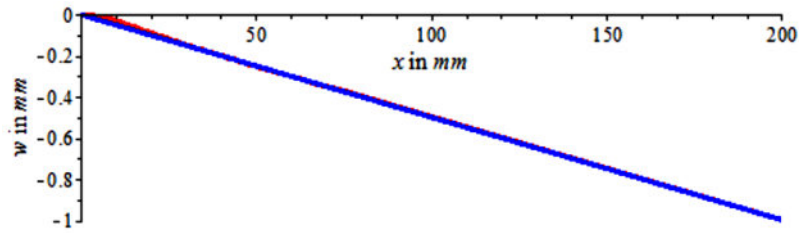


Figure 25.24: Displacement due to rotation of the beam

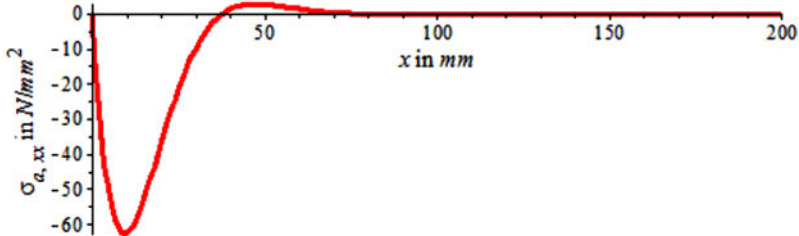


Figure 25.25: Adhesive stress in z-direction due to rotation of the beam

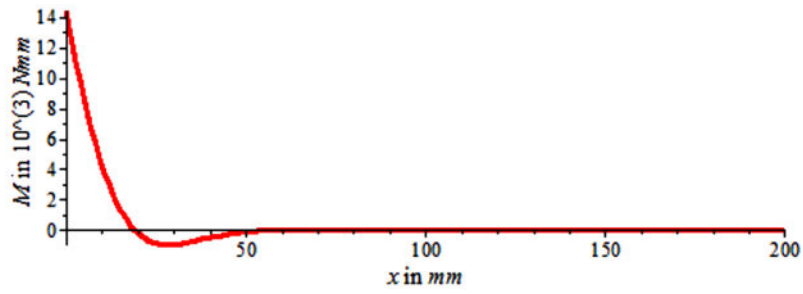


Figure 25.26: Moment due to rotation of the beam

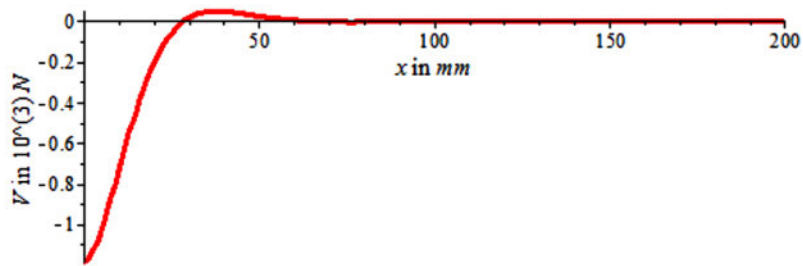


Figure 25.27: Shear force due to rotation of the beam

Note that the stress fades out before $x = 2\pi/\beta \approx 54 \text{ mm}$, just as for the latter sections.

25.7 Uniform translation of the beam at the horizontal plane of outer angle

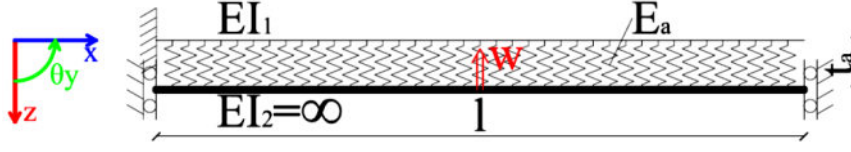


Figure 25.28: Structural diagram per unit width

For the displacement of the upper beam the next equation applies:

$$w_2(x) = -W \quad (25.81)$$

For the lower beam the fourth order, linear DE of the Euler Bernoulli theory is assumed:

$$E_1 I_1 \frac{d^4 w_1(x)}{dx^4} = q_z(x) \quad (25.82)$$

Where the second moment of area for a unit width is given by:

$$I_1 = \frac{bt_1^3}{12} = \frac{t_1^3}{12} \quad (25.83)$$

The load is given by:

$$q_z(x) = k_a (w_2(x) - w_1(x)) \quad (25.84)$$

With the distributed spring stiffness:

$$k_a = \frac{E_a}{t_a} \quad (25.85)$$

Combining (25.81), (25.82) and (25.84), and rearranging gives:

$$\frac{d^4 w_1(x)}{dx^4} + 4\beta^4 w_1(x) = -4\beta^4 W \quad (25.86)$$

With:

$$\beta = \sqrt[4]{\frac{k_a}{4E_1 I_1}} \quad (25.87)$$

The general solution of (25.86) can be written in the form:

$$w_1(z) = e^{\beta z} (C_1 \sin(\beta z) + C_2 \cos(\beta z)) + e^{-\beta z} (C_3 \sin(\beta z) + C_4 \cos(\beta z)) - W \quad (25.88)$$

To solve the integration constants four boundary conditions are necessary. At the left end ($x=0$) the displacement and rotation are zero, at the right end ($z=l$) the moment and shear force are zero, consequently:

$$w_1(0) = 0 \quad (25.89)$$

$$\left. \frac{dw_1(x)}{dx} \right|_{x=0} = 0 \quad (25.90)$$

$$\left. \frac{d^2 w_1(x)}{dx^2} \right|_{x=l} = 0 \quad (25.91)$$

$$\left. \frac{d^3 w_1(x)}{dx^3} \right|_{x=l} = 0 \quad (25.92)$$

This gives:

$$\begin{aligned}
 C_1 &= Ws_1 \left(-e^{-2\beta l} + 2 \cos^2(\beta l) + 2 \sin(\beta l) \cos(\beta l) - 1 \right) \\
 C_2 &= Ws_1 \left(e^{-2\beta l} + 2 \cos^2(\beta l) - 2 \sin(\beta l) \cos(\beta l) + 1 \right) \\
 C_3 &= Ws_1 \left(e^{2\beta l} - 2 \cos^2(\beta l) + 2 \sin(\beta l) \cos(\beta l) + 1 \right) \\
 C_4 &= Ws_1 \left(e^{2\beta l} + 2 \cos^2(\beta l) + 2 \sin(\beta l) \cos(\beta l) + 1 \right)
 \end{aligned}
 \tag{25.93}$$

With:

$$s_1 = \frac{1}{\left(e^{2\beta l} + e^{-2\beta l} + 4 \cos^2(\beta l) + 2 \right)}
 \tag{25.94}$$

The strain in the adhesive is given by:

$$\varepsilon_{a,zz}(x) = \frac{w_2(x) - w_1(x)}{t_a}
 \tag{25.95}$$

For the stress in the adhesive Hooke's law is used:

$$\sigma_{a,zz}(x) = E_a \varepsilon_{a,zz}(x)
 \tag{25.96}$$

Hence:

$$\sigma_{a,zz}(x) = \frac{E_a}{t_a} (w_2(x) - w_1(x))
 \tag{25.97}$$

The distributions of $w_1(x)$, $w_2(x)$, $\sigma_{a,zz}(x)$, $M(x)$, $V(x)$ for the constants $t_a = 4\text{ mm}$, $E_a = 12800\text{ mm}$, $W = 1\text{ mm}$, $l = 100\text{ mm}$, $E_1 = 2.1 \cdot 10^5\text{ N/mm}^2$ and $t_1 = 10\text{ mm}$, can be found in the next figures:

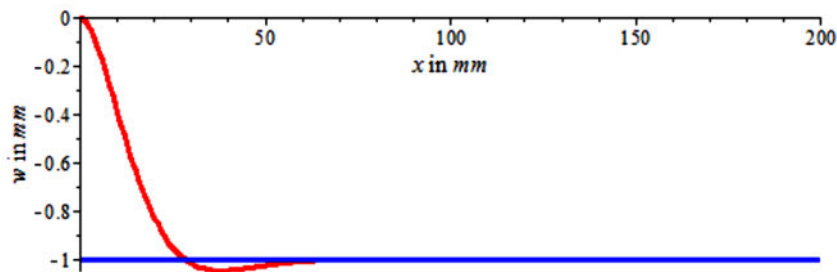


Figure 25.29: Displacement due to translation of the beam

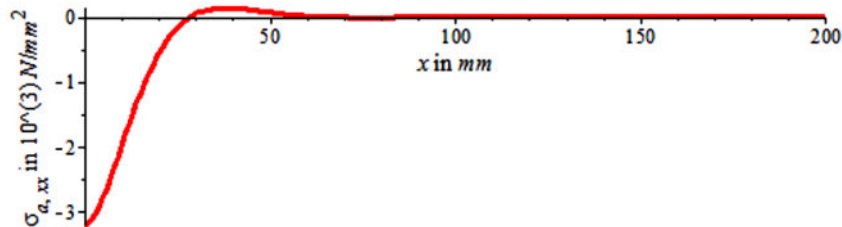


Figure 25.30: Adhesive stress in z-direction due to translation of the beam

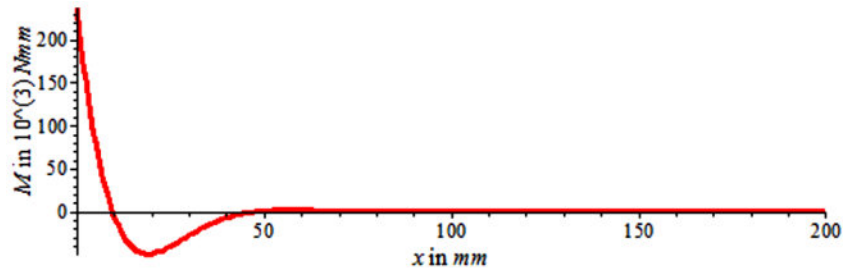


Figure 25.31: Moment due to translation of the beam

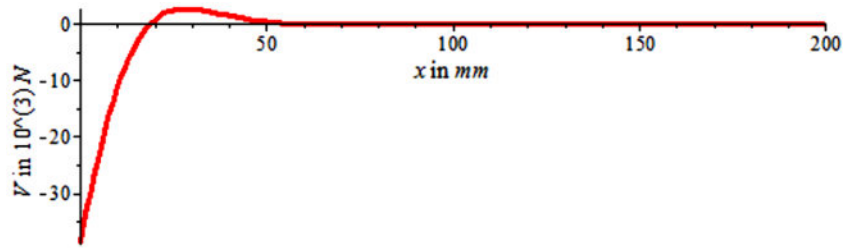


Figure 25.32: Shear force due to translation of the beam

Note that the stress fades out before $x = 2\pi/\beta \approx 54 \text{ mm}$, just as for the latter sections.

25.8 Rotation of the beam at the horizontal plane of outer angle

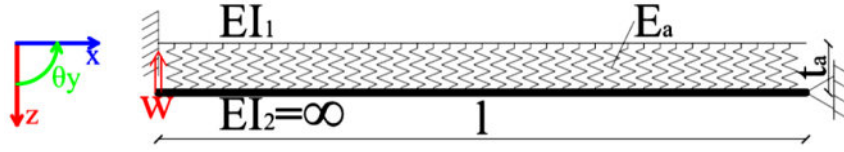


Figure 25.33: Structural diagram per unit width

For the displacement of the upper beam the next equation applies:

$$w_2(x) = -W \left(\frac{l-x}{l} \right) \quad (25.98)$$

For the lower beam the fourth order, linear DE of the Euler Bernoulli theory is assumed:

$$E_1 I_1 \frac{d^4 w_1(x)}{dx^4} = q_z(x) \quad (25.99)$$

Where the second moment of area for a unit width is given by:

$$I_1 = \frac{bt_1^3}{12} = \frac{t_1^3}{12} \quad (25.100)$$

The load is given by:

$$q_z(x) = k_a (w_2(x) - w_1(x)) \quad (25.101)$$

With the distributed spring stiffness:

$$k_a = \frac{E_a}{t_a} \quad (25.102)$$

Combining (25.98), (25.99) and (25.101), and rearranging gives:

$$\frac{d^4 w_1(x)}{dx^4} + 4\beta^4 w_1(x) = 4\beta^4 W \frac{x-l}{l} \quad (25.103)$$

With:

$$\beta = \sqrt[4]{\frac{k_a}{4E_1 I_1}} \quad (25.104)$$

The general solution of (25.103) can be written in the form:

$$w_1(z) = e^{\beta z} (C_1 \sin(\beta z) + C_2 \cos(\beta z)) + e^{-\beta z} (C_3 \sin(\beta z) + C_4 \cos(\beta z)) + \dots \\ \dots + W \frac{x-l}{l} \quad (25.105)$$

To solve the integration constants four boundary conditions are necessary. At the left end ($x=0$) the displacement and rotation are zero, at the right end ($z=l$) the moment and shear force are zero, consequently:

$$w_1(0) = 0 \quad (25.106)$$

$$\left. \frac{dw_1(x)}{dx} \right|_{x=0} = 0 \quad (25.107)$$

$$\left. \frac{d^2 w_1(x)}{dx^2} \right|_{x=l} = 0 \quad (25.108)$$

$$\left. \frac{d^3 w_1(x)}{dx^3} \right|_{x=l} = 0 \quad (25.109)$$

This gives:

$$\begin{aligned}
 C_1 &= \frac{W}{\beta l} s_1 \left(-e^{-2\beta l} (\beta l + 1) + \beta l (2 \cos^2(\beta l) - 1) + 2 \sin(\beta l) \cos(\beta l) (\beta l - 1) - 1 \right) \\
 C_2 &= \frac{W}{\beta l} s_1 \left(\beta l e^{-2\beta l} + (\beta l - 1) 2 \cos^2(\beta l) - 2 \beta l \sin(\beta l) \cos(\beta l) + \beta l \right) \\
 C_3 &= \frac{W}{\beta l} s_1 \left((\beta l - 1) e^{2\beta l} - 2 \beta l \cos^2(\beta l) + (\beta l + 1) 2 \sin(\beta l) \cos(\beta l) + (\beta l - 1) \right) \\
 C_4 &= \frac{W}{\beta l} s_1 \left(e^{2\beta l} + (\beta l + 1) 2 \cos^2(\beta l) + 2 \sin(\beta l) \cos(\beta l) + \beta l \right)
 \end{aligned} \tag{25.110}$$

With:

$$s_1 = \frac{1}{\left(e^{2\beta l} + e^{-2\beta l} + 4 \cos^2(\beta l) + 2 \right)} \tag{25.111}$$

The strain in the adhesive is given by:

$$\varepsilon_{a,zz}(x) = \frac{w_2(x) - w_1(x)}{t_a} \tag{25.112}$$

For the stress in the adhesive Hooke's law is used:

$$\sigma_{a,zz}(x) = E_a \varepsilon_{a,zz}(x) \tag{25.113}$$

Hence:

$$\sigma_{a,zz}(x) = \frac{E_a}{t_a} (w_2(x) - w_1(x)) \tag{25.114}$$

The distributions of $w_1(x)$, $w_2(x)$, $\sigma_{a,zz}(x)$, $M(x)$, $V(x)$ for the constants $t_a = 4 \text{ mm}$, $E_a = 12800 \text{ mm}$, $W = 1 \text{ mm}$, $l = 100 \text{ mm}$, $E_1 = 2.1 \cdot 10^5 \text{ N/mm}^2$ and $t_1 = 10 \text{ mm}$, can be found in the next figures:

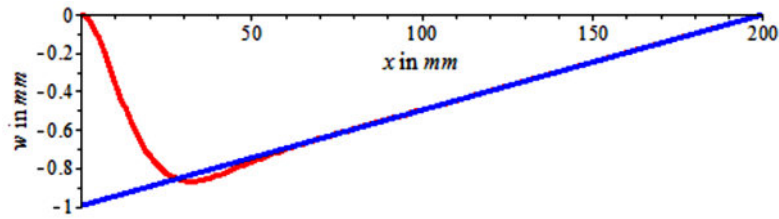


Figure 25.34: Displacement due to rotation of the beam

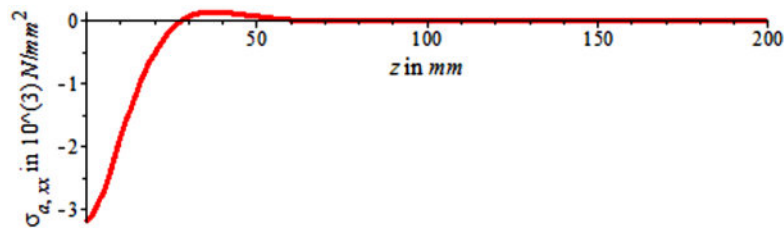


Figure 25.35: Adhesive stress in z-direction due to rotation of the beam

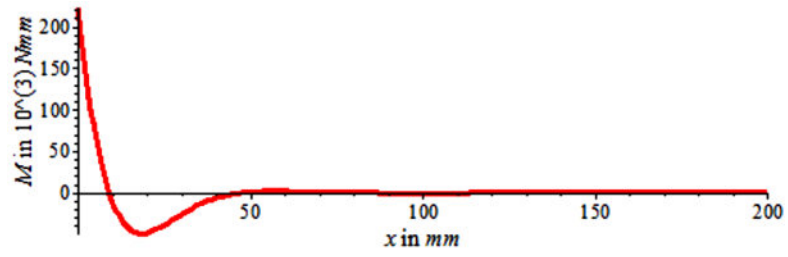


Figure 25.36: Moment due to rotation of the beam

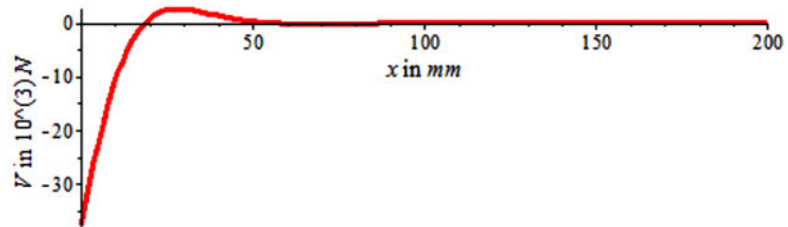


Figure 25.37: Shear force due to rotation of the beam

Note that the stress fades out before $x = 2\pi/\beta \approx 54 \text{ mm}$, just as for the latter sections.

25.9 Rotation of the beam at the vertical plane of outer angle

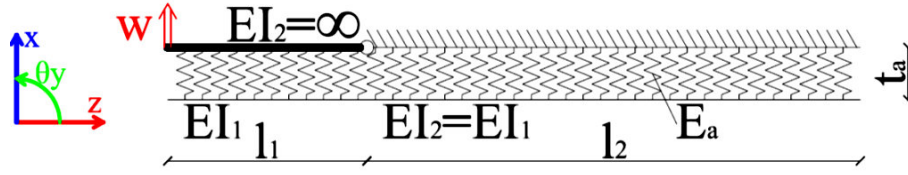


Figure 25.38: Structural diagram per unit width

For the displacement of the upper beam the next equation applies:

$$w_3(z) = W \left(1 - \frac{z}{l_1} \right) \quad (25.115)$$

For the lower beam the fourth order, linear DE of the Euler Bernoulli theory is assumed:

$$E_1 I_1 \frac{d^4 w_1(z)}{dz^4} = q_1(z) \quad \text{for } 0 \leq z \leq l_1 \quad (25.116)$$

$$E_1 I_1 \frac{d^4 w_2(z)}{dz^4} = q_2(z) \quad \text{for } l_1 \leq z \leq l_1 + l_2 \quad (25.117)$$

Where the second moment of area for a unit width is given by:

$$I_1 = \frac{b t_1^3}{12} = \frac{t_1^3}{12} \quad (25.118)$$

The load is given by:

$$q_1(x) = k_a (w_3(x) - w_1(x)) \quad (25.119)$$

$$q_2(x) = -k_a w_2(x) \quad (25.120)$$

With the distributed spring stiffness:

$$k_a = \frac{E_a}{t_a} \quad (25.121)$$

Combining and rearranging (25.116), (25.119) and (25.115), and (25.117) and (25.120) gives:

$$\frac{d^4 w_1(x)}{dx^4} + 4\beta^4 w_1(x) = 4\beta^4 W \left(1 - \frac{x}{l_1} \right) \quad (25.122)$$

$$\frac{d^4 w_2(x)}{dx^4} + 4\beta^4 w_2(x) = 0$$

With:

$$\beta = \sqrt[4]{\frac{k_a}{4E_1 I_1}} \quad (25.123)$$

The general solutions of (25.122) and can be written in the form:

$$w_1(z) = e^{\beta z} (C_1 \sin(\beta z) + C_2 \cos(\beta z)) + e^{-\beta z} (C_3 \sin(\beta z) + C_4 \cos(\beta z)) + \dots \\ \dots + W \left(1 - \frac{x}{l_1} \right) \quad (25.124)$$

$$w_2(z) = e^{\beta z} (C_5 \sin(\beta z) + C_6 \cos(\beta z)) + e^{-\beta z} (C_7 \sin(\beta z) + C_8 \cos(\beta z))$$

To solve the integration constants eight boundary conditions are necessary:

$$\left. \frac{d^2 w_1(z)}{dx^2} \right|_{z=0} = 0 \quad (25.125)$$

$$\left. \frac{d^3 w_1(z)}{dx^3} \right|_{z=0} = 0 \quad (25.126)$$

$$w_1(z) = w_2(z) \quad (25.127)$$

$$\left. \frac{dw_1(z)}{dx} \right|_{z=l_1} = \left. \frac{dw_2(z)}{dx} \right|_{z=l_1} \quad (25.128)$$

$$\left. \frac{d^2 w_1(z)}{dx^2} \right|_{z=l_1} = \left. \frac{d^2 w_2(z)}{dx^2} \right|_{z=l_1} \quad (25.129)$$

$$\left. \frac{d^3 w_1(z)}{dx^3} \right|_{z=l_1} = \left. \frac{d^3 w_2(z)}{dx^3} \right|_{z=l_1} \quad (25.130)$$

$$\left. \frac{d^2 w_2(z)}{dx^2} \right|_{z=l_1+l_2} = 0 \quad (25.131)$$

$$\left. \frac{d^3 w_2(z)}{dx^3} \right|_{z=l_1+l_2} = 0 \quad (25.132)$$

With (25.125)/(25.132) the constants of (25.124) can be solved.

The strain in the adhesive is given by:

$$\varepsilon_1(z) = \frac{w_3(z) - w_1(z)}{t_a} \quad (25.133)$$

$$\varepsilon_2(z) = -\frac{w_2(z)}{t_a} \quad (25.134)$$

For the stress in the adhesive Hooke's law is used:

$$\sigma_i(z) = E_a \varepsilon_i(z) \quad i = 1..2 \quad (25.135)$$

Hence:

$$\sigma_1(x) = \frac{E_a}{t_a} (w_3(z) - w_1(z)) \quad (25.136)$$

$$\sigma_2(x) = -\frac{E_a}{t_a} w_2(z) \quad (25.137)$$

The distributions of $\sigma_1(x)$, $\sigma_2(x)$ and $w_3(z)$ for the constants $t_a = 4\text{mm}$, $E_a = 12800\text{mm}$, $W = 1\text{mm}$, $l_1 = 200\text{mm}$, $l_2 = 500\text{mm}$, $E_1 = 2.1 \cdot 10^5 \text{N/mm}^2$ and $t_1 = 10\text{mm}$, can be found in the next figures:

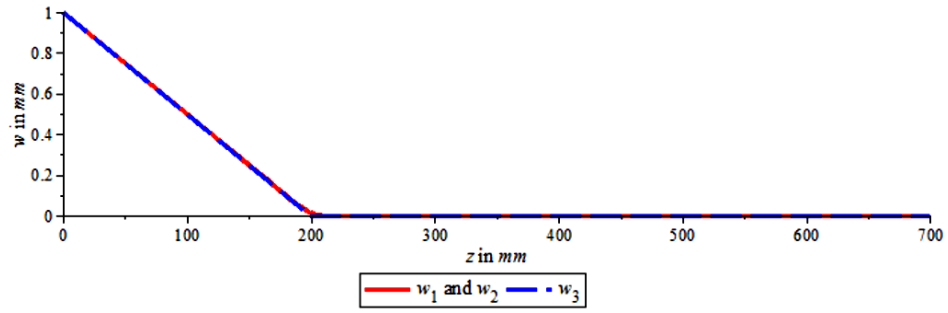


Figure 25.39: Displacement due to rotation of the beam

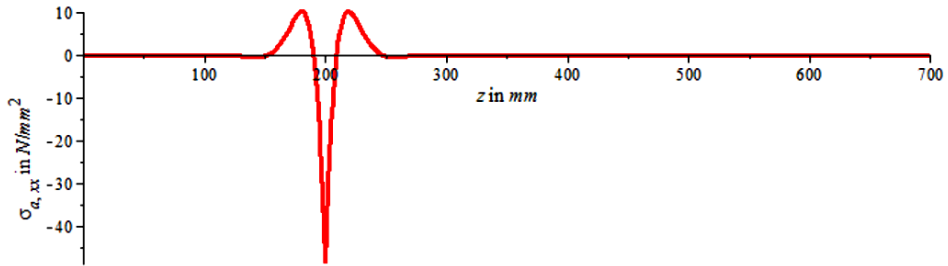


Figure 25.40: Adhesive stress in x-direction due to rotation of the beam

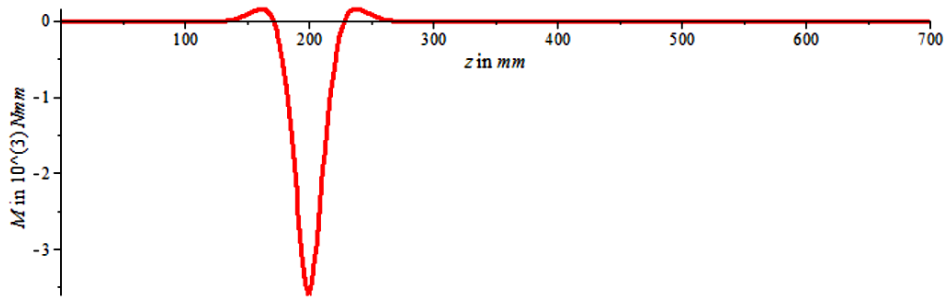


Figure 25.41: Moment due to rotation of the beam

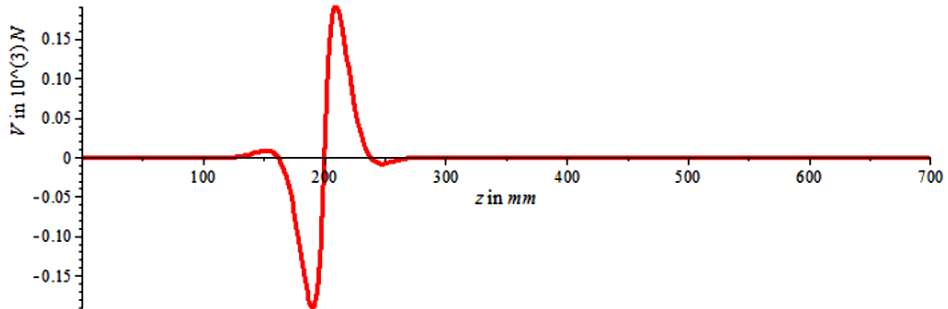


Figure 25.42: Shear force due to rotation of the beam

Note that the stress fades out before $x = 2\pi/\beta \approx 54 \text{ mm}$, just as for the latter sections.

25.10 Uniform translation of the beam at the vertical plane of outer angle

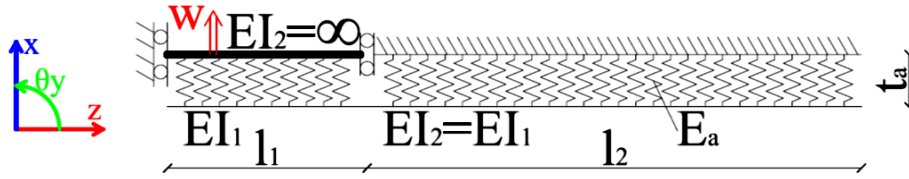


Figure 25.43: Structural diagram per unit width

For the displacement of the upper beam the next equation applies:

$$w_3(z) = W \tag{25.138}$$

For the lower beam the fourth order, linear DE of the Euler Bernoulli theory is assumed:

$$E_1 I_1 \frac{d^4 w_1(z)}{dz^4} = q_1(z) \quad \text{for } 0 \leq z \leq l_1 \tag{25.139}$$

$$E_1 I_1 \frac{d^4 w_2(z)}{dz^4} = q_2(z) \quad \text{for } l_1 \leq z \leq l_1 + l_2 \tag{25.140}$$

Where the second moment of area for a unit width is given by:

$$I_1 = \frac{bt_1^3}{12} = \frac{t_1^3}{12} \tag{25.141}$$

The load is given by:

$$q_1(x) = k_a (w_3(x) - w_1(x)) \tag{25.142}$$

$$q_2(x) = -k_a w_2(x) \tag{25.143}$$

With the distributed spring stiffness:

$$k_a = \frac{E_a}{t_a} \tag{25.144}$$

Combining and rearranging (25.139), (25.142) and (25.138), and (25.140) and (25.143) gives:

$$\begin{aligned} \frac{d^4 w_1(x)}{dx^4} + 4\beta^4 w_1(x) &= 4\beta^4 W \\ \frac{d^4 w_2(x)}{dx^4} + 4\beta^4 w_2(x) &= 0 \end{aligned} \tag{25.145}$$

With:

$$\beta = \sqrt[4]{\frac{k_a}{4E_1 I_1}} \tag{25.146}$$

The general solutions of (25.145) and can be written in the form:

$$\begin{aligned} w_1(z) &= e^{\beta z} (C_1 \sin(\beta z) + C_2 \cos(\beta z)) + e^{-\beta z} (C_3 \sin(\beta z) + C_4 \cos(\beta z)) + W \\ w_2(z) &= e^{\beta z} (C_5 \sin(\beta z) + C_6 \cos(\beta z)) + e^{-\beta z} (C_7 \sin(\beta z) + C_8 \cos(\beta z)) \end{aligned} \tag{25.147}$$

To solve the integration constants eight boundary conditions are necessary:

$$\left. \frac{d^2 w_1(z)}{dx^2} \right|_{z=0} = 0 \quad (25.148)$$

$$\left. \frac{d^3 w_1(z)}{dx^3} \right|_{z=0} = 0 \quad (25.149)$$

$$w_1(z) = w_2(z) \quad (25.150)$$

$$\left. \frac{dw_1(z)}{dx} \right|_{z=l_1} = \left. \frac{dw_2(z)}{dx} \right|_{z=l_1} \quad (25.151)$$

$$\left. \frac{d^2 w_1(z)}{dx^2} \right|_{z=l_1} = \left. \frac{d^2 w_2(z)}{dx^2} \right|_{z=l_1} \quad (25.152)$$

$$\left. \frac{d^3 w_1(z)}{dx^3} \right|_{z=l_1} = \left. \frac{d^3 w_2(z)}{dx^3} \right|_{z=l_1} \quad (25.153)$$

$$\left. \frac{d^2 w_2(z)}{dx^2} \right|_{z=l_1+l_2} = 0 \quad (25.154)$$

$$\left. \frac{d^3 w_2(z)}{dx^3} \right|_{z=l_1+l_2} = 0 \quad (25.155)$$

With (25.148)/(25.155) the constants of (25.147) can be solved.

The strain in the adhesive is given by:

$$\varepsilon_1(z) = \frac{w_3(z) - w_1(z)}{t_a} \quad (25.156)$$

$$\varepsilon_2(z) = -\frac{w_2(z)}{t_a} \quad (25.157)$$

For the stress in the adhesive Hooke's law is used:

$$\sigma_i(z) = E_a \varepsilon_i(z) \quad i = 1..2 \quad (25.158)$$

Hence:

$$\sigma_1(x) = \frac{E_a}{t_a} (w_3(z) - w_1(z)) \quad (25.159)$$

$$\sigma_2(x) = -\frac{E_a}{t_a} w_2(z) \quad (25.160)$$

The distributions of $\sigma_1(x)$, $\sigma_2(x)$ and $w_3(z)$ for the constants $t_a = 4\text{mm}$, $E_a = 12800\text{mm}$, $W = 1\text{mm}$, $l_1 = 200\text{mm}$, $l_2 = 500\text{mm}$, $E_1 = 2.1 \cdot 10^5 \text{N/mm}^2$ and $t_1 = 10\text{mm}$, can be found in the next figures:

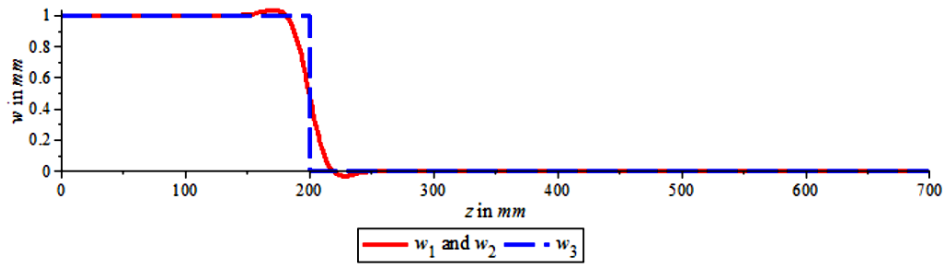


Figure 25.44: Displacements due to uniform translation of the beam

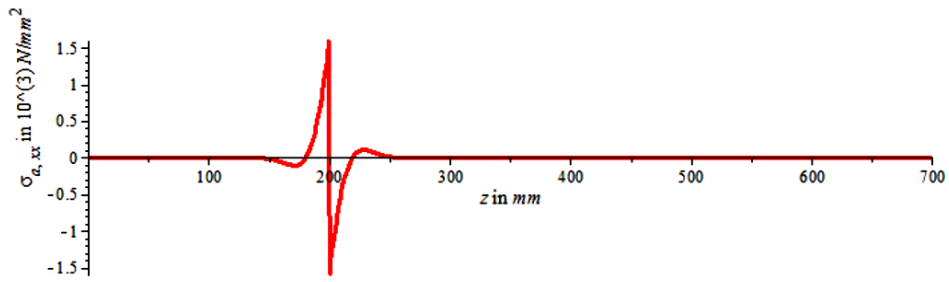


Figure 25.45: Adhesive stress in x-direction due to uniform translation of the beam

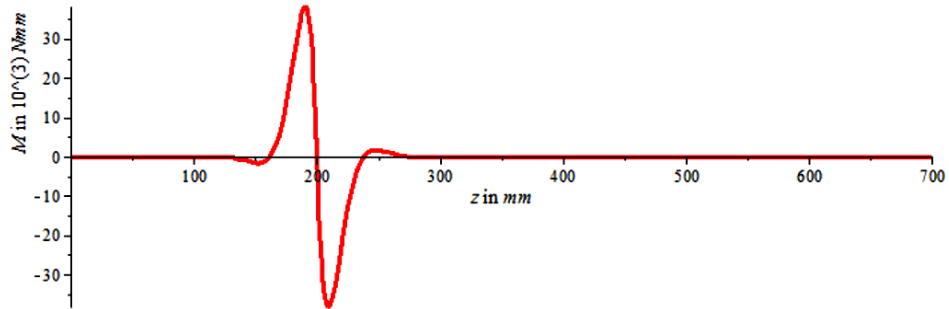


Figure 25.46: Moment due to uniform translation of the beam

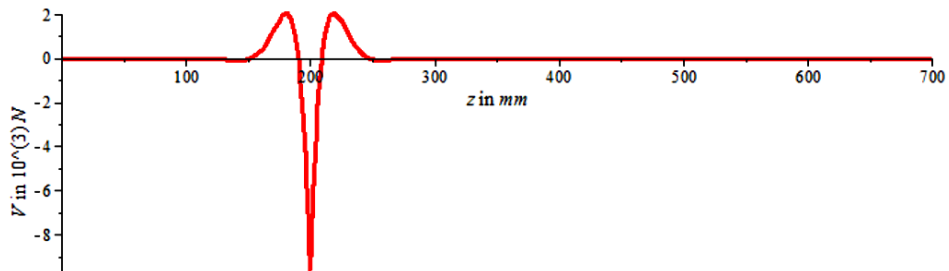


Figure 25.47: Shear force due to uniform translation of the beam

Note that the stress fades out before $x = 2\pi/\beta \approx 54 \text{ mm}$, just as for the latter sections.

26 Appendix J: Design and calculation of bolted double strap

Goal is to design and calculate a double strap connection with a plate with $t_{plate} = 15\text{ mm}$. In the figure below a typical layout for a bolted double strap connection can be found.

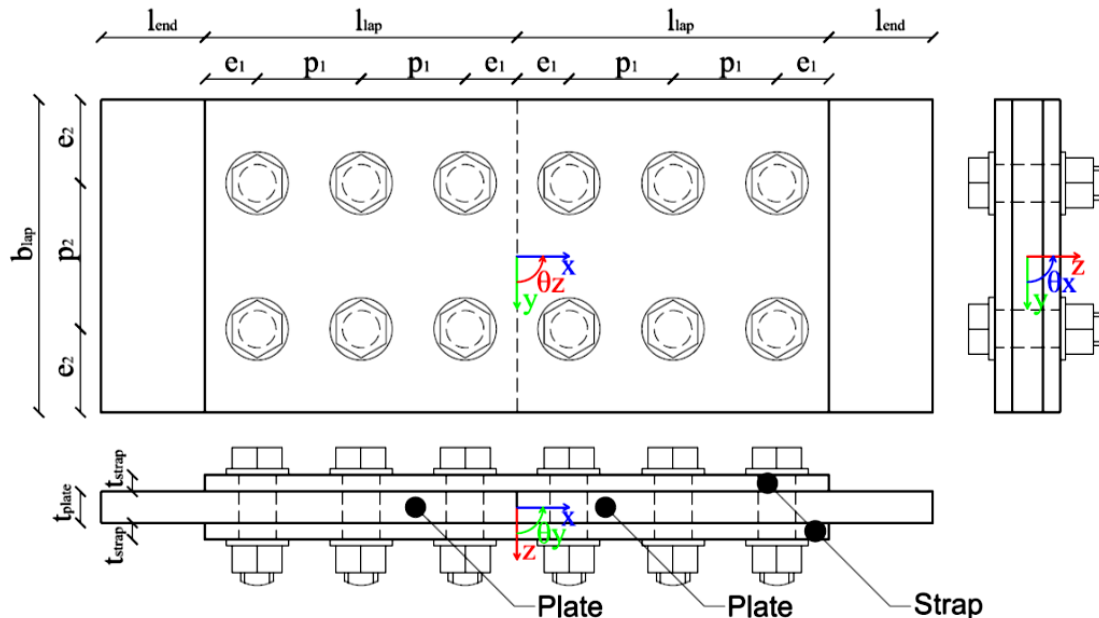


Figure 26.1: Typical bolted double strap connection

26.1 Mechanical properties

For the detail the steel grade S235 and bolt class 8.8 are chosen. The associated mechanical properties can be found in the next two tables:

Bolt class	8.8
f_{yb}	800 N/mm^2
f_{ub}	640 N/mm^2

Table 26.1: Mechanical properties of the bolts [61]

Steel grade	S235
f_y (for $t \leq 40\text{ mm}$)	235 N/mm^2
f_u^* (for $t \leq 40\text{ mm}$)	400 N/mm^2

* according to [61] section 3.6.1 it is allowed to use 400 instead of 360 mentioned in [24] table 3.1

Table 26.2: Mechanical properties of the construction steel [24]

26.2 Measurements

As starting point $t_{plate} = 15\text{ mm}$, which is a standard available plate thickness. For the strap it is obvious to choose an as small as possible standard thickness so that $t_{strap} \geq t_{plate}/2$, which is $t_{strap} = 8\text{ mm}$. The maximum standard available width for hot rolled flat bars is 150mm, which is

chosen for b_{lap} . The value for l_{lap} is chosen to be the same as b_{lap} . The length of l_{end} does not influence the calculation and will be chosen later out of practical reasons.

As starting point for the bolts six M16 bolts are chosen. The nominal clearance of bolt holes is regulated by table 11 of [42]. For normal round holes, M16/M24, the nominal hole diameter is 2mm larger than the nominal bolt diameter.

Type	M16
d_b	16mm
d_0	18mm
$A_{b;s}$	157mm ²

Table 26.3: Overview of measurements of M16

Rules for the position of holes can be found in table 3.3 of [61]. For ordinary construction steel which is not exposed to outside conditions or other corrosive influences the next table applies (see also Figure 26.1):

	Minimal size	Maximum size
e_1	$1.2d_0 = 21.6mm$	-
e_2	$1.2d_0 = 21.6mm$	-
p_1	$2.2d_0 = 39.6mm$	$\min(14t, 200) = 112mm^*$
p_2	$2.4d_0 = 43.2mm$	$\min(14t, 200) = 112mm^*$

*for simplicity for the edge distance of the plate $t = t_{strap}$ is used

Table 26.4: Overview requirements for position of the bolt holes

As starting point the next distances, which meet the requirements of Table 26.4, are used:

e_1	25mm
e_2	40mm
p_1	50mm
p_2	70mm

Table 26.5: Overview of measurements of positioning of the bolts

With the chosen measurements Figure 26.1 becomes:

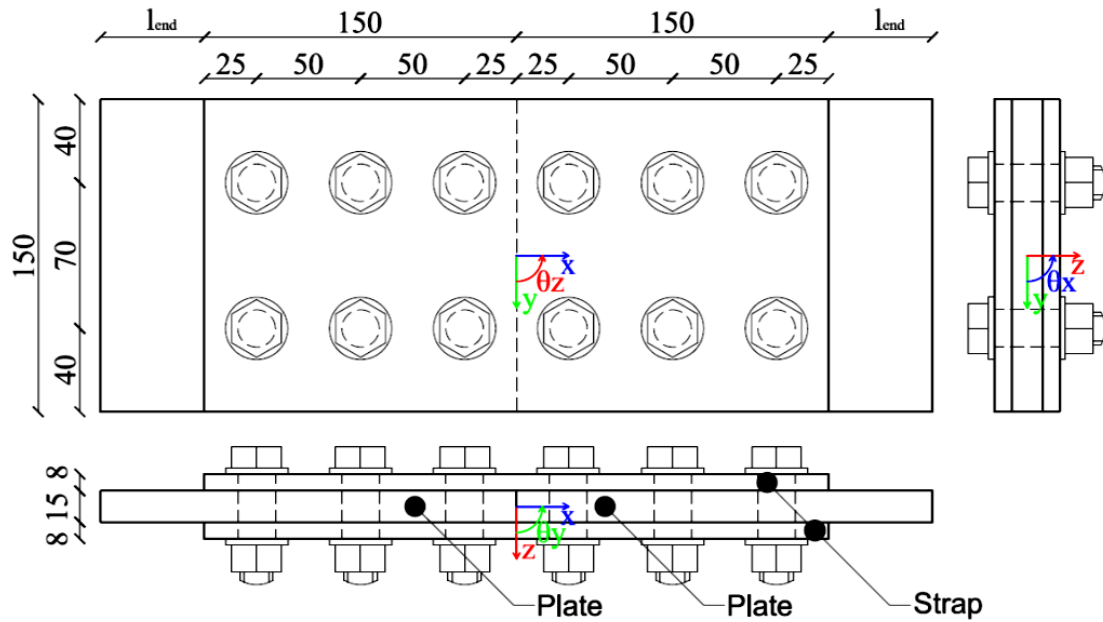


Figure 26.2: Chosen measurements

26.3 Calculation

For the bolted double strap connection depicted in the figure above, four failure modes have to be considered.

1. Yielding of the gross area of the plates/straps
2. Fracture of net area of plates/straps
3. Shear failure of the bolts¹
4. Bearing failure of the plates/straps

Yielding of the gross area of the plate is chosen to be decisive.

26.3.1 Yielding of gross area of plates/straps

For the plates:

$$F_{y,plate,Rd} = b_{lap} t_{plate} f_y = 150 \cdot 15 \cdot 235 = 528.75 \cdot 10^3 \text{ N} \quad (26.1)$$

For the straps:

$$F_{y,strap,Rd} = b_{lap} t_{strap} f_y = 150 \cdot 8 \cdot 235 = 282 \cdot 10^3 \text{ N} \quad (26.2)$$

The yielding of the plate is decisive:

$$F_{y,plate,Rd} \leq 2 \cdot F_{y,splice,Rd} \quad (26.3)$$

26.3.2 Fracture of net area of plates/straps

For centric load connections formula 3.9 of [61] applies:

$$V_{eff,1,Rd} = \frac{f_u A_{nt}}{\gamma_{M2}} + \frac{f_y A_{nv}}{\sqrt{3} \gamma_{M0}} \quad (26.4)$$

According to section 6.1 of [62]:

$$\gamma_{M0} = 1.0 \quad \gamma_{M2} = 1.25 \quad (26.5)$$

¹ Bolts have less deformation capacity than construction steel. To ensure ductile behaviour the failure load due to this type of failure should not be decisive

There are four important failure cases, two for the straps and two for the plates. In the figure below these cases for the right side can be found:

	Case 1	Case 2
Strap		
Plate		

Table 26.6: Failure cases of fracture of net area

For one strap at case 1:

$$A_{nt} = (b_{lap} - 2d_0)t_{strap} \quad (26.6)$$

$$A_{nv} = 0 \quad (26.7)$$

$$V_{eff,1,strap1,Rd} = 2 \left[\frac{f_u A_{nt}}{\gamma_{M2}} + \frac{f_y A_{nv}}{\sqrt{3}\gamma_{M0}} \right] = 583.68 \cdot 10^3 \text{ N} \quad (26.8)$$

For one strap at case 2:

$$A_{nt} = (b_{lap} - 2e_2 - d_0)t_{strap} \quad (26.9)$$

$$A_{nv} = \left(2p_1 + e_1 - \frac{5}{2}d_0 \right)t_{strap} \quad (26.10)$$

$$V_{eff,1,strap2,Rd} = 2 \left[\frac{f_u A_{nt}}{\gamma_{M2}} + \frac{f_y A_{nv}}{\sqrt{3}\gamma_{M0}} \right] = 613.58 \cdot 10^3 \text{ N} \quad (26.11)$$

For the plates at case 1:

$$A_{nt} = (b_{lap} - 2d_0)t_{plate} \quad (26.12)$$

$$A_{nv} = 0 \quad (26.13)$$

$$V_{eff,1,plate1,Rd} = \frac{f_u A_{nt}}{\gamma_{M2}} + \frac{f_y A_{nv}}{\sqrt{3}\gamma_{M0}} = 547.20 \cdot 10^3 \text{ N} \quad (26.14)$$

For the plates at case 2:

$$A_{nt} = (b_{lap} - 2e_2 - d_0)t_{plate} \quad (26.15)$$

$$A_{nv} = \left(2p_1 + e_1 - \frac{5}{2}d_0\right)t_{plate} \quad (26.16)$$

$$V_{eff,1,plate2,Rd} = \frac{f_u A_{nt}}{\gamma_{M2}} + \frac{f_y A_{nv}}{\sqrt{3}\gamma_{M0}} = 575.23 \cdot 10^3 \text{ N} \quad (26.17)$$

As mentioned the yielding of the gross section is chosen to be decisive, hence:

$$\frac{F_{y,plate,Rd}}{\min(V_{eff,1,strap1,Rd}, V_{eff,1,strap2,Rd}, V_{eff,1,plate1,Rd}, V_{eff,1,plate2,Rd})} = 0.97 < 1 \quad (26.18)$$

26.3.3 Shear failure of the bolts

Table 3.4 NEN-en 1993

$$F_{v,Rd} = \frac{\alpha_v f_{ub} A_s}{\gamma_{M2}} \quad (26.19)$$

If the shear plane goes through the thread of the bolt, with the chosen bolt class:

$$\alpha_v = 0.6 \quad (26.20)$$

Hence:

$$F_{v,Rd} = \frac{\alpha_v f_{ub} A_s}{\gamma_{M2}} = 60.29 \cdot 10^3 \text{ N} \quad (26.21)$$

Due to shear lag, the shear resistance of the bolts in long connections have to be reduced (see section 3.8 of [61]). This is the case if the length between the outer bolts in the direction of the load is more than $15d_b$, which is not the case for Figure 26.2:

$$2p_1 = 100 < 15d_b = 240 \quad (26.22)$$

According to section 3.78 of [61] the total resistance is equal to the sum of all shear planes if:

$$F_{v,RD} \geq F_{b,RD} \quad (26.23)$$

There are two shear planes per bolt. So the total resistance is:

$$F_{v,total,Rd} = 2 \cdot n_{bolts} \cdot \frac{\alpha_v f_{ub} A_s}{\gamma_{M2}} = 723.46 \cdot 10^3 \text{ N} \quad (26.24)$$

As mentioned the yielding of the gross section is chosen to be decisive, hence:

$$\frac{F_{y,plate,Rd}}{F_{v,total,Rd}} = 0.73 < 1 \quad (26.25)$$

26.3.4 Bearing failure of plates/straps

According to table 3.4 of [61]:

$$F_{b,Rd} = \frac{k_1 \alpha_b f_u d_b t}{\gamma_{M2}} \quad (26.26)$$

Where:

$$\alpha_b = \min\left(\alpha_d, \frac{f_{ub}}{f_u}, 1\right) \quad (26.27)$$

For bolts at the ends in the direction of the load transfer:

$$\alpha_{d,end} = \frac{e_1}{3d_0} \quad (26.28)$$

For inner bolts in the direction of the load transfer:

$$\alpha_{d,inner} = \frac{p_1}{3d_0} - \frac{1}{4} \quad (26.29)$$

Hence:

$$\alpha_b = \min\left(\frac{e_1}{3d_0}, \frac{p_1}{3d_0} - \frac{1}{4}, \frac{f_{ub}}{f_u}, 1\right) = 0.46 \quad (26.30)$$

For bolts at the edges perpendicular to the direction of the load transfer:

$$k_{1,edge} = \min\left(2.8 \frac{e_2}{d_0} - 1.7, 2.5\right) \quad (26.31)$$

For inner bolts perpendicular to the direction of the load transfer:

$$k_{1,inner} = \min\left(1.4 \frac{p_2}{d_0} - 1.7, 2.5\right) \quad (26.32)$$

Hence:

$$k_1 = \min\left(2.8 \frac{e_2}{d_0} - 1.7, 1.4 \frac{p_2}{d_0} - 1.7, 2.5\right) = 2.5 \quad (26.33)$$

For the plates:

$$F_{b,plate,Rd} = \frac{k_1 \alpha_b f_u d_b t_{plate}}{\gamma_{M2}} = 88.89 \cdot 10^3 \text{ N} \quad (26.34)$$

For the straps:

$$F_{b,strap,Rd} = \frac{k_1 \alpha_b f_u d_b t_{strap}}{\gamma_{M2}} = 47.41 \cdot 10^3 \text{ N} \quad (26.35)$$

According to section 3.7 of [61] the total resistance of the group of bolts is equal to the sum of $F_{b,Rd}$ if for all bolts the next conditions are true:

$$F_{b,Rd} < F_{v,Rd} \quad (26.36)$$

The plates have two shear planes per bolt, hence:

$$F_{b,plate,Rd} = 88.89 \cdot 10^3 \text{ N} < 2 \cdot F_{v,Rd} = 120.58 \cdot 10^3 \text{ N} \quad (26.37)$$

For the strap:

$$F_{b,strap,Rd} = 47.41 \cdot 10^3 \text{ N} < F_{v,Rd} = 60.29 \cdot 10^3 \text{ N} \quad (26.38)$$

Both conditions are met. The total resistance is now allowed to be calculated as the sum of bearing failure per bolt:

$$F_{b,plate,total,Rd} = n_{bolts} \cdot F_{b,plate,Rd} = 533.33 \cdot 10^3 \text{ N} \quad (26.39)$$

$$F_{b,strap,total,Rd} = 2 \cdot n_{bolts} \cdot F_{b,strap,Rd} = 568.89 \cdot 10^3 \text{ N} \quad (26.40)$$

As mentioned the yielding of the gross section is chosen to be decisive, hence:

$$\frac{F_{y,plate,Rd}}{\min(F_{b,plate,total,Rd}, F_{b,strap,total,Rd})} = 0.99 < 1 \quad (26.41)$$

27 Appendix K: Double strap according to Volkersen

Due to symmetry, only a quarter of the double strap has to be considered. The theory of Volkersen only accounts for axial deformation in longitudinal direction of the steel elements and the shear deformation of the adhesive. According to Volkersen the double lap connection is as the following figure:

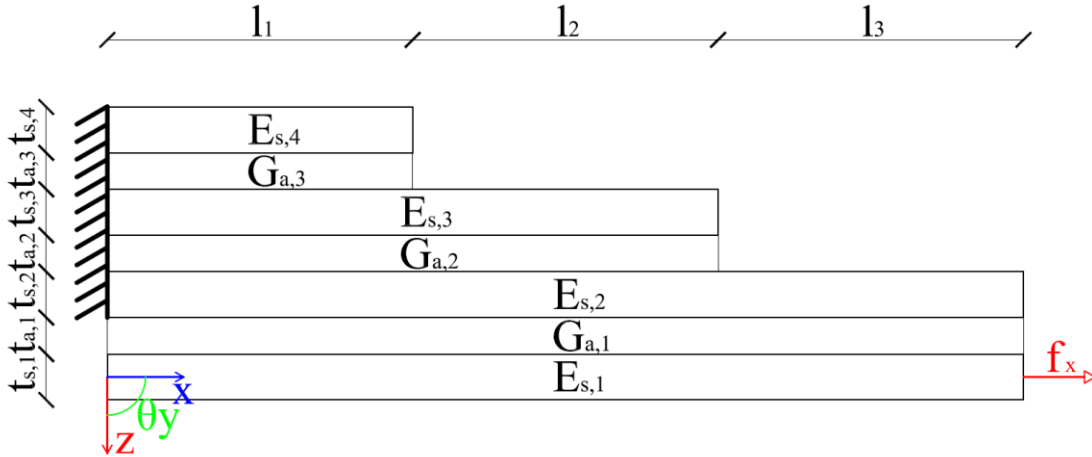


Figure 27.1: Double strap connection according to Volkersen

Due to axial deformation of the steel elements the adhesive will be loaded in shear:

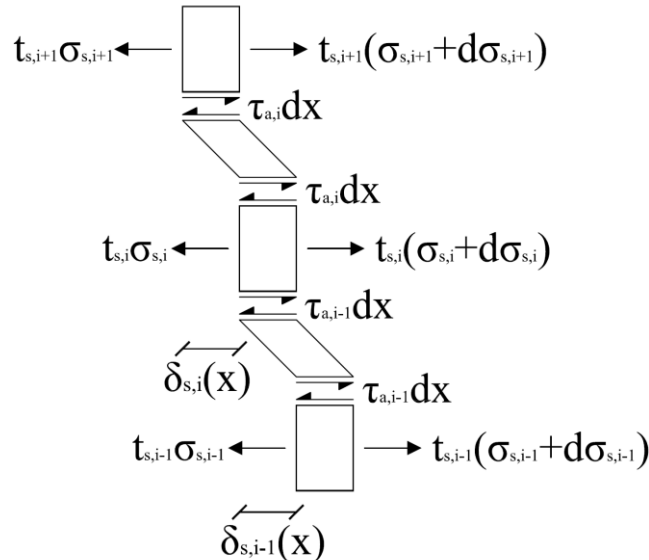


Figure 27.2: Section of displaced unit width according to Volkersen

The constitutive relation (Hooke's law) for the shear of the adhesive is:

$$\tau_{a,i}(x) = G_{a,i} \gamma_{a,i}(x) \quad (27.1)$$

The shear strain is given by the kinematic relation:

$$\gamma_{a,i}(x) = \delta_{s,i}(x) / t_{a,i} \quad (27.2)$$

Where the relative displacement for a unit width of the adherent is given by:

$$\delta_{s,i}(x) = u_{s,i}(x) - u_{s,i+1}(x) \quad (27.3)$$

Combining the latter three equations gives:

$$\tau_{a,i}(x) = \frac{G_{a,i}}{t_{a,i}} \{u_{s,i}(x) - u_{s,i+1}(x)\} \quad (27.4)$$

The constitutive relation (Hooke's law) for the adherents is:

$$\sigma_{s,i}(x) = E_{s,i} \varepsilon_{s,i}(x) \quad (27.5)$$

The kinematic relation for the adherents is:

$$\varepsilon_{s,i}(x) = \frac{du_{s,i}(x)}{dx} \quad (27.6)$$

Combining the latter two equations gives:

$$\sigma_{s,i}(x) = E_{s,i} \frac{du_{s,i}(x)}{dx} \quad (27.7)$$

From the equilibrium of a unit width the next equation follows:

$$t_{s,i} \frac{d\sigma_i(x)}{dx} - \tau_{a,i}(x) + \tau_{a,i-1}(x) = 0 \quad (27.8)$$

For the detail which will be investigated the next conditions apply:

$$G_{a,3} = G_{a,2} = G_{a,1} = G_a = 4273 \text{ N/mm}^2 \quad (27.9)$$

$$E_{s,1} = E_{s,2} = E_{s,3} = E_{s,4} = E_s = 2.1 \cdot 10^5 \text{ N/mm}^2 \quad (27.10)$$

$$t_{s,1} = 7.5 \text{ mm} \quad (27.11)$$

$$t_{s,4} = t_{s,3} = t_{s,2} = 3 \text{ mm} \quad (27.12)$$

$$t_{a,1} = 1.7 \text{ mm} \quad (27.13)$$

$$t_{a,3} = t_{a,2} = 1 \text{ mm} \quad (27.14)$$

$$f_y = 235 \text{ N/mm}^2 \quad (27.15)$$

$$f_x = f_y t_{s,1} = 1762,5 \text{ N/mm} \quad (27.16)$$

$$l_1 = l_2 = l_3 = 100 \text{ mm} \quad (27.17)$$

Due to the three different lengths of the straps and adhesive the system should be solved with the Heaviside function or in three steps which are related to each other by the boundary conditions. The last option is used.

27.1 General solution for $0 \leq x \leq l_1$

For the detail which will be investigated for the region $0 \leq x \leq l_1$, equation (27.8) with (27.4) and (27.7) should be developed for $n = 1 \dots 4$ ($\tau_{a,4}(x) = 0$):

$$\frac{d^2 u_{s,1}(x)}{dx^2} - \frac{G_a}{E_s t_{s,1} t_{a,1}} u_{s,1}(x) + \frac{G_a}{E_s t_{s,1} t_{a,1}} u_{s,2}(x) = 0 \quad (27.18)$$

$$\frac{d^2 u_{s,2}(x)}{dx^2} + \frac{G_a}{E_s t_{s,2} t_{a,1}} u_{s,1}(x) - \frac{G_a (t_{a,1} + t_{a,2})}{E_s t_{s,2} t_{a,1} t_{a,2}} u_{s,2}(x) + \frac{G_a}{E_s t_{s,2} t_{a,2}} u_{s,3}(x) = 0 \quad (27.19)$$

$$\frac{d^2 u_{s,3}(x)}{dx^2} + \frac{G_a}{E_s t_{s,2} t_{a,2}} u_{s,2}(x) - \frac{2G_a}{E_s t_{s,2} t_{a,2}} u_{s,3}(x) + \frac{G_a}{E_s t_{s,2} t_{a,2}} u_{s,4}(x) = 0 \quad (27.20)$$

$$\frac{d^2 u_{s,4}(x)}{dx^2} + \frac{G_a}{E_s t_{s,2} t_{a,2}} u_{s,3}(x) - \frac{G_a}{E_s t_{s,2} t_{a,2}} u_{s,4}(x) = 0 \quad (27.21)$$

The system of (27.18)/(27.21) can be solved in several different ways. One possible way is to express all $u_{s,i}(x)$'s in $u_{s,4}(x)$.

With (27.18), $u_{s,2}(x)$ can be expressed in $u_{s,1}(x)$:

$$u_{s,2}(x) = \left[u_{s,1}(x) \quad \frac{d^2 u_{s,1}(x)}{dx^2} \right] \begin{bmatrix} 1 \\ -\frac{E_s}{G_a} t_{s,1} t_{a,1} \end{bmatrix} \quad (27.22)$$

With (27.19) and (27.22), $u_{s,3}(x)$ can be expressed in $u_{s,1}(x)$:

$$u_{s,3}(x) = \left[u_{s,1}(x) \quad \frac{d^2 u_{s,1}(x)}{dx^2} \quad \frac{d^4 u_{s,1}(x)}{dx^4} \right] \begin{bmatrix} 1 \\ -\frac{E_s}{G_a} (t_{s,1} (t_{a,1} + t_{a,2}) + t_{s,2} t_{a,2}) \\ \frac{E_s^2}{G_a^2} t_{s,1} t_{s,2} t_{a,1} t_{a,2} \end{bmatrix} \quad (27.23)$$

With (27.20) and (27.23), $u_{s,4}(x)$ can be expressed in $u_{s,1}(x)$:

$$u_{s,4}(x) = \left[u_{s,1}(x) \quad \frac{d^2 u_{s,1}(x)}{dx^2} \quad \frac{d^4 u_{s,1}(x)}{dx^4} \quad \frac{d^6 u_{s,1}(x)}{dx^6} \right] \begin{bmatrix} 1 \\ -\frac{E_s}{G_a} (t_{s,1} (t_{a,1} + 2t_{a,2}) + 3t_{s,2} t_{a,2}) \\ \frac{E_s^2}{G_a^2} t_{s,2} t_{a,2} (3t_{s,1} t_{a,1} + t_{s,1} t_{a,2} + t_{s,2} t_{a,2}) \\ -\frac{E_s^3}{G_a^3} t_{s,1} t_{s,2}^2 t_{a,1} t_{a,2}^2 \end{bmatrix} \quad (27.24)$$

With (27.23) and (27.24), (27.21) becomes:

$$\left[\frac{d^2 u_{s,1}(x)}{dx^2} \quad \frac{d^4 u_{s,1}(x)}{dx^4} \quad \frac{d^6 u_{s,1}(x)}{dx^6} \quad \frac{d^8 u_{s,1}(x)}{dx^8} \right] \begin{bmatrix} E_s (t_{s,1} + 3t_{s,2}) \\ -\frac{E_s^2}{G_a} t_{s,2} (3t_{s,1} (t_{a,1} + t_{a,2}) + 4t_{s,2} t_{a,2}) \\ \frac{E_s^3}{G_a^2} t_{s,2}^2 t_{a,2} (t_{s,1} (4t_{a,1} + t_{a,2}) + t_{s,2} t_{a,2}) \\ -\frac{E_s^4}{G_a^3} t_{s,1} t_{s,2}^3 t_{a,1} t_{a,2}^2 \end{bmatrix} = 0 \quad (27.25)$$

The most easy way to find the solution of (27.25) is by substituting $u_{s,1}(x) = Ce^{\omega x}$ and divide by $Ce^{\omega x}$ in (27.25):

$$\begin{bmatrix} \omega^2 & \omega^4 & \omega^6 & \omega^8 \end{bmatrix} \begin{bmatrix} E_s (t_{s,1} + 3t_{s,2}) \\ -\frac{E_s^2}{G_a} t_{s,2} (3t_{s,1} (t_{a,1} + t_{a,2}) + 4t_{s,2} t_{a,2}) \\ \frac{E_s^3}{G_a^2} t_{s,2}^2 t_{a,2} (t_{s,1} (4t_{a,1} + t_{a,2}) + t_{s,2} t_{a,2}) \\ -\frac{E_s^4}{G_a^3} t_{s,1} t_{s,2}^3 t_{a,1} t_{a,2}^2 \end{bmatrix} = 0 \quad (27.26)$$

The solution of (27.25) is:

$$u_{s,1}(x) = \sum_{i=1}^8 C_i e^{\omega_i x} \quad (27.27)$$

Where ω_i are the roots of (27.26). The first two roots of (27.26) are easy to find because each term consists of a multiplication of ω^2 , hence:

$$\omega_1 = \omega_2 = 0 \quad (27.28)$$

The other roots are more difficult to find symbolically¹, moreover the expressions for the roots will be large. Therefore they are numerically solved with the computer and the constants of (27.9)/(27.16):

$$\begin{bmatrix} \omega_1 \\ \omega_2 \\ \omega_3 \\ \omega_4 \\ \omega_5 \\ \omega_6 \\ \omega_7 \\ \omega_8 \end{bmatrix} = \begin{bmatrix} 0 \\ 0 \\ 0.04485184658 \\ -0.04485184658 \\ 0.09715389089 \\ -0.09715389089 \\ 0.1458259682 \\ -0.1458259682 \end{bmatrix} \quad (27.29)$$

Because $\omega_1 = \omega_2$, C_1 or C_2 should be multiplied by x:

$$u_{s,1}(x) = xC_1e^{\omega_1x} + \sum_{i=2}^8 C_i e^{\omega_i x} \quad (27.30)$$

27.2 General solution for $l_1 \leq x \leq l_1 + l_2$

For the region $l_1 \leq x \leq l_1 + l_2$, equation (27.8) with (27.4) and (27.7) should be developed for $n = 1 \dots 3$ ($\tau_{a,3}(x) = 0$). All expressions which depend on x are given a hat to distinguish between those of the other regions.

$$\frac{d^2 \hat{u}_{s,1}(x)}{dx^2} - \frac{G_a}{E_s t_{s,1} t_{a,1}} \hat{u}_{s,1}(x) + \frac{G_a}{E_s t_{s,1} t_{a,1}} \hat{u}_{s,2}(x) = 0 \quad (27.31)$$

$$\frac{d^2 \hat{u}_{s,2}(x)}{dx^2} + \frac{G_a}{E_s t_{s,2} t_{a,1}} \hat{u}_{s,1}(x) - \frac{G_a(t_{a,1} + t_{a,2})}{E_s t_{s,2} t_{a,1} t_{a,2}} \hat{u}_{s,2}(x) + \frac{G_a}{E_s t_{s,2} t_{a,2}} \hat{u}_{s,3}(x) = 0 \quad (27.32)$$

$$\frac{d^2 \hat{u}_{s,3}(x)}{dx^2} + \frac{G_a}{E_s t_{s,2} t_{a,2}} \hat{u}_{s,2}(x) - \frac{G_a}{E_s t_{s,2} t_{a,2}} \hat{u}_{s,3}(x) = 0 \quad (27.33)$$

With (27.31), $\hat{u}_{s,2}(x)$ can be expressed in $\hat{u}_{s,1}(x)$:

$$\hat{u}_{s,2}(x) = \left[\hat{u}_{s,1}(x) \quad \frac{d^2 \hat{u}_{s,1}(x)}{dx^2} \right] \begin{bmatrix} 1 \\ -\frac{E_s}{G_a} t_{a,1} t_{s,1} \end{bmatrix} \quad (27.34)$$

With (27.32) and (27.34), $\hat{u}_{s,3}(x)$ can be expressed in $\hat{u}_{s,1}(x)$:

¹ Cardano's formula can be used to solve the roots of a third order polynomial analytically

$$\hat{u}_{s,3}(x) = \begin{bmatrix} \hat{u}_{s,1}(x) & \frac{d^2 \hat{u}_{s,1}(x)}{dx^2} & \frac{d^4 \hat{u}_{s,1}(x)}{dx^4} \end{bmatrix} \begin{bmatrix} 1 \\ -\frac{E_s}{G_a} (t_{s,1}(t_{a,1} + t_{a,2}) + t_{s,2}t_{a,2}) \\ \frac{E_s^2}{G_a^2} t_{s,1}t_{s,2}t_{a,1}t_{a,2} \end{bmatrix} \quad (27.35)$$

With (27.34) and (27.35), (27.33) becomes:

$$\begin{bmatrix} \frac{d^2 \hat{u}_{s,1}(x)}{dx^2} & \frac{d^4 \hat{u}_{s,1}(x)}{dx^4} & \frac{d^6 \hat{u}_{s,1}(x)}{dx^6} \end{bmatrix} \begin{bmatrix} E_s(t_{s,1} + 2t_{s,2}) \\ -\frac{E_s^2}{G_a} t_{s,2}(t_{s,1}(2t_{a,1} + t_{a,2}) + t_{s,2}t_{a,2}) \\ \frac{E_s^3}{G_a^2} t_{s,1}t_{s,2}^2 t_{a,1}t_{a,2} \end{bmatrix} = 0 \quad (27.36)$$

Substituting $\hat{u}_{s,1}(x) = Ce^{\omega x}$ and divide by $Ce^{\omega x}$ equation (27.36) gives:

$$\begin{bmatrix} \omega^2 & \omega^4 & \omega^6 \end{bmatrix} \begin{bmatrix} E_s(t_{s,1} + 2t_{s,2}) \\ -\frac{E_s^2}{G_a} t_{s,2}(t_{s,1}(2t_{a,1} + t_{a,2}) + t_{s,2}t_{a,2}) \\ \frac{E_s^3}{G_a^2} t_{s,1}t_{s,2}^2 t_{a,1}t_{a,2} \end{bmatrix} = 0 \quad (27.37)$$

The solution of (27.37) is:

$$\hat{u}_{s,1}(x) = \sum_{i=9}^{14} C_i e^{\omega_i x} \quad (27.38)$$

Where ω_i are the roots of (27.37). The first two roots of (27.37) are easy to find because each term consists of a multiplication of ω^2 , hence:

$$\omega_9 = \omega_{10} = 0 \quad (27.39)$$

The other roots can be found by dividing (27.37) by ω^2 , substituting $\omega^2 = r$, solve the equation with the quadratic equation and substituting $\omega = \pm\sqrt{r}$.

$$\begin{bmatrix} \omega_{11} \\ \omega_{12} \\ \omega_{13} \\ \omega_{14} \end{bmatrix} = \begin{bmatrix} \sqrt{\hat{\omega} + \sqrt{\tilde{\omega}}} \\ -\sqrt{\hat{\omega} + \sqrt{\tilde{\omega}}} \\ \sqrt{\hat{\omega} - \sqrt{\tilde{\omega}}} \\ -\sqrt{\hat{\omega} - \sqrt{\tilde{\omega}}} \end{bmatrix} \quad \text{with} \quad \begin{cases} \hat{\omega} = \frac{G_a}{E_s} \frac{(t_{s,1}(2t_{a,1} + t_{a,2}) + t_{s,2}t_{a,2})}{2t_{s,1}t_{s,2}t_{a,1}t_{a,2}} \\ \tilde{\omega} = \hat{\omega}^2 - \frac{G_a^2}{E_s^2} \frac{(t_{s,1} + 2t_{s,2})}{t_{s,1}t_{s,2}^2 t_{a,1}t_{a,2}} \end{cases} \quad (27.40)$$

With (27.9)/(27.16) the numerical value of the roots are:

$$\begin{bmatrix} \omega_9 \\ \omega_{10} \\ \omega_{11} \\ \omega_{12} \\ \omega_{13} \\ \omega_{14} \end{bmatrix} = \begin{bmatrix} 0 \\ 0 \\ 0.1270084415 \\ -0.1270084415 \\ 0.05495048733 \\ -0.05495048733 \end{bmatrix} \quad (27.41)$$

Because $\omega_9 = \omega_{10}$, C_9 or C_{10} should be multiplied by x:

$$\hat{u}_{s,1}(x) = xC_9e^{\omega_9x} + \sum_{i=10}^{15} C_i e^{\omega_i x} \quad (27.42)$$

27.3 General solution for $l_1+l_2 \leq x \leq l_1+l_2+l_3$

For the region $l_1 + l_2 \leq x \leq l_1 + l_2 + l_3$, equation (27.8) with (27.4) and (27.7) should be developed for $n=1..2$ (with $\tau_{a,2}(x) = 0$). All expressions which depend on x are given a tilde to distinguish between those of the other regions.

$$\frac{d^2 \tilde{u}_{s,1}(x)}{dx^2} - \frac{G_a}{E_s t_{s,1} t_{a,1}} \tilde{u}_{s,1}(x) + \frac{G_a}{E_s t_{s,1} t_{a,1}} \tilde{u}_{s,2}(x) = 0 \quad (27.43)$$

$$\frac{d^2 \tilde{u}_{s,2}(x)}{dx^2} + \frac{G_a}{E_s t_{s,2} t_{a,1}} \tilde{u}_{s,1}(x) - \frac{G_a}{E_s t_{s,2} t_{a,1}} \tilde{u}_{s,2}(x) = 0 \quad (27.44)$$

With (27.43), $\tilde{u}_{s,2}(x)$ can be expressed in $\tilde{u}_{s,1}(x)$:

$$\tilde{u}_{s,2}(x) = \left[\tilde{u}_{s,1}(x) \quad \frac{d^2 \tilde{u}_{s,1}(x)}{dx^2} \right] \begin{bmatrix} 1 \\ -\frac{E_s}{G_a} t_{s,1} t_{a,1} \end{bmatrix} \quad (27.45)$$

With (27.45), (27.44) becomes:

$$\left[\frac{d^2 \tilde{u}_{s,1}(x)}{dx^2} \quad \frac{d^4 \tilde{u}_{s,1}(x)}{dx^4} \right] \begin{bmatrix} E_s (t_{s,1} + t_{s,2}) \\ -\frac{E_s^2}{G_a} t_{s,1} t_{s,2} t_{a,1} \end{bmatrix} = 0 \quad (27.46)$$

Substituting $\hat{u}_{s,1}(x) = Ce^{\hat{\omega}x}$ and divide by $Ce^{\hat{\omega}x}$ equation (27.46) gives:

$$\begin{bmatrix} \omega^2 & \omega^4 \end{bmatrix} \begin{bmatrix} E_s (t_{s,1} + t_{s,2}) \\ -\frac{E_s^2}{G_a} t_{s,1} t_{s,2} t_{a,1} \end{bmatrix} = 0 \quad (27.47)$$

The solution of (27.47) is:

$$\hat{u}_{s,1}(x) = \sum_{i=15}^{18} C_i e^{\omega_i x} \quad (27.48)$$

Where ω_i are the roots of (27.48). The first two roots of (27.48) are easy to find because each term consists of a multiplication of ω^2 , hence:

$$\omega_{15} = \omega_{16} = 0 \quad (27.49)$$

The other roots can be found by dividing (27.37) by ω^2 , substituting $\omega^2 = r$ and solve the equation with the quadratic equation.

$$\omega^2 = \frac{G_a(t_{s,1} + 2t_{s,2})}{E_s t_{s,1} t_{s,2} t_{a,1}} \rightarrow \begin{cases} \omega_{17} = \sqrt{\frac{G_a(t_{s,1} + t_{s,2})}{E_s t_{s,1} t_{s,2} t_{a,1}}} \\ \omega_{18} = -\sqrt{\frac{G_a(t_{s,1} + t_{s,2})}{E_s t_{s,1} t_{s,2} t_{a,1}}} \end{cases} \quad (27.50)$$

With (27.9)/(27.16) the numerical value of the roots are:

$$[\omega_{15} \quad \omega_{16} \quad \omega_{17} \quad \omega_{18}] \begin{bmatrix} 0 \\ 0 \\ 0.07473701168 \\ -0.07473701168 \end{bmatrix} \quad (27.51)$$

Because $\omega_{15} = \omega_{16}$, C_{15} or C_{16} should be multiplied by x:

$$\hat{u}_{s,1}(x) = x C_{14} e^{\omega_{14} x} + \sum_{i=15}^{18} C_i e^{\omega_i x} \quad (27.52)$$

27.4 Boundary and matching conditions

For the system the next eighteen conditions apply:

$$t_{s,1} \tilde{\sigma}_{s,1}(0) = 0 \quad (27.53)$$

$$u_{s,1}(l_1) = \hat{u}_{s,1}(l_1) \quad (27.54)$$

$$\sigma_{s,1}(l_1) = \hat{\sigma}_{s,1}(l_1) \quad (27.55)$$

$$\hat{u}_{s,1}(l_1 + l_2) = \tilde{u}_{s,1}(l_1 + l_2) \quad (27.56)$$

$$\hat{\sigma}_{s,1}(l_1 + l_2) = \tilde{\sigma}_{s,1}(l_1 + l_2) \quad (27.57)$$

$$t_{s,1} \tilde{\sigma}_{s,1}(l_1 + l_2 + l_3) = F \quad (27.58)$$

$$u_{s,2}(0) = 0 \quad (27.59)$$

$$u_{s,2}(l_1) = \hat{u}_{s,2}(l_1) \quad (27.60)$$

$$\sigma_{s,2}(l_1) = \hat{\sigma}_{s,2}(l_1) \quad (27.61)$$

$$\hat{u}_{s,2}(l_1 + l_2) = \tilde{u}_{s,2}(l_1 + l_2) \quad (27.62)$$

$$\hat{\sigma}_{s,2}(l_1 + l_2) = \tilde{\sigma}_{s,2}(l_1 + l_2) \quad (27.63)$$

$$t_{s,2} \tilde{\sigma}_{s,2}(l_1 + l_2 + l_3) = 0 \quad (27.64)$$

$$u_{s,3}(0) = 0 \quad (27.65)$$

$$u_{s,3}(l_1) = \hat{u}_{s,3}(l_1) \quad (27.66)$$

$$\sigma_{s,3}(l_1) = \hat{\sigma}_{s,3}(l_1) \quad (27.67)$$

$$t_{s,3} \tilde{\sigma}_{s,3}(l_1 + l_2) = 0 \quad (27.68)$$

$$u_{s,4}(0) = 0 \quad (27.69)$$

$$t_{s,4} \tilde{\sigma}_{s,4}(l_1 + l_2) = 0 \quad (27.70)$$

27.5 Solving the constants

With (27.7), (27.9)/(27.17), (27.22)/(27.24), (27.29)/(27.30), (27.34)/(27.35), (27.41)/(27.42), (27.45), and (27.51)/(27.70) the unknown constants can be solved. The symbolic expression for the constants are large, therefore only the numerical values will be presented:

$$\begin{matrix} C_1 \\ C_2 \\ C_3 \\ C_4 \\ C_5 \\ C_6 \\ C_7 \\ C_8 \\ C_9 \end{matrix} = \begin{bmatrix} 0.0005086580088 \\ 0.008355572484 \\ 0.00003145394259 \\ 0.008889385210 \\ -3.728308918 \cdot 10^{-8} \\ 0.001025371096 \\ 4.114566851 \cdot 10^{-11} \\ 0.00008051396414 \\ 0.0006216931217 \end{bmatrix} \quad \begin{matrix} C_{10} \\ C_{11} \\ C_{12} \\ C_{13} \\ C_{14} \\ C_{15} \\ C_{16} \\ C_{17} \\ C_{18} \end{matrix} = \begin{bmatrix} -0.001388381250 \\ -3.671189786 \cdot 10^{-15} \\ -13.81847832 \\ 5.545297762 \cdot 10^{-8} \\ 0.2020697677 \\ 0.0007993197279 \\ -0.03465605848 \\ 7.832851886 \cdot 10^{-13} \\ 1971.937824 \end{bmatrix} \quad (27.71)$$

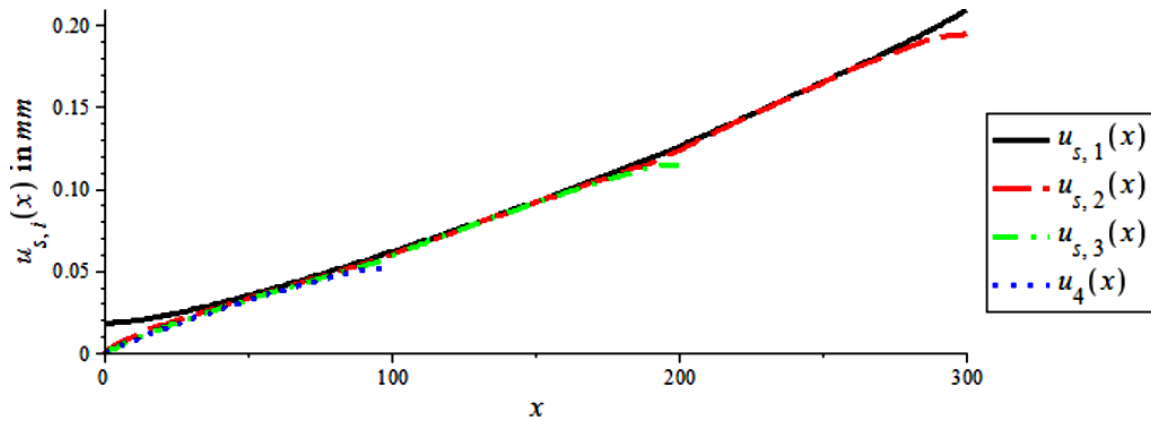


Figure 27.3: Displacement in x-direction of the steel elements

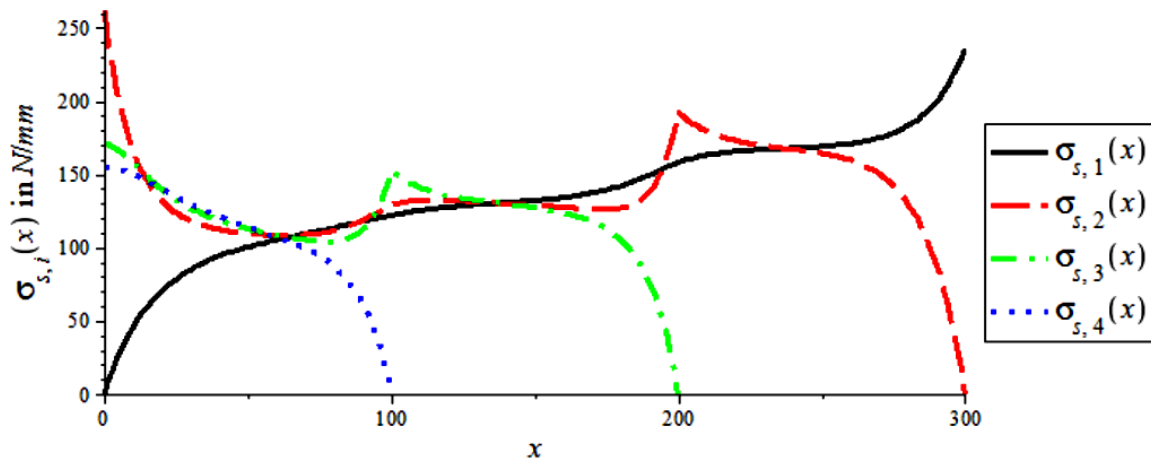


Figure 27.4: Axial stress in x-direction of the steel elements

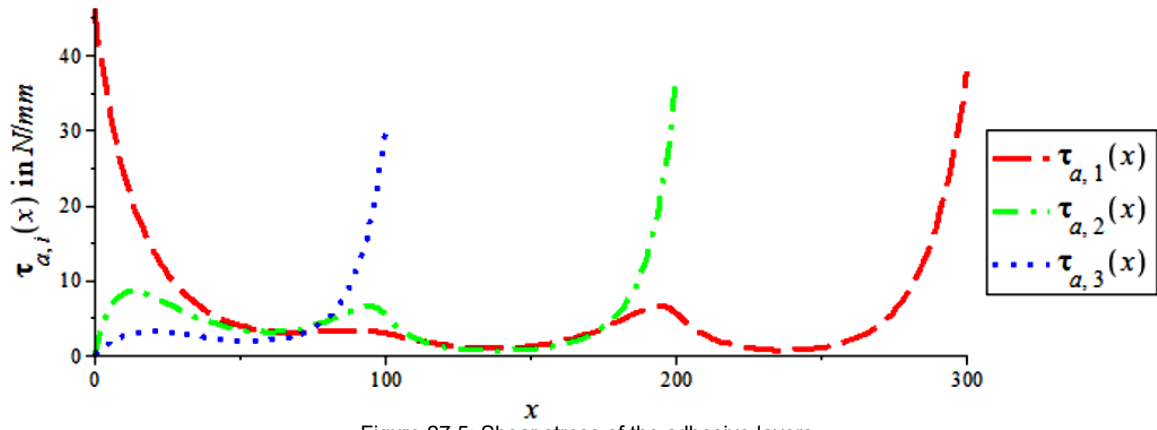


Figure 27.5: Shear stress of the adhesive layers

28 Appendix L: DIANA procedure for double strap connection model

For the double strap, the same DIANA procedure is used as for the entire L-connection, see 'Appendix G: DIANA procedure for entire L-connection model'. However other parameters are used. In this section these parameters are presented.

28.1 Input

For this thesis FX+ for DIANA version 3.1.0 is used to create the input file TNO DIANA version 9.4.4.

28.1.1 Solids

The geometry of the double lap connection is straightforward, the entire connection can be modelled with several rectangular cuboids. The division into the solids is obvious. In x-direction the division is imposed by the end of the laps, in y-direction no division is needed and in z-direction the division is imposed by the material change.

If the nodes of the plate at $x=0$ are the same as those of the adhesive, the plate is automatically restrained in x-direction, because the adhesive nodes are. Therefore the nodes at the corner of the plate are not restrained in x-direction. To reduce this model error smaller solids of 1mm length, instead of 3mm length, are applied.

For several models a butt connection is applied. This butt connection makes use of the same solids 1mm length solids as described above. But for the butt connection this 1mm of the steel plate is changed into adhesive and all the nodes are shared. All the nodes at $x=0$ are restrained in x-direction for the butt connection models.

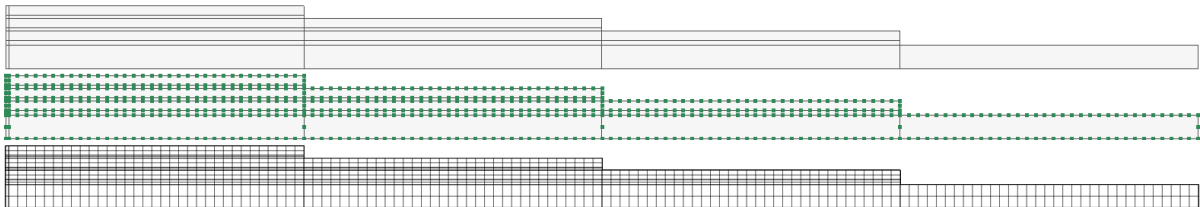


Figure 28.1: Solid, seed and FEM division of double strap

For several models the lap length is 25mm or 50mm longer. To achieve those longer lap lengths, extra solids of 25mm are inserted.

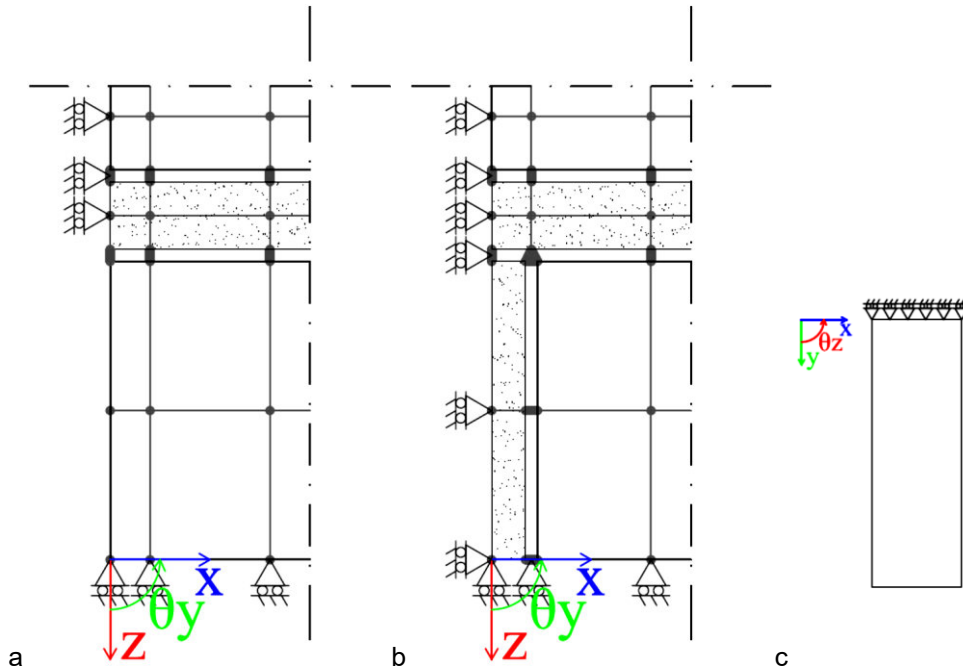


Figure 28.2: a. Element division and shared nodes at left side of double lap without butt connection; b. Element division and shared nodes at left side of double lap with butt connection ; c. Solid to enlarge the lap length

28.1.2 Seeds

In the table below an overview of the applied seed division can be found:

Member	Dimension in mm
Steel strap thickness	1.5
Adhesive thickness of outer two layers	0.5
Adhesive thickness of most inner layer	0.85
Plate thickness	3.75
Length	3.03
Length of enlargement solids	3.13
Width	3

Table 28.1: General applied seed division of double strap connection

28.1.3 Material and properties

For physical non-linear FEM calculation the type of yield criterion and the related parameters should be known.

For steel the Von Mises criterion fits best. For steel grade S235 the Von Mises stress is

$$\sigma_{s,VM} = 235 \text{ N/mm}^2 .$$

For structural adhesives (which are a polymers) the Drucker-Prager criterion fits better than the Von Mises criterion but both are used. For the adhesive the parameters have to be calculated with the strength parameters delivered by the manufacturer. The test will be done shortly after the adhesive is cured. Therefore, for an accurate prediction of the behaviour, the initial strength data should be taken. From Table 9.8 the next data follow: $\sigma_c = 85 \text{ N/mm}^2$, $\sigma_t = 26 \text{ N/mm}^2$ and $\sigma_{sh} = 17 \text{ N/mm}^2$.

28.1.3.1 Von Mises

The FEM program DIANA uses the next formula for the Von Mises criterion¹ ([53]):

$$\sigma_{eq} = \sqrt{\frac{3}{2}(s_{xx}^2 + s_{yy}^2 + s_{zz}^2) + 3(\sigma_{xy}^2 + \sigma_{yz}^2 + \sigma_{zx}^2)} \quad (28.1)$$

With:

$$\begin{aligned} s_{xx} &= \frac{2}{3}\sigma_{xx} - \frac{1}{3}\sigma_{yy} - \frac{1}{3}\sigma_{zz} \\ s_{yy} &= -\frac{1}{3}\sigma_{xx} + \frac{2}{3}\sigma_{yy} - \frac{1}{3}\sigma_{zz} \\ s_{zz} &= -\frac{1}{3}\sigma_{xx} - \frac{1}{3}\sigma_{yy} + \frac{2}{3}\sigma_{zz} \end{aligned} \quad (28.2)$$

For the uniaxial and pure shear stress state the formula simplifies to:

$$\sigma_{xx} \neq 0, \sigma_{yy} = \sigma_{zz} = \sigma_{xy} = \sigma_{yz} = \sigma_{zx} = 0 \rightarrow \sigma_{eq} = \sigma_{xx} \quad (28.3)$$

$$\sigma_{xy} \neq 0, \sigma_{xx} = \sigma_{yy} = \sigma_{zz} = \sigma_{yz} = \sigma_{zx} = 0 \rightarrow \sigma_{eq} = \sqrt{3}\sigma_{xy} \quad (28.4)$$

Hence:

$$\begin{aligned} \sigma_c &= 85 \text{ N/mm}^2 & \rightarrow & \sigma_{eq} = 85 \text{ N/mm}^2 \\ \sigma_t &= 26 \text{ N/mm}^2 & \rightarrow & \sigma_{eq} = 26 \text{ N/mm}^2 \\ \sigma_{sh} &= 17 \text{ N/mm}^2 & \rightarrow & \sigma_{eq} = 29.44 \text{ N/mm}^2 \end{aligned} \quad (28.5)$$

For the calculation the smallest stress ($\sigma_{eq} = 26 \text{ N/mm}^2$) is taken.

28.1.3.2 Drucker-Prager

For the Drucker-Prager yield criterion the cohesion (c), internal friction angle (ϕ) and dilatancy angle (ψ) are input parameters for a FEM calculation. These parameters can be deduced from the data of Table 9.8. In [63] three relations are mentioned:

$$c_1 = \left(1 - \frac{1}{3} \tan(\phi)\right) \sigma_{a,c} \quad (28.6)$$

$$c_2 = \left(\frac{1}{K} + \frac{1}{3} \tan(\phi)\right) \sigma_{a,t} \quad (28.7)$$

$$c_3 = \frac{\sqrt{3}}{2} \left(1 + \frac{1}{K}\right) \sigma_{a,sh} \quad (28.8)$$

By setting $\psi = \phi$ and $K = 1$ the original Drucker-Prager criterion is obtained, which will be used.

From (28.6)/(28.8) three formulas for ϕ which do not depend on c can be derived:

$$\phi_1 = \arctan\left(\frac{3(\sigma_c - \sigma_t)}{\sigma_t + \sigma_c}\right) \quad (28.9)$$

$$\phi_2 = \arctan\left(\frac{3(\sigma_c - \sqrt{3}\sigma_{sh})}{\sigma_c}\right) \quad (28.10)$$

$$\phi_3 = \arctan\left(\frac{3(\sqrt{3}\sigma_{sh} - \sigma_t)}{\sigma_t}\right) \quad (28.11)$$

¹ The Von Mises stress is denoted as equivalent stress in DIANA

The average value will be used:

$$\phi_4 = (\phi_1 + \phi_2 + \phi_3) / 3 \quad (28.12)$$

With: $\sigma_c = 85 \text{ N/mm}^2$, $\sigma_t = 26 \text{ N/mm}^2$ and $\sigma_{sh} = 17 \text{ N/mm}^2$.

	radian	degree
ϕ_1	1.01	57.91
ϕ_2	1.01	62.98
ϕ_3	0.38	21.68
ϕ_4	0.83	47.52

Table 28.2: Calculated values for the internal friction angle

For the FEM calculation the average value, $\psi = \phi = 47.52^\circ$, will be used. Now the value for the cohesion can be determined. In the next table the values of (28.6)/(28.8) and $c_4 = (c_1 + c_2 + c_3) / 3$ can be found:

	N/mm^2
c_1	45.06
c_2	29.44
c_3	35.46
c_4	39.66

Table 28.3: Calculated values for the cohesion

For the calculation the average value, $c_4 = 39.66 \text{ N/mm}^2$, will be used.

28.1.3.3 Overview

The used material and properties used for the solids can be found in the next tables.

Name	Type	Property	Value	Unit	Model Type
Steel LE	Isotropic	E	210000	N/mm^2	Elastic
		ν	0.33		
Steel VM	Isotropic	E	210000	N/mm^2	Von Mises
		ν	0.33		
		σ_y	235	N/mm^2	
Adhesive LE	Isotropic	E	12800	N/mm^2	Elastic
		G	4273	N/mm^2	
Adhesive VM	Isotropic	E	12800	N/mm^2	Von Mises
		G	4273	N/mm^2	
		σ_y	26	N/mm^2	
Adhesive DP	Isotropic	E	12800	N/mm^2	Drucker Prager
		G	4273	N/mm^2	
		c	39.66	N/mm^2	
		ϕ	47.52	Deg	
		ψ	47.52	Deg	

Table 28.4: Material of solids

Name	Type	Sub-Type		Material
Steel	3D	Solid	Regular	Steel
Adhesive	3D	Solid	Regular	Adhesive

Table 28.5: Properties for solids

28.1.4 Mesh

For all elements the brick elements are used (see Table 23.6). For most models the linear variant (HX24L) is used, for some models the quadratic variant (CHX60) is used. Linear elements can be changed into quadratic by the *Mesh/Element/Change Parameter...* command. The solid of the plate butt is remeshed after this change to ensure the right node sharing conditions.

28.1.5 Loads and boundary conditions

In all three directions symmetry conditions apply. The nodes at $y=0$ are all restrained in y -direction and the nodes at $z=0$ are restrained in z -direction. At $x=0$ the nodes of the straps and adhesive layers are restrained in x -direction.

The outer nodes in positive x -direction of the plate are loaded with a displacement controlled load.

28.2 Analysis

For the analysis the exact same procedure is used as for the entire L-connection, see section 23.2. For calculation with nonlinear behaviour the converge criterion, number of iterations and size of the iterations have to be specified. For all nonlinear calculations the same parameters are used. These parameters are saved in a dcf-file. 16 equal steps with Newton regular iteration and the energy converge criterion are chosen. The used dcf-file can be found below:

```

*FILOS
INITIA
*NONLIN
BEGIN EXECUT
  BEGIN LOAD
    LOADNR 1
    STEPS EXPLIC SIZES 0.0625(16)
  END LOAD
  BEGIN ITERAT
    BEGIN CONVER
      DISPLA OFF
      ENERGY
      FORCE OFF
    END CONVER
  END ITERAT
END EXECUT
BEGIN OUTPUT
  FXPLUS
  APPEND
  FILE "Plastic"
END OUTPUT
BEGIN TYPE
  GEOMET
  BEGIN PHYSIC
    CONCEN OFF
    CORROS OFF
    CRACKI OFF
    CREEP OFF
    ELASTI OFF
    HYPERE OFF
    INTERF OFF
    MATURI OFF
    SHRINK OFF
    TEMPER OFF
    TOTCRK OFF
    VISCOE OFF
    VISCOP OFF
  END PHYSIC
END TYPE
*END

```

Figure 28.3: Used dcf-file for the nonlinear double strap FEM calculation

28.3 Output

For the adhesive planes several lines, for which data is generated, are made. Two types of lines are made, lines in longitudinal direction (x-direction) and lines in transverse direction (y-direction). Longitudinal lines are made at $y=0$ (symmetry plane), $y=37.5$ and $y=75$ (outer edge). Transverse lines are made at $x=0$ (symmetry plane), $x=L_1$ (end of lap 1), $x=L_1+L_2$ (end of lap 3) and $x=L_1+L_2+L_3$ (end of lap 3). Both types of lines are made for every adhesive planes at the top interface, in the middle of the adhesive and at the lower interface. The division for the extraction point is 1 per 2mm which is assumed to be enough for accurate data.

To obtain the data for the load-displacement diagrams and to check the load, the support reactions are important. With the command *Results/Structural Linear Static/Load Case 1/Reactions/FBX(V)/Table* (for LE calculations) or with *Results/Structural Nonlinear/Reactions/Load step 1¹/FBX(V)/Table* (for VM or DP calculation) a table with the support reactions can be made.

¹ This number indicates the iteration step

29 Appendix M: FEM results of double strap connection

In the figure below the location of the output lines used in section 29.1/29.4 is depicted.

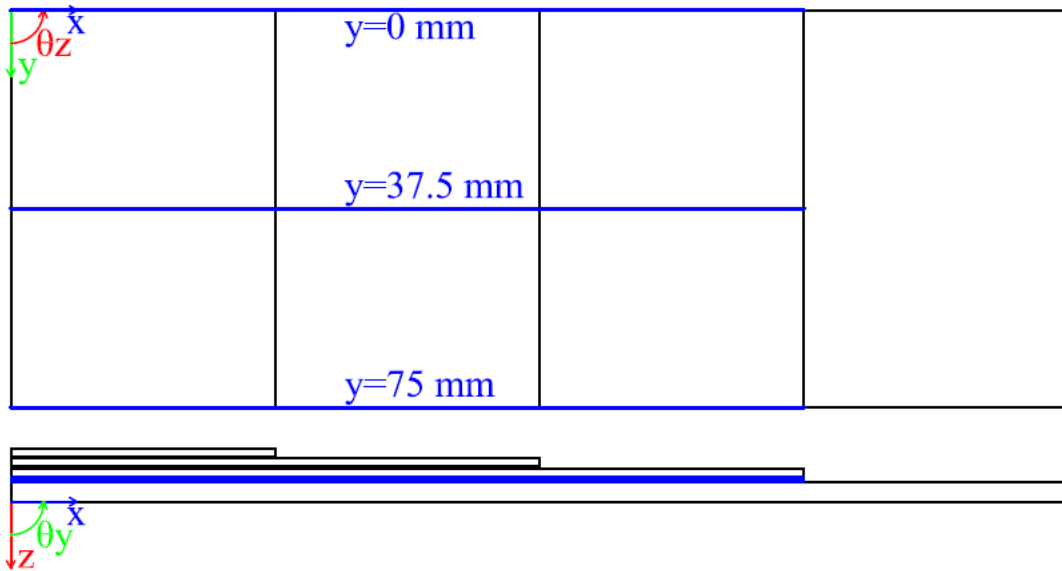


Figure 29.1: Output lines for double strap models

In the figure below the area which is considered in section 29.5 is visible.

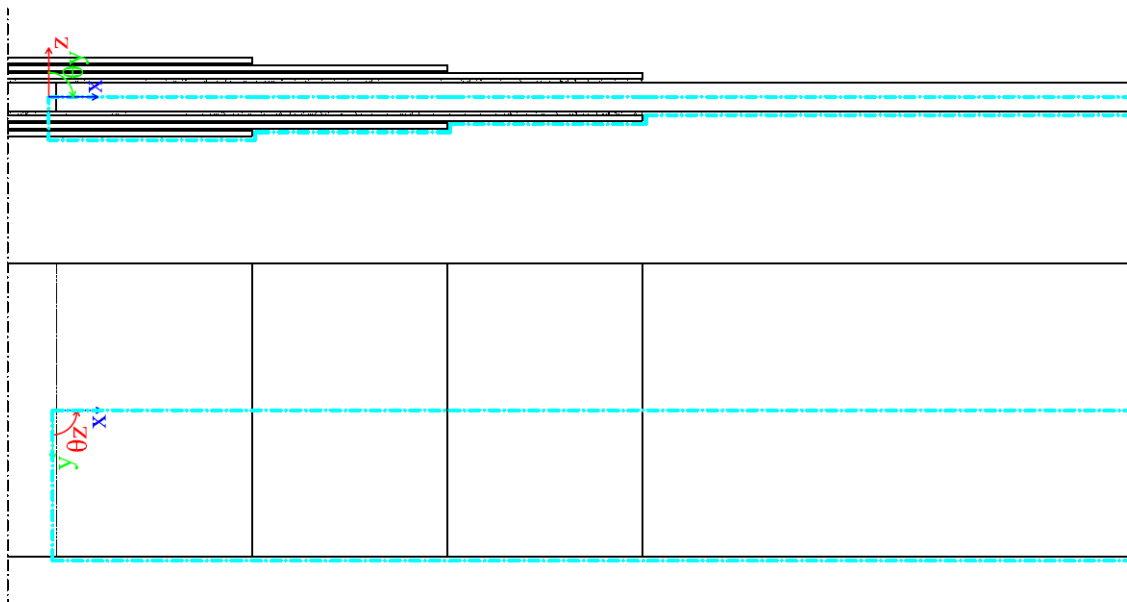


Figure 29.2: FEM area for comparison with DIC

29.1 Shear stress of first adhesive layer at last load step

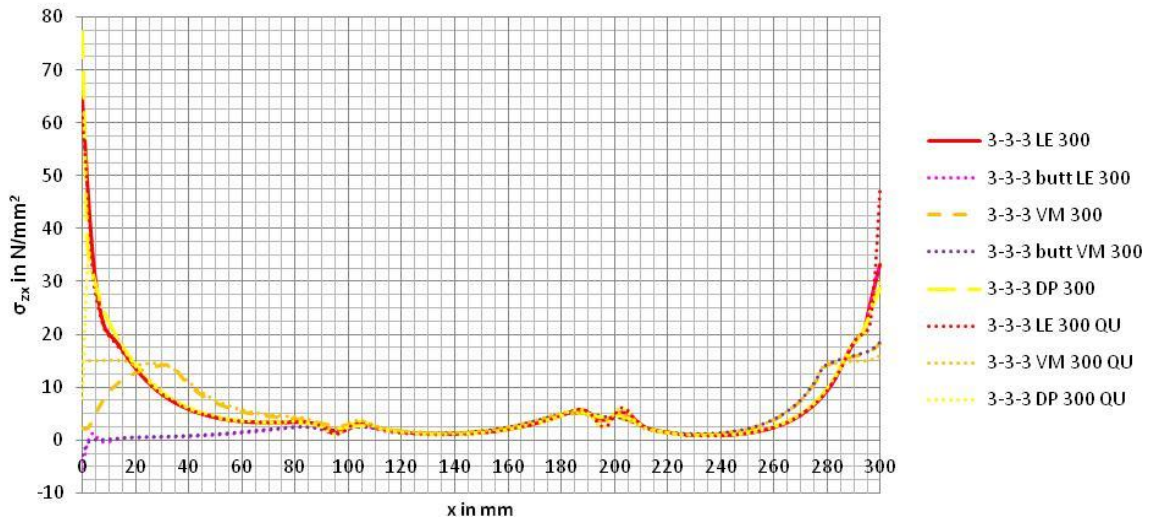


Figure 29.3: Shear stress of double strap at y=0, bottom

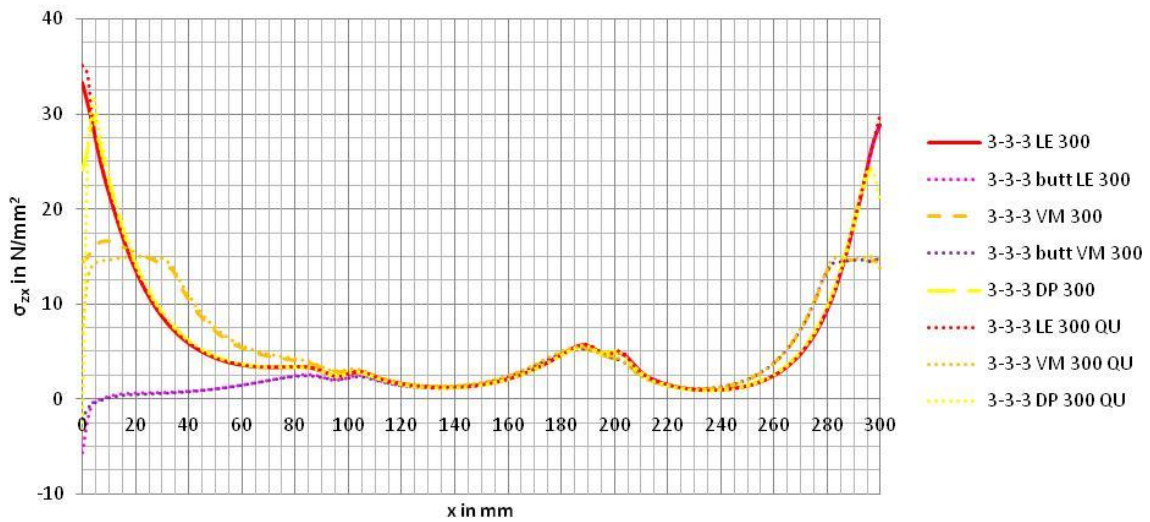


Figure 29.4: Shear stress of double strap at y=0, middle

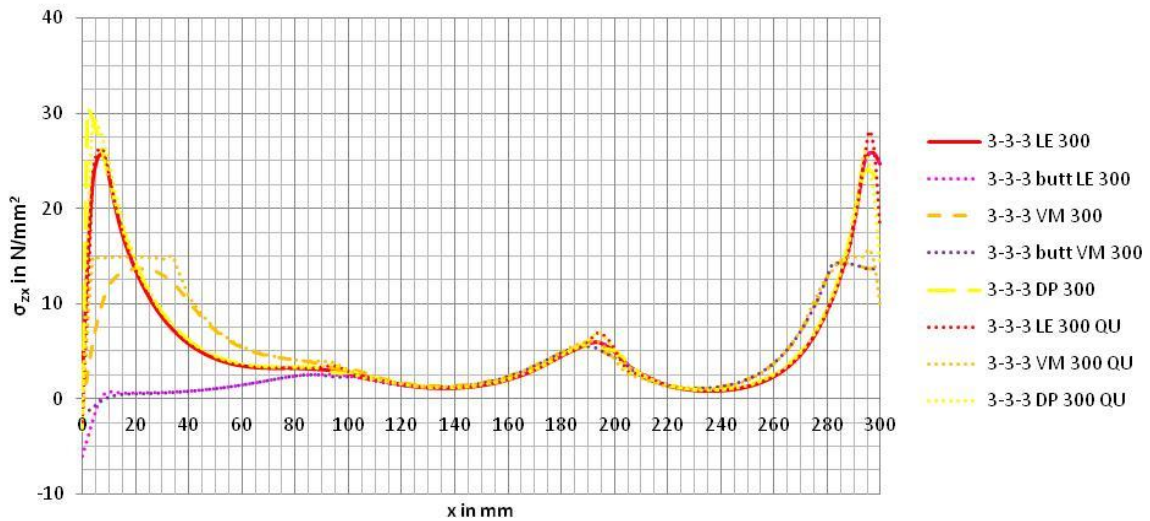
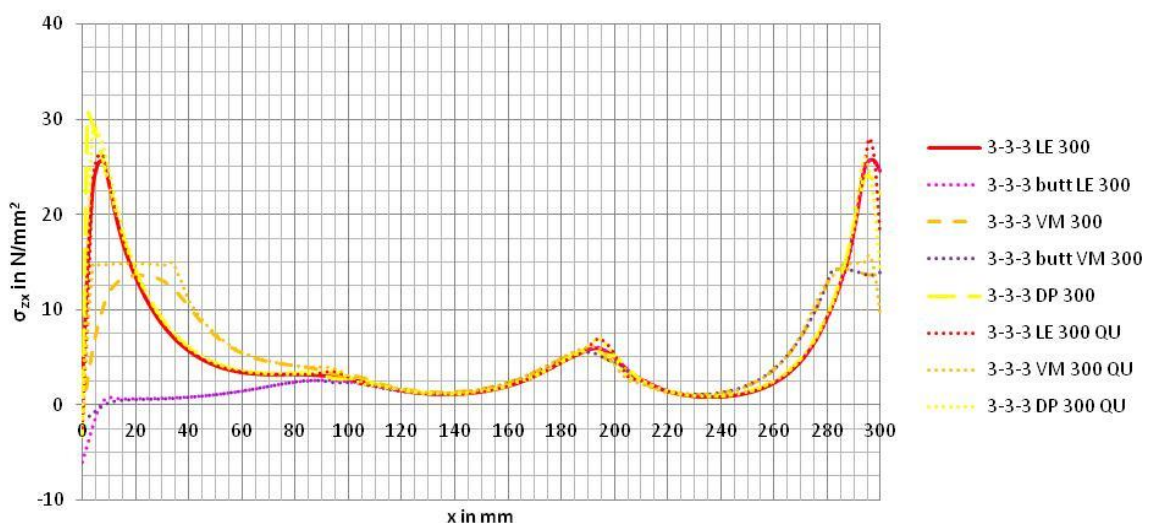
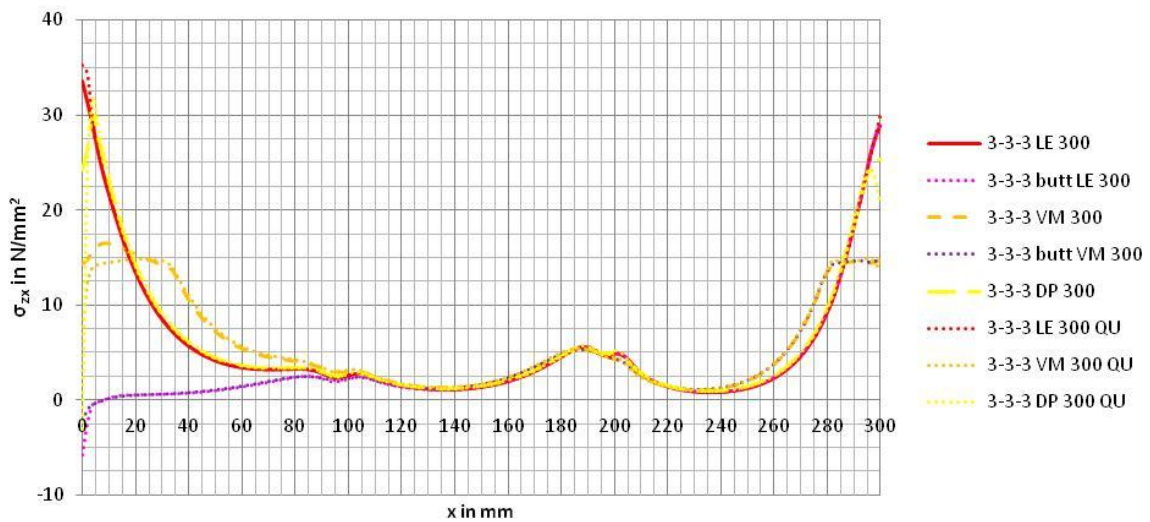
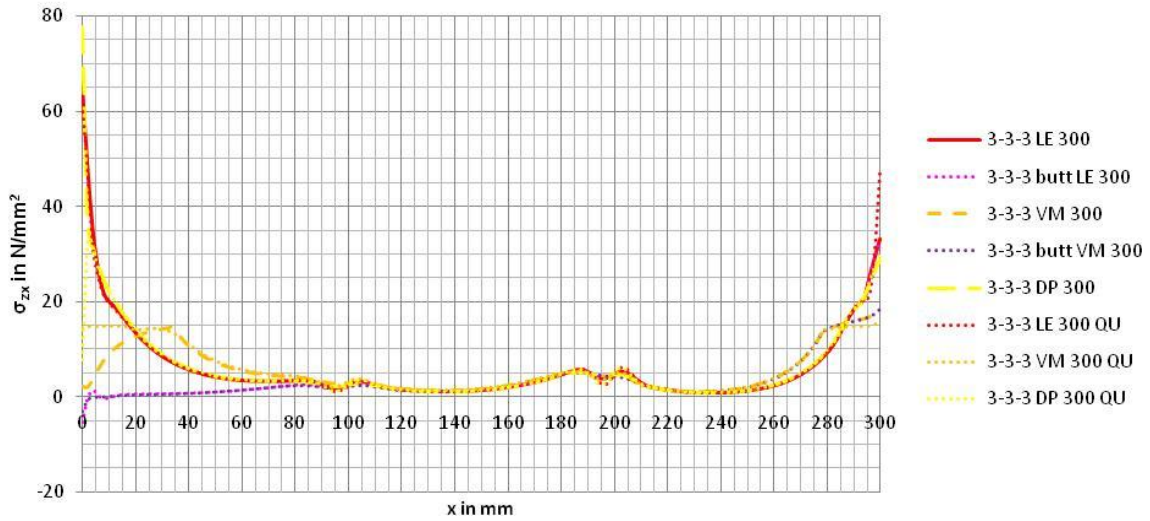


Figure 29.5: Shear stress of double strap at y=0, top



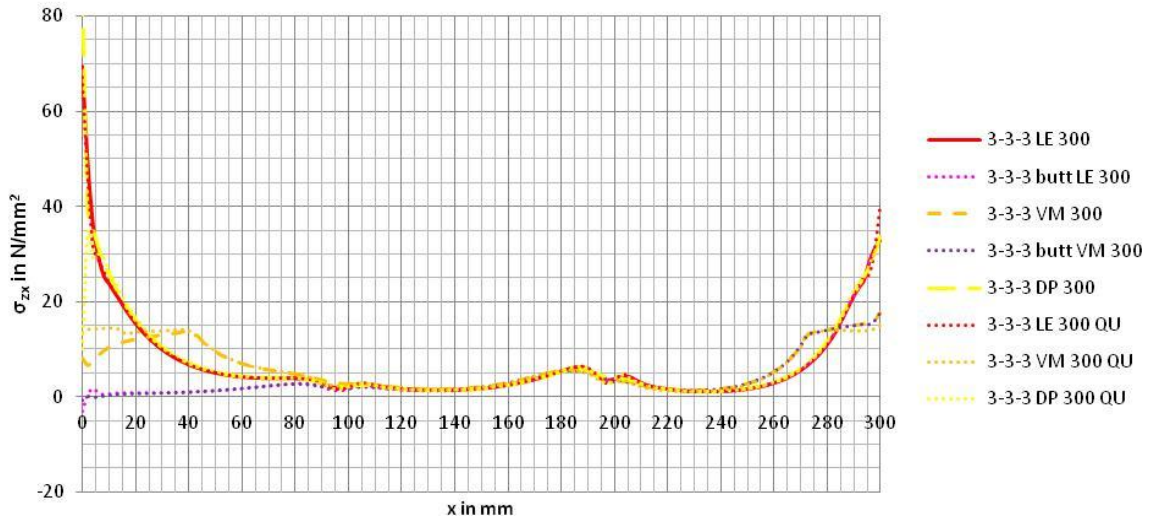


Figure 29.9: Shear stress of double strap at y=75, bottom

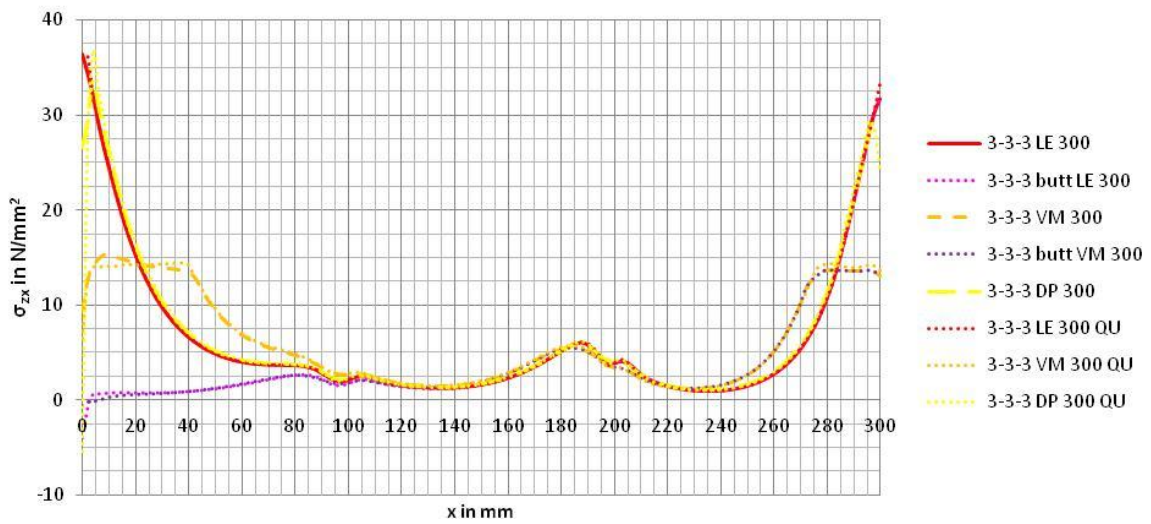


Figure 29.10: Shear stress of double strap at y=75, middle

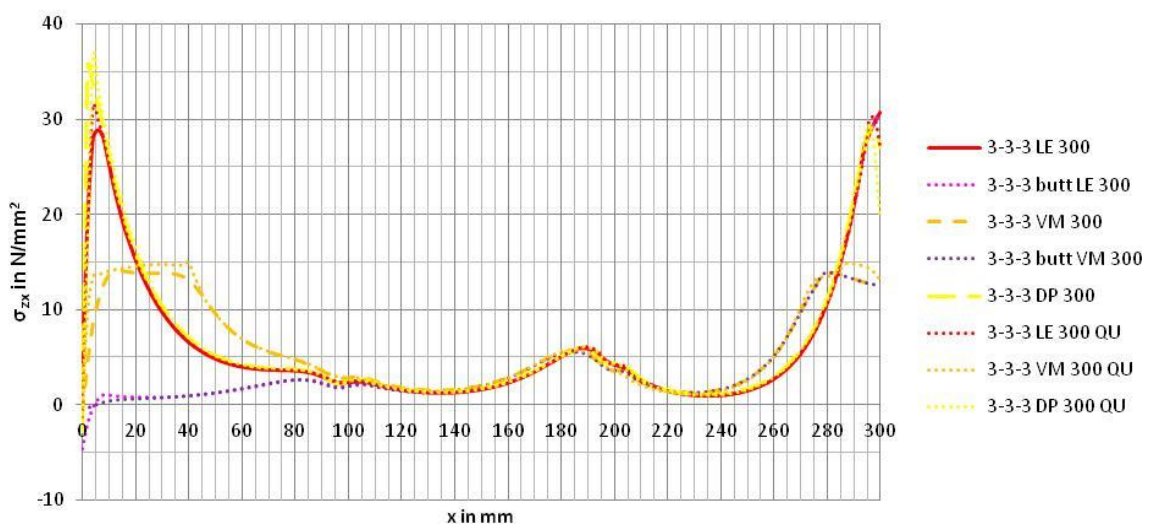


Figure 29.11: Shear stress of double strap at y=75, top

29.2 Peel stress of first adhesive layer at last load step

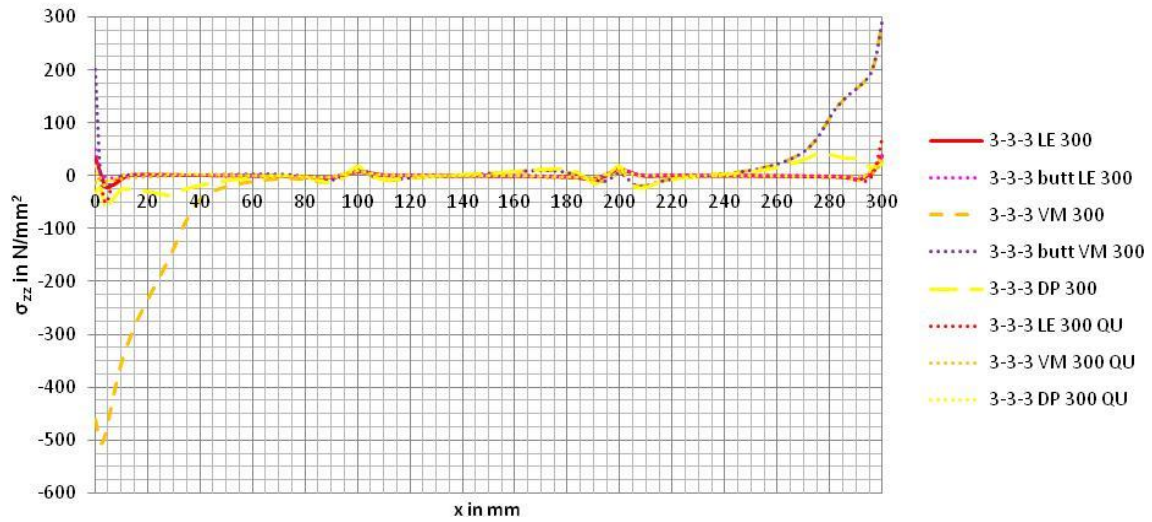


Figure 29.12: Peel stress of double strap at $y=0$, bottom

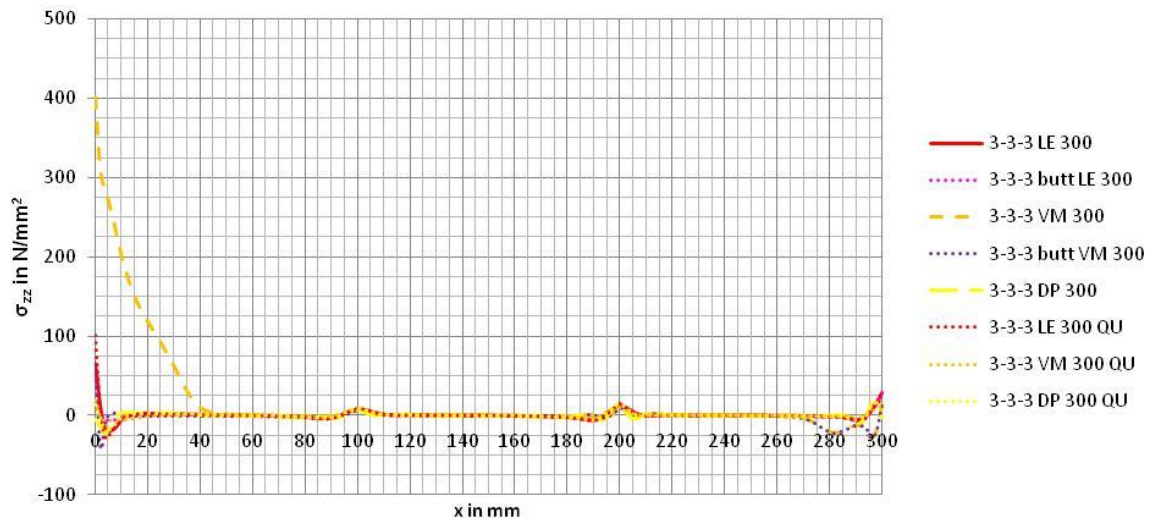


Figure 29.13: Peel stress of double strap at $y=0$, middle

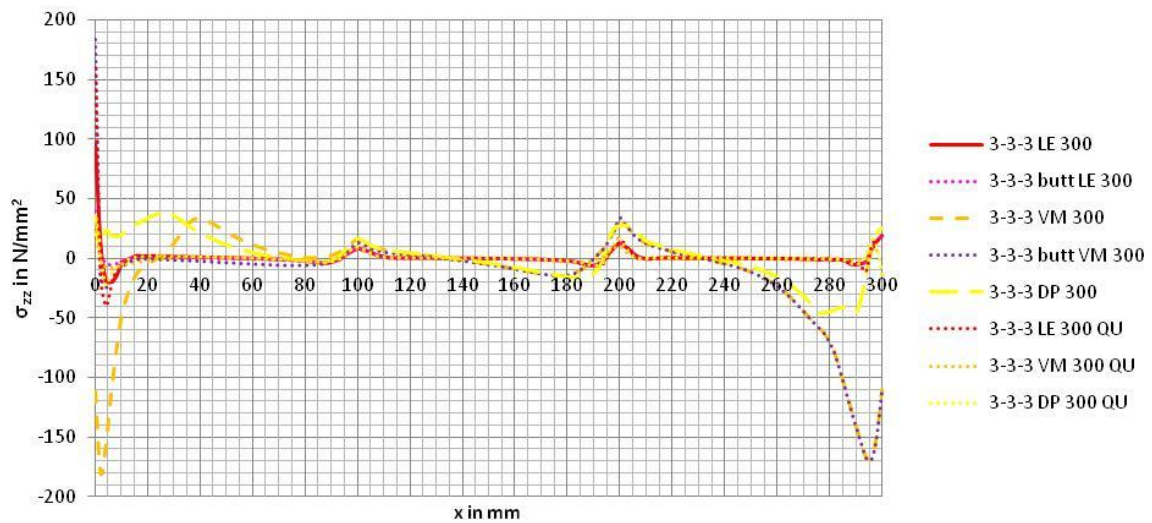
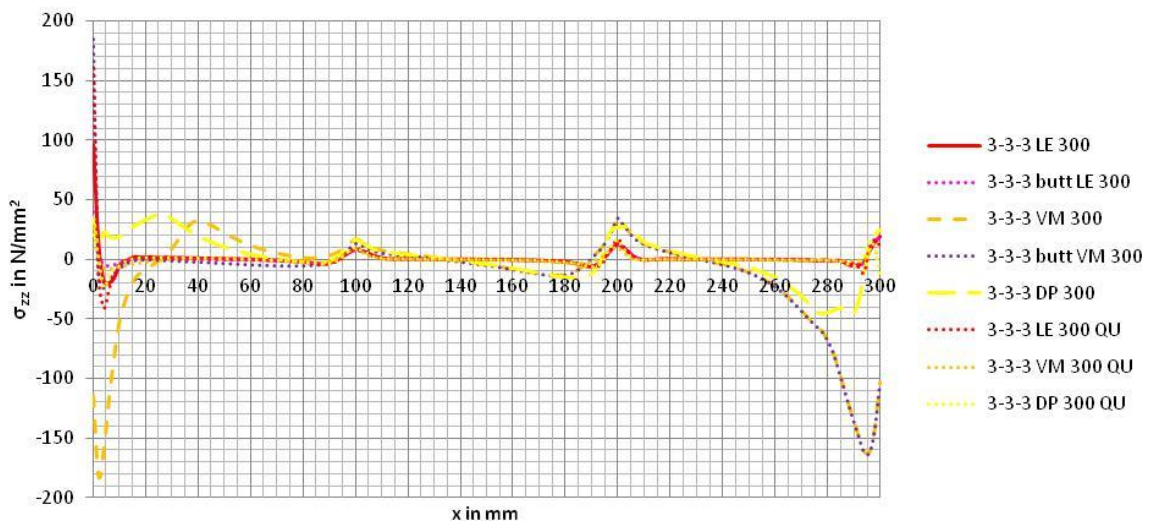
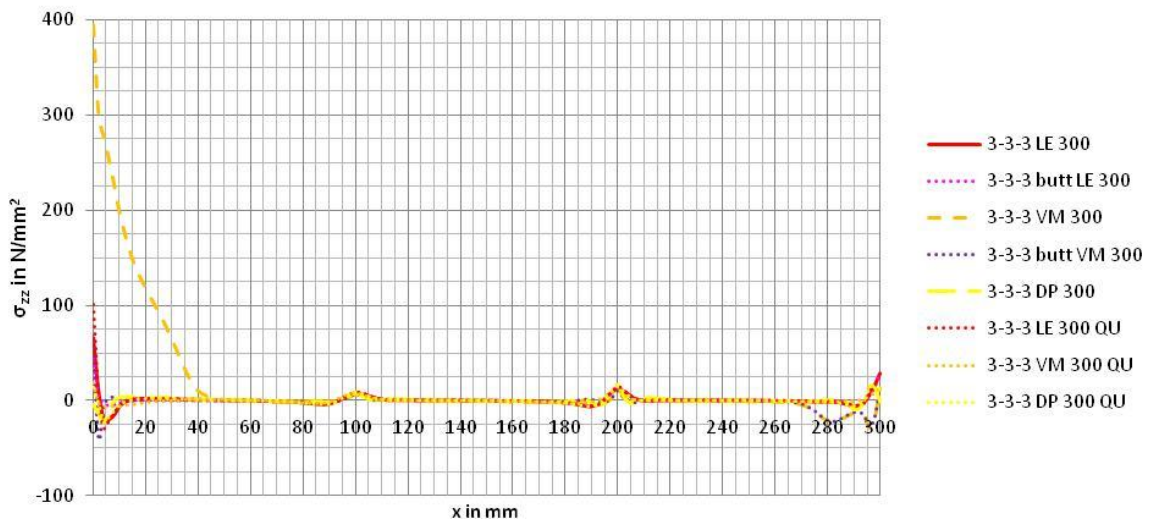
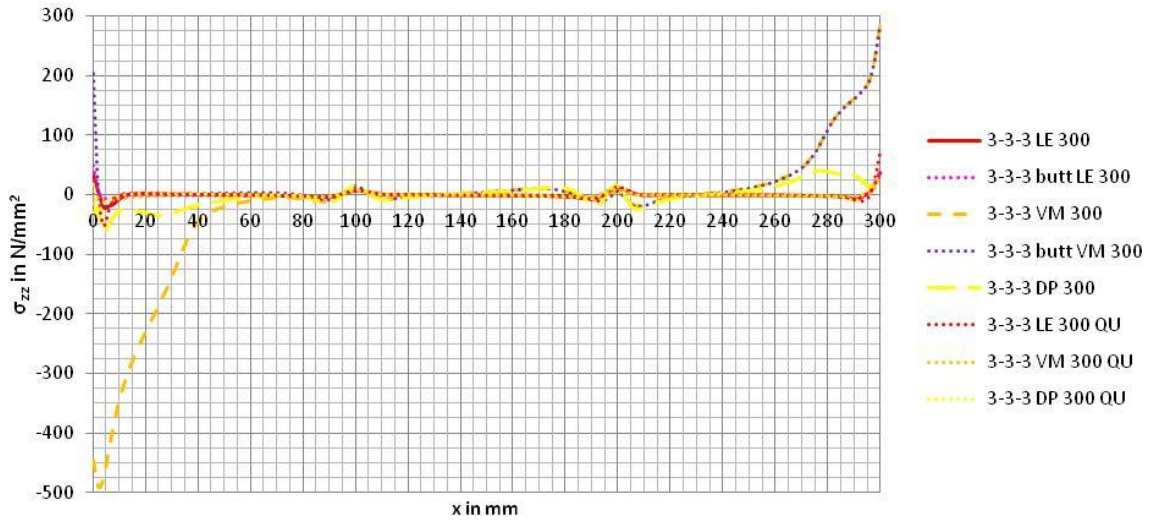


Figure 29.14: Peel stress of double strap at $y=0$, top



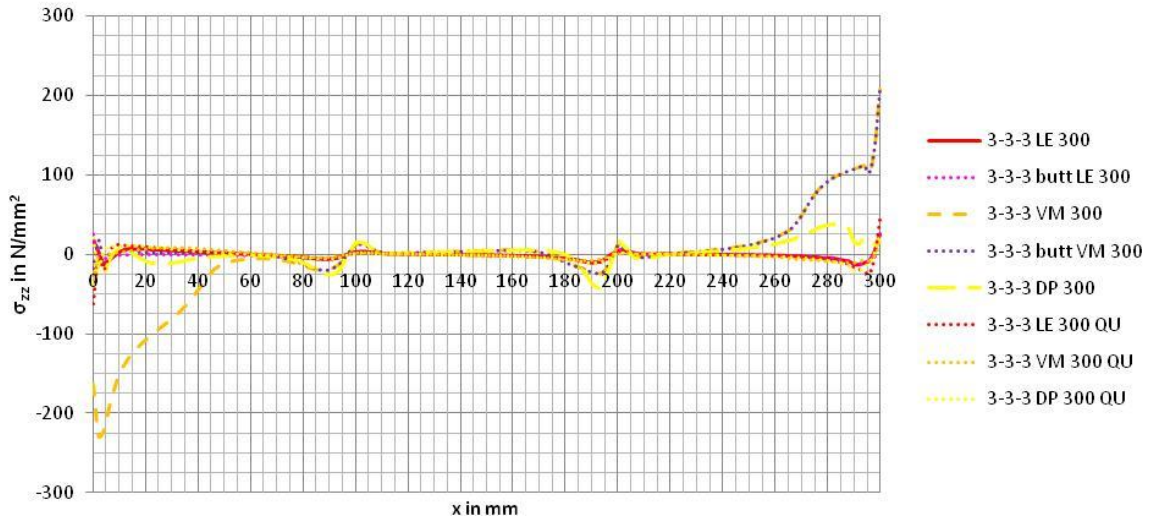


Figure 29.18: Peel stress of double strap at $y=75$, bottom

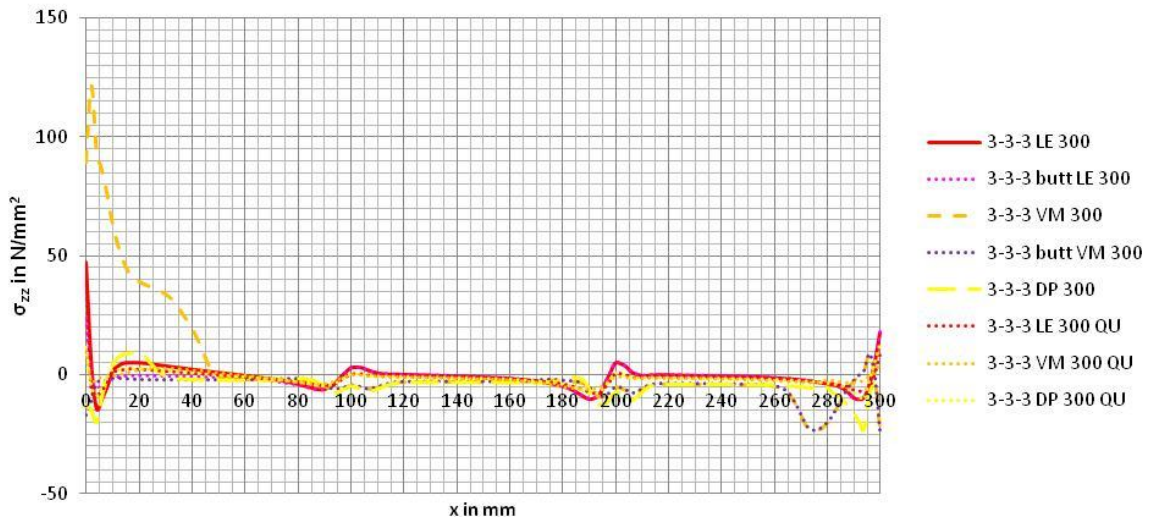


Figure 29.19: Peel stress of double strap at $y=75$, middle

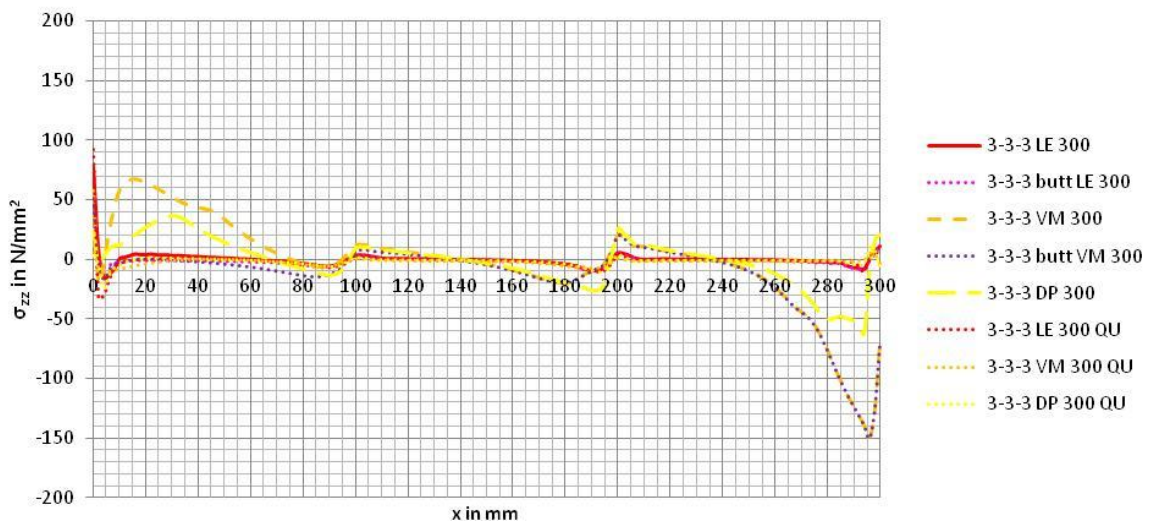


Figure 29.20: Peel stress of double strap at $y=75$, top

29.3 Equivalent stress of first adhesive layer at last load step

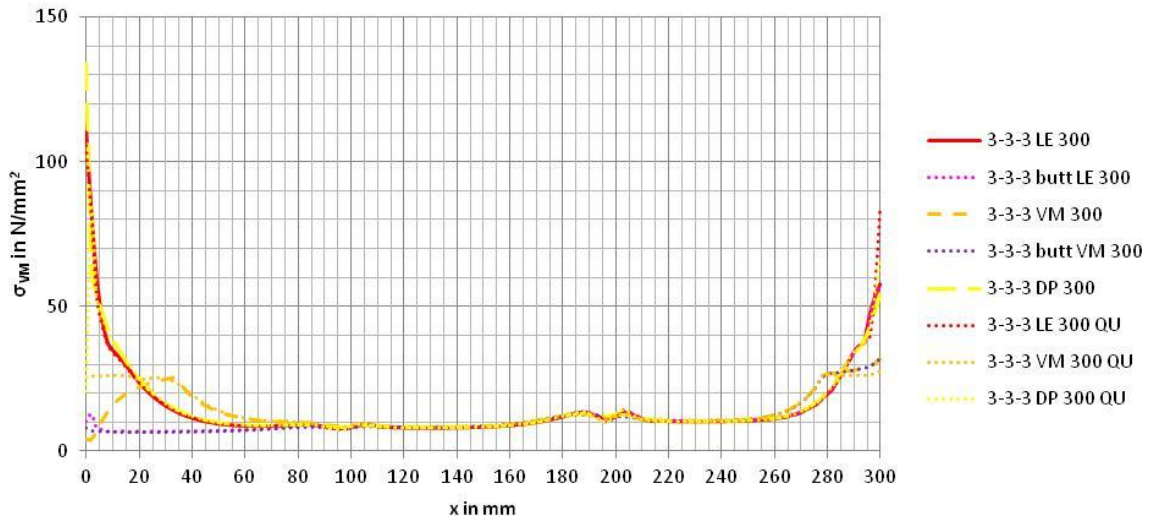


Figure 29.21: Equivalent stress of double strap at y=0, bottom

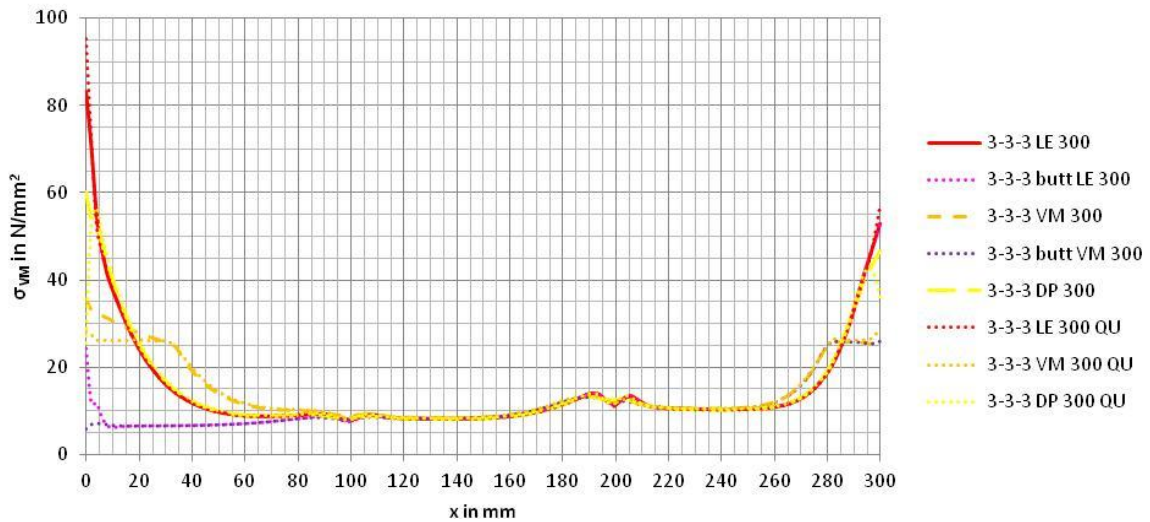


Figure 29.22: Equivalent stress of double strap at y=0, middle

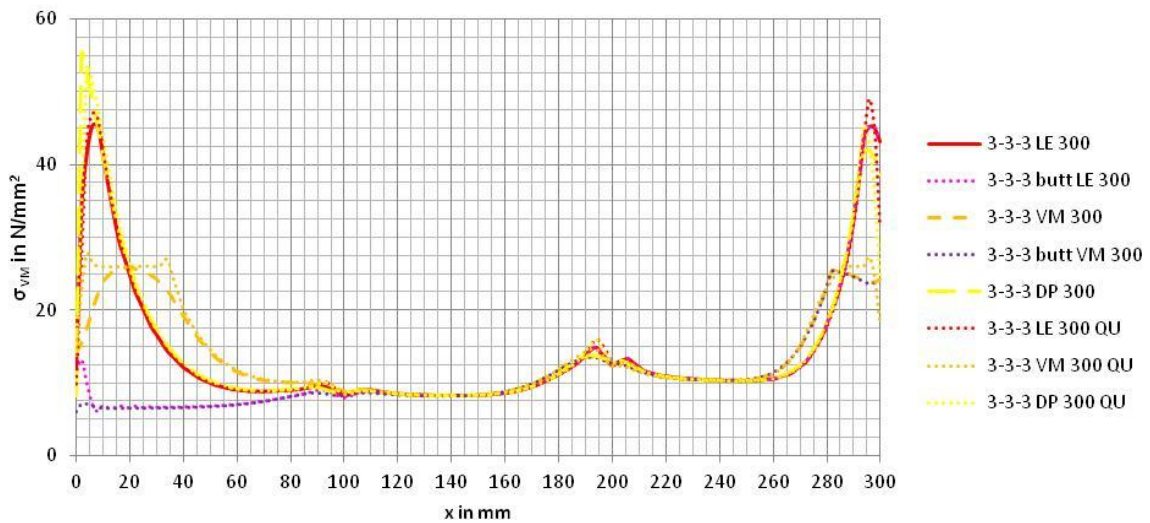


Figure 29.23: Equivalent stress of double strap at y=0, top

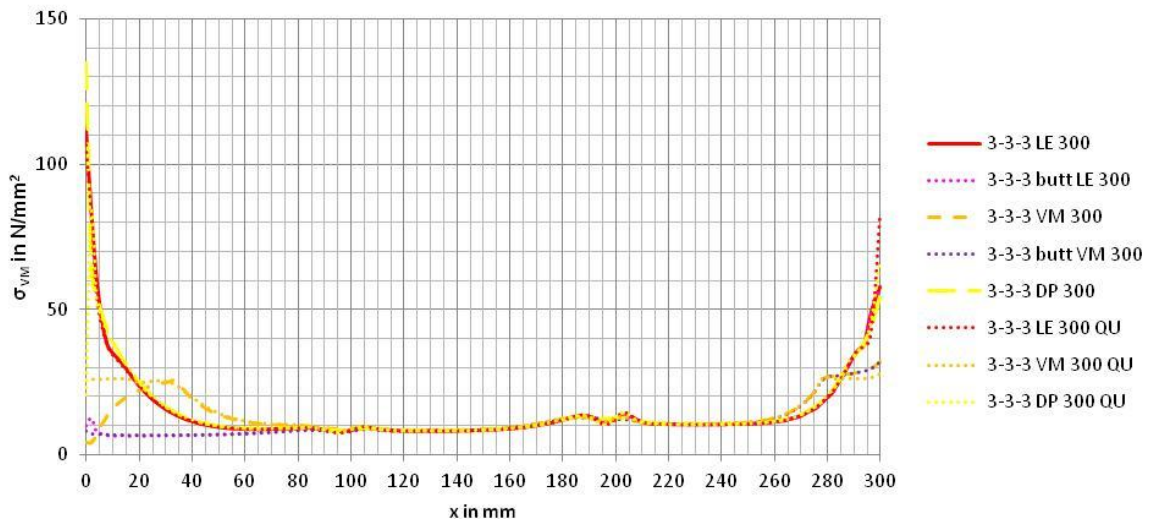


Figure 29.24: Equivalent stress of double strap at y=37.5, bottom

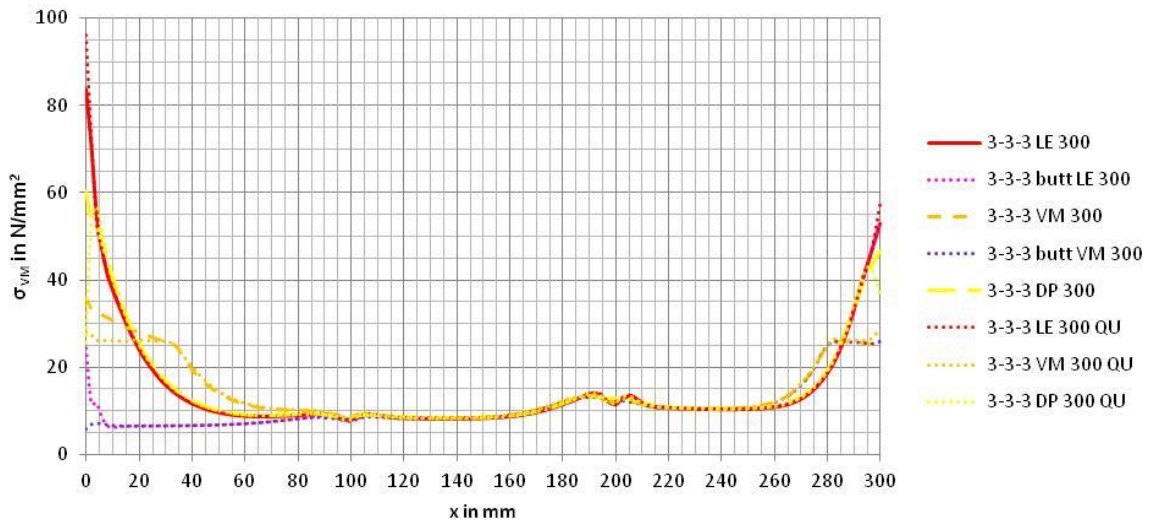


Figure 29.25: Equivalent stress of double strap at y=37.5, middle

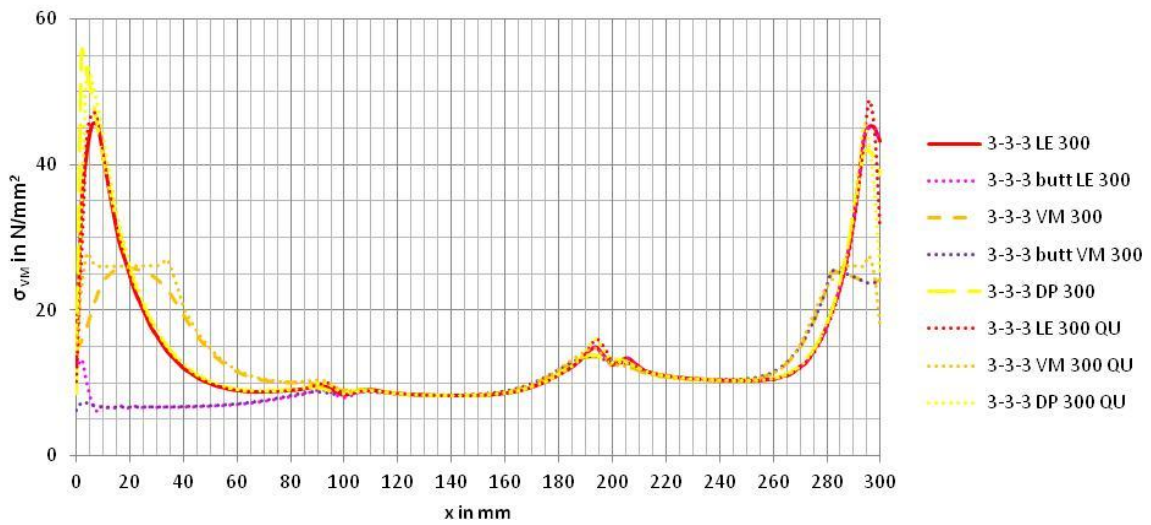


Figure 29.26: Equivalent stress of double strap at y=37.5, top

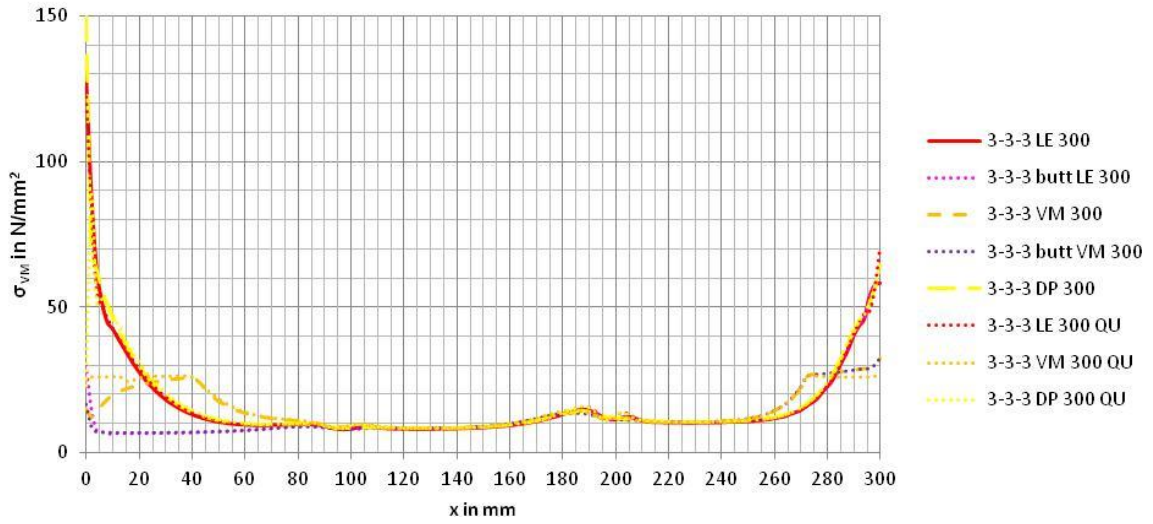


Figure 29.27: Equivalent stress of double strap at y=75, bottom

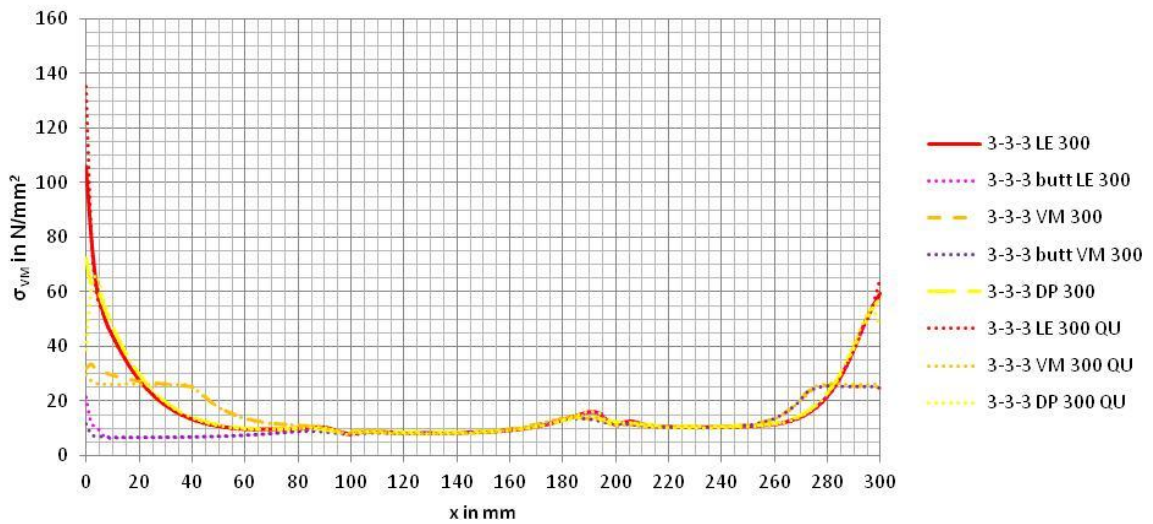


Figure 29.28: Equivalent stress of double strap at y=75, middle

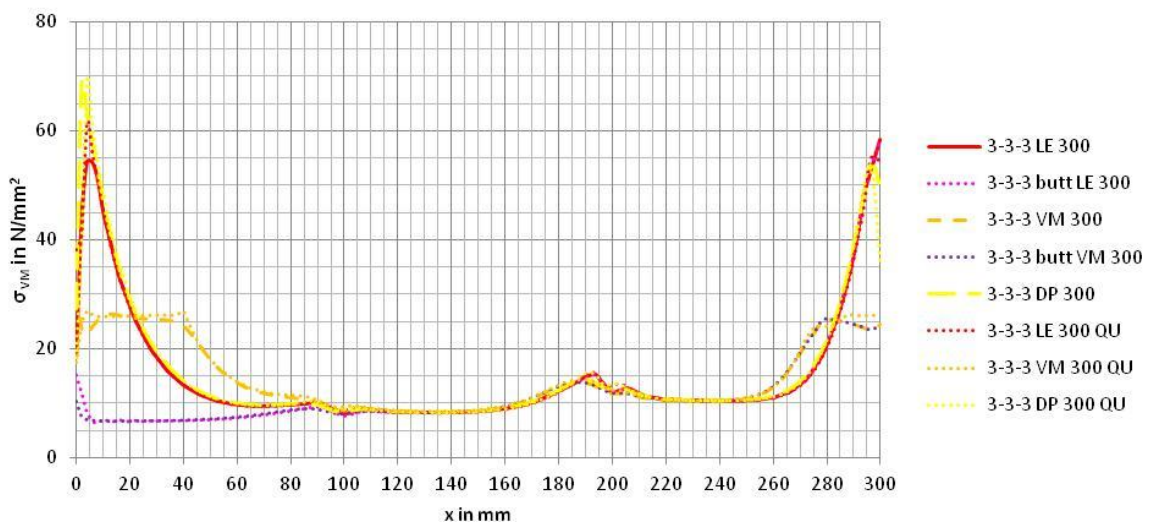


Figure 29.29: Equivalent stress of double strap at y=75, top

29.4 Equivalent strain of first adhesive layer at last load step

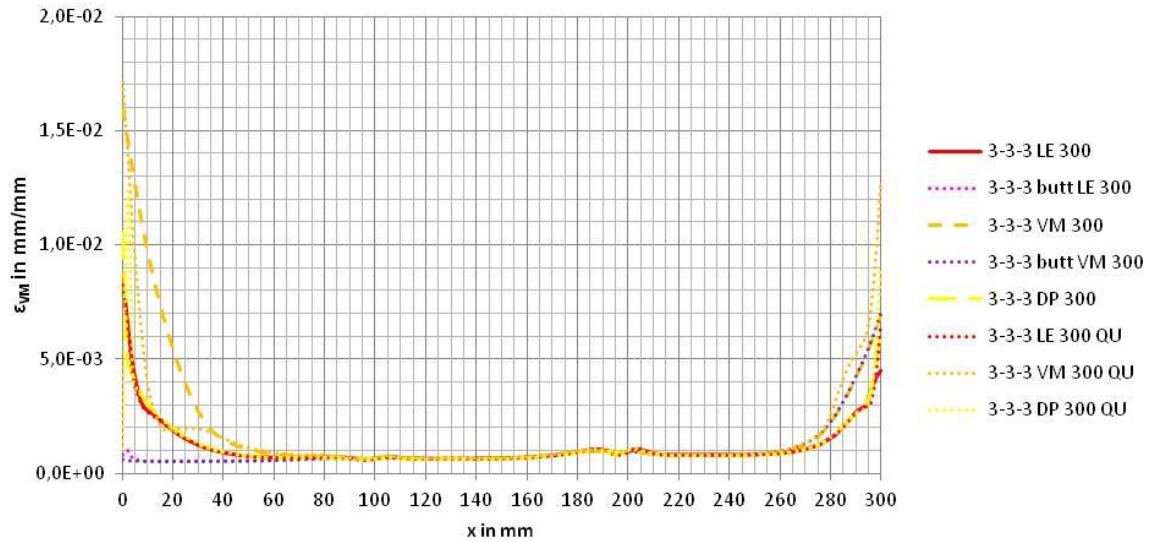


Figure 29.30: Equivalent strain of double strap at y=0, bottom

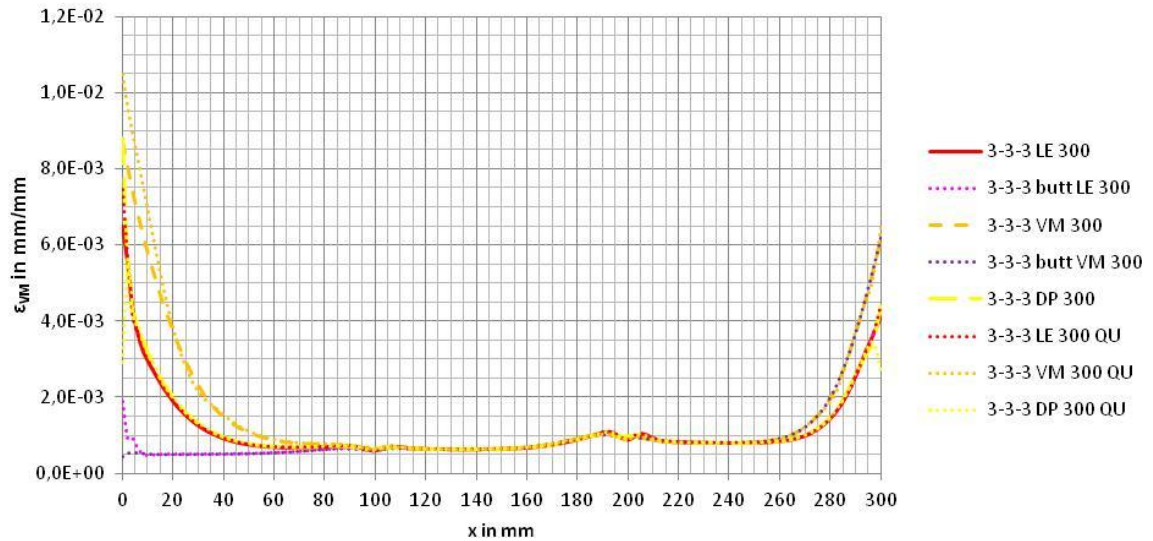


Figure 29.31: Equivalent strain of double strap at y=0, middle

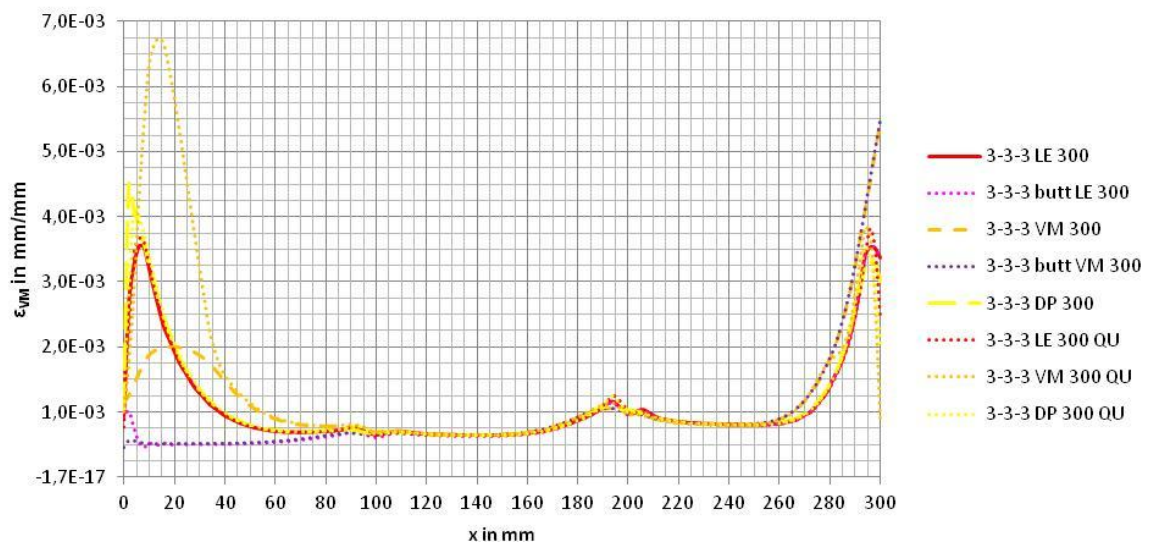


Figure 29.32: Equivalent strain of double strap at y=0, top

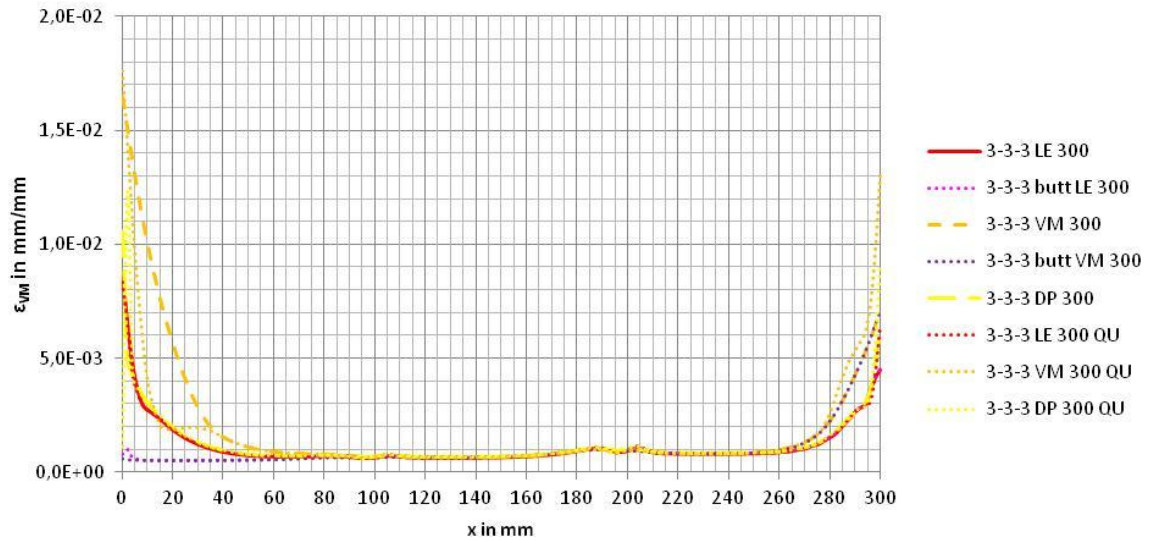


Figure 29.33: Equivalent strain of double strap at y=37.5, bottom

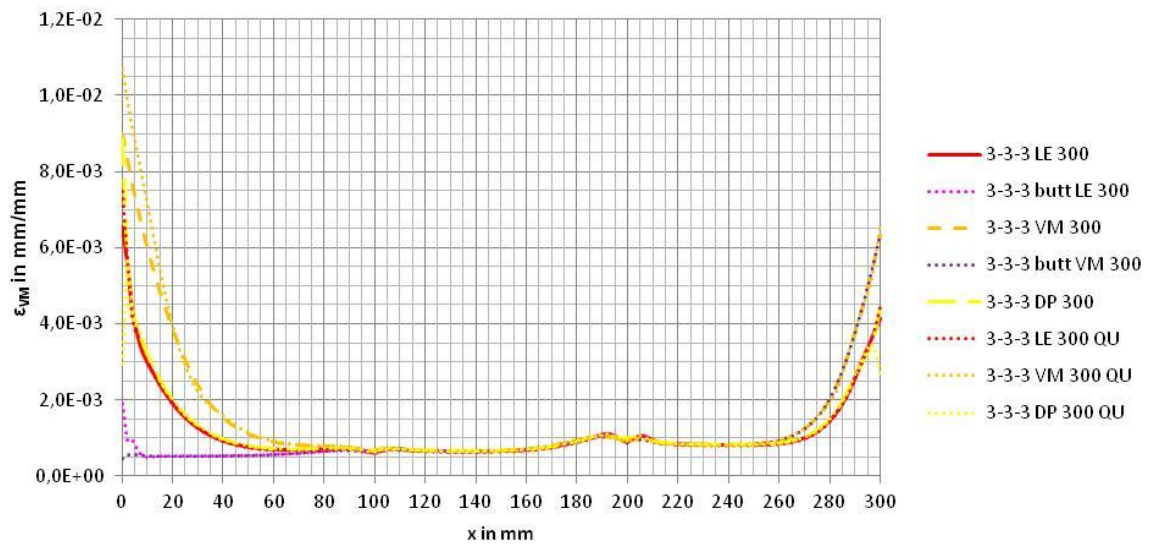


Figure 29.34: Equivalent strain of double strap at y=37.5, middle

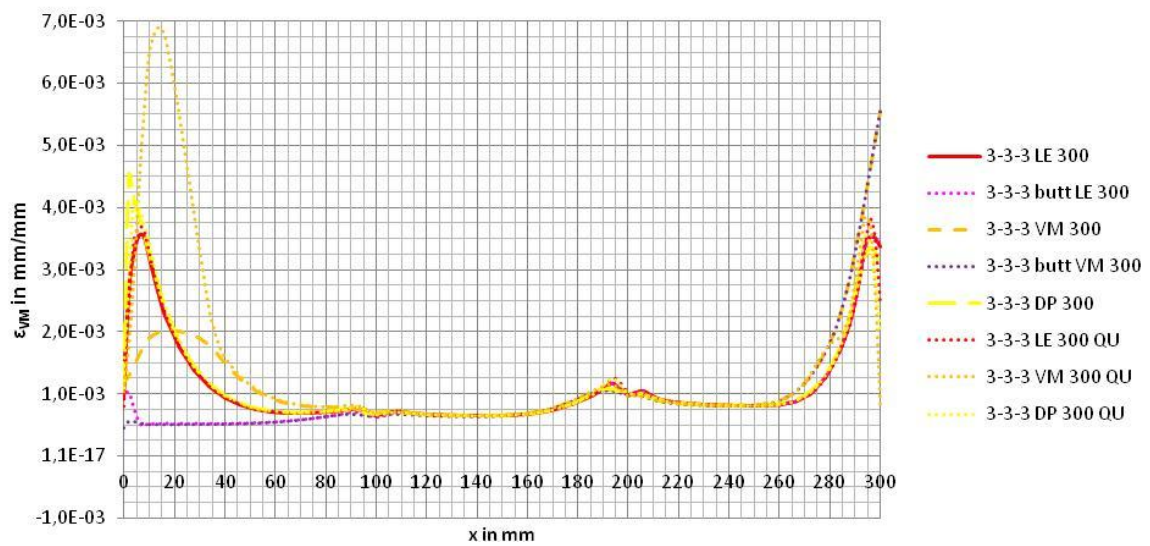


Figure 29.35: Equivalent strain of double strap at y=37.5, top

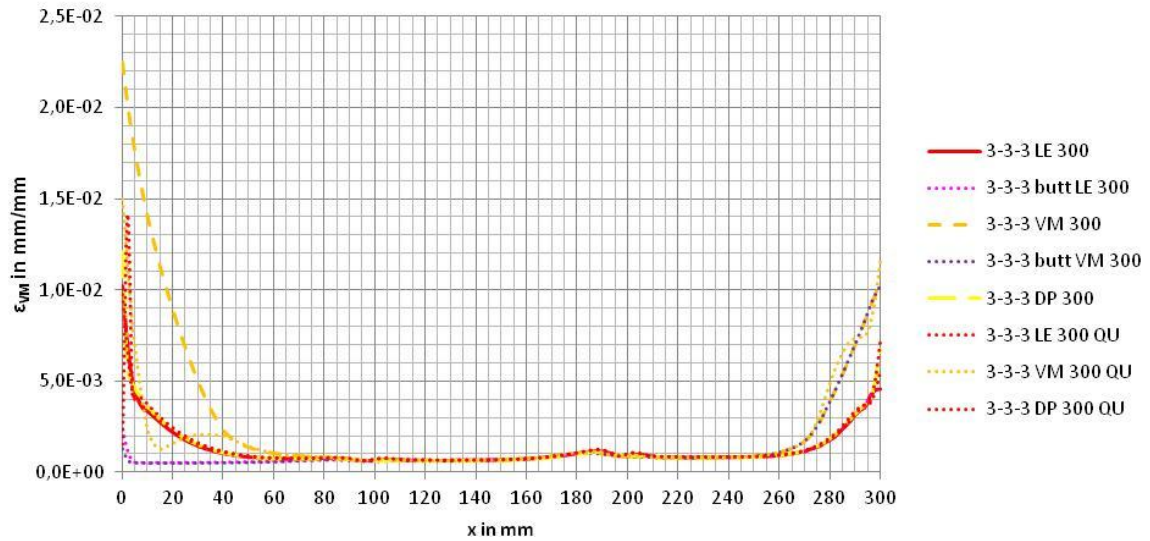


Figure 29.36: Equivalent strain of double strap at y=75, bottom

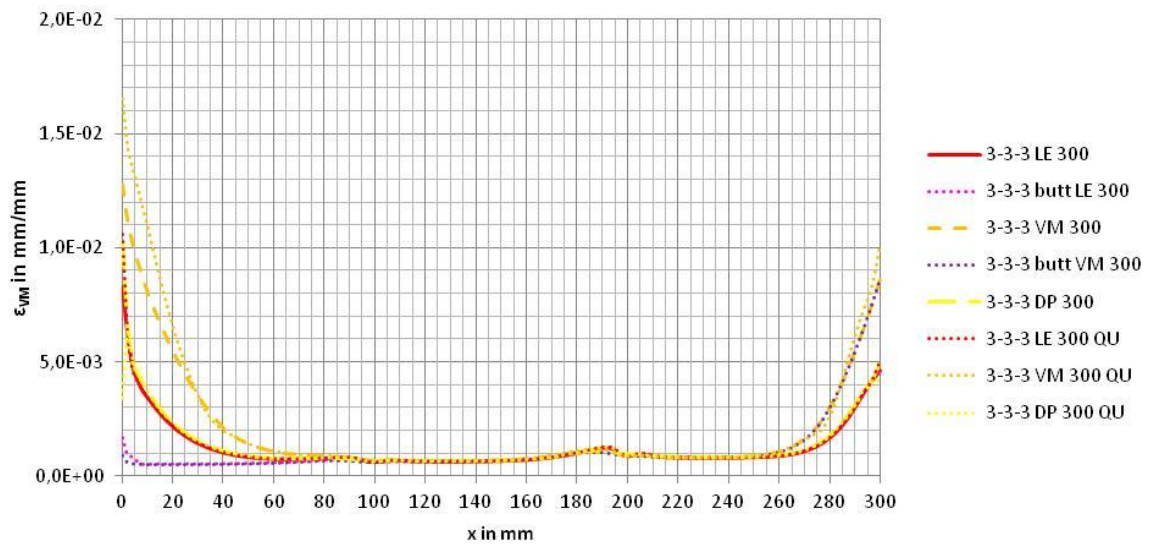


Figure 29.37: Equivalent strain of double strap at y=75, middle

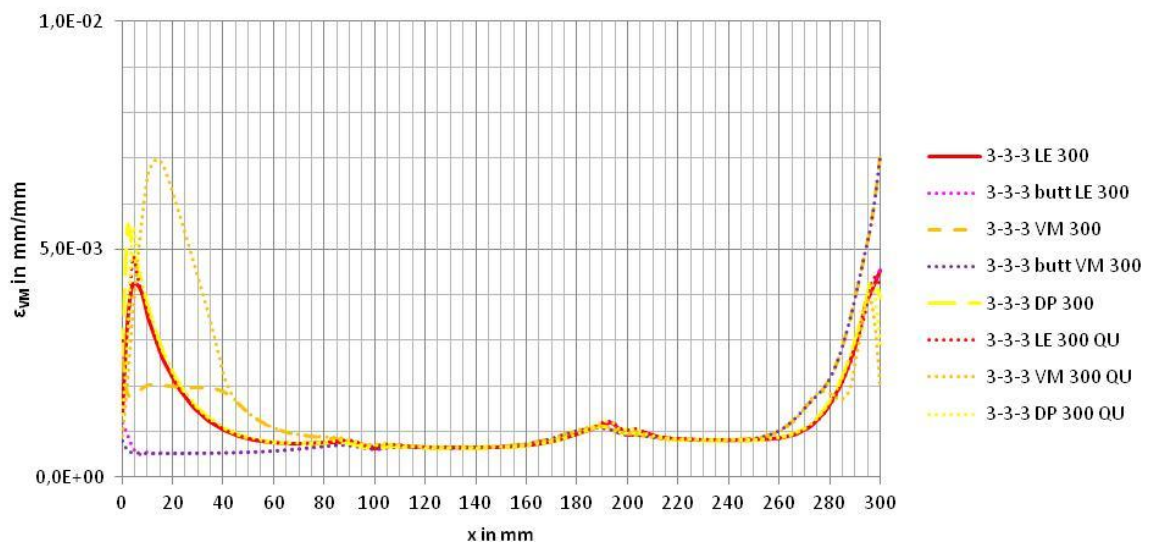


Figure 29.38: Equivalent strain of double strap at y=75, top

29.5 FEM results for comparison with DIC

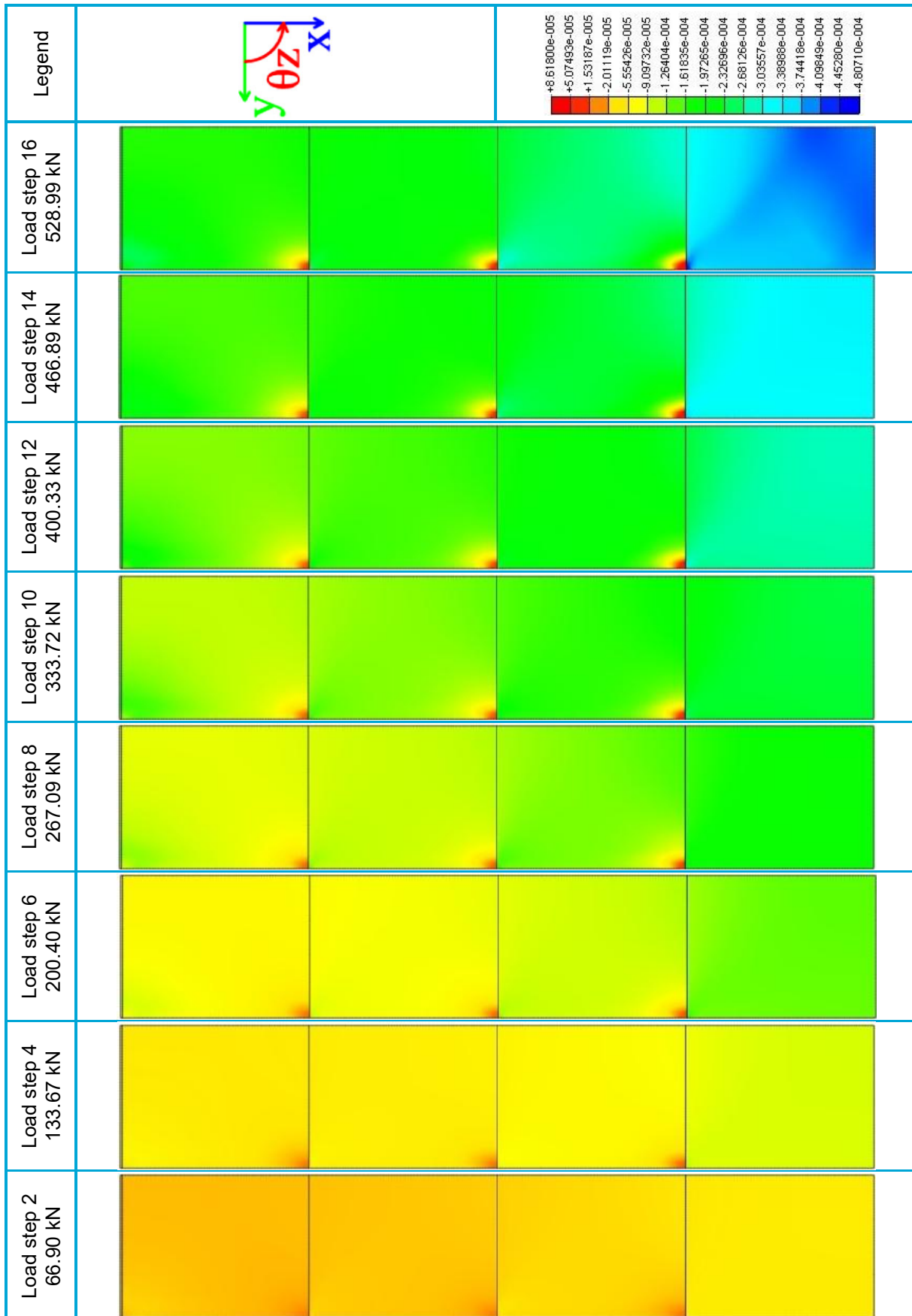


Table 29.1: Top view of ϵ_{yy} strain of FEM model 3-3-3 DP 300 Qu

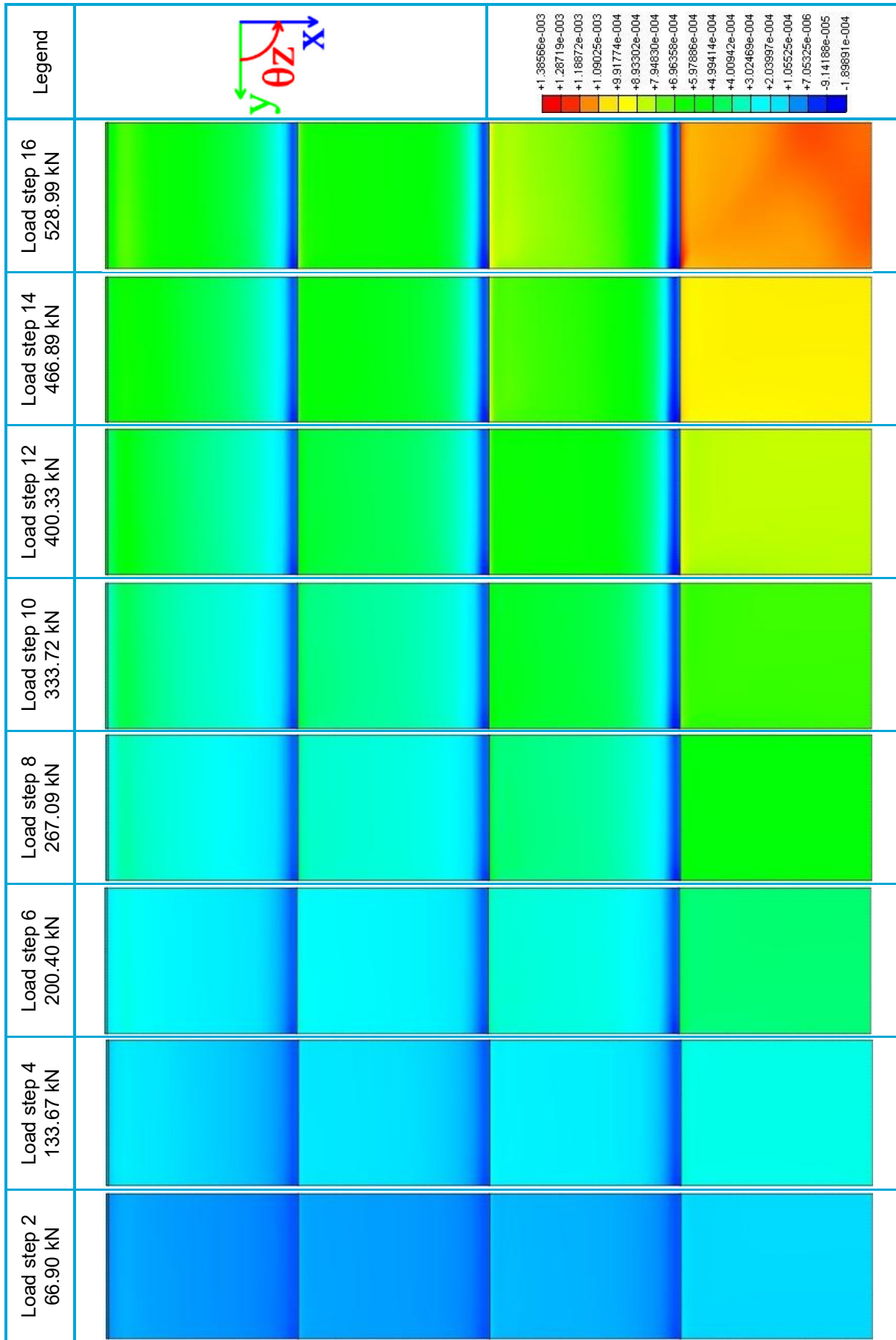


Table 29.2: Top view of ϵ_{xx} strain of FEM model 3-3-3 DP 300 Qu

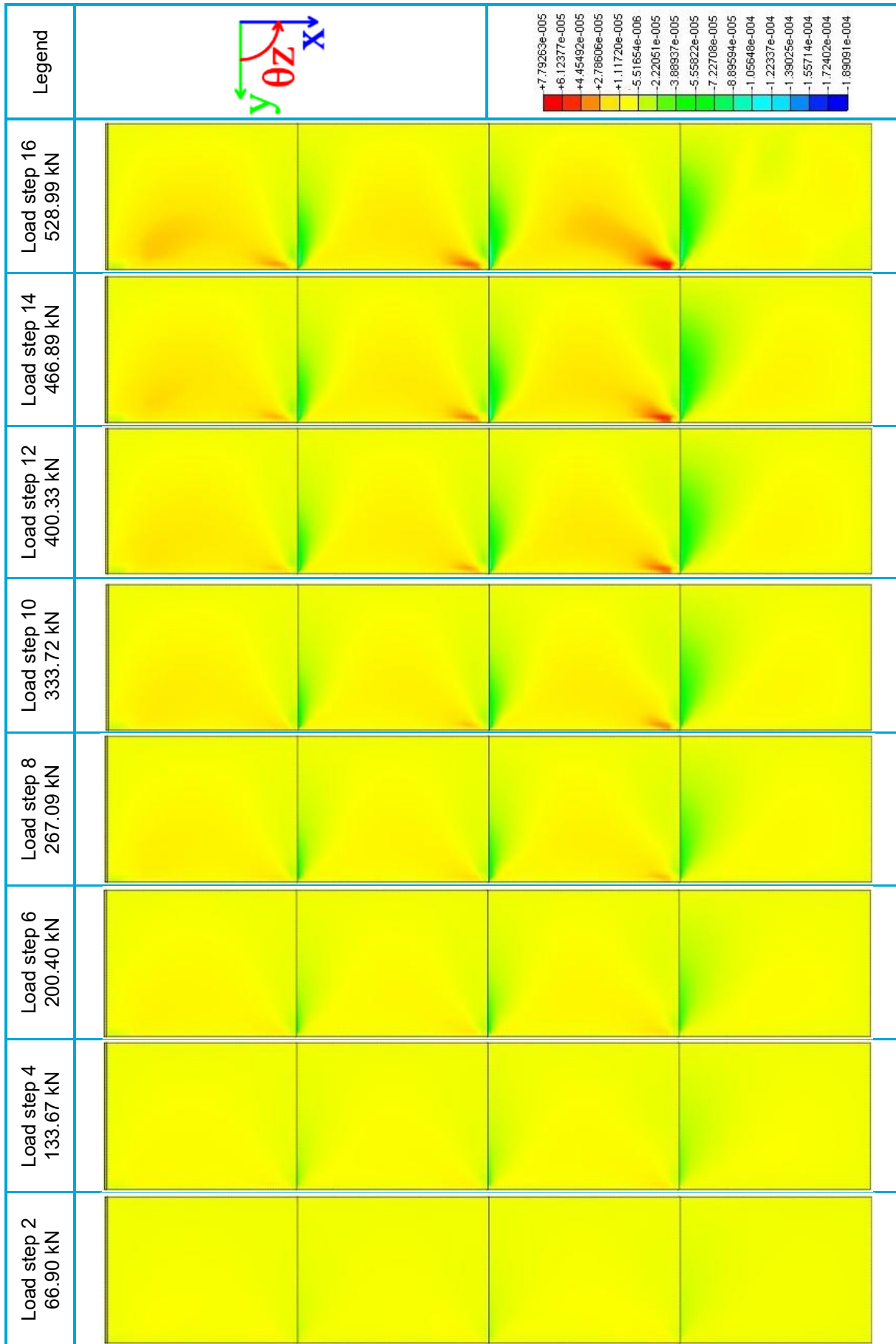


Table 29.3: Top view of γ_{xy} strain of FEM model 3-3-3 DP 300 Qu


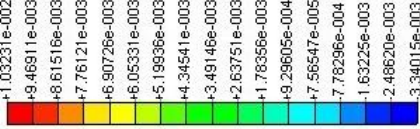
Legend	 	
Load step 16 528.99 kN		
Load step 14 466.89 kN		
Load step 12 400.33 kN		
Load step 10 333.72 kN		
Load step 8 267.09 kN		
Load step 6 200.40 kN		
Load step 4 133.67 kN		
Load step 2 66.90 kN		

Table 29.4: Side view of ϵ_{xx} strain of FEM model 3-3-3 DP 300 Qu

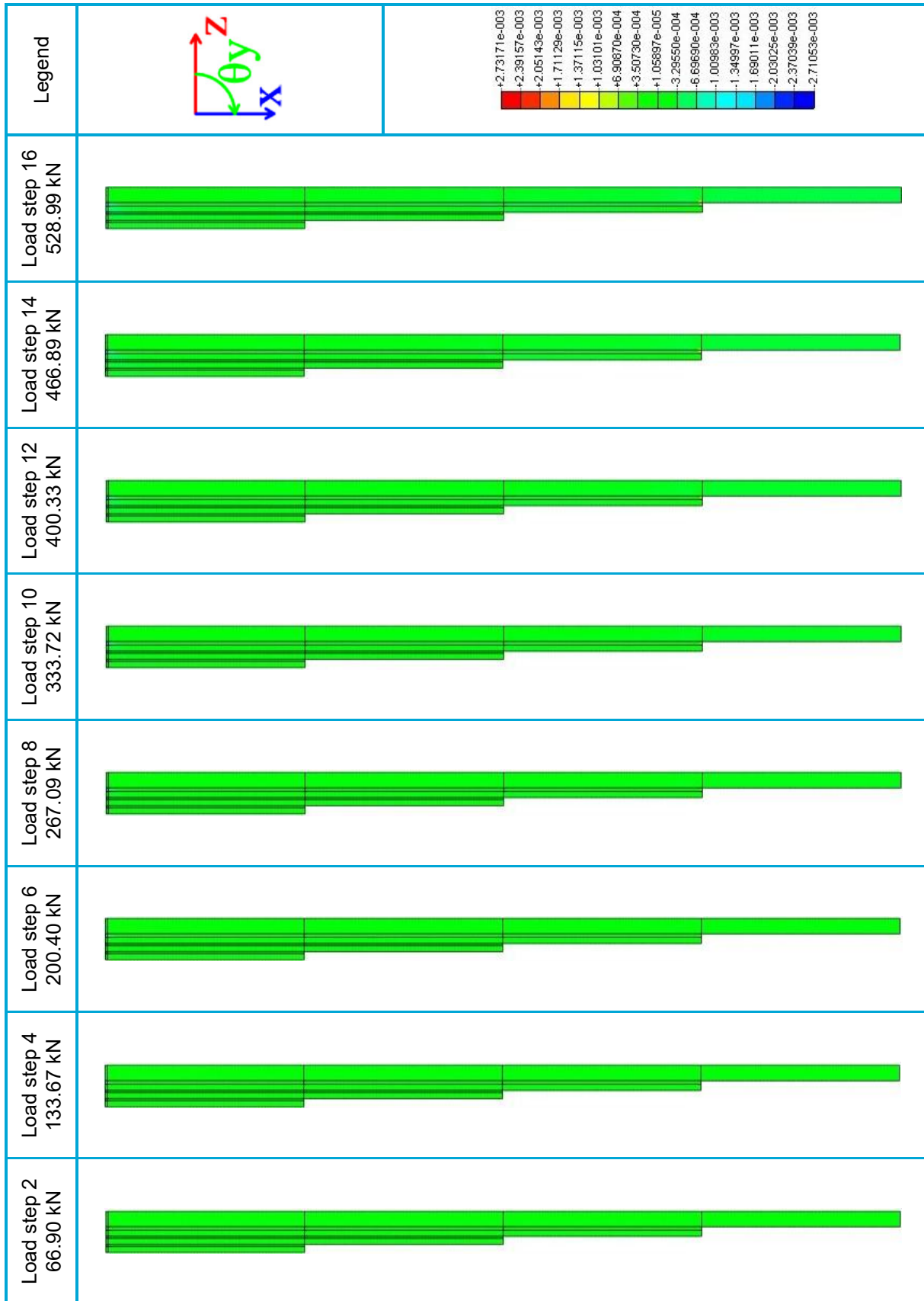


Table 29.5: Side view of ϵ_{zz} strain of FEM model 3-3-3 DP 300 Qu


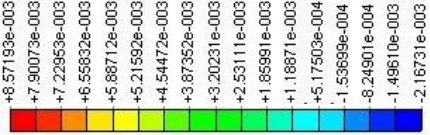
Legend	 	
Load step 2 66.90 kN		
Load step 4 133.67 kN		
Load step 6 200.40 kN		
Load step 8 267.09 kN		
Load step 10 333.72 kN		
Load step 12 400.33 kN		
Load step 14 466.89 kN		
Load step 16 528.99 kN		

Table 29.6: Side view of γ_{xy} strain of FEM model 3-3-3 DP 300 Qu

30 Appendix N: Influence of adhesive thickness

In order to examine the influence of the adhesive thickness, several FEM calculations are made. Due to the rather large tolerances of steel profiles which are used for structural engineering applications, a rather large adhesive thickness will often be applied. Therefore the influence of the adhesive thickness on the behaviour of the connection is of special interest.

30.1 Modelling and calculation

For the adhesive thickness study the same type of models are used as described in 'Appendix L: DIANA procedure for double strap connection model'. The thickness between the thin plates can be controlled rather well. For most applications such stepped straps will be composed of thin plates in a workshop. Therefore small tolerances apply and so the adhesive thickness can be small. The thickness between the strap and plate, or between a strap and a profile, is harder to control. Therefore only this adhesive thickness will vary in the adhesive thickness study. In the table below an overview of the different models can be found.

		Model					
		LE taX.X	LE QU taX.X	VM taX.X	VM QU taX.X	DP taX.X	DP QU taX.X
Parameters (see Figure 11.1)	l_1	100	100	100	100	100	100
	l_2	100	100	100	100	100	100
	l_3	100	100	100	100	100	100
	l_{end}	100	100	100	100	100	100
	$t_{s,1}$	3	3	3	3	3	3
	$t_{s,2}$	3	3	3	3	3	3
	$t_{s,3}$	3	3	3	3	3	3
	$t_{a,1}$	X.X	X.X	X.X	X.X	X.X	X.X
	$t_{a,2}$	1	1	1	1	1	1
	$t_{a,3}$	1	1	1	1	1	1
	Material model adhesive	LE	VM	VM	VM	DP	DP
	Material model steel	LE	VM	VM	VM	VM	VM
	Linear or quadratic elements	Lin	Qu	Lin	Qu	Lin	Qu

Table 30.1: Models for adhesive thickness study

30.2 Results

In the next five tables and one figure the results of the FEM calculations can be found. For the load-displacement curve the displacements of the displacement-controlled load is used (displacement of the rightmost nodes of the plate).

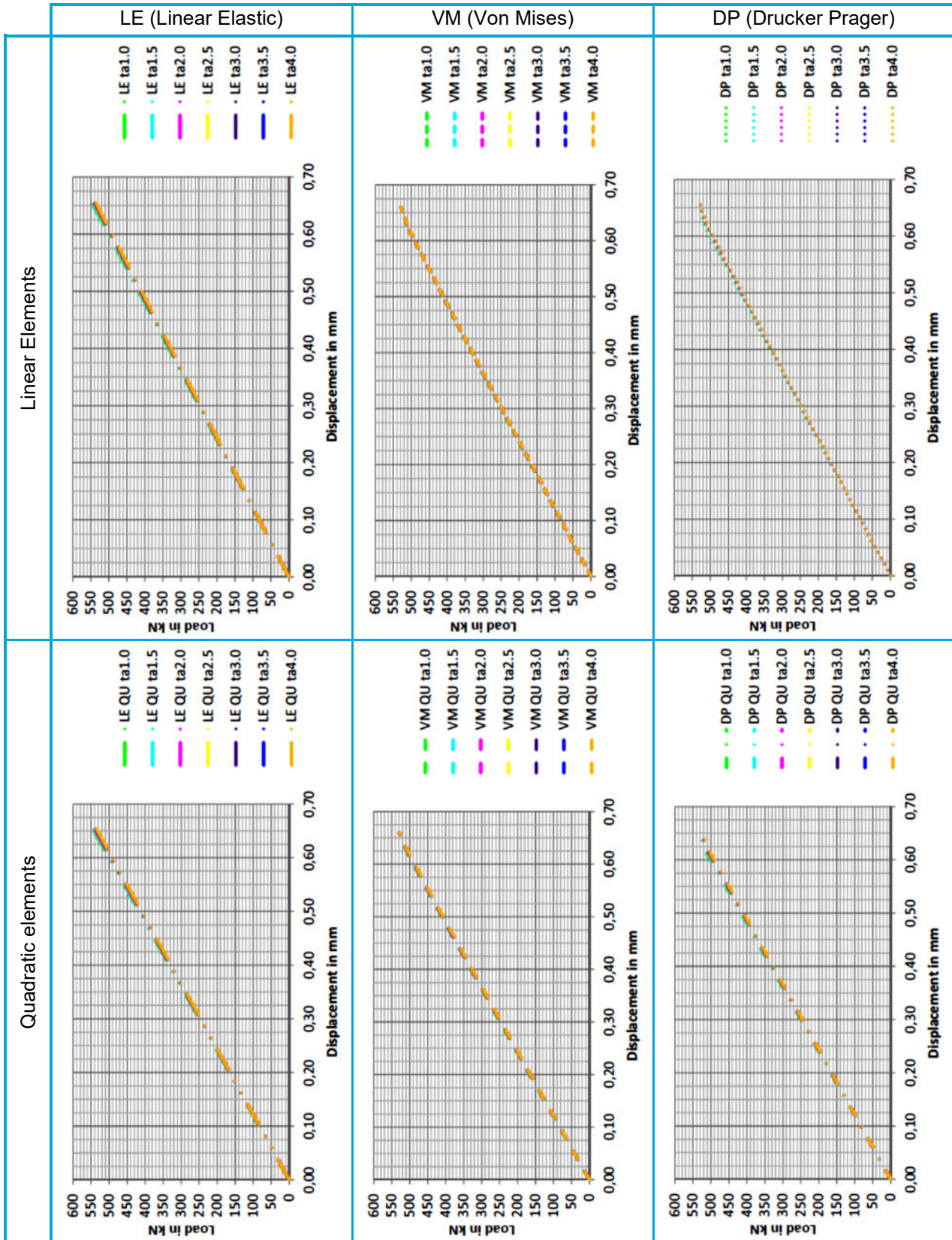


Table 30.2: Load displacement curves for different thicknesses

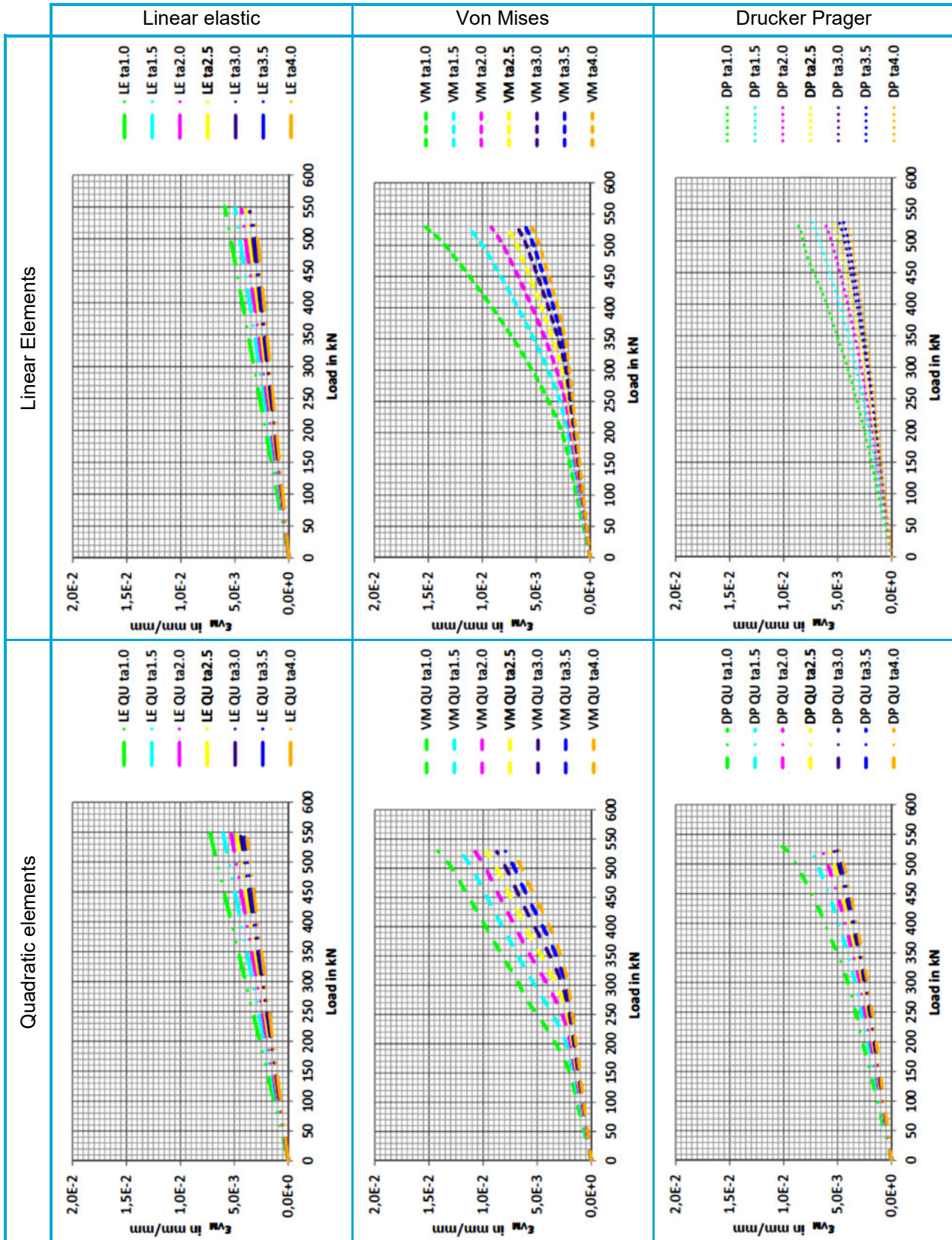


Table 30.3: Strain-load diagram of adhesive thickness study for the top point at $y=75$ and $x=l_{tot}$

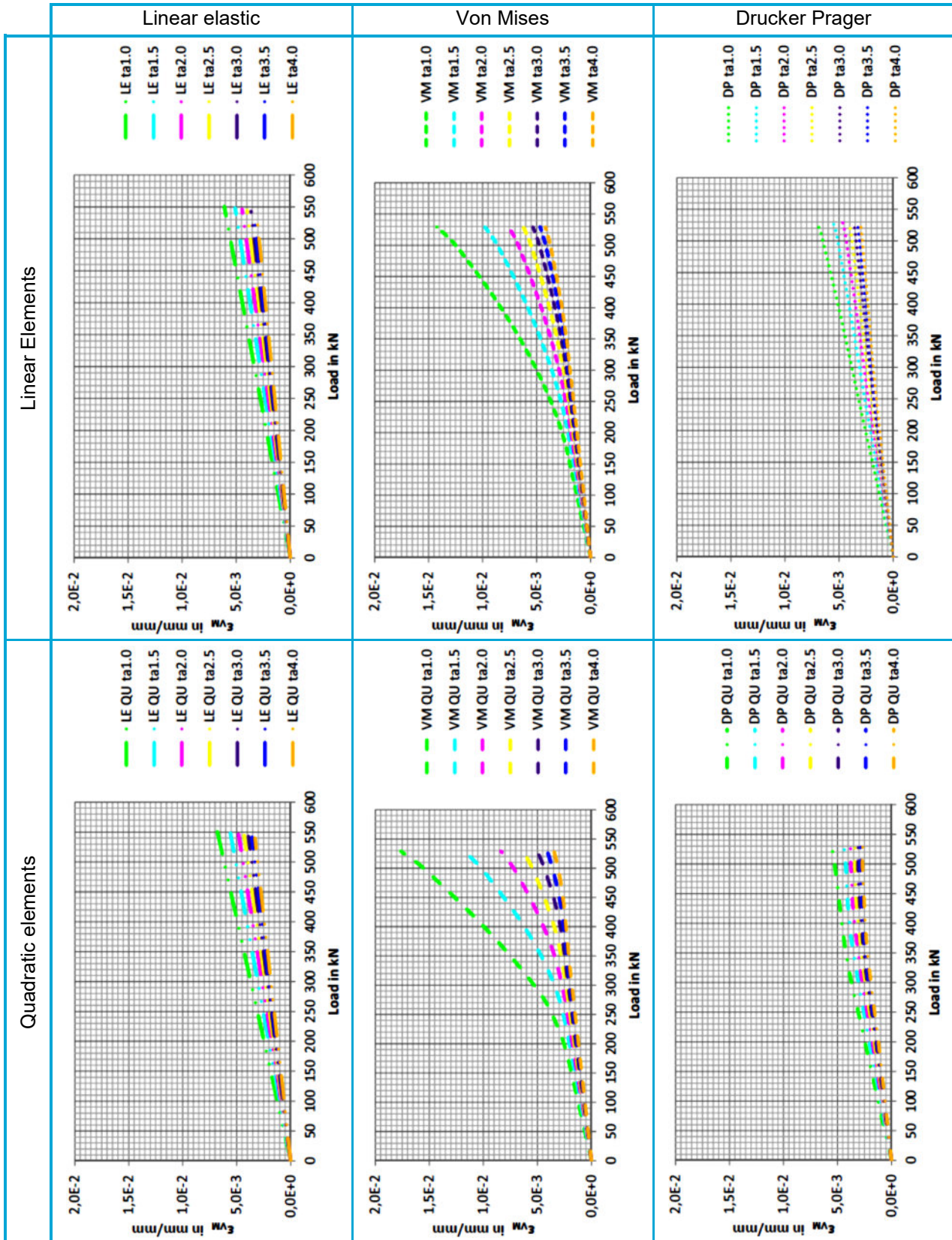


Table 30.4: Strain-load diagram of adhesive thickness study for the midpoint at $y=75$ and $x=l_{tot}$

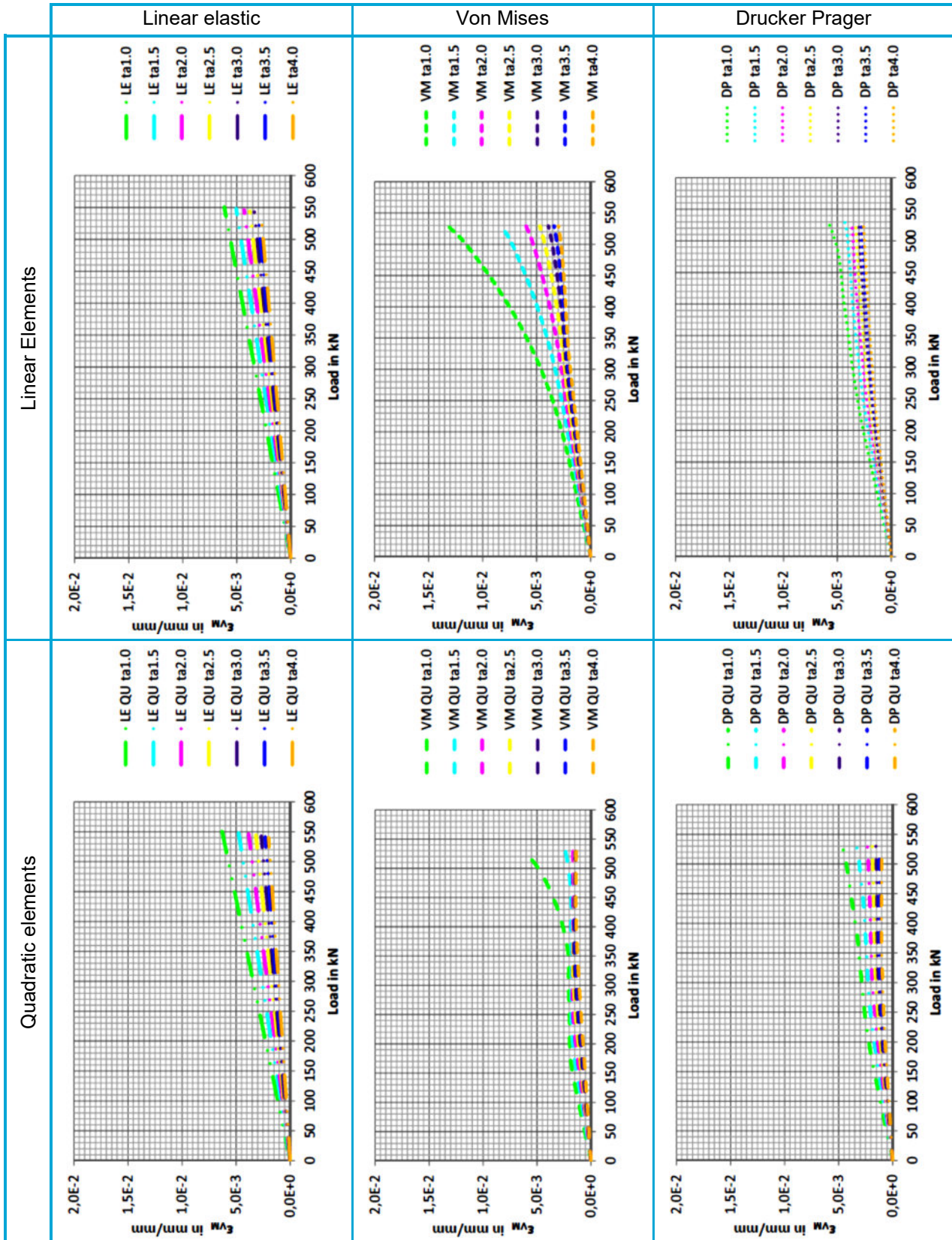


Table 30.5: Strain-load diagram of adhesive thickness study for the bottom point at $y=75$ and $x=l_{tot}$

Adhesive thickness in mm	Linear elastic Linear elements	Linear elastic Quadratic elements	Von Mises Linear elements	Von Mises Quadratic elements	Drucker Prager Linear elements	Drucker Prager Quadratic elements
10	551,06	550,86	529,36	529,26	529,54	529,48
15	548,60	548,42	529,34	529,21	529,52	529,46
20	546,58	546,40	529,33	529,15	529,50	529,58
25	544,82	544,65	529,31	529,09	529,48	0,00
30	543,27	543,10	529,30	528,95	529,46	529,63
35	541,86	541,69	529,28	528,86	529,44	529,64
40	540,56	540,40	529,26	528,76	529,42	529,62

Table 30.6: Overview of loads corresponding to a 0.33mm displacement load

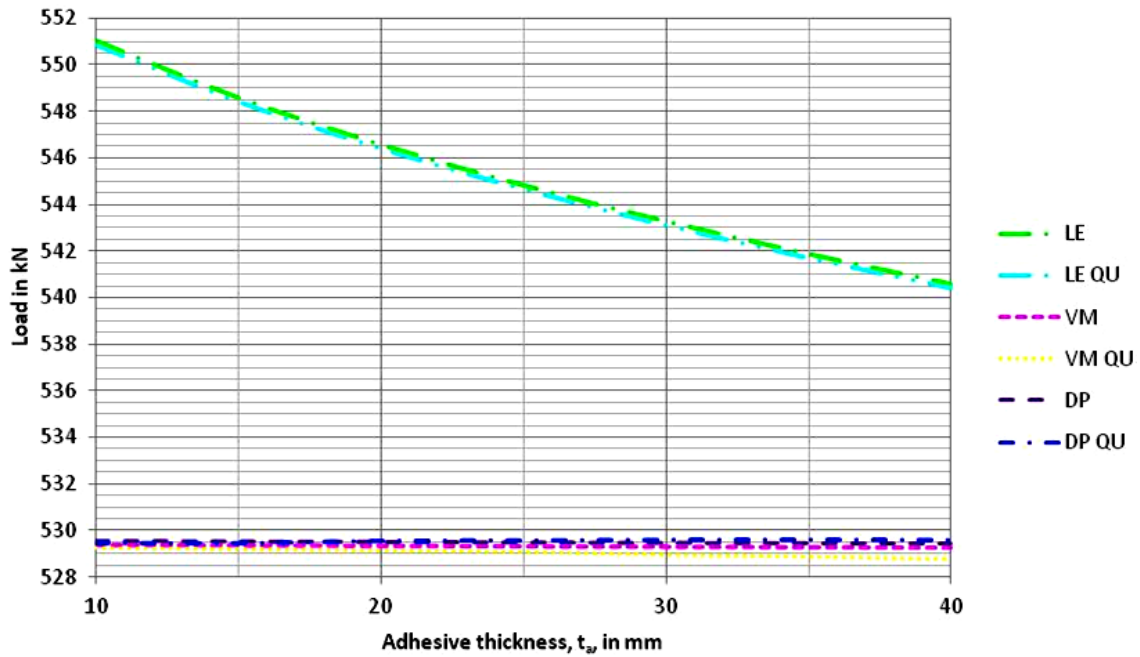


Figure 30.1: Load-adhesive thickness relation corresponding to a 0.33mm displacement load

30.3 Conclusion

Table 30.2, Table 30.6 and Figure 30.1 show that according to the FEM calculations the thickness of the first adhesive layer has no significant influence on the load-displacement behaviour of the connection for non linear material behaviour. The differences are all under a tenth of a percent. For calculations with linear elastic material behaviour the maximum difference is nearly two percent. In Table 30.6 the values of the model with Drucker Prager material behaviour and quadratic elements are remarkable. No clear relationship between the adhesive thickness and the stiffness of the connection seems to exist. Most likely this is a numerical error instead of real behaviour. Note that the differences are very small.

Table 30.3/Table 30.5 show that according to the FEM calculations a larger thickness of the first adhesive layer results in lower strains (and consequently lower stresses). A higher failure load may be expected according to this result. But some remarks have to be made. The effect of the adhesive thickness is hard to predict. According to practice tests and other more extensive research the failure load will not necessarily increase by increasing the adhesive thickness. An optimal adhesive thickness seems to exist. A larger or smaller thickness results in higher stresses at the interface near the end of the lap, in contrast to many theories and these FEM calculations. However, the stresses in the middle of the thickness will decrease by increasing the adhesive thickness, in accordance with most theories. [1]

31 Appendix O: Pictures of practice test

In this section pictures made after the tensile test of the double strap connection can be found.

31.1 Location of pictures

In the figure below an overview of the direction in which the picture are made can be found:

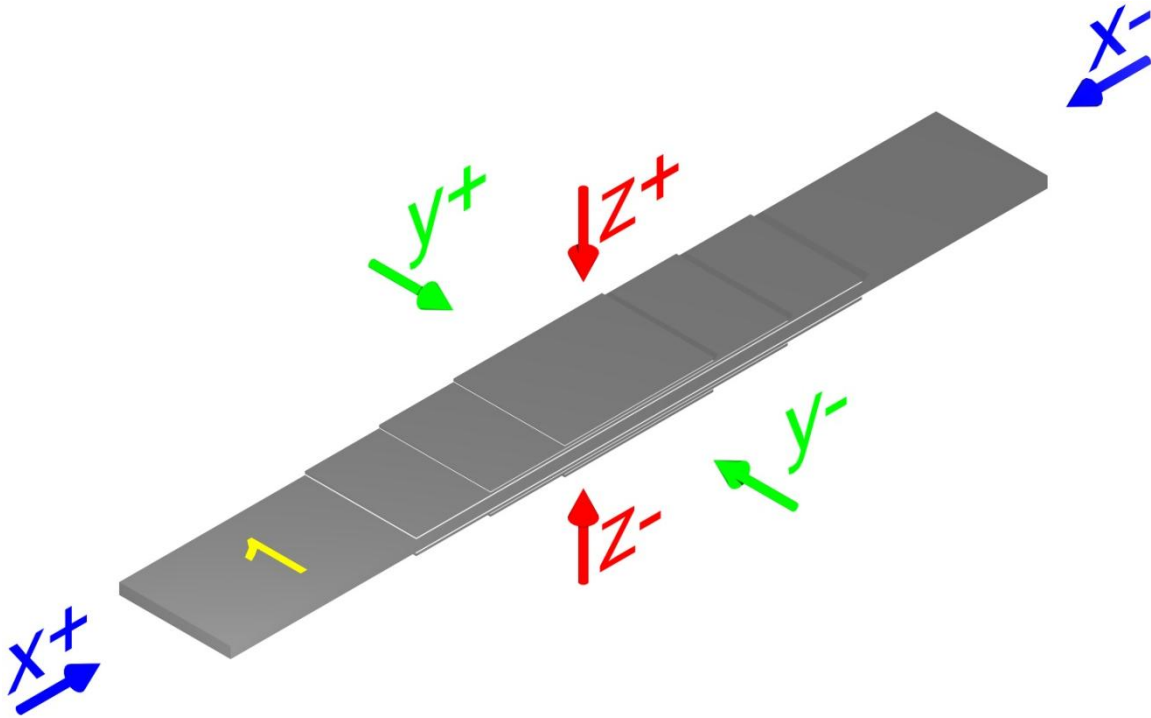


Figure 31.1: Overview from above of direction of pictures

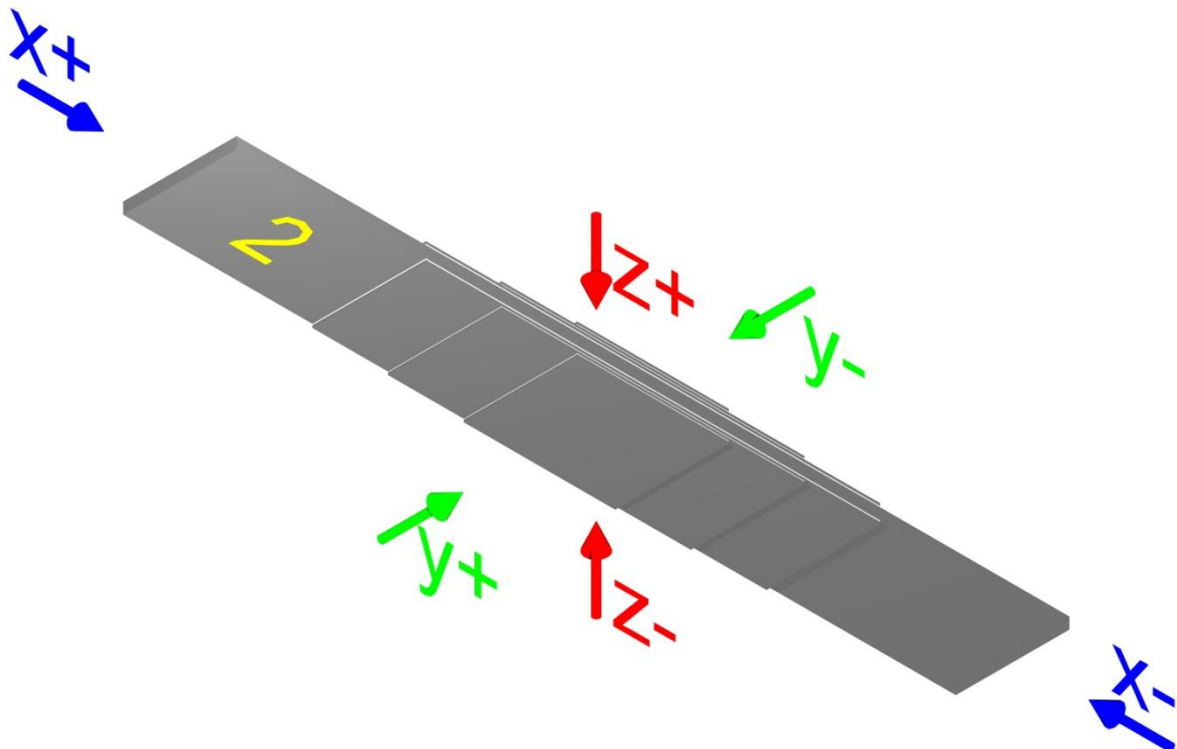


Figure 31.2: Overview from below of direction of pictures

31.2 Test 1

Below the pictures made after testing connection 1 can be found.



Figure 31.3: Connection 1 – side 1 – direction x+ – delamination of adhesive layer 2

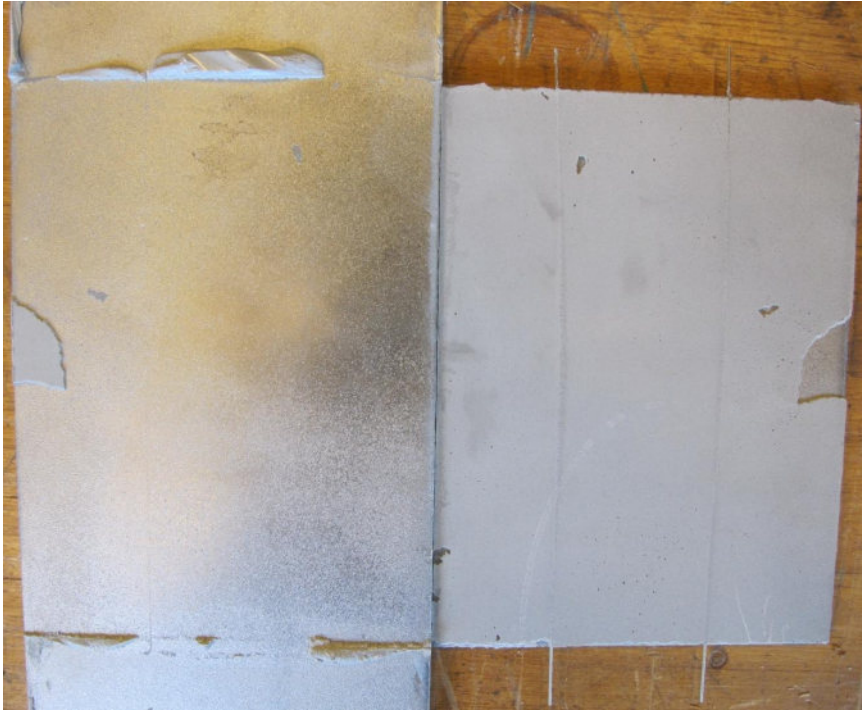


Figure 31.4: Connection 1 – side 1 – direction z+ (left side) and direction z- (right side) – third adhesive layer – complete delamination caused by adhesion failure



Figure 31.5: Connection 1 – side 1 – direction z+ (left side) and direction z- (right side) – first adhesive layer – complete delamination caused by adhesion failure



Figure 31.6: Connection 1 – direction y- – end and second of first lap



Figure 31.7: Connection 1 – direction y- – end of second and third lap



Figure 31.8: Connection 1 – direction y- – end of third lap and middle part



Figure 31.9: Connection 1 – direction y- – middle part and end of third lap

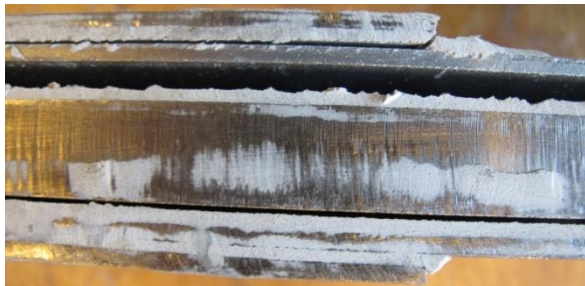


Figure 31.10: Connection 1 – direction y- – end of third and second lap

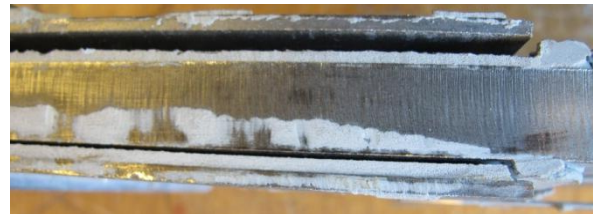


Figure 31.11: Connection 1 – direction y- – end of first and second lap



Figure 31.12: Connection 1 – direction y+ – end and first lap



Figure 31.13: Connection 1 – direction y+ – end of second and third lap



Figure 31.14: Connection 1 – direction y+ – end of third lap and middle part



Figure 31.15: Connection 1 – direction y+ – middle part and end of third lap



Figure 31.16: Connection 1 – direction y^+ – end of third and second lap



Figure 31.17: Connection 1 – direction y^+ – end of second and first lap

31.3 Test 2

Below the pictures made after testing connection 2 can be found.



Figure 31.18: Connection 2 – direction y- – end of first lap



Figure 31.19: Connection 2 – direction y- – end of second and third lap



Figure 31.20: Connection 2 – direction y- – end of third lap and middle part



Figure 31.21: Connection 2 – direction y- – middle part and end of third lap



Figure 31.22: Connection 2 – direction y- – end of third and second lap



Figure 31.23: Connection 2 – direction y- – end of second and first lap



Figure 31.24: Connection 2 – direction y+ – end of first and second lap



Figure 31.25: Connection 2 – direction y+ – second lap



Figure 31.26: Connection 2 – direction y+ – end of third lap and middle part



Figure 31.27: Connection 2 – direction y+ – middle part and end of third lap



Figure 31.28: Connection 2 – direction y+ – end of second and first lap

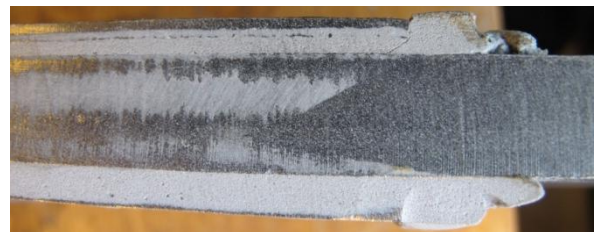


Figure 31.29: Connection 2 – direction y+ – end of first lap

31.4 Test 3

Below the pictures made after testing connection 3 can be found.

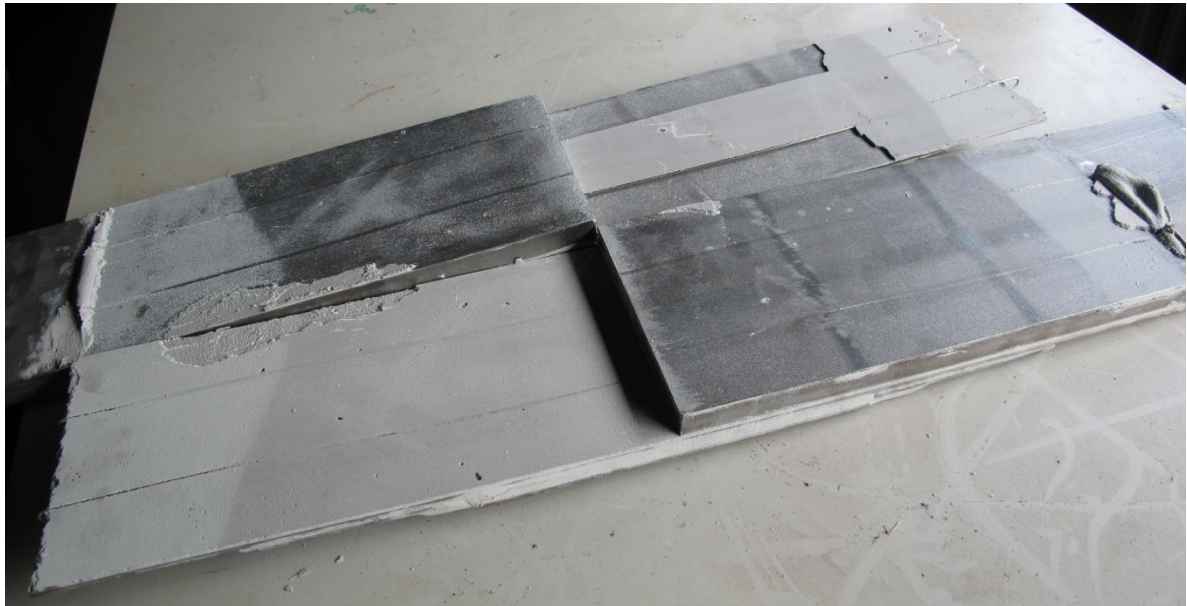


Figure 31.30: Connection 3 – Complete delamination of first adhesive layer in Z-shape

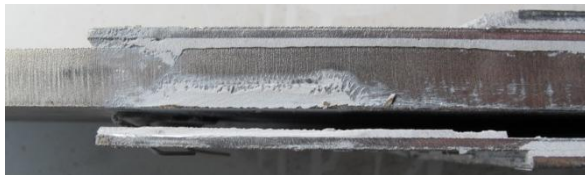


Figure 31.31: Connection 3 – direction y- – end of first and second lap

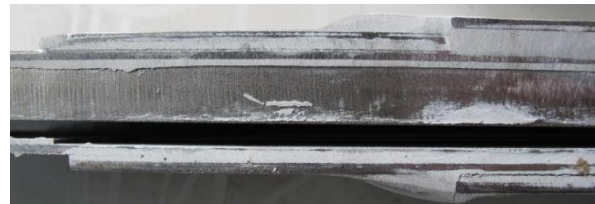


Figure 31.32: Connection 3 – direction y- – end of second and third lap



Figure 31.33: Connection 3 – direction y- – middle part

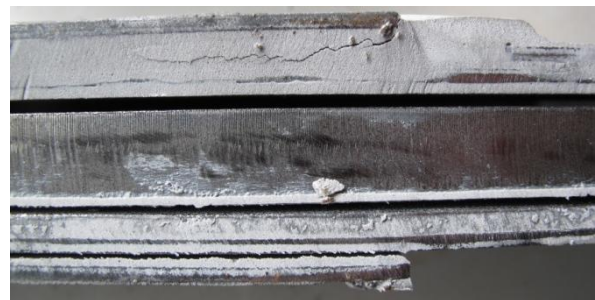


Figure 31.34: Connection 3 – direction y- – end of third lap

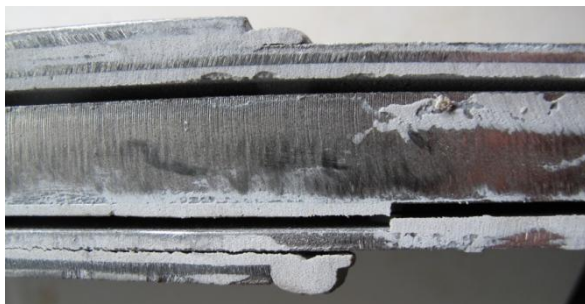


Figure 31.35: Connection 3 – direction y- – end of second lap

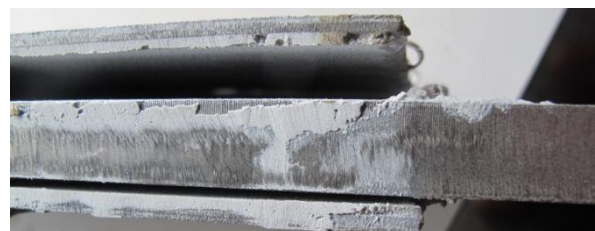


Figure 31.36: Connection 3 – direction y- – end of first lap



Figure 31.37: Connection 3 – direction y+ – end of first lap

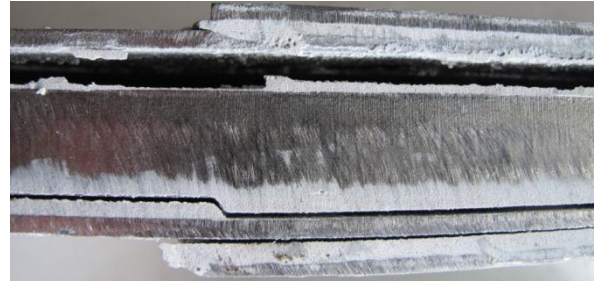


Figure 31.38: Connection 3 – direction y+ –end of second lap

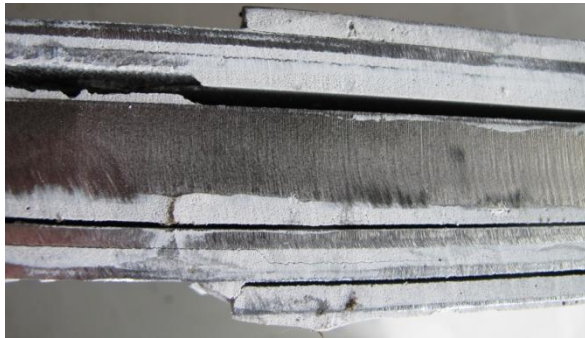


Figure 31.39: Connection 3 – direction y+ – end of third lap

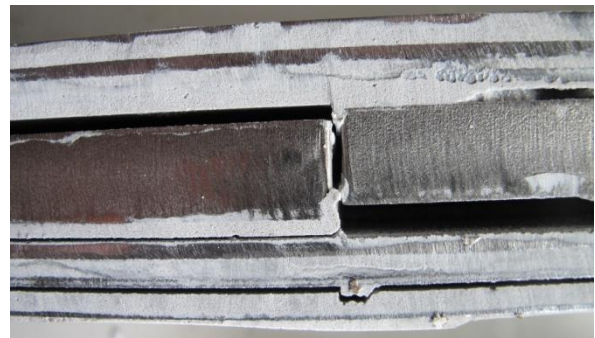


Figure 31.40: Connection 3 – direction y+ – middle part



Figure 31.41: Connection 3 – direction y+ – end of third lap

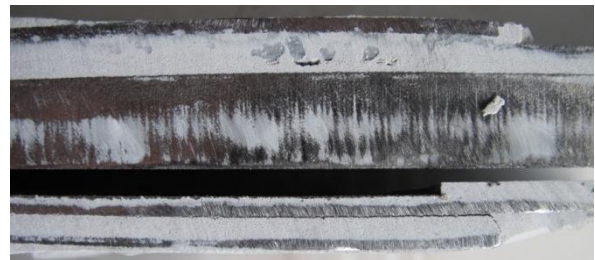


Figure 31.42: Connection 3 – direction y+ – end of second lap



Figure 31.43: Connection 3 – direction y+ – end of first lap

31.5 Test 4

Below the pictures made after testing connection 4 can be found.

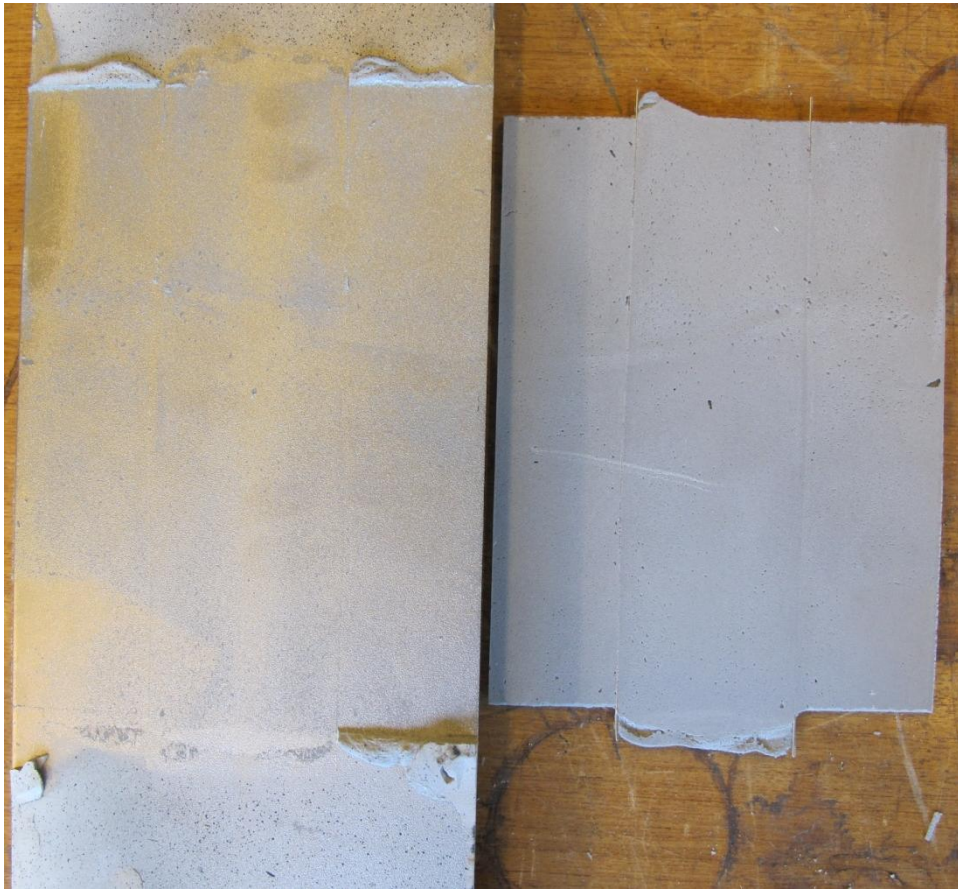


Figure 31.44: Connection 4 – side 1 – direction z+ (left side) and direction z- (right side) – third adhesive layer – complete delamination caused by adhesion failure

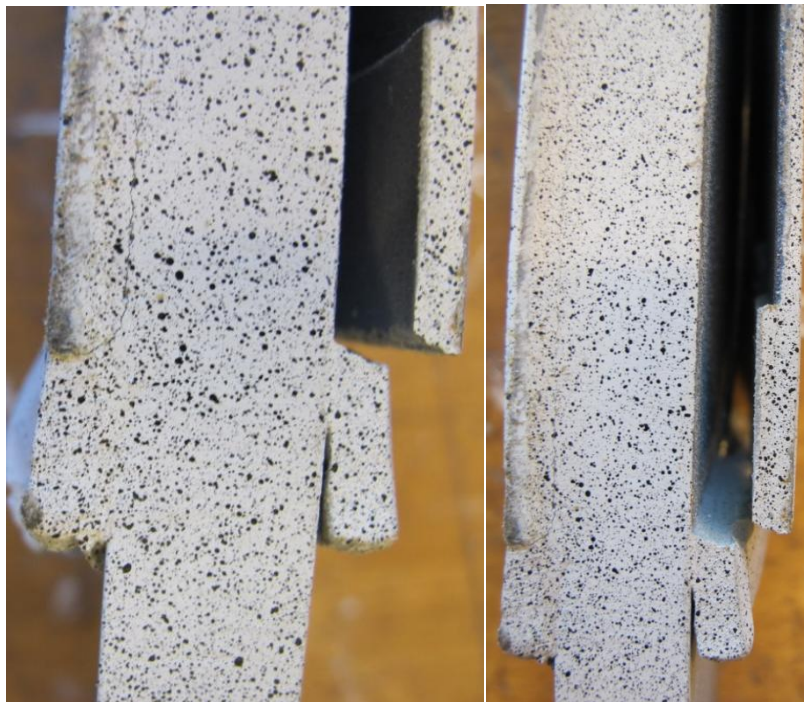


Figure 31.45: Connection 4 – End of adhesive layer 1 which is considered during DIC measurements

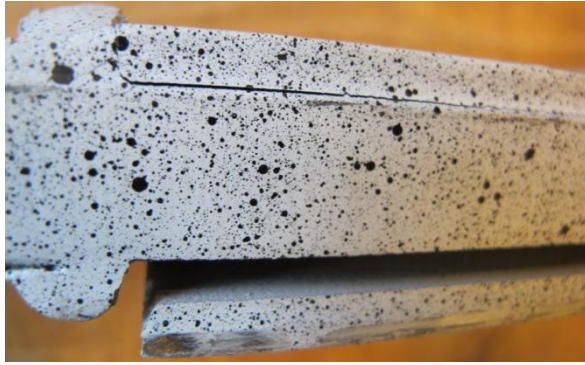


Figure 31.46: Connection 4 – direction y- – end of first lap



Figure 31.47: Connection 4 – direction y- – end of third lap



Figure 31.48: Connection 4 – direction y- – middle part



Figure 31.49: Connection 4 – direction y- – middle part and end of third lap



Figure 31.50: Connection 4 – direction y- – end of second lap

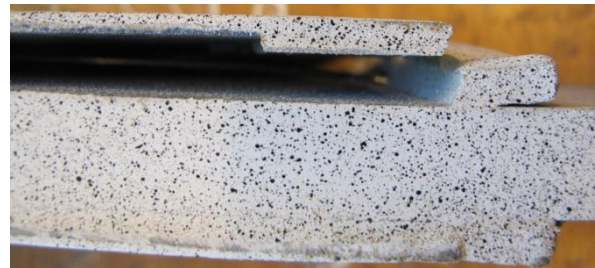


Figure 31.51: Connection 4 – direction y- – end of first lap



Figure 31.52: connection 4 in y+ direction



Figure 31.53: Connection 4 – direction y+ – end of first lap



Figure 31.54: Connection 4 – direction y+ – end of second lap

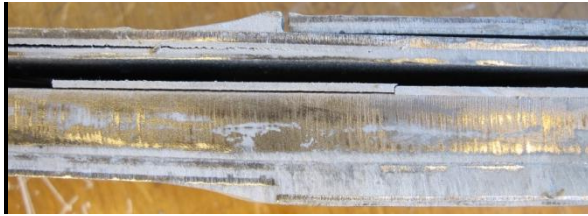


Figure 31.55: Connection 4 – direction y+ – end of third lap

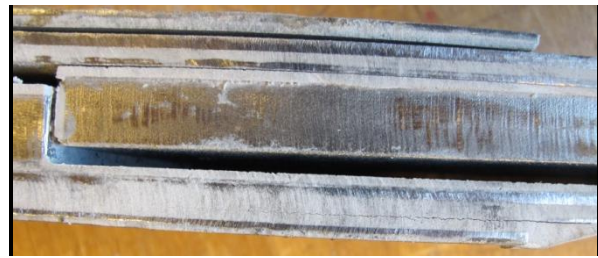


Figure 31.56: Connection 4 – direction y+ – middle part and end of third lap

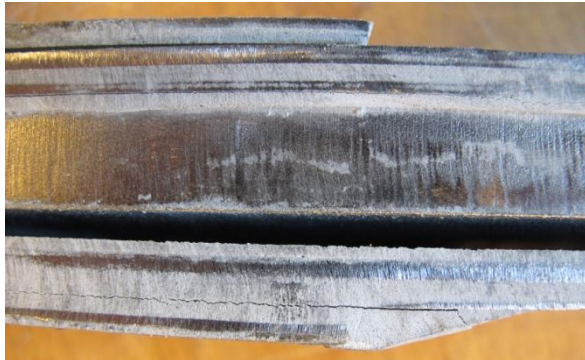


Figure 31.57: Connection 4 – direction y+ – end of second lap

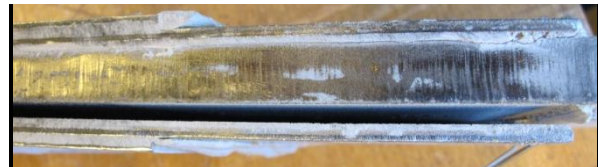


Figure 31.58: Connection 4 – direction y+ – end of second and first lap

31.6 Test 5

Below the pictures made after testing connection 5 can be found.

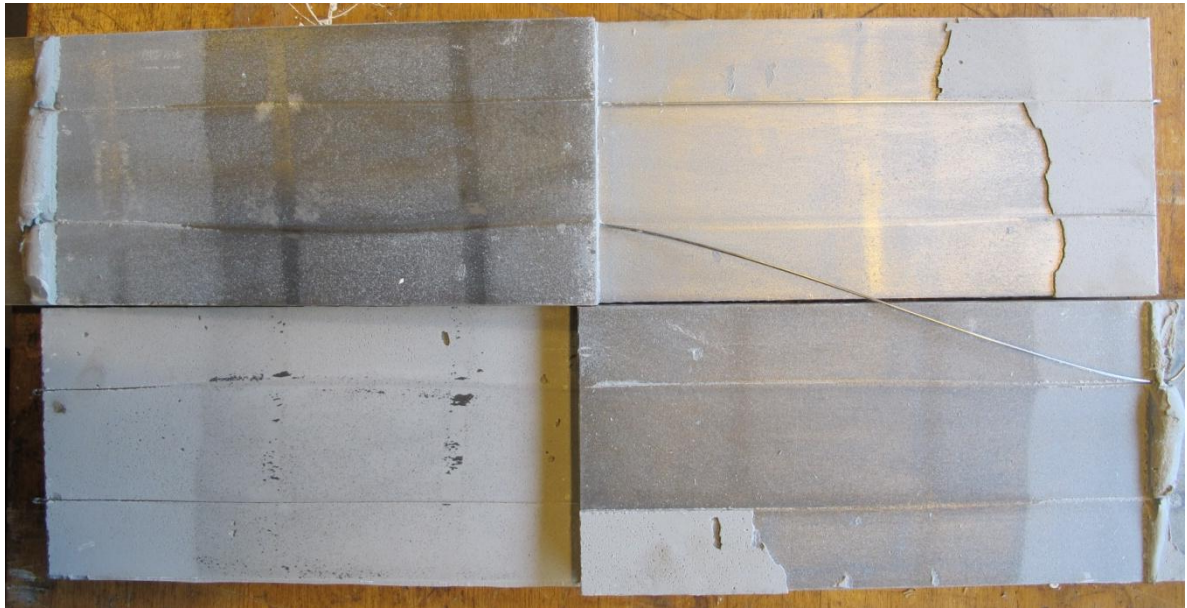


Figure 31.59: Connection 5 – complete delamination at first adhesive layer in Z-shape



Figure 31.60: Connection 5 – Failure in Z-shape

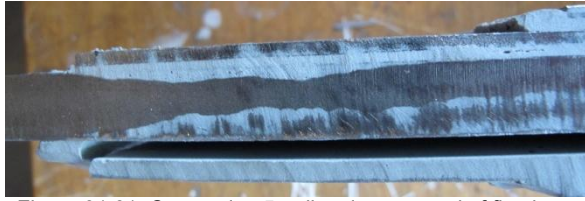


Figure 31.61: Connection 5 – direction y- – end of first lap

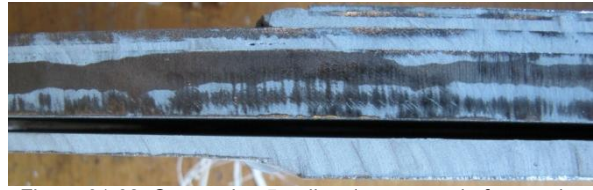


Figure 31.62: Connection 5 – direction y- – end of second lap

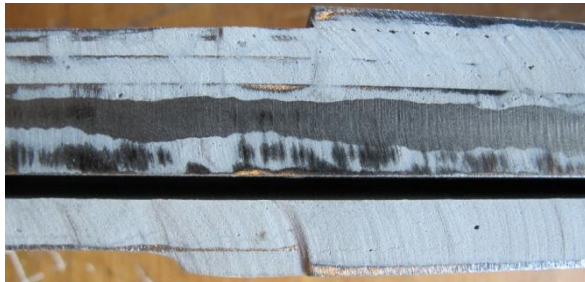


Figure 31.63: Connection 5 – direction y- – end of third lap

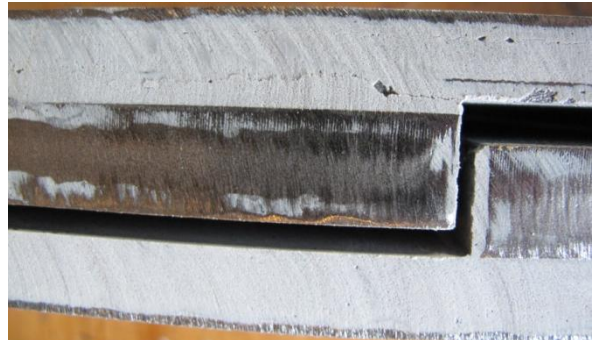


Figure 31.64: Connection 5 – direction y- – middle part



Figure 31.65: Connection 5 – direction y- – end of second lap

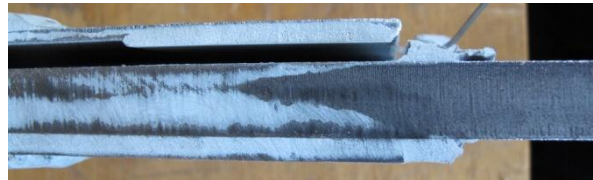


Figure 31.66: Connection 5 – direction y- – end of first lap



Figure 31.67: Connection 5 – direction y+ – end of first lap



Figure 31.68: Connection 5 – direction y+ – end of second lap



Figure 31.69: Connection 5 – direction y+ – middle part



Figure 31.70: Connection 5 – direction y+ – end of third lap



Figure 31.71: Connection 5 – direction y+ – end of second lap



Figure 31.72: Connection 5 – direction y+ – end of first lap

32 Appendix P: DIC results

In the figure below the area which is considered with DIC is visible. For a proper DIC calculation a somewhat smaller area is considered than the area with the spackle pattern. For the front view the area around the rod of the LVDT is not considered. The rod has no spackle pattern and therefore the DIC program has difficulties with the calculation of it. Due to the correlation process some scatter arise in all DIC results. The outflow of the adhesive gives rise to some high peak stresses but due to its irregularities it is hard to say if this is due to correlation problems or real behaviour. The chosen images correspond best with the steps in section 29.5 and the image right before failure is added.

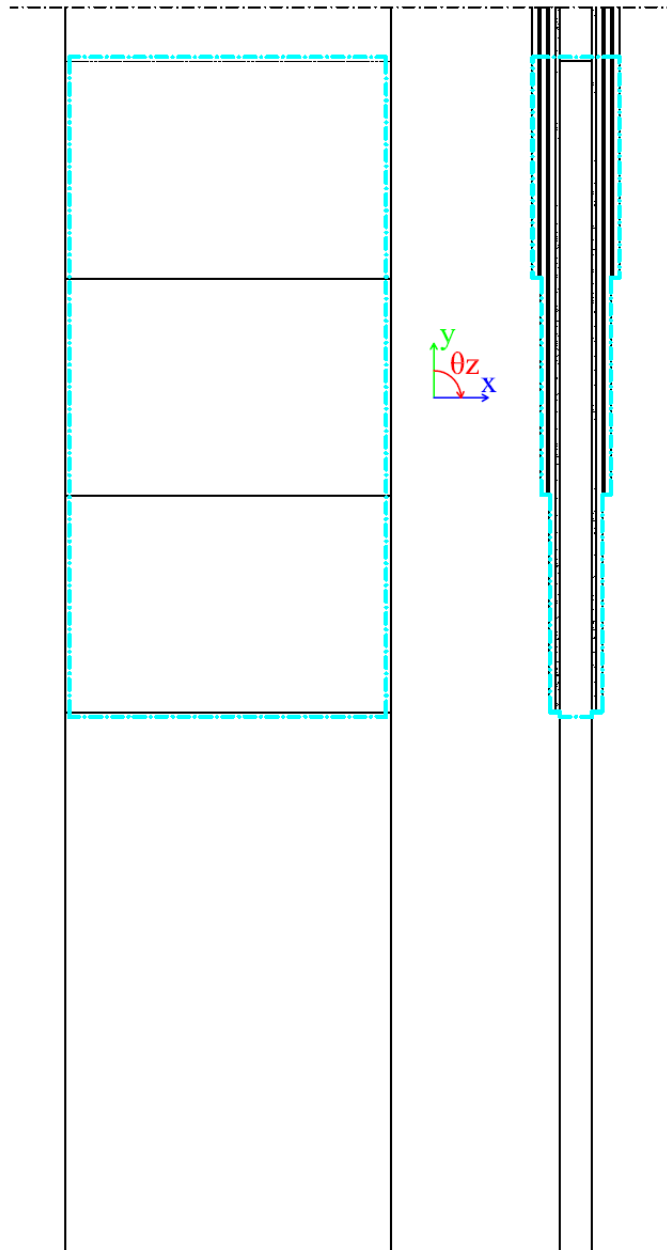


Figure 32.1: DIC area

32.1 Connection 2; DIC measurement of the front

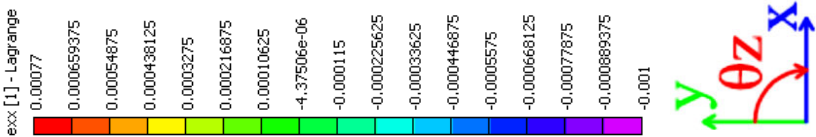
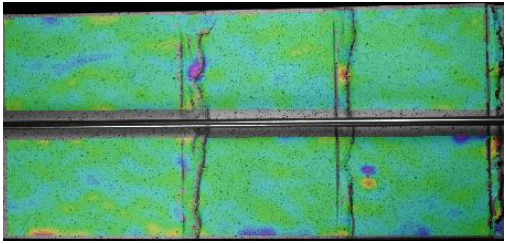
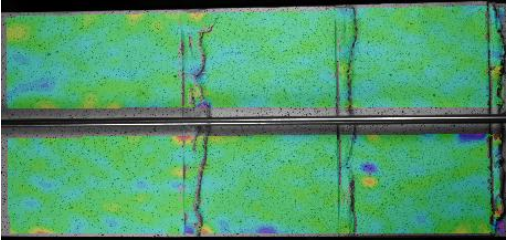
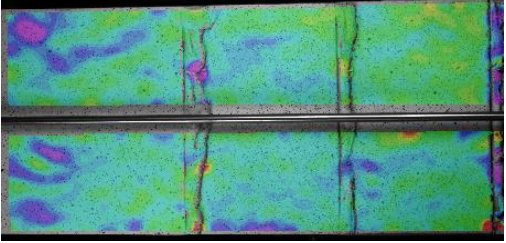
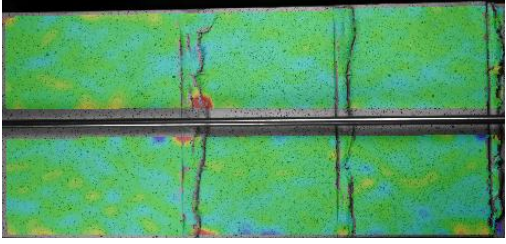
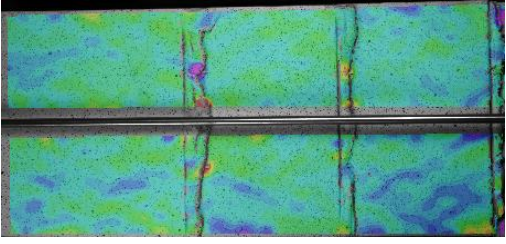
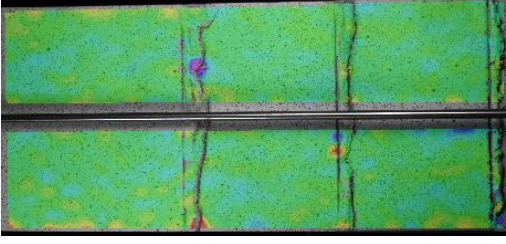
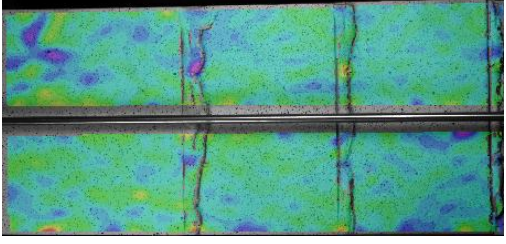
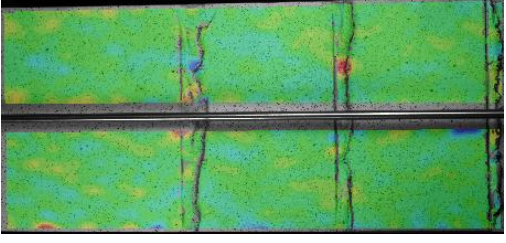
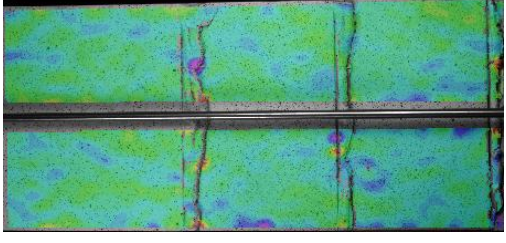
Legend		
Photo 127: 300.38 kN		
Photo 92: 232.85 kN		Photo 397: 569.66 kN 
Photo 63: 166.92 kN		Photo 276: 500.07 kN 
Photo 37: 98.32 kN		Photo 215: 433.98 kN 
Photo 16: 33.55 kN		Photo 169: 367.94 kN 

Table 32.1: Connection 2 DIC results of ϵ_{xx}

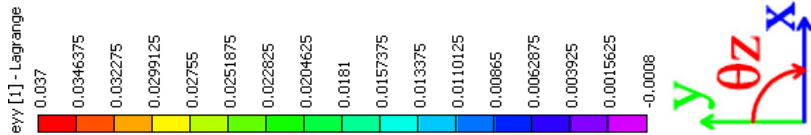
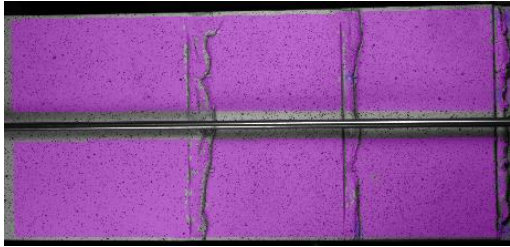
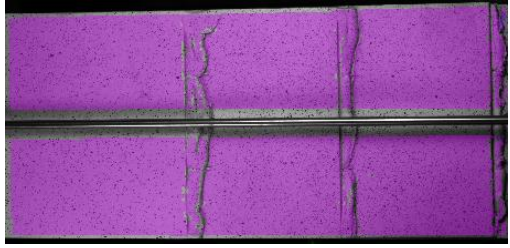
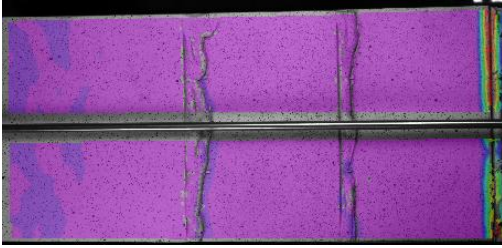
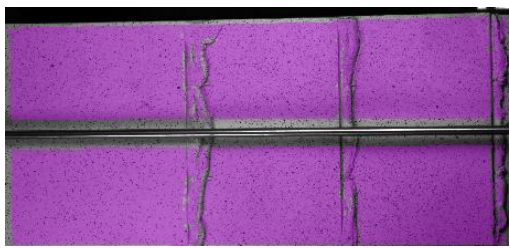
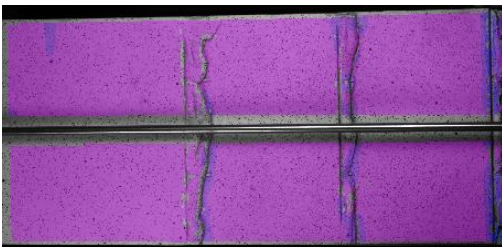
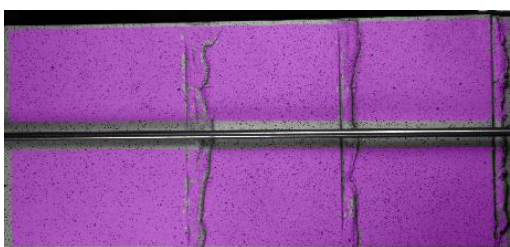
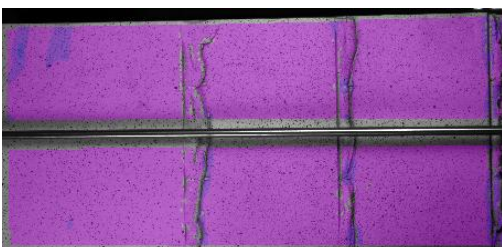
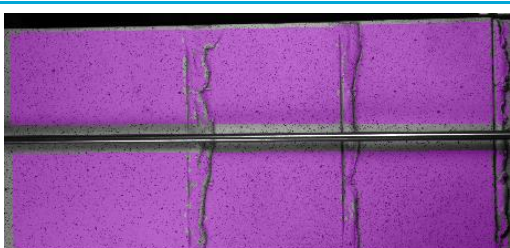
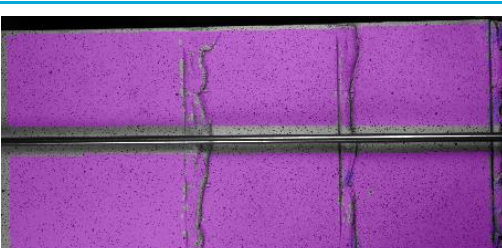
Legend		
Photo 127: 300.38 kN		
Photo 92: 232.85 kN		
Photo 63: 166.92 kN		
Photo 37: 98.32 kN		
Photo 16: 33.55 kN		
	Photo 169: 367.94 kN	
	Photo 276: 500.07 kN	
	Photo 397: 569.66 kN	

Table 32.2: Connection 2 DIC results of ϵ_{yy}

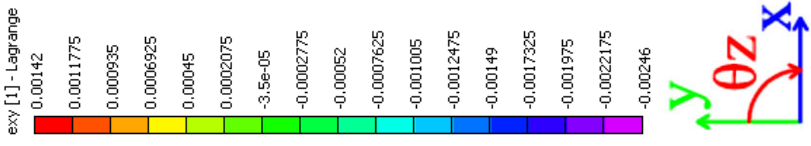
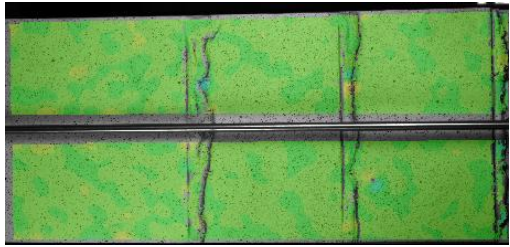
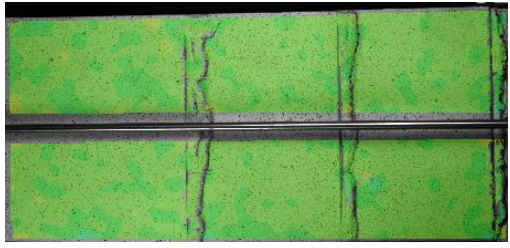
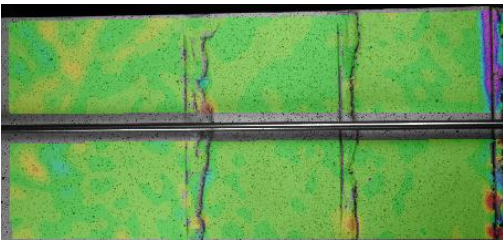
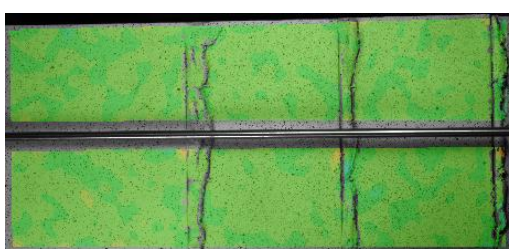
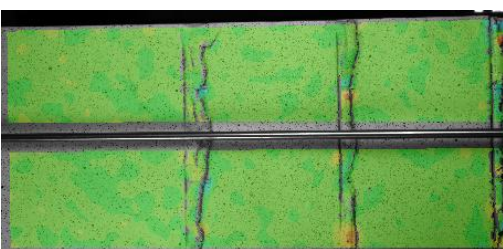
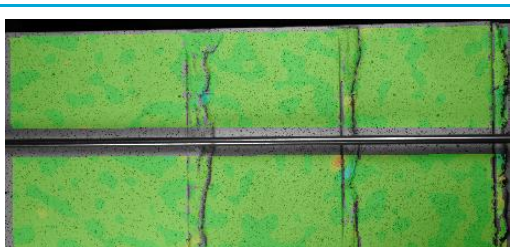
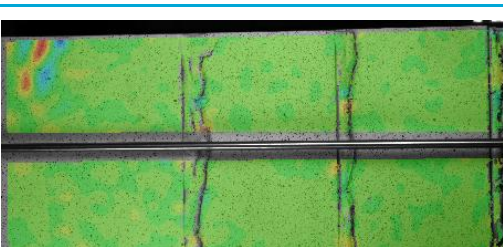
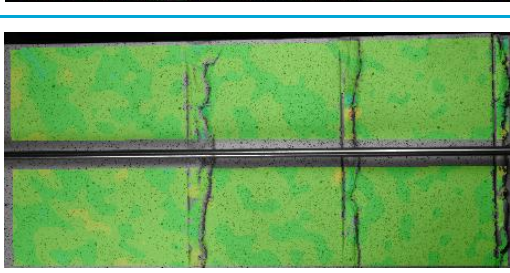
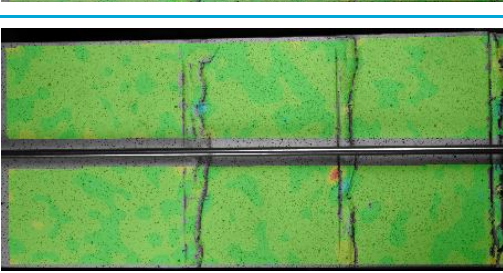
Legend		
Photo 127: 300.38 kN		
Photo 92: 232.85 kN		
Photo 63: 166.92 kN		
Photo 37: 98.32 kN		
Photo 16: 33.55 kN		

Table 32.3: Connection 2 DIC results of γ_{xy}

32.2 Connection 4; DIC measurement of the side

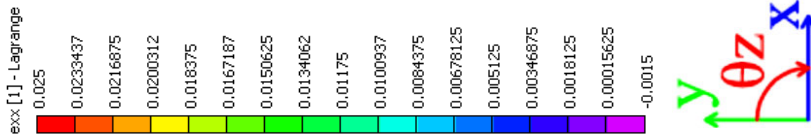

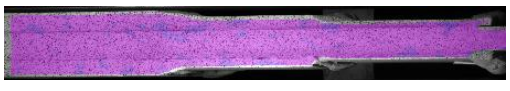

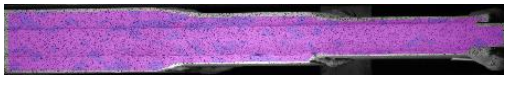
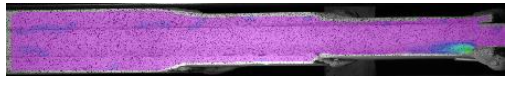
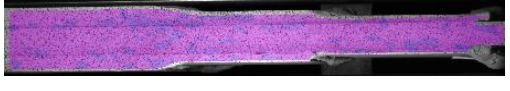
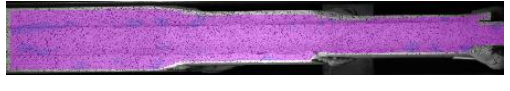
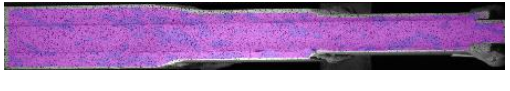
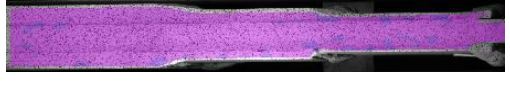
Legend		
Photo 157: 333.38 kN		
Photo 115: 266.98 kN		Photo 433: 576.29 kN 
Photo 80: 200.89 kN		Photo 331: 528.36 kN 
Photo 40: 101.85 kN		Photo 263: 465.38 kN 
Photo 18: 34.16 kN		Photo 204: 400.43 kN 

Table 32.4: Connection 2 DIC results of ϵ_{xx}

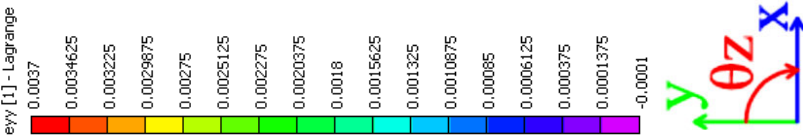
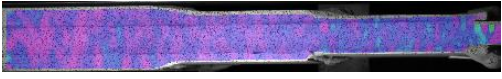
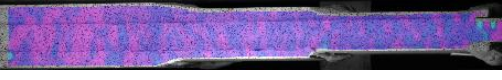
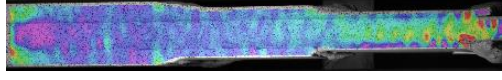
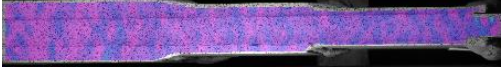
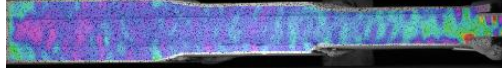
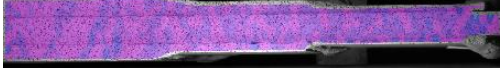
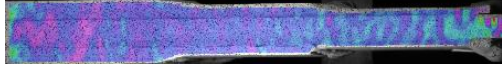
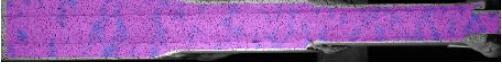
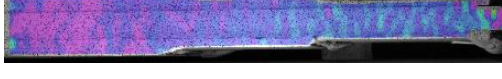
Legend		
Photo 157: 333.38 kN		
Photo 115: 266.98 kN		Photo 433: 576.29 kN 
Photo 80: 200.89 kN		Photo 331: 528.36 kN 
Photo 40: 101.85 kN		Photo 263: 465.38 kN 
Photo 18: 34.16 kN		Photo 204: 400.43 kN 

Table 32.5: Connection 2 DIC results of ϵ_{yy}

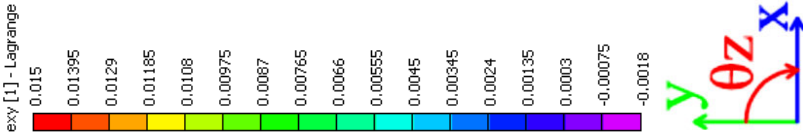
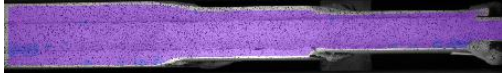
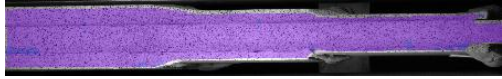
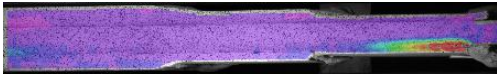
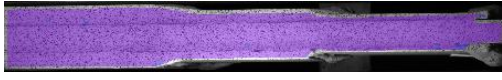

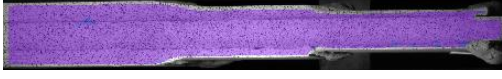
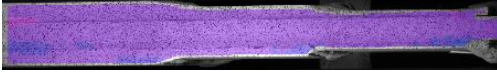
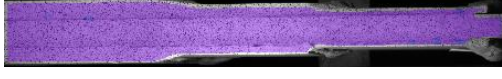
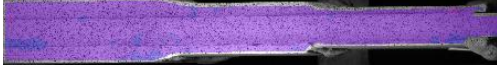
Legend		
Photo 157: 333.38 kN		
Photo 115: 266.98 kN		Photo 433: 576.29 kN 
Photo 80: 200.89 kN		Photo 331: 528.36 kN 
Photo 40: 101.85 kN		Photo 263: 465.38 kN 
Photo 18: 34.16 kN		Photo 204: 400.43 kN 

Table 32.6: Connection 2 DIC results of γ_{xy}